SYNTHESIS AND CHARACTERISATION OF NOVEL STAR-SHAPED OLIGOFLUORENES FOR ORGANIC SEMICONDUCTOR LASERS

Submitted by

Clara Orofino Peña

A thesis submitted in fulfilment of the requirements for the degree of Doctor of Philosophy in Department of Pure and Applied Chemistry, University of Strathclyde

2013

This thesis is the result of the author's original research. It has been composed by the author and has not been previously submitted for examination, which has led to the award of a degree.

The copyright of this thesis belongs to the author under the terms of the United Kingdom Copyright Acts as qualified by University of Strathclyde Regulation 3.50. Due acknowledgement must always be made of the use of any material contained in, or derived from, this thesis.

Signed:

Date:

Acknowledgement

I would like to thank the Basque Government for providing the funding for my PhD and for spending four months of my research in Montreal. I would like to thank Prof. Peter Skabara for giving me the opportunity to develop my PhD within his group at the University of Strathclyde in a state of the art lab. Also a big thanks to Prof. Dimitrii Perepichka (McGill University) for the excellent time spent in his group. I would also like to thank the collaborators from the University of St Andrews, Institute of Photonics (Strathclyde) and Imperial College London for the photophysics and lasing studies performed on my molecules. I am also very greatful to Dr. Filipe Vilela (Max Plank, Potsdam) for his help at the beginning of my PhD and for our recent collaboration. I would like to dedicate a very special thank you to Dr. Alexander Kanibolotsky and Dr. Neil Findlay for their supervision and support throught my PhD. Moreover, the remarkable job both of them have done correcting my thesis in record time has been extraordinary. All the members of the Skabara group with whom I have had the pleasure to share my PhD days have helped me during these years, providing a great working environment and support. The technical staff of the Department has been key for the completion of my PhD. Thank you very much Denise Gilmour for the elemental analysis, Pat Keating for the mass spectrometry, Lindsay McCulloch for the TGA measurements and Craig Irvine for taking care of the NMR facilities.

Finally, I would like to thank the most important people in my life, who have supported me all the way here in the good moments and especially in the bad ones.

Thank you very much Zuzka and Sandie, for making me see the positive side of things and the nice chit-chat in and outside the lab. Your friendship has been the best result of this PhD!

Thank you Tom for your incredible support and understanding, and for making me forget about Chemistry (at least for a while)! I would not have made it without you!

Soni, Io, Fer y Pau, mil gracias pore star siempre ahí mandando vuestro apoyo ante cualquier bajón. Koadrilla Enpanadilla betiko!

Gracias amatxo, aitatxo, Elena, Vita, Ana y amama. Si he conseguido llegar aquí, es principalmente por vosotros. ¡Sois la major familia que hubiera podido pedir!

Abstract

The vast efforts dedicated to the improvement of light emitting semiconductors for light emitting diodes (LEDs) led to the leap of these materials into lasing applications. Organic semiconductor lasers (OSLs) quickly became an excellent complement to their inorganic counterparts as compact, low cost visible lasers that can even be produced on flexible substrates. The simple processability of organic semiconductors, coupled with excellent optical properties such as strong absorbance and emission profiles, high photoluminescence quantum yields and especially the possibility to tune such properties in a simple manner through chemical or physical modifications has enabled the use of OSLs in a wide variety of applications such as spectroscopical light sources, visible light communications or chemical sensors. Monodisperse oligomers allow perfect chemical control of the optoelectronic properties of the materials, which lead to high-performance reproducible lasers. Furthermore, the increase in dimensionality of these oligomers through the introduction of a central core to obtain star-shaped materials provides a greater degree of anisotropy of their properties as well as enhanced control of the morphology in the condensed state. Star-shaped oligomeric materials have featured in OSLs with excellent performance and research in this area is becoming widespread.

Chapter 1 provides an overview of the properties of organic semiconductor light emitting materials and the basic principles of organic semiconductor lasers, including the applications and the ultimate goal of this class of device. A very short overview of the principles behind OLED operation is also described.

Chapter 2 introduces developments in oligofluorenes and the concept of star-shaped oligomeric materials. The synthesis and properties of two families of such star-shaped oligofluorene truxene compounds with butyl and octyl chains (**Tn**) are introduced and compared with the already published **Tn (hexyl)** series. The impact of the length of the alkyl chains of these materials on their synthesis, thermal and photophysical properties is discussed and this comparative study is extended to an explosive sensing study based on OSL.

The importance of the position of an acceptor BT unit within the oligofluorene arms of a star-shaped quaterfluorene truxene molecule is discussed in Chapter 3. The structural symmetry

around the BT unit leads to three distinctive locations with important implications on the photophysical properties.

Chapter 4 describes the attempt to avoid aggregation previously observed in a family of materials with 9,9-dihexyloligofluorene arms and DPP cores through the enlargement of the solubilising alkyl chains (octyl). The importance of the excitation wavelength in the photophysical properties of this class of materials is also assessed.

Chapter 5 presents the synthesis and characterisation of two star-shaped compounds with four oligofluorene arms and a tetraphenylethene core. The materials are efficient emitters in the aggregated state, but not in solution, due to their aggregation induced enhanced emission (AIEE) properties. Furthermore, their lasing capabilities and the effect of pressure on their emission properties is discussed, indicating that they could be used in a new generation of pressure sensor devices.

The importance of the substitution pattern in T- and Y-shaped materials with BODIPY cores and oligofluorene arms is discussed in Chapter 6. The variation of the location of two of the arms within the core has a dramatic effect on the optical properties of the materials, which are promising for lasing applications such as visible light communications.

The experimental procedures for chapters 2-6 are presented in Chapter 7.

Abbreviations and symbols

1/2/3D	one/two/three dimensional
A	absorbance/substituent
Å	angstrom
A(*λ*)	emission cross section constant
ACQ	aggregation-caused quenching
AIE	aggregation induced emission
AIEE	aggregation induced enhanced emission
AFM	atomic force microscopy
aq	aqueous
ASE	amplified spontaneous emission
a.u.	arbitrary units
b	pathlength
BLA	bond length alternation
BHJ	bulk-heterojunction
BODIPY	boron-dipyrromethene
BT	benzothiadiazole
c	concentration/speed of light (constant)
°C	degrees centigrade
C_{60}	fullerene
C_n	rotational symmetry
CD	compact disc
CHDV	1,4-cyclohexanedimethanol divinyl ether
CIEE	crystallisation induced enhanced emission
cm	centimetre
CMOS	complementary metal oxide semiconductor
CT	charge transfer
CV	cyclic voltammetry
cw	continuous wave
d	doublet
D	diffusion coefficient
DC LCL	dye cholesteric liquid crystal laser
DD CLC	dye-doped cholesteric liquid crystals

DDQ	2,3-dichloro-5,6-dicyanobenzoquinone
DFB	Distributed feedback
DFT/TD-DFT	density functional theory/time dependent-density functional theory
DLS	dynamic light scattering
DMF	dimethylformamide
DNA	deoxyribonucleic acid
DNB	dinitrobenzene
DNT	dinitrotoluene
DPP	diketopyrrolopyrrole
DSC	differential scanning calorimetry
DVD	digital videodisk
e	number e, constant
E	energy/redox potential
E_a	acceptor band
E_{BLA}	bond length alternation
E_d	donor band
E_f	Fermi level
E_g	HOMO-LUMO energy gap
E_{Int}	interchain/intermolecular coupling energy
E_{ox}	oxidation potential
E_{red}	reduction potential
E_{Res}	aromatic resonance energy of a monomer unit
E_{Sub}	substituent influence on the HOMO-LUMO gap
E_θ	distortions from planarity in a polymer/oligomer chain
EDOT	3,4-ethylenedioxythiophene
EL	electroluminescent
Eq	equivalents
Et	ethyl
eV	electron volt
ex	excitation
F6	9,9-dihexylfluorene
F8BT	poly(9,9-dioctylfluorene-co-benzothiadiazole)
Fc/Fc^+	ferrocene/ferrocenium
F_{th} (avg)	average pumping threshold

FET	field effect transitor
Fl	fluorene
FWHM	full width at half maximum
g	gain coefficient
HOMO	highest occupied molecular orbitals
h	Planck's constant
h	hours
hex	hexane
I	intensity of transmitted light
I_0	intensity of incident light
ICT	intramolecular charge transfer
IR	infrared
ISC	intersystem crossing
ITO	indium tin oxide
IUPAC	International Union of Pure and Applied Chemistry
J	Joule/coupling constant
K	Kelvin
kJ	kilojoule
l	litre/length
L_{1D}	one-dimensional exciton diffusion length
LCD	liquid crystal display
LED	light emitting diode
LFET	light emitting field effect transistor
LUMO	lowest unoccupied molecular orbitals
M	molar (mol/litre)
m	multiplet/metre/mili/*meta*/order of diffraction
MALDI-TOF	matrix-assisted laser desorption ionisation-time of flight
min	minute
mL	millilitre
mm	milimetre
MMA	methylmethacrylate
mmol	milimole
MOD	modified
mol	mole

m.p.	melting point
MS	mass spectrometry
MW	microwave
N	Newton/population inversion density
n	non-bonding orbital/ number of fluorene units
n	refractive index
N_0	excited population density
NBS	*N*-Bromossucinimide
n-BuLi	*n*-butyllithium
n-doped	negatively doped
NIR	near infra-red
nm	nanometre
NTO	natural transition orbital
OF	oligofluorene
OFET	organic field effect transistor
OLED	organic light emitting diode
OPV	organic photovoltaic
OSL	organic semiconductor laser
Ox	oxidation
P	*para*-/pressure
PCE	power conversion efficiency
PDI	perylenetetracarboxydiimide
p-doped	positively doped
PF	polyfluorene
Ph	phenyl
PL	Photoluminescence
PLED	polymeric light emitting diode
PLQY	Photoluminescence quantum yield
PMMA	polymethylmethacrylate
POSS	polyhedral oligomeric silesquioxane
ppb	parts per billion
ppm	parts per million
PPP	poly(*para*-phenylene)
PPV	poly-*para*-phenylenevinylene

R	substituent group
R_{avg}	average intermolecular spacing
Red	reduction
RIR	restriction of intramolecular rotation
rpm	revolutions per minute
s	second/singlet
S	singlet electronic level
SEM	scanning electron microscopy
st	standard
STM	scanning tunnelling microscopy
t	time
T	temperature/transmittance/triplet electronic level
T_c	crystallisation temperature
T_m	melting point
T_d	decomposition temperature
T_g	glass transition temperature
$TBAPF_6$	tetrabutyl ammonium fluoride
TCTA	triscarbazol-9-yl-triphenylamine
TCSPC	time-correlated single photon counting
TEM	transmission electron microscopy
TFA	trifluoroacetic acid
TGA	thermogravimetric analysis
THF	tetrahydrofuran
TLC	thin layer chromatography
TMS	trimethylsilyl
TNT	trinitrotoluene
TPA	triphenylamine
TPE	tetraphenylethene
UP VLC	ultra-parallel visible light communications
UV	ultra-violet
V	Volt
v	vibrational level
vis	visible
vs.	*versus*

W	Watt
x	distance
XRD	X-ray diffraction
z	distance

Greek

α	1st position on heterocycle/optical loss coefficient/absorptivity
β	2nd position on heterocycle
δ	chemical shift
ε	molar extinction coefficient
Φ	Photoluminescence quantum yield
θ	dihedral angle
π	pi bonding orbital
π^*	pi anti-bonding orbital
σ	sigma bonding orbital
σ^*	sigma ant-bonding orbital
Δ	increment/shift
Λ	periodicity
λ	wavelength
ν	frequency
μ	micro
Φ	photoluminescence quantum efficiency
τ	photoluminescence lifetime/pulse duration
Υ_{avg}	annihilation rate

Table of contents

1. Introduction

1.1 Organic electronics

1.1.1 Band theory

Band theory is a model that describes the electronic structure of solid-state materials (Figure 1-1). In metals there are a large number of atoms with their atomic orbitals so close in energy that they overlap, forming continuous *bands* of energy. The electrons in the outer shells of the atoms (valence electrons) are free to flow along the metal lattice. Due to the *Aufbau principle*, electrons fill first the lowest available energy levels and additional electrons fill subsequently higher levels. At 0 K the electrons of the outer shells of the atoms fill the *valence* band up to the *Fermi level* (E_f), defined as the highest energy level occupied at 0 K. At this temperature the *conduction* band is empty. Given that there is no bandgap between the valence and the conduction band, above 0 K electrons start to move and populate energy levels in the conduction band, leaving behind vacancies or "holes" (which are considered positively charged) in the valence band. The movement of electrons and holes confers conductivity to metals, which decreases with the increase of temperature due to the vibrations of the atoms in the metal lattice, which increase the number of colisions and scattering of the moving electrons, increasing the resistance of the material.[1]

On the other hand, valence and conduction bands in insulators are separated by such a large energy gap (E_g) that electrons are localised in the valence band and cannot undergo transitions to the conduction band, and therefore these materials present no conductivity (Figure 1-1).[2]

Semiconductors present a smaller bandgap than that of insulators, but still greater than the one of metals (Figure 1-1). Thermal excitations or photoexcitations of the material allow the promotion of some electrons from the valence band to the conduction band, leaving holes in the valence band. The increase of temperature implies the promotion of more electrons to the conduction band, and therefore the generation of more charge carriers. For this reason, conductivity of semiconductors increases with temperature, unlike metals.[2, 3]

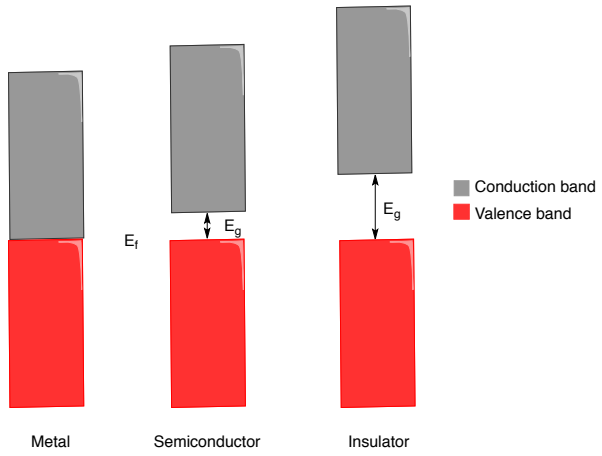

Figure 1-1 Representation of the valence and conduction bands in solids according to *band theory*. E_f is the Fermi level and E_g is the energy bandgap between the valence and the conduction bands.

Conductivity in semiconductors with relatively large bandgaps can be improved by doping the materials with elements that contain additional or fewer electrons than the semiconductor (in the case of inorganic semiconductors) or *via* oxidation or reduction of the material (in organic semiconductors). This process leads to the generation of an additional energy level between the valence and conduction bands (the acceptor band (E_a) and the donor band (E_d)), thus reducing the bandgap. These types of materials are called extrinsic semiconductors and they can be positively doped (p-doped) oxidising the material or introducing an electron-withdrawing group or an element with less electrons than the extrinsic semicondutors. They can also be negatively doped (n-doped) reducing the material or embedding an electron-donating group or element with additional electrons in the molecule or lattice (Figure 1-2). Doping is not enough to overcome the large bandgap of insulators.[2, 3]

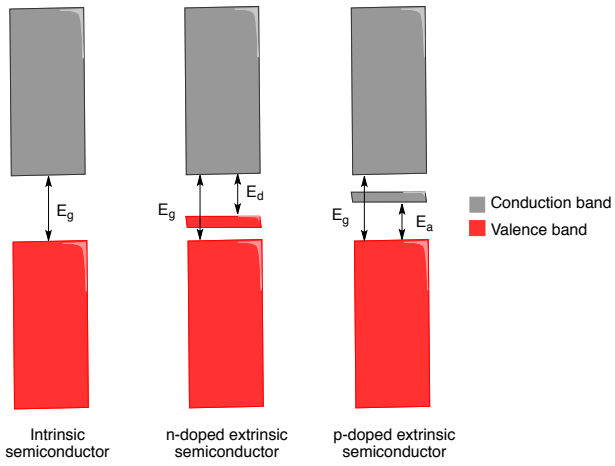

Figure 1-2 Schematic representation of intrinsic and extrinsic semiconductors. E_g is the bandgap of the intrinsic semiconductor, E_d is the bandgap n-doped semiconductors and E_a is the bandgap in p-doped semiconductors.

1.1.2 Organic semiconductors

Organic semiconductors are carbon-based materials (polymers or small molecules) that present semiconductive properties due to the alternation of single and double bonds. The sp^2 hybridisation of carbon leads to the formation of a trigonal arrangement between the three sp^2 orbitals, which are in plane, and the P_z orbital, which lies perpendicular to the aforementioned plane. When two sp^2 orbitals overlap, a σ-bond is formed between them. The energy gap between the highest occupied molecular orbital (HOMO, in this case the σ bonding orbital) and the lowest unoccupied molecular orbital (LUMO, the σ* antibonding orbital) is quite large in this type of bond. Nevertheless, when a second bond is formed between the P_z orbitals of two atoms (π bond), the HOMO-LUMO gap or energy difference between the HOMO (π-bonding orbital) and the LUMO (π*-antibonding orbital) is much smaller (Figure 1-3).[3]

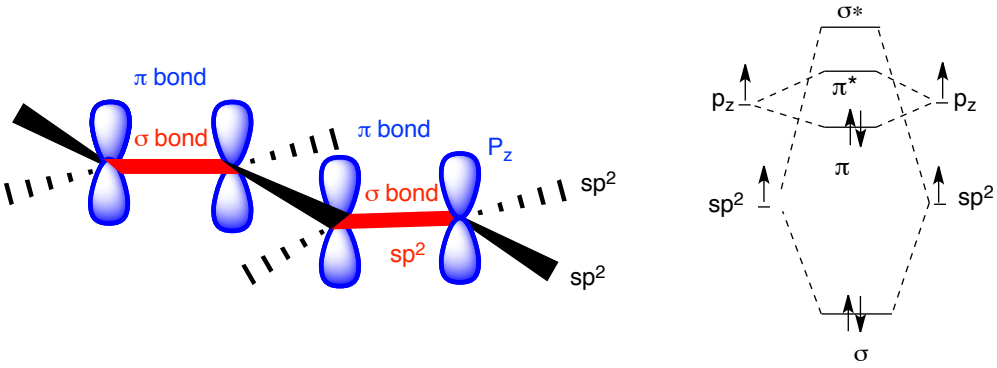

Figure 1-3 Orbitals of sp^2 hybridised carbon atoms (left). Molecular orbitals involved in a C=C bond.

In systems where there is a long chain of carbon atoms with alternating single and double bonds, the P_z orbitals of the conjugated molecule overlap, forming two bands of energy, the HOMO (π band, or valence band) and the LUMO (π* band, or conduction band). Generally, the HOMO-LUMO gap of a large conjugated system is narrower than that of a localised C=C bond. The electrons in the P_z orbitals (π-electrons) become delocalised along the electronic system and this confers them with semiconductivity. The degree of conductivity of these molecules relies on their energy levels and their HOMO-LUMO gap.[3] The conductivity of this class of compounds confers them with very desirable characteristics for application in electronics, such as charge-carrier generation and transport, light absorption and emission and electroluminescence.[4, 5]

Organic semiconductors have attracted attention in recent research as an alternative to their inorganic analogues because of their flexibility, low cost, easy processability (that permits the attainment of thin films of the material over large areas) and the tunability of their properties through chemical modification or variation of their morphology in the condensed state.[6] They have been used for electronic and photonic devices such as organic light-emitting diodes (OLEDs),[5] organic semiconductor lasers (OSLs),[7] organic field effect transistors (OFETs),[8] solar cells,[9] sensors[10] and electrochromic devices.[11]

1.1.3 Bandgap engineering in π-conjugated systems

In general, applications in organics electronics require organic semiconductors with low bandgaps, but the positions of the HOMO and LUMO levels are also important to match the requirements of each application individually. For this reason, fine control or engineering of the bandgap of organic semiconductors is of extreme importance when it comes to designing new materials. The bandgap of organic semiconductors is composed by five energy terms that can be addressed individually in order to tailor the energy gap in the material: contribution of bond length alternation (E_{BLA}), resonance energy of aromatic cycles (E_{Res}), the contribution from the introduction of electron-donating or -withdrawing substituents (E_{Sub}), the mean deviation from planarity (E_{θ}) and the energy derived from intermolecular interactions (E_{Int}) (Equation 1-1).[6] These energetic terms are represented in a linear oligothiophene chain in Figure 1-4.

$$E_g = E_{BLA} + E_{Res} + E_{Sub} + E_{\theta} + E_{Int} \qquad \textbf{Equation 1-1}$$

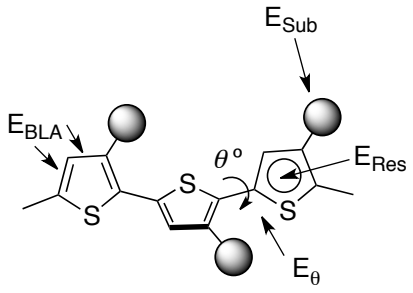

Figure 1-4 Schematic representation of the factors that affect the bandgap of linear π-conjugated oligothiophenes.

In the ideal case of an infinitely delocalised system for *trans*-polyacetylene, all the C-C bonds would have the same length with negibly narrow bandgap, providing metallic conductivity

along the chain. These 1D systems are unstable and therefore in reality there is alternation of bond lengths along the system (BLA). The bond length alternation provides the greatest contribution to the bandgap of the material (E_{BLA}).[12]

The term E_{Res} is derived from the difference in energy between the aromatic and the quinoidal mesomeric forms of aromatic rings. The resonance of aromatic systems tends to maintain the π-electrons within the ring, decreasing the delocalisation across the whole conjugated molecule. The quinoidal form is required in order to achieve electon-delocalisation and an E_{Res} energy is then added to the bandgap. Furthermore, the E_{BLA} term is also reduced in the quinoidal form.[6] The rotation of consecutive aromatic rings around a single bond also introduces an energy destabilisation derived from the loss of planarity of the conjugated system. Polyaromatic systems can be converted to their quinoidal states if the aromatic rings are fused with aromatic units with higher resonance energy, since the aromatic sextet normally localises on the ring with higher E_{Res}. The E_{Res} of a six membered aromatic ring is greater than that of a five membered one. Therefore, fused benzothiophenes adopt a quinoidal state in the thiophene in order to maintain the aromaticity of the benzene. This decreases the E_{Res} contribution to the E_g of the benzothiophene ring, which is conjugated through the thiophenes (Figure 1-5 a).[6]

The mean dihedral angle (θ) between consecutive rings decreases their conjugation, thus increasing the bandgap by an E_θ energy term. In the case of thiophenes, for example, both E_{Res} and E_θ can be stabilised by the introduction of ethylenic linkers between the rings. This reduces the overall aromaticity of the thiophenes and confers an increased planarity on the chain (Figure 1-5 b).[12] Effective planarisation of the system can also be obtained by covalent rigidification of the structure, binding the conjugated units through methylene bridges (Figure 1-5 c). This leads to a reduction of the BLA, enhancement of the electron delocalisation, and therefore a reduction of the bandgap. The drawback of this approach is that it involves long and complex synthetic procedures that limit the ultimate application of the material for mass-produced devices, where large scale and low-costs are required.[6]

As commented above, the introduction of electron-withdrawing or -donating substituents is a direct way to modify the bandgap by an energy factor E_{Sub}. Electron-withdrawing groups (acceptors) decrease the reduction potential of the material, stabilising the LUMO level and therefore reducing the E_g (Figure 1-5 d). Electron-donating groups (donors) lower the oxidation

potential and increase the HOMO level of the system, thus reducing the bandgap of the material (Figure 1-5 e). The number of donor and acceptor units that can be introduced in the π-conjugated system and their location must be carefully controlled since an excess of such units can affect the solubility of the material, hinder their polymerisations if the redox potentials are greatly influenced and affect the molecular conformation.[12] Regular alternation of donors and acceptors in conjugated systems tends to broaden their valence and conduction bands and therefore lowers the bandgaps of the materials. This is due to the generation of a charge transfer state from the donor to the acceptor, which leads to an increase in the double bond character of the bond between donor and acceptor units, decreasing the BLA (Figure 1-5 f).[13]

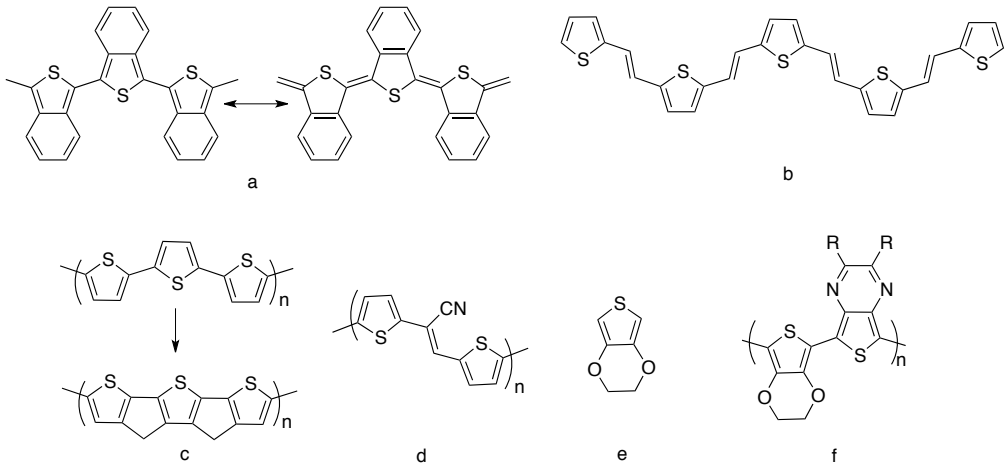

Figure 1-5 Synthetic approaches to lower the bandgap. a) Increasing the quinoid character, b) Decreasing the BLA and planarising the system, c) covalent rigidification of the system, d) introducing electron withdrawing groups, e) introducing electron donating groups, f) alternating donor and acceptor units in the structure.

These four energy terms affect the bandgap of isolated linear π-conjugated systems. The different approaches to control each of the parameters have advantages and drawbacks, but the synergistic effect of several of the parameters can be more beneficial than the absolute optimisation of each of them individually, in order to achieve a compromise and tailor the energy levels as required.[12] The final term, E_{Int} is derived from intermolecular interactions of the chains in the solid state. In some cases, such interactions can be strong and lead to planarisation of the systems, with a considerable stabilisation of the bandgap. This effect, on the other hand, can also have a negative impact on the solubility of the materials.[6]

1.1.4 Light absorption and emission in organic semiconductors

Optical excitations of organic semiconductor molecules promote electronic transitions from the valence band to the conduction band. The energy required for that transition must be sufficient to overcome the bandgap and, in this type of molecule, normally falls within the UV or visible region, but the range can even be increased to the near infrared (NIR) in materials with very low bandgaps.

Electronic delocalisation in organic semiconductors is weaker than that of their inorganic counterparts. For this reason, they present well-defined spin states: singlet in which the spin of the electrons located in the π* orbital after the transition and the one remaining in the π orbital are anti-parallel, and triplet, in which the spin of those electrons is parallel.[14, 15] The Jablonski diagram (Figure 1-6) represents the electronic states of organic molecules. Molecules in their ground state have a singlet spin (S_0) and optical excitations promote electrons to another singlet state (*absorption*, solid red arrows in Figure 1-6), normally to an excited vibrational level of the the first excited singlet state ($S_{1,x}$). The lifetetimes of these excited states are short (around 10^{-15} s) and the molecules relax to lower energy levels. The excitation can also be induced by electric current and the fluorescence obtained in this case is called electroluminescence.[16]

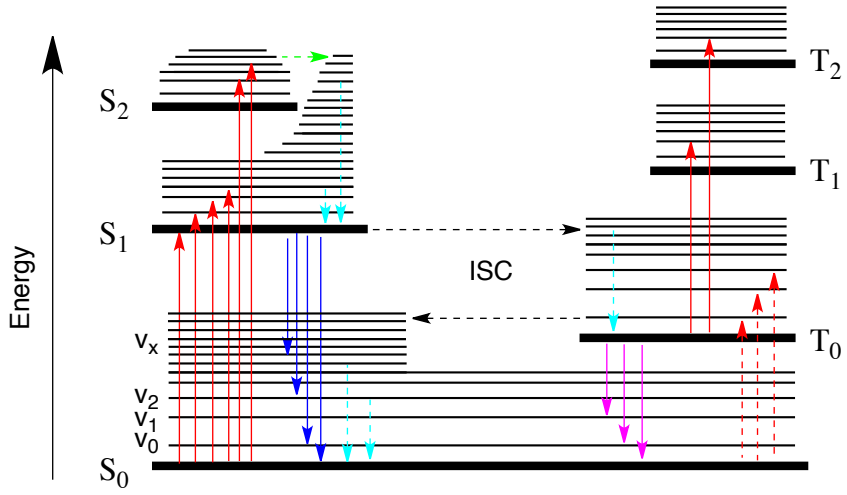

Figure 1-6 Jablonski diagram (energy level scheme of an organic molecule). On the left hand side the energy manifolds of the singlet electronic levels (S_n) are represented. On the right hand side, the triplet electronic levels (T_n) are represented. Each electronic level is divided in vibronic sublevels (v_n). Transitions represented with solid arrows are radiative and those with dashed arrows are non-radiative. Red arrows represent absorption, dark blue arrows represent fluorescence, sky blue arrows represent vibrational relaxation, green arrows represent internal conversion, black arrows represent intersystem crossing (ISC) and pink arrows represent phosphorescence.

Vibrational relaxations convert the excitation energy to kinetic energy for the bonds to vibrate. This process is very fast (between 10^{-14} s and 10^{-11} s) and therefore it is likely to occur immediately after the absorption. This energy deactivation mechanism (represented by sky blue dashed lines in Figure 1-6) normally occurs between the excited vibrational levels within each electronic level, even though vibrational relaxation can also occur between two electronic levels if there is a large energetic overlap between them. The transition in the latter case is called *internal conversion* (dashed horizontal green arrow in Figure 1-6) and it is more likely to occur between higher energy states (eg. S_3-S_2) because the energy levels are more closely distributed at higher energies. The energy gap between the S_1 and S_2 levels is very large for molecules to deactivate through this mechanism and, even if it is possible, faster mechanisms normally take place. Once the molecules have relaxed to the lowest vibrational level of the first electronic excited state ($S_{1,0}$) they can relax to any of the vibrational levels of the ground electronic state ($S_{0,x}$) by *fluorescence* (solid dark blue arrows in Figure 1-6). This process is slower than vibrational relaxations, but the larger energy gap for this transition allows competition between them in terms of timescale. Fluorescence is an allowed radative process that involves the release of photons with energy equal to the difference in energy between the levels involved in the transition. Given the fact that both absorption and fluorescence (also known as emission or photoluminescence) can occur between multiple vibrational levels within two electronic states, they are often observed over a wide range of wavelengths (broad absorption and emission spectra). The energy of the fluorescence photons is normally lower than that of the absorptions due to the intial energetic deactivation *via* vibrational relaxation processes. For this reason, fluorescence bands appear at longer wavelengths than absorption and the separation between the two is known as Stokes shift.[17]

Molecules in the $S_{1,0}$ state can also undergo *intersystem crossing* (ISC, horizontal black dashed line in Figure 1-6), a very weakly allowed transition in which the multiplicity of the molecule changes ($S_{1,0}$ - $T_{1,x}$). This process is non-radiative but after vibrational relaxations to the $T_{1,0}$ level, a radiative process to the ground singlet energy level ($S_{0,x}$) can occur. This decay is called *phosphorescence* (solid pink arrows in Figure 1-6) and it is a longer-lived process (10^{-4} - 10^{-1} s) that normally cannot be observed at room temperature.[15] ISC is faster than phosphorescence (10^{-8} - 10^{-3} s) and sometimes a two-way ISC process can occur, after which delayed fluorescence can be observed. Molecules can also decay *via* other processes such as intermolecular collisions (10^{-13} s), formation of dimers (excimers) or energy transfer to other molecules.[17]

UV-Vis spectroscopy is a technique employed to study the electronic optical transitions of molecules. The energy levels of the molecules define the wavelengths of light required in order to obtain an electronic transition. As discussed above, the electrons in π orbitals require less energy for a transition than those in σ orbitals because their HOMO-LUMO gap is narrower. Organic molecules with heteroatoms also have lone electron pairs that are located in non-bonding orbitals (n). Transitions between the bonding and non-bonding orbitals to antibonding orbitals give rise to absorptions in different regions of the spectrum (Figure 1-7).

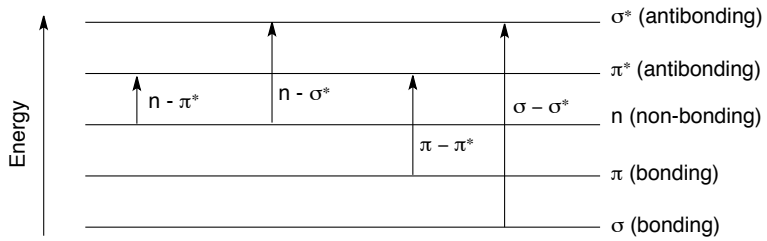

Figure 1-7 Possible electronic transitions in organic molecules.

The energy of the photons involved in these electronic transitions is described by:

$$E = h\vartheta = \frac{hc}{\lambda} \qquad \textbf{Equation 1-2}$$

where *h* is Planck's constant ($6.63 \cdot 10^{-34}$ J·s), ϑ is the frequency of the photon, *c* is the speed of light ($3 \cdot 10^{8}$ m·s^{-1}) and λ is the wavelength of the photon. Transitions that involve high energy occur at low wavelengths and low energy transitions appear at longer wavelengths. $\sigma \longrightarrow \sigma^*$ transitions occur below 150 nm and $n \longrightarrow \sigma^*$ transitions between 150 nm and 250 nm. These high energy transitions are sometimes difficult to observe given the spectral region of study (normally from 200 nm to 900 nm). On the other hand, $n \longrightarrow \pi^*$ and $\pi \longrightarrow \pi^*$ transitions occur in the region of 200 – 700 nm, and therefore they are usually observed in the spectra. These transitions involve π electrons and therefore the molecules that absorb in this region (chromophores) must possess unsaturated bonds.[18]

A UV-Vis spectrophotometer has two light beams that hit the sample and a blank simultaneously. When the light of the right wavelength interacts with the molecules of the sample, some of its photons are absorbed in order to yield electronic promotions and this leads to a decrease of its intensity. The intensity of the beam before and after passing through the sample (I_0 and I respectively) is measured at each wavelength. The ratio of I/I_0 is called

transmittance (T) and it is expressed as a percentage (Equation 1-3). UV-Vis spectra are more commonly expressed in terms of absorbance (A), which is a unitless value calculated as the negative logarithm of the transmittance (Equation 1-4).[18]

$$T = \frac{I}{I_0} x\ 100 \quad \textbf{Equation 1-3}$$

$$A = -\log(\%\ T) \quad \textbf{Equation 1-4}$$

In dilute solutions (up to ≈ 10^{-2} mol·L^{-1}), the absorbance is directly proportional to the concentration according to the Lambert-Beer law (Equation 1-5).

$$A = \varepsilon \cdot b \cdot c \quad \textbf{Equation 1-5}$$

where A is absorbance, ε is the molar absorptivity of the material (expressed in mol·L^{-1}·cm^{-1}), b is the pathlength of the cell that contains the solution (expressed in cm) and c is the concentration of the solution (expressed in mol·L^{-1}). The molar absorptivity (also known as molar extinction coefficient) is a value characteristic of each material at a specific wavelength. It represents the magnitude of intensity of absorbance originated from the nature of the electronic transition. Allowed transitions lead to large molar absorptivities and therefore much greater absorbances than forbidden transitions.[18]

Absorption spectra are displayed as a plot of the intensity of absorbance *versus* the wavelength at which such absorbance was recorded. Absorption spectra of organic molecules are typically broad bands with a maximum intensity at a given wavelength (λ_{max}) due to the distribution of the absorbed energies (explained with the Jablonski diagram). Similarly, fluorescence emission spectra are recorded by measuring the intensity of the photons emitted over a range of wavelengths when the sample is excited at a certain wavelength. They are normally also broad bands with an emission maximum (λ_{em}) but it is more common to observe vibronic structure (different maxima within the band) because in general the molecules acquire a more planar structure in their excited state, which leads to more well-defined transitions rather than a broad average.[18] For reference, the normalised absorption and emission spectra of **T4 (butyl)** are presented in Figure 1-8.

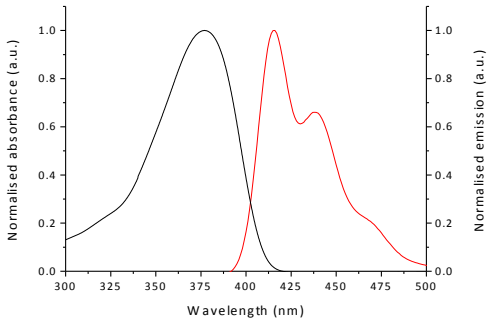

Figure 1-8 Normalised absorption and emission spectra of **T4 (butyl)** in 1:2 acetonitrile:benzene.

This project is focused on the synthesis of organic semiconductor light emitting materials for lasing applications, but they are also applicable in other optoelectronic devices such as OLEDs. For this reason, the principles of operation for organic semiconductor lasers are discussed in more depth, but some characteristics of OLEDs are also outlined.

1.2 Organic Light Emitting Diodes (OLEDs)

Since the first observation of electroluminescence (EL) from an organic material in 1963,[19] intensive research has been carried out to achieve light-emitting diodes (LEDs) based on organic materials with efficiencies and lifetimes comparable to their inorganic counterparts. Tang and Van Slyke,[20] and Saito and Tsutsui[21] developed thin films of efficient dye-based LEDs. The use of highly fluorescent conjugated polymers as the active layer of LEDs was revolutionary because it overcame the high cost of vapour deposition of fluorescent dyes and inorganic materials and it enabled the production of large area displays by simple coating techniques.[22]

OLEDs are advantageous over their inorganic counterparts because their production cost is much lower. They can be processed as very thin films allowing flexible display technology and can be illuminated uniformly over a large area. Importantly, the materials operate at much lower power than inorganic LED or liquid crystal displays (LCDs). The manufacturing of these devices is more facile as simple processing methods such as roll-to-roll or standard printing techniques provide well-defined complex patterns. Nevertheless, the main advantage of OLEDs over their inorganic analogues is the tunability of the emitted light through structural modifications of the organic emissive layer.[16]

In single-layer OLEDs a thin film of the active EL material is sandwiched between two electrodes, one of which needs to be semi-transparent to allow the generated light to be observed (usually an indium tin oxide (ITO)-coated glass substrate is used as the anode). The cathode is made out of electropositive metals with low work functions, such as Al, Ca, Mg or In to inject charges efficiently.

When a voltage between the electrodes is applied, charge carriers are injected into the organic layer (holes at the anode and electrons at the cathode). Charge carriers move towards the oppositely charged electrode in the presence of an electric field releasing non-radiative energy, but if an electron and a hole encounter and recombine while travelling through the organic layer, then excitons are formed. Singlet excitons undergo radiative-relaxation (fluorescence) resulting in the emission of visible light (see Figure 1-9).[16]

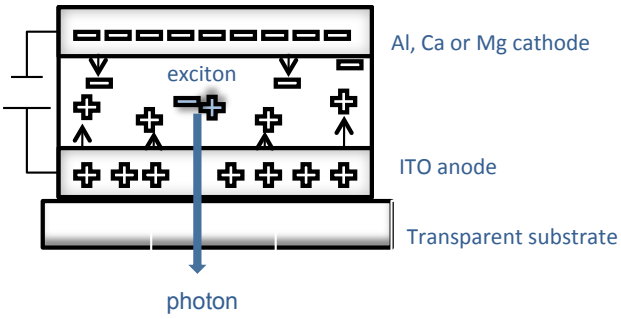

Figure 1-9 -Schematic representation of a single-layer OLED.

Most organic semiconductors are p-type conductors and show greater efficiency for hole mobility than for electron transport. As a result, electrons and holes recombine in the vicinity of the cathode, leading to limited lifetimes and efficiencies. To overcome this problem, multilayer OLED structures have been studied, involving electron and hole transport in layers of different materials. In a two-layer OLED, the *conductive layer* is sandwiched between the anode and the *emissive layer*, after which the cathode is placed. The holes coming from the conductive layer are transported into the emissive layer where they recombine with electrons and emit light.[16] Another approach to improve the efficiency and lifetime of the device is to synthesise oligomers and polymers with higher electron affinity to obtain a balanced charge injection.[16]

1.3 Lasers

The acronym laser stands for light amplification by stimulated emission of radiation. Lasers are devices that generate or amplify coherent electromagnetic radiation at wavelengths that vary from the long infrared to the vacuum ultraviolet or even X-ray regions.[23] Laser technology has improved and spread in various and very different fields since the report of the first ruby laser in 1960. They are used on a daily basis, from CD/DVD players, printers, supermarket scanners to medicine, telecommunications and spectroscopy.[24]

To understand the operation of lasers it is necessary to introduce the concept of *stimulated emission*. Let us consider an atom with any two energy levels, **1** and **2**, E_1 and E_2 being the respective energies of those levels ($E_1<E_2$) (Figure 1-10). When the atom is in an excited state **2**, it tends to decay to achieve a lower energy state **1**. If the transition **2**→**1** occurs via a *radiative decay* process the difference in energy (E_2-E_1) is released as an electromagnetic wave or photon and the process is called *spontaneous emission* (fluorescence). The frequency of the emitted radiation (v) is given by the following expression:

$$\vartheta_0 = \frac{(E_2 - E_1)}{h} \quad \textbf{Equation 1-6}$$

where h is Planck's constant. The excess of energy can also be dissipated to the kinetic or internal energy of the surrounding atoms or molecules via *nonradiative* decay.

When electromagnetic radiation with the same frequency as the spontaneously emitted wave of the atom ($\vartheta = \vartheta_0$) is incident to the atom in the excited state **2** there is a probability that the atom will be forced to undergo the transition **2**→**1**. In this case two photons that have the same frequency, direction and phase as the incident radiation are released (in contrast with spontaneous emission, where the radiation emitted by different atoms is not necessarily in phase). This process is called *stimulated emission*.[24] When the atom is in the lower energy state (i.e. ground level) and an external stimulus is applied (e.g. an electromagnetic wave of frequency $\vartheta = \vartheta_0$), the atom will probably raise to the excited level **2** and the difference in energy between final and initial levels E_2-E_1 will be provided by the absorption of a photon of the incident radiation. This process is called *absorption* and was described in the previous section.[25]

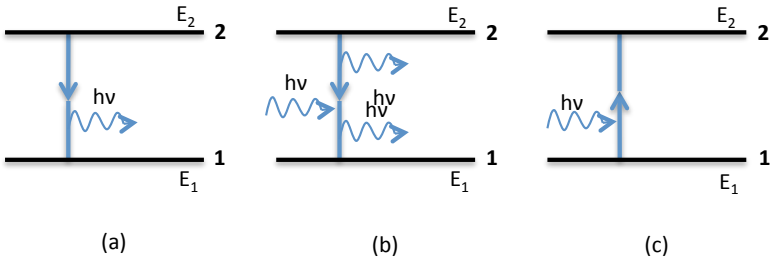

Figure 1-10 Schematic illustration of (a) spontaneous emission, (b) stimulated emission and (c) absorption.

Lasers consist of a *laser gain medium* that contains atoms, molecules, ions or semiconductor crystals, a *pumping system* to excite the gain medium to higher energy levels and an *optical feedback* system that reflects the incident beam of radiation back and forth to force it to travel through the gain medium several times (*optical resonator or optical cavity*). The laser action takes place when the gain medium is excited via pumping to achieve *population inversion* so that there are more atoms or molecules in the excited state (**2**) than in lower energy levels. If then an external electromagnetic radiation is directed to the gain medium, it can be amplified coherently via a stimulated emission process. The feedback is due to the oscillation of the amplified light coming from the gain medium in the resonator. The loss of energy in each bounce on the surface of the resonator must be small to provide a very directional and monochromatic output beam.[23]

The main properties of the lasers output beam are:

Monochromaticity: in near-ideal lasers the output beam consists of a very stable single-frequency wave of constant amplitude. The atomic or molecular transitions of the gain medium during lasing provide very narrow emission linewidth, up to 10 orders of magnitude compared to the usual linewidth of the transition **2**→**1**.[23, 24]

Spatial Coherence: The obtained beam oscillates in a *single transverse-mode pattern* that has a definite and specific amplitude and phase pattern across any transverse plane inside the laser, and particularly across the output mirror.[23, 24]

Temporal Coherence: The signal must show correlation between the amplitude and phase of the wave at any given time (t) and any moment earlier or later than t.[24]

Beam divergence and size: Laser output beams have constant phase and uniform amplitude and therefore can travel short distances with very little diffraction. However, as the beam travels further, it spreads slightly beyond the radius of the initial beam, but it can still be focused into a spot of only a few wavelengths in diameter.[23, 26] This spreading is called divergence and it is measured as half the full angle at which the beam spreads and it is measured in miliradians.[26]

Output power: Also called brightness, it is defined as the power emitted per unit surface area, per unit solid angle. The brightness of laser beams (even the ones with moderate power) is several orders of magnitude greater than that of even the brightest conventional sources (e.g. incandescent lamps), due to the high directionality of laser beams.[24]

Pulsed and continuous output: Lasers can emit a steady beam of light but if the *mode locking* technique is applied, light pulses of duration approximately the inverse of the linewidth of the laser transition $\mathbf{2} \rightarrow \mathbf{1}$ can be generated. The duration of the laser pulses ranges from milliseconds (in gas lasers) to femtoseconds (in solid-liquid and liquid lasers).[24]

Lasers can be classified according to the physical state of their active material as *solid-state*, *semiconductor*, *liquid* or *gas lasers*. Another possible classification is according to the wavelength of the emitted beam and in this case *infrared lasers*, *visible lasers*, *ultraviolet* (UV) *lasers* and *x-ray lasers* can be named and their emission wavelengths range from 1 mm to 1 nm.[23]

1.3.1 Semiconductor lasers

Semiconductor lasers are one of the most important types of lasers due to their multiple applications.[27] Their active layer consists of a direct-gap material and it is usually a combination between elements of the third and fifth groups of the Periodic Table (*III-V compounds*). The continuous wave (cw) laser emission typically ranges from 630-1600 nm, but emission at lower wavelength (≈ 410 nm) has also been achieved with an InGaN laser. Other semiconductor lasers employ wide-gap semiconductors (*II-VI compounds*) for the blue-green region of the spectrum and *IV-VI compounds* or quantum cascade lasers for the mid-infrared.[24]

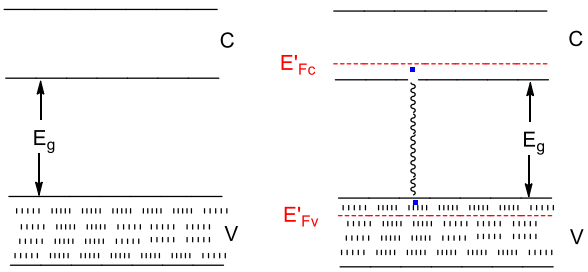

Figure 1-11 Operation principle of a semiconductor laser.

In organic semiconductor lasers, some electrons can be excited via a pumping mechanism to the conduction band and, after a short time (≈ 1 ps), the electrons in the conduction band drop to the lowest unoccupied level of the band. The same event occurs in the valence band, and some holes at the top of the valence band are generated. At this stage, if an electron from the conduction band falls to the valence band to recombine with a hole, light emission can occur (principle of LED operation). If gain from simulated emission exceeds absorption losses (when the density of electrons in the conduction band by achieved by efficient pumping is high enough), the semiconductor exhibits net gain and spontaneous emission from the recombination radiation can also occur. If the active medium is placed in a cavity and the net gain exceeds the cavity losses, laser action occurs.[24]

The light output intensity in these lasers is proportional to the drive or pump current and the output wavelength depends on the bandgap of the semiconductor material (i.e., the energy difference between the top of the valence and the bottom of the conduction bands). Amplified emission can occur in any direction but it is confined to a single direction by means of feedback structures.[26]

1.3.2 Organic Semiconductor Lasers (OSLs)

Although inorganic semiconductor lasers are dominant in everyday life in applications such as technology, medicine and materials science, they do not cover a considerable part of the visible spectrum. Organic materials, on the contrary, present tailored properties for optoelectronic applications.[28] Furthermore, they are excellent candidates for a laser gain medium due to the simple processability for device fabrication and the possibility of tuning their optoelectronic properties.[25]

The rapid development of light emitting conjugated polymers enhanced greatly the improvement of light emitting diodes (LEDs) compared to their inorganic equivalents.[22] Following this work, a great effort has been devoted to the development of organic semiconductor lasers (OSLs, also known as plastic lasers) as compact, low cost visible lasers.[25]

Organic lasers began their development with the emergence of dye lasers in 1985.[29] Solid-state organic lasers were first demonstrated by Soffer *et al* in 1967, employing dye-doped polymers.[30] This was followed by organic materials doped in single crystals in 1972[31] and on pure anthracene crystals in 1974 (Figure 1-12 a).[32] OSLs provide an alternative to high-quality single crystals, which are difficult to grow, and they have opened the door to easily fabricated lasers.[25] The first OSL, reported in 1992, employed a conjugated polymer in solution[33] and in 1996 several solid-state conjugated polymer lasers were reported.[34] Since then, intensive work to develop OSLs with conjugated polymers[28] and evaporated films of small molecules[35] has been performed.

Conjugated polymers with suitable electronic and optical properties for OSL are derived from arrays of randomly oriented chromophores that are located in the conjugated segments of the backbone. The main three families of conjugated polymers suitable for lasing applications are poly(p-phenylenevinylene)s (PPV) (Figure 1-12 b), poly(p-phenylene)s (PPP) and polyfluorenes (PF) (Figure 1-12 c).[25, 36] These materials are suitable for easy device fabrication because they are usually soluble in common organic solvents and can be deposited from solution by ink-jet printing or spin-coating. The fabrication of OSLs with electroluminescent small molecules is more complicated than with conjugated polymers since it involves the deposition of evaporated films of these molecules.[20] Conjugated dendrimers have also been used as the light amplification layer (Figure 1-12).[37] They consist of a chromophore at the core, that defines the colour of the emitted light, conjugated branches or dendrons, and surface solubilising groups.[38] Spiro-compounds (consisting of two oligomers linked by a spiro bridge) have also been employed as active materials in OSLs (Figure 1-12 e).[39]

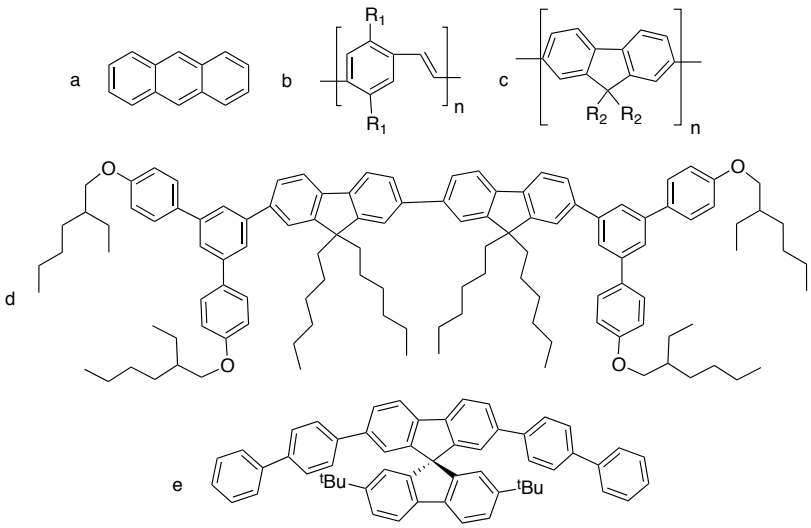

Figure 1-12 Chemical structures of some typical organic semiconductors employed in lasers: a) Anthracene; b) generic poly(p-phenylene vinylene) derivative; c) generic polyfluorene derivative; d) bisfluorene cored dendrimers; e) spiro-linked oligomer.

1.3.2.1 Photophysics in OSLs

Organic semiconductors present strong absorption at the maximum of the band (λ_{max}) even in thin films (≈ 100 nm). This characteristic is useful for lasing applications since the stimulated emission process is closely related to absorption and thus they are very likely to achieve high gain.[34] Organic materials show broad fluorescence spectra that can be easily tuned by changing the chemical structure to cover the visible, infrared and near-UV spectrum. This characteristic also enables short pulse generation[40] and broad-band optical amplification.[41]

The most appealing characteristic of organic semiconductors in laser applications is their fluorescence. The efficiency of fluorescence is measured by the *photoluminescence quantum yield* (PLQY, Φ) and it is defined as the ratio of the number of photons emitted to the number of photons absorbed by the material.[25] Many organic semiconductors and organic dyes present high PLQY in dilute solution, but at high concentrations or in the solid state intermolecular interactions between the chromophores lead to the formation of dimers, aggregates or excimers that quench the emitted light (π-π* stacking), thus decreasing dramatically the PLQY (this effect is known as aggregation-caused quenching, ACQ).[25] The strategy to avoid these intermolecular interactions is to increase the space between the chromophores. In conjugated polymers, rather bulky side chains are employed to confer solubility as well as to ensure the formation of amorphous films in which the light emitting units are kept distant.[5] In small molecules the problem is approached by blending them with a

host material.[42] In the case of dendrimers, the dendrons themselves act as spacing units between the chromophore cores[38] and in spiro compounds the spiro linkage avoids regular packing of the molecules in the solid state and the amorphous nature of their films controls intermolecular interactions.[39]

Another important photophysical parameter of organic semiconductor materials is their fluorescence lifetime (τ), which is the time that a material can fluoresce after the excitation. The fluorescence lifetime is determined by time-resolved photoluminescence studies, exciting the material with a pulse of light of the appropriate wavelength (at t = 0 s) and monitoring fluorescence as a function of the the time after the excitation pulse. Figure 1-13 represents a typical time-resolved photoluminescence plot. The decay can be monoexponential or it can present two regions, a fast decay and a slow decay in complex systems. The PL lifetime of the material corresponds to the time in which the fluorescence of the material decays by a factor "e^{-1}".[43]

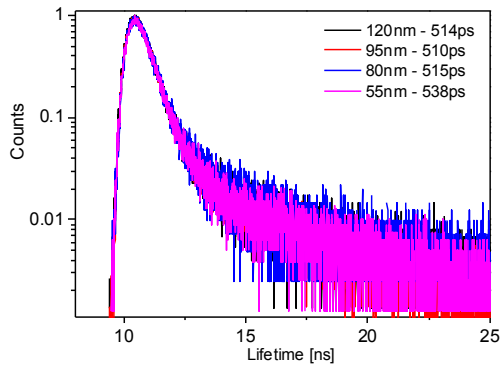

Figure 1-13 Time-resolved photoluminescence plot for the determination of the fluorescence lifetime of the oligofluorene truxene **T6**. Note that the photon count is normalised and the ordinate axis is unitless.

1.3.2.2 Gain in organic semiconductors

Organic semiconductors employed in OSLs are capable of undergoing stimulated emission when the material has already been excited and light of enough energy is incident on the material. As light travels through the gain medium it stimulates the emission of more photons and therefore the intensity of the output beam increases exponentially with distance:

$$I(z) = I(z = 0)\exp(gz) \quad \textbf{Equation 1-7}$$

where $I(z)$ is the intensity of the emitted light as a function of distance (z) and g is the gain coefficient of the medium.[25]

The probability of occurrence (cross-section) of stimulated emission is similar to the absorption, so in order to decrease the latter a population inversion must be favoured (keeping the molecules in an excited state rather than in ground state). The gain coefficient is calculated by Equation 1-8, where σ is the stimulated emission cross-section and N is the population inversion density.[24]

$$g = \sigma N \qquad \textbf{Equation 1-8}$$

The typical lowest singlet energy levels of an organic semiconductor are shown in Figure 1-14, which is a simplified version of the Jablonski diagram previously presented. The vibrational sub-levels of each electronic level are separated by about 0.2 eV and therefore at room temperature the population is mainly in the S_0 level. When a light source hits a molecule, it forces an transition from the ground state ($S_{0,0}$) to an excited vibrational state in the next singlet energy level (e.g. to $S_{1,1}$, transition (1)). The molecule undergoes quick vibrational relaxation (transition (2)) to the $S_{1,0}$ level and from there it decays to a vibrationally excited level of the ground electronic state $S_{0,n}$ (transition (3)). This is the lasing transition and it is followed by vibrational relaxation to the ground state $S_{0,0}$ (transition (4)).

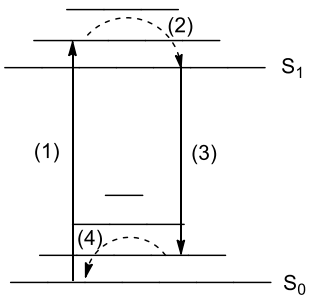

Figure 1-14- Diagram of the lowest singlet energy levels of organic semiconductors- transitions (1) and (3) are optical absorption and emission respectively and transitions (2) and (4) are thermal relaxations.

The energy levels of organic semiconductors allow them to act as four-level lasers that can achieve population inversion even if most molecules are in the ground state. They do not require high rates of excitation and therefore they present low lasing thresholds. Furthermore, the fact that vibrational relaxation processes are involved explains the shift between emission and absorption spectra.[25] This separation is beneficial for lasing because it reduces re-

absorption at the lasing wavelength. In films of organic semiconductors this shift is also increased by the distribution of environments, and thus energy states. Upon pumping, a wide range of energy levels become excited but there is quick energy transfer to the molecules with lowest energy, causing red-shifted emission.[44] Other strategies to enhance this effect have been employed. For example, blends of materials with different energy gaps can be prepared in order to excite the substance with a larger energy gap and obtain a red-shifted lasing emission that comes from the lower energy material of the blend after an energy transfer process.[45] The same principle is applied in copolymers with wider and narrower energy chromophores (donor-acceptor systems).[46]

Gain in organic semiconductors can be studied by *transient absorption measurements*, that provide information about gain and its time evolution, as well as photoexcitations and their time evolution, but *amplified spontaneous emission* (ASE) is much more widely used.[24] In this technique, a slab waveguide of the material is created, pumped with pulsed laser light in a stripe near the edge of the sample, and the light emitted from the edge of the slab is measured. Some of the light spontaneously emitted by the material is waveguided along the length of the excitation stripe and amplified by stimulated emission before emerging from the edge of the film. Narrowing of the emission occurs above a certain value of pumping intensity, which is known as the ASE threshold. ASE experiments are typically performed over ≈ 500 pulses and the threshold is calculated as an average over the 500 pulses. It is more accurate to describe the threshold in terms of fluence, the energy threshold divided by the area of the pumped stripe (the units of fluence are J·cm^{-2}). The the threshold can also be expressed in terms of pumping density in W·cm^{-2} if the duration of the excitation pulse is taken into account. When the intensity of this emission is monitored as a function of the stripe length, the wavelength-dependent gain of the material (*g(λ)*) can be calculated from:

$$\boldsymbol{I(\lambda) = \frac{A(\lambda) I_p}{g(\lambda)} [\exp(g(\lambda) l) - 1]} \qquad \textbf{Equation 1-9}$$

where *I(λ)* is the wavelength-dependent output intensity, $A(\lambda)$ is a constant related to the emission crossection, I_p is the pumping intensity and l is the length of the stripe.

This technique is important for evaluating the suitability of a material for lasing because it demonstrates the ability of the material to strongly amplify light at a certain wavelength, usually corresponding to a 0-1 transition of the gain material, which is consistent with the four-

level lasing diagram (**Figure 1-14**). ASE determines the material's threshold without involving the resonator effect on the final lasing threshold. Therefore, low ASE thresholds usually correspond to low lasing thresholds.[47] It also enables to measure the waveguide losses of light that propagates through an unpumped region by progressively moving the stripe away from the edge of the film.[25] In this ASE setting the output intensity is given by Equation 1-10:

$$I_{out} = I_o \exp(-\alpha x) \qquad \textbf{Equation 1-10}$$

where α is the optical loss coefficient and x is the distance from the end of the stripe to the end of the film.

1.3.2.3 Laser resonators

The second key element in lasers is the optical resonator that provides feedback to the amplified light by passing the resonant light repeatedly through the gain medium to establish an intense, coherent optical field in the laser.[25] The Fabry-Perot cavity is the simplest arrangement. It consists of two parallel mirrors sandwiching the gain medium. Another simple configuration is the optical ring resonator, in which the light travels along a circular pathway defined by three or more mirrors.[23, 24] The resonator defines the resonant frequencies (and therefore the lasing wavelength) allowed in the device, always within the gain medium's emission spectrum and it also affects the power characteristics of the laser. The gain must be equal to or larger than the optical losses of the cavity, which are due to transmission losses through the mirrors and absorption and scattering in the cavity components.[25]

The population inversion density that leads to gain depends on the external pumping rate. If it is too low, the gain cannot exceed the round-trip losses and the light is radiated in all directions as spontaneous emission. At threshold pump rate, the gain is equal to the round trip losses and at higher rates a coherent light field is created in the cavity and some of that light escapes out as the output laser beam, whose intensity increases linearly with the excess of pump rate. The output power of the laser can be maximised by converting the maximum fraction of the optical losses in useful output-coupling losses.[25]

The most popular types of resonator commonly used in OSLs at present are planar microcavities, Fabry-Perot waveguides, microring and microsphere resonators and diffractive

resonators.[25] For the scope of the project, diffractive resonators are explained in more detail. For more information about the other types of oscillator structures, see the books of Svelto[24] and Siegmann.[23] Diffractive resonators use periodic, wavelength-scale microstructures that diffract or Bragg-scatter the light over planar organic semiconductor waveguides. The corrugation creates a structure that reflects the propagating waveguide modes. The most typical example of this kind of resonators is the distributed feedback resonator (DFB), which is schematized in Figure 1-15. A high refractive index organic semiconductor film is placed over the corrugated silica or UV-transparent polymer substrate and the light propagating in a waveguide mode is scattered by the corrugation.

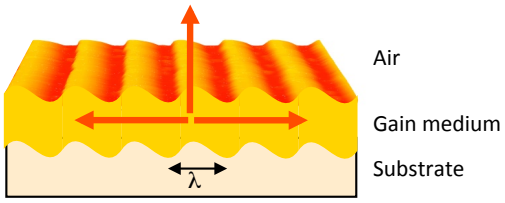

Figure 1-15 Schematic structure of a distributed feedback resonator.

The scattered light combines coherently to create a "Bragg-scattered" radiation that propagates in a new direction and with a wavelength dependent angle. The group of wavelengths that can be diffracted from a propagating mode in the direction opposite to that of the propagation must satisfy the Bragg condition:

$$m\lambda = 2n_{eff}\Lambda \qquad \textbf{Equation 1-11}$$

where λ is the wavelength of the light, Λ is the period of the structure, m represents the order of diffraction and n_{eff} is the effective refractive index of the waveguide.[25]

The periodicity of the grating creates a photonic stop-band centred at the Bragg frequency, so that the propagation of the wave with a wavelength that satisfies the Bragg condition is forbidden in the direction orthogonal to the grating groves. For this reason, DFB lasers oscillate on two wavelengths at both ends of the stop-band and the separation between them depends on the diffractive coupling of the waves that propagate in opposite directions. This type of resonator structure provides good spectral selection of the resonant light and low oscillation threshold due to a large resonator length in which the optical field interacts with the gain medium.[25]

Fabrication of diffractive OSLs is simpler than that of OSLs with other resonators because simple spin-coating of organic semiconductor solutions provides good quality amorphous films. Holography or electron beam lithography can be used in laboratory scale for the reproduction of well-defined patterns in the substrate, over which the organic semiconductor is deposited, but for large production soft lithographic techniques like nanoimprint lithography (NIL)[48] and micromolding[49] can be used to pattern the active layer directly.

1.3.2.4 Future developments to improve OSLs

As mentioned, intensive research is being carried out in the field of OSLs to optimise their fabrication cost, size, output characteristics and efficiency. Lower threshold lasers are desirable in order to utilise lower pumping intensities to achieve improved output energies. Therefore, refined cavity designs minimise the losses and extract the maximum of the amplified light as a useful output beam.[50] The gain materials are also a matter of research to ensure maximised optical gain and low optical losses. The latter can be achieved either by using energy transfer in the materials in order to increase the shift between absorption and emission wavelengths or by improving the amorphous morphology of the gain medium to diminish scattering.[51] Better processability properties and endurance are also desired, since some organic semiconductors are prone to photo-oxidation at the pumping energies employed.[25]

The greatest challenge in OSLs is the fabrication of an electrically pumped laser. The low mobility of many light-emitting organic semiconductors hinders smooth transport of the high current densities that would be necessary to achieve population inversion. Moreover, the injection of such high currents would probably overheat the gain layer and degrade it.[50] The threshold in electrically pumped OSLs would be even higher than that of optically pumped OSLs due to optical losses associated with the contacts and the formation of a significant portion of polarons and triplet states during charge injection.

1.3.2.5 Applications of OSLs

The tunability of OSLs and their ability to generate short optical pulses of medium pulse energy makes them useful for a wide range of applications. For example, they can be employed in

spectroscopy as excitation light sources for absorption, fluorescence and time resolved studies, given that the spectral range in which they operate matches the wavelengths used in organic molecules and biological systems.[52]

Organic semiconductors are suitable optical amplifiers for the field of short haul data communications in fibres serving the home/workplace and in data transfer in automobiles.[53] They can also be applied in optical switching providing all-optical wavelength switching between the near-infrared and visible data communications channels.[54]

Finally, OSLs also find applications in chemical sensing.[55] For example, they have been used for the detection of vapour of 2,4,6-trinitrotoluene (TNT) and 2,4-dinitrotoluene (DNT) with fluorescent conjugated polymers in thin films[56] and for detecting particular DNA sequences[57] and metal ions[58] at ultralow concentrations.

2 Star-shaped oligofluorene truxenes

2.1 Abstract

Star-shaped oligofluorene truxenes are very promising materials and have demonstrated excellent properties as the gain medium in organic semiconductor lasers OSLs.[47, 59, 60] Alkyl chains in oligofluorene truxenes act as solubilising groups as well as spacers to prevent intermolecular π-π stacking that leads to quenching of the emitted light. A new series of star-shaped systems analogous to the hexyl oligofluorene truxenes[59] with alkyl chains of different lengths (butyl chains and octyl chains) was synthesised. The objective of this study was to investigate the effect of alkyl chain length on the film forming properties of oligofluorene truxene materials and, as a result, on their optoelectronic properties for applications as the gain medium in organic semiconductor lasers.

Furthermore, the conjugation length of the arms in oligofluorene truxenes with hexyl and octyl chains was increased to six fluorene units (**T6** (**hexyl** and **octyl**)) in order to obtain a greater insight to the effective conjugation length of the oligofluorene-truxene family.

The performance of the **T3** (**butyl**, **hexyl** and **octyl**) materials as the gain medium in explosive detection devices was also investigated in order to determine the optimal oligofluorene-truxene material for this purpose.

2.2 Introduction

2.2.1 Oligofluorene truxenes and other similar star-shaped oligomers

Star polymers and oligomers consist of three or more linear polymer/oligomer arms joined together by a central core. They possess two or three dimensional architechture depending on the nature of the core (flat rigid cores with rigid-rod like arms attached provide a 2D geometry whereas non planar cores give rise to 3D structures).[61] 1D conjugated polymers and oligomers show anisotropic properties due to the conjugation along the linear backbone, but not along the other two dimensions. This issue leads to anisotropic properties in aligned chains of these 1D systems and limitations in their electronic characteristics when they are disordered in the bulk. The increase in dimensionality of star-shaped conjugated systems represents a clear advantage from their 1D analogues.[62] The characteristic shape of these materials together with

the conjugated character within the arms provides new electrical, optical and morphological properties that make them attractive for optoelectronic applications.[59]

The core of star-shaped macromolecules defines the shape and the symmetry of the whole molecule.[61] If a linear oligomer possesses a symmetry point group that includes rotational operations with an order greater than two, the application of such symmetry operations to the whole linear molecule leads to the construction of the corresponding star-shaped system. The application of a C_3 or C_6 symmetry operation to oligo-*p*-phenylene leads to star-shaped systems with 3 or 6 arms respectively.[61] If only part of the monomer has rotational symmetry, the application of the symmetry operation generates a star-shaped system with a new core. In the case of oligofluorenes, the application of C_3 symmetry operations at the centre of the benzene fragment of the monomer leads to star-shaped systems with benzene and truxene cores. Rotational symmetry C_n (with $n \geq 3$) of the molecule imparts the electronic properties of features such as the degeneracy of HOMO and LUMO levels.[61]

Cores with the point group D_{2h} and four arms can provide diagonal conjugation along the arms through the core, offering an additional means of tuning the band gap of the materials and enhancing the dimensionality of donor-acceptor interactions.[63]

10,15-Dihydro-5H-diindeno[1,2-a;1',2'-c]fluorene] (truxene) is a polycyclic aromatic system with C_3 symmetry that can be perceived as three overlapping fluorene fragments[64] (see Figure 2-1). The truxene unit can easily be functionalised at C-2, C-7 and C-12 positions and at C-5, C-10 and C-15 positions. The C-5, C-10 and C-15 positions are usually derivatised with alkyl chains to increase the solubility and processability of the truxene moiety and to reduce the intermolecular π-π stacking.[65]

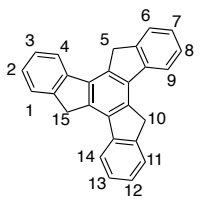

Figure 2-1 Truxene core.

Truxene has been employed as starting material for the construction of bowl-shaped fragments of fullerenes,[66] liquid crystalline compounds[67] and C_3 tripodal materials for chiral

recognition.[68] Some truxenes have shown self-assembly properties in solution through arene-arene interactions[69] and a 3D core based on truxene was employed as scaffold for the generation of self-assembled organogels.[70]

The core has also been employed to synthesise star-shaped oligomers and dendritic truxene derivatives with π-conjugation to the aromatic core.[59, 71] Truxene-based donor acceptor systems for use as multifunctional fluorescent probes have also been described.[72] It has been utilised as a platform for several phosphorescent transition metal complexes.[73] Truxene has featured in multichromophoric systems with difluoroborondipyrromethene (BODIPY) species as a photoactive core of light harvesting antennae for application in solar energy conversion devices. In these molecules, both the truxene and the BODIPY harvest light but all of it is transferred to the BODIPY through energy transfer processes.[74, 75] Truxenes have also been employed in dye sensitised solar cells as a coadsorbent[76] and as an organic sensitiser.[77] In an interesting report from Scherf *et al.*, truxene has featured in a hyperbranched polytruxene end-capped with donor dyes for optical applications.[78] Sánchez and co-workers described the use of truxene connected to [60]fullerene (C_{60}) as electron and energy transduction antennae.[79] Lavelée *et al.* have recently developed highly absorbing truxene-based photoinitiators for polymerisation.[80] Truxene has featured as antennae in a multiluminescent organometallic polymer to provide slow energy transfer.[81] It was also employed in a star-shaped chromophore with two-photon excited fluorescence properties.[82]

Polyfluorenes have been extensively used as electroluminescent materials because they are efficient blue emitters in both the solution and solid state, they show high hole mobility, great thermal and electrochemical stability. Furthermore, they are easily synthesised and their properties are tunable through modification of the structure or copolymerization.[5] They have been extensively used as electroluminescent materials in polymeric light emitting diodes (PLEDs),[83] photovoltaics,[83] field-effect transistors (FETs)[84] and solid state lasers.[85]

Chemical purity is a key issue in the performance of optoelectronic devices because impurities and degradation during synthesis, processing and device operation can lead to quenching of the emission. For example, polyfluorenes suffer from formation of fluorenone moieties in the polymer backbone (the unalkylated or partially alkylated methylene of the fluorene undergoes the formation of C=O bonds via oxidative degradation).[86] This defect acts as a charge or energy trap and quenches the emission efficiency; an undesirable green emission appears, losing the

saturated blue emission of polyfluorenes.[87] This defect, that can be aggravated by insufficient monomer purification, is mitigated in the case of oligofluorenes because superior chemical purity of the latter can be achieved by column chromatography.[88]

Monodisperse π-conjugated oligomers are characterised by a relatively short and uniform chain length, precise HOMO/LUMO energy levels, good solubility and chemical purity, and ease of processing.[89, 90] Linear oligofluorenes have been synthesised to study the correlation between the chemical structure and molecular conformation, as well as the electronic, thermal, optical and morphological properties of rod-shaped π-conjugated polyfluorene systems, providing an insight to the photophysics of this class of conjugated polymers.[91] The superior environmental stability of monodisperse oligofluorenes compared to their polymeric counterparts has enabled their use as efficient light emitters in organic light emitting diodes (OLEDs),[92] dye-doped cholesteric liquid crystal lasers (DD CLC)[93] and organic field effect transistors (OFETs).[94]

Linear oligofluorenes co-oligomerised with other building blocks have also been intensively studied. For example, Bryce's group synthesised dibenzothiophene-S,S-dioxide-fluorene co-oligomers Figure 2-2 a) as efficient blue light emitters (Φ_{PL}(sol) ≈ 0.65 – 0.67; Φ_{PL}(film) ≈ 0.44 - 0.63) with improved electron affinity and stability towards p- and n- doping compared to their oligofluorene analogues.[95] They also studied the donor-acceptor properties of an oligofluorene donor terminated with a C_{60} fullerene acceptor on one or on both sides (C_{60}-Fl_n or C_{60}-Fl_n-C_{60}).[96] Furthermore, they isolated a single C_{60}-Fl_2-C_{60} molecule on a gold surface with a Scanning Tunneling Microscope (STM) tip and monitored the conductance of the single molecule and elongated it at the junction.[97] They then reported the use of an oligofluorene molecular wire with a zinc porphyrin as an electron donor and a C_{60} fullerene as an acceptor at either side (Figure 2-2 b). The molecules undergo long-range electron transfer from the donor to the acceptor in the excited state due to the increased conjugation through the oligofluorene wire. Furthermore, the charge transfer mechanism can be controlled with temperature.[98]

Findlay *et al.* described linear oligofluorenes attached to a 4,4-di-fluoro-4-borata-3a-azonia-4a-aza-s-indacene (BODIPY) unit either in the *meso*-position (Figure 2-2 c) or in the *beta*-position, and demonstrated the suitability of the materials as down-converters to absorb high energy light and emit at longer wavelengths.[99] Aldred and co-workers described the synthesis and properties of a series of oligofluorenes encapped with tetraphenylethene (TPE) moieties

(Figure 2-2 d). The materials showed fluorescence quenching in solution but efficient blue fluorescence in the solid state (Φ_{PL} = 0.68). Furthermore, solutions of the materials in tetrahydrofuran:water mixtures with high percentage of water showed high emission through aggregation induced emission (AIE).[100] Feng *et al.* developed a series of linear diphenylamino-endcapped oligofluorenes with a 1,2,3-triazole electron-withdrawing core (Figure 2-2 e). These donor-π-acceptor-π-donor materials exhibit strong three-photon absorption properties, while the PhN-OFn-NPh analogue shows deep blue lasing.[101]

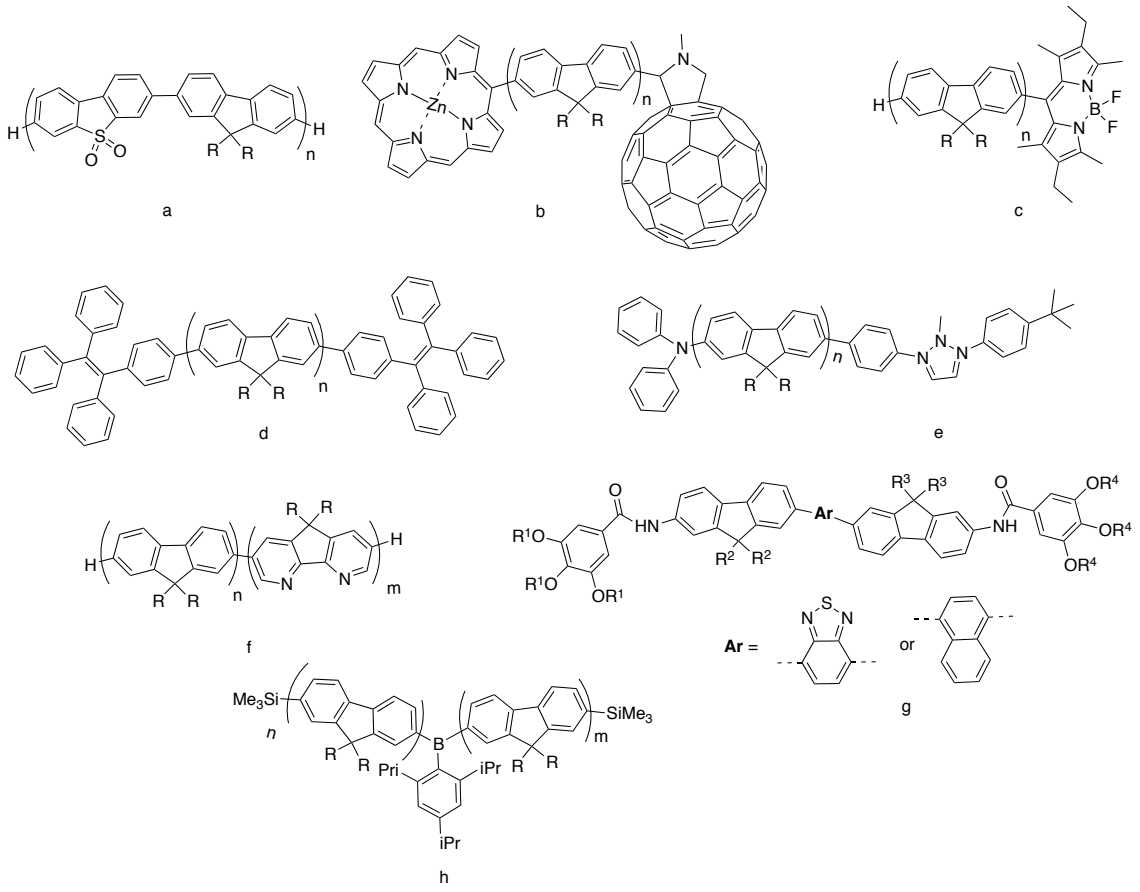

Figure 2-2 Some linear oligofluorenes reported in the literature.

Huang *et al.* described the synthesis and characterisation of donor-acceptor diazafluorene-fluorene co-oligomers and co-polymers (Figure 2-2 f) with lowered LUMOs with respect to the corresponding oligofluorenes.[102] Kaeser and co-workers described a series of fluorene-benzothiadiazole or naphthalene co-oligomers (Figure 2-2 g) with different hydrophilic and hydrophobic alkyl chains that lead to the self-assembly of the oligomers into fluorescent nanoparticles.[103] Jäkle's group described a new iterative procedure for the synthesis of a series of oligo(fluorene boranes) (Figure 2-2 h) with decreased LUMO levels and red-shifted

absorption and emission properties for the longer analogues.[104] The incorporation of 4-carbazolephenyl groups in the oligofluorene backbone yielded Kieffer's group blue OLEDs with maximum external efficiencies of 4.99 – 7.40 % in the undoped architectures (compared with the 2.00 % obtained with oligofluorenes) and up to 9.40 % in a doped device.[105]

The use of oligofluorenes as substituents of 2-phenylpyridine and 1-phenylisoquinoline in Ir(III) complexes was reported by Zhao's group and their photophysical properties at room temperature and at 77 K were compared.[106] Zhou and co-workers described the synthesis of linear oligofluorenevinylenes attached to an anthracene core. Their study suggests that long oligomeric arms can suppress the formation of excimers, beneficial for device fabrication.[107]

The functionalisation of the C-2, C-7 and C-12 positions of truxene with oligofluorenes provides an ideal scenario for the synthesis of virtually no-core two-dimensional star-shaped oligofluorenes (see Figure 2-3).[59, 108]

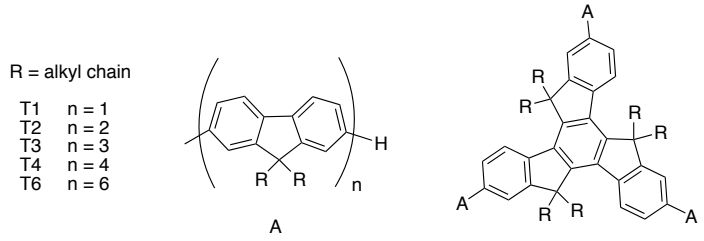

Figure 2-3 Oligofluorene truxene with the arm length rising from one fluorene unit (**T1**) to four (**T4**) and six (**T6**).

These nanosized macromolecules show advantages over conjugated polymers because they contain monodisperse oligomers with a well-defined and uniform molecular structure that enables the investigation of the impact of molecular structure on the condensed phase electronic, photonic and morphological properties of the materials.

The absorption spectra of these oligofluorene truxenes in solution and in the solid-state presents strong π-π* absorption bands that are red-shifted as the number of oligofluorene units in the arms increases (the maximum absorption peaks rising from 343 nm for **T1** to 374 nm for **T4**). They are highly fluorescent in solution and solid-state with PLQY (Φ_{PL}) for the longer oligomers ranging from 0.70 to 0.86 in solution and from 0.43 to 0.59 in solid state, close to those of polyfluorenes. These molecules are bright blue emitters and their photoluminescence (PL) spectra are red-shifted as the length of the oligofluorene arms

increases (λ_{PL}≈ 400 - 420 nm). They all show the typical vibronic structure for polyfluorenes, whose shape is independent of the conjugation length in solution but their relative intensity varies in the solid-state.[59, 109]

Cyclic voltammetry (CV) studies have proved that these materials have good electrochemical stability both to p- and n-doping and have shown that all the oligomers are high band-gap materials (in the range of 3.20 - 3.40 eV).[109]

Thermal and morphological stability are key issues for device performance. Thermogravimetric analysis (TGA) of oligofluorene truxene materials shows stability up to 400 °C in an inert atmosphere, increasing slightly as the oligofluorene arm length increases. All the oligomers are amorphous materials at room temperature (although **T1** shows some crystallinity), and present increasing glass transition temperatures from **T1** to **T4**.[59]

T4 (≈ 4 nm molecular radius) has been employed to produce fluorescent microstructures when blended with the UV-photoresist material, 1,4-cyclohexanedimethanol divinyl ether (CHDV), which can be cross-linked by direct laser writing.[110] This encapsulation process enables individual photoprocessing of nanoscopic organic light-emitting molecules, reduces oxygen diffusion and photo-oxidation and makes possible the creation of all-organic optical devices, which had not been achieved so far due to the incompatibility of organic light-emitting molecules with conventional photolithography materials. Furthermore, a fluorescent microstructure of **T4**/CHDV was micropatterned on silicon dioxide using DIP-pen nanolithography.[111] **T3** (3.1 nm molecular radius) has also been blended with CHDV to provide a micro-patterned composite over GaN light-emitting devices (LEDs) as micro pixels, *via* solvent-free inkjet printing. This hybrid GaN/organic device allows the conversion of UV light emitted by the inorganic LED to blue emission (in the visible spectrum) by the oligofluorene truxene material.[112] Additionally, free-standing membranes of **T3**/CHDV blends were prepared, showing ASE thresholds around 80 kW·cm^{-2}.[113] The same group described the first use of a monodisperse star-shaped oligofluorene encapsulated and in a mechanically flexible format. The **T3**/CHDV was employed in a DFB laser with an increased stability from 11.5 J·cm^{-2} energy dosage (in ambient conditions) to 53 J·cm^{-2}.[114]

Guilhabert and co-workers fabricated and characterised a flexible 4x4 array of organic semiconductor lasers with **T3** as the gain medium. The lasers presented wavelength uniformity

across the array with a lasing threshold of 14 kW·cm^{-2} and the output could be tuned 10 nm upon flexing the substrate due to a change in the periodicity of the resonator.[115] Samuel's group developed DFB lasers employing the oligofluorene truxene materials as gain the medium. Their **T3** laser presented a lasing threshold of 515 W·cm^{-2} and a very broad wavelength tunability across 51 nm (422 – 473 nm) in the deep-blue region, with lower ASE threshold and higher solid-state PLQY (Φ_{PL} (film) = 0.86), neat gain coefficient and lasing tunability than **T4**.[60] On the other hand, **T4** (Φ_{PL} (film) = 0.73) was employed in a DFB laser with lower lasing threshold than for **T3** (270 W·cm^{-2}). This low threshold was attributed to a low ASE threshold and low waveguide loss coefficient of 2.3 cm^{-1} due to the amorphous nature of the **T4** films (the waveguide optical losses of this material within a thin waveguide film are reduced by more than a third in comparison to polyfluorene). Moreover, lasing wavelength tunability was achieved across 25 nm in the blue part of the spectrum by changing the period of the corrugated substrate of the DFB resonator.[47]

Radial oligofluorene truxenes with six arms (**Tr1** - **Tr4**) in the C2, C3, C7, C8, C12 and C13 positions of the truxene core (Figure 2-4 a) have also proved to have high luminescence in the solid state, amorphous characteristics, good solubility in common solvents, well-defined molecular size and structure, and high purity achieved *via* column chromatography. They exhibit efficient deep-blue emission with high PLQY (Φ_{PL} = 0.60 – 1.00 in solution and 0.50 – 0.90 in films) and their absorption and emission spectra are blue shifted with respect to their oligofluorene truxene analogues with three arms (**T1** - **T4**), due to steric hindrance between the core and arms, that leads to a decrease in the degree of conjugation. A DFB laser of **Tr3** afforded a low threshold (109 W·cm^{-2}) and wavelength tunability from 421 to 442 nm, achieved by the control of the film thickness (100 - 150 nm).[108]

Truxene has also been employed as a core for other star-shaped materials with other oligomeric arms. Zhou *et al.* developed a family of star-shaped oligo(fluorene vinylenes) with truxene core showing two-photon absorption properties (Figure 2-4 b).[116] Pei's group has investigated extensively the properties of truxenes coupled to different types of oligomeric arms. They developed a series of oligo(*p*-phenylene) functionalised truxenes (Figure 2-4 c) with 1-4 phenylene units per arm as efficient blue emitters with high glass transition temperatures, good solubility in common organic solvents and good film-forming properties.[117] They also synthesised the oligo(fluorene ethynylene truxenes) TOEFE1-TOEFE4 (Figure 2-4 d), that possessed efficient green-blue light emission for OLED applications.[118] Similarly, Chen and co-

workers described a series of star-shaped oligofluorenes (n = 1 - 3) with a tri(ethynyl)truxene core. The materials show a small bathochromic shift in the absorption spectra (both in solution and solid state) and solution PL spectra with respect to their **T1** - **T4** analogues, but a large red shift in the solid-state PL spectra, possibly due to some extent of ordering in the condensed phase.[119] In both types of star-shaped systems an unexpected blue shift and a change in the shape of the solid-state PL spectra occurs when the length of the arms is increased to n ≥ 3. This effect might be a consequence of greater disorder in the condensed state due to the flexible ethynylene linkers between the core and the arms.[61]

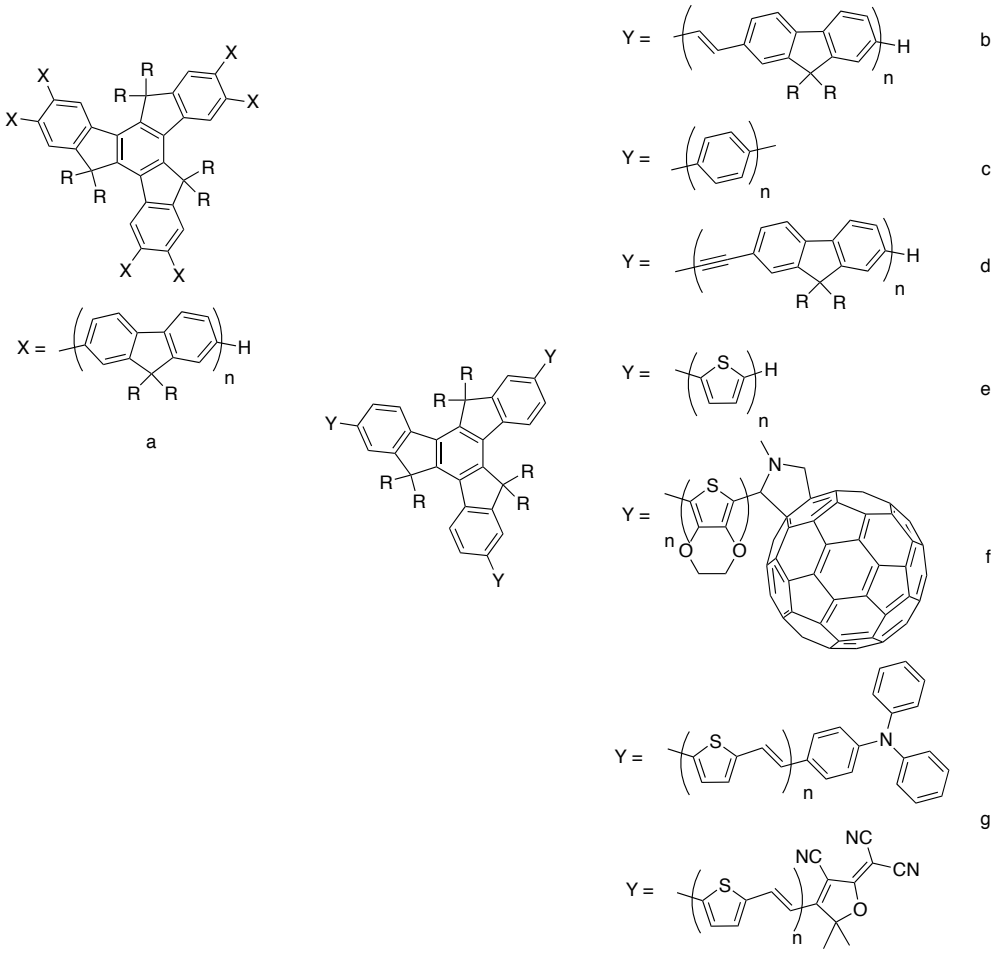

Figure 2-4 Some star-shaped truxene-cored materials with oligomeric arms reported in the literature.

A series of star-shaped truxenes derivatised with oligothiophenes (Figure 2-4 e) were also synthesised[71] and applied in OFETs by Pei and co-workers.[120] The same group also investigated the use of star-shaped truxene cored materials for organic photovoltaics. Their materials with a truxene core and 3,4-ethylenedioxythiophene (EDOT) units in the arms with C_{60} end groups

(Figure 2-4 f) have given rise to donor-acceptor systems.[121] They developed dendritic star-shaped systems with the truxene core as a branching point and thienyleneethynylene arms as linkers.[121] They then designed more complex asymmetric truxene-cored materials substituted with mono and di(ethylene-2,5-thiophene) arms endcapped with triphenylamine (TPA) donors or 2-dicyano-methylen-3-cyano-4,5,5-trimethyl-2,5-dihydrofuran acceptors with potential applications in OPVs (Figure 2-4 g).[122] A shape persistant truxene-cored molecule with thiophene-functionalised terpirydine-Ru(II) complex was also developed by this group for light harvesting applications.[123]

Star-shaped oligofluorene architectures with other cores have also been synthesised. Starburst oligofluorene benzene materials (Figure 2-5 a) are deep-blue emitters and have high PLQYs both in solution and solid state (Φ_{PL} = 0.41 - 0.82 in solution and 0.43 - 0.58 in films).[124] They present good thermal stability and form amorphous films. Their PL spectra show the vibronic structure characteristic of linear oligofluorenes, presenting a bathochromic shift with an increase in conjugation length along the arms. CV experiments show good stability towards oxidation and reduction giving evidence of independent processes in the arms, which are not cross-conjugated through meta-connections in the core. Tsiminis and co-workers reported the use of a family of starbust materials with benzene core and three oligofluorene arms (B1 – B4) as the gain medium in blue emitting DFB lasers with low lasing thresholds (1.1 $kW \cdot cm^{-2}$) and high efficiencies (6.6 %). Furthermore, combinations of the B2-B4 materials in the gain medium enable up to 60 nm spectral tunability.[125] A series of highly twisted materials with a benzene core and six oligofluorene arms has recently been reported. An OLED fabricated with these electroactive materials has shown an external quantum efficiency of 6.8 %, the highest efficiency reported so far for undoped star-shaped deep blue electroactive materials.[126]

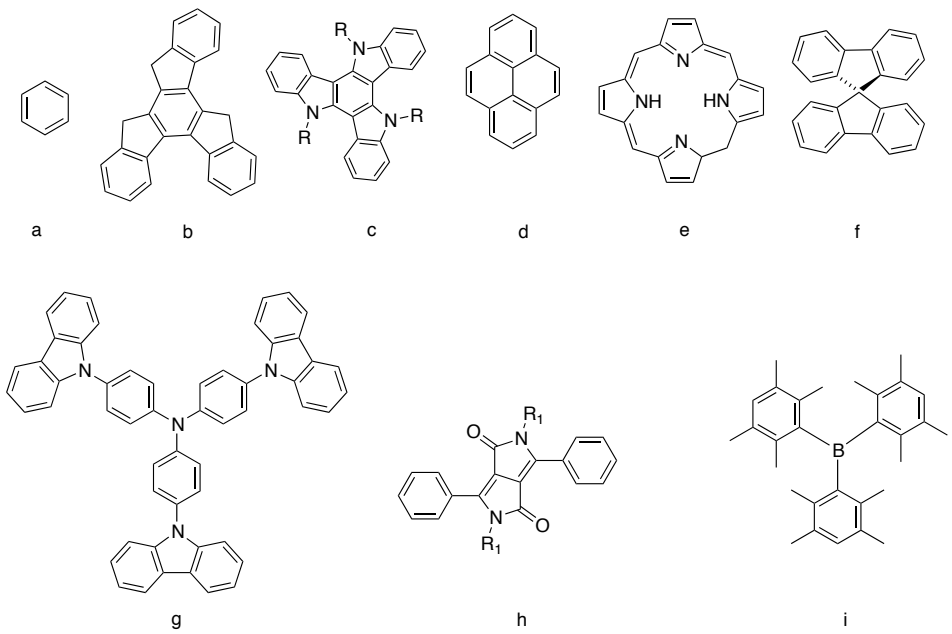

Figure 2-5 Some cores for star-shaped architectures reported in the literature: a) benzene, b) isotruxene, c) triazatruxene, d) pyrene, e) porphyrin, f) spirofluorene, g) TCTA, h) DPP, i) tridurylborane.

Yang *et al.* synthesised star-shaped oligofluorenes with an isotruxene core (see Figure 2-5 b). Isotruxene is an isomer of truxene that simultaneously possesses the *para*-, *meta*-, and *ortho*-substituted patterns for the phenylene rings.[127] The breakage of the C_3 symmetry leads to stronger electronic couplings between the phenylene rings than in truxene derivatives, in which only *meta*-linkages are present. This effect is reflected in broader and red-shifted absorption spectra compared to that of truxenes. Star-shaped oligofluorene isotruxene derivatives present excellent thermal and electrochemical stability, with blue light emission and high PLQYs (Φ_{PL} = 0.77 - 0.79). They show higher glass transition temperatures and lower oxidation potentials for generating the hole carrier than their truxene analogues. Furthermore, they require shorter solubilising alkyl chains (ethyl groups are enough) and they have little chain length dependence for the oxidation and reduction potentials and PL spectra (saturation in conjugation with n = 2 - 3). This effect arises from the fact that the isotruxene core is integrated into the conjugated pathway between the arms. This contrasts with oligofluorene truxene systems, in which *meta*-conjugation interactions are negligible and the properties of the whole molecule are more similar to a single oligofluorene arm.[128] More recently, a series of materials with an isotruxene core and several oligophenylene arms with full two-dimensional conjugation both in the ground and excited state has been described.[129] Similarly, they synthesised star-shaped ladder-type oligo(*p*-phenylenes) containing an isotruxene core with up to four benzene rings in the arms. These blue emitters present high PLQYs

(Φ_{PL} = 0.79 - 0.89) and a bathochromic shift with respect to linear oligo(*p*-phenylenes), indicating good delocalisation of the excitons along the 2D conjugated backbone, owing to the *para*/*ortho* branching in the isotruxene core.[130]

Tri- and hexa-(oligofluorene)triazatruxenes (Figure 2-5 c) have also been synthesised, showing bright blue emission, high quantum efficiencies (up to 1.00 in solution and 0.90 in the solid state) and enhanced hole-injection transport properties compared to oligofluorene truxenes due to the higher HOMO level of the oligomers attached to a triazatruxene core. These systems have been employed in OLEDs, achieving deep blue electroluminescence with high efficiency and brightness. Their properties as promising gain materials have also been investigated.[131, 132]

The same group investigated a series of star-shaped cruciform oligofluorenes with a pyrene core (Figure 2-5 d) as light blue emitters for OLEDs.[133] The materials were also employed as the gain medium in DFB lasers obtaining low lasing threshold (even when increasing the temperature up to 50 °C above their glass transition temperature) and wide wavelength tunability.[134]

Star-shaped oligofluorenes with a porphyrin core (Figure 2-5 e) and four arms present blue absorption and red emission due to an energy transfer process, which is enhanced with the increase in the chain length of the arms.[135] The same group also synthesised analogous porphyrin-cored oligocarbazole star shaped materials of up to 7.2 nm radius as efficient red emitters for optical applications.[136]

Monodisperse starburst systems with tris(carbazol-9-yl)-triphenylamine (TCTA, Figure 2-5 g) and six oligofluorene arms of length n= 2 - 4 show bright fluorescence in solution and solid state, high PLQYs and an increased hole mobility due to the presence of the TCTA core, which reduces the energy difference between the HOMO and the work function of ITO. They have been used for the fabrication of OLEDs using the oligomers as emitters and hole-transporting materials.[137]

Kanibolotsky and co-workers described the synthesis and properties of linear and star-shaped materials with a diketopyrrolopyrrole (DPP) cores (Figure 2-5 h) and quaterfluorene arms. The

materials were efficient red emitters but the star and linear non-conjugated analogues suffered from aggregation and only the linear-conjugated DPP possessed efficient ASE.[138] Recently two star-shaped tridurylboranes (Figure 2-5 i) with three mono or bifluorene arms (DBF1 and DBF2) were described. The materials have excellent solubility and thermal stability and DBF1 has been employed as a host material in a green phosphorescent OLED.[139]

Spiro oligofluorenes, in which the two fluorenes of the core have a relative 90° orientation (Figure 2-5 f) possess good thermal stability towards crystallinity and excellent amorphous film-forming properties. These systems are blue emitters with similar spectroscopic characteristics in the solution and condensed state, and present $\Phi_{PL} \approx 0.50$.[140]

Other 3D star-shaped oligofluorenes have been described, for example with an adamantane core of tetrahedral architecture,[141] 1,3,5-triazine core, *N,N,N',N'*-tetraphenylbenzidine core with flexible spacers[142] or a water soluble material with a polyhedral oligomeric silsesquioxane (POSS) core for cellular imaging.[143] These three dimensional star-shaped oligoflourene materials have not been studied in as much depth as their two dimensional counterparts.

2.2.2 Convergent and divergent synthetic approaches for star-shaped oligomers

The synthesis of star-shaped oligomers has been developed by both convergent and divergent approaches (see Figure 2-6). The divergent approach follows a repetitive sequence: (i) coupling of the monomer to the core; (ii) terminal functionalisation of the arms; (iii) extension of the arms by further aryl-aryl coupling. Repetition of steps (ii) and (iii) can be performed successively until the desired length of the arms is achieved. This approach presents the advantage of coupling reactions with a simple monomer, but purification of the product from partially reacted by-products is problematic, especially when the length of the oligomer arms increases, because the properties of the elements present in the reaction mixture converge when the molecular weight of the target molecule increases.[61]

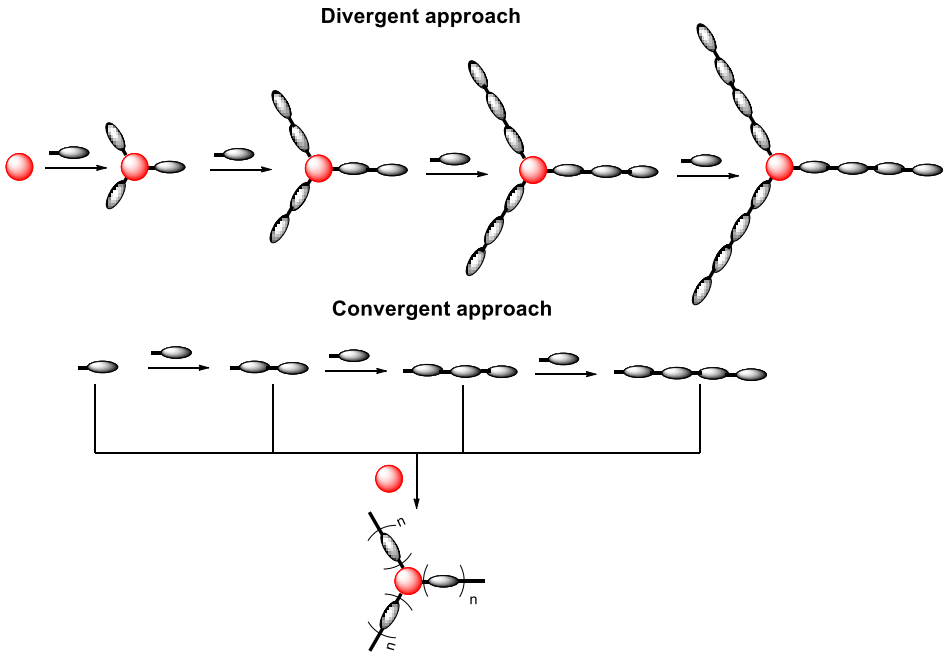

Figure 2-6 Divergent and convergent approaches for the synthesis of star-shaped oligomers.

The convergent approach employs the same synthetic strategy for the arms as for linear oligomers. The star-shaped molecule is then synthesised in a single step, coupling the oligomeric arms to the central core. The advantages of this approach over the divergent one are the simpler synthesis and accessible coupling of the arms to the core and the possibility of using this procedure with cores that are not stable towards halogenation.[61] A variation of the convergent method is to create the core in the final step employing suitable functionalities of the arms.[61] This methodology can lead to star-shaped systems with a benzene core and three arms, (using $SiCl_4$- or $TiCl_4$-mediated trimerisation of oligomers with a terminal acetyl functionality)[124] or six arms (e.g. by Diels-Alder reaction of tetrasubstituted cyclopentadienones with disubstituted acetylenes),[144] or to four or eight-armed systems with porphyrin[145] and phthalocianyne[146] cores, respectively.

In the case of the synthesis of oligofluorene truxenes, the divergent method leads to poor yields and difficult separation from mono- and di-substituted by-products and/or homocoupled products, while the convergent approach has proven to be much more efficient and convenient.[59]

2.3 Results and discussion

2.3.1 Synthesis

Initially, the truxene core was synthesised following the procedure depicted in Scheme 2-1. The procedure involved generation of truxene by cyclisation of commercially available 1-indanone under acidic conditions in high yield, followed by alkylation of the methylenic positions (lithiation with n-BuLi followed by the addition of the bromoalkyl chains in one pot) in high yields. Final bromination of the C2, C7 and C12 positions with bromine afforded **2.2 B** and **2.2 O** products in high yields. Note that "**B**" refers to butyl chain and "**O**" to octyl chain. This terminology will be carried throughout the rest of the section.

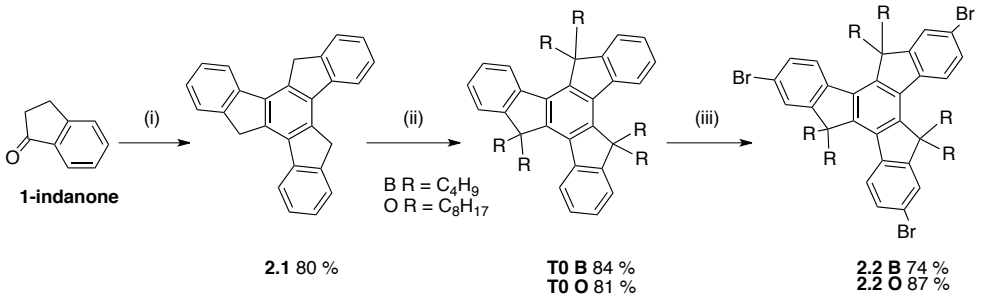

Scheme 2-1 Synthesis of the truxene core. Reagents and conditions: (i) CH_3COOH, HCl, 100 °C, 16 h; (ii) (1) n-BuLi/THF (0 °C), (2) RBr, 3) R.T., 18 h; (iii) Br_2/CH_2Cl_2 (R.T.), 12 h.

For the synthesis of the oligofluorene arms (Scheme 2-2, page 44), initial bromination of fluorene was carried out on large scale, instead of alkylation followed by bromination to avoid an additional step due to the use of two different alkyl chains. The bromination was carried out with bromine, and $KBrO_3$ was added to the reaction mixture to regenerate bromine from the HBr that is formed during the bromination reaction. Compound **2.3** was obtained in high yield but the dark colour of the product suggests that a small percentage of the oxidised form (fluorenone) might have been formed due to slightly high addition rate of the $KBrO_3$.

Subsequent deprotonation of the 9-position with potassium tert-butoxide followed by nucleophilic substitution on the corresponding alkyl bromide (RBr) yielded the 9,9-dialkyl-2,7-dibromofluorene (**2.4 B** and **2.4 O**) in one pot in relatively high yields. Compound **2.4** was used as the building block for the synthesis of the oligofluorene chain throughout the iterative Suzuki cross-coupling and conversion to boronic acid procedure that is described below.

The following step consisted of the substitution of one bromine with a trimethylsilyl group and the conversion of the other one to a boronic acid functionality in one pot, as opposed to the standard two step procedure.[147] This was achieved by lithiation of the dibromoderivative with one equivalent of n-BuLi, addition of chlorotrimethylsilane, and a second lithiation with one equivalent of n-BuLi, followed by quenching with triisopropylborate. Final hydrolysis with deionised water afforded **F_1 B** and **F_1 O** in high yields. The ^{1}H NMR of all the boronic acids described (**F_n** and **F_n'**) was complex due to a mixture of dimers of fluorenylboronic acid (formed *via* hydrogen bonds) and boroxines (the tricyclic anhydride). Unlike in the standard synthetic path,[59] the TMS protecting group was carried along the synthesis of the oligofluorene chain for two reasons: it provides easier purification and handling that makes scaling up easier and it provides a platform for easy modification of the protecting group into other functional groups, for example through bromination. The deprotection of the trimethylsilyl group was achieved by simple acid treatment followed by aqueous work-up, generating the deprotected product in almost quantitative yields without the need for purification by column chromatography.

The fluoreneboronic **F_1 B** and **F_1 O** acids were coupled *via* the Suzuki protocol with 2,7-dibromo-9,9-dialkylfluorene derivatives (**2.4 B** and **2.4 O** respectively), affording the next generation of 2-bromo-oligofluorenes, **2.5 B** and **2.5 O**, in high yields. The following steps involved repetitive lithiation – boronation sequences, yielding the boronic acids **F_2**, **F_3** and **F_4** and converting the boronic acids **F_2** and **F_3** into the corresponding elongated 2-bromo-oligofluorenes *via* palladium catalysed Suzuki cross-coupling with **2.4**. The yields obtained for the synthesis of the oligofluorene boronic acids were around 80 % with the exception of **F_4**. In the case of the butyl analogue (**F_4 B**), the large molecular weight and the short length of alkyl chain decreased dramatically the solubility of the molecules in tetrahydrofuran, especially at the low temperatures required for lithiation. As a result, the dilution factor employed had to be increased and this might have affected the yield of the reaction. Similarly, a low yield was obtained for the octyl analogue of quaterfluorenylboronic acid (**F_4 O**). Deprotection of the TMS group to provide **2.8** in high yield, followed by conversion to the boronic acid afforded **F_4' O** in a much more acceptable 73 % yield. The yield for the synthesis of **F_2 O** is also relatively low (64 %), probably due to the difficulty to handle the oily bifluorenylbromide **2.5 O**, whose recrystallisation was not possible because the material invariably crashed out as an oil despite the multiple crystallisation conditions tried. The yields obtained for the synthesis of the oligofluorene bromides were comparable with the ones described in the original publication with hexyl chains,[59] compound **2.6 O** being the only lower yielding material.

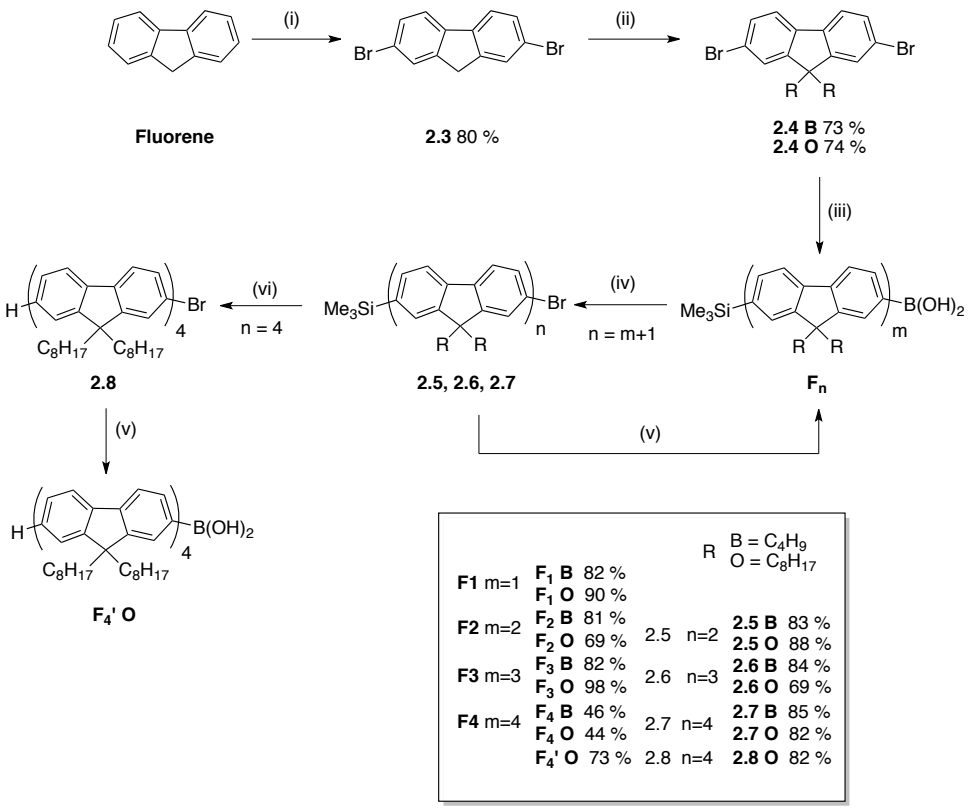

Scheme 2-2 Synthesis of the oligofluorene arms. Reagents and conditions: (i) Br_2, $KBrO_3$, H_2SO_4, AcOH, 44 – 55 °C, 4 h; (ii) RBr, THF, ^{t}BuOK/THF, 4 h, R.T; (iii) (1) n-BuLi, THF, -80 °C, (2) $SiMe_3Cl$, -95 °C – 20 °C, (3) n-BuLi, -85 °C, (4) $(^iPrO)_3B$, -100 °C, (5) R.T., 18 h; (iv) (1) $Pd(PPh_3)_4$, **2.4**, toluene, (2) 2M Na_2CO_3 (aq), 80 °C, 18 h; (v) (1) n-BuLi, THF, -80 °C, (2) $(^iPrO)_3B$, -100 °C, (3) R.T., 18 h; (vi) CF_3COOH, CH_2Cl_2, R.T., 2 h.

Following the previous results obtained in the Skabara group,[59] the convergent approach was chosen for the synthesis of the oligofluorene truxenes **T1** – **T4**, attaching the oligofluorene arms of different lengths directly onto the hexaalkylated brominated truxene core (**2.2**). Nevertheless, a semi-convergent route was employed for the synthesis of **T6 O** in 69 % yield, coupling a quaterfluorene boronic acid (**F_4' O**) to **T2Br O**. This approach avoided the conversion of a quaterfluorene into a hexafluorene, saving three extra synthetic steps onto an already precious compound, itself the product of a ten step synthetic route (Scheme 2-3).

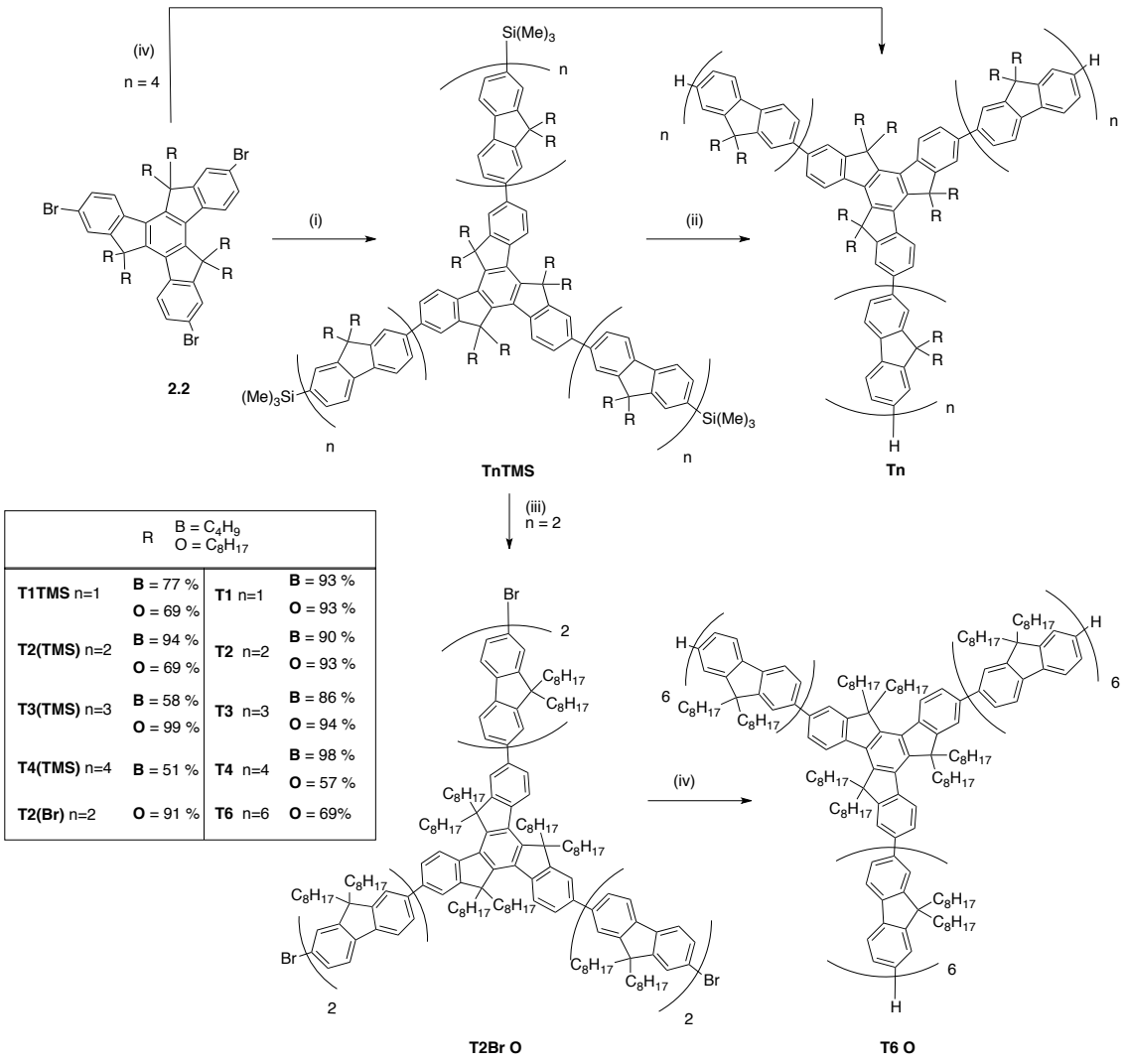

R	B = C_4H_9 O = C_8H_{17}		
T1TMS n=1	**B** = 77 % **O** = 69 %	**T1** n=1	**B** = 93 % **O** = 93 %
T2(TMS) n=2	**B** = 94 % **O** = 69 %	**T2** n=2	**B** = 90 % **O** = 93 %
T3(TMS) n=3	**B** = 58 % **O** = 99 %	**T3** n=3	**B** = 86 % **O** = 94 %
T4(TMS) n=4	**B** = 51 %	**T4** n=4	**B** = 98 % **O** = 57 %
T2(Br) n=2	**O** = 91 %	**T6** n=6	**O** = 69%

Scheme 2-3 Synthesis of tris(oligofluorenyl) truxenes **Tn**. Reagents and conditions: (i) $\mathbf{F_n}$, $Pd(PPh_3)_4$, $Ba(OH)_2{\cdot}8H_2O$, H_2O, THF or DME, 70 °C, 18 h; (ii) CF_3COOH, CH_2Cl_2, R.T., 2 h; (iii) AcONa, Br_2, THF, R.T., 2 h; (iv) $\mathbf{F_4'}$ **O**, $Pd(PPh_3)_4$, $Ba(OH)_2{\cdot}8H_2O$, H_2O, THF, 70 °C, 18 h.

T1TMS –T4TMS B and **T1TMS – T3TMS O** were synthesised following a modified Suzuki cross-coupling of the tribromotruxene **2.2** and the corresponding trimethylsilyl-oligofluorenyl boronic acid ($\mathbf{F_n}$) employing barium hydroxide as an efficient base. The number of equivalents of boronic acid per coupling position was increased from 1.14 eq (used in the original publication)[59] to 1.70 eq in order to improve the efficiency of the coupling. The solvent initially chosen for the reaction was anhydrous dimethoxyethane but upon addition of the solvent the reaction mixture turned dark brown and the yields obtained were rather low (around 50 %). Previous experience in the group employing anhydrous dimethoxyethane for modified Suzuki coupling under similar conditions had provided high yields and it was finally determined that the solvent was either contaminated or no longer oxygen free. Changing the solvent to tetrahydrofuran dramatically improved the coupling to up to almost quantitative yields. **T4 O**

(octyl) was directly synthesised following the same modified Suzuki coupling procedure between the tribromotruxene **2.2 O** and the quaterfluorene boronic acid **F_4' O** with a low yield (54 %) despite the use of tetrahydrofuran. It is worth noting that a previous attempt to synthesise **T4TMS O** (not described here) afforded the product in an 88 % yield. This is an indicator that the low yield achieved for **T4 O** should not imply that coupling of large oligofluorenes to the truxene core is less efficient. The final step consisted of the deprotection of the TMS functionality in acidic conditions in almost quantitative yield.

T2TMS O was brominated under mild conditions with bromine and sodium acetate to eliminate the HBr formed during the bromination. The yield was almost quantitative and simple recrystallisation afforded the product in high purity and almost quantitative yield. The semiconvergent modified Suzuki cross-coupling of quaterfluorene boronic acid (**F_4' O**) with **T2Br O** yielded the largest member of the oligofluorene truxene series, **T6 O** in a moderate yield (69 %).

The synthesis of the materials proceeded with good yields in general but it is noteworthy to mention the difficulties associated to handling the butyl and octyl oligofluorenes. In general, the butyl analogues seemed more crystalline and the yields obtained during the synthesis were generally lower than for the octyl series. This resulted in the need to repeat the whole synthetic sequence several times in order to obtain large enough quantities of oligofluorenes for the final couplings with truxene. The main problem arose during the synthesis of the boronic acids in which the low temperatures required tended to trigger the precipitation of the materials from solution. Nevertheless, their purification did not cause major problems.

The octyl derivatives, on the other hand, were very soluble in common organic solvents but their longer alkyl chains made the purification of the compounds much harder. For example, in the Suzuki coupling reactions for the synthesis of the oligofluorenyl bromides (**2.5 O**, **2.6 O** and **2.7 O**) the separation of the product from the homocoupling product was very poor, resulting in the need to perform several column purifications or use large quantities of silica for the column and employ very slow polarity increases. Furthermore, after the column the oligofluorene bromides were normally recrystallised from acetone to eliminate any traces of impurities or silicon grease from the column. Despite the multiple attempts of recrystallisation of **F_2 O**, an oil was consistently obtained. Low temperature treatment with liquid nitrogen

triggered the material to solidify but upon reaching room temperature, it once again it became an oil.

The petroleum ether employed in the column chromatographies was previously distilled to remove the grease that is often dissolved in the grade of solvent employed. Despite these efforts to avoid grease, the octyl chains often trapped traces of it that could be observed in the ^{1}H NMR and several recystallisations were necessary in order to obtain the pure product.

2.3.2 Physical properties

The properties of the **Tn** (hexyl) series have previously been described,[59, 109] except for **T6** (**hexyl**), that was recently synthesised and characterised by Alexander Kanibolotsky. All the **T1- T6** materials presented excellent film forming properties, but the solubility of the butyl analogues at low temperature was lower than for the octyl and hexyl analogues. The thermal behaviour and molecular weights of the materials are presented in Table 2-1. The first obvious difference in the physical properties of the butyl, hexyl and octyl analogues are the molecular weights. These monodisperse macromolecules have molecular weights of up to 8000 g·mol^{-1} (**T6 O**) and this affects their thermal behaviour.

The stability of the molecules was studied by thermogravimetric analysis (TGA) heating the materials under argon from 0 °C to 600 °C. All the materials are stable and show a 5 % mass loss above 400 °C. The only compound that had a slightly lower stability was **T4 B** (butyl), with a 5 % mass loss at 370 °C. The main mass loss for the butyl analogues was 35 - 38 % of the total mass. For the hexyl analogues it was 45 – 50 % and for the octyl analogues 50 – 55 %. This is in good agreement with the loss of the alkyl chains.

The materials were also studied by diferential scanning calorimetry (DSC) to have a better insight on their morphology. All the materials are amorphous, with no hint of crystallisation. This was also confirmed by powder X-ray diffraction (XRD) experiments performed on the materials by Dr. Fiona Coomer.

Table 2-1 Physical properties of the **Tn (butyl, hexyl** and **octyl)** series. M_w is the molecular weight of the compounds; T_g is the glass transition temperature of the compounds as measured by differential scanning calorimety; T_d is the decomposition temperature measured by thermogravimetric analysis (TGA).

Compound	M_w (g·mol^{-1})	T_g (°C)	T_d (°C) [TGA, 5 % mass loss]
T1 (butyl)	1287.51	126	419
T1 (hexyl)	1844.95	63	401
T1 (octyl)	2179.90	11	414
T2 (butyl)	2337.56	155	429
T2 (hexyl)	2842.52	86	408
T2 (octyl)	3347.48	34	422
T3 (butyl)	3166.81	169	427
T3 (hexyl)	3840.08	101	413
T3 (octyl)	4511.75	47	421
T4 (butyl)	3996.05	163	370
T4 (hexyl)	4837.65	116	413
T4 (octyl)	5679.20	51	434
T6 (hexyl)	6862.85	106	436
T6 (octyl)	8011.01	56	428

Focusing first on each series of alkyl chain, the glass transition temperature (T_g) increases with the addition of every fluorene unit, but the effect is more noticeable for the first addition, i.e. from **T1** to **T2** (ΔT_g = 29, 23 and 23 °C for butyl, hexyl and octyl respectively). Thereafter the increase in T_g per fluorene unit is more moderate (around 14 °C for **T3** and between 4 and 15 °C for **T4**). As expected, the modification of the length of the alkyl chains by two methylene units also affects the glass transition temperature because longer alkyl moieties have a larger free volume, which results in lower T_g. This has a major impact on the materials, especially for the octyl derivatives, that present very low glass transition temperatures from 11 °C for **T1 O** (it is a very sticky oil at room temperature) to 56 °C for **T6 O**. This is detrimental for device fabrication, where a stable morphology is required. When the materials are employed as the

gain medium in an optically pumped laser, the incident energy and the non-radiative losses will cause the gain material to heat. If the materials heat up above their glass transition temperature, the film can become rubbery, allowing the molecules to move slightly. This may induce greater losses and therefore increased lasing thresholds and poorer device performance. On the other hand, the butyl derivatives present exceptionally high glass transition temperatures, from 126 °C for **T1 B** to 163 °C for **T4 B**. This is promising for their device performance, but the difficulty of their synthesis makes the use of these compounds as gain media for OSLs unfeasible on a larger scale.

Based on the thermal data presented here, it seems that the hexyl chain, the alkyl chain initially chosen for developing star-shaped oligofluorene truxenes, was the best choice due to easier synthesis and purification, as well as good thermal properties.

2.3.3 Cyclic voltammetry

The electrochemical properties of the materials were studied by cyclic voltammetry in ≈ 10^{-4} M solutions of the materials in 1:2 acetonitrile:benzene. Despite the compounds being soluble in most common organic solvents, it is known from the previous studies performed on the **Tn (hexyl)** family that the electrochemical reduction of the compounds occurs at lower potentials than the reduction of those solvents. Acetonitrile has a lower reduction potential than the **Tn** compounds but it is not able to solvate them. Benzene assists in the solvation of the materials and does not interfere in the electrochemical study. Therefore it was found that the ideal solvent mixture for the electrochemical studies was 1:2 acetonitrile:benzene.

The oxidation waves of the **Tn** (**butyl**) and **Tn** (**octyl**) are presented Figure 2-7 and Figure 2-9 respectively and all the electrochemical properties are summarised in Table 2-2. In both cases the smallest analogues (**T1** and **T2**) present two well-resolved reversible anodic peaks separated by 0.22 – 0.25 V. These transitions seem one electron processes and are well defined. **T3** also presents two consecutive reversible oxidation peaks separated by around 0.14 – 0.16 V. The **T4** analogues showed a more complex electrochemical behaviour with poor resolution between the first two oxidation peaks (both being quasi reversible). **T4** (**butyl**) presents a hint of a third irreversible peak that involves less current than the first two oxidation processes. Note that the irreversible peak at around 1.40 V is probably related with oxidation of the solvent rather than the **T4**. **T6** also has two quasi reversible oxidation peaks

separated 0.20 V from each other and a rather softened profile. The increase in the size of the molecules generally involves a lowering of the oxidation potentials in the **Tn** series. Additionally, the fact that **T1** and **T2** present better defined voltammograms might be an indication that the core is more present in the electrochemistry whereas in the larger analogues the arms play a more important role and the charge is more delocalised along the arms.

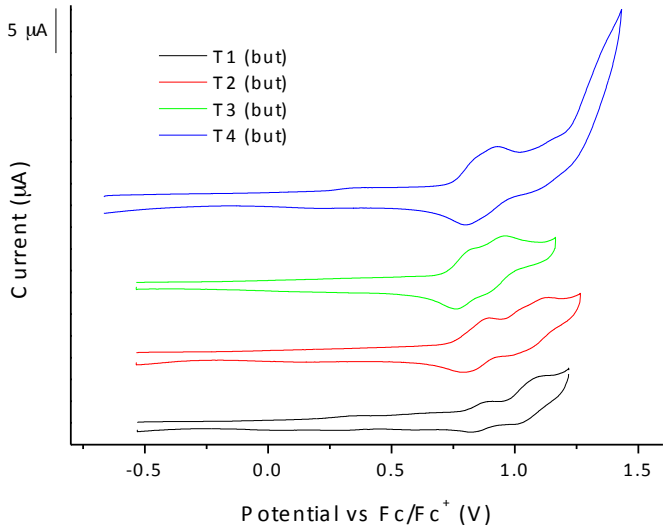

Figure 2-7 Oxidation waves of the **Tn (butyl)** series in 1:2 acetonitrile:benzene. The cyclic voltammogram was obtained employing a glassy carbon working electrode, a platinum wire counter electrode and a silver wire reference electrode. All the waves were referenced to ferrocene.

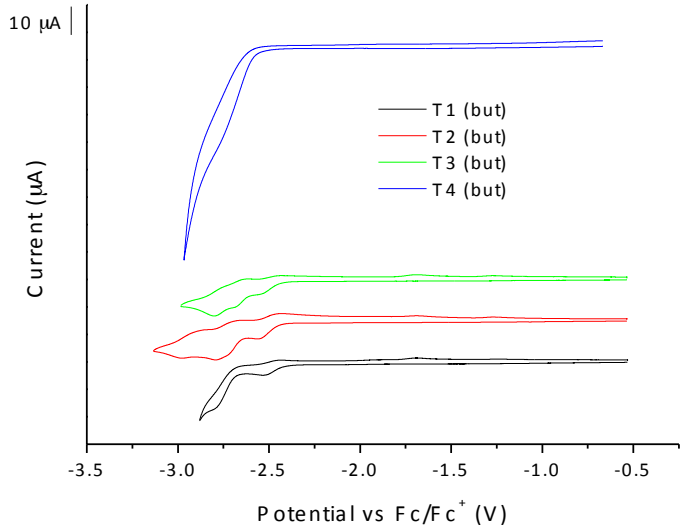

Figure 2-8 Reduction waves of the **Tn (butyl)** series in 1:2 acetonitrile:benzene. The cyclic voltammogram was obtained employing a glassy carbon working electrode, a platinum wire counter electrode and a silver wire reference electrode. All the waves were referenced to ferrocene.

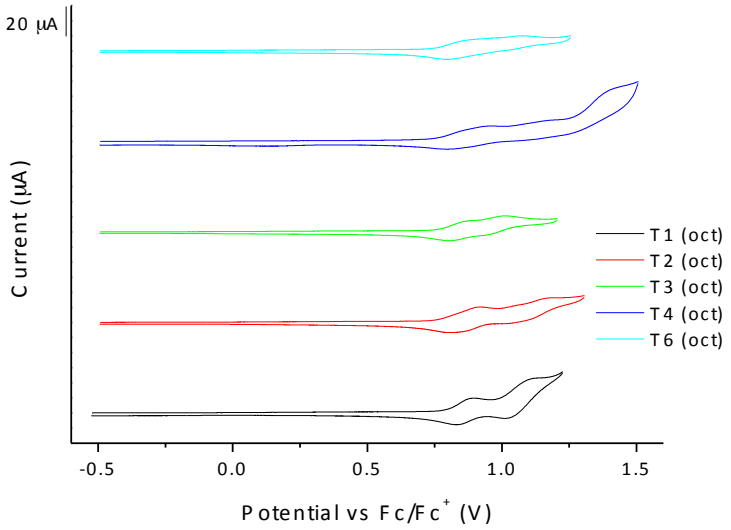

Figure 2-9 Oxidation waves of the **Tn (octyl)** series in 1:2 acetonitrile:benzene. The cyclic voltammogram was obtained employing a glassy carbon working electrode, a platinum wire counter electrode and a silver wire reference electrode. All the waves were referenced to ferrocene.

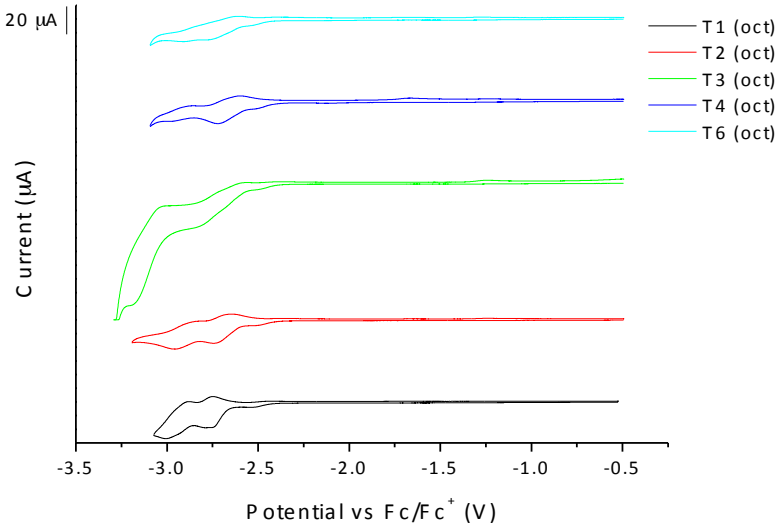

Figure 2-10 Reduction waves of the **Tn (octyl)** series in 1:2 acetonitrile:benzene. The cyclic voltammogram was obtained employing a glassy carbon working electrode, a platinum wire counter electrode and a silver wire reference electrode. All the waves were referenced to ferrocene.

Table 2-2 Cyclic voltammetry results in 1:2 acetonitrile:benzene for the **Tn (butyl, hexyl** and **octyl)** series.[a] HOMO and LUMO levels were calculated from the onset of the corresponding redox wave and are referenced to ferrocene, which has a HOMO of -4.8 eV. [b] The electrochemical HOMO-LUMO gap ($E_{g, CV}$) is the energy gap between the HOMO and LUMO levels. The optical HOMO-LUMO gap ($E_{g, opt}$) is calculated from the onset of the long wavelength-edge of the absorption band.

Compound	E_{ox} vs Fc/Fc^+ (V)	E_{red} vs Fc/Fc^+ (V)	HOMO[a] (eV)	LUMO[a] (eV)	$E_{g, CV}$[b] (eV)	$E_{g, opt}$ (eV)
T1 (butyl)	0.90, 1.12	-2.50, -2.78, -2.97	-5.53	-2.36	3.17	3.05
T1 (hexyl)	0.80, 1.05	-2.80	-	-	3.40	3.29
T1 (octyl)	0.89, 1.11	-2.53, -2.76, -3.00	-5.59	-2.37	3.22	3.27
T2 (butyl)	0.90, 1.14	-2.56, -2.79, -2.97	-5.54	-2.36	3.18	3.11
T2 (hexyl)	0.76, 0.84, 1.03	-2.74	-	-	3.30	3.14
T2 (octyl)	0.92, 1.17	-2.50, -2.74, -3.00	-5.56	-2.41	3.15	3.12
T3 (butyl)	0.82, 0.96	-2.54, -2.68, -2.80	-5.51	-2.38	3.13	3.12
T3 (hexyl)	0.76, 0.94	-2.70, -2.83	-	-	3.24	3.08
T3 (octyl)	0.86, 1.01	-2.49, -2.82, -3.16	-5.56	-2.41	3.15	3.05
T4 (butyl)	0.82, 1.27, 1.31	-2.75	-5.54	-2.22	3.33	3.03
T4 (hexyl)	0.74, 0.87	-2.66, -2.74	-	-	3.20	3.05
T4 (octyl)	0.93, 1.16	-2.50, -2.72, -2.97	-5.55	-2.41	3.14	3.01
T6 (hexyl)	0.88, 0.97, 1.09	-2.71, -2.87	-5.55	-2.41	3.14	3.01
T6 (octyl)	0.88,1.08	-2.52, -2.77, -2.91	-5.55	-2.37	3.18	2.99

The reduction voltammograms for **Tn (butyl)** and **Tn (octyl)** are presented in Figure 2-8 and Figure 2-10 respectively. The reduction peak around -2.5 V (highlighted in red Table 2-2) is present in the voltammograms of all the **Tn (butyl** and **octyl)** series, but its intensity differs between voltammograms and is not consistent with a one electron process. This observation, together with the fact that such peak was not present in the electrochemical studies of the **Tn (hexyl)** family, might be an indication that it is a process that does not belong to the **Tn** molecules and it might be due to environmental factors such as the reduction of some impurity of the solvent or the electrolyte. For this reason, these peaks are not taken into

account in the discussion of the electrochemical properties of these materials. **T1** (**butyl**) presents an irreversible reduction peak at -2.78 V, while **T1** (**octyl**) has two quasi-reversible reduction peaks (-2.76 V and -3.00 V respectively) involving significantly more current. Similarly, **T2** (**butyl** and **octyl**) present two quasi reversible processes at around -2.75 V and -3.00 V respectively. The reduction of **T3** (**butyl**) presents two quasi-reversible peaks at -2.68 V and -2.80 V whereas the voltammogram of **T3** (**octyl**) features an irreversible readuction at -2.82 V, and a final irreversible reduction at -3.16 V that might be caused by the reduction of the solvent. The reduction of **T4** (**butyl**) involves a single irreversible transition at -2.75 V, whereas **T4** (**octyl**) presents two well-defined quasi reversible reduction peaks at -2.72 V and -2.97 V (the fist reduction process seems to involve more than one electron). Similarly, **T6** (**octyl**) shows two reduction peaks that are not very well resolved at -2.77 V and -2.91 V.

All the compounds have relatively high HOMO-LUMO gaps (around 3.18 eV) that are generally slightly reduced with the increase of the conjugation length in the arms. The optical HOMO-LUMO gap was calculated from the onset of the absorption band and in general there is a good agreement between it and electrochemical HOMO-LUMO gap, the latter being generally slightly higher.

The solubilising alkyl chains should not have a major effect on the electrochemical processes of organic semiconductor materials and the differences in reversibility of some of the peaks should be studied in more depth in order to ensure that they arise from the molecules and not from any environmental conditions.

2.3.4 Optical and photophysical properties

The optical properties of the materials were studied in solutions of the compounds in 1:2 acetonitrile:benzene (in order to compare the optical and electrochemical HOMO-LUMO gaps) and concentrations in the region of 10^{-6} M.

The normalised absorption and emission spectra of the **Tn (butyl)** family are depicted in Figure 2-12 (page 56) and for the **Tn (octyl)** series in Figure 2-13 (page 57). The data for the absorption and emission maxima as well as the logarithm of the molar absorptivity of each material (log (ε)) are presented in Table 2-3, together with the results previously obtained for the **Tn (hexyl)** series and the new **T6 (hexyl)** compound. As expected, the length of the

solubilising alkyl chain does not have a major effect on the optical properties of the series in solution. For each member of the family, the results are comparable for butyl, octyl and hexyl chains.

Table 2-3 Optical properties of the **Tn (butyl, hexyl** and **octyl)** series. λ_{abs} is the wavelength of maximum absorbance; λ_{em} is the wavelength of maximum emission; ε is the molar absorptivity at $\lambda_{abs,\ solution}$.

Compound	$\lambda_{abs,\ solution}$ (nm)	$\lambda_{abs,\ film}$ (nm)	$\lambda_{em,sol}$ (nm)	$\lambda_{em,film}$ (nm)	log(ε)
T1 (butyl)	344	343	-	-	5.64
T1 (hexyl)	343	343	377, 398, 416	380, 398, 420	5.27
T1 (octyl)	344	343	-	-	5.26
T2 (butyl)	364	363	405, 431, 461	407, 426, 454	5.47
T2 (hexyl)	362	359	400, 424, 452	404, 426, 449	5.37
T2 (octyl)	362	363	406, 429, 463	405, 427, 454	5.24
T3 (butyl)	373	373	411, 432, 463	417, 437, 467	5.58
T3 (hexyl)	372	369	410, 434, 457	417, 436, 462	5.41
T3 (octyl)	370	373	410, 430, 464	416, 438, 469	5.58
T4 (butyl)	377	378	416, 438, 470	420, 442, 475	5.72
T4 (hexyl)	377	362	414, 438, 467	422, 442, 467	5.53
T4 (octyl)	376	379	414, 441, 467	423, 444, 471	5.72
T6 (hexyl)	391	374	415.5, 439, 470	420, 446, 480	5.87
T6 (octyl)	381	376	415, 437, 470	420, 446, 478	5.84

The increase in the number of fluorenes in the arms results in a red shift of the absorption. This effect is greater for the first fluorene addition (there is a shift of ≈ 19 nm from **T1** to **T2**) and it decreases as the number of fluorene units increases. The addition of two more fluorenes from **T4** to **T6** does not have a great effect on the energy of the absorption. This effect denotes the fact that 6 fluorene units are close the saturation of the conjugation length for the absorption in star-shaped oligofluorene truxenes (the effective conjugation length for linear oligofluorenes reported by Jo and co-workers is fourteen fluorene units).[148] A further

increase in the number of fluorenes (e.g. **T8**, **T10** or **T12**) would be beneficial to determine the exact conjugation length of these systems. Nevertheless, the slight improvement in the properties of the **T6** probably does not justify the increased synthetic effort required to obtain this molecule compared with **T4** (and this subsequently applies to the proposed larger members of the family). Figure 2-11 represents the energy of the maximum of absorption (in eV) related to 1/n, where n is the number of fluorene units. This type of representation has previously been employed to determine the conjugation length in oligomeric systems.[148] The energies are in linear correlation with the inverse of the number of fluorenes for the three alkyl chains (r^2 = 0.993 – 0.998), and the absorption maxima extrapolating to n = ∞ would be $\lambda_{n=\infty}$ = 401 nm for the octyl series and 406 nm for the hexyl series. This falls in the region of the extrapolated value for linear oligofluorenes ($\lambda_{n=\infty}$ = 401 nm) and the experimental value for poly(9,9)-dihexylfluorene (λ_{max} = 383 nm).[149]

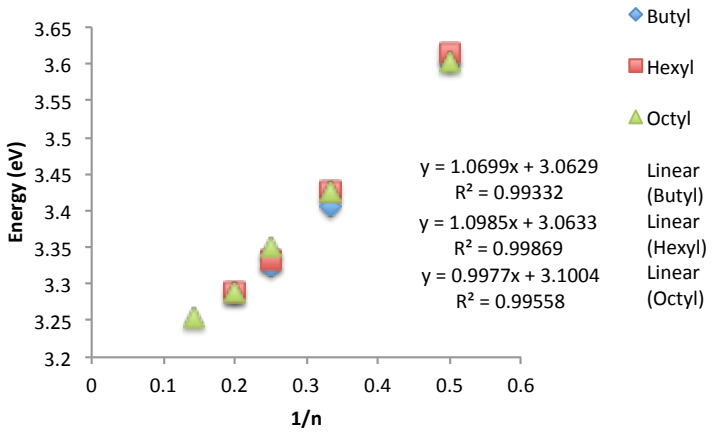

Figure 2-11 Representation of the energy of absorption (eV) *versus* the number of fluorene units in the arm one fluorene from the truxene core in the **Tn (butyl, octyl** and **hexyl)** series.

A previous study on the **Tn (hexyl)** series discussed the effect of the number of fluorenes on the absorption transitions of the **Tn** series and attributed the red shift associated to the increase of the fluorene units to the stabilisation of the LUMO and destabilisation of the HOMO of the molecule.[150] This narrowing of the HOMO-LUMO gap is less pronounced for the truxene series than for the oligofluorenes of equivalent length of the arm. The reason behind this effect is the conjugation pattern between the fluorenes. In an oligofluorene chain all fluorenes are connected to each other by *para* links, whereas in the truxenes the arms are not conjugated through the core because they are connected to the *meta*-position in the truxene.

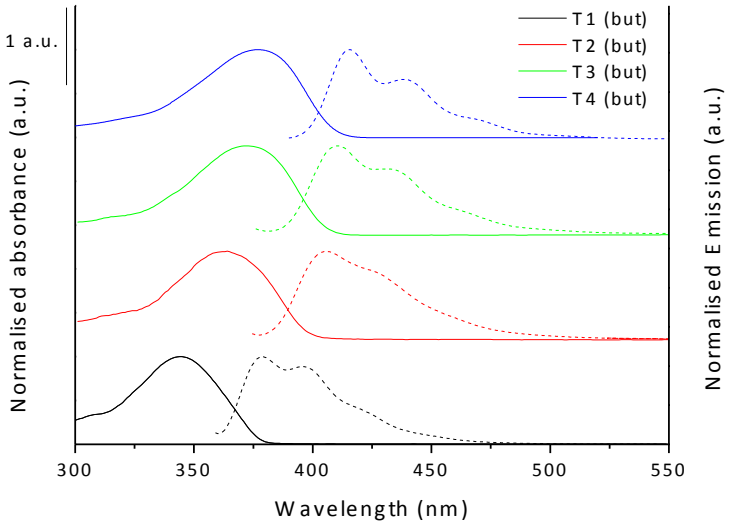

Figure 2-12 Normalised absorption (continuous line) and emission (dashed line) spectra of the members of the **Tn (butyl)** family (10^{-6} M solutions in 1:2 acetonitrile:benzene).

All the compounds exhibit large molar absorptivities that increase with the length of the arm. There is certain variation in the molar absorptivity of the same member of the **Tn** family with different alkyl chains. As previously discussed in a study performed on the hexyl analogues, the length of the alkyl chain should not affect the optical properties, as demonstrated by DFT calculations performed on benzene-cored star-shaped oligofluorenes with three arms. Calculations of the molecules with the full hexyl chain and with methyl groups in the C9 position of the fluorenes only changed the absorption energy and dipole of the molecules by 0.6 % to 2.4 %, depending on the basis set employed for the calculation.[151] It should be then concluded that the observed differences must be due to experimental errors, but the trends observed for the each arm length are still maintained. Taking into account that the truxene core increases the effective conjugation length of each arm by one fluorene, an arm of **T1** is comparable with bifluorene, **T2** with terfluorene, etc. The same publication by Montgomery and co-workers also discussed the direct threefold increase of the molar absorptivity of the **Tn** compounds compared to the corresponding oligofluorenes. This is easily explained by the fact that the truxene molecules absorb energy with three oligofluorene arms simultaneously.[151]

The absorption spectra for the **Tn** series present a broad featureless band arising from strong π-π* interactions between the HOMO and LUMO of the molecules. The loss of spectral vibronic resolution compared with **T0** arises from the lack of rigidity of the structure, in which the C-C single bonds between fluorenes allow for rotation, as previously discussed by Moreno

Oliva and co-workers.[150] Their theoretical study predicted that the S_0-S_1 transition is forbidden and the first dipole-allowed transition is the S_0-S_2, with a large oscillator strength, which would explain the large molar absorptivities associated with these molecules.

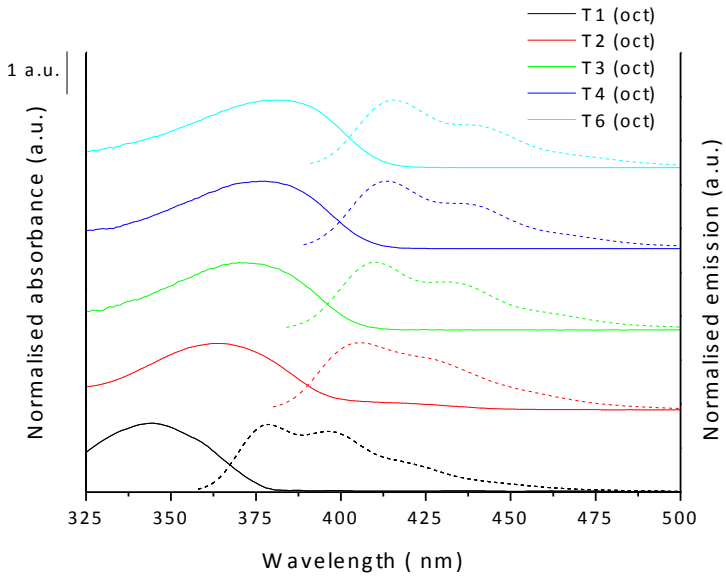

Figure 2-13 Normalised absorption (continuous line) and emission (dashed line) spectra of the members of the **Tn (octyl)** family (10^{-6} M solutions in 1:2 acetonitrile:benzene). $\lambda_{ex} = \lambda_{max}$.

All the molecules in the **Tn** series present efficient fluorescence behaviour represented by a broad band with vibrational structure (a main band corresponding to the 0-0 vibronic emission and two red-shifted shoulders related to the 0-1 and 0-2 transitions respectively).[148] TD-DFT calculations previously reported assigned the fluorescence to the S_2-S_0 transition. The authors imply that the efficient fluorescence of these molecules might arise from the strong coupling between the S_2 and the ground state.[150] The theoretical calculations performed in the same study also predicted that in the excited quinoidal-state the C-C bonds between the fluorene and the truxene core have a bonding nature that enables greater conjugation and rigidifies the system.[150] This could be the reason behind the vibronic structure of the fluorescence band.

In every example there is a large Stokes shift between the absorption and the emission maxima (an average of 38 nm), with little spectral overlap. This is beneficial for optical applications because it minimises the re-absorption of the emission, thus maximising the photoluminescence quantum efficiency and improving the device performance. The increase of the number of fluorene units in the arms induces a bathochromic shift in the emission which, as observed in the absorption properties, is more pronounced for the first fluorene

addition (≈ 26 nm shift from **T1** to **T2**) than for the larger members of the series (≈ 7 nm shift from **T2** to **T3** , ≈ 4 nm from **T3** to **T4** and 1 nm from **T4** to **T6**). This effect was also discussed by Montgomery and co-workers, that attributed the smaller transition energies (both for absorption and emission) in compounds **T2** to **T4** than in **T1**, to the fact that the core is a greater fraction of the molecule in the smaller members of the series.[151] Interestingly, the same publication described a TD-DFT study on the change in electron density by absorption of circularly polarised light and/or fluorescence for a benzene-cored analogue to **T2** (**B2**). They concluded that the change in electron density during absorption and emission was larger in the middle of the arms, but for the absorption it was delocalised over the entire molecule while in the emission it was localised on a single arm. They found three equivalent energy minima in the excited state, which would imply that the emission in benzene or truxene cored tris(oligofluorenes) could come from any of the three arms, but only from one arm at a time.[151]

The solid state optical and photophysical properties of the **T1-T4** (**butyl**, **octyl** and **hexyl**) series were studied by Neil Montgomery at the Organic Semiconductor Optoelectronics group in the University of St Andrews. Likewise, all the photophysical and lasing measurements of **T6** (**hexyl** and **octyl**) were performed by John McGurk at the Experimental Solid State Physics group in Imperial College London.

The photoluminescence quantum yields (PLQY, Φ) of the **Tn** series are presented in Table 2-4. All the materials show high PLQYs in solution (≈ 80 %), film (≈ 60 %) and powder (≈ 50 %), being generally higher for the larger analogues (**T2**-**T4**). The film and powder PLQYs for the butyl analogues were generally lower than for the materials with hexyl and octyl alkyl chains. The derivatives with hexyl chains were normally the most efficient emitters, but their PLQYs were similar to those of the octyl analogues, except for **T6**. The photoluminescence quantum efficiency for the **T6** compounds was measured in films of different thicknesses and **T6** (**octyl**) consistently showed higher PLQY than **T6** (**hexyl**). At the thickness chosen for the photophysical studies (141 nm for **T6** (**hexyl**) and 147 nm for **T6** (**octyl**)), the PLQY for **T6** (**octyl**) was 1.8 times greater than that of **T6** (**hexyl**). This effect might be due to a closer packing of the chromophores with shorter alkyl chains in the solid state, leading to a certain degree of quenching of the emission by reabsorption from a neighbouring molecule.

Table 2-4 Photoluminescence quantum yields of the **Tn (butyl, hexyl, octyl)** series in solution, film and powder.

Compound	$\Phi_{solution}$	Φ_{film}	Φ_{powder}
T1 (butyl)	0.73	0.40	0.31
T1 (hexyl)	0.78	0.55	0.47
T1 (octyl)	0.79	0.52	0.61
T2 (butyl)	0.85	0.47	0.52
T2 (hexyl)	0.81	0.66	0.49
T2 (octyl)	0.71	0.58	0.49
T3 (butyl)	0.85	0.50	0.45
T3 (hexyl)	0.79	0.66	0.71
T3 (octyl)	0.73	0.59	0.64
T4 (butyl)	0.87	0.31	0.23
T4 (hexyl)	0.87	0.70	0.69
T4 (octyl)	0.86	0.68	0.66
T6 (hexyl)	-	0.37	-
T6 (octyl)	-	0.67	-

The solid state absorption and emission bands (Figure 2-14 for **T2**-**T4** (**butyl**) and Figure 2-15 for **T2**-**T4** (**octyl**)) are very similar to the ones in solution, with barely no shift in the absorption maxima and a slight red shift in the emission peaks (see Table 2-3, page 54). It should be noted that the high energy peak at around 215 nm corresponds to the S_0-S_2 transition of the oligofluorenes and it could not be observed in solution due to the cutoff of the solvent. The emission profiles of the compounds present variable intensities in the vibronic splitting, probably due to differences in morphology in the solid state derived from the different lengths of the alkyl chains. Furthermore, the vibronic peaks are slightly better resolved than in solution.

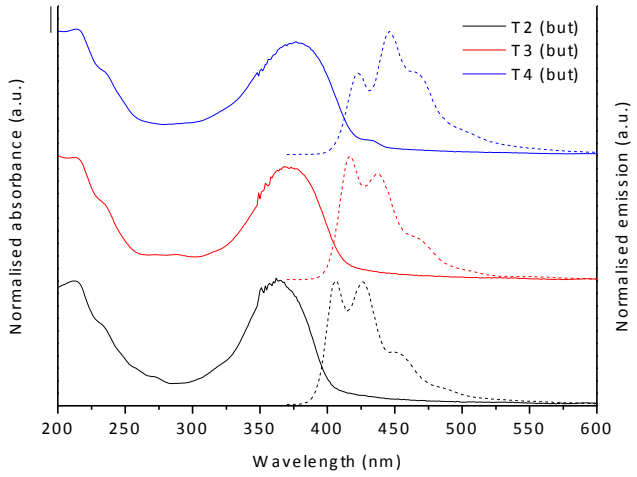

Figure 2-14 Solid state absorption spectra of the **Tn (butyl)** series.

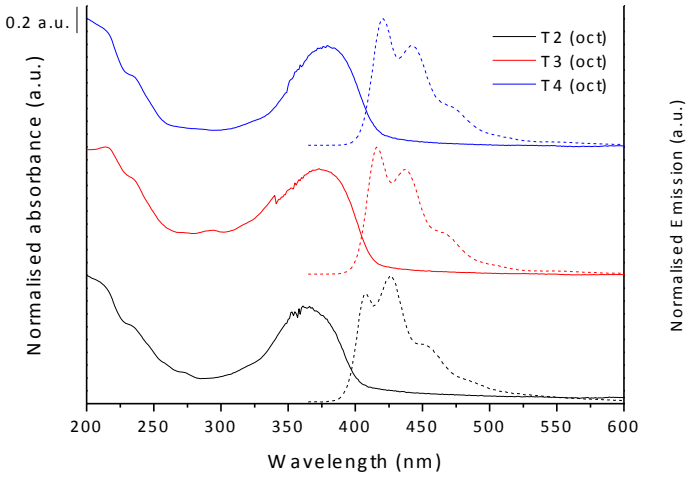

Figure 2-15 Solid state absorption spectra of the **Tn (octyl)** series.

The solid state spectra of **T6** (**hexyl** and **octyl**) recorded from thin films (141 nm and 147 nm respectively) are presented in Figure 2-16. Despite both films having marginally different thicknesses, **T6** (**hexyl**) presents an 18 % greater absorption coefficient than **T6** (**octyl**) ($2.26 \cdot 10^5$ cm^{-1} and $1.91 \cdot 10^5$ cm^{-1} respectively). This might be due to a closer packing of the hexyl derivatives because of the shorter length of their alkyl chain. This could lead to a greater concentration of the chromophores in a film of similar thickness, allowing the sample to absorb more radiation. As previously discussed for the rest of the members of the **Tn** family, the absorption band is featureless and broad and the short wavelength absorption of the fluorenes is observed in the solid state.

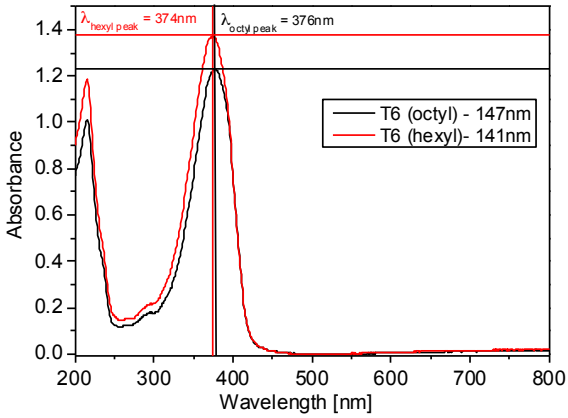

Figure 2-16 Solid state absorption spectra of **T6 (hexyl** and **octyl).** The thickness of the spin coated films was 141 nm for **T6 (hexyl)** and 141 nm for **T6 (octyl)**.

The solid state emission spectra of the **T6** (**hexyl** and **octyl**) materials were measured on the same films as the absorption spectra (Figure 2-17). The vibronic structure is clearly observed and the intensities of the three peaks follow the same pattern as in the solution spectrum for **T6** (**octyl**), with the greatest intensity for the 0-0 band, followed by the 0-1 band and the 0-2 band presenting the lowest intensity. Interestingly, **T6** (**hexyl**) breaks that pattern having an increased intensity of the 0-1 vibronic peak at 446 nm, despite the small thickness difference of the film between both compounds. Again, this effect might come from the closer packing of the molecules **T6** (**hexyl**) in the film.

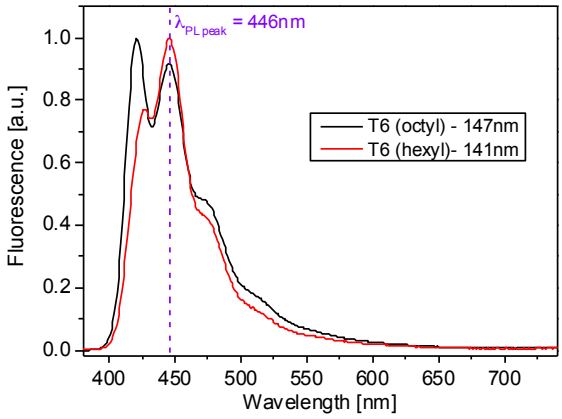

Figure 2-17 Solid state fluorescence spectra of **T6 (hexyl** and **octyl)**. The thickness of the spin coated films was 141 nm for **T6 (hexyl)** and 141 nm for **T6 (octyl)**. λ_{ex} = 374 nm.

The determinations of the threshold for amplified spontaneous emission (ASE) for the **T6** (**hexyl** and **octyl**) materials are presented in Figure 2-18 a) and b) respectively. The ASE measurements were performed by pumping the material across a range of power intensities

employing a set strip length for the pumping. This method is called the variable strip length (VSL) at variable power (VP) configuration. In Figure 2-18 it can be observed that the ideal strip length is 4 mm for both compounds. The ASE threshold for **T6** (**hexyl**) was determined to be ≈ 90 μJ·cm^{-2} and for **T6** (**octyl**) it was much lower at 30 μJ·cm^{-2} (the lowest threshold obtained for the oligofluorene truxenes was 16 μJ·cm^{-2} for **T4** (**hexyl**)).[47] In general, it seems advantageous to use hexyl chains for the **Tn** materials due to their thermal properties and their synthetic feasibility, as discussed above, but it seems that for **T6** materials octyl chain offers advantages in terms of device performance and presenting higher PLQY and lower ASE threshold than the hexyl derivative.

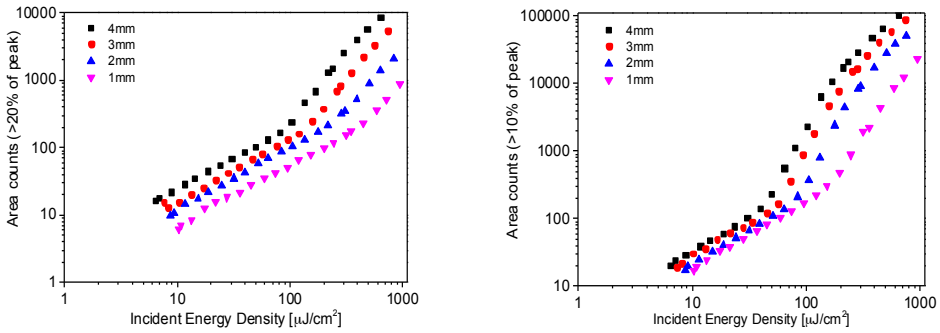

Figure 2-18 ASE measurement at various strip lengths for a) **T6 (hexyl)** and b) **T6 (octyl)**. The legend corresponds to the length of the strip pumped for the determination of the ASE threshold.

The ASE spectra for **T6** (**hexyl**) and **T6** (**octyl**) are represented in Figure 2-19 (top row and bottom row respectively). It can be observed that when pumping both compounds with low energies the output is simply the photoluminescence spectrum with the 0-1 vibronic band intensified. When pumping just above the ASE threshold energy (obtained when the ASE output intensity is twice the fluorescence intensity) the emission profile narrows around the ASE wavelength. Note that the narrowing is more obvious in the case of **T6** (**hexyl**) because the pumping energy is 46 μJ·cm^{-2} higher than the threshold, whereas for **T6** (**octyl**) it is only 20 μJ·cm^{-2} higher. Pumping above those energies a narrowed emission peak can be observed for both compounds and gain is obtained. For both materials the ASE wavelength is centred at 449 nm (the 0-1 vibronic peak). The gain for both **T6** materials was studied pumping at a constant energy (150 μJ·cm^{-2}), while varying the length of the pumped stripe. The gain coefficient for **T6** (**hexyl**) was extracted to be 9.29 cm^{-1} and for **T6** (**octyl**) 15.66 cm^{-1} at the cited experimental conditions (the maximum gain value obtained for an oligofluorene truxene was 23 cm^{-1} for **T4**).[47]

The photoluminescence lifetime (τ) is defined as the time that a molecule remains in excited state before falling to the ground state. The lifetimes of the **T6** materials were measured by time resolved photoluminescence experiments following a time-correlated single photon counting (TCSPC) setup. This method is based on the registration of all the fluorescence photons obtained from the moment the sample is excited with a pulse of certain energy (this would represent the time = 0 ns). The measured average lifetime for **T6** (**hexyl**) was 580 ps and for **T6** (**octyl**) 515 ps. These lifetimes are broadly similar and slightly shorter than the lifetime obtained for **T4** (**hexyl**) (630 ps).[151]

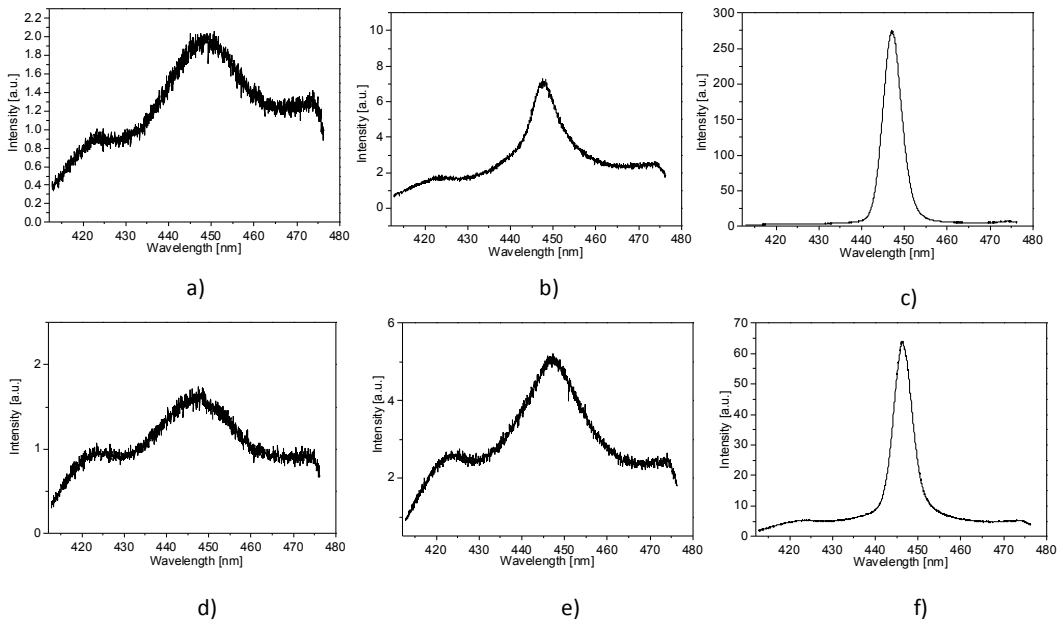

Figure 2-19 ASE measurements on the **T6** compounds with a 4 mm stripe. The top row corresponds to **T6 (hexyl)** pumping at a) 24 μJ·cm^{-2} (photoluminescence); b) 136 μJ·cm^{-2} (just above threshold); c) 303 μJ·cm^{-2} (gain). The bottom row belongs to T6 (octyl) pumping at d) 23 μJ·cm^{-2} (photoluminescence); e) 50 μJ·cm^{-2} (just above threshold); f) 136 μJ·cm^{-2} (gain).

2.3.5 Explosive vapour sensing

The fast and reliable detection of explosives is a major concern in our current society in terms of security in airports and public buildings, or to assist with the detection of landmines. Fluorescent polymers have previously been employed as sensors for nitroaromatic explosives like trinitrotoluene (TNT) or dinitrotoluene (DNT).[7] The challenge in the field is to improve the selectivity, detection limits, speed of response and portability.[152] Nitroaromatic explosives are electron deficient molecules whose LUMO lies below the LUMO of electron-rich organic

semiconductors. When vapour of an electron deficient explosive is in contact with a light emitting organic semiconductor, it induces quenching of the emission because the photoexcitation of the conjugated material is followed by energy transfer to the lower-lying LUMO of the explosive. Several sensing mechanisms have exploited this quenching effect by measuring the increase of the ASE and lasing threshold, the decrease of photoluminescence lifetime or the photoluminescence intensity of the semiconductor amongst others.[152-154]

Samuel and co-workers previously described the use of a polyfluorene-based organic semiconductor laser as an explosive detection method. They observed an increase in the lasing threshold (1.8 times) and a threefold decrease in the slope efficiency of the device after exposure to dinitrobenzene (DNB) vapour (9.8 ppb). Moreover, they achieved a maximum sensing efficiency (ratio of the emission intensity before and after the exposure to the explosive vapour) of 82 %, 1.2 times greater than simply measuring the fluorescence from a planar film of polyfluorene of the same thickness exposed to the same concentration of DNB. Their device was recoverable after evacuating the chamber or flushing it with clean nitrogen for just 32 seconds.[152] The same group developed an ultraportable explosive detection system based on the on-site measurement of the fluorescence lifetime of a commercial CDT Green copolymer and a CMOS PL lifetime detection system built in-house.[153] They also reported the use of an explosive detection device based on the measurement of PL lifetimes, lasing thresholds, slope efficiencies and sensing efficiencies of a laser that employed the intrinsically porous polybenzodioxane PIM-1 polymer. They obtained a greater response than with their polyfluorene laser in all fields after exposure to 10 ppb DNB vapour.[154]

Following these studies and the previous work performed on the use of star-shaped oligofluorene truxenes as efficient gain media in OSLs, the performance of **T3** (**butyl**, **hexyl** and **octyl**) in lasers for explosive detection was tested by Yue Wang of the Organic Semiconductor Optoelectronics group at the University of St Andrews. As already discussed for polyfluorene, the deeper the explosive molecules can penetrate through the film, the more sensitive the device becomes.[152] For this reason the goal of this study was to determine the effect of the alkyl chain length in the packing of the molecules within the film and hence on the sensitivity of the explosive detection device. From the lasing studies performed on the **T6** analogues it had been anticipated that the longer the alkyl chain, the less dense the packing of the molecules was in the film. In principle this should allow for a better diffusion of the explosive

throughout the film and therefore a better performance of the octyl analogues over the hexyl and the butyl ones was anticipated.

Initially, spin-coated films of the materials were exposed to 10 ppb DNB vapour for 500 seconds, followed by flushing with clean nitrogen for the same amount of time to study the recovery while monitoring photoluminescence intensity over time. Figure 2-20 represents two of these cycles. For comparison, the study was also performed on films of the benzene-cored analogue of **T3** (**hexyl**) (**B3**).

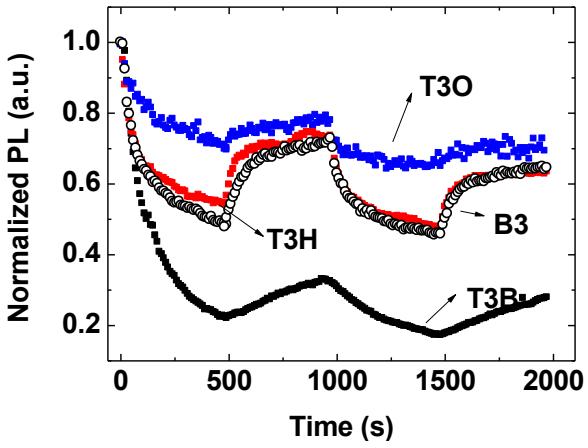

Figure 2-20 PL sensing comparison between the **T3 (butyl, hexyl** and **octyl)** compounds. The benzene-cored tris(terfluorene) **B3** analogue is presented for comparison. In the legend "B" stands for butyl, "H" for hexyl and "O" for octyl.

After the first contact with the explosive vapour all the materials suffer a quenching of the emission, which is most pronounced for the butyl analogue (quenching of 78 % of its PL) and least effective for the octyl derivative (quenching of 30 % of its PL). Both T3 and B3 (hexyl) behave similarly with a 46 % quenching of their emission intensity (the results are summarised in Table 2-5). Flushing the films with clean nitrogen leads to a partial recovery of the emission in all cases. A second cycle of explosive vapour/nitrogen leads to quenching to approximately the same levels as after the first exposure and the same partial recovery. The fact that **T3** and **B3** (**hexyl**) behave almost identically indicates that the permanent partial photobleaching is not due to the truxene core. Furthermore, polyfluorenes also show some permanent quenching after the first explosive vapour exposure, which indicates that in this case the effect should come from the oligofluorene arms.

Table 2-5 Sensing based on the PL intensity given as the percentage of PL quenching.

	T3 (butyl)	T3 (hexyl)	T3 (octyl)
1st exposure	78%	46%	30%
1st recovery	10%	19%	8%
2nd exposure	15%	36%	13%
2nd recovery	11%	17%	7%

The next stage of the study consisted of developing lasers by spin-coating films of the T3 materials (80 – 110 nm thick) onto a 2D silicon grating with emission wavelengths around 445 nm. The lasers where photoexcited with a Q-Swip microchip laser at 355 nm with a 500 Hz repetition rate and an excitation diameter of ≈ 1.8 mm. The lasing threshold was measured before and after exposure to 16 ppb DNB vapour (see Table 2-6). Again, the laser developed with **T3** (**butyl**) was the most responsive (an almost tenfold increase in the lasing threshold was observed), followed by the hexyl derivative. It should be noted that the thinnest film employed was for the **T3** (**butyl**) analogue and, as discussed in a previous publication,[152] thinner films lead to greater sensitivities because the quenching of the emission occurs only in the areas where the explosive molecules have been in contact with the emissive material. Even if the penetration of the molecules is the same in thick and thin films, the former have more "un-quenched" chromophores that can continue emitting light after exposure to the vapour, and their PL and threshold is therefore less affected. Nevertheless, the small thickness difference (30 nm in the most extreme case) cannot explain the great increase in threshold on its own and it should be therefore concluded that the length of the alkyl chain plays a very important role in the interaction of the film and the explosive vapour.

Against the initial prediction, **T3** (**butyl**) is the best material for explosive detection sensing. In order to explain this result, a series of photophysical studies were performed on films of ≈ 70 nm thickness dropcast from 20 $mg \cdot mL^{-1}$ solutions in toluene onto a quartz substrate, exciting at 355 nm. The results are summarised in Table 2-7.

Table 2-6 Sensing based on DFB lasers**.**

Compound	Film thickness (nm)	λ_{lasing} (nm)	Threshold before ($W \cdot cm^{-2}$)	Threshold after ($W \cdot cm^{-2}$)	Lasing threshold increase (times)
T3 (butyl)	80	459	99	987	9.97
T3 (hexyl)	110	456	156	248	1.59
T3 (octyl)	103	451	156	197	1.26

The PLQYs measured from these films are much higher than the results presented in Table 2-4 (page 59), which were around 0.60, but the pattern of a much lower PLQY for the butyl analogue compared with the hexyl and octyl analogues is repeated.

Table 2-7 Photophysical properties of the **T3** series.

Compound	PLQY	λ_{abs} (nm)	λ_{em} (nm)
T3 (butyl)	0.63	364	413, 437
T3 (hexyl)	0.83	367	412, 435
T3 (octyl)	0.80	368	412, 435

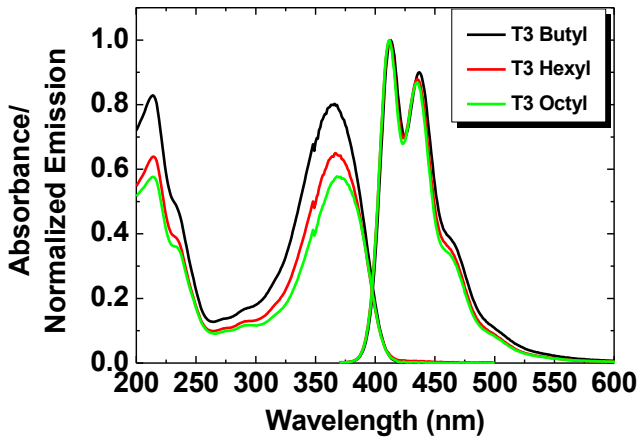

Figure 2-21 Absorption (left axis) and emission spectra (right axis) of spin-coated films of **T3 (butyl, hexyl** and **octyl)**.

The absorption and emission spectra of the **T3** analogues are presented in Figure 2-21. It can be observed that the butyl analogue shows higher absorption intensities than the hexyl and both of them are more intense than the octyl derivative. As already discussed for **T6** (**hexyl** and **octyl**), the shorter length of the alkyl chain probably allows for a greater concentration of

chromophores in films of the same thickness, promoting a greater absorption for the analogues with the shortest alkyl chains. In this case the emission profile resembles that of the solution.

The refractive index was also higher for **T3** (**butyl**), followed by **T3** (**hexyl**) and finally **T3** (**octyl**) (see Figure 2-22). This might reinforce the hypothesis that the shorter alkyl chains lead to a closer packing of the molecules in the isotropic thin films.

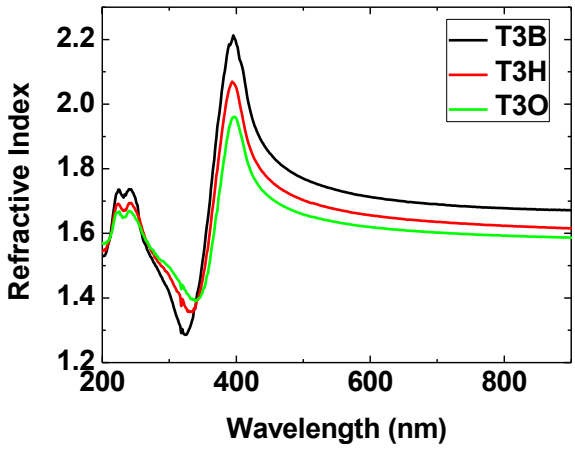

Figure 2-22 Refractive index of **T3 (hexyl, butyl** and **octyl)**.

To prove this hypothesis, the film densities of films of the **T3** materials were measured. Solutions of 20 $mg \cdot mL^{-1}$ of the materials in toluene were spin coated onto silicon wafers of known dimensions and the edges were cut in order to ensure uniform thickness throughout the samples. The films were then dissolved in the same known amount of toluene and the absorbance was measured and compared with the absorbance of dilute solutions of known concentrations. The absorbances were integrated between 310 nm and 415 nm and the film thicknesses were measured and modelled by ellipsometry. The results summarised in Table 2-8 indicate that, as previously discussed, the film density of the butyl analogues was greater than for the hexyl ones and films of **T3** (**octyl**) had the greatest average intermolecular distance.

Table 2-8 Film density measurements and intermolecular distance for films of the **T3 (butyl, hexyl and octyl)** compounds spin-coated from 20 mg·mL^{-1} solutions in toluene.

Compound	Average film density ($\cdot 10^5$ g·m^{-3})	M_w (g·mol^{-1})	Molecules/cubic meter (average) ($\cdot 10^{25}$ molecules·m^{-3})	Average intermolecular spacing R_{avg} (nm)
T3 (butyl)	7.38	3166.81	14.04	1.92
T3 (hexyl)	5.90	3840.08	9.25	2.21
T3 (octyl)	5.52	4513.36	7.36	2.39

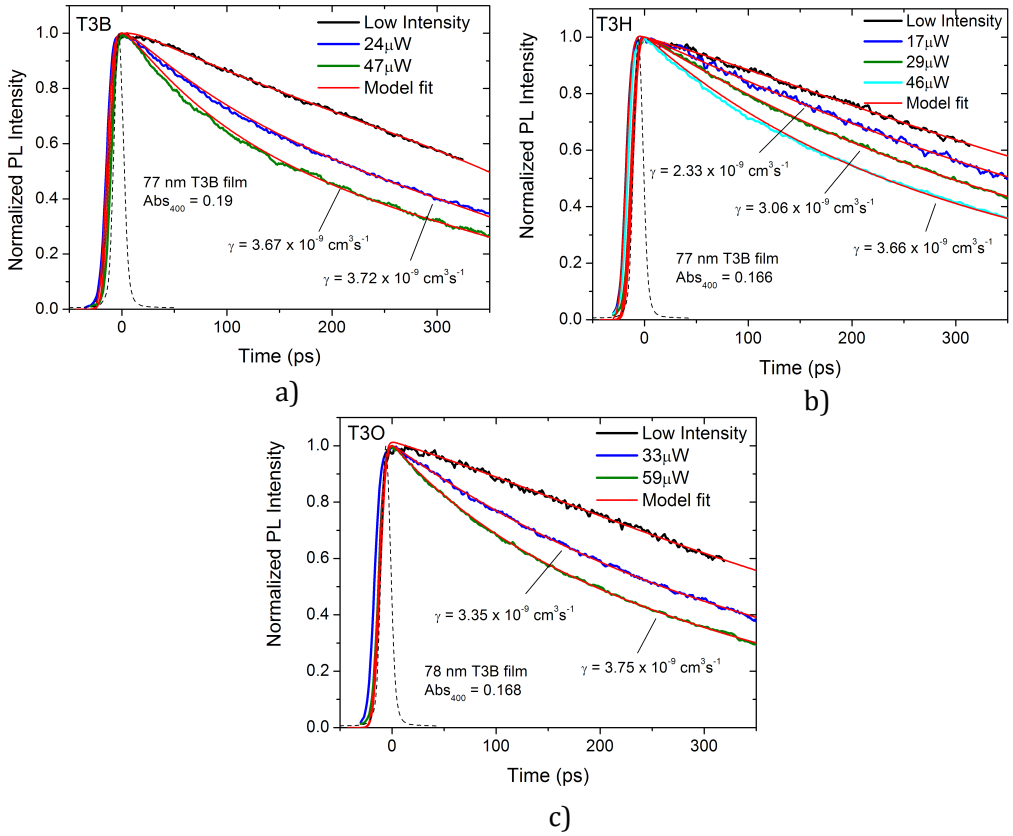

Figure 2-23 Time-resolved PL decay spectra at different pumping energies of a) **T3 (butyl)**, b) **T3 (hexyl)** and c) **T3 (octyl).**

The higher response of the devices with **T3** (**butyl**) might be explained because the closer packing of the molecules in the condensed state might lead to a more efficient exciton diffusion length and therefore to a higher quenching efficiency. To investigate this further exciton-exciton annihilation experiments were carried out on ≈ 77 nm thick films of the

materials employing 400 nm excitation wavelengths and increased pumping energies. The time-resolved PL decay spectra for **T3** (**butyl**, **hexyl** and **octyl**) are presented in Figure 2-23 a), b) and c) respectively. The red line corresponds to the model fit for the decay at each pumping energy and it matches the experimental results very well. The dotted black peak represents the excitation pulse at time zero. A faster decay occurs in all cases upon increasing the pumping intensity.

Table 2-9 Exciton-exciton annihilation parameters. τ_{avg} is the average decay time, γ_{avg} is the annihilation rate, R_{avg} is the average intermolecular spacing, D is the diffusion coefficient and L_{1D} is the 1D- diffusion length.

Compound	τ_{avg} (ps)	γ_{avg} ($\times 10^{-9}$ cm^{3}s^{-1})	R_{avg} (nm)	D ($\cdot 10^{-3}$ cm^{2}s^{-1})	L_{1D} (nm)
T3 (butyl)	518	3.70	1.92	1.53	8.9
T3 (hexyl)	585	3.02	2.21	1.09	8.0
T3 (octyl)	551	3.55	2.39	1.18	8.1

Table 2-9 summarises the results from the exciton-exciton annihilation experiments. The average decay times are similar for all three materials but **T3** (**butyl**) has the shortest lived photoluminescence (518 ns). The annihilation rate, diffusion coefficient and the one-dimensional diffusion length are greater for the butyl derivative, indicating that the shorter intermolecular distance in the film is leading to a greater degree of exciton diffusion and therefore a larger degree of quenching. After this study it can be concluded that even though the **T3 (butyl)** analogue might be the least suitable candidate as a gain medium for lasing applications, it is the best material for explosive vapour detection. It shows the fastest response and greatest sensitivity of all three **T3** materials. In order to complete this study it would be beneficial to investigate the effect of film thickness on the sensitivity of the devices with the three materials.

2.4 Conclusion

In conclusion, a series tris(oligofluorene) truxenes (**Tn**) with butyl and octyl chain were synthesised in order to study the effect of the length of the solubilising side chains in the properties of the materials, through morphological variations. A larger member of the family

(**T6**) was also synthesised with hexyl and octyl chains in order to have a better insight on the effective conjugation length of these star-shaped materials. The synthesis of the butyl analogues proved to be difficult due to the reduced solubility of the materials in organic solvents, especially at low temperatures. On the other hand, the purification of the octyl derviatives was more challenging due to poorer separation from their byproducts on silica and their tendency to trap grease.

The compounds are thermally stable and amorphous materials. The length of the solubilising alkyl chains affects the glass transition temperatures dramatically and for the octyl derivatives the T_g values are so low that it could affect their device performance. The electrochemical properties of the compounds are not largely affected by the length of the solubilising chains, although this would be confirmed by further investigation. The optical properties of the materials in solution are very similar, but their photophysical characteristics in the condensed state are greatly affected by the size of the alkyl chain. Hexyl chains are optimal for the performance of the **Tn** materials in the condensed state, taking into account the synthetic, thermal and photophysical properties of the materials. Nevertheless, for the greater analogues (**T6**) the octyl chain offers a better performance in the solid state, reducing the re-absorption of the emission and providing higher PLQY and lower ASE threshold than the one for **T6** (**hexyl**).

Finally, the performance of the **T3 (butyl**, **hexyl** and **octyl)** materials in explosive vapour sensors based on PL decay or increase of lasing threshold was tested. The materials are suitable for the application because they provide a fast and sensitive response, but **T3 (butyl)** is the strongest candidate because it provides the greatest response to the presence of the analyte across a range of testing protocols.

3 Star-shaped oligofluorene-BT truxene: T4BT isomers

3.1 Abstract

A series of monodisperse star-shaped tris(oligofluorene) truxenes containing the fused bicyclic acceptor unit 2,1,3-benzothiadiathole (BT) within the oligofluorene arm were synthesised. In these **T4BT-X** isomers (**T4BT-A** to **T4BT-E**), the BT unit is sequentially introduced at each possible position within the oligofluorene arms, enabling a thorough study of the structure-property relationship. The electronic behaviour of the series members is related to substitution pattern of BT unit within the oligofluorene arm, which provides pairwise correspondence in the optical properties of these isomers, with three distinct "locations" for the BT moiety within the **T4** structure. This work was published in Advanced Functional Materials and the experimental for the synthesis as well as further studies and additional information can be found in the publication.[155]

T4BT-E, the isomer with BT at the terminal position of the oligofluorene arm, exhibits the fastest radiative decay, a decreased PLQY when compared with the other members of the series and shows no ASE when excited under the same conditions as the other four materials.

Theoretical calculations explain the differences in the optical properties of the **T4BT-X** family, especially related to their photoluminescence decay time.

3.2 Introduction

Following the previous study on the effects of the length of the solubilising alkyl chains and the number of oligofluorene units in the tris(oligofluorene)truxene series, it was decided to investigate the effect of the introduction of an acceptor unit within the oligofluorene chain of **T4**, one of the oligofluorene truxene materials that has proven to be most effective for lasing applications.[47]

The fused bicyclic unit 2,1,3-benzothiadiazole (BT) is an electron-deficient heterocycle that can stabilise and spatially localise the LUMO of simple conjugated materials.[156] A BT-fluorene copolymer was first synthesised of by Woo and co-workers at the Dow Chemical Company.[157] Since then, the copolymer poly(9,9-dioctylfluorene-co-benzothiadiazole) copolymers (**F8BT**) has been employed as an excellent green emissive material with efficient electron-

transporting properties for OLED,[158, 159] light emitting field effect transistor (LFET)[84] and lasing applications.[84, 160] **F8BT** on its own shows lower electron injection barriers than poly(9,9-dioctylfluorene) (PF8)[159] and blends with PF8[161] and copolymers containing fluorene, BT and arylamine comonomers have improved the OLED performance.[162, 163]

BT and thiophene based copolymers, such as the triad thiophene-benzothiadiazole-thiophene developed by Dow Chemicals for their Dow Ref F dye, have been employed as red emitters in optoelectronic applications.[158, 164, 165] BT and benzobisthiadiazole based monomers have also been copolymerised with thiophene and other donor monomers promoting high efficiencies in organic photovoltaics.[166-169]

Although BT has featured in many conjugated polymers and molecular based materials, little is understood about the intricate association and electronic interplay between the donor and acceptor components of these materials. This understanding would be beneficial for the structural design of new organic semicondutors for optical applications. To this end, a series of structural isomers featuring three oligofluorene arms with one BT unit appended to a truxene core was synthesised.[59] In these isomers (**T4BT-A** to **T4BT-E**), the BT unit is located at each possible position within the oligofluorene arms, initially directly connected to the truxene core (**T4BT-A**), then subsequently shifted outwards until it is located at the terminal position (**T4BT-E**) (see Figure 3-1). This study allows a thorough investigation of the effect of subtle variation of the donor environments around the BT unit within an oligofluorene arm in derivatives of **T4**.

Furthermore, the distribution of the BT moiety in a fluorene-BT copolymer is not well defined and slight variations in the environment of the BT are averaged over the whole polymer. On the other hand, the **T4BT-X** series presents a well-defined symmetry derived from the trigonal structure containing monodisperse oligomers, allowing a better explanation of the structure-property relationship.

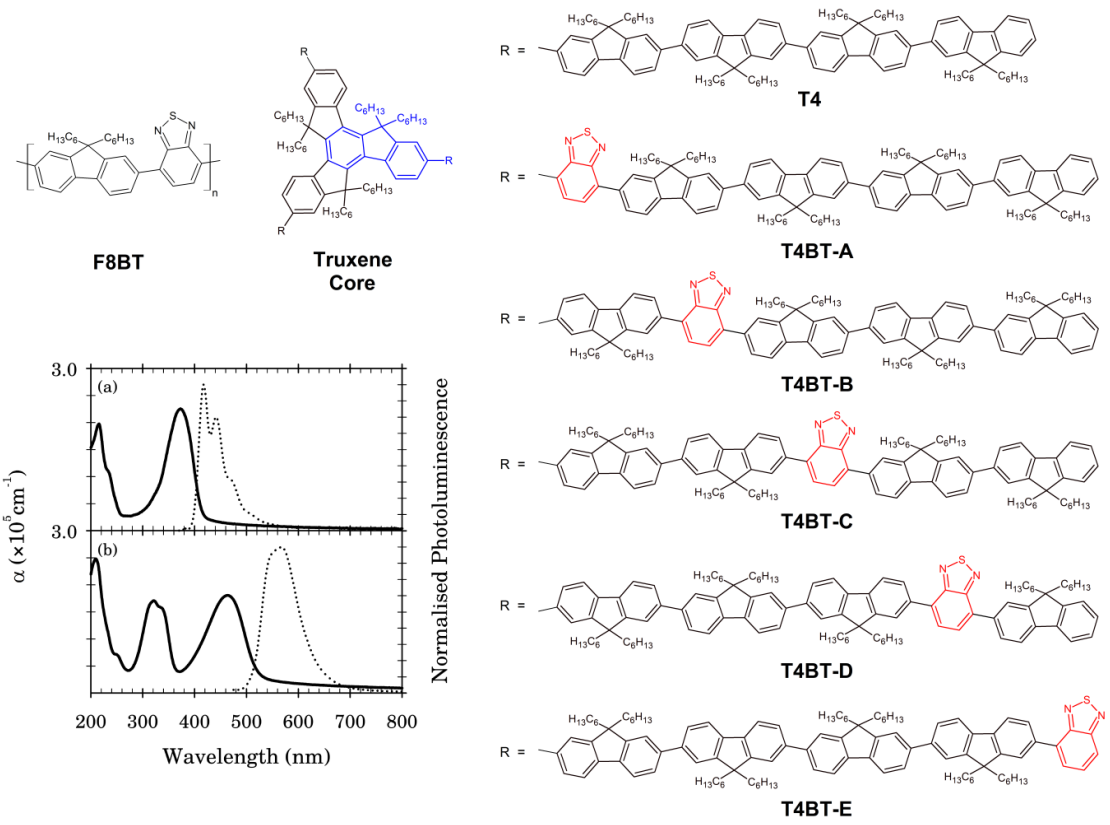

Figure 3-1 Chemical structure of the **F8BT** alternating copolymer, the parent truxene **T4**, and the members of the **T4BT-X** series. The blue highlighted part in the truxene represents the 9,9-dihexylfluorene that is attached to the arm and takes part in the effective conjugation length of the arm. The BT moiety is highlighted in red. The inset graphs show the absorption (solid line) and emission (dotted line) spectra of the truxene **T4** (a) and **F8BT** (b).

The materials were designed and synthesised within the Skabara group (University of Strathclyde), mainly by Dr. Alexander Kanibolotsky, and were characterised by absorption, emission and cyclic voltammetry by Saadeldin Elmasly. Further photophysics, amplified spontaneous emission and lasing studies were performed in the Bradley group (Imperial College London) by Colin Belton. DFT calculations were performed by James Kirkpatrick at Imperial College London.

The members of the **T4BT-X** family are highly efficient green emitters with excellent solubility and film-forming properties. The absorption and emission spectra of the materials show a pair-wise relationship between **T4BT-A** and **–D** and **T4BT-B** and **–C** due to the similar symmetry around the BT moiety in each of the two pairs. **T4BT-E** presents very distinct properties from the rest of the members of the series due to a completely different conjugation pattern around the acceptor unit. Density functional theory/time-dependent density functional theory (DFT/TD-DFT) calculations allowed to determine the distribution of the HOMO/occupied

Natural Transition Orbital (NTO) amplitude within the arm and the proportion of wavefunction present on the BT unit. The results of DFT calculations shed a light on the peculiarity of intramolecular charge transfer (ICT) interaction in the conjugated system of BT series.

3.3 Results and discussion

3.3.1 Synthesis

The synthetic strategy for creating the set of C_3 symmetric star-shaped truxene-oligofluorene-BT conjugated systems involved the synthesis of the tris(bromooligofluorene)truxene derivatives (**TnBr**) following the procedure introduced in Chapter 0. Convergent Suzuki or Negishi coupling of trimethylsilyl terminated oligofluorenes (**TMS-F$_n$-B(OH)$_2$** or **TMS-F$_n$-ZnCl** respectively) with tribromohexahexyltruxene (**3.1**) yielded the **TnTMS** products. Both cross-coupling reactions were very high yielding but Suzuki proved to be more efficient (yields above 90 %) than Negishi (84 and 87 %). **T4TMS** was synthesised by both methods *via* a semiconvergent coupling of **T2Br** with **TMS-F$_2$-B(OH)$_2$** or **TMS-F$_2$-ZnCl**, affording the product with an 84% yield in both cases. Bromination of the **TnTMS** compounds under mild conditions yielded the **TnBr** scaffold with almost quantitative yields.

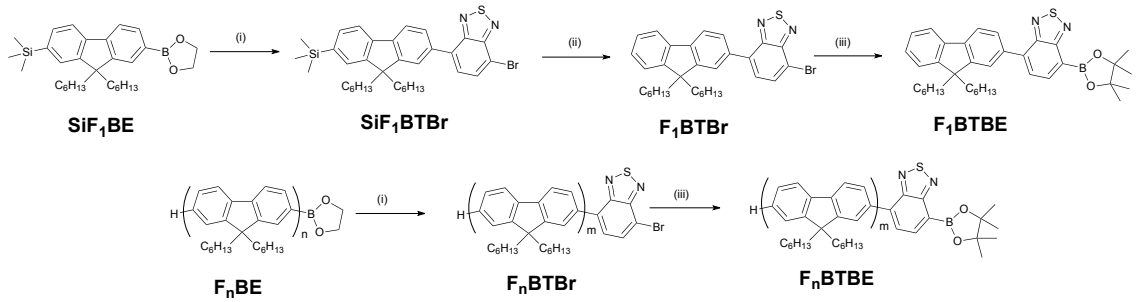

Scheme 3-1 Synthesis of the oligofluorene-BT arm precursors **F$_1$BTBE-F$_3$BTBE**. Reagents and conditions: (i) $BTBr_2$, K_3PO_4, $Pd(PPh_3)_4$, DMF, 80 °C, 24 - 32 h; (ii) CF_3COOH, CH_2Cl_2; (iii) bis(pinacolato)diboron, [1,1'-bis(diphenylphosphino)ferrocene]dichloropalladium, CH_3COOK, dioxane, 105 °C, 21 h.

The arm precursors **SiF$_1$BTBr** and **F$_n$BTBr** were synthesised in high yields using the anhydrous modified Suzuki cross-coupling procedure with 3 equivalents of 4,7-dibromobenzothiadiazole **BTBr$_2$** and the corresponding oligofluorene boronic ester **F$_n$BE**, K_3PO_4 as a base and dimethylformamide to efficiently solubilise **BTBr$_2$**. Note that after the coupling to the BT unit the terminology for the number of fluorenes in the oligofluorene chain changes from n to m. This is done in order to distinguish the length of the arm from the arm length of the **TnBr**

compounds. Further coupling with bis(pinacolato)diboron in the presence of a weak base (CH_3COOK) yielded the **F_nBTBE** (see Scheme 3-1).

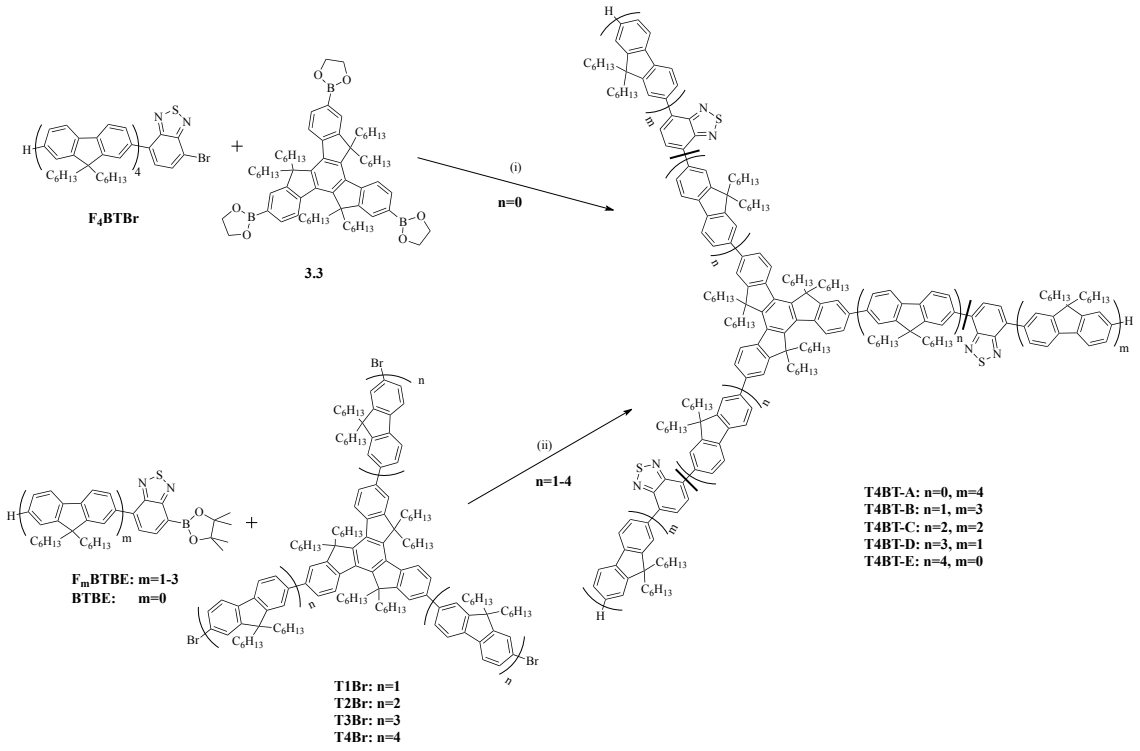

Scheme 3-2 Synthesis of the **T4BT-X** family. The disconnection sites are represented by bold lines. Reagents and conditions: (i) $Pd(PPh_3)_4$, $Ba(OH)_2{\cdot}8\ H_2O$, THF, DME, H_2O, 80 °C, 41 h; (ii) $Pd(PPh_3)_4$, $Ba(OH)_2{\cdot}8\ H_2O$, DME, H_2O, 80 °C, 24 h.

The synthesis of the first member of the family (**T4BT-A)** involved the coupling of truxenetriboronic ester **3.3** with bromo(quarterfluorenyl)benzothiadiazole **F_4BTBr** *via* Suzuki coupling (Scheme 3-2, top). With this approach the conversion of **F_4BTBr** (product of a nine step synthetic route) to boronic ester is avoided. Furthermore, the Suzuki coupling using a more nucleophilic bromo-containing compound (**F_4BTBr** as opposed to tribromotruxene) is more efficient. The ester **3.3** was synthesised from tribromohexahexyltruxene **3.1** (Scheme 3-3) *via* lithiation with n-BuLi, followed by quenching with triisopropylborate and hydrolysis in acidic conditions. Compound **3.2** presented low solubility due to the formation of polymeric anhydrous forms and conversion to the boronic ester **3.3** solved the issue.

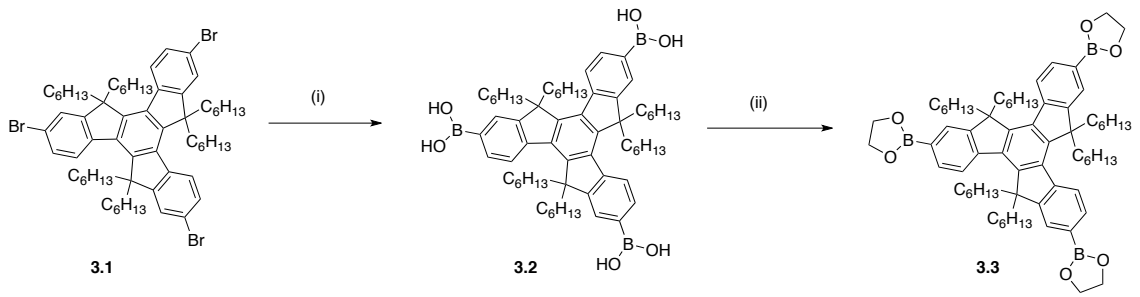

Scheme 3-3 Synthesis of truxenetriboronic ester **3.3**. Reagents and conditions: (i) THF, BuLi (-78 °C), $(^{i}PrO)_3B$ (-100 °C), 20 h (R.T.); (ii) ethyleneglycol, toluene,reflux, 16 h.

The other four members of the family (**T4BT-B** to **T4BT-E**) were synthesised in high yields (70 - 84 %) by Suzuki cross-coupling between tribrominated oligofluorene truxenes (**T1Br** to **T4Br**) and oligofluorene boronic esters containing a BT unit in the required position (**F_mBTBE**), using barium hydroxide as a base in dimethoxyethane (Scheme 3-2, bottom).

The **T4BT-X** family is promising for device fabrication because its members are soluble in common organic solvents and present high thermal stability with high decomposition temperatures (418 - 428 °C) measured by TGA. Furthermore, DSC studies show that the materials possess good morphological stability with high glass transition temperatures (T_g = 107 - 111 °C) and no obvious crystallisation.

3.3.2 Absorption and photoluminescence properties

The absorption and normalised emission spectra of the members of the **T4BT-X** series are presented in Figure 3-2. Absorption spectra were recorded on films of 50 ± 5 nm thickness, whereas the films employed for the emission spectra were 30 ± 7nm thick. For comparison, the corresponding spectra for the parent truxene **T4** (on films of 50 nm thickness) and the fluorene-BT copolymer **F8BT** (65 nm thick) are presented in Figure 3-1.

The **T4** parent presents two main absorption features at 220 nm and 370 nm that correspond to the π-π* HOMO to LUMO transitions of the oligofluorene arms/core. The first transition corresponds to feature I in Figure 3-2 and is a localised-localised transition. The absorption at 370 nm corresponds to feature II in Figure 3-2 and is a delocalised-delocalised transition.

The copolymer **F8BT** also presents an absorption band at 220 nm related to the feature I (π-π* localised-localised transition). It possesses two lower energy absorption bands. The first band at 330 nm involves a transition from the HOMO to the highest energy unoccupied molecular orbitals (and it can be compared to the delocalised-delocalised transition in **T4**, feature II). The second band involves a transition from the HOMO to a LUMO localised on the BT unit.[156]

The **T4BT-X** series presents absorption spectra with characteristics of both reference materials **T4** and **F8BT**, but **T4BT-E** shows unexpected behaviour. All the materials have an absorption band around 220 nm (feature I) corresponding to the localised-localised π-π* transition. They also show the absorption band corresponding to feature II, but in the case of **T4BT-E** this band is red shifted to 376 nm, is broader and it does not show any sign of the presence of BT (feature III).

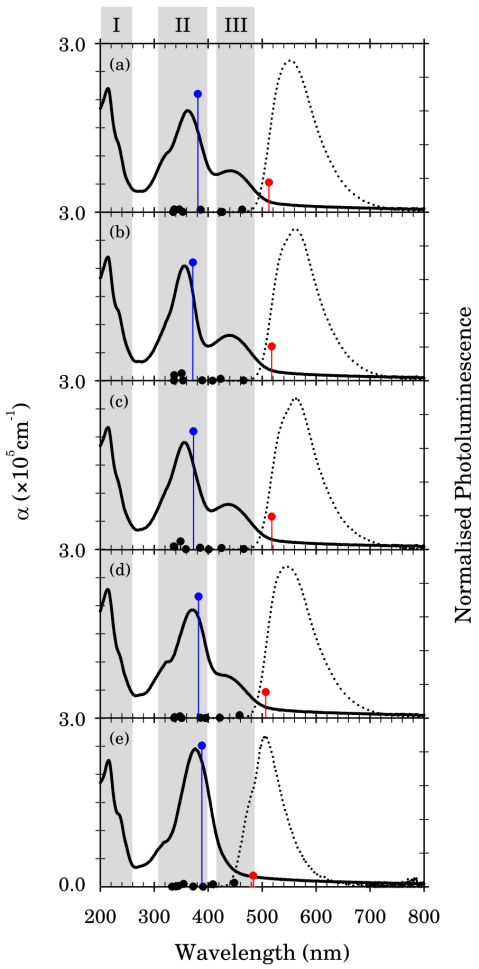

Figure 3-2 Absorption coefficient (α, 10^5 cm^{-1}) (solid line) and normalised PL emission spectra (dotted lines) of thin films of the compounds **T4BT-A** (a), **-B** (b), **-C** (c), **-D** (d) and **–E** (e). The grey highlighted areas are the three absorption features of the **T4BT-X** series. The red and blue circles represent the oscillator strengths for transitions II and III respectively, as calculated by TD-DFT. The black dots represent the oscillator strengths for the many low-lying optical transitions.

The spectra of the other four compounds can be explained as two pairs: (i) **T4BT-A** and **–D** and (ii) **T4BT-B** and **–C**.

The **T4BT-A** and **T4BT-D** possess a similar conjugation pattern around the BT unit: F6'-BT-F6-F6-F6-F6 (**T4BT-A**) and F6'-F6-F6-F6-BT-F6 (**T4BT-D**). Similarly, the conjugation pattern for the second pair is: F6'-F6-BT-F6-F6-F6 (**T4BT-B**) and F6'-F6-F6-BT-F6-F6 (**T4BT-C**). Note that F6' corresponds to the fluorene unit integrated in the truxene core that is highlighted in blue in Figure 3-1.

The transitions between the HOMO and the higher lying unoccupied delocalised molecular orbitals (feature II) in **T4BT-A** and **T4BT-D** are split into a main band (362 nm and 370 nm respectively) and a higher energy shoulder at ≈ 320 nm. **T4BT-B** and **T4BT-C** show a blue shifted main band in feature II (≈ 356 nm) and a hint of a poorly resolved shoulder, again at ≈ 320 nm.

The longer wavelength location of feature II and the greater splitting between the main band and the shoulder in **T4BT-A** and **T4BT-D** can be rationalised by the long conjugation length of the oligofluorenes attached to the BT unit. There are four fluorenes in a row on one side of the BT and one fluorene on the other side, compared to the three fluorenes on one side and two fluorenes on the other side of the BT found in the **T4BT-B** and **T4BT-C** pair. The band in feature II is most red shifted in **T4BT-E** and **T4** because they possess the longest effective conjugation length between oligofluorenes (five fluorenes in a row).

As it can be observed in Table 3-1, the HOMO-LUMO transition (feature III) appears around 445 nm for the **T4BT-A** and **T4BT-D** pair and it has a peak absorption coefficient (α_{III}) much smaller than that of the absorption feature II (α_{II}). For the **T4BT-B** and **T4BT-C** pair the band appears at 440 nm and its peak absorption coefficient (α_{III}) is also very reduced in comparison to that of the absorption feature II (α_{II}). In **F8BT** the HOMO-LUMO transition appears at 445 nm (similar to the results obtained for both pairs of materials) but the absorption coefficient α_{III} is slightly larger than α_{II}, as it can be observed in the inset graph b) of Figure 3-1.

A previous study in which the fractions of fluorene and BT in a $F8_{(1-x)}BT_{(x)}$ copolymer were varied (x = 0.06 - 0.5) described that the polymers containing lower fractions of BT presented decreased intensity of the absorption band in feature III, which is associated to the BT

moiety.[170] Following those results, the 17 % content of BT in the **T4BT-X** family predicts a weaker transition III than for **F8BT** (with 50 % content of BT). Furthermore, the weaker character of the transition III in the **T4BT-X** compounds in comparison with **F8BT** can be explained by the increase of the oscillator strength when the spatial overlap between the molecular orbitals of the oligofluorenes and BT increases. **T4BT-E** presents an anomalous behaviour with no obvious transition in the feature III region. If any transition occurs in this region, it must have a much smaller oscillator strength and therefore no absorption band is observed.

Table 3-1 Experimental and calculated optical properties of the **T4BT-X** family. λ_{II} and λ_{III} are the absorption wavelengths associated with features II and III respectively and α_{II} and α_{III} are the corresponding absorption coefficients. S_{II} and S_{III} are the absorption integrals defined as $\boldsymbol{S = \int \alpha(E) dE}$ where $\boldsymbol{\alpha(E)}$ is the absorption coefficient and E the photon energy. $\lambda_{PL\ max}$ is the wavelength of maximum emission. Φ_{PL} (λ_{II} *ex*) and Φ_{PL} (λ_{II} *ex*) are the photoluminescence quantum yields for excitations at the transition II and III respectively. <τ> is the first temporal moment of the transient decay. *n* ($\lambda_{PL\ max}$) is the refractive index measured at $\lambda_{PL\ max}$.

Material	T4BT-A	T4BT-B	T4BT-C	T4BT-D	T4BT-E
λ_{II} (nm)	364	357	358	372	376
α_{II} ($\times 10^5$ cm^{-1})	1.8	2	1.9	1.9	2.4
S_{II} ($\times 10^4$ eV·cm^{-1})	7.7	7.3	7.8	8.0	11.1
λ_{III} (nm)	445	440	440	444	_
α_{III} ($\times 10^5$ cm^{-1})	0.7	0.8	0.8	0.7	_
S_{III} ($\times 10^4$ eV·cm^{-1})	2.4	3.2	3.0	1.9	_
$\lambda_{PL\ max}$ (nm)	553	561	562	546	507
Φ_{PL} (λ_{II} *ex*) (%)	43 ± 4	39 ± 2	41 ± 3	41 ± 4	27 ± 4
Φ_{PL} (λ_{III} *ex*) (%)	54 ± 7	53 ± 6	55 ± 7	52 ± 6	_
<τ> (ns)	3.45	3.58	3.62	3.99	3.34
n ($\lambda_{PL\ max}$)	1.753	1.747	1.746	1.762	1.785

The pair-wise relationship can also be observed in the emission properties, but the similarities are not as obvious as in the absorption. Compounds **T4BT-A** to **–D** show emission spectra similar to **F8BT** (one broad featureless band with maximum at 569 nm). The **T4BT-A** and **T4BT-D** pair has a shorter emission wavelength at 553 nm and 546 nm respectively and presents a featureless band. The **T4BT-B** and **T4BT-C** pair has the most red-shifted emission of the whole family (562 nm) and also shows a hint of a blue shifted shoulder. **T4BT-E** has a significantly

blue shifted emission (507 nm) compared with the rest of the members of the family but, unlike the structured emission of **T4** (417 nm), the emission band of **T4BT-E** is featureless. In all cases the emission comes solely from the BT unit and no fluorene fluorescence can be observed.

The greater Stokes shift observed between the absorption and emission spectra of the **T4BT-A** to **-D** compounds compared with **T4** is a consequence of the energy transfer in the donor-acceptor system with an extra BT acceptor unit. In the case of **T4BT-E**, it might be due to a significant structural relaxation after the compounds are excited at the wavelength of transition II.

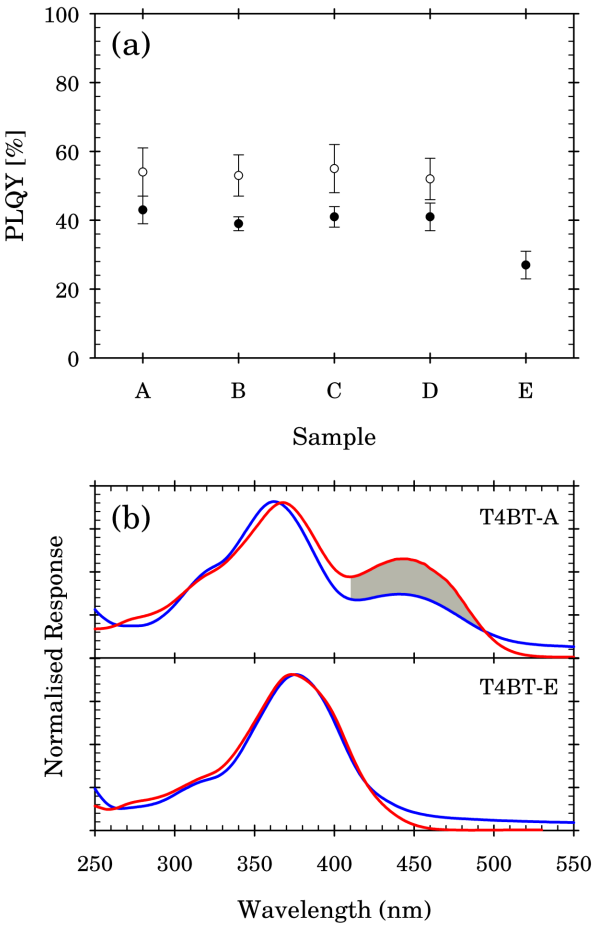

Figure 3-3 a) PLQY values for the **T4BT-X** family under excitation at the wavelengths of features (II) (filled circles) and (III) (empty circles). (b) Photoluminescence excitation (PLE) spectra (red lines for **T4BT-A** (600 nm PL detection) and **T4BT-E** (550 nm PL detection) are shown. The corresponding absorption spectra normalised at the peak of transition II (blue lines) are shown for comparison. The shaded area in the spectrum of **T4BT-A** highlights the increase in the PLE compared with the absorption spectrum.

The PLQY of compounds **T4BT-A** to **–D** is very similar despite the slight differences in the emission profiles of the materials. Nevertheless, as observed in **Figure 3-3** (a), when the materials are excited at the wavelength of the transition III, a higher efficiency is obtained compared to when the material is pumped at the wavelength of the transition II ($\Phi = 0.55 \pm 0.07$ versus $\Phi = 0.40 \pm 0.04$). This effect is also observed for **F8BT**.[171] **Figure 3-3** (b) shows the enhancement of the photoluminescence excitation spectrum compared with the absorption spectrum when **T4BT-A** is excited in the region of transition III (the spectra are normalised at the wavelength corresponding with transition II). The increased intensity of the long wavelength band in the excitation spectrum compared with the absorption one is an indication that the photoluminescence is obtained predominantly from the lower energy region of the spectrum, in this case from the BT.[171] The lower PL efficiency obtained for **T4BT-A** to **–D** when exciting at the wavelength of the π-π^* of fluorenes is a consequence of the energy transfer that the molecules undergo in order to emit from the BT moiety. In the case of **T4BT-E**, on the other hand, it could be derived from the charge transfer character of the transition.

T4BT-E presents a significantly smaller PLQY than the other members of the series ($\Phi = 0.27 \pm 0.04$) and its PL excitation and absorption spectra match almost perfectly (**Figure 3-3**). It should also be noted that the long tail in the absorption spectrum disappears in the PL excitation spectrum. This might be an indication that it is not due to real absorption, but to scattering and/or reflection, because excitation at that wavelength does not generate any photoluminescence. This is further confirmation that transition III is either not present in **T4BT-E**, very weak or so blue shifted that is embedded in the broad transition II and it cannot be observed.

Photoluminescence decay was studied by measuring the transients of 50 nm thick films of the **T4BT-X** members after applying 1 MHz, 70 ps excitation pulse at 405 nm. The transients of **T4BT-A** to **T4BT-D** follow a mono-exponential decay allowing a numerical convolution approach to obtain the excited lifetime of the materials. Despite **T4BT-E** not showing a truly mono-exponential decay, the same procedure to obtain the decay times was applied. Other fitting procedures, including the statistical first moment measure, revealed the same trend with small variations in the absolute values (8% or less).

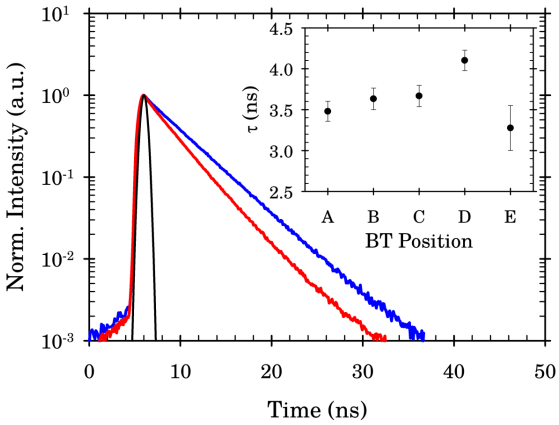

Figure 3-4 PL decay transients for **T4BT-D** (blue line) and **T4BT-E** (red line) under 405 nm pulsed excitation (70 ps, 1MHz laser diode excitation). Inset: Lifetimes for **T4BT-A** to **-E**, extracted using a convolution of a mono-exponential fit with the instrument response function (shown by a black line in the main figure).

As shown in Figure 3-4 and Table 3-1, **T4BT-A** to **–E** show longer lifetimes than **T4** (τ = 0.6 ns)[151] and **F8BT** (τ = 2 ns).[172] This is explained by the reduced oscillator strength of the longest absorption wavelength (feature III) as compared with the reference materials. The pair **T4BT-B** and **T4BT-C** have very similar decay times ($\tau \approx 3.6$ ns) but the pair **T4BT-A** and **T4BT-D** show a very different trend. **T4BT-D** has a ≈ 18 % longer lived species ($\tau \approx 4$ ns) than **T4BT-A** ($\tau \approx 3.4$ ns). This is consistent with the calculated lowest oscillator strength for transition III for **T4BT-D** compared with the rest, but it does not account for the magnitude of the increase in PL decay time. Further investigation recording the transients of each compound after exciting it at its particular wavelength for transitions II and III would be required in order to obtain a better understanding of the behaviour.

T4BT-E presents the fastest decay ($\tau \approx 3.3$ ns). The large Stokes-shift between absorption and emission, the lack of vibrational structure in the PL spectrum and the TD-DFT calculations (see next section) suggest that the emission has charge transfer character and involves a significant geometry relaxation after excitation. This explains why the material has a longer decay time than **T4**, despite having a much smaller PLQY ($\Phi_{PL} \approx 0.27$ for **T4BT-E** *versus* 0.43 for **T4**).

In all the other members of the series the variation of the PL decay is small in relation to the magnitude of their PLQY. This indicates that despite the τ of **T4BT-E** being the shortest of the whole family, the fact that it has a significantly lower PLQY might indicate that it would actually have the longest radiative lifetime of the whole series. This explanation is consistent with a

significant charge transfer character[172] and implies the presence of non-radiative decay processes, which might have induced the non-mono-exponential decay (Figure 3-4).

3.3.3 TD-DFT calculations

The electronic structures of molecules containing 9,9-dialkylfluorene covalently bonded to BT have been previously modelled[170] and two main optical transitions originating in the HOMO have been described. The first type involves a transition from the HOMO to a spatially localised LUMO (feature III) and it is considered to present a degree of charge transfer character. The second type (feature II) is a transition between the HOMO to higher lying delocalised unoccupied molecular orbitals.[170]

The geometry of the **T4BT-X** family was initially subjected to ground state geometry optimisation of the simplified structures (with H in the 9,9-positions instead of hexyl chains). The electronic structure of the molecular orbitals was calculated employing a Natural Transition Orbital (NTO)[173] representation. An occupied NTO represents a state in which an electron is excited for a certain transition and a virtual NTO is the empty state to which the electron is promoted. The absorption transition intensities were calculated between 320 nm and 520 nm and are represented in Figure 3-2 as filled dots. The predicted transitions match the experimental bands that are observed in features II and III reasonably well (they are red shifted 12-17 nm for transition II and 63-78 nm for transition III). The larger deviations obtained for the longest wavelength transition can be explained by the limitations of the chosen theoretical approach to explain the charge transfer state energies.[174]

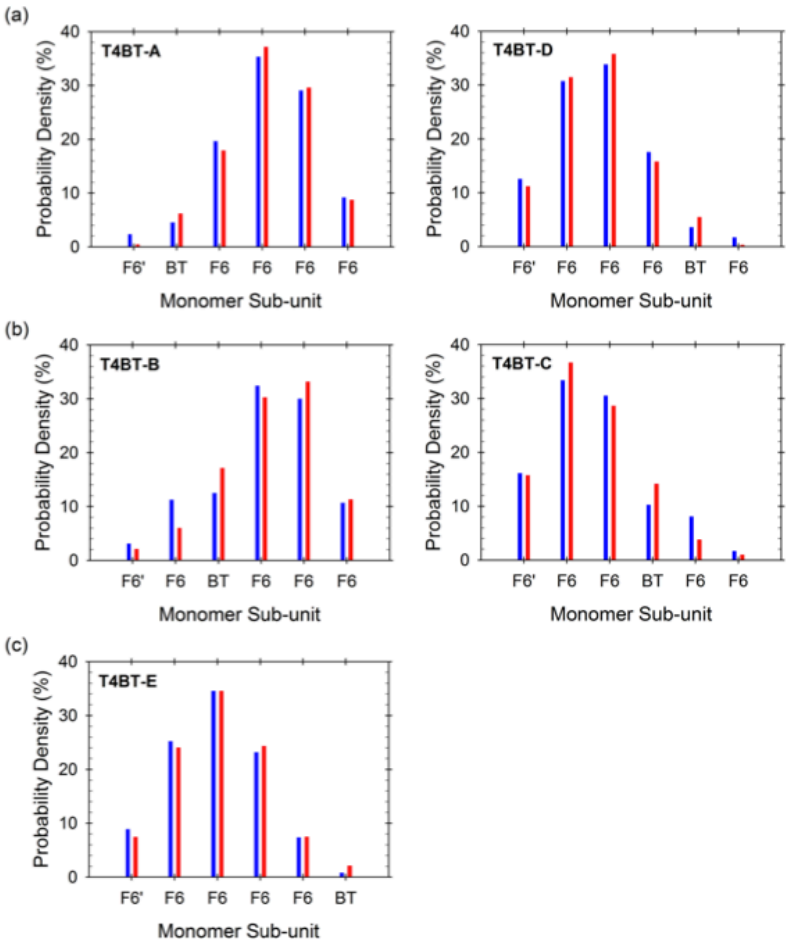

Figure 3-5 TD-DFT calculated probability density distributions for the occupied (blue bars) and unoccupied (red bars) NTOs associated with transition II for the **T4BT-X** family. (a) **T4BT-A** and **–D** pair; (b) **T4BT-B** and **–C pair**; (c) **T4BT-E**. Due to unavailability of the original data while writing this thesis, the poor quality of the image arises from copying it from the original publication**.**

The molecular orbitals involved in the transition occurring in the region II are delocalised along the fluorene arm (see Figure 3-5), as previously calculated for **F8BT**.[156] The transition occurring at longer wavelength (feature III) involves a HOMO delocalised along the oligofluorene arm to a LUMO that is spatially localised on the BT (Figure 3-6). In both figures the bar charts are plotted in relation to each monomer unit within the oligofluorene-BT chain in the **T4BT-X** series, starting on the left with the fluorene unit embedded in the truxene core (F6'). From these charts the pair-wise association can be clearly observed, as well as the relative strengths of the overlaps between occupied and unoccupied molecular orbitals being the strongest for the pair **T4BT-B** and **T4BT-C** and weakest for **T4BT-E**.

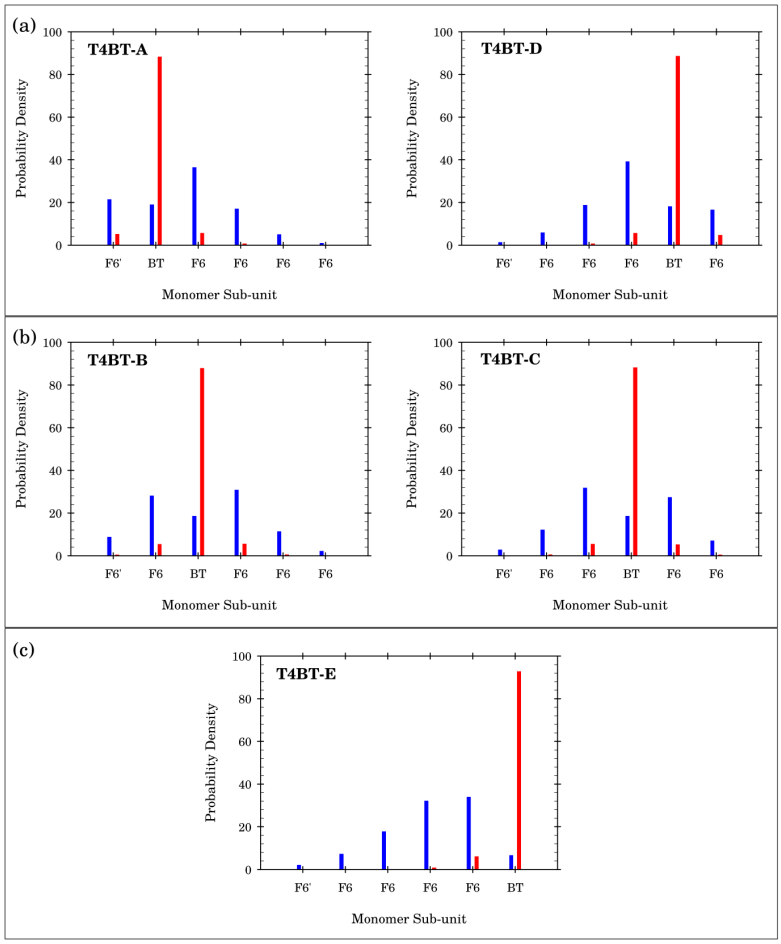

Figure 3-6 TD-DFT calculated probability density distributions for the occupied (blue bars) and unoccupied (red bars) NTOs associated with transition III for the **T4BT-X** family. (a) **T4BT-A** and **–D** pair; (b) **T4BT-B** and **–C** pair; (c) **T4BT-E**.

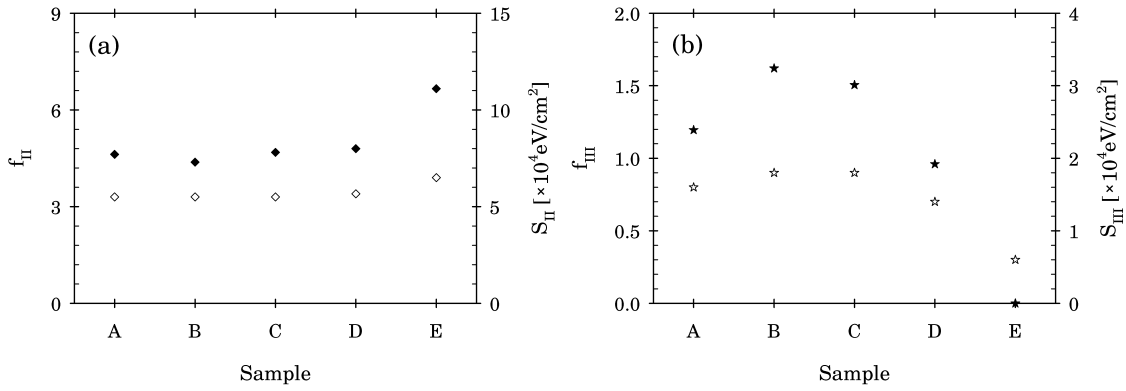

Figure 3-7 Comparison between oscillator strength as calculated by DFT (f, open symbols) and the experimentally determined absorption integral (S, filled symbols) for transition II (a) and transition III panel (b).

The calculated oscillator strengths of the **T4BT-X** family for transitions II and III are presented in **Figure 3-7** in comparison with the experimental absorption integrals. The lower energy of

transition II for **T4BT-E** as well as the increase in its oscillator strength for this transition in comparison with the rest of the members of the family are predicted by the TD-DFT calculations (see **Figure 3-7**). Furthermore, transition III is also predicted but its oscillator strength is significantly reduced in relation to **T4BT-A** to **–D** and the predicted separation between transitions II and III is smaller (see Figure 3-2). An explanation for this reduction in the oscillator strength is the small overlap between the occupied and unoccupied orbitals located in the BT unit. The LUMO is located at the BT, but the probability density distribution for the occupied NTO on the BT is significantly smaller than for the rest of the members of the series. On the other hand, the weaker oscillator strength of **T4BT-E** would predict a longer radiative decay as opposed to the experimental results. This might be explained by additional non-radiative pathways for the decay of the exited state of **T4BT-E**, which could contribute greatly to the short overall lifetime and to make the decay non-monoexponential.

3.3.4 Electrochemistry

The cyclic voltammetry study of the series in dichloromethane solution (Table 3-2) reveals that the HOMO-levels are in the range of 5.4 - 5.6 eV. The highest HOMO-levels are observed for the compounds that do not present resolved ICT features (**T4BT-E** and **T4BT-D**). Charge transfer leads to a deepening of the HOMO level (**T4BT-A**, **T4BT-B** and **T4BT-C**). The deepest HOMO level (compound **T4BT-C**) is a consequence of both the ICT effect and the fact that this compound has the shortest conjugation length of oligofluorene donor units. The LUMO levels are quite stable between 2.95 eV and 3.08 eV.

Compounds **T4BT-A**, **T4BT-B** and **T4BT-C** and **T4BT-D** exhibit a good agreement between their electrochemical and optical HOMO-LUMO gaps. However, a difference of 0.48 eV is observed between the optical and electrochemical HOMO-LUMO gap for the compound **T4BT-E**. This large difference might be attributed to the poor conjugation between donor and acceptor units which is revealed by DFT/TD-DFT calculations as a poor overlap between the HOMO (occupied NTO) and LUMO (non-occupied NTO).

Table 3-2 Electrochemical properties of the truxene-oligofluorene-BT series. [a] HOMO and LUMO levels were calculated from the onset of the corresponding redox wave and are referenced to ferrocene, which has a HOMO of -4.8 eV. [b] The electrochemical HOMO-LUMO gap ($E_{g, CV}$) is the energy gap between the HOMO and LUMO levels. The optical HOMO-LUMO gap ($E_{g, opt}$) is calculated from the onset of the red-edge of the absorption band (in brackets).

Material	E_{ox} vs Fc/Fc^+ (V)	HOMO[a] (eV)	E_{red} vs Fc/Fc^+ (V)	LUMO[a] (eV)	$E_{g, CV}$[b] (eV)	$E_{g, UV}$[b] (eV)
T4BT-A	0.86, 1.0	-5.56	-1.93	-3.02	2.54	2.53 (490)
T4BT-B	0.88, 0.99, 1.14	-5.56	-1.90	-3.07	2.49	2.53 (491)
T4BT-C	1.01	-5.62	-1.83	-3.08	2.54	2.55 (486)
T4BT-D	0.77, 0.91	-5.45	-1.96	-2.95	2.50	2.59 (478)
T4BT-E	0.75, 0.86	-5.43	-1.98	-2.95	2.48	2.96 (419)

3.3.5 Amplified Spontaneous Emission

Amplified spontaneous emission studies were performed on thin films of the **T4BT-X** series. The samples were pumped systematically with an increased incident energy, causing the broad PL spectrum to collapse to a line-narrowed peak. The reference materials **T4** and **F8BT** have previously been reported to provide optical gain (i.e., show efficient ASE).[47, 160]

The representative results for **T4BT-B** are shown in Figure 3-8. The ASE spectrum appeared at a slightly higher energy than for **F8BT** (561 nm *versus* 575 nm).[160] In the inset of Figure 3-8 it can be observed that the onset before the line becomes a plateau coincides with the pumping energy that triggered the ASE narrowing of the PL spectrum. This is the ASE threshold and it corresponds to ≈ 60 $\mu J \cdot cm^{-2}$. The typical ASE onset for **F8BT** is ≈ 40 $\mu J \cdot cm^{-2}$. **T4BT-A** to **–D** provided similar results but **T4BT-E** did not show any evidence of ASE narrowing for incident pump energies up to 500 $\mu J \cdot cm^{-2}$, the limit of the pump system. Blends of of regioregular

poly(3-hexylthiophene) with **F8BT** (20:80 wt %) present a similar PLQY to **T4BT-E** (Φ_{PL} ≈ 25 %) but show efficient ASE and lasing.[175]

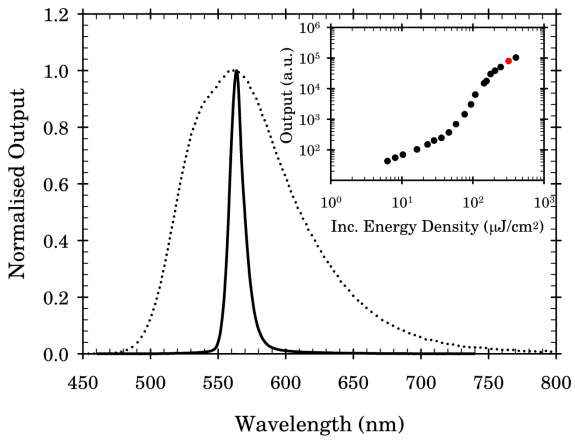

Figure 3-8 Normalised amplified spontaneous emission spectrum (solid line) and normalised PL spectrum (dotted line) of a **T4BT-B** film (120 ± 10 nm) at an incident pump energy density of 320 μJ·cm^{-2}. The inset shows the dependence of the amplified spontaneous emission as a function of the incident pump energy density plotted in black dots; The red dot highlights that pumping at 320 μJ·cm^{-2} triggers a gain narrowed spectrum.

According to Kasha's rule, the PL spectra show the emission that occurs after the relaxation of the excited state and, as long as the relaxation processes occur quick enough not to overlap with the radiative decay, they generally do not need to be taken into consideration.[176] The radiative decay time is much shorter in ASE and lasing due to emission stimulation and the structural relaxation might contribute greatly to non-radiative processes. In this case non-radiative relaxation of the excited state can compete with emission and this might be the cause for the lack of ASE in **T4BT-E**, that presents a significant relaxation of the excited state as explained in the sub-chapter 3.3.2.

3.4 Conclusion

In conclusion, a series of tris(oligofluorene-BT)truxene isomers was synthesised (**T4BT-X** family) to study the effect of the introduction of a strong acceptor unit within every single position of the quaterfluorene chain in a star shaped **T4** molecule. The BT unit was initially introduced directly attached to the truxene core (**T4BT-A**) and it was moved outwards along the chain to synthesise **T4BT-B**, **-C**, **-D** and **–E**, where the BT moiety endcaps the

quaterfluorene arm. The compounds are efficient green emitters with good solubility in most common organic solvents, good thermal stability and excellent film forming properties.

The properties of the molecules were studied by UV-Vis absorption and emission spectroscopy, electrochemistry, PL decay and ASE. Regarding the symmetry and the optical properties of these compounds, a pair-wise association can be observed between (i) **T4BT-A** and **T4BT-D** and (ii) **T4BT-B** and **T4BT-C**. **T4BT-E** is the only member of the series that possesses the BT unit in a terminal position and this difference in its structure is the reason for its different properties in comparison with the rest of the family. Therefore, there are three main *locations* in which the BT can be introduced within the arms of a **T4**. The radiative lifetimes of the series cannot be explained in terms of the three locations because **T4BT-A** and **T4BT-D** no longer behave as a pair (**T4BT-D** is has the slowest PL decay of the whole series, while **T4BT-A** is the second shortest lived species) and **T4BT-E** presents the fastest decay, against the theoretical predictions. DFT/TD-DFT modelling was also performed on the proxy structures of the **T4BT-X** family, providing calculated values that back up the experimental results in most cases, except for the raditiative lifetime of **T4BT-E**, probably due to non-radiative losses that are not taken into account in the theoretical calculations.

The precise structural design and synthetic reproducibility of these monodisperse star-shaped compounds offer an advantage over fluorene-BT copolymers because the structure-property relationship can be accurately studied. The influence of the location of the BT unit along the chain on the properties of the material is not averaged over a range of slightly different chemical structures. Furthermore, the study of this series of compounds isolates the role of the location of the BT from other factors like interchain interactions because these star shaped materials are completely amorphous and they are distributed randomly within the bulk.

4 Linear and star-shaped oligofluorene DPPs

4.1 Abstract

Following previous work developed in the Skabara group,[138] three new oligofluorene DPP molecules (**Star** and **Linear-c DPP** with octyl chains and **Linear-c DPP MOD** with hexyl chains) were synthesised in order to further study the aggregation effects observed in the hexyl analogues. The increase in the length of the solubilising alkyl chain did not solve the problem, but this study confirmed the hypothetical aggregation mechanism proposed in the original publication. Furthermore, it provided greater understanding of the photophysics of these compounds, concluding that the best excitation pathway of **Linear-c DPP** for lasing applications is through the DPP absorption band, in order to avoid energy losses associated with the charge transfer from the oligofluorenes to the DPP core.

4.2 Introduction

1,4-Diketo-3,6-diphenyl-pyrrolopyrrole (DPP) is a well known electron deficient moiety initially reported by Farnum and coworkers in 1974 as a by-product in a failed attempt to synthesise azetinone.[177] Investigations by the Ciba-Geigy company modified the structure of the DPP moiety by attaching substituents at the *meta*- and *para*-positions of the phenyl rings, leading to a wide variety of bright coloured pigments with excellent durability and resistance to light, weather, heat and chemicals, that were used in a variety of industrial applications.[178] DPP is a high electron-affinity compound (derived from its lactam units) and tends to form intermolecular hydrogen bonds between the lactams and π-π stacking through the aryl rings, resulting in poor solubility in organic solvents.[179] The addition of solubilising groups to the molecules enabled the leap to a wide variety of applications such as organic field effect transistors (OFETs),[180] organic photovoltaics (OPVs),[181] organic light emitting diodes (OLEDs),[182] sensors or microporous networks.[183] The increased solubility can be achieved by *N*-alkylation, arylation or acylation of the lactams to prevent the formation of hydrogen bonds.[179]

DPP cores have been widely employed in copolymers. The most commonly used chromophores have phenyl rings or thiophenes at the 3,6-positions of the DPP cores (Figure 4-1 a and b respectively), but lately there have been reports of the use of furan,[184] thienothiophene,[185] selenophene[186] and thiazole[187] in those positions (Figure 4-1 c, d, e and f). The side aryl substituent can influence the HOMO and LUMO levels of the whole molecule, as well as the conjugation pattern.[181]

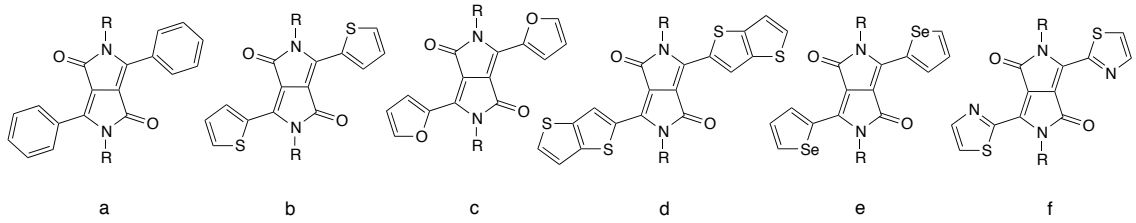

Figure 4-1 DPP chromophores employing the following aryl-substituents in the 3,6-positions: a) phenyl; b) thiophene; c) furan; d) thienothiophene; e) selenophene; f) thiazole. R represents alkyl, acyl or aryl substituents.

DPP chromophores can be introduced to conjugated polymers by attaching polymerisable groups (such as halogens, aldehydes or hydroxyl groups) onto the aryl substituents on the 3,6-positions or on the lactams (2,5-positions, see Figure 4-3).[179] The first copolymer containing the *N*-alkylated 1,4-diketo-3,6-diphenyl-pyrrolopyrrole (DPP) was synthesised by Stille cross-coupling and was reported in 1993 by Yu and coworkers for photorefractive applications.[188] Since then, several conjugated moieties such as *p*-phenylenevinylene, fluorene, anthracene, benzothiadiazole, carbazole or triarylamine have been introduced to the *para*-position of the phenyl ring of the DPP chromophore *via* Suzuki cross-coupling (see Figure 4-2 a-f). These yellow to red fluorescent polymers have PLQYs of up to 0.86 and their absorption and emission characteristics present large bathochromic shifts when compared to the monomers because of the increase in the conjugation length.[189] Other aromatic units such as thiophene or ethylenedioxythiophene (EDOT) (Figure 4-2 g and h) have also been introduced *via* Stille cross couplings.[190] The replacement of the phenyl rings on the DPP core by thienyl groups has led to a series of monomers and polymers with red-shifted absorptions and emissions, with low bandgaps and high carrier mobility properties,[179] making them suitable for OFET applications.[180] The thienyl- and bithienyl-DPP monomers have also been copolymerised with other aromatic moieties such as thiophene, fluorene, carbazole, dithienopyrrole or dibenzosilole (Figure 4-2 g, b, e, I and h).[179]

Tieke and co-workers published a very comprehensive review in 2010 detailing the role of DPP in multiple conjugated polymers.[179] In this review it can be observed that in recent years the polymerisation techniques have become more varied, including Stille, Suzuki, Heck, Buchwald Hartwig or Sonogashira protocols.[179] More recently Nielsen, Turbiez and McCulloch published and interesting review on the development of DPP containing conjugated polymers for use in OFETs.[180] Chandran and Lee have also written a review on the use of DPP for organic solar cells.[181]

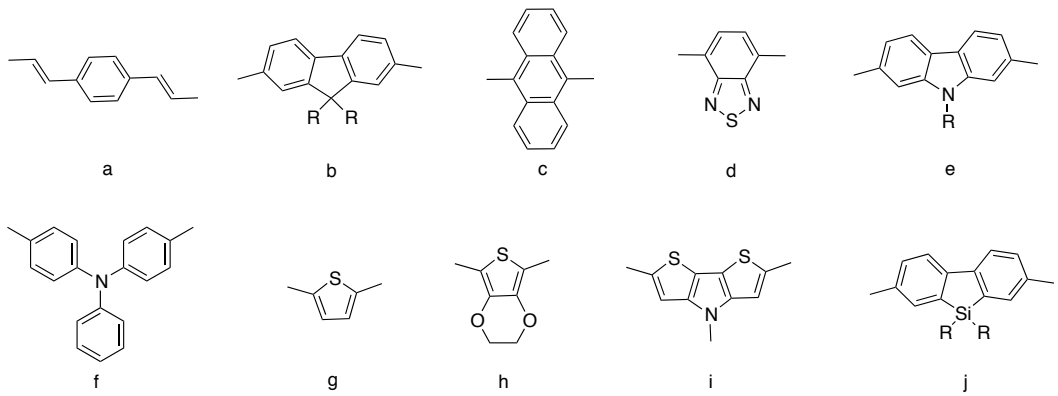

Figure 4-2 Some aryl groups copolymerised with DPP in semiconducting polymers. a) Phenylenevinylene, b) fluorene, c) athracene, d) benzothiadiazole, e) carbazole, f) triphenylamine, g) thiophene, h) ethylenedioxythiophene, i) dithienopyrrole, j) diphenylsilole.

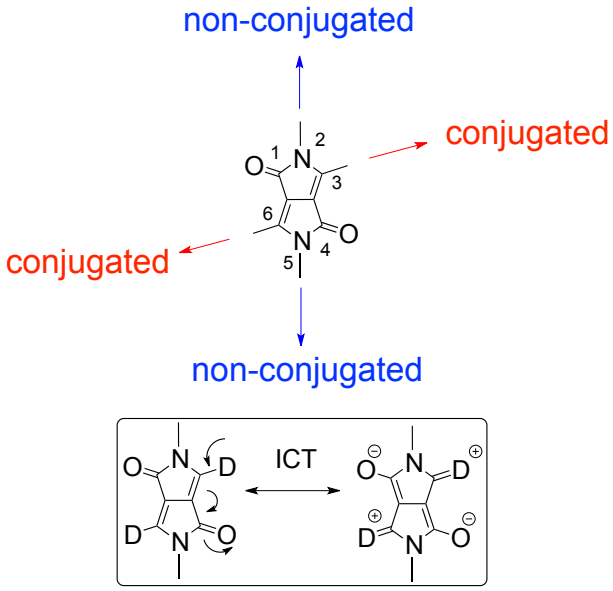

Figure 4-3 Conjugation pattern through the DPP core. The inset depicts the intramolecular charge transfer (ICT) character of the bonds between a donor (D) and the DPP core in the 3,6-positions.

Zhang and Tieke where the first to report *N*-arylated DPPs as monomers. They studied the effect of the Suzuki polymerisation of DPP at the 2,5- lactam position and compared it to polymerisation at the 3,6-positions (Figure 4-3).[191] They prepared fluorene-DPP and fluorene-2,5-di-hexyloxyphenylene-DPP copolymers and found that although polymerisation at the 3,6-positions led to conjugated polymers with bathochromic shifts in their optical properties, polymerisation through the 2,5-positions provided polymers with similar optical properties to the corresponding monomers. This was due to the breakage of conjugation at the lactam units in the DPP chromophore. Cao and coworkers also studied the effect of polymerisation location in 3,6-diphenyl-DPP:fluorene copolymers in which the polymerisable functional groups in the

DPP where located in the *meta* and the *para* positions of the phenylene rings of the DPP.[192] The *meta*-conjugated polymer had well defined optical features attributable to the separate monomers and thermal properties characteristic of a more flexible backbone, whereas the *para*-conjugated polymer presented a broader and more continuous absorption, with the position of the DPP absorption transition red shifted with respect to the monomer. Furthermore, preliminary electroluminescence studies proved that the *para*-conjugated polymer was a promising material for polymer light emitting diodes (PLEDs), while the *meta*-conjugated polymer presented poor behaviour. The more linear structure of the polymer containing *p*-phenylene rings leads to a greater degree of conjugation than for the polymer with *m*-phenylene rings, which explains its physical and optical properties.

In recent years there has been an increased number of reports of small molecules containing DPP moieties, especially for OPV applications, since the ease of synthesis, the well-defined structure and the inherent high purity of these molecules can lead to high charge carrier mobilities and avoid differences between batches.[181] Ngoyen and coworkers reported the synthesis of a series of small molecules containing a DPP core and two oligothiophene arms (with one to three thiophene units) on the 3,6-positions of the DPP and hexyl or dodecyl chains on the lactam nitogens.[193] They then synthesised an analogous molecule with terthiophene arms bearing hexyl chains at the 5-position of the terminal thiophene, and thus developed the first DPP-based small molecule OFET.[194] They also reported the synthesis of an analogous molecule with *t*-Boc solubilising chains for its use in bulk heterojunction (BHJ) OPVs with power conversion efficiencies of up to 2.33 %.[195] Another analogue with ethylhexyl solubilising alkyl chains on the 2,5-positions possessed higher thermal stability and better film forming properties than the *t*-Boc analogue, yielding a BHJ device with 3 % power conversion efficiency (Figure 4-4 a).[196] Their 3,6-dithienoDPP with benzofuran moieties attached to the thiophenes led to the fabrication of a very high efficiency BHJ solar cell (4 % power conversion efficiency).[197]

Other groups have also investigated the potential of DPP-based small molecules in organic photovoltaics. Izawa and co-workers reported the synthesis and characterisation of DPP-terthiophene small molecules bearing C_{70} fullerenes at the end of their N-solubilising alkyl chains.[198] Yao's group developed an acceptor-donor-acceptor system with a benzodithiophene core terminated by two 3,6-dithienoDPP units. The use of this molecule in organic solar cells led to a 5.29 % power conversion efficiency (PCE), the highest PCE reported to date for a

solution-processable DPP containing material (Figure 4-4 b).[199] The same group synthesised a series of star-shaped triphenylamine-cored small molecules terminated with 3,6-dithienoDPP directly attached or coupled to a bridging thiophene unit (Figure 4-4 c). Both molecules undergo intramolecular charge transfer (ICT) from the triphenylamine to the DPP but the extra thiophene in the second molecule increases the extinction coefficient of the molecule, triggers a red shift in the absorption profile, reduces the bandgap of the molecule and improves the power conversion efficiency in BHJ solar cells.[200]

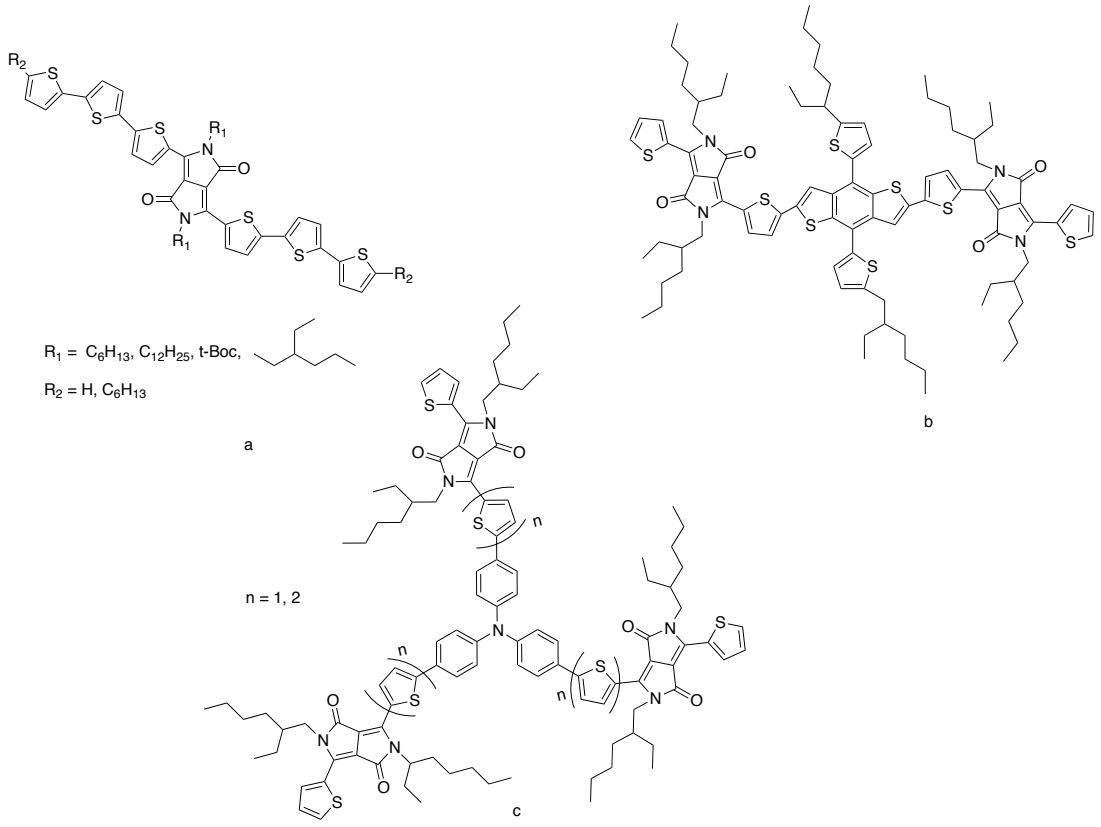

Figure 4-4 Structures of some DPP-based small molecules employed in organic solar cells.

Kanibolotsky and co-workers described the synthesis of monodisperse linear and star-shaped oligofluorenes with a 3,6-diphenylDPP core in the first report of a DPP-containing macromolecular single molecule.[138] The largest molecule of the family is the **Star DPP** (Figure 4-5 a) that contains a 2,3,5,6-tetraphenylDPP core terminated with four 9,9-dihexylquaterfluorene arms. As discussed before, the arms located in the 3,6-positions are conjugated through the core but the arms in the 2,5-positions act independently because the conjugation is disrupted at the lactam nitrogen. Additionaly, two linear DPP analogues were reported, a conjugated version (**Linear-c DPP**, Figure 4-5 b), with the oligofluorene arms at the

3,6-position and hexyldecyl solubilising alkyl chains at the nitrogens, and a non-conjugated compound (**Linear-nc DPP**, Figure 4-5 c) in which the oligofluorene arms were attached to a phenylene ring on the nitrogen and phenyl rings at the 3,6- conjugated positions.

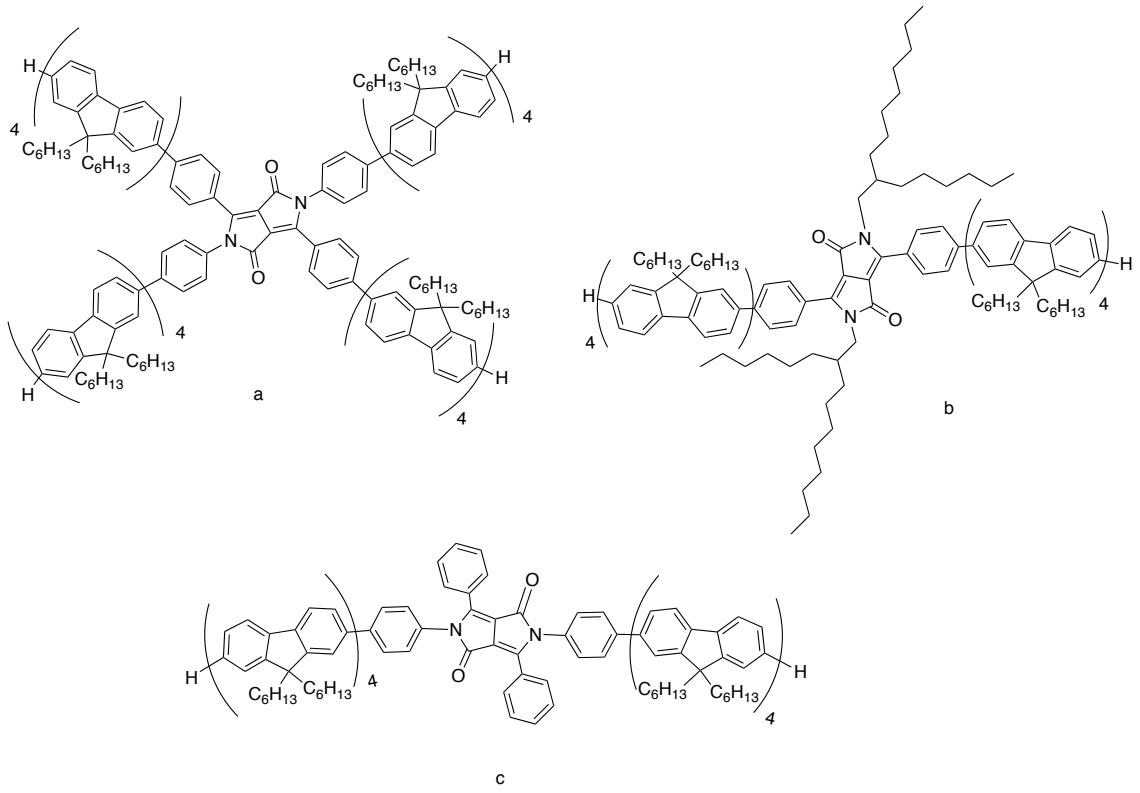

Figure 4-5 Oligofluorene DPP systems. a) **Star DPP,** b) **Linear-c DPP**, c) **Linear-nc DPP.**

Star and **Linear-nc DPP** were amorphous materials, whereas **Linear-c DPP** presented crystalline character with a well-defined melting point and two crystallisation points. All the compounds presented broad absorption spectra, with a band associated to the absorption of the oligofluorene arms around 368 nm and a lower energy band related to the absorption of the DPP core. The position of the latter band varied in the three compounds because of the different conjugation patterns through the core (Figure 4-3).[138]

Concentration dependence studies of the molecules in non-polar hexane solutions followed the Lambert-Beer law for the linear derivatives, whereas **Star DPP** deviated from linearity at higher concentrations. The authors postulated that this behaviour was due to aggregation of the molecules in concentrated solutions and a change in the conformation around the DPP core. In the ground state the phenyl rings at the 3,6-positions remain planar and in the aggregated state they adopt a propeller-like conformation in which all four phenyl rings are

twisted equally. Furthermore, the hydrophobic interactions between the solubilising alkyl chains hinder the longitudinal displacement of adjacent **Star-DPP** molecules, assisting aggregation in hexane.[138] The authors proposed that the crystallinity of **Linear-c** and its lack of aggregation in solution would be a result of quadrupole-quadrupole interactions in the condensed phase, which lead to 1D alignment of the quadrupoles in one direction (Figure 4-6 a). **Star DPP** would also present quadrupole-quadrupole interactions but in this case in two dimensions because the phenylene rings located in the 2,5-positions are electron rich and the ones in the 3,6-positions are electron deficient, leading to alignment of the quadrupole ellipsoids in one plane but in two directions. As observed in Figure 4-6 b, the electron-rich quadrupole of the 2,5-position (represented in blue) aligns with the electron deficient one (3,6-positions, represented in red) of the adjacent molecule, reducing the ICT character. Figure 4-6 c represents a molecular model of two aggregated **Star DPP** molecules. **Linear-nc DPP** presents a similar pattern as **Star DPP** in the condensed state due to the 2D aggregation, but to a lesser extent, because the initial lower ICT character of this band and the linear shape of the molecule do not allow such strong interactions as in **Star DPP**.

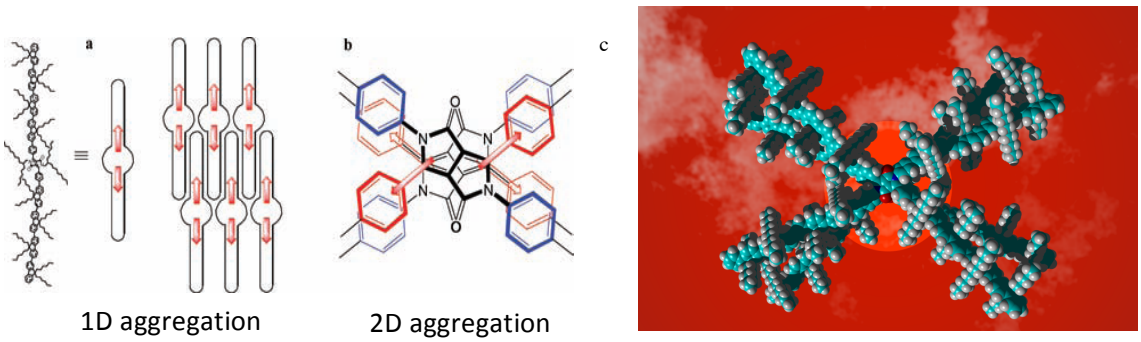

Figure 4-6 Schematic representation of a) 1D and b) 2D interactions between molecules in DPP aggregates. c) Molecular modelling representation of two **Star DPP** molecules aggregated. Figure presented with permission of the original authors.[138]

The emission properties of the three compounds also have ICT character with emission maxima bathochromically shifted from the emission of the core. Interestingly, only **Linear-c DPP** showed ASE narrowing of the emission (λ_{ASE} = 627 nm) and the threshold obtained when pumping at the ICT band was much lower than when the oligofluorene band was used as the excitation wavelength (42 $\mu J \cdot cm^{-2}$ vs 106 $\mu J \cdot cm^{-2}$) because energy lossess during the energy transfer from the oligofluorenes to the DPP were avoided. Despite the large absorption cross-section provided by the four oligofluorene arms and the 2D shape of **Star DPP** suggesting good lasing behaviour, its propensity to aggregate led to a lack of ASE. Avoiding aggregation would

allow the chromophores to emit light more efficiently and therefore improve their lasing capabilities. Blends of light emitting materials with UV-transparent photoresists have proven to prevent aggregation of materials and increase the stability of the devices compared to the naked materials.[110, 112]

Following the study on the length of the alkyl chains of star-shaped oligofluorene truxenes, a new series of oligofluorene-DPPs with octyl solubilising alkyl chains were synthesised. As discussed in Chapter 0, the increase of the length of the alkyl chain by only two carbons has a deep impact on the morphology of the films, providing a greater distance between chromophores. The goal of the study was to try to avoid the aggregation observed in the DPP materials and improve the lasing properties of the family. The DPP analogues where the oligofluorene arms are conjugated through the core have the most promising optical properties for lasing applications and therefore only the **Star DPP** and **Linear-c DPP** analogues with octyl chains where synthesised (Figure 4-7 a and b respectively). For comparison, a new linear conjugated compound with a phenyl ring as solubilising agent in the 2,5-positions (**Linear-c DPP MOD**, Figure 4-7 c, isomer of **Linear-nc**) was synthesised.

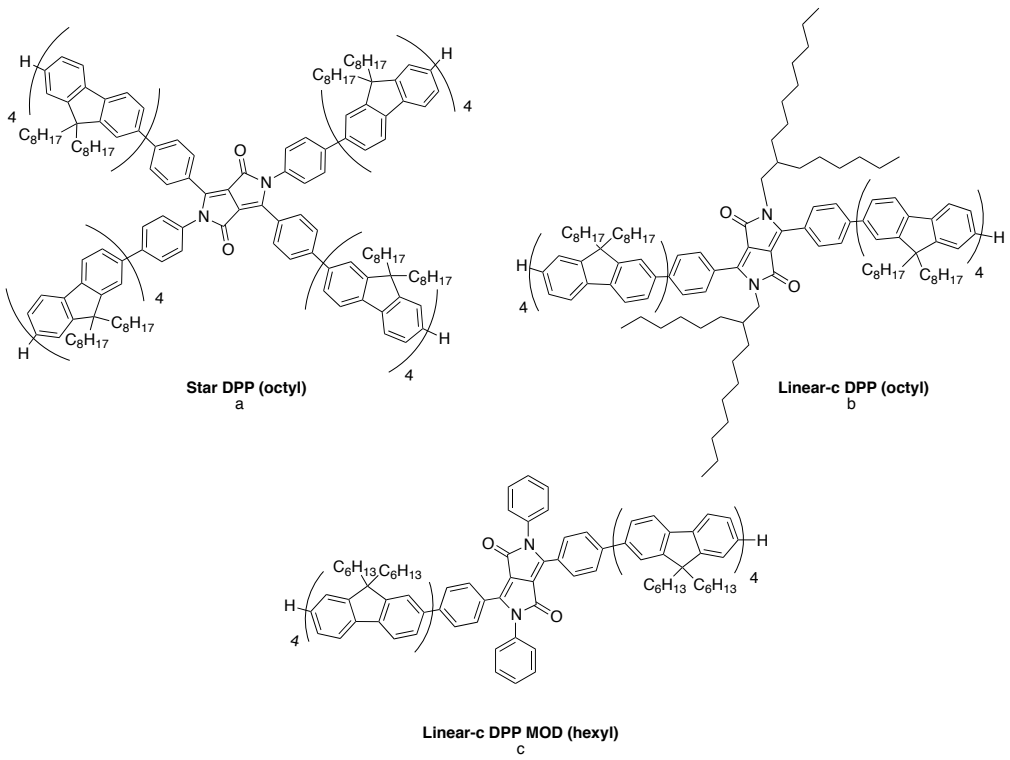

Figure 4-7 Structures of the new oligofluorene DPP compounds synthesised. a) **Star DPP (octyl)**, b) **Linear-c DPP (octyl)**, c) **Linear-c DPP MOD (hexyl).**

4.3 Results and discussion

4.3.1 Synthesis

The synthesis of the cores for the oligofluorene DPP molecules is depicted in Scheme 4-1. The synthesis of the 2,3,5,6-tetraphenylDPP cores (**DPPBr$_4$** and **DPPBr$_2$-c MOD**) involved the condensation of *p*-bromoacetophenone (**4.1**) with diethylcarbonate to yield compound **4.2** in a moderate yield. The batch of **4.2** was split into two, one of which was brominated and the other was deprotonated with sodium hydride. Both modified batches were then reacted together to obtain the dimer **4.3** by nucleophilic substitution in 68 % yield. Compound **4.3** was heated to 300 °C under vacuum and the molten tar was allowed to cool down to 220 °C and heated to 300 °C to form the diketofurofuran **BrDFF** in low yield (33 %). The final step consisted of the condensation of the dilactones of **BrDFF** with primary amines (bromoaniline for **DPPBr$_4$** and aniline for **DPPBr$_2$-c MOD**), the yield being significantly lower for **DPPBr$_4$** (25 % *versus* 60 %).

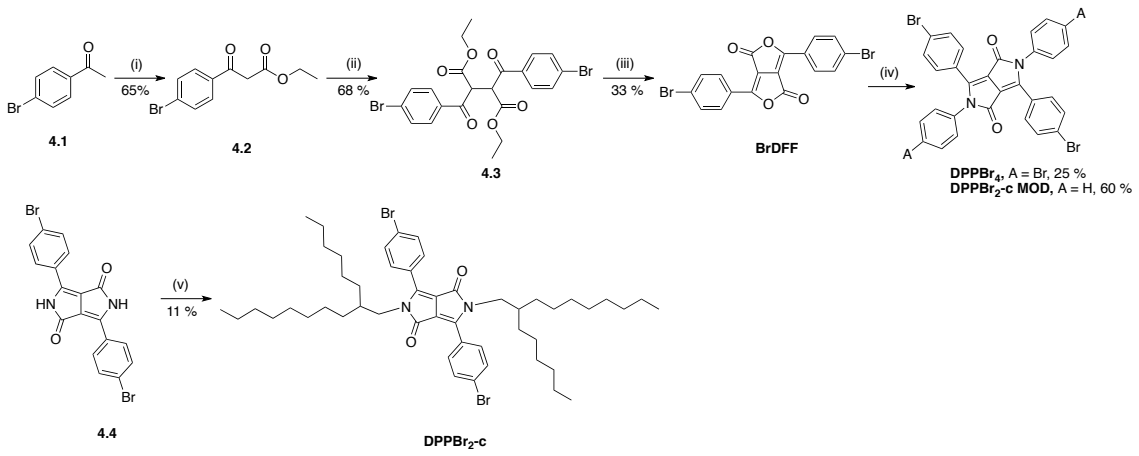

Scheme 4-1 Synthesis of the DPP cores **DPPBr$_4$**, **DPPBr$_2$-c** and **DPPBr$_2$-c MOD**. Reagents and Conditions: (i) diethyl carbonate, NaH, toluene, 80 °C, 18 h; (ii) (1) Br_2, CH_2Cl_2 (2) NaH, CH_2Cl_2, reflux, 3 h; (iii) 300 °C, 20 min; (iv) *p*-bromo-aniline (for A = Br) or aniline (for A = H), *N,N-dicyclohexylcarbodiimide,* CF_3COOH, $CHCl_3$, 3 days; (v) (1) KO^tBu, DMSO, 60 °C, 30 min, (2) 1-bromo-2-hexyldecane (slow addition), 60 °C, 20 h.

The purification of these cores was very challenging due to their low solubility in toluene. The products were purified by column chromatography eluting with toluene but there was an impurity that would consistently co-elute with the product. Furthermore, a large degree of the product was lost on every column. To avoid this problem the purification of **DPPBr$_2$-c MOD** was carried out in hot toluene with a jacketed column attached to a thermostat bath. The losses were not as significant (and therefore the yield is higher) but the product tended to

crystallise on the stem of the column. After this observation it was found that the best way to purify these cores after a preliminary small column was by recrystallisation in a large volume of hot toluene.

The synthesis of **DPPBr$_2$-c** was achieved by basic treatment of 3,6-di(bromophenyl) DPP (**4.4**) with potassium tert-butoxide followed by the addition of 1-bromo-2-hexyldecane, obtaining the product in a very poor 11 % yield. Several other bases were tried for the alkylation but no product was obtained.

The arms with hexyl chains were synthesised following the iterative procedure described in Chapter 0; i.e., generation of the fluorene boronic acid by lithiation with n-butyllithium and quenching with triisopropylborate, followed by Suzuki cross-coupling with 9,9-dihexyl-2,7-dibromofluorene (**4.6**). Note that "**H**" represents hexyl chain, following the terminology employed in Chapter 0, where "**B**" stands for butyl and "**O**" for octyl alkyl chains. In this case **4.6** was synthesised by initial alkylation of the fluorene followed by bromination of compound **4.5**, instead of brominating first and then alkylating, as explained in Chapter 0. Note that the alkylation yield was higher here than for the butyl and octyl analogues (84 % *versus* 73 % and 74 %), probably because of the initial increased purity of the non-brominated fluorene derivative.

The yields of the generation of the boronic acids (**F$_n$ H**) were generally high (above 80 %) except for the quaterfluorene derivative, which was synthesised in a poor 44 % yield, probably due to losses during the purification process, where not all the product was recovered from the column. In this case, the bromo-oligofluorenyltrimethylsilane derivatives **4.7**, **4.8** and **4.9** were split into two batches, one of which was employed for the synthesis of the next generation of TMS-protected oligofluorene (**F$_n$ H**) and the other one was deprotected in acidic conditions and converted to the corresponding boronic acid (**F$_n$' H**). Unlike the case of the oligofluorene truxenes, the TMS group cannot be deprotected once the arms are coupled to the DPP core because the harsh acidic conditions would affect the DPP core and lead to possible ring opening. For this reason, the arms had to be deprotected beforehand and converted to the boronic acids for the final Suzuki coupling to the core. Note that **F$_2$' H** and **F$_3$' H** were not employed for the synthesis of the DPPs but they were used in the synthesis of the oligofluorene BODIPYs in Chapter 6; their synthesis is presented here for conciseness.

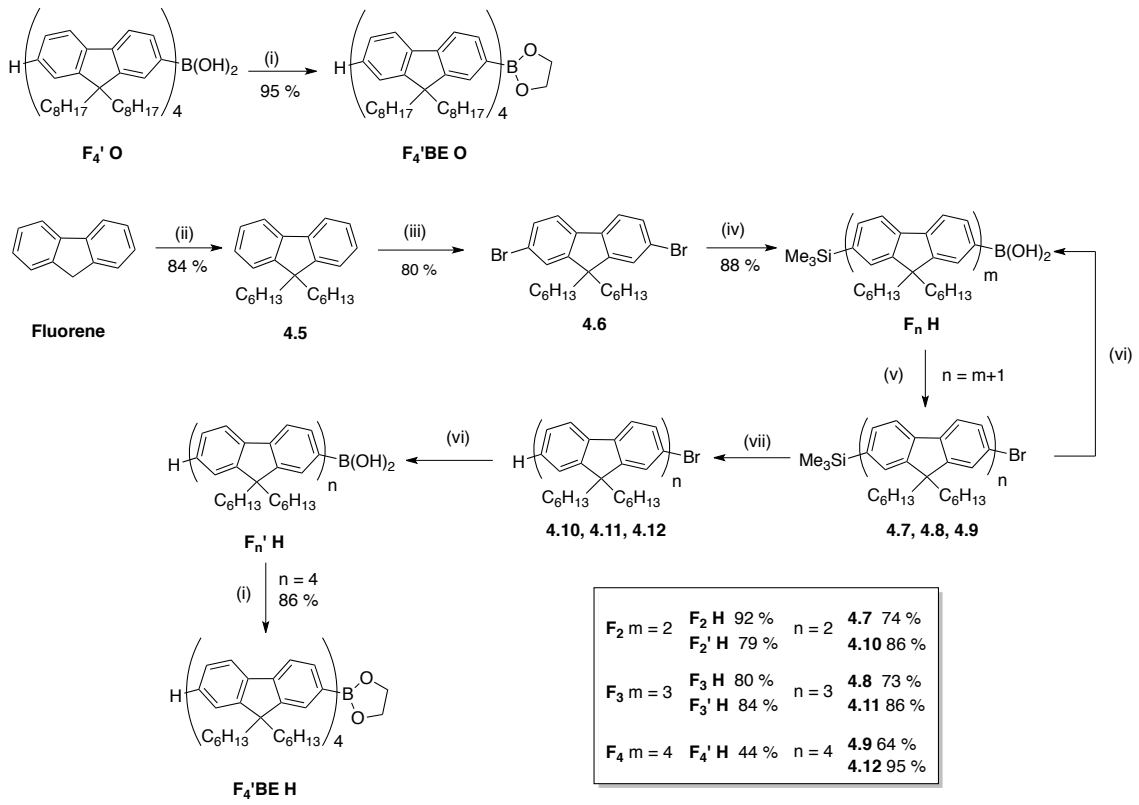

Scheme 4-2 Synthesis of the oligofluorene arms. Reagents and conditions: (i) Ethylene glycol, toluene, reflux, 18 h; (ii) RBr, THF, ^{t}BuOK/THF, 4 h, R.T; (iii) Br_2, $KBrO_3$, H_2SO_4, AcOH, 44 – 55 °C, 4 h; (iv) (1) BuLi, THF, -80 °C, (2) $SiMe_3Cl$, -95 °C – 20 °C, (3) BuLi, -85 °C, (4) $(^{i}PrO)_3B$, -100 °C, (5) R.T., 18 h; (v) (1) $Pd(PPh_3)_4$, **4.6**, toluene, (2) 2M Na_2CO_3 (aq), 80 °C, 18 h; (vi) (1) BuLi, THF, -80 °C, (2) $(^{i}PrO)_3B$, -100 °C, (3) R.T., 18 h; (vii) CF_3COOH, CH_2Cl_2, R.T., 2 h.

The yields of the Suzuki couplings were slightly lower than those obtained for the butyl and octyl derivatives, however they were all above 70 % except for the quaterfluorene **4.9**, which was obtained in 64 % yield. Both deprotected quaterfluorene boronic acids with octyl and hexyl chain (**F_4' O** and **H**) were converted to the corresponding boronate ester **F_4'BE O** and **H** in order to increase the yields when employing Suzuki cross-coupling under anhydrous conditions. This step involved a simple condensation of the boronic acid with ethylene glycol at high temperatures in high yields (95 % and 84 % respectively).

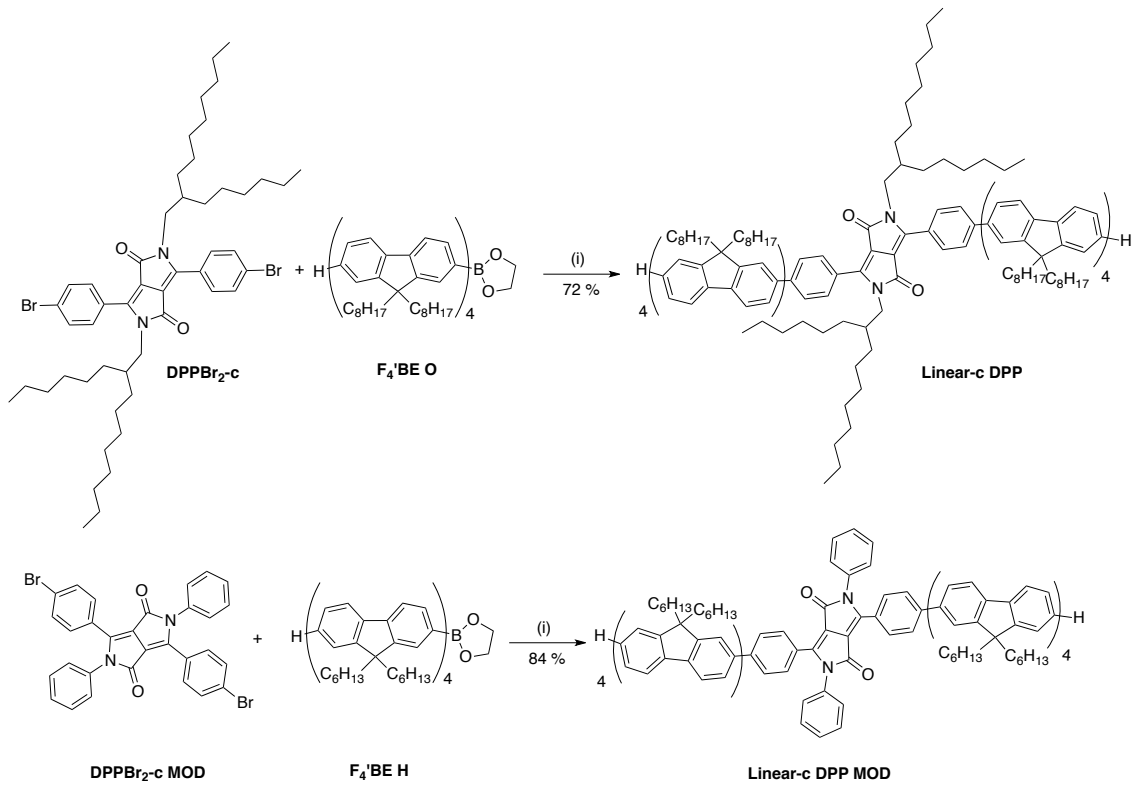

Scheme 4-3 Synthesis of **Linear-c DPP** and **Linear-c DPP MOD**. Reagents and conditions: (i) $Pd(PPh_3)_4$, K_3PO_4, DMF, 80 °C, 40 h.

The synthesis of the two linear analogues of oligofluorene DPP are presented in Scheme 4-3. Modified Suzuki cross-coupling under anhydrous conditions proved to be the most efficient method for the synthesis of **Linear-c** and **Linear-c MOD DPP**, using potassium phosphate as a base and *N,N*-dimethylformamide as a strong solubilising agent. The use of a boronate ester instead of a boronic acid functionality improved the yield dramatically leading to the synthesis of the bright red **Linear-c DPP** in 72 % yield (instead of the 13 % yield obtained with the boronic acid) and **Linear-c DPP MOD** in 84 % yield, higher than the original publication (63 %).[138]

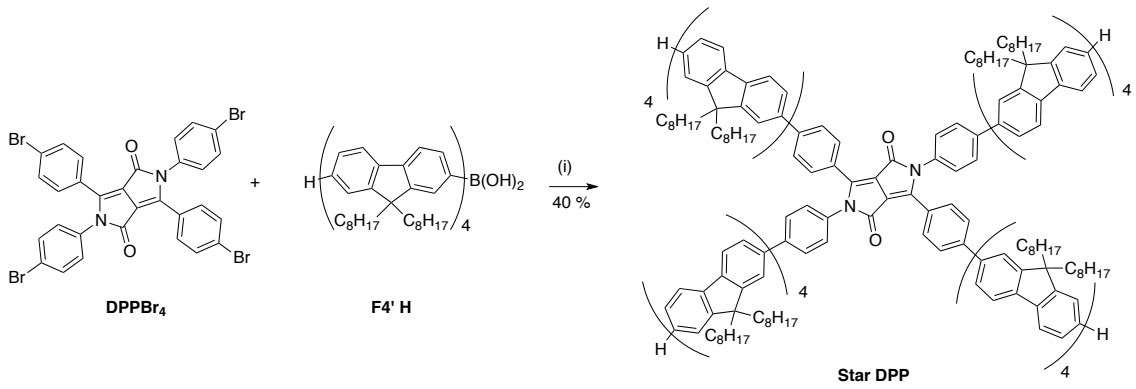

Scheme 4-4 Synthesis of **Star DPP**. Reagents and conditions: (i) $Pd(PPh_3)_4$, K_2CO_3 (aq), toluene, reflux, 3 days.

Star DPP was synthesised by Suzuki cross-coupling, employing an aqueous solution of potassium phosphate as base. The coupling was less efficient than that reported by Kanibolotsky *et al.* for the derivative with hexyl chain (40 % *versus* 50 % yield) and perhaps the anhydrous modified Suzuki coupling would improve the efficiency of the reaction.

4.3.2 Physical properties

All the DPP-containing compounds were bright red powders readily soluble in common organic solvents. The stability of the materials was tested by thermogravimetric analysis, revealing that all are stable up to 396 - 460 °C (Table 4-1). The morphology of the solid materials was studied by differential scanning calorimetry and all the materials present a certain degree of crystallinity. Both **Star DPP** and **Linear-c DPP MOD**, which share a common substitution pattern around the DPP core with four phenyl rings, present a glass transition temperature (at 48 °C and 108 °C, respectively) and a melting point (at 130°C and 208 °C, respectively). The star analogue has four oligofluorene arms with octyl chains instead of two oligofluorene arms with hexyl chains, providing a greater free volume that accounts for the much lower temperature at which the thermal events occur. The thermal events of **Linear-c DPP MOD** occur at temperatures comparable with those of its isomer **Linear-nc DPP** (T_g = 101 °C and T_c = 164 °C).[138] **Linear-c DPP**, as its published hexyl analogue, only shows a well-defined melting point at 88.5 °C, with no sign of amorphous character. The thermal events for the octyl derivatives of **Star** and **Linear-c DPP** occur at much lower temperatures than for the hexyl derivatives due to the increased free volume associated with the extra two carbons in the alkyl chains.[138] On the other hand, powder X-ray diffraction studies of the molecules (performed by Dr. Fiona Coomer) showed completely amorphous diffractograms.

Table 4-1 Physical properties of the oligofluorene DPP series. M_w is the molecular weight of the compound, T_g is the glass transition temperature and T_m is the melting point as measured from differential scanning calorimetry (DSC). T_d is the decomposition temperature measured by thermogravimetric analysis (TGA).

Compound	M_w (g·mol^{-1})	Thermal event (°C)	T_d (°C) [5% mass loss]
Star DPP (octyl)	6658.53	48 (T_g); 130 (T_m)	396
Linear-c DPP (octyl)	3846.17	88.5 (T_m)	426
Linear-c DPP MOD (hexyl)	3100.66	108 (T_g); 209 (T_m)	460

Figure 4-8 represents the DSC plots of the three compounds. Only the third heat cycle is presented for **Star DPP** and **Linear-c DPP** but for **Linear-c DPP MOD** the cooling and third heating cycles are presented to show that no crystallisation is observed. Note that the sharp peak at ≈ 60 °C on the cooling cycle in Figure 4-8 c is background noise.

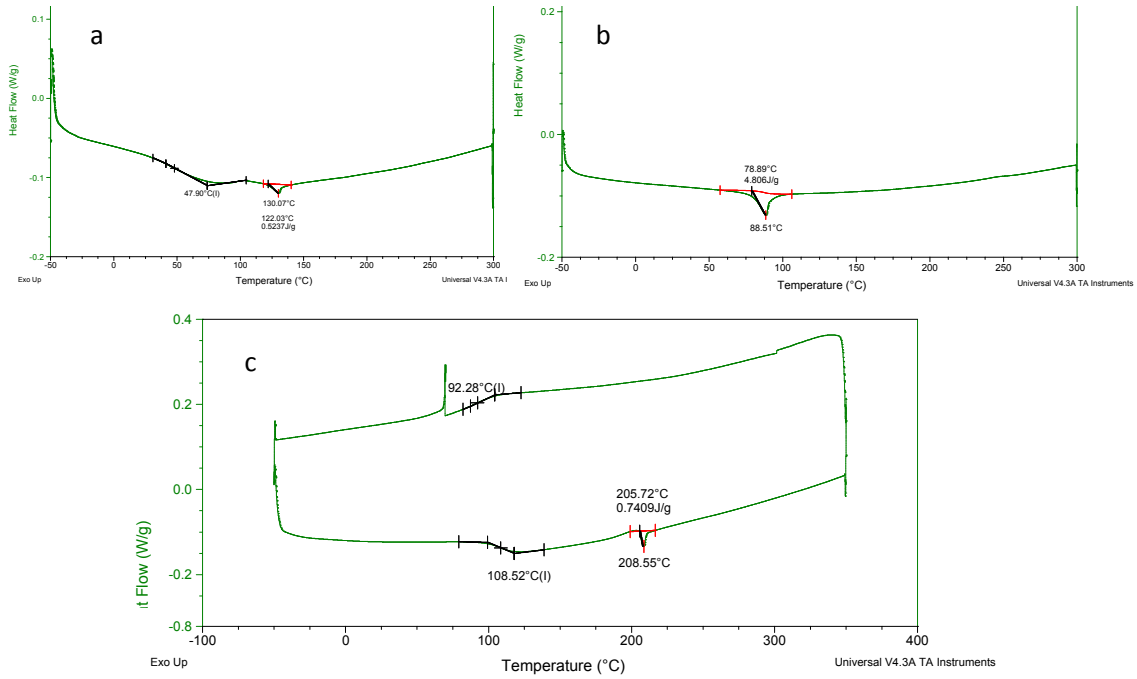

Figure 4-8 DSC plots of the oligofluorene DPP molecules. a) **Star DPP**, b) **Linear-c DPP**, c) **Linear-c DPP MOD**.

4.3.3 Electrochemistry

The electrochemical properties of the oligofluorene DPP materials were studied in 10^{-4} M solutions in dichloromethane and the results are summarised in Table 4-2. Figure 4-9 shows the oxidation curves of the three materials with all the compounds presenting two reversible oxidation processes spaced 0.17 – 0.21 V, except for **Linear-c DPP (octyl)** that presents an extra peak at 0.78 V. All compounds possessed similar HOMO levels (around -5.48 eV), which could be explained since the oxidation of these compounds probably occurs on the quaterfluorene arms, and all three materials possess the same length of oligofluorene arms.

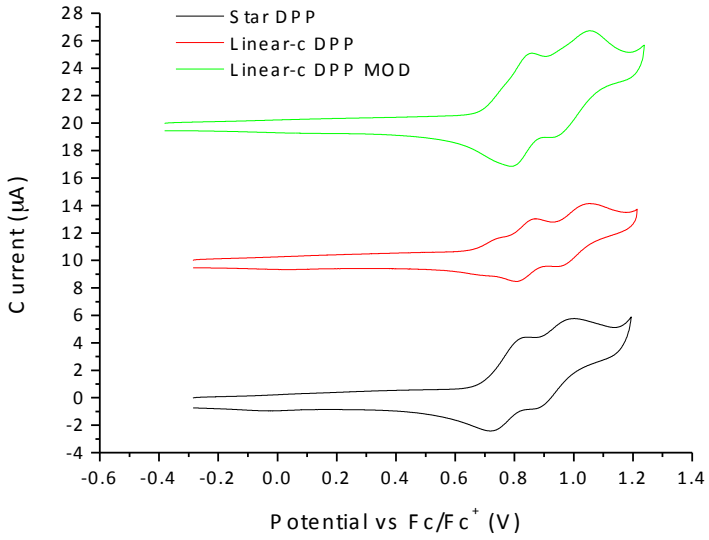

Figure 4-9 Oxidation curves of the 10^{-4} M solutions of the oligofluorene DPP compounds in dichloromethane. The cyclic voltammogram was obtained employing a glassy carbon working electrode, a platinum wire counter electrode and a silver wire reference electrode. All the waves were referenced to ferrocene.

The reduction waves of the materials are presented in Figure 4-10. **Star** and **Linear-c DPP (octyl)** present a single irreversible reduction peak around -2.03 V, which lies at a more negative potential than that of their hexyl analogues (≈ -1.90 V).[138] On the other hand, **Linear-c DPP MOD** possesses an extra quasi-reversible reduction peak at -1.64 eV and presents a more stable LUMO (-3.35 eV) than **Star** and **Linear-c DPP** (-2.97 eV and -3.08 eV respectively). The optical and electrochemical HOMO-LUMO gaps are in relatively good agreement for the linear analogues but they differ by 0.33 eV for **Star DPP**. In order to clarify this issue the electrochemical studies should be repeated. They lie around 2.20 eV, which is comparable with the HOMO-LUMO gaps of their hexyl analogues.[138] In all compounds, the DPP core is responsible for the reduction band. In **Star DPP**, the oligofluorene arms donate electron-density to the core, raising the reduction potential to more negative values. In **Linear-c DPP MOD** there are only phenyl groups attached to the 2,5-positions, which could decrease the electron-density on the DPP core via mesomeric effect, lowering the reduction potential to a less negative value compared to **Linear-c DPP**.

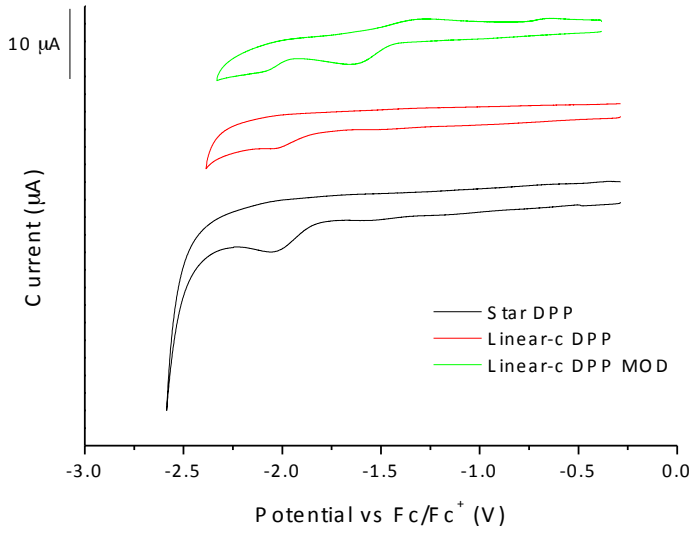

Figure 4-10 Reduction curves of the 10^{-4} M solutions of the oligofluorene DPP compounds in dichloromethane. The cyclic voltammogram was obtained employing a glassy carbon working electrode, a platinum wire counter electrode and a silver wire reference electrode. All the waves were referenced to ferrocene.

Table 4-2 Electrochemical properties of the oligofluorene DPP series in dichloromethane. [a] HOMO and LUMO levels were calculated from the onset of the corresponding redox wave and are referenced to ferrocene, which has a HOMO of -4.8 eV. [b] The electrochemical HOMO-LUMO gap ($E_{g,\,CV}$) is the energy gap between the HOMO and LUMO levels. The optical HOMO-LUMO gap ($E_{g,\,opt}$) is calculated from the onset of the red-edge of the absorption band (in brackets).

Compound	E_{ox} vs Fc/Fc^+ (V)	HOMO[a] (eV)	E_{red} vs Fc/Fc^+ (V)	LUMO[a] (eV)	$E_{g,\,CV}$[b] (eV)	$E_{g,\,opt}$[b] (eV)
Star DPP (octyl)	0.83, 1.00	-5.49	-2.03	-2.97	2.52	2.19 (566)
Linear-c DPP (octyl)	0.78, 0.87, 1.05	-5.46	-2.04	-3.08	2.37	2.23 (557)
Linear-c DPP MOD (hexyl)	0.85, 1.06	-5.49	-1.64, -2.03	-3.35	2.14	2.20 (563)

4.3.4 Optical and lasing properties

The absorption and emission spectra of 10^{-6} M solutions of the compounds in dichloromethane are presented in Figure 4-11. All the compounds present a main absorption band related to the

π-π* transition of the quaterfluorene arms, centred at 366 nm for the linear compounds and slightly red shifted at 369 nm for **Star DPP**. A second red-shifted broad transition ascribed to the ICT band from the donor arms to the acceptor DPP core appears between 491 nm and 512 nm. As with the hexyl analogues, **Linear-c DPP** presents a symmetric featureless band at 491 nm, while **Star DPP** presents a flattened absorption band (centred at 512 nm) with the vibronic structure not as well resolved as for the hexyl analogue.[138] **Linear-c DPP MOD** possesses a similar absorption profile as **Star DPP**, but slightly blue shifted to 509 nm. In this case, the substitution pattern around the DPP is the same as for **Star DPP**, except for the extra two oligofluorene arms. Compared to **Linear-c DPP**, the modified version has a phenyl ring that can enhance the charge transfer from the arms at the 3,6-positions to the carbonyl of the core by withdrawing electron-density *via* mesomeric effects and therefore making the core more electropositive. This, combined with the symmetry of the molecule can contribute to a greater quadrupole-quadrupole interaction, similar to that occurring in **Star DPP**.

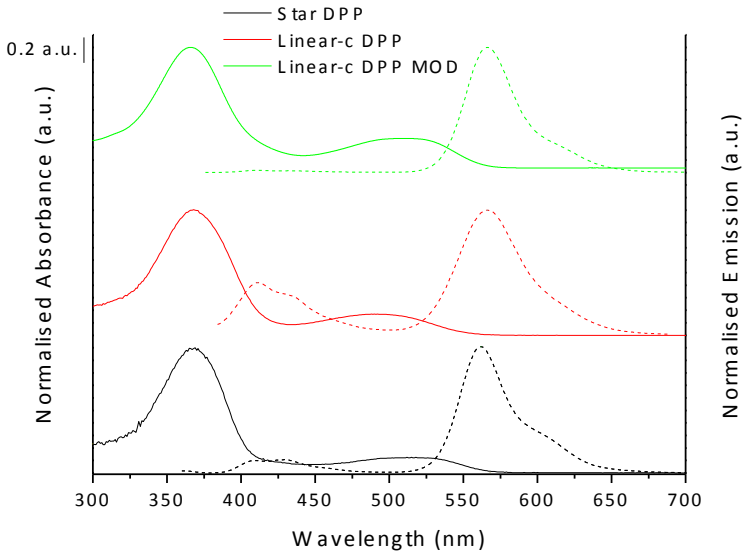

Figure 4-11 Absorption (solid line) and emission (dashed line) spectra of the oligofluorene DPP series (10^{-6} M solutions in dichloromethane). λ_{ex} = 360 nm.

The emission spectra of **Star** and **Linear-c DPP** show a weak fluorescence band with vibronic structure around 415 nm, characteristic of the oligofluorene emission. This indicates that in solution the charge transfer is not complete for these analogues, whereas **Linear-c MOD** does not present any sign of emission in that region, indicating a complete charge transfer from the arms to the core. In the case of **Star DPP**, it is possible that the charge transfer is also happening to the same extent in the 3,6-positions and the emission in that region might only

come from the arms coupled in the non-conjugated locations of the core. In the case of **Linear-c DPP** the lower degree of ICT is possibly caused by the positive inductive effect that the solubilising alkyl groups exert on the core, reducing its electron affinity, but mainly by the greater degree of twisting of the phenylene spacers in 3- and 6-positions of the DPP core due to steric hindrance from the branched alkyl substituents. The less planar structure of the ground state of **Linear-c DPP** is evidenced by the featureless profile of its DPP absorption band. The short wavelength emission band overlaps partially with the absorption profile of DPP and to a lesser extent with the oligofluorene band. This is detrimental for optoelectronic applications because it can lead to partial re-absorption of the emission, leading to lower PLQYs. The main emission band in all compounds comes from the DPP and is centred around 566 nm for the linear analogues and slightly red-shifted to 569 nm for **Star DPP**. It is rather broad and presents vibronic structure with a well-resolved shoulder for **Star DPP** and to a lesser extent for **Linear-c DPP MOD**. **Linear-c DPP** presents a tail in the emission rather than an obvious shoulder.

Table 4-3 Optical properties of the oligofluorene DPP series (10^{-6} M solutions in dichloromethane and films). ε is the molar absorption coefficient in the film, measured for both fluorene and DPP absorption bands. Φ_{film} is the PLQY of the materials in the film, measured exciting at the wavelength of maximum absorbance for the oligofluorenes (380 nm) and the DPP (520 nm).* The longer excitation wavelength employed for **Linear-c DPP MOD** was 450 nm rather than 520 nm.

Compound	$\lambda_{abs,\ sol}$ (nm)	$\lambda_{abs,\ film}$ (nm)	$\lambda_{em,\ sol}$ (nm)	$\lambda_{em,\ film}$ (nm)	log(ε) [Fluorene/DPP]	Φ_{film} [λ_{ex} 380/520 nm]
Star DPP (octyl)	369, 512	371, 509	408, 569	630	5.79/4.88	0.16/0.28
Linear-c DPP (octyl)	366, 491	365, 506	420, 567	630	5.12/4.34	0.23/0.46
Linear-c DPP MOD (hexyl)	366, 509	362, 506	566	580	5.37/4.76	0.48/0.45*

The shape of the DPP band for **Star DPP** and **Linear-c DPP MOD** in their solid state absorption spectra indicates aggregation due to the increased intensity of the short-wavelength vibronic peak (509 nm) with respect to the red-shifted one (≈ 540 nm). Unfortunately, this implies that the increase in the length of the alkyl chain to eight carbons (in the case of **Star DPP**) is not enough to force the chromophores away from each other in thin films. The DPP absorption

band for **Linear-c DPP** also reveals its aggregation in the condensed state. The broader and less symmetric absorption profile, as well as the 12 nm bathochromic shift observed for the DPP band in the film compared to the solution are typical characteristics of the aggregated states. This tendency to aggregate in the solid state is expectable, given the crystalline nature of the material. As explained by Kanibolotsky *et al.*, the quadrupole-quadrupole interactions between molecules and the π-π stacking of the four phenyl rings in these compounds induce very strong intermolecular interactions that change the conformation of the molecule from almost planar to a propeller-like structure.[138]

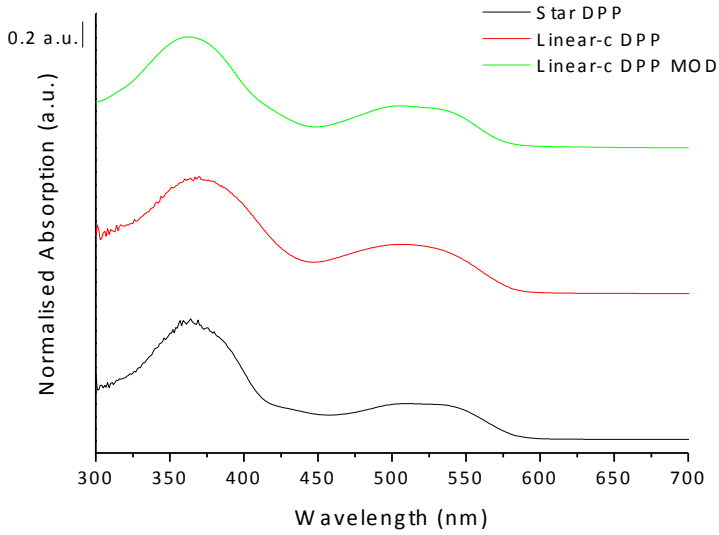

Figure 4-12 Absorption spectra of the oligofluorene DPP series measured on films dropcast from 10 mg·mL^{-1} in toluene.

Figure 4-13 presents the absorption spectra of the oligofluorene DPP compounds in the region of the DPP absorption band. These spectra were recorded in hexane solutions as a concentration study to assess the aggregation of the compounds in solution. Both linear derivatives follow the Lambert-Beer law with a linear increase in the absorbance when increasing the concentration of the solution. Note that instead of absorbance, the molar absorptivity is presented as cuvettes of different pathlengths were employed for this study in order to avoid saturation of the absorption in very concentrated solutions. **Star DPP (octyl)**, as it occurred with its hexyl analogue, aggregates in hexane solution at high concentrations. This can be observed by an increased intensity of the short wavelength vibronic feature (≈ 500 nm) at higher concentrations and a certain degree of quenching, while at low concentrations the long wavelength vibronic peak (≈ 530 nm) is dominant.[138]

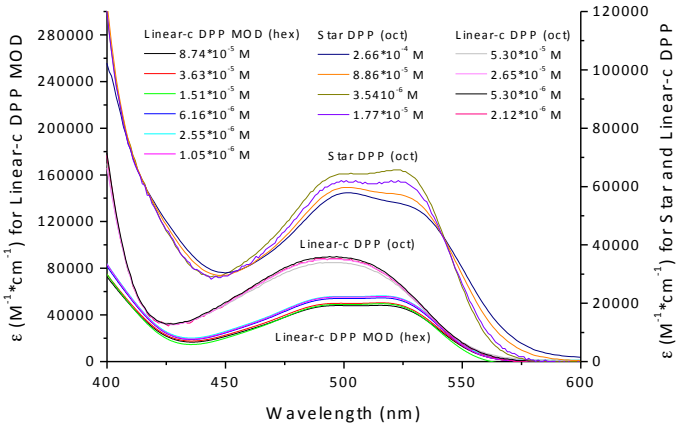

Figure 4-13 Concentration studies on the oligofluorene DPP compounds in hexane solutions. The absorption band of DPP for the three compounds is presented. Note that the left axis corresponds only to **Linear-c DPP MOD** and its scale is much larger than that of the right axis (corresponding to **Star DPP** and **Linear-c DPP**) in order to plot clearly the three compounds in one graph. *ε* represents the molar absorptivity of the compounds.

In order to compare the aggregation of the three compounds in hexane solution and in the solid state, a plot of the normalised absorption of the DPP band of the compounds in hexane and in the film was plotted (Figure 4-14). The red shift, broadening and change of shape of the DPP band in the film is obvious for the three compounds, confirming the aggregation in the condensed state. On the other hand, only **Star DPP** aggegates in hexane, as discussed above.

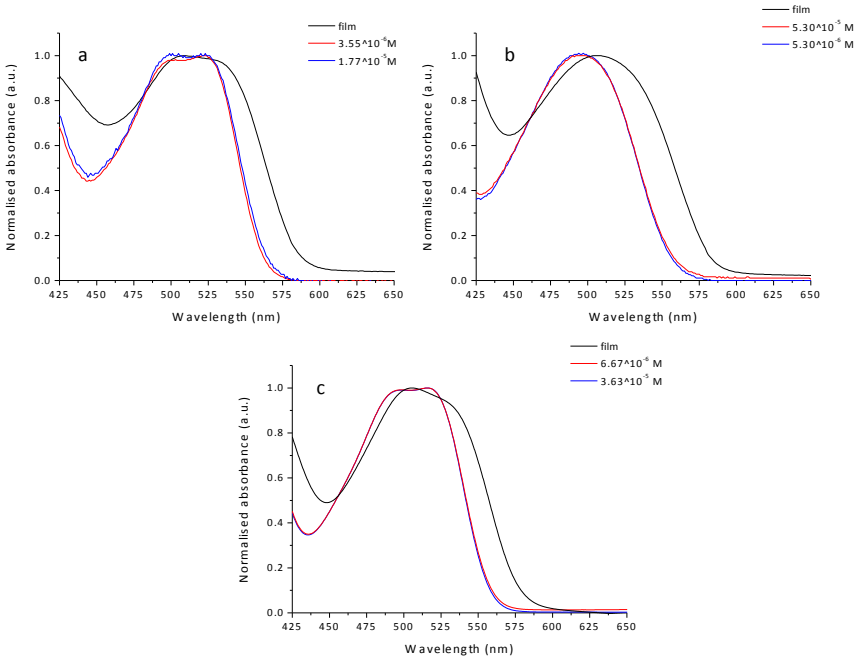

Figure 4-14 Normalised absorption spectra of the DPP band of a) **Star DPP**, b) **Linear-c DPP** and c) **Linear-c DPP MOD** in hexane and films.

The photophysical properties of **Star-DPP** and **Linear-c DPP** were studied by Dr. Colin Belton of the Experimental Solid State Physics group at Imperial College London (**Linear-c DPP MOD** was synthesised at a later date and no photophysical properties were recorded in order to be included in this thesis). Given the fact that the octyl chain had not solved the aggregation issues, the goal of the study was to determine the differences between the fluorene excitation pathway (at 370 nm) and the direct excitation of the DPP band (510 nm). Figure 4-15 presents the emission spectra of films of the octyl derivatives of **Linear-c** (left) and **Star DPP** (right) of two thicknesses (50 nm and 230 nm) excited at 370 nm. The PL spectra shows exclusively emission from the DPP band (demonstrating complete charge transfer in this case) and presents vibronic structure for both compounds, the 0-1 transition being the most intense in both cases. Note that the thinner film shows a hint of emission from the fluorenes at around 450 nm but the resolution is much poorer for both compounds than in the case of the thicker films.

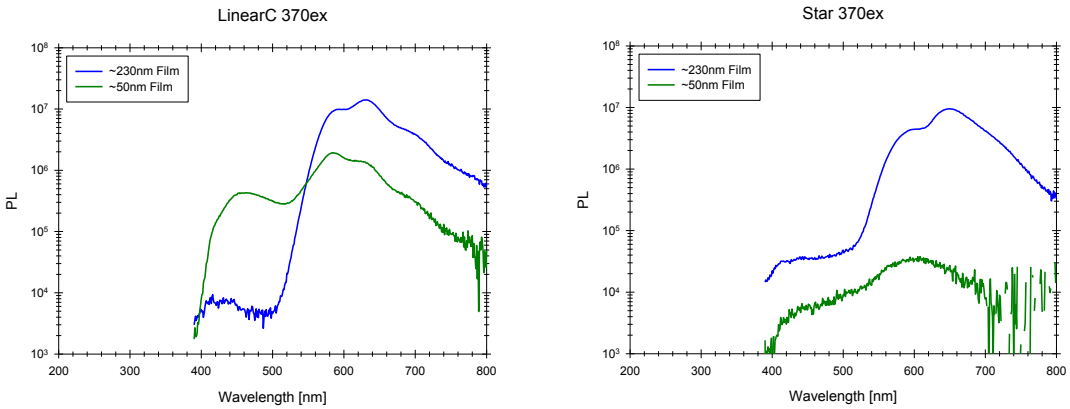

Figure 4-15 Emission spectra of **Star DPP** and **Linear-c DPP (octyl)** measured on 50 nm thick films (green line) and 230 nm thick film (blue line). λ_{ex} = 370 nm.

The PLQY of both compounds was measured on 230 nm thick films *via* exciting at the fluorene and the DPP absorption bands (see Table 4-3, page 110). **Linear-c** presents a PLQY twice that of **Star DPP** and for both compounds it is higher when the DPP band is excited directly, which implies that there are energy losses associated with the charge transfer process from the fluorene to the DPP. The PLQY of **Linear-c DPP MOD** was measured at the University of St Andrews, exciting at 360 nm and 450 nm and it did not show a large variation with the different excitation wavelength (note that the longer excitation wavelength does not excite exactly the DPP band due to experimental restrictions). In both cases the PLQY is quite high for an emissive material in the condensed state ($\Phi \approx 0.46$).

The PL decay studies performed by exciting the molecules in the region of absorption of the fluorenes (379 nm) and in that of the DPP (465 nm) shows that for **Linear-c DPP** a monoexponential decay is obtained with almost no dependence on the excitation wavelength, which indicates a fast charge transfer process (Figure 4-16). **Star DPP** presents an almost mono-exponential decay with a more dispersive result when the film is excited at 379 nm. This might be due to dispersive recombination caused by the inclusion of the non conjugated arms at the 2,5-positions of the DPP, or to extra losses induced by these two arms during the charge transfer process. The lifetime of **Linear-c DPP** is 2.85 ns independent of the excitation wavelength, but **Star DPP** has a longer lived PL when excited at 465 nm than at 379 nm (3.00 ns *versus* 2.55 ns).

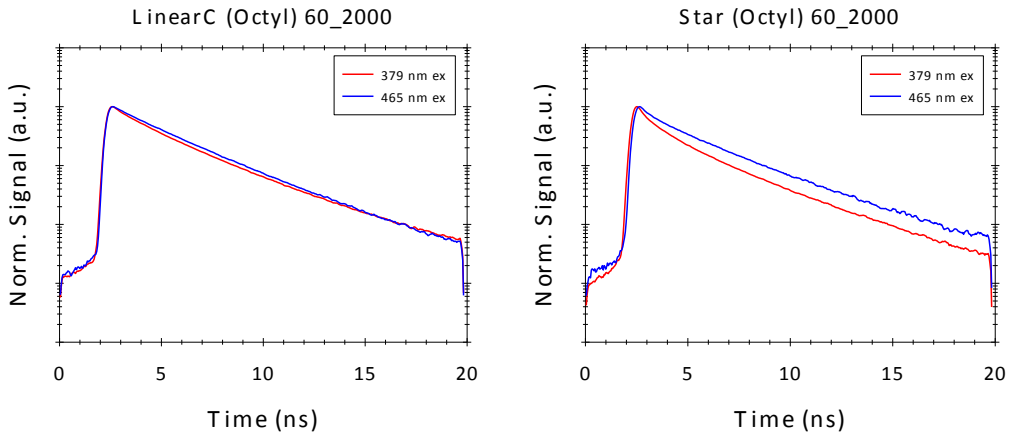

Figure 4-16 PL decay of **Linear-c DPP** (left graph) and **Star DPP** (right graph) excited at 379 nm (red line) and 465 nm (blue line).

ASE studies on the two octyl analogues only provided ASE narrowing for **Linear-c DPP** and therefore the in depth study of the photophysical properties was only performed for this compound. Figure 4-18 presents the output PL intensity against the pumping energy for stripes of different lengths (presented in the legend of the graph) to determine the ASE threshold using the variable stripe length method (VSL) with variable power (VP) configuration. It can be observed that the 4 mm stripe length provides the sharpest change in the slope of the curve and the lowest ASE threshold independently of the excitation wavelength employed. The ASE narrowing (λ_{ASE}) appears at almost the same wavelength for both excitation wavelengths (630 nm when exciting the film at 355 nm and at 631 nm when exciting at 532 nm), corresponding with the 0-1 vibrational peak (Figure 4-17). Given the fact that the absorption coefficient for the oligofluorenes ($1.36 \cdot 10^5$ cm^{-1}) is much greater than that of the DPP ($0.19 \cdot 10^5$ cm^{-1}), the ASE threshold is calculated on the basis of the excited population density at the film surface where

the laser is first incident. The excited population density (N_0) can be calculated following Equation 4-1.

$$N_0 = \frac{E_0 \cdot \alpha(v) \cdot \tau_{SP}}{h \cdot v \cdot \tau_L} \qquad \textbf{Equation 4-1}$$

Where E_0 is the incident energy, α(ν) is the absorption coefficient, τ_{SP} is the fluorescence lifetime, h·ν is the photon energy and τ_L is the excitation laser pulse duration.

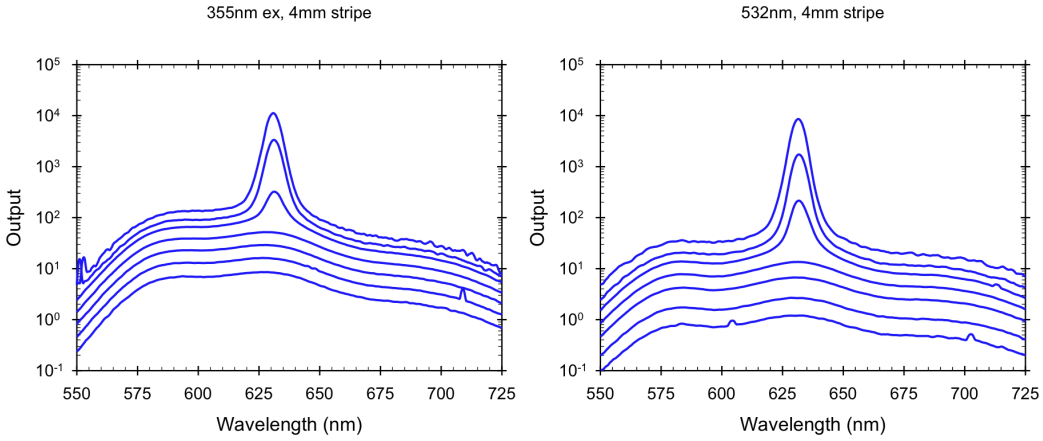

Figure 4-17 ASE narrowing of **Linear-c DPP** films pumped at a 4 mm stripe with excitation pulses at 355 nm (left graph) or 532 nm (right graph).

The pumping energy threshold for ASE narrowing, pumping at the fluorene excitation wavelength is ≈ 80 μJ·cm^{-2}, while for excitation at the DPP band it is ≈ 200 μJ·cm^{-2}. Nevertheless, if we take into account the much greater absorption coefficient for the oligofluorenes than for the DPP (explained by a greater percentage of fluorenes than of DPP in the molecule) it is better to explain the ASE threshold in this case in terms of the maximum excitation density (bottom abscissa axis in Figure 4-18). The maximum excitation density required for pumping at the fluorene excitation wavelength is 8·10^{18} cm^{-3}, whereas for the DPP excitation wavelength it is 3·10^{18} cm^{-3}. Therefore the real threshold required for pumping at 355 nm is 2.6 times greater than for pumping at 532 nm, which might be explained by extra energy losses involved in the energy transfer process, as observed for the PLQY values.

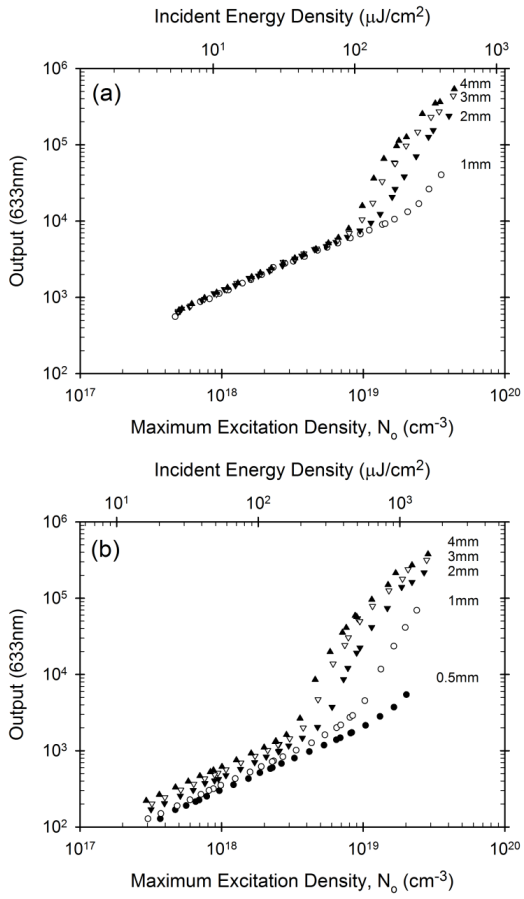

Figure 4-18 Power dependence of ASE of **Linear-c DPP** (integrated signal from 620 nm to 638 nm) for (a) 355 nm excitation and (b) 532 nm excitation. The data are shown for different excitation beam stripe lengths.

4.4 Conclusion and further work

In conclusion, two new oligofluorene DPP compounds with octyl chains (**Star DPP** and **Linear-c DPP**) were synthesised in order to avoid the 1D and 2D aggregation issues that arose in their hexyl analogues, as reported by Kanibolotsky and co-workers.[138] Unfortunately the longer alkyl chain did not solve the issue. **Linear-c DPP** presented crystalline character although it did not aggregate in solution, whereas **Star DPP** had only a low degree of crystallinity (observed by a small melting point and the presence of T_g) but aggregated in concentrated hexane solutions as well as in the film. Following this study, the next step to avoid the aggregation would be to encapsulate the molecules in UV-transparent photoresist materials to separate the chromophores from each other. Another interesting approach would be to synthesise a new DPP core with fluorenes attached directly to the 3,6- and/or 2,5-positions of the DPP (Figure 4-19). The quaterfluorene arm would then be built by coupling terfluorene arms onto the core, obtaining a new oligofluorene DPP analogue without phenylene spacers. This approach would avoid the π-π stacking between the phenyl rings and, hence the adoption of a propeller-like

conformation due to the alkyl chains of the fluorene. Thus it would help to prevent aggregation, allowing these compounds to achieve their maximum potential for optoelectronic applications.

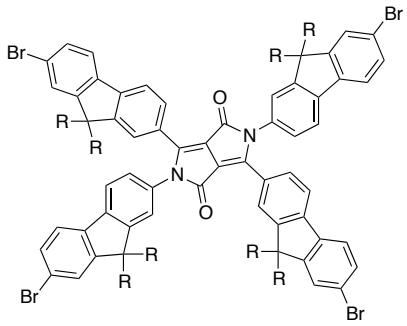

Figure 4-19 New **Star-DPP** core.

A new linear oligomer, an isomer of the compound **Linear-nc DPP** published by the Skabara group, but with the oligofluorene arms coupled in the 3,6-conjugated positions (**Linear-c MOD DPP**), was also synthesised in order to confirm the aggregation mechanism postulated in the original publication.[138] The properties of this analogue were a compromise between **Linear-c DPP** (as it has the same shape and arms in the 3,6-positions) and **Star DPP** (because it shares the same substitution pattern around the core). Further work with this compound will involve performing photophysical and lasing studies to observe if the lasing thresholds could be lowered in comparison with **Linear-c DPP**, since it has a lower degree of crystallinity.

Linear-c DPP was the only octyl derivative that showed ASE narrowing and a photophysical study to determine the best excitation pathway for this compound was performed. Despite the greater absorption coefficient of the oligofluorene absorption band, direct excitation at the DPP band provided higher PLQYs and lower ASE thresholds (measured in terms of the maximum excitation density to account for the difference in absorption coefficient). This indicates that there are energy losses in the charge transfer from the fluorene to the DPP and it is better to excite these molecules directly at the DPP band.

5 Star-shaped oligofluorene TPEs

5.1 Abstract

Two novel star-shaped oligofluorene tetraphenylethene materials (**TPE1** and **TPE4**) were synthesised in order to explore their suitability for OSLs. The monodisperse materials present low fluorescence efficiency in solution but they are efficient emitters in the solid state. The addition of water to THF solutions triggers the formation of nanoaggregates of the materials with enhanced emission intensities (this effect is commonly known as aggregation induced enhanced emission, AIEE). **TPE1** is capable of undergoing ASE and lasing, and its ASE wavelength is linearly responsive to the application of pressure. This opens up the opportunity for the development of new ASE-based pressure sensing devices with AIEE active materials.

5.2 Introduction

Many light emitting materials present efficient fluorescence in dilute solutions, whereas in concentrated solutions or the solid state their emission is quenched. This is due to the aggregation of the chromophores *via* π-π stacking that leads to the formation of species that undergo decay *via* non-radiative pathways.[7] This effect is commonly known as aggregation-caused quenching (ACQ) and it can be mitigated by spacing the chromophores by means of bulky alkyl chains, dendrimers, spyro links or blends of the materials in non-conjugated transparent polymers such as poly(methyl methacrylate).[110] These approaches may avoid aggregation but can also be detrimental for the properties of the materials as they can lead to an increase in the torsion of the molecules and a decrease in the conjugation (which affects the optical and electronic properties of the molecules) or the hole and electron mobility in the bulk.[201]

In 2001, Ben Zhong Tang's group discovered a material that barely fluoresced in dilute solutions but became an efficent emitter in the condensed state.[202] They first observed the phenomenon during the purification of a silole: a fresh spot on a TLC plate did not show emission under UV ilumination, but upon drying it became fluorescent (Figure 5-1 a). Interested by this behaviour, they investigated the effect of the addition of different fractions of water, a non-solvent for the material, into solutions of the compound in ethanol and tetrahydrofuran. After the addition of a critical amount of water the fluorescence of the compound was dramatically enhanced. Furthermore, the absorption profile also increased

dramatically in intensity, suffered a bathochromic shift and its shape changed, revealing a tail above the baseline characteristic of nanoparticle suspensions. This confirmed the existence of nano-aggregates whose effective conjugation length was greater than that of the isolated species. Furthermore, they also prepared solid solutions of the material in PMMA and observed the same trend of an increase in the luminescence efficiency and a red-shift in the absorption maximum with an increase in the concentration of the silole.[202]

They named this phenomenon aggregation induced emission (AIE) and since then they have investigated in depth the mechanism behind it, its applications and a diversity of materials that can undergo AIE.[201, 203, 204] Initially they postulated that the PL enhancement might be due to conformational planarisation of the molecules in the condensed state, but this would imply that both absorption and emission would suffer bathochromic shifts and this is not the case. Furthermore, X-ray diffraction measurements reveal that the molecules remain in a twisted conformation in the solid state. Similarly, the AIE effect could not be due to the formation of *J* aggregates because the molecules did not have donor-acceptor components that would induce the push-pull mechanisms required for the formation of such aggregates. Moreover, this would also discard the possibility of a twisted intramolecular charge transfer, which is also confirmed by a lack of solvatochromism.[203] They then postulated that the fluorescence enhancement was a result of the restriction of intramolecular rotations (RIR) of the five phenyl rings attached to the silole *via* single bonds. Intramolecular rotations act as non-radiative relaxation pathways for the decay of the excited state, thus quenching the fluorescence. In solution, the molecules are free to rotate and the material is barely fluorescent. In the condensed state (solid, films, aggregates), the rotations are restricted and the fluorescence of the materials is dramatically enhanced.[204]

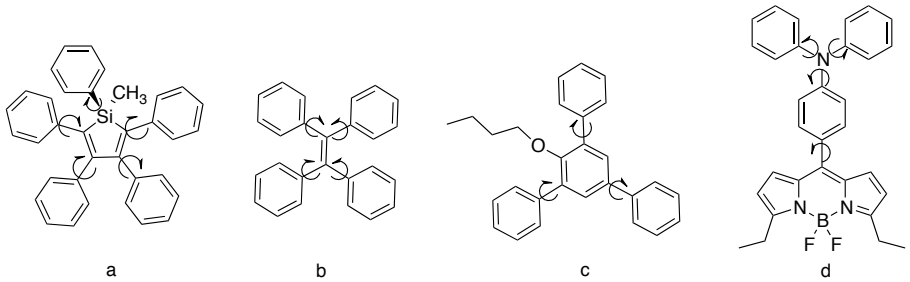

Figure 5-1 Some AIE active cores. a) 1-methylphenyl-2,3,4,5-tetraphenylsilole, b) tetraphenylethene (TPE), c) 2-butoxy-1,3,5-triphenylbenzene, d) *meso*-triphenylamineBODIPY.

In order to support this mechanism, the viscochromism of the molecules in solvent mixtures of increased viscosity was tested. The greater viscosity of the medium slowed down the molecular rotations that quench the emission and therefore the AIE effect was observed.[205] Then the piezofluorochromism was tested by applying increased pressure to thick films of AIE active materials and an increase in the PL intensity was observed without changes in the position and shape of the emission. The increased pressure diminished the intermolecular spacing, thus permitting a RIR process. Nevertheless, at very high pressures the PL decreased again because the close proximity of the chromophores under pressure induced π-π stacking.[206] Furthermore, the effect of temperature on the PL of solutions of the siloles in tetrahydrofuran, whose viscosity is largely independent from temperature, was tested. As expected, at lower temperatures the PL of the materials increased since the intramolecular rotations and vibrations occur at a lower rate. This was once again a confirmation of the proposed mechanism for AIE.[205] Additionally, the fluorescence decay dynamics were tested, realising that the nanoaggregate formation in water-dimethylformamide mixtures led to a change in the PL decay from a fast monoexponential decay in pure DMF solutions, to a decay with two-relaxation pathways: a fast channel, associated with the molecules free to rotate and a slow channel, related to the aggregates. Increased amounts of water in the solvent mixture led to a greater degree of the slow channel decay, increasing the PL lifetime of the materials. This supports the restriction of the non-radiative decay pathways that occur *via* intramolecular rotations, supporting the AIE mechanism.[207] In order to obtain further support for the proposed mechanism, novel silole analogues with isopropyl groups attached to the peripheral phenyl rings of hexaphenylsilole were designed. The bulky groups exert steric hindrance, thus restricting the intramolecular rotations. As a result, the materials are highly fluorescent both in the condensed state and in dilute solutions and their PL lifetimes increase from 40 ps to 6.18 ns.[208]

Once the mechanism behind AIE was elucidated, it was easier to design different AIE cores based on the restriction of their intramolecular rotations. Tang's group designed a wide variety of cores including the well-know tetraphenylethene (TPE) unit, in which the four phenyl rings attached to a central ethene can rotate freely in solution but not in the condensed state (Figure 5-1 b), as well as phenyl rings directly attached to each other by single bonds (Figure 5-1 c) or rotamers containing heteroatoms that can undergo not only RIR, but also charge transfer processes (Figure 5-1 d).[203]

Multiple modifications of these architectures with other groups can lead to spectral tuning of the emission to tailor the properties of the materials in order to match the requirements of each application. Amongst others, AIE active materials have been widely employed in OLEDs because they can provide both efficient emission and mobility in their aggregated state.[201] They have also been employed as chemical sensors, biological probes for cell imaging, for the formation of microstructured aggregates such as nanowires, liquid crystals or smart mechanochromic and thermochromic materials.[204]

Together with silole, TPE (Figure 5-1 b) is one of the most widely employed AIE active cores. The four phenyl rings are twisted (≈ 50°), adopting a propeller-like conformation that avoids π-stacking in the condensed state, and the conformation is further stabilised by multiple C-H···π bonds between the hydrogens of the phenyl rings and the π-electrons of an adjacent ring. This molecular conformation enables the strong AIE effect that TPE experiences in the condensed state.[201]

The introduction of TPE into systems that suffer ACQ leads to new materials with AIE or aggregation induced enhanced emission (AIEE); materials that presented poor luminscence before the introduction of the AIE-active chromophore and become efficient emitters after.[201] For example, TPE has been introduced as a side chain through flexible linkers in polyacetylene backbones, activating their fluorescence in the aggregated state.[209] TPE hyperbanched poly(tetraphenylethene) has been described as a polymer soluble in most organic solvents, that does not emit in solution but upon the addition of 60 % of water or higher fractions it becomes an efficient blue emitter.[210] Furthermore, the crosslinked polymer shows high transmittance when it is pumped at low laser imputs but low transmittance at high imputs, acting as an optical barrier that could be used in order to protect eyes or skin from damaging irradiation. Moreover, solutions or aggregates of the polymers in water/THF mixtures are sensitive to explosive vapours. Monitoring the decay of their PL could be used as an explosive sensor. Xu and co-workers described the synthesis of microporous polymers of TPE with enhanced fluorescence due to the permanent restriction of the intramolecular rotations in the three-dimensionally interlocked skeleton of the polymer.[211]

TPE-modified oligomers have also been described. For example, Aldred and co-workers described the synthesis and characterisation of a linear oligofluorene end-capped at both sides with TPE (Figure 5-2 a). The molecules presented an AIEE effect with an enhancement of their

fluorescence from 0.3 % to 2.1 % in THF solution, depending on the length of the oligofluorene core, to up to 41 % upon the formation of nanoagregates with the addition of water to the solution and 68 % in the solid state. The AIEE effect decreases in greater oligomers because the percentage of TPE in the molecules is reduced. The materials could be employed in solid state vapour sensors as they experience a reversible turn-off of their PL upon contact with dichloromethane vapour, that increases the possibilities of molecular rotation. Furthermore, the authors described the use of the materials in OLED devices that unfortunately presented high turn-on voltages.[100] Tang's group described the synthesis of a of TPE-triphenylamine (TPE-TPA) oligomer that presents AIE and good hole transporting properties (Figure 5-2 b). The material was used as the emissive layer in OLEDs and for photopatterning, and its high quantum yields coupled with its good mobilities could be employed in a future generation of electrically pumped lasers.[212]

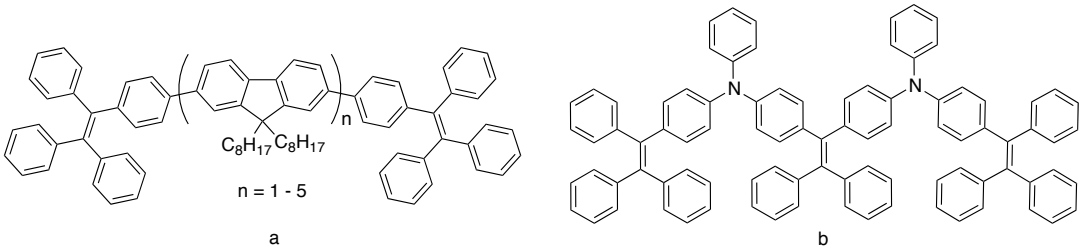

Figure 5-2 Some TPE-containing oligomers.

Several star-shaped materials containing TPE are described in the literature. For example Tang's group described the synthesis of a star-shaped material containing three TPEs merged by a central benzene core (Figure 5-3 a).[213] It presents AIE with increased water fractions in water-THF mixtures and the types of aggregates formed vary from crystalline at lower water fractions to amorphous at higher water fractions, leading to a red-shift in the emission of the latter. The emission of the crystal of the materials is hypsochromically shifted, probably due to the additional twist of its phenyl rings that the molecule must undergo in order to fit in the crystal lattice. This further prevents the aggregation of the molecule, which is normally associated with a red-shift in the emission of crystals. It presents a 100 % PLQY in the solid state but its EL efficiency is much poorer than that of a more linear analogue with ony two TPEs merged by a benzene core. Moreover, the PL of the compound is quenched by picric acid vapour, which is an analogue of DNT or TNT explosive vapour, and selectively by Ru^{3+} ions, opening the opportunity for sensing applications.

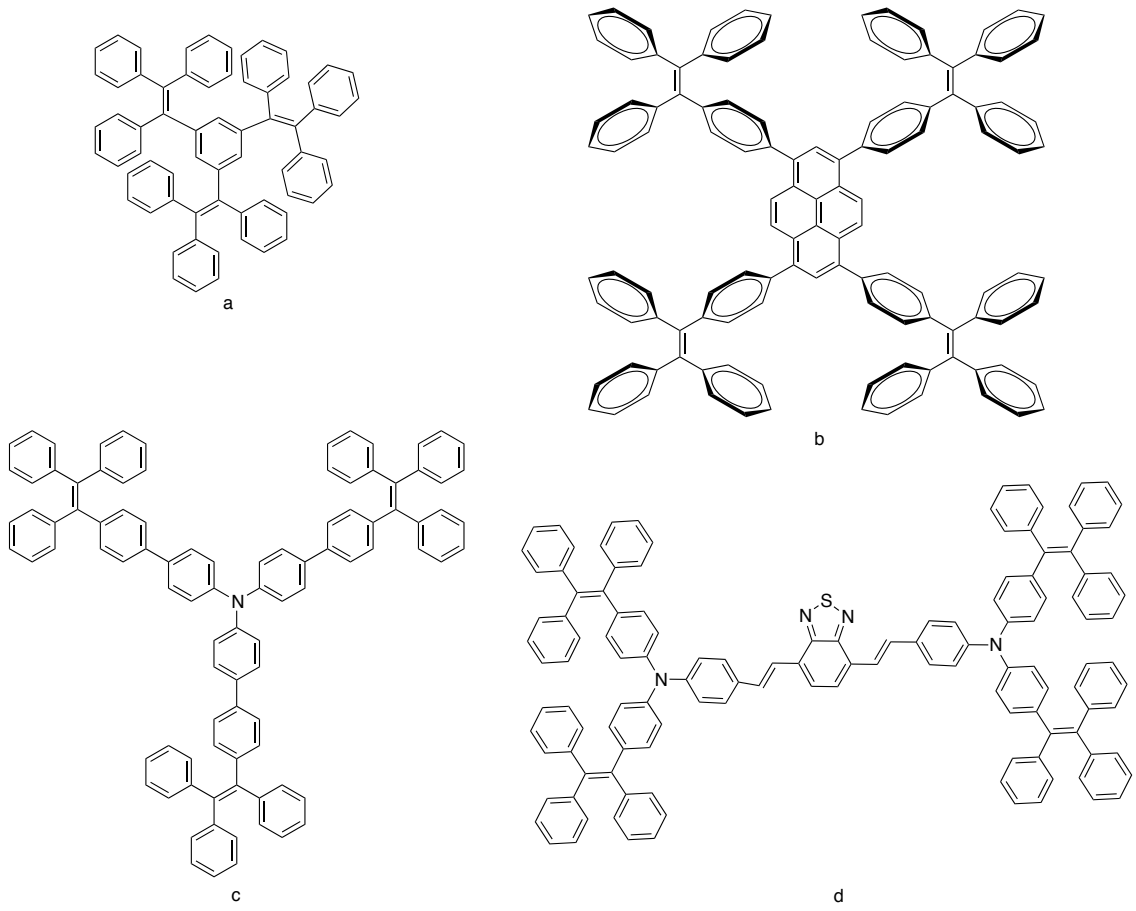

Figure 5-3 Some star-shaped materials with TPE arms.

The same group reported the synthesis of a star-shaped material with a pyrene core and four TPE arms (Figure 5-3 b).[214] Pyrene is a strong fluorophore in dilute solutions but in the condensed state its fluorescence is quenched by π-π stacking. Decoration of the molecule with AIE active TPEs turns it into a strong fluorescent material (Φ_{film} = 0.70). In dilute solution, the fluorescence of the pyrene core is not completely quenched by the molecular rotations of TPE, but the addition of water or lowering the temperature triggers a dramatic increase in PL intensity, the material being AIEE active rather than AIE as the parent TPE. They also constructed an OLED device with the material, obtaining even better efficiencies than with the commonly used Alq_3 emissive layer. TPA (Figure 5-3 c) and di-triphenylamine ((D)TPA) were also employed as cores of star-shaped materials containing three and four TPE peripheries respectively. Both materials present an AIE effect, with a PLQY around 40 % for their nanoaggregates in THF/water mixtures and up to 100 % in the film. The excellent hole transport properties of TPA are maintained in these materials, with the added bonus of a very efficient emission. This led to simplified OLED devices in which the materials acted both as the emissive and the hole transporting layer.[215] Li *et al.* reported the synthesis of a star-shaped

material with a benzothiadiazole (BT) core, a TPA spacer at either side and two perfipheral TPE units attached to each TPA (Figure 5-3 d).[216] The material presented strong red light emission with marked solvatochromism of the emission, leading to red-shifts and a reduction of the fluorescence intensity in high polarity solvents, due to the charge transfer nature of the emission of the materials containing donor TPA and acceptor BT units in conjugation. It also presented AIEE in water/DMF mixtures, obtaining a maximum PL enhancement with a 40 % water fraction. An OLED constructed employing the material as the emissive layer obtained the highest current and power efficiencies reported for red-emitting AIEE active materials up to that point.

TPE has also been used as a core in larger star-shaped materials. Tang's group reported the synthesis of a new AIE core with increased dimensionality from TPE by replacing the phenyl rings with naphthalenes (Figure 5-4 a).[217] The material still shows an AIE effect, but it is less dramatic than for TPE due to the greater size of the naphthalene, that enables a greater degree of π-π stacking in the condensed state. On the other hand, it shows enhanced thermal properties and carrier mobilities compared with TPE, which is translated into better EL performances. The same group recently reported a series of TPE-cored molecules coupled to TPE, spiro[bifluorene] and TPA arms (Figure 5-4 b, c and d respectively).[218] The compounds present very weak fluorescence in dilute solutions (but greater than the parent TPE core due to an increase in conjugation length) and PLQYs close to 100 % in the solid state. The materials are AIEE active in 1,4-dioxane/H_2O mixtures and present efficient green electroluminescence, performing better than pristine TPE or bisTPE as the emissive layer in OLEDs. Vyas and Rathore described the synthesis of a star-shaped *tetrakis*(oligo-*p*-phenylene)ethylene molecule which is effectively a TPE core with four ter-*p*-phenylene arms (Figure 5-4 e).[219] The increase in the number of phenylene rings triggers a bathochromic shift in the absorption properties of the materials and the emission intensity increases slightly, but is almost non existent due to deactivation *via* non-radiative pathways. In order to improve the emission properties of the material, they synthesised a new hindered analogue in which the central phenylene ring of a *tetrakis*(ter-*p*-phenylen)ethylene molecule was substituted with four extra phenyl rings (Figure 5-4 f).[220] Their aim was to block the intramolecular rotations *via* steric hindrance and reduce the C=C bond twisting in the excited state, which also leads to non-radiative decay pathways. The absorption spectrum presents characteristic features of TPE and hexaphenylbenzene, indicating poor conjugation between the arms and the core. The emission wavelength of the molecule is similar to its non-hindered parent, but the intensity is much greater, which leads to

the conclusion that the steric hindrance exerted by the phenyl substituents is enough to overcome the non-radiative decay pathways by restricting the intramolecular rotations.

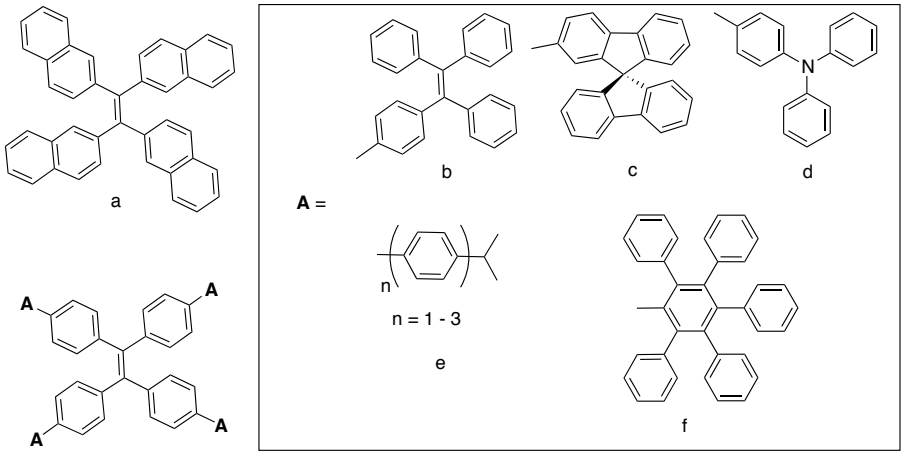

Figure 5-4 Some TPE- and anthracene-cored star-shaped molecules.

As already mentioned above, some AIE-active materials can undergo piezochromism upon the application of pressure. Tangs's group reported the synthesis of two AIE and crystalisation induced emission enhancement (CIEE) active molecules with mechanochromic properties (Figure 5-5 a and b).[221] The molecules are crystalline in nature and present efficient emission in the crystalline phase. Grinding the molecule yields an amorphous powder in which the emission is red-shifted and largely quenched. Re-heating the ground material in order to anneal it returns the fluorescence through re-crystallisation, and the process for turning on and off the fluorescence can be repeated many times. Furthermore, the compound with two phenyl substituents (Figure 5-5 a) shows a recovery of the emission at room temperature after three hours, indicating its great tendency to crystallise. This is very promising as a self-healing material. The replacement of one phenyl ring with a biphenyl substituent (Figure 5-5 b) stabilises the material in the amorphous phase, decreasing its self-healing potential. Li and co-workers described a series of materials with an anthracence core attached to two TPA moieties that are connected to TPE units through oligo-*p*-phenylene linkers (Figure 5-5 c).[222] The materials are AIE active and the only material that presents a certain degree of crystallinity (that with m = n = 2) shows piezofluorochromism. The emission spectrum suffers a 22 nm red-shift upon grinding the sample, which results in a colour change from yellow to orange. XRD confirms that the material presents a certain degree of crystallinity before the application of a mechanical force, but it is amorphous afterwards. The materials that were initally amorphous do not show this effect because grinding does not induce any conformational change of the

molecules. Park *et al.* published a very interesting report of piezochromism with AIE active distyrylbenzene-based molecules (Figure 5-5 d).[223] As yellow single crystals, the molecules arrange themselves in slip-stacks within planar molecular sheets and emit green light but, upon thermal annealing, the crystals turn blue transparent and emit in the blue region of the spectrum. This effect is due to a displacement of the sheets in the crystal lattice. Quick crystallisation from ethanol yields directly the blue crystals but, upon grinding, they undergo piezofluorochromism and return to the green-emissive conformation. Furthermore, thermal annealing of the ground crystals or exposure to solvent vapour turns the crystals into the blue-emissive state once more. Bu and co-workers have recently described the synthesis of three AIE materials with a central anthracene and ethylene-fluorene at either side (Figure 5-5 e).[224] The compounds differ in the length of the solubilising alkyl chain on the fluorene (C_3, C_5 or C_{12}) and present different degrees of piezofluorochromism with an increase in the length of the chain. The materials were ground together with KBr to dilute the chromophores and were pressed with a KBr press, undergoing a colour change that could be reversed by thermal annealing or exposure to solvent vapour. Furthermore, the compound with C_{12} chains underwent the greatest fluorescence shifts after the pressurisation and could self-recover the original colour due to its low melting point.

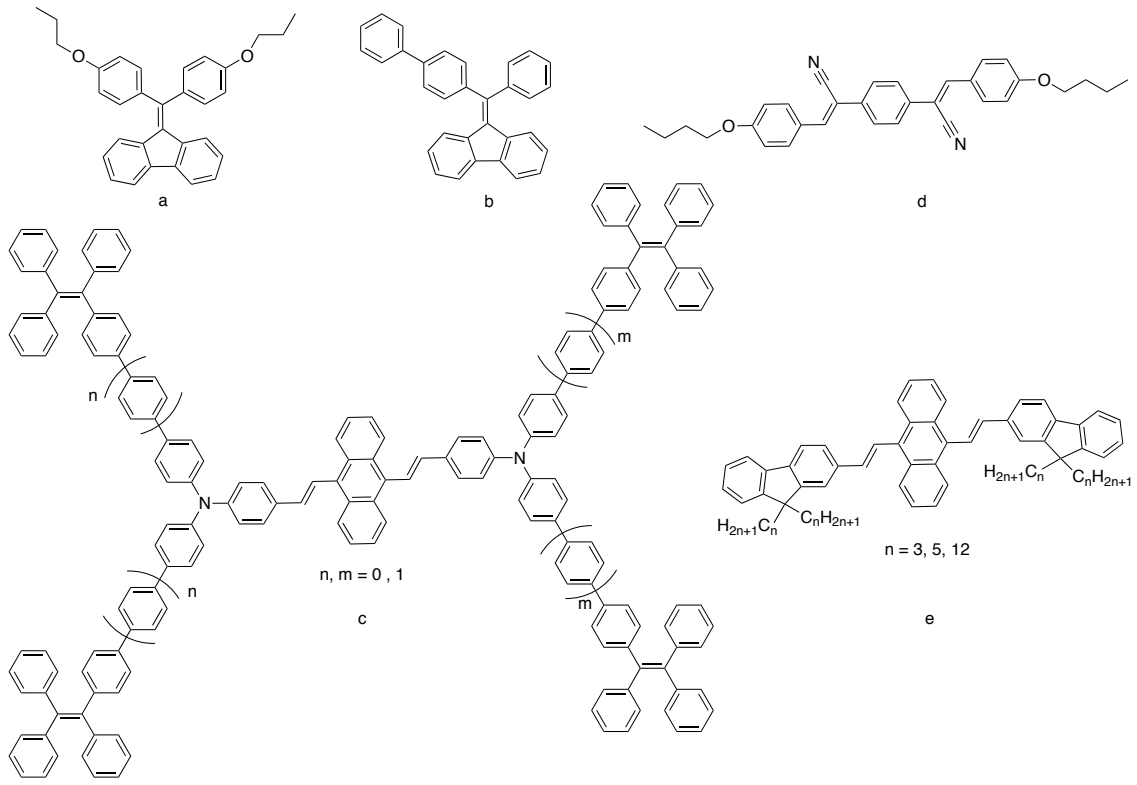

Figure 5-5 Some AIE-active molecules that undergo piezofluorochromism.

Following the interest in the fascinating phenomenon of AIE and monodisperse star-shaped architectures with oligofluorenes, two novel materials with a TPE core and mono- or quaterfluorene arms (**TPE1** and **TPE4**, Figure 5-6) were synthesised and their application in organic semiconductor lasers was tested.

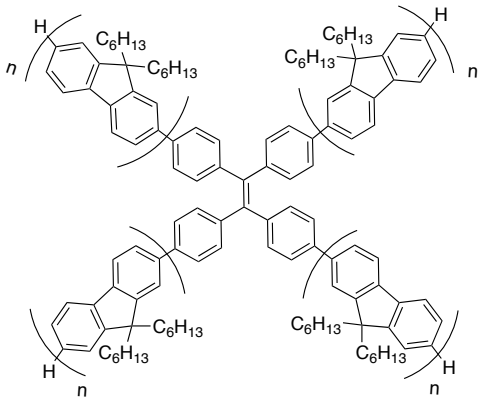

Figure 5-6 Structure of the star-shaped oligofluorene TPE molecules **TPE1** and **TPE4**.

5.3 Results and discussion

5.3.1 Synthesis

One of the outcomes of the research on the effect of the alkyl chain length in oligofluorene truxene molecules described in Chapter 0 was that, in general, the hexyl chains provide the best compromise between the ease of synthesis, the thermal properties and the photophysics for OSL applications. For these reasons, the hexyl chain was selected for the synthesis of the oligofluorene TPE analogues. The materials were synthesised in high yields (80 % for **TPE1** and 90 % for **TPE4**) following the modified Suzuki coupling procedure with barium hydroxide as base and $Pd(PPh_3)_4$ as catalyst (Scheme 5-1). Note that the synthesis of the quaterfluorene boronic acid **F_4' H** has previously been described in Chapter 4, **$TPEBr_4$** and **F_1' H** were kindly provided by colaborators (for more information, see Chapter 7).

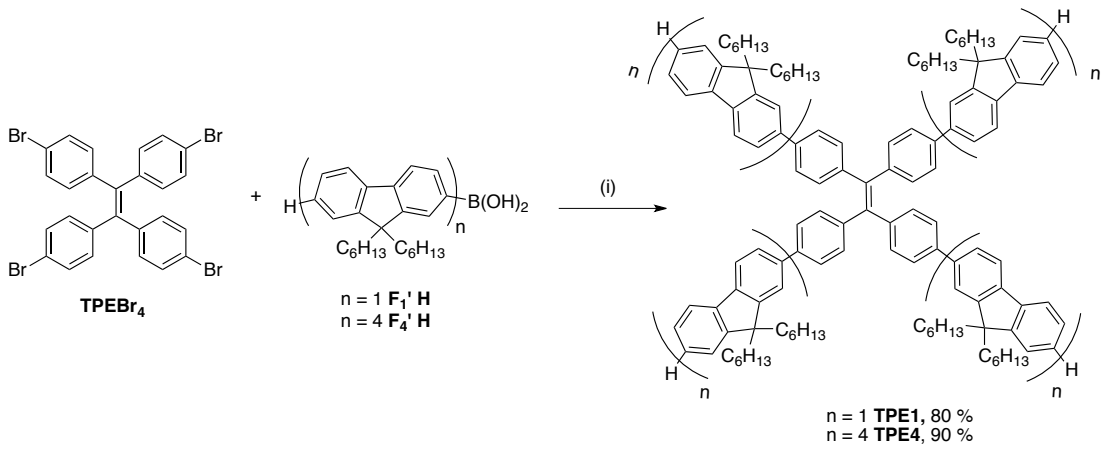

Scheme 5-1 Synthesis of the oligofluorene TPE analogues (**TPE1** and **TPE4**). Reagents and conditions: (i) $Pd(PPh_3)_4$, $Ba(OH)_2 \cdot 8H_2O$, THF, reflux, 18 h.

5.3.2 Physical and thermal properties

The materials were obtained as bright yellow powders in high purity and their physical properties are summarised in Table 5-1. Their thermal stability was assessed by thermogravimetric analysis, revealing that the compounds were stable above 400 °C. The decomposition temperature of **TPE4** was 32 °C higher than that of **TPE1** and its chemical robustness also seemed to be higher: **TPE1** suffered partial decomposition when its solution in the slightly acidic deuterated chloroform was left in an NMR tube overnight, while solutions of **TPE4** could stand for serveral days without showing any sign of decomposition. The DSC analysis of the materials revealed their amorphous character, which was confirmed by powder XRD measurements performed by Dr Fiona Coomer. The T_g of **TPE4** was 23 °C higher than that of **TPE1** due to the increase in molecular weight (almost 4000 $g \cdot mol^{-1}$ greater).

Table 5-1 Physical properties of the oligofluorene TPE compounds. M_w is the molecular weight of the compound, T_g is the glass transition temperature and T_m is the melting point as measured from differential scanning calorimetry (DSC). T_d is the decomposition temperature measured by thermogravimetric analysis (TGA).

Compound	M_w ($g \cdot mol^{-1}$)	T_g (°C)	Td (°C) [TGA, 5% mass loss]
TPE1	1662.52	82	438
TPE4	5652.78	105	470

5.3.3 Electrochemistry

The electrochemical properties of the materials were studied in ≈ 10^{-4} M solutions of the compounds in 1:2 acetonitrile:benzene in order to be able to observe the reduction peak, which was anticipated to be rather low, as it occurred in the oligofluorene truxene materials. The results are summarised in Table 5-2 and the oxidation voltammograms are presented in Figure 5-7. Both compounds present a first reversible peak around 0.90 V, probably associated with the oxidation of the central double bond, which is less stable towards oxidation than the aromatic fluorenes and phenylene spacers. **TPE4** has an extra reversible peak at 1.03 V due to the increased length of the oligofluorene arm, and both compounds present a third irreversible oxidation around 1.30 V. This last oxidation wave is probably due to overoxidation of the molecules, given the much greater current that it involves in both cases.

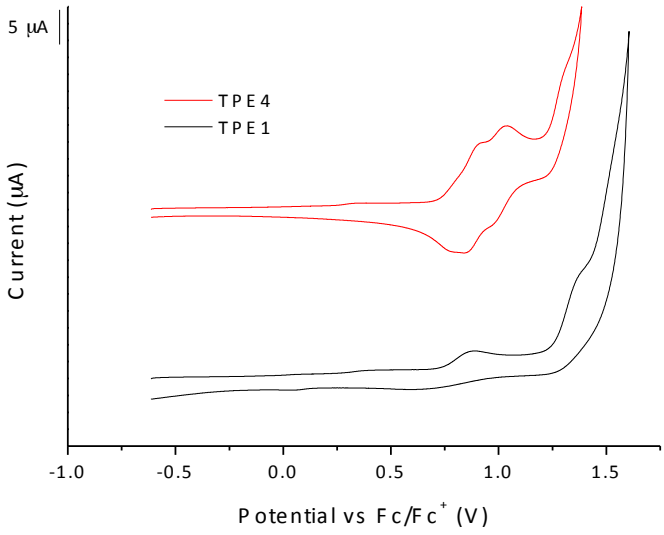

Figure 5-7 Oxidation waves of **TPE1** and **TPE4** in 1:2 acetonitrile:benzene. The cyclic voltammogram was obtained employing a glassy carbon working electrode, a platinum wire counter electrode and a silver wire reference electrode. All the waves were referenced to ferrocene.

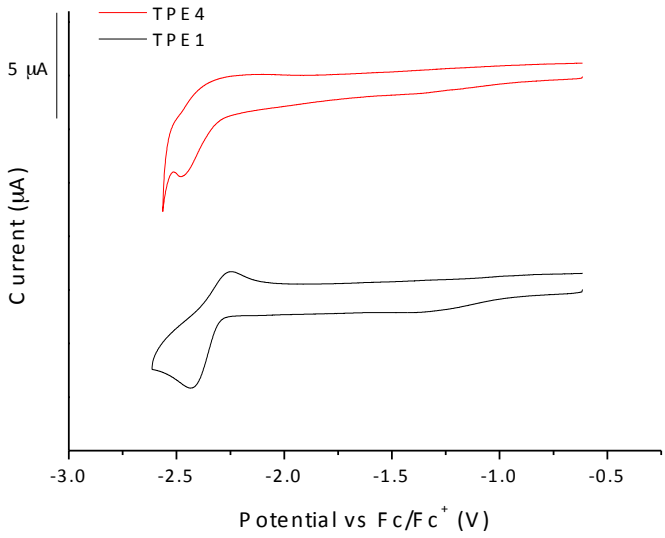

Figure 5-8 Reduction waves of **TPE1** and **TPE4** in 1:2 acetonitrile:benzene. The cyclic voltammogram was obtained employing a glassy carbon working electrode, a platinum wire counter electrode and a silver wire reference electrode. All the waves were referenced to ferrocene.

The reduction waves of the materials are presented in Figure 5-8. Both compounds present a single reduction wave at around -2.45 V, being quasi-reversible for **TPE1** and irreversible for **TPE4**. The low stability of the ethylene bond towards electrochemical processes suggests that the reduction also occurs on the TPE core.

Table 5-2 Electrochemical properties of the **TPE1** and **TPE4** compounds in dichloromethane. . [a] HOMO and LUMO levels were calculated from the onset of the corresponding redox wave and are referenced to ferrocene, which has a HOMO of -4.8 eV. [b] The electrochemical HOMO-LUMO gap ($E_{g,\,CV}$) is the energy gap between the HOMO and LUMO levels. The optical HOMO-LUMO gap ($E_{g,\,opt}$) is calculated from the onset of the red-edge of the absorption band (in brackets).

Compound	E_{ox} vs Fc/Fc^+ (V)	HOMO[a] (eV)	E_{red} vs Fc/Fc^+ (V)	LUMO[a] (eV)	$E_{g,\,CV}$[b] (eV)	$E_{g,\,opt}$[b] (eV)
TPE1	0.87, 1.35	-5.52	-2.43	-2.50	3.02	2.95 (421)
TPE4	0.91, 1.03, 1.30	-5.52	-2.47	-2.49	3.03	3.01 (413)

There is good agreement between the optical and electrochemical HOMO-LUMO gaps of both compounds, which barely differ despite the increase in the length of the oligofluorene arm. This is a further indication that the HOMO and the LUMO are primarily located on the TPE core.

5.3.4 Optical properties

The optical properties of the materials were initially studied in 1:2 acetonitrile:benzene in order to compare the optical and electrochemical bandgaps measured in the same solvent. The properties were also assessed in several concentrations of the materials in dichloromethane, hexane and tetrahydrofuran, to study whether the materials presented solvatochromism. The normalised absorption and emission spectra of the compounds in dichloromethane are presented in Figure 5-9 but the rest of the spectra have been omitted because the shapes of the bands are similar and it does not provide any additional information. The absorption and emission properties obtained in different solvents and in films of the materials dropcast from 20 mg·mL^{-1} solutions in toluene are summarised in Table 5-3 and Table 5-4 respectively.

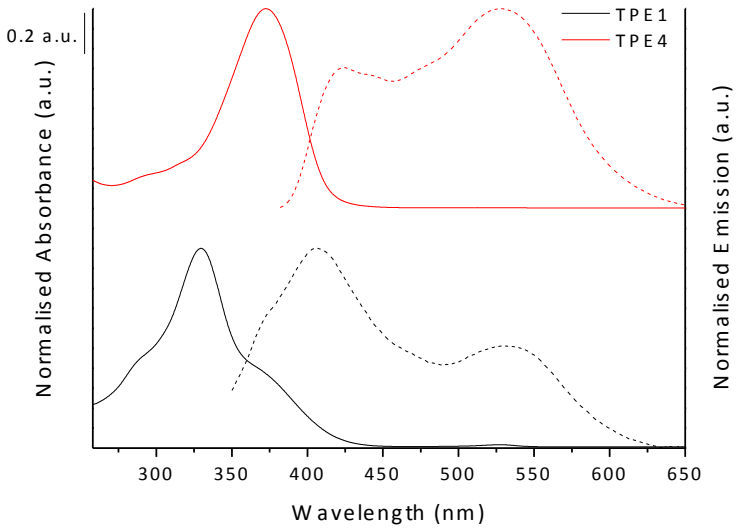

Figure 5-9 Absorption (solid line) and emission (dashed line) spectra of the **TPEn** compounds measured in ≈ 10^{-6} M solutions of the compounds in dichloromethane. λ_{ex} (**TPE1**) = 330 nm, λ_{ex} (**TPE4**) = 370 nm.

TPE1 presents a broad absorption band centred at 329 nm with a shoulder at either side (at 287 nm and 371 nm respectively). The short wavelength shoulder corresponds to the absorption of the TPE core,[225] the maximum of absorption is related to the absorption of the fluorenylphenylene units independently and the long wavelength shoulder is derived from the absorption of the whole conjugated molecule. On the other hand, the absorption band of **TPE4** (λ_{max} = 373 nm) is broad and featureless, probably dominated by the π-π* transition of the much longer quaterfluorenephenylene moieties. Furthermore, there is a considerable

bathochromic shift in the absorption of both materials (44 nm) associated with the increase in the conjugation length of the materials. This also affects the molar absorptivity of **TPE4**, whose logarithm increases from 5.08 to 5.76 as there are twelve more chromophores per molecule that can absorb UV light. It is worth noting that **T1** had a greater value for the logarithm of its molar absorptivity (5.27) probably attributable to the greater absorption efficiency of the truxene core, but the value for **T4** (5.41) is lower than that of **TPE4** because the effect of one extra quaterfluorene arm is greater than that of the core. The positions of the absorption bands in both families of compounds are comparable because the absorption is associated with the π-π* of the oligofluorenes. In the case of **TPE1**, the influence of the TPE core in the absorption profile can only be observed in the shoulder at 287 nm that both of them share, but the maximum of absorption of TPE (320 nm) is embedded within the absorption band of the fluorenes(330 nm).[225] In the case of **TPE4**, only a small shoulder can be observed at 320 nm, but its absorption is negligible in comparison with the absorption band associated with the quaterfluorenes. The position of the absorption band is also comparable with that obtained by Aldred *et al.* for their linear oligofluorenes endcapped with two TPEs (353 nm for the monofluorene analogue and 370 nm for the quaterfluorene analogue).[100] The greater deviation in the case of their monofluorene analogue could be due to the greater percentage of TPE in that molecule compared with **TPE1**, where there is only one TPE moiety and four fluorenes.

Table 5-3 Absorption properties of **TPE1** and **TPE4**.

Property	TPE1	TPE4
$\lambda_{abs,\ Benzene:MeCN}$ (nm)	288, 330, 372	372
$log(\varepsilon)_{Benzene:MeCN}$	5.04	5.74
$\lambda_{abs,\ CH2Cl2}$ (nm)	287, 329, 371	373
$log(\varepsilon)_{CH2Cl2}$	5.08	5.76
$\lambda_{abs,\ hex}$ (nm)	284, 327, 373	368
$log(\varepsilon)_{hex}$	4.99	5.79
$\lambda_{abs,\ THF}$ (nm)	286, 330, 374	373
$log(\varepsilon)_{THF}$	5.12	5.74
$\lambda_{abs,\ film}$ (nm)	288, 329, 384	370

The emission of the materials in solution is poor due to non-radiative decay associated with the rotation of arms around the ethene central bond (the maximum intensity obtained for

both compounds was around 50 a.u. in 10^{-6} M solutions and the increase in concentration of the solutions did not have an associated increase in fluorescence intensity). For both compounds, two emission bands are observed, one around 400 nm associated with the emission of fluorenes and a second one that appears around 530 nm for both compounds. Interestingly, at low concentrations (up to ≈ 10^{-6} M) the fluorene band dominates the spectrum and as the concentration of the materials increases, the intensity of this band diminishes and the red-shifted band becomes dominant (at around $6{\cdot}10^{-5}$ M). This might be a consequence of a greater degree of aggregation of the molecules in concentrated solutions. The longer wavelength emission band cannot be attributed to an energy transfer to the TPE core since the emission of the oligofluorenes, which occurs in the region of 400 - 470 nm, does not overlap with the absorption of the core (320 nm). Furthermore, this emission is red-shifted with respect to the fluorescence of TPE (its reported emission wavelength in the crystal is 453 nm)[225] and with that of the oligofluorenes. It can therefore be attributed to the emission of the whole molecule in which the conjugation length has been elongated with the arms conjugated through the core. This emission wavelength is comparable to those obtained by Aldred and co-workers for the linear oligofluorene-TPEs[100] and by Tang *et al.* for analogous TPE-cored star-shaped materials with spiro[bifluorene] and triphenylamine (≈ 530 nm).[218]

Table 5-4 Emission properties of **TPE1** and **TPE4**.

Compound	$\lambda_{em,Benzene:MeCN}$ (nm)	$\lambda_{em,DCM}$ (nm)	$\lambda_{em,hex}$ (nm)	$\lambda_{em,THF}$ (nm)	$\lambda_{em,film}$ (nm)	Φ_{powder}
TPE1	368, 410, 510	408, 530	401, 543	543	513	0.29
TPE4	508	423, 528	534	527	508	0.77

The Stokes shift between the absorption and emission can be calculated taking into consideration both emission bands, since their intensity can be modulated with the concentration of the solution. For **TPE1**, the Stokes Shift is 79 nm considering the fluorene emission band and 201 nm taking into consideration the longer emission wavelength. For **TPE4**, the Stokes shifts are reduced but they are still considerably large (50 nm and 155 nm respectively). The compounds barely offer any solvatochromism as can be observed in Table 5-3 and Table 5-4. They only experience small hypsochromic shifts in their absorption in hexane since the less polar solvent can increase the energy of the π* level. On the other hand, the emission in hexane occurs at slightly longer wavelengths. A similar event occurred for the linear oligofluorene TPEs previously described,[100] and the authors postulated that the cause

could be an increased planarisation of the TPE molecules in the excited state in hexane solution.

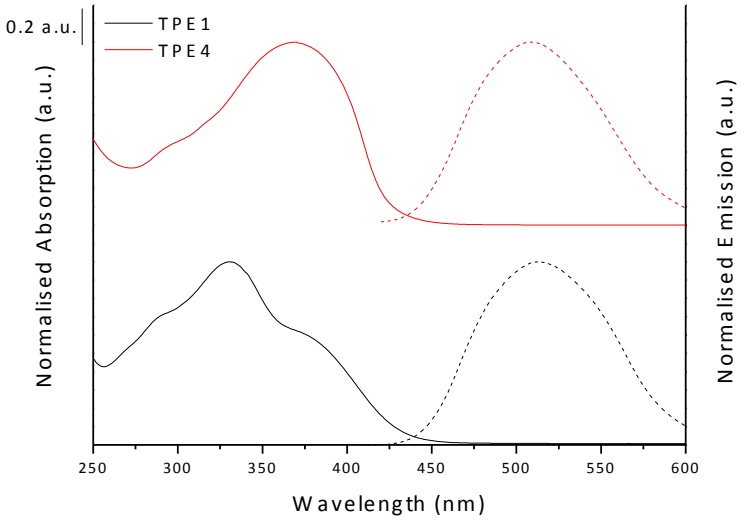

Figure 5-10 Absorption (solid line) and emission (dashed line) spectra of the **TPEn** compounds measured in films dropcast from 10 mg·mL^{-1} toluene solutions. λ_{ex} (**TPE1**) = 330 nm, λ_{ex} (**TPE4**) = 370 nm.

The absorption and emission spectra of films of the materials dropcast from 20 mg·mL^{-1} solutions in toluene are presented in Figure 5-10. The profiles of the absorption bands follow the same pattern as in solution but are slightly broader. The position of the absorption barely changes (it is maintained for **TPE1** and hypsochromically shifted by only 3 nm for **TPE4**). Interestingly, the emission profile does not show any hint of fluorescence from the isolated arms and only one broad symmetric band is obtained for both compounds. The position of this band is hypsochromically shifted for both compounds with respect to the solution emission profile, 17 nm for **TPE1** and 20 nm for **TPE4**, considering the emissions in dichloromethane. This shift is even greater if the emissions in hexane or tetrahydrofuran are taken into account (30 nm for **TPE1** and 26 nm for **TPE4**). Planarisation of the structure in the excited state leads to bathochromic shifts in the emission. In solution, the twisted TPE moieties have a greater freedom of movement and probably can achieve a greater degree of planarisation than in the film, where there is a spacial constraint, which would explain the shorter emission wavelengths obtained in the films. The Stokes shift in the film is considerable (184 nm for **TPE1** and 138 nm for **TPE4**) and the absorption and emission profiles present barely any overlap. The PLQYs of powders of the materials were recorded at the Max Planck Centre for Colloids and Interfaces (Potsdam). The quantum efficiency of **TPE1** is moderate and only slightly higher that of the TPE core (Φ_{film} = 0.25).[225] This rather low value is surprising because Tang and co-

workers reported a PLQY of 0.93 for a similar system with TPE core and four spiro[bifluorene] peripheries.[218] The quantum yield is significantly enhanced in **TPE4** (0.77) in comparison with **TPE1**, but it is still lower than that of the spiro[bifluorene]-substituted TPE. It is worth mentioning that the PLQY of **TPE4** was also measured on a 70 nm thick film of the material at St Andrews University and the obtained value was comparable with that of the powder (0.70). The emission is dramatically enhanced for both **TPE1** and **TPE4** in the condensed state due to the RIR effect and the molecules are therefore AIEE active.

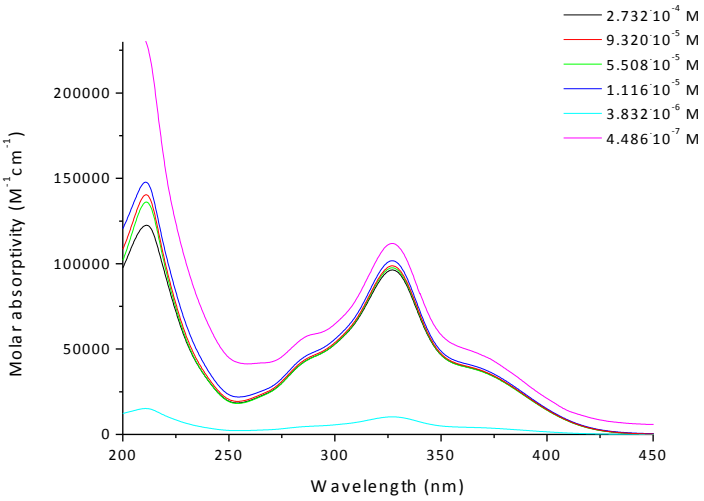

Figure 5-11 Concentration studies of **TPE1** in hexane**.**

In order to clarify whether the molecules suffer any degree of aggregation in solution, concentration studies in hexane were performed, because the conjugated materials have a greater tendency to aggregate in hexane than in more polar solvents such as dichloromethane. The results for **TPE1** are presented in Figure 5-11 and for **TPE4** in Figure 5-12. The molar absorptivity and the shape of the absorption band for both compounds are largely unnaffected at high concentrations indicating that the molecules do not suffer aggregation. The only deviations observed occur at very low concentrations, probably due to the sensitivity of the spectrophotometer at such low concentrations.

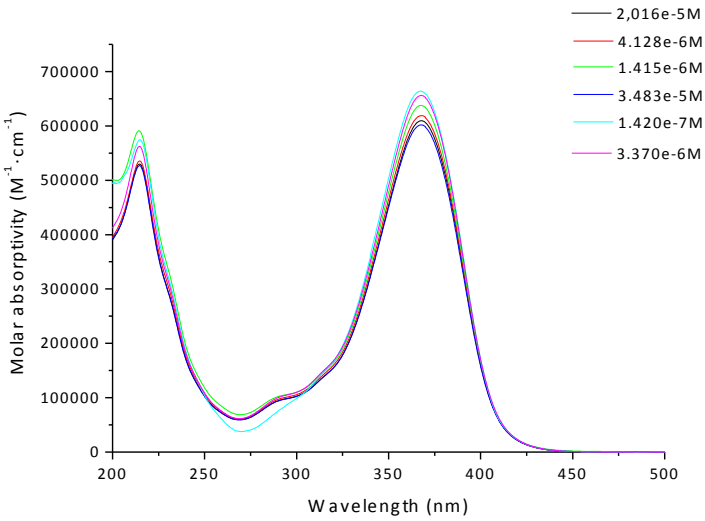

Figure 5-12 Concentration studies of **TPE4** in hexane.

5.3.5 Aggregation induced enhanced emission (AIEE)

As already discussed above, **TPE1** and **TPE4** experience an enhancement of their emission in the condensed state that is due to the RIR effect in a constrained environment. Their AIEE in THF:H_2O solutions was also tested, where the concentration of the molecules was kept constant but the fraction of water in the mixture was increased stepwise. The effect was tested at 10^{-5} M, $5{\cdot}10^{-7}$ M and $2{\cdot}10^{-8}$ M. The AIEE was observed at all concentrations but the degree of emission enhancement is reduced at $2{\cdot}10^{-8}$ M because at that concentration the number of molecules that can aggregate is reduced. Note that only the most representative results (10^{-5} M) are presented here. The AIEE effect can be visually observed in Figure 5-13 a (for **TPE1**) and b (for **TPE4**). The solutions of the materials with increasing water fractions are placed from right to left. The solutions of **TPE1** in THF are barely emissive and their fluorescence is only boosted when 50 % of water is added to the solvent mixture. The fluorescence becomes brighter up to 80 % water content and it then decreases at 90 % water. **TPE4** also shows an enhancement of its emission that can be observed at only 20 % water content, being brighter and greener (rather than yellow) at 30 – 70 % water contents, before it decreases again upon the addition of greater amounts of water to the mixture. The solutions that present AIEE become turbid, especially for **TPE4**, but no precipitation or obvious agglomerates can be observed with the naked eye. The effect is probably due to the formation of nanoaggregates in which the **TPEn** molecules are forced to be close to each other,

restricting the intramolecular rotations of the phenyl rings around the central double bond upon the addition of water.

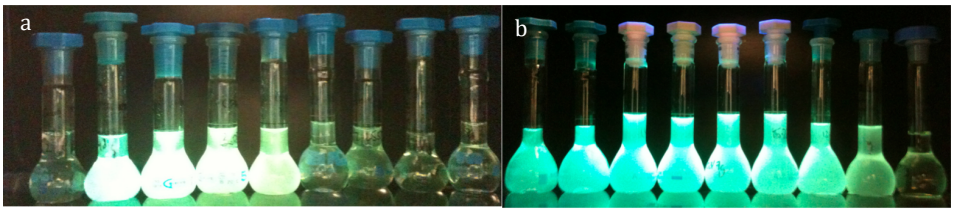

Figure 5-13 10 µM solutions of **TPE1** (a) and **TPE4** (b) in THF:H_2O mixtures with increasing water fractions under UV illumination. From right to left 10 %, 20 %, 30 %, 40 %, 50 %, 60 %, 70 %, 80 % and 90 % water in THF.

The absorption spectra of 10^{-5} M solutions of **TPE1** in different water:THF mixtures is presented in Figure 5-14. The spectra of the solutions with up to 40 % water content do not change compared to the pure THF solution. Nevertheless, the addition of 50 % water to the mixture triggers a sudden lowering in the absorption intensity and broadening of the profile (the area of absorption is actually larger), accompanied by a bathochromic shift of all the peaks and an increase in the intensity of the shoulder located at the red-edge of the absorption maximum. Moreover, the absorption profile levels off from the baseline at longer wavelengths. This is known as the Mie effect, and it is caused by the diffraction of light by particles of similar size as the wavelength of the incident radiation.[100] All of these effects are an indication of the formation of nano-aggregates in the solution. At greater water fractions, the absorption spectra also reveal the presence of nanoparticles, but they are possibly smaller or less abundant because the absorption profiles become more similar to the ones obtained for the non-aggregated state.

The emission spectra of the same solutions (Figure 5-15) are very faint (10 a.u.) up to the addition of 40 % of water to the mixture but they increase in intensity with greater additions of water, being maximised at 80 % water fraction. Interestingly, the emission maxima suffer a slight hypsochromic shift with the increase of the water content, which could be due to the formation of clusters or crystals in which the geometry of the molecules is more twisted due to spacial constraint. The fact that the emission of the aggregates does not suffer bathochromic shifts could be an indication that the molecules do not form excimers through π-π stacking, which typically show red-shifted emissions.

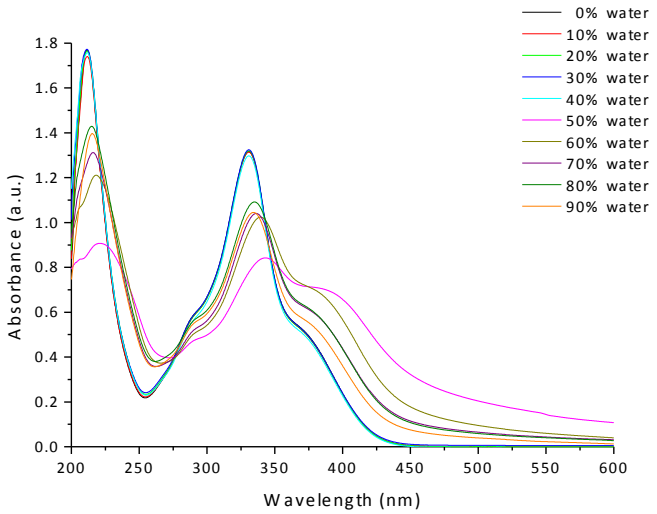

Figure 5-14 Absorption spectra of 10^{-5} M solutions of **TPE1** in THF:H_2O mixtures with increasing water fraction for the AIEE studies.

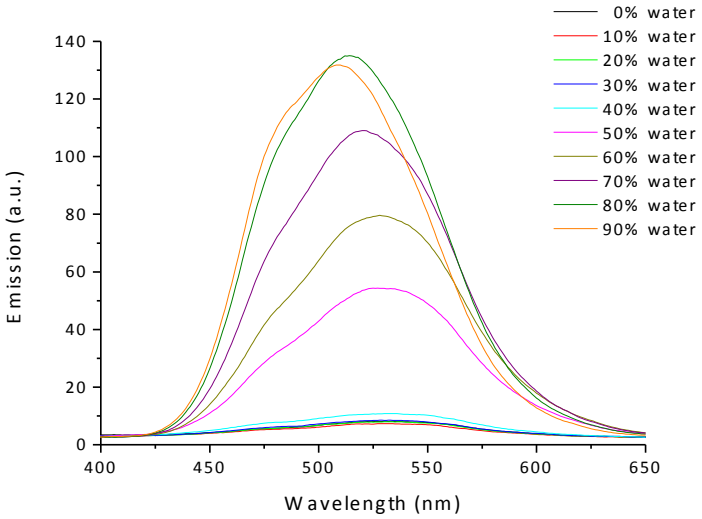

Figure 5-15 Emission spectra of 10^{-5} M solutions of **TPE1** in THF:H_2O mixtures with increasing water fraction for the AIEE studies. λ_{ex} = 330 nm.

The absorption spectra of 10^{-5} M solutions of **TPE4** in in water:THF mixtures with increasing water fractions is presented in Figure 5-16. In this case the addition of 20 % water is enough to trigger the nanoaggregate formation, which is again associated with the Mie effect, and a broadening of the absorption profile accompanied by a decrease in its intensity. **TPE4** is much larger than **TPE1** and it contains 32 hexyl chains *versus* the 8 hexyl chains present in **TPE1**. This confers **TPE4** with a more non-polar character and the addition of a small portion of a polar

solvent such as water triggers the formation of clusters or vesicles where the molecules lay next to each other solvated by THF.

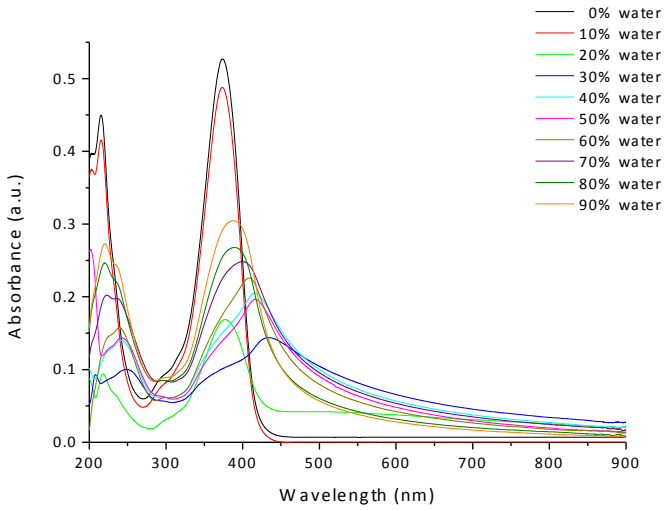

Figure 5-16 Absorption spectra of 10^{-5} M solutions of **TPE4** in THF:H_2O mixtures with increasing water fractions for the AIEE studies.

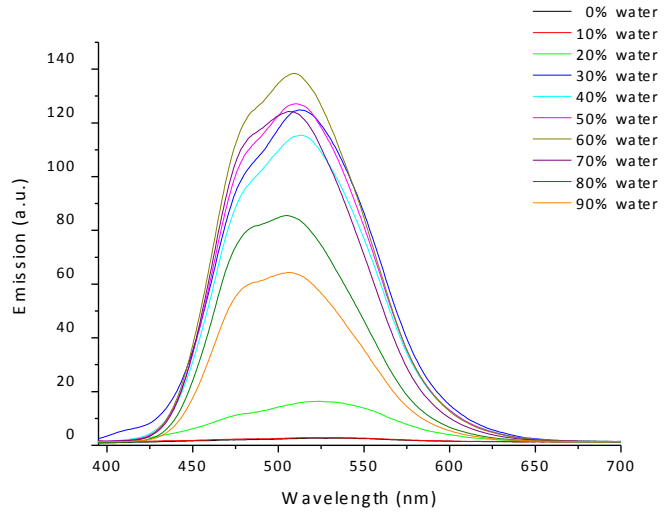

Figure 5-17 Emission spectra of 10^{-5} M solutions of **TPE4** in THF:H_2O mixtures with increasing water fractions for the AIEE studies. λ_{ex} = 370 nm.

The emission spectra of the same solutions (Figure 5-17) do not show a linear tendency in PL enhancement. Only 20 % of water is enough to increase the fluorescence of the solution slightly, but the addition of 30 % of water triggers a great leap of the emission intensity, which then decreases slightly at 40 % water, and increases once more at 50 % and 60 %, to then fall

back again at 70 %, 80 % and 90 % water content. The same AIEE experiments performed on $5 \cdot 10^{-7}$ M solutions provided reproducible results in the emission enhancement for **TPE1,** but for **TPE4** there was less fluctuation than at 10^{-5} M and the increase in the intensity was more linear, being maximised at 80 % water content. When the absorption and emission spectra of solutions aged for one month were recorded, there was little variation in their profiles or intensities, indication that the particles that are formed are stable over time. In order to obtain further information about the size of the nano-aggregates formed at each water fraction, dynamic light scattering (DLS) measurements of the solutions are currently being recorded by Dr Filipe Vilela at Max Plank Centre for Colloids and Interfaces in Potsdam.

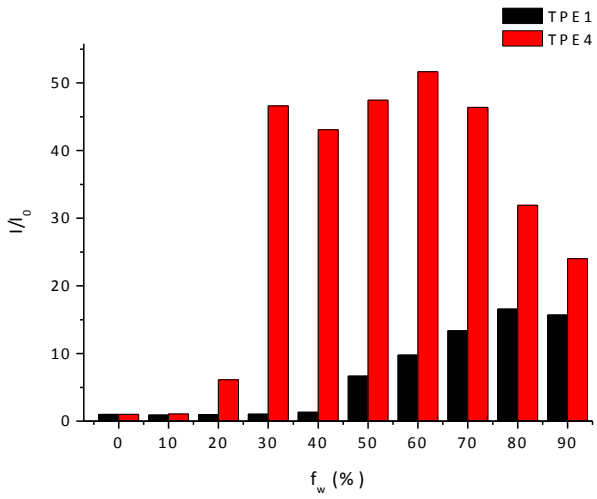

Figure 5-18 Intensity of emission (I) relative to the intensity of emission of the **TPEn** materials in pure THF solution (I_0) *versus* the water fraction (f_w).

The AIEE effect is commonly represented as the fluorescence intensity of each solution relative to that of the solution with 0 % water fraction. Such representation for **TPE1** and **TPE4** is shown in Figure 5-18. It is clear that the AIEE is much greater for **TPE4** than for **TPE1** and the enhancement starts at 20 % water and is maximised at 60 % water fraction, as already discussed above. For **TPE1** the enhancement starts at 50 % water fraction and has a maximum with 80 % water content. Nevertheless, it seems that this representation does not consider the whole effect because the amount of light that a sample emits is related to the amount it absorbs, and therefore the emission should be calibrated with the absorptivity of the system at the wavelength of excitation to account for the formation of nanoaggregates. For this reason, Figure 5-19 should be a better representation of the AIEE effect as it accounts for the area of emission and the molar absorptivity of the aggregates in the solutions. According to

this representation, the AIEE effect for **TPE1** is maximised at 90 % water fraction, whereas the enhancement for **TPE4** is maximum at 30% water content and the effect decreases at greater water fractions. The overall enhancement of emission is greater for **TPE4**, which experiences a 91.5 fold increase in the emission for the 30 % water fraction, compared to the pure THF solution. On the other hand, the calibrated emission of the 90 % water fraction solution of **TPE1** is 11.6 times more intense than that in pure THF.

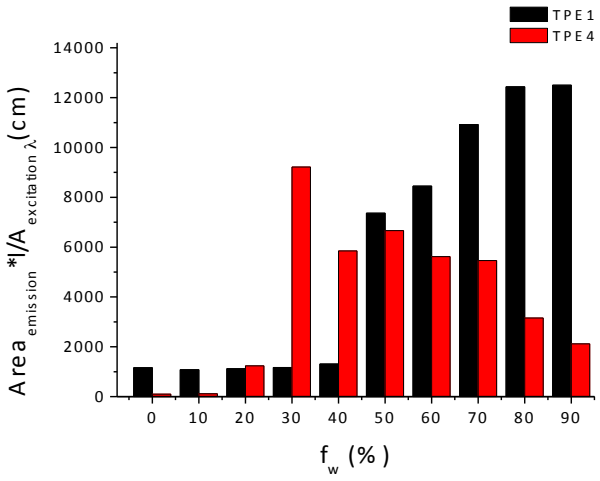

Figure 5-19 Area under the emission curve ($A_{emission}$) relative to the absorbance at the excitation wavelength ($A_{excitation\ \lambda}$)/pathlength (l) for the **TPEn** materials *versus* the water fraction (f_w).

In order to determine the efficiency of emission of the aggregates of **TPE1** and **TPE4**, the PLQY of the solutions that trigger the greatest enhancement of emission was determined. Due to the lack of a fluorimeter with an integrating sphere, the PLQY was determined employing Equation 5-1, and quinine sulphate in 0.05 M H_2SO_4 (aq) as a standard. The refractive indexes of the different THF:water mixtures and that of the 0.05 M H_2SO_4 solution were measured with a refractometer obtaining good reproducibility of the tabulated values of pure water and THF (see Table 5-5). The refractive indexes are also needed for the determination of the particle size by DLS.

$$\boldsymbol{\Phi(\lambda_{ex})} = \frac{\int \boldsymbol{I_d^*(\lambda_{ex},\lambda_{ex})d\lambda_{em}}\ \boldsymbol{\phi_{st}}(\mathbf{1}-\boldsymbol{e^{-\alpha_{st}(\lambda_{ex})d\lambda_{ex}}})}{(\mathbf{1}-\boldsymbol{e^{-\alpha(\lambda_{ex})d\lambda_{ex}}})\int \boldsymbol{I_{d,st}^*(\lambda_{ex},\lambda_{ex})d\lambda_{em}}} \frac{\boldsymbol{n_{sample}^2}}{\boldsymbol{n_{st}^2}} \qquad \textbf{Equation 5-1}$$

where Φ is the PLQY, $\int I_d^*(\lambda_{ex},\lambda_{ex})d\lambda_{em}$ is the area of the emission spectrum, $-\alpha(\lambda_{ex})d\boldsymbol{\lambda}_{ex}$corresponds to the absorbance at the excitation wavelength ($A(\lambda_{ex})$) and *n* is the refractive index of the solvent. Note that "st" represents the standard, in this

case quinine sulphate. The PLQY of quinine sulphate measured with an integrating sphere on a 10^{-5} M solution in 0.05 M H_2SO_4 (aq) was reported to be 0.60 ± 0.02.[226]

Table 5-5 Refractive index (*n*) of the different solvent mixtures employed in the AIEE studies.

Solvent mixture	*n*
THF	1.407
10 % H_2O:THF	1.403
20 % H_2O:THF	1.397
30 % H_2O:THF	1.392
40 % H_2O:THF	1.385
50 % H_2O:THF	1.376
60 % H_2O:THF	1.369
70 % H_2O:THF	1.361
80 % H_2O:THF	1.352
90 % H_2O:THF	1.343
H_2O	1.333
0.05 M H_2SO_4 in H_2O	1.334

In order to obtain a reliable PLQY value, the absorption and emission spectra of a series of solutions of the quinine sulphate standard in 0.05 M H_2SO_4 (aq) and the analytes (**TPE1** and **TPE4**) in 80 % and 60 % water fractions respectively were recorded. The concentrations of the solutions had to be such that the absorbance lay between 0.02 and 0.2 in order to avoid re-absorption of the emission, which could lead to deviations from linearity in a representation of the area of emission versus $1\text{-}10^{A(\lambda ex)}$. Such representations are shown in Figure 5-20, Figure 5-21 and Figure 5-22 for quinine sulphate, **TPE1** and **TPE4** respectively. The representations present a good linearity except for **TPE4**, which deviates from linearity from the fifth datapoint, probably due to the formation of aggregates at higher concentrations.

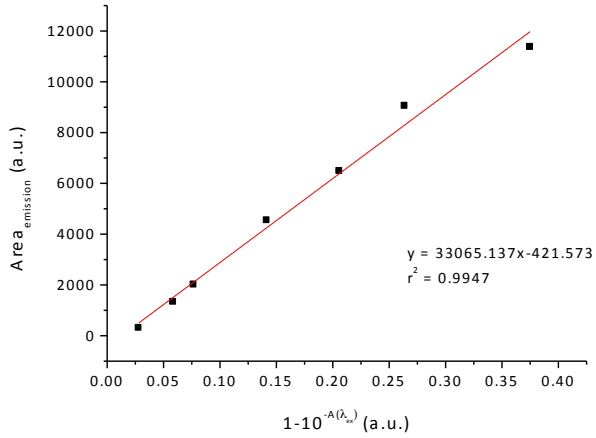

Figure 5-20 Relationship between the area of emission and $1\text{-}10^{A(\lambda ex)}$ of quinine sulphate solutions of different concentrations in 0.05 M H_2SO_4 (aq).

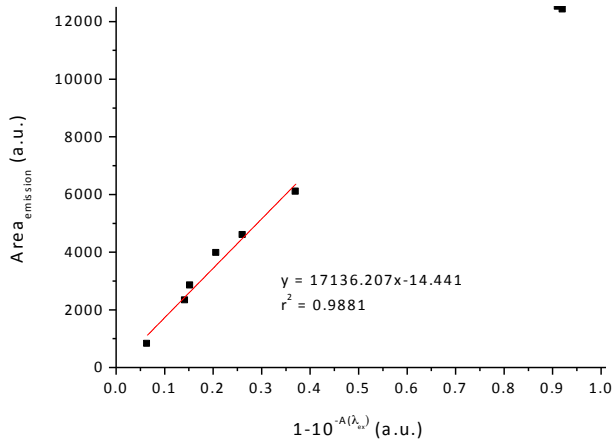

Figure 5-21 Relationship between the area of emission and $1\text{-}10^{A(\lambda ex)}$ of **TPE1** solutions of different concentrations in 80 % H_2O:THF mixtures.

The PLQYs of **TPE1** and **TPE4** at 80 % and 60 % water fractions respectively were obtained from Equation 5-1 (Φ_{TPE1} = 0.32 and Φ_{TPE4} = 0.31). The determination of the PLQY by this method is too time consuming to perform on ten solutions for each compound and it is also prone to the introduction of errors. An absolute determination of the PLQY of each solution using an integrating sphere would be much more beneficial and it will be performed alongside the DLS studies. Nevertheless, a rough approximation of the PLQYs for each solution can be obtained taking into account the measured PLQYs of **TPE1** and **TPE4** at 80 % and 60 % water content respectively and the relative AIEE obtained for the solutions at each water fraction. These approximated PLQY values are presented in Table 5-6 and give an idea of the enhancement of the emission that these molecules can undergo in the condensed state.

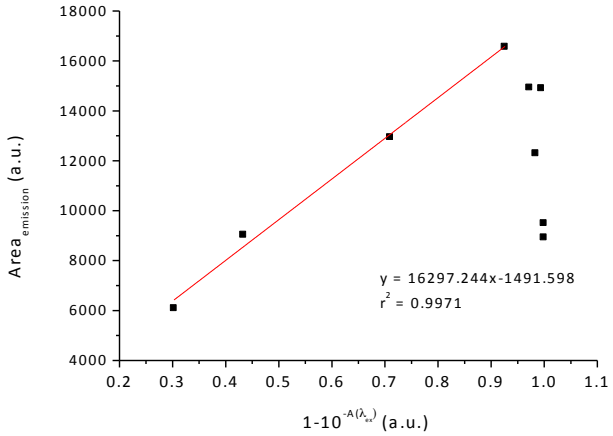

Figure 5-22 Relationship between the area of emission and $1\text{-}10^{A(\lambda ex)}$ of **TPE4** solutions of different concentrations in 60 % H_2O:THF mixtures.

Table 5-6 Approximated photoluminescence quantum efficiencies (Φ) for **TPE1** and **TPE4** in the different water:THF mixtures (f_w is the fraction of water in the mixture).

f_w (%)	Φ_{TPE1}	Φ_{TPE4}
0	0.03	0.01
10	0.03	0.01
20	0.03	0.07
30	0.03	0.51
40	0.03	0.32
50	0.19	0.37
60	0.22	0.31
70	0.28	0.30
80	0.32	0.17
90	0.32	0.12

5.3.6 Photophysical, lasing and pressure studies

In order to test the suitability of the materials for lasing applications, Caroline Foucher developed a series of lasing studies at the Institute of Photonics (IoP) in the University of Strathclyde. The first test consisted of determining whether the materials undergo spectral narrowing of their PL spectrum associated with ASE. Solutions of the materials (30 $mg{\cdot}ml^{-1}$) in tetrahydrofuran were spin-coated at 1000 rpm for one minute onto acetate sheet substrates covered with an epoxy (NOA65) and the films were left to dry at room temperature overnight.

Stripes of the films (0.29x2.79 mm) were pumped with a Q-switched laser at 355 nm. Surprisingly, **TPE4** did not show ASE despite its much greater PLQY, probably due to the non-ideal excitation wavelength. After multiple optimisation efforts, the material was sent to St Andrews University, where studies with a more suitable excitation laser are currently being performed. **TPE1**, on the other hand, showed ASE narrowing around 510 nm with a 13.09 µJ average pumping threshold (Figure 5-23) corresponding to a 719.5 µJ·cm^{-2} fluence threshold. It should be noted that the pumped stripe is not a perfect rectangle but a Gaussian distribution and the fluence is calculated taking into account the pumping threshold and the dimensions of the pumped stripe:

$$A = \frac{ln2*2*F_{th}(avg)}{\pi*0.029*0.279} \qquad \textbf{Equation 5-2}$$

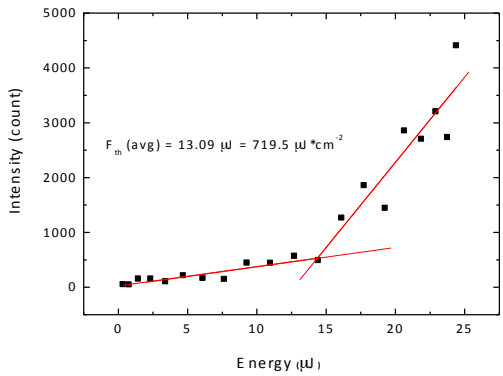

Figure 5-23 ASE threshold measurement for **TPE1** pumping 1.82·10^{-2} cm^2 stripes on films of the material at 355 nm.

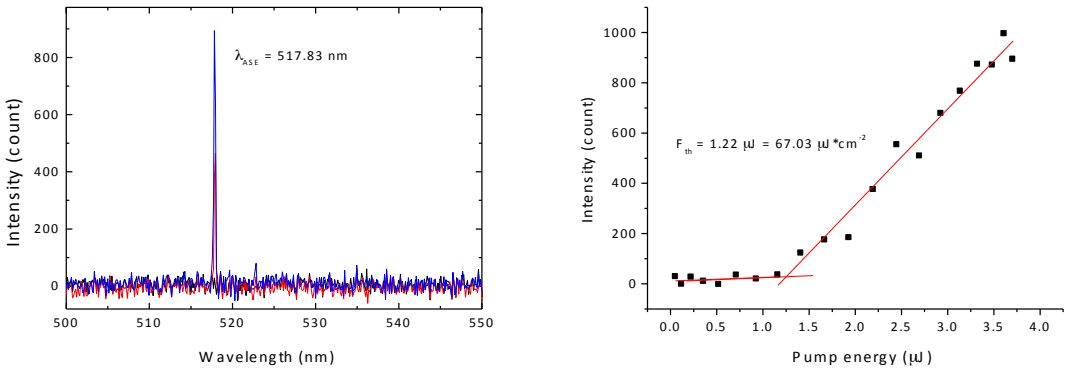

Figure 5-24 TPE1 lasing spectrum (left) and threshold determination (right) measured pumping 1.82·10^{-2} cm^2 stripes on 110 ± 10 nm thick films of the material at 355 nm.

Lasers of **TPE1** were developed by spin-coating 30 mg·mL^{-1} solutions of the material at 4000 rpm for one minute onto an epoxy grating (NOA65) with 330 nm periodicity (Λ). The thickness of the films under these spin-coating conditions was 110 ± 10 nm (measured by AFM). Maintaining the same pumping conditions as for the ASE experiment, a single mode laser emitting at 517.83 nm and an average lasing threshold uniform across the surface of the laser of 60.1 μJ·cm^{-2} was obtained (see Figure 5-24).

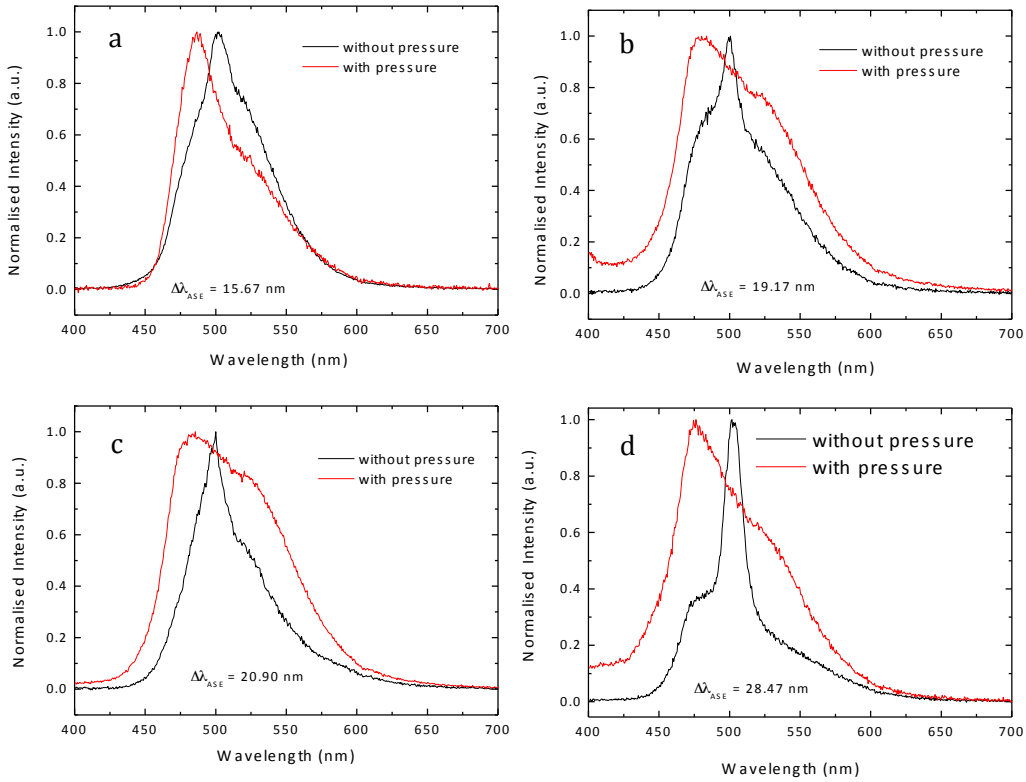

Figure 5-25 Piezofluorochromic studies performed on the ASE of films of **TPE1** applying pressure with a manual hydraulic press on the film for 1 minute. The pressures applied on 1 cm^2 films and the associated spectral shifts of the ASE peaks were the following: (a) 1.90 N·m^{-2}/15.67 nm, (b) 2.45 N·m^{-2}/19.17 nm, (c) 2.94 N·m^{-2} /20.90 nm, (d) 4.90 N·m^{-2}/28.47 nm.

Given the fact that the **TPEn** materials are AIEE active and this class of materials sometimes presents piezofluorochromic behaviour, as discussed in the introduction, a series of studies were carried out in order to determine the effect of pressure on the ASE of **TPE1**. Initially, the spin-coated films were subjected to different pressures with an old manual hydraulic press. The ASE of the films was measured before and just after the application of pressure and a hypsochromic shift that increased with the applied pressure was observed (Figure 5-25). The blue shift might be related to the greater constraint of the molecules within a pressurised film, leading to a less planar conformation, which results in higher energies of emission.

The relationship between the spectral shift observed in the ASE and the amount of pressure applied is linear and therefore **TPE1** is a promising material for ASE-based pressure sensing devices. Furthermore, the effect of the pressure is reversible, since the ASE profiles are recovered in just one night after applying pressure (Figure 5-26).

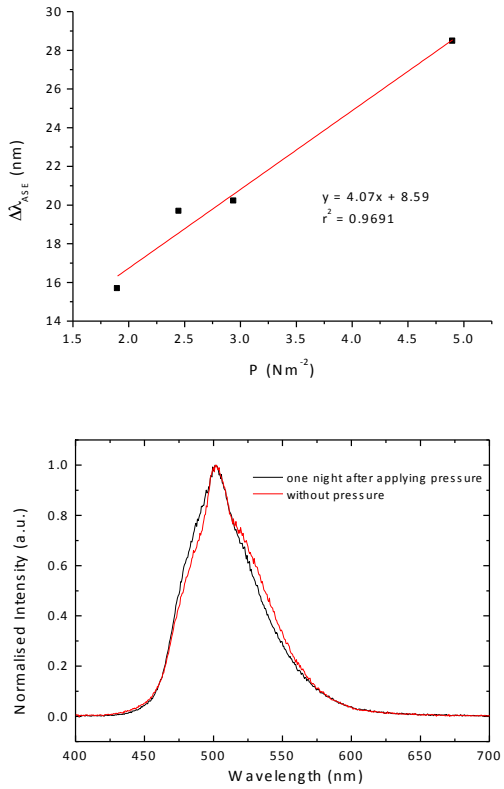

Figure 5-26 Top: Relationship between the spectral shift obtained in the ASE of **TPE1** after the application of pressure and the applied pressure. Bottom: ASE of **TPE1** showing the reversibility on the piezofluorochromic properties after only one night of the application of pressure (1.90 N·m^{-2}).

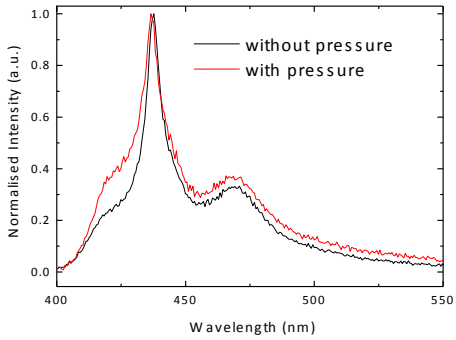

Figure 5-27 ASE spectra of **T3 (hexyl)** before and after the application of pressure (1.90 N·m^{-2}) with a manual hydraulic press over a 1 cm^2 film.

In order to assess whether **TPE1** was responsible for the spectral shift obtained after the application of pressure or if this effect would occur on other non-AIEE active materials, a control with **T3 (hexyl)** was performed applying 1.90 $N \cdot m^{-2}$ pressure (Figure 5-27). Only 1 nm blue shift was obtained, possibly due to small variations in the thickness of the film after the application of pressure. **TPE1**, on the other hand, experienced 15 nm blue shift when the same pressure was applied. This confirmed that the spectral shifts obtained for **TPE1** were due to the gain material and not to film effects such as change in thickness or refractive index.

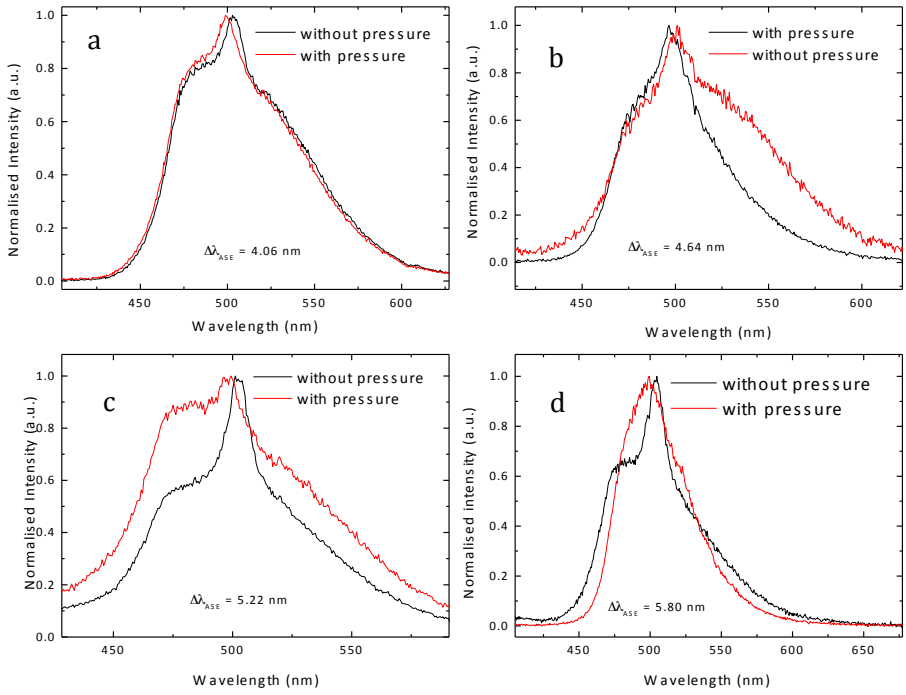

Figure 5-28 Piezofluorochromic studies performed on the ASE of films of **TPE1** applying pressure with a torque press on $1cm^2$ films for 1 minute. The pressures applied and the associated spectral shifts of the ASE peaks were the following: (a) $2.74 \cdot 10^{-2}$ $N \cdot m^{-2}$/4.06 nm, (b) $5.49 \cdot 10^{-2}$ $N \cdot m^{-2}$/4.64 nm, (c) $8.23 \cdot 10^{-2}$ $N \cdot m^{-2}$/5.22 nm, (d) $1.10 \cdot 10^{-1}$ $N \cdot m^{-2}$/5.80 nm.

Unfortunately the reproducibility of the experiments was limited by the manual hydraulic press due to the lack of absolute control of the applied pressure. In order to solve the problem, a torque press was fabricated in-house in order to apply known pressures onto 1 cm^2 films. The ASE spectra measured after applying pressure with the torque also suffer hypsochromic shifts (Figure 5-28) that are linearly related to the applied pressure and in this case are reproducible ($r^2 = 1$ for this linear relationship) (Figure 5-29). It should be noted that the slope of the line that relates the spectral shift with the applied pressure is five times greater at low pressures than at high pressures. There are two possible explanations for this

effect: a) the experiments at high pressure were performed with the hydraulic press and the errors introduced in the pressure measurement were much greater, and/or b) the response to pressure is much greater at low pressures because the molecules have more space within the film to rearrange than at high pressures, where their movements could be much more restricted. In order to investigate this effect further, a series of experiments over a wider range of pressures should be performed employing the torque press. On the other hand, the ASE thresholds after the application of pressure suffer random variations in these prototype experiments. This issue should be addressed in order to be able to use this parameter for pressure sensing. Nevertheless all threshold values are between 467 μJ·cm^{-2} and 684 μJ·cm^{-2}, lower than for the unpressed film. This is an indication that the application of pressure can have a positive effect on the lasing properties of the **TPEn** materials.

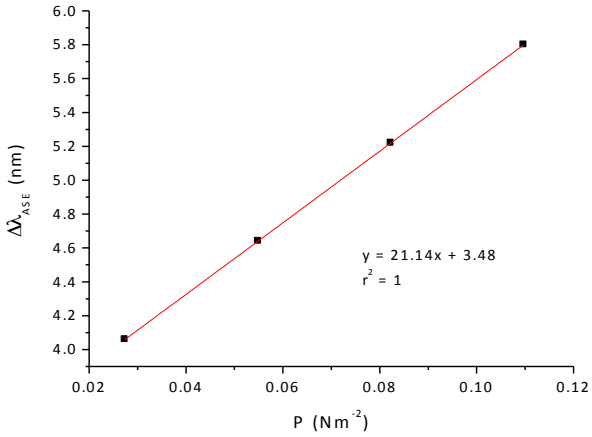

Figure 5-29 Linear relationship between the applied pressure on 1 cm^2 films of **TPE1** and the associated blue shift.

5.4 Conclusion and further work

In conclusion, two new star-shaped oligofluorene TPE materials (**TPE1** and **TPE4**) were efficiently synthesised. The materials are very poor emitters in solution but become efficient yellow-green luminogens in the condensed state (Φ_{TPE1} = 0.29 and Φ_{TPE4} = 0.77). They have a large absorption cross section and large Stokes shifts (184 nm and 138 nm for **TPE1** and **TPE4**, respectively), which makes them promising candidates for down-converter applications. Their AIEE properties were proven in water:THF mixtures in which **TPE1** shows emission enhancement after the addition of 50 % of water to the mixture, being maximised with 90 % water fraction. The effect is observed at 20 % H_2O:THF for **TPE4** and is maximised at 30 %

H_2O:THF due to its lower solubility in polar solvents. Lasing studies performed on **TPE1** reveal that it is a good lasing material and its ASE wavelength varies linearly with the application of pressure, which opens the opportunity for the development of new lasing-based pressure sensors.

Ongoing work involves the determination of the particle size of the **TPEn** compounds in different water:THF mixtures, as well as their associated PLQY. Studying the morphology of the aggregates by transmission electron microscopy (TEM) or scanning electron microscopy (SEM) would provide a better insight on the mechanism of aggregation of the molecules. Photophysics and lasing studies are also being performed on **TPE4** in the Organic Semiconductor Optoelectronics group at the University of St Andrews. Pressure studies will also be performed on this material in order to establish the best possible candidate for pressure sensing. The ultimate goal would be the development of a sensor in which the change in ASE wavelength can be monitored while the pressure is increased, but the equipment for such studies is currently not available within the collaborator's laboratories.

6 T- and Y-shaped oligofluorene BODIPYs

6.1 Abstract

Two families of T-shaped and Y-shaped oligofluorene BODIPY molecules have been synthesised (**T-Bn** and **Y-Bn**). The location of the arms on the BODIPY core (*α*- or *β*-positions) has a great influence on the optical properties of the compounds and this effect is discussed. Furthermore, DFT calculations back up the experimental results and provide a better understanding of the structure/property relationship. The materials are amorphous and present high thermal stability, large Stokes shifts and high PLQYs, making them promising materials for lasing applications.

6.2 Introduction

4,4-Difluoro-4-bora-3a,4a-diaza-s-indacene (BODIPY) is a structural motif (or unit) for a highly versatile class of fluorescent dye that possesses a strong UV-vis absorption, relatively sharp emission with high quantum yields, high thermal, chemical and photochemical stability and low triplet state formation.[227] Figure 6-1 represents the IUPAC nomenclature for the BODIPY core (left), which follows the same numbering rules as indacene, the completely carbon-substituted aromatic moiety (BODIPY is often described as bora-diazaindacene). Another common nomenclature employed for BODIPYs is represented on the right hand side and it is given by analogy with dipyrromethenes: *α* corresponds to the 3,5-positions, whereas *β*- is employed to describe most commonly the 2,6-positions (and less often also the 1,7-positions) and *meso*- corresponds to the 8-position.[228] This dye offers the possibility of structural modification at the *α*-, *β*- and *meso*-positions, allowing fine-tuning of the properties of its derivatives. Furthermore, substitution of the fluorines at the boron (4-position) is also possible.[227]

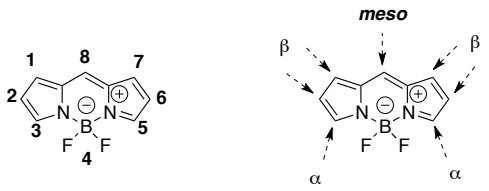

Figure 6-1 Alternative nomenclatures of BODIPY dyes.

Since the first synthetic report of these molecules by Treibs and Kreuzer,[229] the potential of BODIPY derivatives was initially focused on biological labelling, since the strong UV-Vis

absorption and efficient emission properties of the molecules are ideal for such applications. Furthermore, the small size of the dye enables permeability through the cellular membranes, minimising the concentration of the fluorophore required for biological imaging and thus reducing its cytotoxicity compared to other dyes. Functionalisation of the moiety to achieve water-soluble dyes or enabling its chelating ability has also increased the use of these molecules in biochemistry.[230] BODIPY's derivatives have become so popular in life-sciences imaging that the registered trademark "Molecular Probes" has launched a complete catalogue of dyes (the "BODIPY Dye Series") with a broad diversity of emissive properties as well as chemical functionalities to target different biomolecules.[231]

The role of BODIPY derivatives in dye lasers has also been widely studied. Arbeloa and co-workers have dedicated great effort to the study of the effect of structural changes of the BODIPY on its photophysical properties in liquid dye lasers as well as hosts in polymeric dye lasers.[232] For example, they have performed a photophysical study of a series of BODIPY dyes with different types of substituents on their *meso*-position, concluding that the electron-withdrawing or -donating groups have a great impact on the emissive properties of the molecules.[233] Furthermore, they observed a decrease in the PLQY of the molecules due to non-radiative deactivation processes associated with rotations of the aryl substituents in the *meso*-positions. This effect can be reduced *via* substitution of the 1,7-positions in order to block the free rotations of the substituents in the *meso*-position due to steric hindrance.[234] In a recent study, the introduction of amino groups at the 8-position led to hypsochromic shifts in the optical properties of the molecules due to destabilisation of the LUMO without affecting the HOMO levels of the dyes. They obtained higher lasing efficiencies and photostability than the commercial blue dye *coumarin*, widely used for dye lasing applications.[235] They have also tuned the substituents at the *α*-positions to obtain a series of red-emitting dyes that present red-shifts in the absorption and emission spectra compared to the un-substituted parent molecule and lead to photostable and efficient lasers.[232] Solid-state dye lasers with BODIPYs have also been investigated by creating "solid solutions" of BODIPY in UV-transparent polymers like poly(methylmethacrylate) (PMMA) or attaching polymerisable groups to alkyl side chains of the BODIPY to form stable copolymers with methylmethacrylate (MMA), achieving efficient and photostable lasers.[236]

Several comprehensive reviews have described in depth the chemistry of BODIPY[227, 228] and more recently several reviews have focused on specific applications of these molecules such as

fluorescent indicators,[230] sensors[237] or as sensitizers in photodynamic therapy for the localised treatment of illnesses such as cancer.[238, 239] BODIPY derivatives have also been employed in other applications such as sensitisers for dye sensitised[240] and bulk heterojunction solar cells,[241] OLEDs,[242] molecular rotors[243] or electrogenerated chemiluminescence.[244]

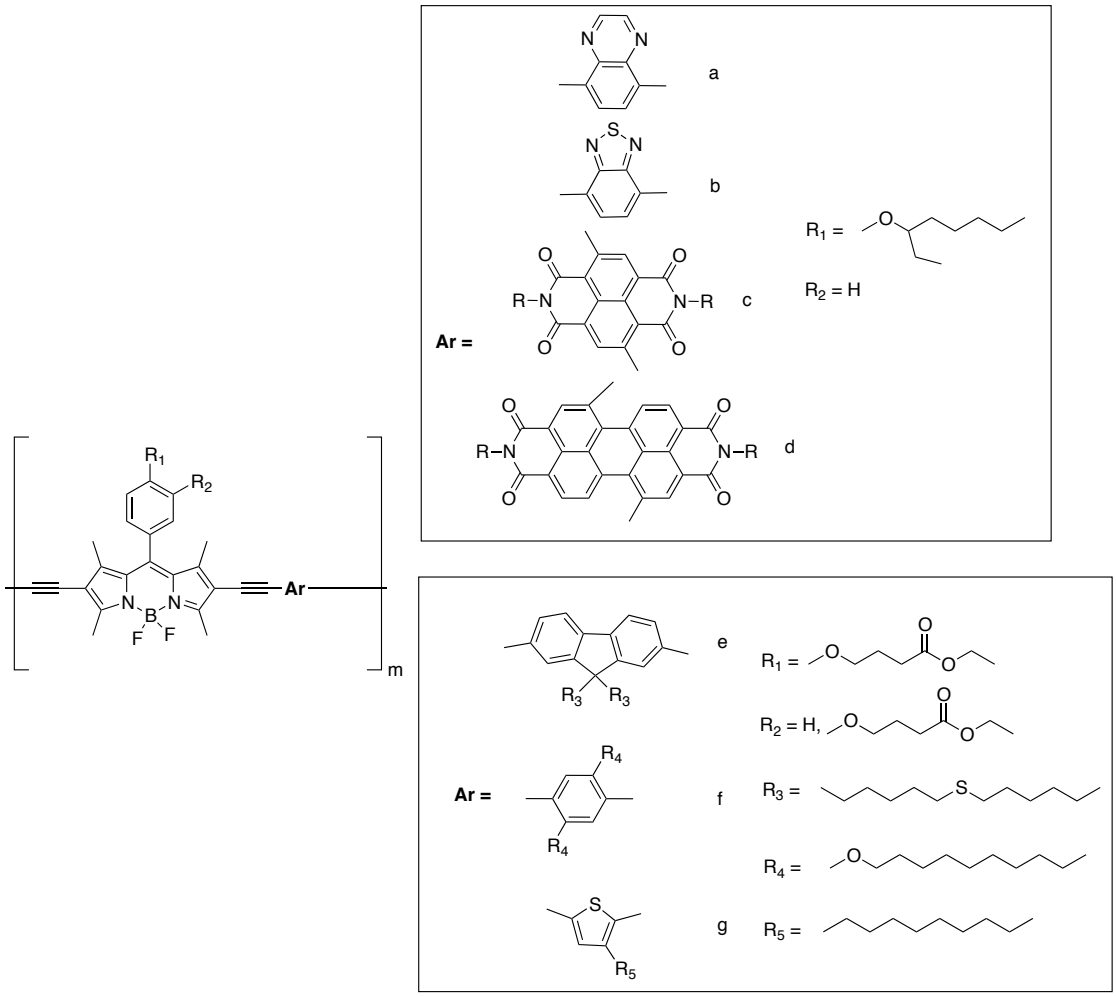

Figure 6-2 Some copolymers containing BODIPY.

Despite BODIPY has been primarily used in small molecules, it has also featured in polymers, both within the polymeric backbone and as a pendant group. Generally, it is polymerised *via* the 2,6-positions. For example, Popere and co-workers described the synthesis of copolymers in which BODIPY acted as the donor and quinoxaline, benzothiadiazole, naphthalene(tetracarboxylic diimide), or perylene(tetracarboxylic diimide) (PDI) acted as acceptors (Figure 6-2 a, b, c and d respectively). The properties of these low bandgap polymers varied with the acceptor unit and the copolymer with PDI absorbed over the whole visible spectrum and was a promising n-type polymer.[245] Donuru and co-workers also described the

synthesis of a BODIPY homopolymer as well as copolymers with fluorene, *p*-phenylene or thiophene by Sonogashira cross-coupling (Figure 6-2 e, f, g). The ethynyl linkers enabled a greater degree of conjugation, acting as a spacer between comonomers to reduce the steric hindrance of the methyl groups placed in the 1,3,5,7-positions. The homopolymers presented deep-red emission through extension of the conjugation length compared with the monomers and the co-polymers provided different shades of red emission, depending on the HOMO-LUMO gaps of the comonomers.[246] Burgess and co-workers described the synthesis of a series of fluorene-BODIPY copolymers in which the BODIPY moiety was "pending" from the main polymeric chain by copolymerisation through the *meta*-positions of the phenyl substituent in the *meso*-position of BODIPY. The twist between the polymer backbone and the BODIPY did not allow effective conjugation, but there was energy transfer from the donor backbone to the acceptor BODIPY, thus providing materials with very the well defined emission of the BODIPY.[247] Scherf *et al.* described the use of BODIPY as an end-capping agent in hyperbranched polytruxene and polytruxene-thiophene block copolymers in order to obtain energy transfer from the excited polymers to the peripheral dyes.[78]

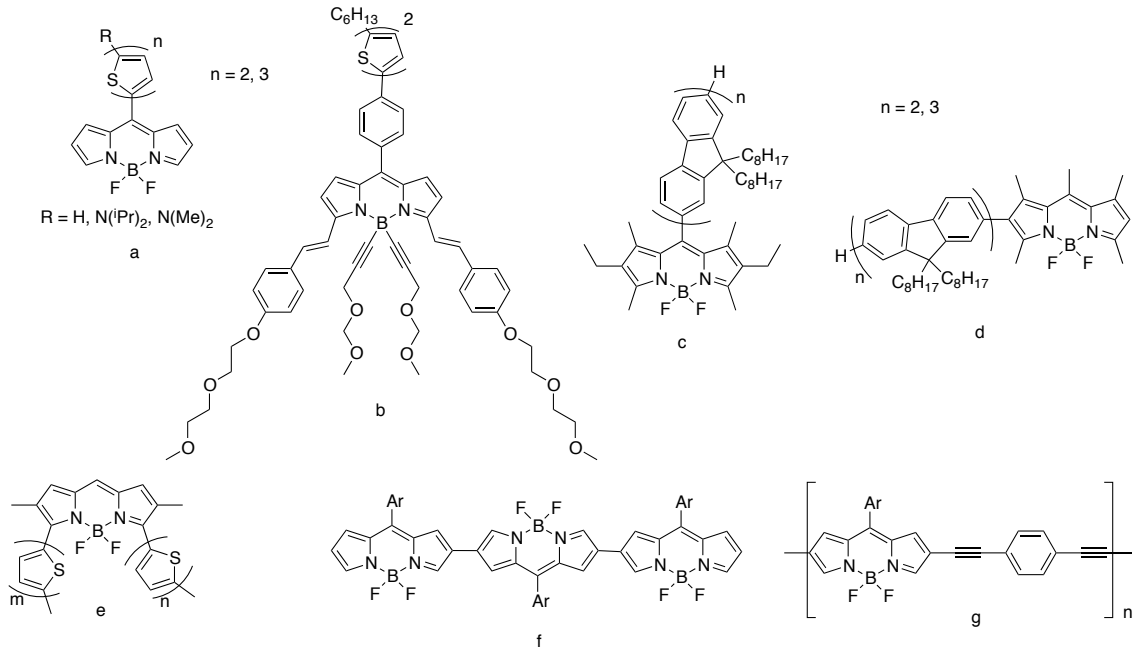

Figure 6-3 Some small BODIPY molecules modified with oligomers.

Small molecules of BODIPY modified with oligomeric chains have also been reported. For example, Collado and co-workers described the synthesis of BODIPY coupled with bithiophene and terthiophene donors at the *meso*-position to study the effect on the photophysical, electrochemical and vibrational properties (Figure 6-3 a).[248] The oligothiophene chains were

modified with *N,N*-dialkylamino functionalities to increase their donor ability and to study the push-pull effect from the amino donors to the BODIPY acceptors through the oligothiophene chain. They were NIR dyes and presented amphoteric redox characteristics. Moreover, their response to selective chemical oxidations and proton accepting ability could be employed in sensing applications. Furthermore, Roncali and co-workers published a similar BODIPY system modified with bithiophene at the *meso*-position through a phenylene linker and *p*-ethenylphenyl linkers in the *α*-positions for bulk heterojunction solar cells with 2.20 % power conversion efficiency (Figure 6-3 b).[241] Similarly, Findlay and co-workers reported the synthesis of ter- and quaterfluorene BODIPY systems in which the oligofluorene chain is attached to the BODIPY either directly onto the *meso*- or on the *β*-position (Figure 6-3 c and d).[99] All the materials presented strong absorption at short wavelength and efficient emission at long wavelengths through energy transfer from the oligofluorenes to the BODIPY. The *meso*-quaterfluorene BODIPY proved the ability of these materials to work efficiently as down-converters for LEDs emitting in the UV region of the spectrum to visible light. Poirel, De Nicola, and Ziessel published the synthesis of asymmetric oligothiophene-modified BODIPYs in which the oligomers were coupled to the 3,5-positions of the BODIPY (Figure 6-3 e).[249] They managed to shift the optical properties of the materials until they obtained NIR emitters by increasing the number of thiophenes in the pending arms, but this change had an associated decrease of the PLQY. They also attached a bisthiophene to the 1-position of the BODIPY obtaining little variation in the properties of the molecule.

Oligomeric BODIPYs have also been described. For example, Hayashi and coworkers published the synthesis of bis- and ter-BODIPY molecules in which the monomers are directly connected *via* their *β*-position (Figure 6-3 f).[250] The monomers are almost co-planar in the dimer and in all cases the absorption and emission properties of the oligomers present bathochromic shifts derived from the increase in the conjugation length. Nevertheless, the PLQY and the fluorescence lifetimes of the oligomers were reduced in comparison with the monomer due to the increase of non-radiative decay pathways associated with a lowered HOMO-LUMO gap. Cakmak and Akaya reported the synthesis of phenylethynyl-BODIPY oligomers in which the monomer unit consisted of an aryl *meso*-substituted BODIPY linked to a phenyl ring *via* an ethynyl linker in the *β*-position of the BODIPY (Figure 6-3 g).[251] They modified the number of monomers from one to four and in all cases they end-capped the oligomer with a terminal BODIPY unit. The increase of the conjugation length led to red-shifts in the optical properties of the molecules but the PLQYs in this case remained high, even for the longer oligomers, due

to the rigidity of the ethynyl linkers. Furthermore, Sakamoto and co-workers published the synthesis of oligo(*p*-phenylene-BODIPY) molecules with one to five monomeric units in which the phenylene is connected to the BODIPY by the α-position.[252] The molecules presented zig-zag structures with almost co-planar BODIPY moieties and the increase in the oligomeric chain led to an increase in Stokes shifts of up to 100 nm, which is remarkable for BODIPY molecules that normally present very small Stokes shifts. The addition of Cs^+ ions to solutions of the oligomers triggered a colour change from blue to pink that was reversible upon the addition of an ether crown to complex the metal ions. The colour tunability was a consequence of a conformational change from unfolded to folded state upon the addition of Cs^+, which has a potential application in biosensors.

Diring and co-workers have studied star-shaped multichromophoric arrays containing BODIPY on truxene platforms. For example, they published the synthesis of a truxene coupled to one, two, three or six BODIPY acceptors through ethynylphenyl linkers at the *meso*-position of the BODIPY (B1-B3 and B6). They also functionalised B6 further by coupling ethylenepyrene residues to the boron in the 4-position of the BODIPY. All the molecules presented intense absorption bands ascribed to the BODIPY residues as well as the truxene moieties. The emission bands showed complete intramolecular energy transfer from either the truxene or the pyrene to the BODIPYs, since the only emission band observed was that of BODIPY, independently of the excitation wavelength employed.[253] They also synthesised star-shaped multichromophoric arrays with three different BODIPY acceptor moieties attached to the truxene core *via* an ethylenephenyl linker at the *meso*-position. The molecule presents a broad absorption that covers the majority of the UV-vis spectrum and an emission dominated by the lowest energy BODIPY unit, with small bands associated with the other two BODIPY moieties. This indicates that in this molecule fast and efficient energy transfer occurs, both from the truxene to the BODIPY as well as between the BODIPYs.[75] Furthermore, Sugimoto and co-workers also synthesised star-shaped molecules with a subporphyrin core and three biphenylene- or phenylene-ethynylene-phenylene-BODIPY arms (with the BODIPY attached at the *meso*-position). All the molecules presented efficient intramolecular energy transfer that could be observed due to independence of the emission from the excitation wavelength. The molecules with methyl substituents in the 1,7-positions had enhanced PLQYs in comparison with their analogues with hydrogen substituents in those positions because the increased steric hindrance that they exert blocks the non-radiative losses associated with the free rotation along the covalent bond in the *meso*-position.[254]

Following the interest of the Skabara group in the BODIPY dye as well as the monodisperse star-shaped materials with oligofluorenes, two new families of materials with BODIPY cores and three 9,9-dihexyloligofluorene arms were synthesised. Both families have an arm coupled to the *meso*-position through a phenyl linker, but the location of the other two arms varies from *β*-position in the family of T-shaped compounds (**T-Bn**), to the *α*-position in the family of Y-shaped materials (**Y-Bn**) (Figure 6-4). The effect of the increase of the oligofluorene length in each family, as well as the location of the arm substitution in the BODIPY core was studied. Moreover, the T-shaped BODIPY family has methyl substituents in the 1,3,5,7-positions, whereas Y-shaped family has no additional substitution, which can also have an effect in the properties of the materials.

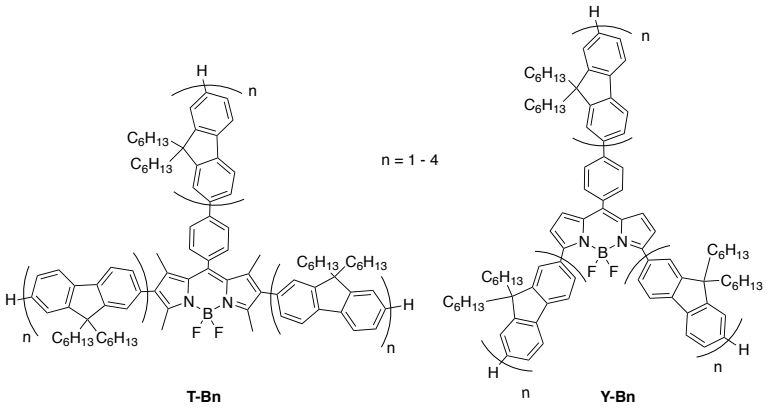

Figure 6-4 The T-shaped and Y-shaped oligofluorene BODIPY families.

6.3 Results and discussion

6.3.1 Synthesis

The synthesis of the BODIPY core for the T-shaped oligofluorene BODIPY series (**T-Bn**) is depicted in Scheme 6-1. It was performed in one pot by condensation of the commercially available *p*-bromobenzaldehyde (**6.1**) and 2,4-dimethylpyrrole (**6.2**) in acidic conditions, followed by oxidation with 2,3-dichloro-5,6-dicyanobenzoquinone (DDQ) and complexation with boron using $BF_3{\cdot}OEt_2$. The product **6.3** was obtained in a moderate 47 % yield, probably due to losses in the workup process derived from the formation of emulsions difficult to separate, as well as partial decomposition during the purification stage due to instability of the material on silica gel. Findlay and co-workers reported slightly improved yields performing the synthesis of their BODIPY core following a pseudo-one pot strategy.[99] Performing a work-up

after the oxidation step reduced the formation of emulsions in the final step, leading to easier workup of the product after the complexation with boron. Compound **6.3** was brominated in the *β*-positions with *N*-bromosuccinimide (NBS) to afford the T-shaped BODIPY core (**6.4**) in a reasonable 63 % yield.

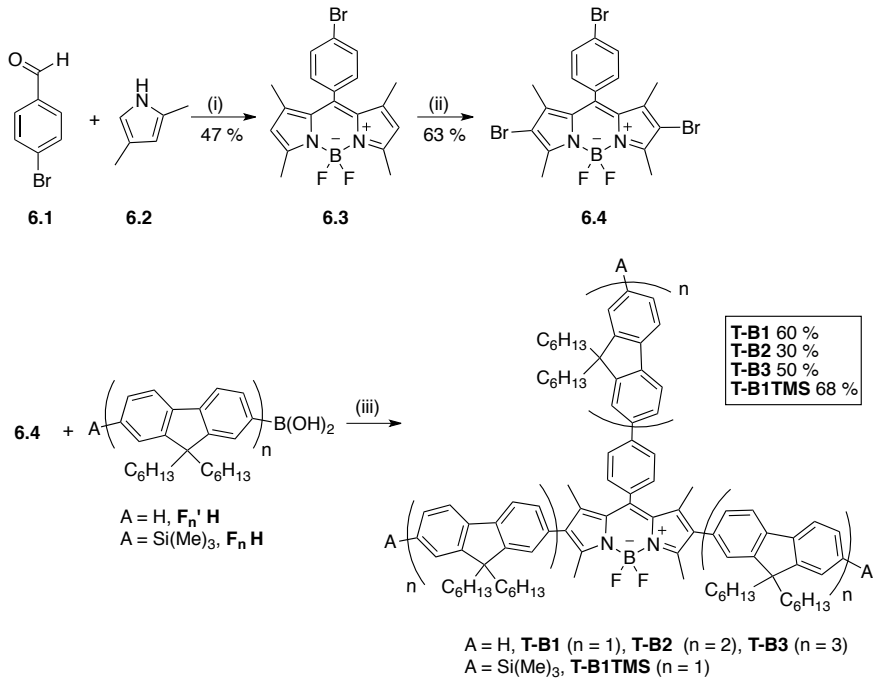

Scheme 6-1 Synthesis of the T-shaped oligofluorene BODIPY family (**T-B1** to **T-B3**). Reagents and conditions : (i) (1) CH_2Cl_2, TFA, R.T., 18 h, (2) DDQ, 4 h, (3) *N,N*-diisopropylethylamine, 10 min, (4) $BF_3{\cdot}OEt_2$, 18 h; (ii) *N*-Bromosuccinimide, CH_2Cl_2, R.T., 18 h; (iii)$Pd_2(dba)_3$, $P^tBu_3{\cdot}HBF_4$, THF, K_3PO_4 1.44 M (aq), reflux, 2 days.

The synthesis of the oligofluorene boronic acid derivatives with hexyl chains was described in Chapter 4 (the nomenclature employed was **F_n H** for the TMS protected hexyl derivatives and **F_n' H** for the deprotected analogues). The **T-B1**, **T-B2**, **T-B3** and **T-B1TMS** analogues were synthesised by modified Suzuki cross-coupling employing $Pd_2(dba)_3$ as a catalyst assisted by the ligand $P^tBu_3{\cdot}HBF_4$. Aqueous potassium phosphate was employed as a base because the sensitivity of BODIPY towards strong bases did not allow the use of the more effective barium hydroxide. The smaller analogues **T-B1** and **T-B1TMS** were obtained in reasonable yields (≈ 60 %) whereas the yield for the larger analogues was poorer (30 % for **T-B2** and 50 % for **T-B3**), probably due to the steric hindrance that the methyl groups in the 1,3,5,7-positions exert on larger oligofluorene moieties. Nevertheless, the yield for **T-B3** is much higher than that of **T-B2** and the reason for this is unclear. It might be due to the larger scale of the synthesis of **T-B3**, but the couplings should be repeated in order to determine whether the trend is consistent.

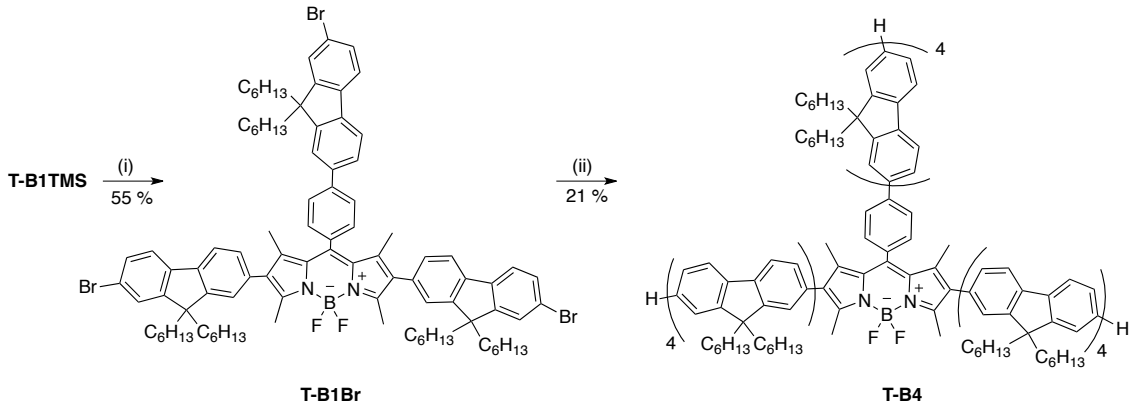

Scheme 6-2 Synthesis of **T-B4**. Reagents and conditions: (i) (1) Sodium acetate, THF, 0 °C, dark, (2) Br_2/CH_2Cl_2, 30 min; (ii) **F_3' H**, $Pd(PPh_3)_4$, THF, K_3PO_4 1.44 M (aq), reflux, 3 days.

In order to avoid using significant quantities of quaterfluorene boronic acid in a low yielding coupling, terfluorene boronic acid (**F_3' H**) was coupled to **T-B1Br** employing the traditional Suzuki coupling that has been described for fluorene-fluorene coupling with $Pd(PPh_3)_4$ as a catalyst, but using K_3PO_4 as a base to ensure the stability of the core (Scheme 6-2). Unfortunately, **T-B4** was obtained in a very modest 21 % yield and the conditions for this coupling should be optimised in the future to improve its efficiency. Poirel and co-workers employed a similar semi-convergent approach to increase the length of the oligothiophene arms at the α-positions and Suzuki coupling under anhydrous conditions, as well as Stille coupling, provided higher yields (36 % - 80 %).[249] **T-B1Br** was obtained in 55 % yield by bromination of **T-B1TMS** with bromine in mild conditions, using sodium acetate to neutralise the HBr formed during the bromination reaction.

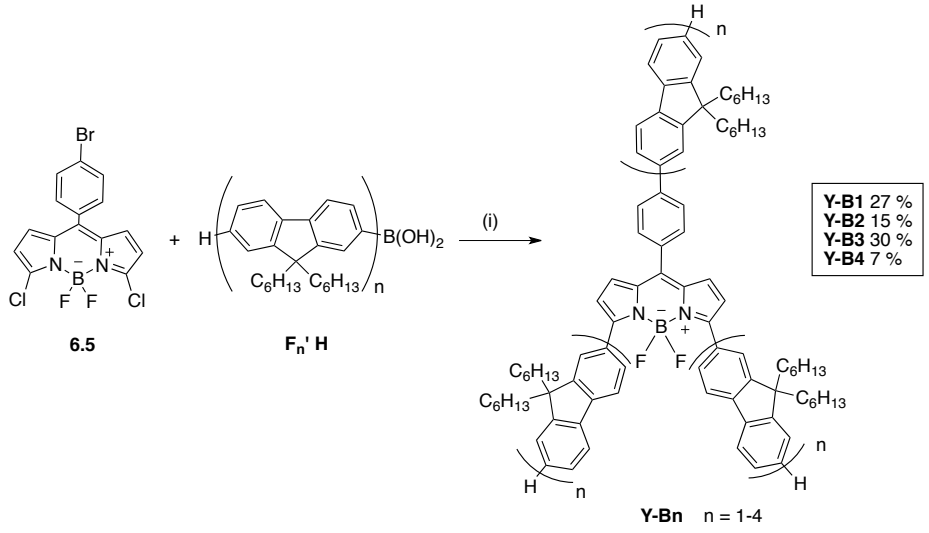

Scheme 6-3 Synthesis of the Y-shaped oligofluorene BODIPY family (**Y-Bn**). Reagents and conditions: (i) $(A\text{-}^{ta}Phos)_2PdCl_2$, K_3PO_4 1.44 M (aq), reflux, 24 h.

The synthesis of the Y-shaped BODIPY family (**Y-Bn**) was performed by another modified Suzuki coupling and it is represented in Scheme 6-3. The lower reactivity of the chlorine substituents compared to the bromine was anticipated and therefore the catalyst (A-^{ta}Phos)$_2$PdCl$_2$ was employed due to its greater affinity for chlorine substituents.[255] Using this catalyst it was possible to obtain the final products in high purity, but the yields for all the couplings were very low (30 % or below) and the increase of the length of the oligofluorene arm resulted in lower yields (7 % for the **Y-B4** analogue). Surprisingly, **Y-B3** was obtained in higher yield than any of the other analogues but this might be due to the greater scale in which the coupling was performed, as occurred for the **T-B3** analogue. Further optimisation of the couplings is required in order to obtain the materials in reasonable yields to study the applications of the materials. It is worth noting that Boens and co-workers reported the synthesis of several BODIPY dyes modified at the α-positions by palladium catalysed cross-couplings, obtaining yields above 60 % with Suzuki coupling under microwave irradiation, whereas the reactions did not work without irradiation.[256] Nevertheless, following a modular coupling approach they obtained yields above 90 % for a mono-substituted BODIPY in the 3-position by Suzuki coupling under classic conditions.[257] This may indicate that the coupling of two large oligofluorene arms at the 3,5-positions is unfavourable due to steric hindrance since the coupling locations are relatively close and might interfere with each other. The same group has recently reported the palladium catalysed direct C-H arylation of BODIPY dyes at the 3- or 3,5-positions, obtaining the products in yields up to 40 % both under conventional heating and under MW-irradiation.[258] These results offer the possibility to investigate new synthetic procedures in order to improve the efficiency of the couplings for the synthesis of the **Y-Bn** family.

6.3.2 Physical properties

The physical properties of the members of the **T-Bn** and **Y-Bn** families are summarised in Table 6-1. The materials have molecular weights ranging between 1300 and 4300 g·mol^{-1} and all are soluble in common organic solvents. Their thermal stability was evaluated by thermogravimetric analysis and all the compounds present decomposition temperatures around or above 400 °C. Despite the compounds being thermally stable it is worth mentioning that they are sensitive to strong bases as well as acids (when the NMR was performed in slightly acidic chloroform precipitation was consistently observed).

Table 6-1 Physical properties of the **T-Bn** and **Y-Bn** families. M_w is the molecular weight of the compound, T_g is the glass transition temperature and T_m is the melting point as measured from differential scanning calorimetry (DSC). T_d is the decomposition temperature measured by thermogravimetric analysis (TGA).

Compound	M_w (g·mol^{-1})	T_g (°C)	Td (°C) [5% mass loss]
T-B1	1321.74	83	396
T-B2	2305.28	93	426
T-B3	3316.87	99	440
T-B4	4314.43	96	413
Y-B1	1265.63	63	438
Y-B2	2263.20	80	421
Y-B3	3260.76	87	442
Y-B4	4258.33	96	423

The materials are amorphous and present reasonably high glass transition temperatures that increase with the number of fluorenes in the arms. It is worth noting that the T_g of the **Y-Bn** family appears at lower temperatures than for the **T-Bn** series. The amorphous character of the molecules was confirmed by powder X-ray diffraction experiments performed by Dr. Fiona Coomer.

6.3.3 Electrochemistry

The electrochemical properties of the materials were investigated in ≈ 10^{-4} M solutions in dichloromethane and they are summarised in Table 6-2. The oxidation curves of the **T-Bn** family are represented in Figure 6-5. **T-B1** and **T-B2** present a first oxidation peak around 0.67 V, which is too low to be related to the oxidation of the fluorenes[259] or the BODIPY unit isolated.[260] It is probably due to the oxidation of the oligofluorene-BODIPY-oligofluorene structural unit. This first oxidation wave appears at slightly higher potentials for **T-B3** and **T-B4** (around 0.78 V). These results are analogous to those obtained for the oligofluorene-BODIPY systems published by Findlay *et al.*[99] The **T-Bn** materials have oligofluorene arms both in the *meso*-position and in the *β*-positions, sharing structural characteristics with both their meso-OF-BOD and beta-OF-BOD (Figure 6-3 c and d respectively, page 156). The second oxidation peak is more intense than the first one in all cases. It probably also involves the oxidation of the OF-BODIPY-OF unit, but the larger intensity indicates a greater involvement of the oligofluorene in the *meso*-position. **T-B3** and **T-B4** present a third quasi-reversible oxidation

peak related to the formation of a radical dication on the oligofluorenes.[259] The second and third oxidation peaks appear at lower potentials in the larger analogues due to the longer effective conjugation length of the molecules. The irreversible peaks that the materials show between 1.30 V and 1.55 V are probably due to over-oxidation of the molecule.

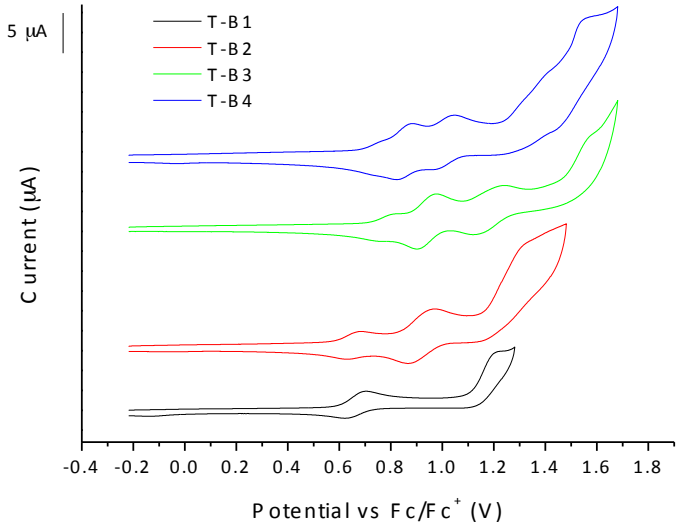

Figure 6-5 Oxidation waves of the **T-Bn** family in dichloromethane. The cyclic voltammogram was obtained employing a glassy carbon working electrode, a platinum wire counter electrode and a silver wire reference electrode. All the waves were referenced to ferrocene.

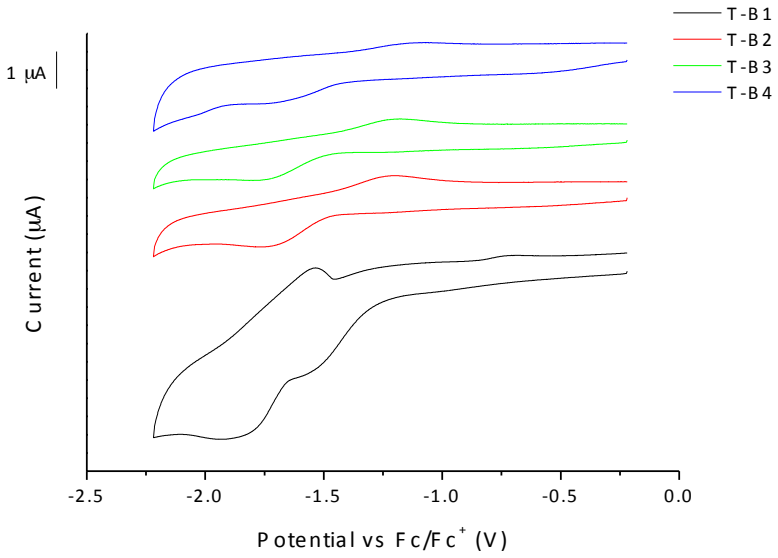

Figure 6-6 Reduction waves of the **T-Bn** family in dichloromethane. The cyclic voltammogram was obtained employing a glassy carbon working electrode, a platinum wire counter electrode and a silver wire reference electrode. All the waves were referenced to ferrocene.

The reduction waves of the **T-Bn** family are presented in Figure 6-6. **T-B1** presents a first irreversible reduction peak at -1.55 V followed by a quasi-reversible reduction at -1.88 V. All the other compounds present a single quasi-reversible peak around -1.70 V, associated with the reduction of the BODIPY core.[261]

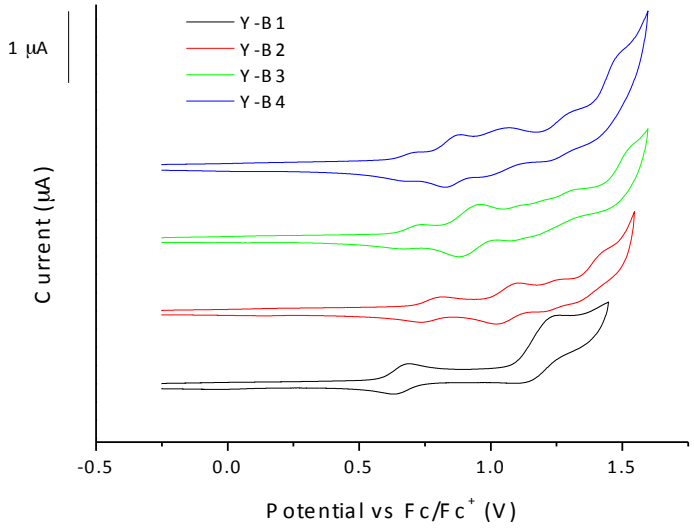

Figure 6-7 Oxidation waves of the **Y-Bn** family in dichloromethane. The cyclic voltammogram was obtained employing a glassy carbon working electrode, a platinum wire counter electrode and a silver wire reference electrode. All the waves were referenced to ferrocene.

The oxidation voltammograms of the **Y-Bn** series are presented in Figure 6-7. A similar behaviour to that observed for the **T-Bn** family is observed, with all the compounds presenting an initial reversible oxidation peak, related to the formation of the radical cation in the (*α*)OF-BODIPY-(*α*)OF unit, followed by a second oxidation peak around 1 V that appears at lower potentials when the arm length is increased from **Y-B2** to **Y-B4**. This peak is once more associated with the formation of a radical dication on the OF-BODIPY-OF, but the greater current involved in the oxidation process indicates that there could be a greater involvement of the OF in the *meso*-position. Furthermore, the oxidation potential in the larger analogues is is decreased due to an increase in the conjugation length of the oligofluorenes.[259] The increase in the oligofluorene chain length also leads to more complex oxidation voltamogramms, due to additional oxidation processes on the oligofluorene arms.[259] The peaks that appear from 1.30 V to 1.50 V involve much greater current and are likely due to over-oxidation of the materials.

The reduction waves of the compounds are presented in Figure 6-8. All the materials present a first reduction peak associated to the formation of a radical anion in the BODIPY core,[261] but its

position varies for the different members of the family, being reversible and at a less negative potential for **Y-B1**. This could be explained by the lower electron density exerted by one fluorene in each arm, as opposed to the oligofluorenes in the other members of the series. Due to the conjugation between the arms in the α-position and the BODIPY core, the increase in the oligofluorene arm length provides greater electron density to the core, which leads to more negative reduction potentials. The first reduction peak for the rest of the materials is quasi-reversible while the second one is irreversible for all the compounds and appears at lower potentials with the increase of the length of the arms. This second reduction probably occurs on the oligofluorene arms.

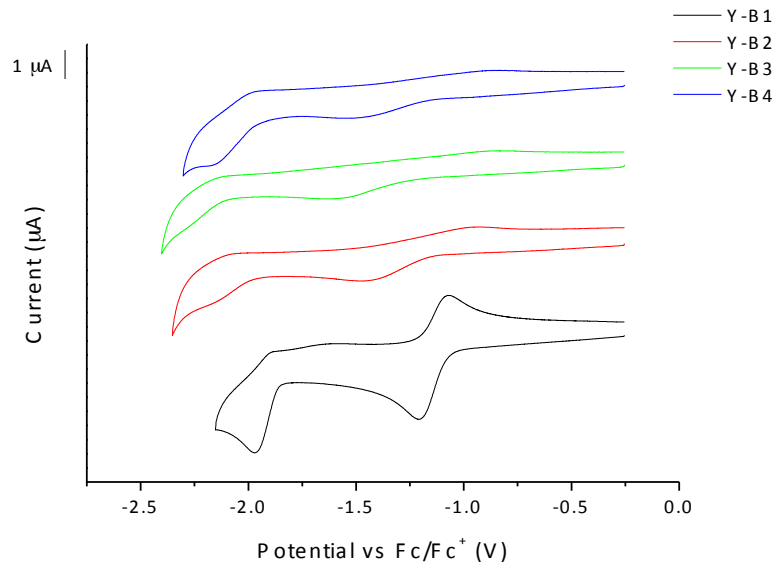

Figure 6-8 Reduction waves of the **Y-Bn** family in dichloromethane. The cyclic voltammogram was obtained employing a glassy carbon working electrode, a platinum wire counter electrode and a silver wire reference electrode. All the waves were referenced to ferrocene.

In general, the oxidation peaks occurred at a similar potential for the analogues of both families, whereas the reduction for the **Y-Bn** family occurred at less negative potentials. This could be a result of two factors: firstly, the oligofluorene arms in the α-positions are conjugated through the BODIPY core and therefore the radical anion formed upon reduction can be delocalised to a greater extent throughout the molecule, facilitating the reduction, whereas it is more localised on the BODIPY in the **T-Bn** family. Secondly, the **T-Bn** family possesses four extra methyl groups directly attached to the BODIPY and the positive inductive effect that they exert decreases the electron affinity of the core, thus hindering the reduction process. The optical and electrochemical HOMO-LUMO gaps are in good agreement for most compounds, the difference being greater for the **T-B1** and **Y-B1** analogues (around 0.25 eV).

The HOMO levels for both families were similar, whereas the in general the LUMO levels of the **Y-Bn** family were lower, leading to narrower HOMO-LUMO gaps (up to 0.39 eV difference for the greater analogues).

Table 6-2 Electrochemical properties of the **T-Bn** and **Y-Bn** families in dichloromethane. [a] HOMO and LUMO levels were calculated from the onset of the corresponding redox wave and are referenced to ferrocene, which has a HOMO of -4.8 eV. [b] The electrochemical HOMO-LUMO gap ($E_{g,\,CV}$) is the energy gap between the HOMO and LUMO levels. The optical HOMO-LUMO gap ($E_{g,\,opt}$) is calculated from the onset of the red-edge of the absorption band (in brackets).

Compound	E_{ox} vs Fc/Fc^+ (V)	HOMO[a] (eV)	E_{red} vs Fc/Fc^+ (V)	LUMO,[a] (eV)	$E_{g,\,CV}$[b] (eV)	$E_{g,\,opt}$[b] (eV)
T-B1	0.67, 1.20	-5.36	-1.55, -1.88	-3.49	1.87	2.14 (579)
T-B2	0.68, 0.96, 1.31	-5.36	-1.75	-3.33	2.03	2.13 (583)
T-B3	0.78, 0.96, 1.22, 1.56	-5.51	-1.76	-3.31	2.20	2.12 (584)
T-B4	0.77, 0.88, 1.04, 1.35, 1.55	-5.55	-1.71	-3.37	2.18	2.13 (583)
Y-B1	0.68, 1.24	-5.38	-1.21, -1.97	-3.72	1.66	1.91 (650)
Y-B2	0.81, 1.10, 1.26, 1.42	-5.50	-1.46, -2.13	-3.63	1.87	1.86 (667)
Y-B3	0.73, 0.95, 1.10, 1.20, 1.31, 1.52	-5.43	-1.60, -2.25	-3.53	1.90	1.85 (670)
Y-B4	0.70, 0.87, 1.07, 1.29, 1.47	-5.41	-1.49, -2.16	-3.62	1.79	1.86 (668)

6.3.4 Optical and photophysical properties

The optical properties of the materials were studied in solutions in dichloromethane and in films dropcast from toluene solutions. An image of toluene solutions of both families under ambient conditions and UV-illumination is presented in Figure 6-9 a) and b) respectively. The effect of the location of the oligofluorene arms (either at the α- or β-positions) on the optical properties of the materials can be observed with the naked eye. The powders and solutions of the **T-Bn** family are bright pink and present bright orange fluorescence, while the compounds of the **Y-Bn** family are dark green powders and present a dark red colour in concentrated

solutions and green when diluted. Their deep-red fluorescence seems less efficient to the naked eye than that of the **T-Bn** family. The optical properties of the **T-Bn** and **Y-Bn** families are summarised in Table 6-3.

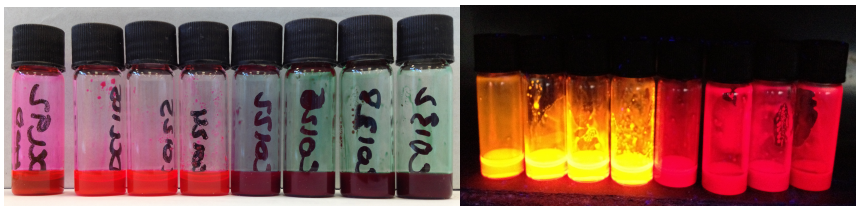

a) b)

Figure 6-9 T- and Y-shaped oligofluorene BODIPY solutions in toluene. From left to right, **T-B1**, **T-B2**, **T-B3**, **T-B4**, **Y-B1**, **Y-B2**, **Y-B3** and **Y-B4**. a) Under ambient light. b) Under UV illumination (254 nm).

Table 6-3 Optical properties of the **T-Bn** and the **Y-Bn** families. ε is the absorption coefficient in the film, measured for the fluorene and the two BODIPY absorption bands.

Compound	$\lambda_{abs,\ sol}$ (nm)	$\log(\varepsilon)_{sol}$	$\lambda_{em,sol}$ (nm)	$\lambda_{abs,\ film}$ (nm)	$\lambda_{em,\ film}$ nm)
T-B1	313, 399, 539	4.66, 4.00, 4.74	585	315, 402, 544	605
T-B2	341, 399, 542	5.24, 4.23, 4.94	591	343, 413, 544	601
T-B3	357, 421, 542	5.44, 4.25, 4.97	589	358, 430, 546	598
T-B4	367, 430, 542	5.50, 4.11, 4.94	592	368, 436, 546	606
Y-B1	317, 443, 599	4.83, 4.54, 4.80	646	319, 446, 610	662
Y-B2	346, 465, 612	5.20, 4.66, 4.81	661	346, 471, 618	674
Y-B3	360, 470, 614	5.38, 4.65, 4.78	664	359, 474, 620	672
Y-B4	368, 469, 614	5.54, 4.69, 4.81	663	367, 476, 620	674

The normalised absorbance and emission spectra of the **T-Bn** family in dichloromethane solution is presented in Figure 6-10. All the compounds have an intense short-wavelength band associated to the π-π* transition of the fluorene.[59] This band is broad and quasi-symmetrical and it only presents vibronic structure in **T-B1**, probably due to a more rigid conformation of the molecule, where the methyl groups of the BODIPY restrict the free rotation of the fluorene, whereas in the longer oligomers, the rest of the fluorenes can undergo rotations, relaxing the structure of the molecule. As the number of fluorene units in the arm increases, the band becomes more intense (as can be observed by its greater logarithm of the molar absorptivity) and presents a bathochromic shift. The band around 400 nm belongs to the S_0-S_2 transition in the BODIPY[256] and it is only clearly resolved in **T-B1**; it becomes a shoulder of the fluorene band as the latter red-shifts in the larger molecules. The

broad, symmetric, featureless band around 540 nm corresponds to the S_0-S_1 transition in the BODIPY.[256] It can be observed that despite the increase in the arm length, the position of the band barely suffers a bathochromic shift because the arms are not conjugated with the core.

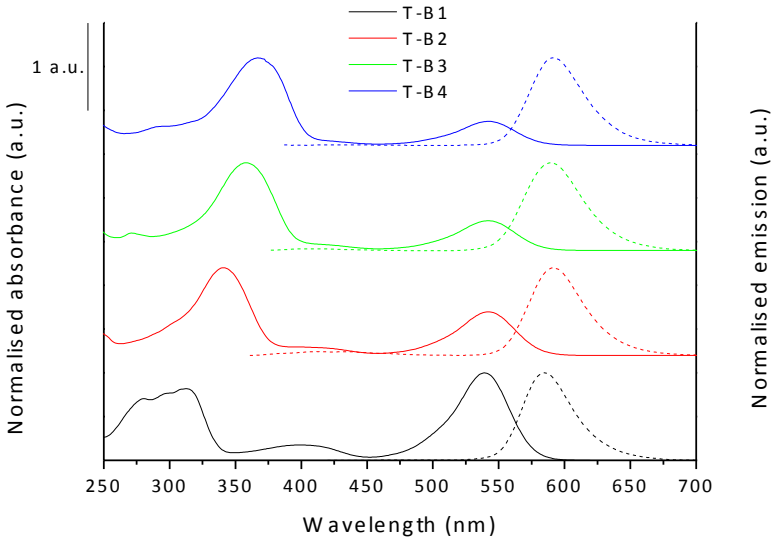

Figure 6-10 Normalised absorption (solid line) and emission (dashed line) spectra of the **T-Bn** family in dichloromethane solution. λ_{ex} = 541 nm.

The emission spectra of the molecules reveals a single band with no vibronic structure around 600 nm. This band arises from the BODIPY[99] and its position and shape does not change with the excitation wavelength, but it is more intense when the fluorene band is excited, indicating a complete energy transfer from the peripheral oligofluorene arms to the BODIPY core. The position of this band barely changes with the increase of oligofluorene arms because of the lack of conjugation between the arms through to the core. The solid state absorption and emission spectra of the **T-Bn** series (Figure 6-11) are very similar to those in solution but the shape of the fluorene band is slightly flattened (perhaps due to an excessive thickness of the film) and the S_0-S_2 band of the BODIPY is better resolved. Moreover, the positions of the absorption peaks are slightly red-shifted in comparison with the solution spectra. The same trend applies to the emission spectra. The coupling of oligofluorene arms to the BODIPY core implements the Stokes shift of the BODIPY to around 50 nm, with reduced overlap between the absorption and emission bands. Furthermore, taking into consideration the distance from the main absorption band (oligofluorene) to the emission band, the Stokes shift is very large (from 225 nm to 272 nm). This presents a great opportunity to apply these materials as down-converters that absorb UV light but emit well into the visible spectrum.

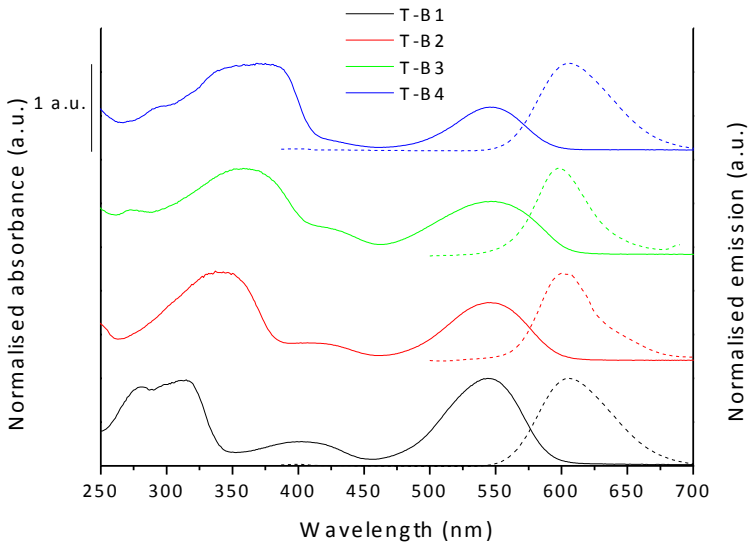

Figure 6-11 Normalised absorption (solid line) and emission (dashed line) spectra of films of the **T-Bn** family dropcasted from 10 mg·mL^{-1} solutions in toluene. λ_{ex} = 410 nm.

Figure 6-12 represents the absorption and emission spectra of the **Y-Bn** series in dichloromethane solution. The same three absorption bands are observed in this family and the only one that presents resolved vibronic structure is the π-π* band in **Y-B1**. The band around 400 nm appears better resolved in this case, although it also becomes a shoulder of the fluorene band in **Y-B3** and especially in **Y-B4**. As occurred in the **T-Bn** family, the increase in the number of oligofluorene arms results in greater intensities and bathochromic shifts of the π-π* transition. In these compounds, the positions of the bands associated to the BODIPY core suffer a bathochromic shift when moving from **T-B1** to **T-B2** (22 nm for the S_0-S_2 transition and 13 nm for the S_0-S_1 transition) and to a lesser extent from **T-B2** to **T-B3** (5 nm and 2 nm respectively). In this case the arms are conjugated through the core and the increase into the conjugation length results in lower HOMO-LUMO gaps, which is translated in bathochromic shifts. This also explains the longer absorption wavelengths of the BODIPY for all the members of the **Y-Bn** family compared to their **T-Bn** analogues, while the π-π* transition appears at similar wavelengths.

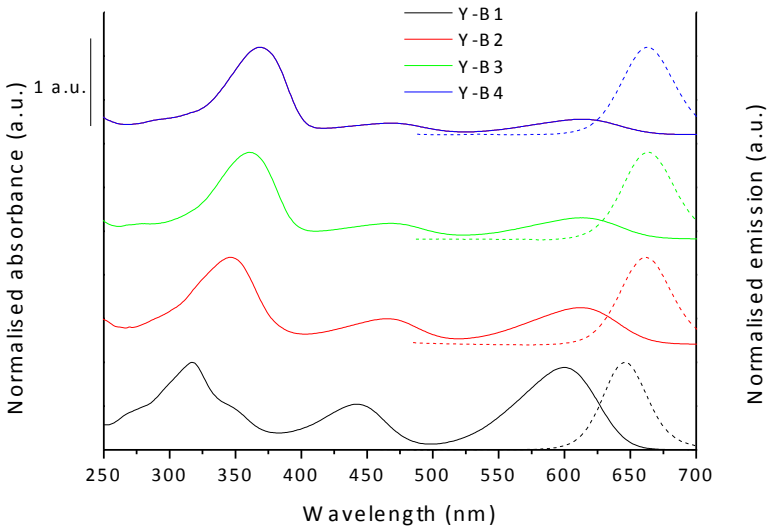

Figure 6-12 Normalised absorption (solid line) and emission (dashed line) spectra of the **Y-Bn** family in dichloromethane solution. λ_{ex} = 465 nm.

The emission spectra of these compounds are also broad and featureless bands that appear around 650 nm and suffer bathochromic shifts with an increase in arm length. The Stokes shift from the S_0-S_1 band of the BODIPY is around 50 nm, but considering the distance between the oligofluorene absorption and the emission, it is between 295 nm and 329 nm, even greater than for the **T-Bn** family.

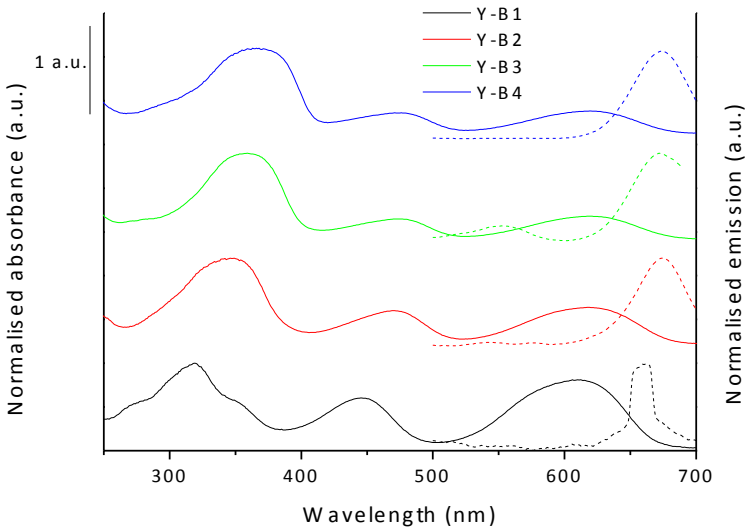

Figure 6-13 Normalised absorption (solid line) and emission (dashed line) spectra of films of the **Y-Bn** family dropcasted from 10 mg·mL^{-1} solutions in toluene. λ_{ex} = 541 nm.

The normalised solid state absorption and emission spectra of the **Y-Bn** family are presented in Figure 6-13. As occurred for the **T-Bn** family, all the features become broader and the band around 450 nm appears better resolved. The emission of **Y-Bn** compounds is less intense than that of their **T-Bn** analogues. The shape of the emission band of **Y-B1** is much narrower and less smooth than for the rest of the compounds due to the low intensity of the band, independently of the excitation wavelength employed. The emission bands shifted 12-16 nm bathochromically from solution to the solid state whereas the only absorption band that showed a slight red-shift in the condensed state was that of the S_0-S_1 transition of the BODIPY.

Table 6-4 Photophysical properties of some members of the **T-Bn** and **Y-Bn** families measured on films of the materials spin-coated from 20 mg·mL^{-1} toluene solutions. τ is the measured lifetime after an ecitation pulse at 400 nm, τ_N is the natural radiative lifetime and Φ is the photoluminescence quantum yield at 360 nm and 450 nm excitation wavelengths.

Compound	τ, ns	τ_N, ns	Film thickness, nm	Φ (360 nm)	Φ (450 nm)
T-B3	0.490	0.96	100	0.51	0.48
Y-B3	0.786	1.64	75	0.43	0.41

Preliminary photophysical studies were performed on **T-B3** and **Y-B3** by Dimali Vithanage in the Organic Semiconductor Optoelectronics group at the University of St Andrews (Table 6-4). Both compounds present a monoexponential fluorescence decay following an excitation pulse at 400 nm and the lifetime for **Y-B3** is much longer than that of **T-B3** (786 ps *versus* 490 ps). The PLQY for both materials is relatively high for organic semiconductors in the condensed state, being only slightly lower for the **Y-B3** analogue. The PLQY was also tested at 450 nm in order to investigate the suitability of the materials for ultra-parallel visible light communication applications (UPVLC) in which the excitation wavelength provided by the LED is 450 nm. The PLQY barely decreases at the longer wavelength indicating that the materials are promising for UPVLC applications and also for organic semiconductor lasers (OSLs).

6.3.5 DFT calculations

Joseph Cameron (from the Skabara group) perfomed theoretical calculations on the structures and molecular orbitals of **T-B1** and **Y-B1** using Density Functional Theory (DFT) in order to achieve a better understanding of the structure/property relationships as a function of the substitution pattern of the BODIPY core. The structures were optimised using the program Gaussian 09[262] using the CAM-B3LYP[263] functional with the TZVP[264] basis set. Solvent effects

were considered with the inclusion of the SMD[265] solvent model. In order to increase the computational efficiency of the optimisations, the alkyl chains on the fluorene units were shortened to methyl groups.

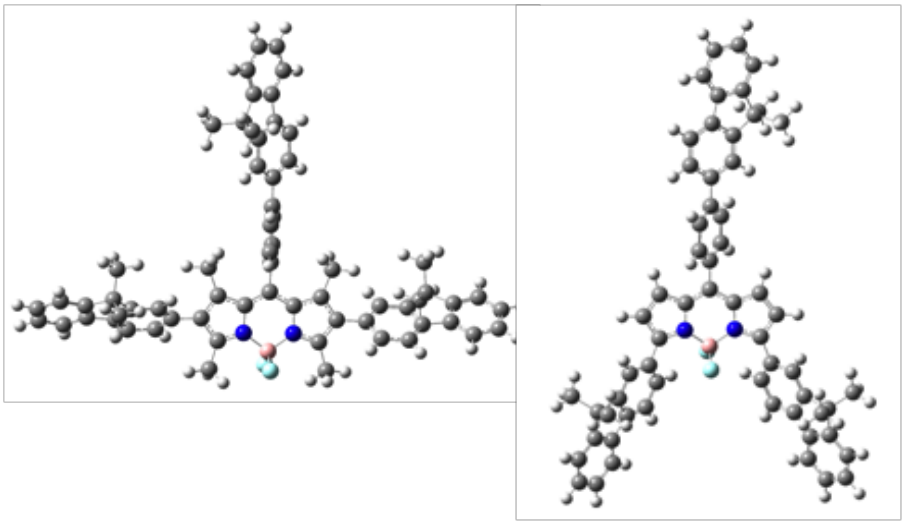

Figure 6-14 Optimised structures of **T-B1** (left) and **Y-B1** (right).

The twist between the β-fluorenes and BODIPY in **T-B1** (56.6°) is greater than that obtained for the fluorenes in α-positions in **Y-B1** (42.9°), probably due to steric restrictions imposed by the methyl substituents at the 1,3,5,7-positions (Figure 6-14). The distance between the hydrogens of the fluorene and the fluorines of the BODIPY in **Y-B1** are 2.20 Å and 2.23 Å. These distances are shorter than the sum of the Wan der Waals radii of H (1.20 Å) and F (1.47 Å), which is 2.67 Å. This implies that there are H-F interactions between the fluorene and the BODIPY core, which could also contribute to stabilise the planarisation of the structure. In the case of **T-B1**, the H-F distances between the hydrogens of the methyl substituents at the 3,5-positions and the fluorines at the 4-position of the BODIPY (2.42 Å and 2.44 Å) are also smaller than the sum of the Van der Waals radii, also indicating the possibility of H-F interactions. The greater degree of planarity in **Y-B1** leads to increased conjugation and therefore a lower HOMO-LUMO gap, which is predicted from the DFT calculations and is observed in the electrochemical and optical data. This explains the red shifts in the absorption spectrum of **Y-B1** compared to that of **T-B1** ($\Delta\lambda$ = 60 nm). It is likely that the greater degree of planarisation is also present in the rest of the members of the **Y-Bn** family, which would account for their bathochromically shifted optical transitions compared with their T-shaped analogues. The phenyl linker attached to the *meso*-position is also more twisted in **T-B1** (80.8°) than in **Y-B1** (58.0°) because the

methyl groups in the 1,7-positions exert greater steric hindrance than the hydrogen substituents of **Y-B1**.

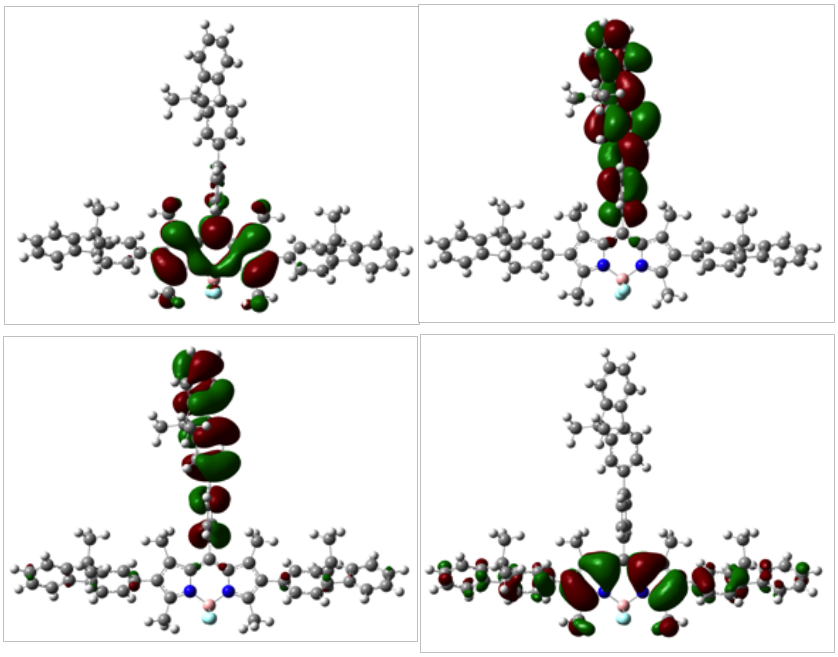

Figure 6-15 HOMO-1 (bottom, left), HOMO (bottom, right), LUMO (top, left) and LUMO+1 (top, right) of **T-B1**.

The greater degree of conjugation of the fluorenes with the core in **Y-B1** compared with **T-B1** is also evident from the examination of their frontier orbitals. The HOMO of **Y-B1** shows increased electron-density over the fluorene units (Figure 6-16) with respect to the analogous units in **T-B1** (Figure 6-15). Also, the LUMO of **Y-B1** shows some delocalisation over the fluorenes, but the LUMO of **T-B1** is localised on the BODIPY unit, which supports the idea that the increase in fluorene twist reduces conjugation in **T-B1**, hence its absorption spectrum is hypsochromically shifted with respect to **Y-B1**. The calculated energies of the HOMO and LUMO levels do not match the experimental values but they show the trend of lower HOMO-LUMO gaps for **Y-B1**.

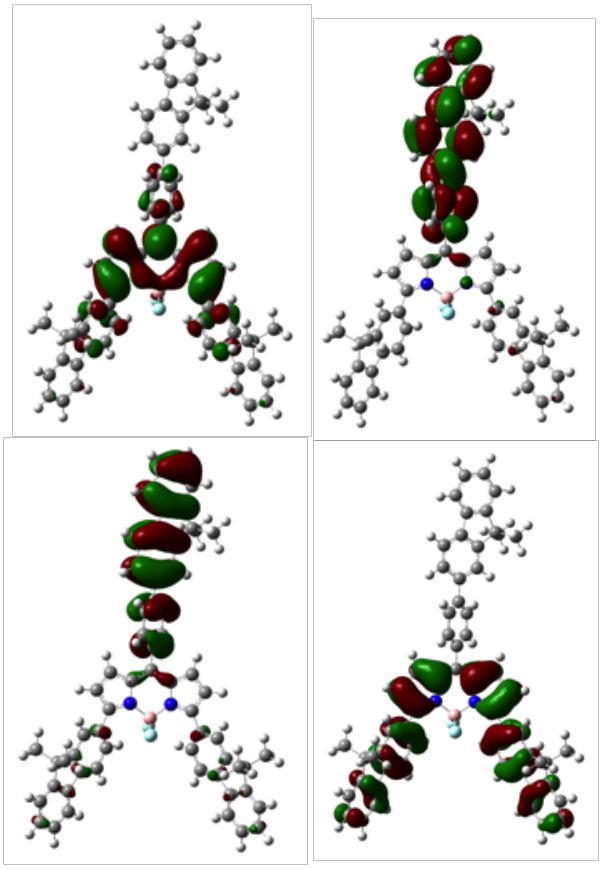

Figure 6-16 HOMO-1 (bottom, left), HOMO (bottom, right), LUMO (top, left) and LUMO+1 (top, right) of **Y-B1**.

The HOMO-1 represents the energy level right below the HOMO and the LUMO+1 that immediately above the LUMO. These frontier orbitals are localised primarily over the phenyl-fluorene located on the *meso*-position for both compounds and they have the almost the same calculated energies. The absorption band that occurs in the region of 400 – 450 nm has previously been described as the S_0-S_2 transition of the BODIPY.[256] It is likely that this transition is represented by the HOMO – LUMO+1 orbitals and the fact that this band presents a 44 nm bathochromic shift for **Y-B1** compared to that of **T-B1** is probably due to the lower energy of the HOMO for the latter.

6.4 Conclusion and further work

Two families of T-shaped and Y-shaped oligofluorene BODIPY molecules have been synthesised (**T-Bn** and **Y-Bn**). The materials vary in the position of the oligofluorene arms directly attached to the BODIPY core from the α- to β-position, and both families possess a third arm attached to the *meso*-position through a phenyl linker. The **T-Bn** family possesses four extra methyl

substituents in the 1,3,5,7-positions that induce steric hindrance and can reduce the electron affinity of the core *via* positive inductive effect. All the materials are amorphous and present high thermal stability. The increase in the length of the oligofluorene arms triggers a bathochromic shift in the absorption band of the oligofluorenes and their location dramatically affects the optical properties. The arms are fully conjugated through the core only in the **Y-Bn** family and this results in bathochromically shifted absorption and emission properties with respect to the **T-Bn** family. DFT calculations support the experimental results. The presence of the oligofluorene arms leads to Stokes shifts of around 50 nm for both families and the shift between the maximum absorbance (at the oligofluorene absorption band) and the emission band is as large as 272 nm in the **T-Bn** family and 329 nm in the **Y-Bn** family. The materials are very efficient emitters with solid state PLQYs around 0.40-0.50.

Current work is being performed in order to study the photophysics of the rest of the members of the **T-Bn** and **Y-Bn** families, and the materials will shortly be employed in UPVLC studies at Oxford University. Furthermore, the potential of these materials as gain medium in OSLs will also be tested, opening the opportunity for a generation of new explosive vapour detection devices based on these lasers.

7 Experimental

General: ^{1}H and ^{13}C NMR spectra were recorded on a Bruker Avance DPX400 at 400.13 and 100.61 MHz or a Bruker Avance DRX500 at 500 MHz and 125.75 MHz in $CDCl_3$ or CD_2Cl_2. Proton NMR chemical shifts are reported as δ values in ppm relative to deuterated solvents: $CDCl_3$ (7.26) or CD_2Cl_2 (5.30). Data are presented as follows: chemical shift, integration, multiplicity (s = singlet, b.s. = broad singlet, d = doublet, t = triplet, q = quartet, m = multiplet), and coupling constant(s) (*J*) are in Hz. Multiplets are reported over the range (in ppm) they appeared. Carbon NMR data were collected relative to the following solvent signals $CDCl_3$ (77.36) or CD_2Cl_2 (53.52). MS MALDI-TOF spectra were recorded on a Shimadzu Axima-CFR spectrometer (mass range 1-150 000 Da). Elemental analyses were obtained on a PERKIN ELMER 2400 elemental analyser. Commercial TLC plates (Silica gel 60 F254) were used for TLC chromatography and column chromatography was carried out on silica gel Zeoprep 60 Hyd (40-63 µm mesh). Solvents were removed using a rotary evaporator (vacuum supplied by low vacuum pump) and, when necessary, a high vacuum pump was used to remove residual solvent. Distillation to remove excess 1-bromoalkane was performed on a Kugelrohr Z24 with a high vacuum pump. Dry solvents (dichloromethane, tetrahydrofuran, toluene, hexane and diethyl ether) were obtained from a solvent purification system (SPS 400, innovative technologies) using alumina as the drying agent; any other dry solvents were purchased from Sigma Aldrich. All reagents and solvents were purchased commercially from Sigma Aldrich or Alfa Aesar and were used without any purification, with the exception of petroleum ether, which was distilled in a rotary evaporator at atmospheric pressure prior to its use as eluent for column chromatography. The following compounds were kindly provided by collaborators: **F_1' H** (Dr. Alexander Kanibolotsky); **4.5** and 1-bromo-2-hexyldecane (Dr. Neil Findlay); **$TPEBr_4$** (Dr. Filipe Vilela); **6.5**, **T-B1**, **T-B1-TMS** and **T-B2** (Diego Cortizo Lacalle).

Optical properties: UV-Vis absorption spectra were recorded on a UNICAM UV 300, a Jasco V-660 or a Shimazdu UV-2600 spectrophotometer. Baselines of solvents were measured before analysis and solution spectra were recorded in 1 cm or 1 mm path length quartz cells between 190 and 900 nm. Emission spectra were measured on a Perkin Elmer LS45 or a Jasco FP-6500 fluorescence spectrometers. Films for studying the optical properties of star-shaped molecules were prepared from 30 mg/mL toluene solutions, which were spin cast onto spectrosil quartz substrates (UQG optics). Absorption measurements were taken using a Shimadzu UV2550 spectrophotometer, with a clean spectrosil quartz substrate as reference. Photoluminescence measurements were taken using a Jobin-Yvon Fluoromax-3 spectrometer. Quantum yield measurements were carried out using this spectrometer and an integrating sphere. The

spectral measurements were corrected for the response of the integrating sphere and spectrometer using a calibrated blackbody emitter. Amplified Spontaneous Emission studies were carried out in air by exciting the structures using a Spectra-Physics GCR 11 Nd:YAG laser which produced pulses of 25 ns duration (FWHM) with a repetition rate of 10 Hz at λ = 355 & 532 nm. The pump beam was shaped into a uniform beam profile using a beam homogeniser (Suss MicroOptics). The output was spatially filtered using a slit, which was then imaged onto the surface of the sample to produce a stripe of 100 µm width and approx. 2 mm length. This configuration produced a uniform beam profile where the variation of the intensity along the length of the stripe was <10%. The beam profile was measured using a Gentec Beamage CCD-12 beam profiler to determine the exact beam dimensions (evaluated at FWHM). Neutral density filters were used to control the energy of the pump light incident on the sample during ASE measurements. The output from the ASE structures was coupled into a spectrometer with CCD camera, using a liquid light-guide (aperture size = 5 mm), which was placed transverse to the pump stripe at the end of the sample film, so that waveguided emission was collected.

Electrochemistry. CV measurements were performed on a CH Instruments 660A electrochemical workstation with *iR* compensation using anhydrous solvents (dichloromethane or 1:2 acetonitrile:benzene). The electrodes were glassy carbon, platinum wire, and silver wire as the working, counter, and reference electrodes, respectively. All solutions were degassed (Ar) and contained monomer substrates in concentrations *ca.* 10^{-4} M, together with $TBAPF_6$ (0.1 M) as the supporting electrolyte. All measurements are referenced against the $E_{1/2}$ of the Fc/Fc^+ redox couple.

Thermogravimetric Analysis. The sample (approx. 5 mg) was placed on a standard platinum pan and loaded at 35 °C to be analysed with a *Perkin Elmer Thermogravimetric Analyzer TGA7* under a constant flow of helium (20 mL/min). The temperature was raised to 50 °C followed by an isothermal period of 5 minutes. The temperature was raised again at a rate of 10 °C/min until 500 °C when the material was left for an isothermal period of 30 minutes. The percentage weight loss over time was recorded at this temperature and the data was processed using the *Pyris Series Software.*

Differential Scanning Calorimetry was conducted on a TA Instruments Q1000 with a RC-90 refrigerated cooling unit attached. The calibration was conducted using Indium (melt temperature 156.42°C, ΔHf 28.42 J/g). The test procedure used was a standard Heat-Cool-

Reheat, that allows the removal of thermal history on the first heat allowing examination of any thermal processes on the cooling and second heat scan. The temperature range was from -50 °C to 300 °C at 10 °C/min.

2,7-Dibromofluorene (**2.3**) [266]

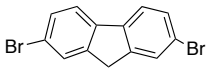

To a mechanically stirred solution of fluorene (97.30 g, 0.58 mol) in acetic acid (870 mL) H_2SO_4 (95 - 97 %, 9.0 mL) was slowly added at 70 °C. The reaction was cooled to 55°C and a solution of bromine (50 mL, 0.97 mol) in acetic acid (67 mL) was added dropwise for 3 h, keeping the temperature at 40 - 55 °C to avoid crystallisation of the fluorene. After the addition of ~1/3 of the amount of bromine, $KBrO_3$ (33.34 g, 0.20 mol) was added in small portions with vigorous stirring to promote the precipitation of 2,7-dibromofluorene. The rest of the bromine was then added dropwise. The mixture was stirred at 50 °C for 4 h and then allowed to reach room temperature before cooling down to 10 °C. The white precipitate was filtered off, washed with 70% acetic acid (1.0 L) and water until a pH of 7 was reached, yielding 177.71 g of crude solid. The material was purified by stirring in acetic acid (340.0 mL) at reflux under N_2 for 4 h. The solid was left to reach room temperature, filtered off, washed with acetic acid and dried to afford (**CO6**) as a dark creamy solid (151.70 g, 0.47 mol, 80 %). ^{1}H NMR ($CDCl_3$) δ (ppm): 7.68 (2 H, s), 7.62 (2 H, d, J = 8.0 Hz), 7.52 (2 H, d, J = 8.0 Hz). The analysis was comparable with that from the literature. [266]

General procedure A: Synthesis of 2,7-dibromo-9,9-dialkylfluorene (**2.4 B**, **2.4 O**) [267]

To a mixture of 2,7-dibromofluorene (**2.3**) (1 eq) and 1-bromoalkane (4 eq) in tetrahydrofuran (8 mL per gram), a solution of potassium *tert*-butoxide (2.25 eq) in dry tetrahydrofuran (200 mL) was added dropwise at 0 °C - +5 °C over 1.5 h with vigorous stirring. The reaction was then stirred at room temperature for 4 h and the mixture was filtered through a silica plug to remove the KBr precipitate, and was washed with dichloromethane. After evaporation of the solvent, the crude product was treated with activated carbon in methanol, filtered by gravity and allowed to crystallise, obtaining the product that was recrystallised from hexane to remove traces of methanol.

2,7-Dibromo-9,9-dibutylfluorene (**2.4 B**)

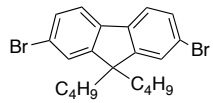

Using the general procedure A, the quantities used were: 2,7-Dibromofluorene (**2.3**) (26.00 g, 0.08 mol), 1-Bromobutane (34.0 mL, 0.32 mol), tetrahydrofuran (200 mL), potassium *tert*-butoxide (20.20 g, 0.18 mol) in dry tetrahydrofuran (200 mL). The product was afforded as white crystals (25.67 g, $59 \cdot 10^{-3}$ mol, 73 %). ^{1}H NMR ($CDCl_3$) δ (ppm): 7.53 (2 H, d, J = 8.0 Hz), 7.45 (4 H, d, J = 8.0 Hz), 1.95–1.91 (4 H, m), 1.09 (4 H, m), 0.70 (6 H, t, J = 8.0 Hz), 0.62-0.54 (4 H, m). Anal. calcd. for $C_{21}H_{22}Br_2$: C, 57.82; H, 5.55, Br; 36.63. Found: C, 57.85; H, 5.43; Br, 36.44. The analysis was comparable with that from the literature.[268]

2,7-Dibromo-9,9-dioctylfluorene (**2.4 O**)

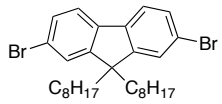

Using the general procedure A, the quantities used were: 2,7-Dibromofluorene (**2.3**) (26.00 g, 0.08 mol), 1-Bromooctane (55 mL, 0.31 mol) tetrahydrofuran (200 mL), solution of potassium *tert*-butoxide (20.20 g, 0.18 mol) in tetrahydrofuran (200 mL). After evaporation of the solvent, residual 1-bromooctane was removed *in vacuo* (45 °C, $1.6 \cdot 10^{-3}$ atm). The product as was afforded as a white-yellowish solid (32.563 g, $59.3 \cdot 10^{-3}$ mol, 74 %). ^{1}H NMR ($CDCl_3$) δ (ppm): 7.53 (2 H, d, J = 8.0 Hz), 7.46 (4 H, d, J = 8.0 Hz), 1.94–1.89 (4 H, m), 1.28-1.06 (20 H, m), 0.84 (6 H, t, J = 8.0 Hz), 0.65-0.54 (4 H, m). The analysis was comparable with that from the literature.[268]

9,9-Dihexylfluorene (**4.5**)[267]

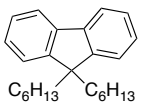

9 H- fluorene (40.00 g, 0.24 mol) was dissolved in dry tetrahydrofuran (400 mL). The solution was cooled to 0 °C and 1-Bromohexane (131 mL, 0.92 mol) was added to the reaction mixture.

A suspension of potassium tert-butoxide (72.4 g, 0.63 mol) in dry tetrahydrofuran (700 mL) was added under nitrogen over 3 hours with vigorous stirring. The reaction mixture was stirred under nitrogen for 18 h and it was then filtered through a silica plug. The filtrate was evaporated and the excess of 1-bromohexane was removed in vacuo (85 °C, 6 mm Hg) for 4 hours. The yellow oil was treated with activated carbon in methanol under reflux, filtered by gravity and allowed to crystallise. 9,9-dihexylfluorene was obtained as a white crystalline powder (64.84 g, 0.19 mol, 80%). ^{1}H NMR ($CDCl_3$) δ (ppm): 7.72 (2 H, d, J =6.0 Hz), 7.36-7.28 (6 H, s), 2.00-1.93 (4 H, m), 1.16-0.99 (12 H, m), 0.77 (6 H, t, J = 5.6 Hz), 0.67-0.58 (4 H, m). The analysis was comparable with that from the literature. [269]

2,7-Dibromo-9,9-dihexylfluorene (**4.6**)[266]

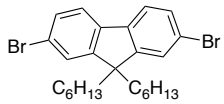

9,9-Dihexylfluorene (**4.5**) (67.50 g, $201.8 \cdot 10^{-3}$ mol) and catalytic iodine (511 mg, $2.02 \cdot 10^{-2}$ mol) were dissolved in dichloromethane and the reaction mixture was protected from the light. Bromine (23.8 mL, 0.46 mol) was added over 90 minutes and the reaction mixture was stirred at room temperature for 18 h. It was then cooled to 0 °C for 15 minutes, quenched with a saturated aqueous solution of Na_2SO_3 (150 mL) and extracted with dichloromethane (3 x 100 mL). The combined organic fractions were washed with a saturated aqueous solution of $NaHCO_3$ (2 x 100 mL) and with water (1 x 100 mL). The organic fraction was dried over $MgSO_4$ and solvent evaporated to yield 92.31 g of white solid. The crude product was treated with activated carbon in ethanol under reflux, filtered by gravity and allowed to crystallise. The 66.60 g of white crystals obtained were recrystallized from hexane yielding 2,7-dibromo-9,9-dihexylfluorene as a white crystalline solid (83.66 g, 0.17 mol, 84 %).^{1}H NMR ($CDCl_3$) δ (ppm): 7.56-7.49 (2 H, m), 7.48-7.42 (4 H, m), 1.95 1.86 (4 H, m), 1.18-0.98 (12 H, m), 0.78 (6 H, t, J = 7.0 Hz), 0.64-0.52 (4 H, s). The analysis was comparable with that from the literature. [269]

General procedure B: Synthesis of 9,9-Dialkyl-7-trimethylsilylfluoren-2-ylboronic acid (**F_1**) [155]

A solution of 2,7-Dibromo-9,9-dialkylfluorene (**2.4**, **4.6**) (1 eq) in dry tetrahydrofuran (20 mL per gram) was prepared under N_2 and at -80 °C a solution of n-BuLi in n-hexanes (1 eq) was added dropwise, carefully maintaining the temperature below -78 °C. The reaction mixture

was stirred at -80 °C for 5 min and then cooled down to -95 °C. Chlorotrimethylsilane (1 eq) was added dropwise and the mixture was left to warm up to room temperature and cooled back to -80 °C. A second portion of n-BuLi in hexanes (1.2 eq) was added dropwise. At -100 °C, triisopropylborate (3 eq) was added slowly and the system allowed to reach room temperature and stirred for 18 h. The mixture was poured over deionised water and extracted with diethyl ether (4 times). The combined organic fractions were washed with water, dried over anhydrous $MgSO_4$ and the solvent evaporated to yield the crude material. The product was purified by flash chromatography with a silica gel column eluting first with toluene to isolate the by-products, then by elution with diethyl ether to isolate the product.

9,9-Dibutyl-7-trimethylsilylfluoren-2-ylboronic acid (**F_1 B**)

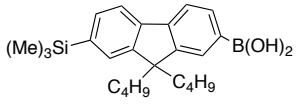

Using the general procedure B, the quantities used were: 2,7-dibromo-9,9-dibutylfluorene (**2.4 B**) (12.20 g, 28.07 mmol), dry tetrahydrofuran (250 mL), n-BuLi (2.38 M in hexanes, 11.8 mL, $28.07 \cdot 10^{-3}$ mol), chlorotrimethylsilane (3.6 mL, $28.07 \cdot 10^{-3}$ mol), n-BuLi (2.38 M in hexanes, 14.15 mL, $33.68 \cdot 10^{-3}$ mol), triisopropylborate (19.8 mL, $84.20 \cdot 10^{-3}$ mol). The product was obtained as a white foamy solid (9.11 g, $23.10 \cdot 10^{-3}$ mol, 82 %). ^{1}H NMR ($CDCl_3$) δ (ppm): 8.32-8.24 (1 H, m), 8.18-7.68 (3 H, m), 7.10-7.45 (2 H, m), 2.20-1.92 (4 H, m), 1.25-0.90 (4 H, m), 0.62-0.54 (10 H, m), 0.32 (9 H, s). The analysis was comparable with that from the literature. [270]

9,9-Dihexyl-7-trimethylsilylfluoren-2-ylboronic acid **F_1 H**

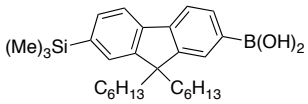

Using the general procedure B, the quantities used were: 2,7-dibromo-9,9-dihexylfluorene (**4.6**) (50.00 g, 0.10 mol), dry tetrahydrofuran (700 mL), n-butyllithium (2.5 M, 40.6 mL, 0.10 mol), chlorotrimethylsilane (13 mL, 0.10 mol), n-BuLi (2.5 M, 48.8 mL, 0.12 mol), triisopropylborate (71.8 mL, 0.30 mol). The product was isolated as a white foamy solid (40.04 g, $88.87 \cdot 10^{-3}$ mol, 88 %). ^{1}HNMR ($CDCl_3$) δ (ppm): 8.30 (1 H, d, J = 7.5 Hz), 8.23 (1 H, s), 7.89 (1 H, d, J = 7.5 Hz), 7.80 (1 H, d, J = 7.7 Hz), 7.56 (1 H, d, J = 6.7 Hz), 7.54 (1 H, s), 2.07-2.13 (4 H,

m), 1.06-1.15 (12 H, m), 0.77 (4 H, m), 0.77 (6 H, t, *J* = 6.6 Hz), 0.35 (9 H, s). The analysis was comparable with that from the literature. [271]

9,9-Dioctyl-7-trimethylsilylfluoren-2-ylboronic acid (**F_1 O**)

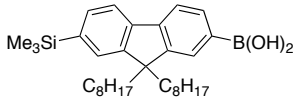

Using the general procedure B, the quantities used were: 2,7-dibromo-9,9-dioctylfluorene (**2.4 O**) (8.04 g, $15 \cdot 10^{-3}$ mol), tetrahydrofuran (100.0 mL), n-butyllithium (2.5 M in n-hexanes, 6.0 mL, $15 \cdot 10^{-3}$ mol), chlorotrimethylsilane (1.9 mL, $15 \cdot 10^{-3}$ mol), n-BuLi (2.5 M in n-hexanes, 7.3 mL, $18 \cdot 10^{-3}$ mol), triisopropylborate (10.6 mL, $46 \cdot 10^{-3}$ mol). The product was afforded as a white foamy solid (6.25 g, $12 \cdot 10^{-3}$ mol, 90 %). ^{1}H NMR ($CDCl_3$) δ (ppm): 8.32 (1 H, d, *J* = 8.0 Hz), 8.24 (1 H, s), 7.91 (1 H, d, *J* = 8.0 Hz), 7.81 (1 H, t, *J* = 8.0 Hz), 7.57-7.53 (2 H, m), 2.18-2.04 (4 H, m), 1.05-0.96 (18 H, m), 0.80 (6 H, t, *J* = 8.0 Hz), 0.78-0.65 (4 H, m), 0.35 (9 H, t, *J* = 8.0 Hz). The analysis was comparable with that from the literature. [141]

General procedure C: Synthesis of 7'-bromo-9-alkyl-oligofluorenyltrimethylsilanes (**TMS-F_n-Br**) by Suzuki cross-coupling (**2.5 B**, **2.6 B**, **2.7 B**, **2.5 O**, **2.6 O**, **2.7 O**, **4.7**, **4.8**, **4.9**)[59]

A solution of 2,7-dibromo-9,9-dialkylfluorene (**2.4**, **4.6**) (3 eq) and $Pd(PPh_3)_4$ (0.03 eq) in dry toluene (2.6 mL per gram) was stirred under a N_2 atmosphere for 20 min. A solution of 9,9-dialkyl-7-trimethylsilyloligofluoren-2-ylboronic acid (**F_n**) (1 eq) in dry toluene (2.5 mL per gram) was added to the mixture. The flask previously containing **F_n** was washed with an additional portion of dry toluene and added to the reaction mixture. A 2M aqueous solution of Na_2CO_3 (2.3 eq) was added and the system was stirred under N_2 at 80 °C for 18 h. The reaction mixture was washed with water and extracted with dichloromethane (5 times). The combined organic fractions were washed with water, dried over anhydrous $MgSO_4$ and the solvent evaporated yielding the crude product as a yellow oil. The material was purified by column chromatography on silica gel and then crystallised in acetone to afford the product.

7'-Bromo-9,9,9',9'-tetrabutyl-2,2'-bifluoren-7-yl) trimethylsilane (**2.5 B**)

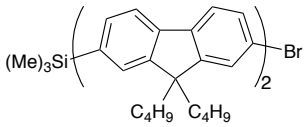

Using the general procedure C, the quantities used were: 2,7-dibromo-9,9-dibutylfluorene (**2.4 B**) (26.69 g, $61.19 \cdot 10^{-3}$ mol), $Pd(PPh_3)_4$ (0.71 g, $6.12 \cdot 10^{-4}$ mol), dry toluene (70 mL), 9,9-dibutyl-7-trimethylsilylfluoren-2-ylboronic acid (**F_1 B**) (8.05 g, $20.40 \cdot 10^{-3}$ mol), dry toluene (40 mL), 2M aqueous solution of Na_2CO_3 (24 mL, $47.94 \cdot 10^{-3}$ mol). Column chromatography petroleum ether. The product was obtained as a white crystalline solid (10.41 g, 14.74 mmol, 72 %). ^{1}H NMR ($CDCl_3$) δ (ppm): 7.80-7.72 (3 H, m), 7.67-7.59 (5 H, m), 7.54-7.47 (4 H, m), 2.10-1.95 (8 H, m), 1.18-1.08 (8 H, m), 0.79-0.67 (20 H, m), 0.34 (9 H, t, J = 8.0 Hz). ^{13}C NMR ($CDCl_3$) δ (ppm): 150.60, 149.67, 140.84, 140.46, 139.96, 139.79, 139.35, 138.70, 138.63, 131.37, 129.50, 127.13, 125.73, 125.70, 125.38, 120.95, 120.86, 120.59, 120.48, 119.54, 119.51, 118.52, 54.95, 54.45, 39.65, 39.46, 25.56, 25.47, 22.53, 13.33, 13.29, -1.33. (MALDI/TOF, m/z): [M^+] calcd. for $C_{45}H_{57}BrSi$: 705.9; found, 704.4. Anal. calcd. for $C_{45}H_{57}BrSi$: C, 76.56; H, 8.14, Br; 11.32. Found: C, 76.74; H, 8.53; Br, 11.23.

2-Bromo-9,9,9',9',9'',9''-hexabutyl-2,2'-terfluorenyl-7-trimethylsilane (**2.6 B**)

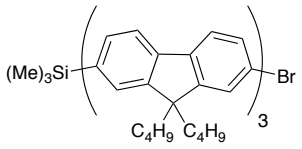

Using the general procedure C, the quantities used were: 2,7-dibromo-9,9-dibutylfluorene (**2.4 B**) (13.07 g, $29.96 \cdot 10^{-3}$ mol), $Pd(PPh_3)_4$ (346 mg, $3.00 \cdot 10^{-4}$ mol), toluene (70 mL), 9,9,9',9'-tetrabutyl-2,2'-bifluoren-7-trimethylsilylboronic acid (**F_2 B**) (6.70 g, $23.47 \cdot 10^{-3}$ mol), toluene (60 mL), 2M solution of Na_2CO_3 (11.73 mL, $23.47 \cdot 10^{-3}$ mol). Column chromatography with petroleum ether. The product was obtained as a white solid (6 g, $6.11 \cdot 10^{-3}$ mol, 61 %). ^{1}H NMR ($CDCl_3$) δ (ppm): 7.85-7.58 (12 H, m), 7.55-7.46 (6 H, m), 2.18-1.94 (12 H, m), 1.23-1.06 (12 H, m), 0.85-0.65 (30 H, m), 0.34 (9 H, s). ^{13}C NMR ($CDCl_3$) δ (ppm): 153.60, 152.19, 152.12, 152.05, 151.48, 141.75, 141.30, 140.90, 140.86, 140.71, 140.54, 140.26, 140.20, 139.58, 139.40, 132.20, 130.36, 127.98, 126.57, 126.46, 126.32, 121.81, 121.74, 121.42, 121.33, 120.36, 120.33, 119.34, 55.80, 55.61, 55.38, 40.54, 40.47, 40.31, 26.47, 26.42, 26.33, 14.14, 14.11, -

0.50. (MALDI/TOF, m/z): [M^+] calcd. for $C_{90}H_{129}BrSi$: 1318.9; found, 1318.3. Anal. calcd. for $C_{90}H_{129}BrSi$: C, 8.70; H, 8.31, Found: C, 8.05; H, 6.93.

7-Bromo-9,9,9',9',9'',9'',9''',9'''-octabutyl-2-trimethylsilylquaterfluorene (**2.7 B**)

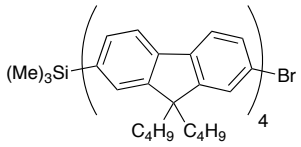

Using the general procedure C, the quantities used were: 2,7-dibromo-9,9-dibutylfluorene (**2.4**) (1.38 g, $3.17\cdot10^{-3}$ mol), $Pd(PPh_3)_4$ (37 mg, $3.20\cdot10^{-5}$ mol), toluene (25 mL), 9,9,9',9',9'',9''-hexabutyl-2,2'-terfluorenyl-7-trimethylsilyl-boronic acid (**F_3 B**) (1.00 g, $1.06\cdot10^{-3}$ mol), toluene (6 mL), 2M solution of Na_2CO_3 (1.24 mL, $2.48\cdot10^{-3}$ mol). Column chromatography eluting first with petroleum ether and then 30:1 petroleum ether:toluene. The product was afforded as a creamy solid, with low solubility in most solvents (0.70 g, $3.71\cdot10^{-3}$ mol, 52 %). ^{1}H NMR ($CDCl_3$) δ (ppm): 7.88-7.59 (20 H, m), 7.57-7.47 (4 H, m), 2.19-1.95 (16 H, m), 1.23-1.08 (16 H, m), 0.87-0.63 (40 H, m), 0.34 (9 H, s). ^{13}C ($CDCl_3$) δ (ppm): 140.44, 140.02, 139.88, 139.85, 139.70, 139.59, 139.49, 139.46, 139.35, 138.76, 138.55, 131.37, 129.53, 127.14, 125.74, 125.63, 125.49, 120.96, 120.89, 120.60, 120.51, 119.54, 118.51, 54.97, 54.78, 54.55, 39.74, 39.66, 39.49, 25.64, 25.58, 25.49, 22.62, 22.55, 13.36, 13.33, 13.30, -1.32. (MALDI/TOF, m/z): [M^+] calcd. for $C_{66}H_{81}BrSi$: 1258.0; Found: 1259.0; Anal. calcd. for $C_{66}H_{81}BrSi$: C, 83.01; H, 8.41; Br, 6.35; Found: C, 81.80; H, 8.24; Br, 6.12.

7'-Bromo-9,9,9',9'-tetrahexyl-2,2'-bifluoren-7-yl) trimethylsilane (**4.7**)

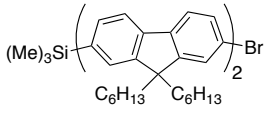

Using the general procedure C, the quantities used were: 2,7-dibromo-9,9-dihexylfluorene (**4.6**) (107.00 g, 218 mmol), $Pd(PPh_3)_4$ (3.00 g, 2.66 mmol), toluene (200 mL), 9,9-dihexyl-7-trimethylsilylfluoren-2-ylboronic acid (**F_1 H**) (40.00 g, 88.8 mmol), toluene (200 mL), Na_2CO_3 (2 M, 104 mL, 209.7 mmol). Column chromatography with petroleum ether. The product was obtained as a white solid (53.80 g, 65.70 mmol, 74 %). ^{1}H NMR ($CDCl_3$) δ (ppm): 7.81-7.70 (3 H,

m), 7.67-7.57 (5 H, m), 7.55-7.46 (4 H, m), 2.94-2.10 (8 H, m), 1.20-1.03 (24 H, m), 0.83-0.66 (20 H, m), 0.34 (9 H, m). The analysis was comparable with that from the literature.[271]

2-Bromo-9,9,9',9',9'',9''-hexahexyl-2,2'-terfluorenyl-7-trimethylsilane (**4.8**)

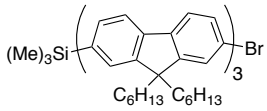

Using the general procedure C, the quantities used were: 2,7-dibromo-9,9-dihexylfluorene (**4.6**) (10.94 g, $22.2 \cdot 10^{-3}$ mol), $Pd(PPh_3)_4$ (257 mg, $2.20 \cdot 10^{-4}$ mol), toluene (100 mL), 9,9,9',9'-tetraoctyl-2,2'-bifluoren-7-trimethylsilylboronic acid (**F_2 H**) (5.80 g, $7.41 \cdot 10^{-3}$ mol), toluene (70 mL), Na_2CO_3 (2 M, 8.7 mL, $17.4 \cdot 10^{-3}$ mol). Column chromatography with petroleum ether:toluene (10:1). The product was obtained as a white crystalline solid (6.26 g, $5.44 \cdot 10^{-3}$ mol, 73 %). ^{1}H NMR ($CDCl_3$) δ (ppm): 7.85-7.71 (5 H, m), 7.71-7.59 (9 H, m), 7.55-7.47 (4 H, m), 2.14-1.96 (12 H, m), 1.20-1.05 (36 H, m), 0.86-0.68 (30 H, m), 0.34 (9 H, s). ^{13}C NMR ($CDCl_3$) δ (ppm): 153.42, 151.98, 151.92, 151.86, 151.27, 150.33, 141.56, 141.20, 140.77, 140.48, 140.43, 140.32, 140.05, 140.01, 139.36, 139.15, 132.00, 130.15, 127.79, 126.43, 126.37, 126.32, 126.17, 121.67, 121.60, 121.22, 121.13, 120.13, 119.16, 55.69, 55.48, 55.26, 40.48, 40.44, 40.28, 31.60, 31.51, 29.78, 29.72, 23.98, 23.88, 22.70, 22.63, 14.15, -0.70. (MALDI/TOF, m/z): [M^+] calcd. for $C_{78}H_{105}BrSi$: 1148.7; Found: 1148.0; Anal. calcd. for $C_{66}H_{81}BrSi$: C, 81.42; H, 9.20; Br, 6.94; Found: C, 81.34; H, 9.12; Br, 6.97.

7-Bromo-9,9,9',9',9'',9'',9''',9'''-octahexyl-2-trimethylsilylquaterfluorene (**4.9**)

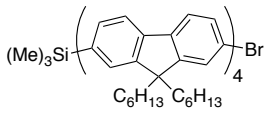

Using the general procedure C, the quantities used were: 2,7-dibromo-9,9-dihexylfluorene (**4.6**) (5.59 g, $11.35 \cdot 10^{-3}$ mol), $Pd(PPh_3)_4$ (0.13 g, $1.14 \cdot 10^{-4}$ mol), toluene (70 mL), 9,9,9',9',9'',9''-hexahexyl-2,2'-terfluorenyl-7-trimethylsilyl-boronic acid (**F_3 H**) (4.22 g, $3.79 \cdot 10^{-3}$ mol), toluene (50 mL), Na_2CO_3 (2 M, 4.5 mL, $8.90 \cdot 10^{-3}$ mol). Column chromatography eluting first with petroleum ether and then with petroleum ether:toluene (9:1). The product was obtained as a white solid (3.62 g, $2.44 \cdot 10^{-3}$ mol, 64 %). ^{1}H NMR ($CDCl_3$) δ (ppm): 7.88-7.57 (20 H, m), 7.55-

7.46 (4 H, m), 2.19-1.92 (16 H, m), 1.23-1.02 (48 H, m), 0.90-0.66 (40 H, m). The product contained a small impurity seen by TLC and it was used without further purification.

7'-Bromo-9,9,9',9'-tetraoctyl-2,2'-bifluoren-7-yl) trimethylsilane (**2.5 O**)

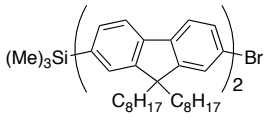

Using the general procedure C, the quantities used were: 2,7-dibromo-9,9-dioctylfluorene (**2.4 O**) (19.74 g, $36 \cdot 10^{-3}$ mol), $Pd(PPh_3)_4$ (416 mg, $3.60 \cdot 10^{-4}$ mol), toluene (40 mL), 9,9-dioctyl-7-trimethylsilylfluoren-2-ylboronic acid (**F_1 O**) (6.05 g, $12 \cdot 10^{-3}$ mol), toluene (20 mL), 2M solution of Na_2CO_3 (14 mL, $28 \cdot 10^{-3}$ mol). Column chromatography with petroleum ether. The product was obtained as a white solid (8.06 g, $8.67 \cdot 10^{-3}$ mol, 88 %). ^{1}H NMR ($CDCl_3$) δ (ppm): 7.78 (1 H, d, *J* = 8.0 Hz), 7.73 (2 H, t, *J* = 6.0 Hz), 7.66-7.59 (5 H, m), 7.53-7.47 (4 H, m), 2.05-1.93 (8 H, m), 1.20-1.09 (40 H, m), 0.84-0.66 (20 H, m), 0.34 (9 H, m). ^{13}C NMR ($CDCl_3$) δ (ppm): 39.77, 39.62, 31.28, 29.43, 28.66, 28.61, 23.28, 22.11, 13.58, 3.00. (MALDI/TOF, m/z): [M^+] for $C_{53}H_{73}BrSi$: 930.6. The analysis was comparable with that from the literature. [272]

2-Bromo-9,9,9',9',9'',9''-hexaoctyl-2,2'-terfluorenyl-7-trimethylsilane (**2.6 O**)

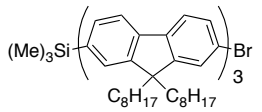

Using the general procedure C, the quantities used were: 2,7-dibromo-9,9-dioctylfluorene (**2.4 O**) (17.77 g, $32.40 \cdot 10^{-3}$ mol), $Pd(PPh_3)_4$ (374 mg, $3.00 \cdot 10^{-5}$ mol), toluene (60 mL), 9,9,9',9'-tetraoctyl-2,2'-bifluoren-7-trimethylsilylboronic acid (**F_2 O**) (9.71 g, $10.80 \cdot 10^{-3}$ mol), toluene (40 mL), Na_2CO_3 (2 M, 13 mL, $25.92 \cdot 10^{-3}$ mol). Column chromatography eluting with petroleum ether. The product as was obtained as a white crystalline solid (10.98 g, $8.01 \cdot 10^{-3}$ mol, 74 %). ^{1}H NMR ($CDCl_3$) δ (ppm): 7.84-7.74 (5 H, m), 7.67-7.61 (9 H, m), 7.55-7.49 (4 H, m), 2.14-1.97 (12 H, m), 1.28-1.60 (60 H, m), 0.89-0.67 (30 H, m), 0.35 (9 H, s). ^{13}C NMR ($CDCl_3$) δ (ppm): 140.91, 140.53, 140.09, 139.82, 139.75, 139.68, 139.40, 139.36, 138.71, 138.49, 131.35, 129.50, 127.16, 125.78, 125.73, 125.66,125.52, 120.99, 120.92, 120.57, 120.47, 119.49, 119.46, 118.51, 55.04, 54.84, 54.61, 39.86, 38.78, 39,65, 31.28, 29.52, 29.45, 28.70, 28.62, 23.40, 23.31, 23.27, 22.10, 13.56, -1.34. (MALDI/TOF, m/z): [M^+] calcd. for $C_{90}H_{129}BrSi$: 1318.9;

found, 1318.3. Anal. calcd. for $C_{90}H_{129}BrSi$: C, 81.95; H, 9.86, Br, 6.06; Found: C, 82.11; H, 9.75; Br, 6.50.

7-Bromo-9,9,9',9',9'',9'',9''',9'''-octaoctyl-2-trimethylsilylquaterfluorene (**2.7 O**)

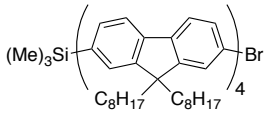

Using the general procedure C, the quantities used were: 2,7-dibromo-9,9-dioctylfluorene (**2.4 O**) (7.48 g, $13.63 \cdot 10^{-3}$ mol), $Pd(PPh_3)_4$ (158 mg, $1.40 \cdot 10^{-4}$ mol), toluene (60 mL), 9,9,9',9',9'',9''-hexaoctyl-2,2'-terfluorenyl-7-trimethylsilyl-boronic acid (**F_3 O**) (6.06 g, $4.54 \cdot 10^{-3}$ mol), toluene (50 mL), Na_2CO_3 (aq) (2 M, 6.8 mL, 13.63 mmol). Column chromatography eluting first with petroleum ether and then petroleum ether:toluene (30:1). The product was afforded as a creamy solid (6.32 g, $3.71 \cdot 10^{-3}$ mol, 82 %). ^{1}H NMR ($CDCl_3$) δ (ppm): 7.86-7.61 (20 H, m), 7.57-7.48 (4 H, m), 2.19-1.96 (16 H, m), 1.32-1.07 (80 H, m), 0.91-0.67 (40 H, m), 0.36 (9 H, s). The analysis was comparable with that from the literature. [272]

General procedure D: Deprotection of the trimethylsilane group of 2-bromoligofluorenyl-7-trimethylsilanes (**4.10**, **4.11**, **4.12**, **2.8**)

To a solution of 2-bromo-9,9-alkyl-2,2'-oligofluorenyl-7-trimethylsilane (**TMS-F_n-Br**) (1 eq) in dichloromethane (16 mL per gram), CF_3COOH (15 eq) was added and the mixture stirred at room temperature for 2 h. Basic work up was carried out with water (2 times), saturated $NaHCO_3$ solution (2 times) and final washing with water. The organic fraction was dried over anhydrous $MgSO_4$ and filtered through a silica plug to remove polar by-products and crystallised from acetone to yield the product.

7'-Bromo-9,9,9',9'-tetrahexyl-2,2'-bifluorene (**4.10**)

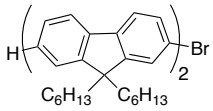

Using the general procedure D, the quantities used were: 2-bromo-9,9,9',9'-tetrahexyl-2,2'-bifluorenyl-7-trimethylsilane (**4.7**) (8.00 g, $9.78 \cdot 10^{-3}$ mol), dichloromethane (130 mL), CF_3COOH (10.3 mL). The product was obtained as a white crystalline solid (6.28 g, $8.43 \cdot 10^{-3}$ mol, 86 %). ^1H NMR ($CDCl_3$) δ (ppm): 7.81-7.71 (3 H, m), 7.68-7.55 (5 H, m), 7.51-7.45 (2 H, m), 7.40-7.29 (3 H, m), 2.10-1.91 (8 H, m), 1.20-0.99 (24 H, m), 0.83-0.62 (20 H, m). The analysis was comparable with that from the literature. [59]

7-Bromo-9,9,9',9',9'',9''-hexahexyl-2,2'-terfluorene (**4.11**)

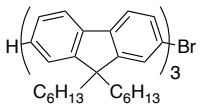

Using the general procedure D, the quantities used were: 2-bromo-9,9,9',9',9'',9''-hexahexyl-2,2'-terfluorenyl-7-trimethylsilane (**4.8**) (7.50 g, $6.52 \cdot 10^{-3}$ mol), dichloromethane (100 mL), CF_3COOH (6.8 mL). The product was obtained as a white crystalline solid (6.03 g, $5.60 \cdot 10^{-3}$ mol, 86 %). ^1H NMR ($CDCl_3$) δ (ppm): 7.86-7.73 (5 H, m), 7.69-7.58 (9 H, m), 7.51 (2 H, m), 7.39-7.29 (3 H, m), 2.14-1.92 (12 H, m), 1.21-1.00 (36 H, m), 0.88-0.63 (30H, m). The analysis was comparable with that from the literature. [59]

7-Bromo-9,9,9',9',9'',9'',9''',9'''-octahexyl-2,2'-quaterfluorene (**4.12**)

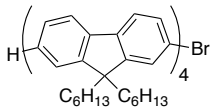

Using the general procedure D, the quantities used were: 7-bromo-9,9,9',9',9'',9'',9''',9'''-octahexyl-2-trimethylsilylquaterfluorene (**4.9**) (3.51 g, $2.42 \cdot 10^{-3}$ mol), dichloromethane (56 mL), CF_3COOH (2.6 mL). The product was obtained as a white solid (3.25 g, $2.30 \cdot 10^{-3}$ mol, 95 %). ^1H NMR ($CDCl_3$) δ (ppm): 7.90-7.74 (7 H, m), 7.74-7.59 (13 H, m), 7.52-7.30 (5 H, m), 2.18-1.95 (16 H, m), 1.29-1.05 (48 H, m), 0.90-0.65 (40 H, m). The analysis was comparable with that from the literature. [59]

7-Bromo-9,9,9',9',9'',9'',9''',9'''-octaoctyl-2,2'-quaterfluorene (**2.8**)

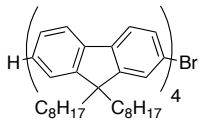

Using the general procedure D, the quantities used were: 7-bromo-9,9,9',9',9'',9'',9''',9'''-octaoctyl-2-trimethylsilylquaterfluorene (**2.7 O**) (2.96 g, $1.74 \cdot 10^{-3}$ mol), dichloromethane (56 mL), CF_3COOH (1.8 mL). The product was obtained as a white crystalline solid (2.74 g, $1.68 \cdot 10^{-3}$ mol, 96 %). ^{1}H NMR ($CDCl_3$) δ (ppm): 7.86-7.59 (20 H, m), 7.52-7.30 (5 H, m), 2.20-1.96 (16 H, m), 1.29-1.05 (80 H, m), 0.90-0.65 (40 H, m). ^{13}C NMR ($CDCl_3$) δ (ppm): 140.78, 140.75, 140.68, 140.56, 140.48, 140.38, 140.27, 140.19, 140.16, 140.07, 139.44, 130.22, 129.00, 127.43, 127.21, 127.01, 126.50, 126.38, 126.26, 123.15, 121.70, 121.62, 121.29, 121.21, 120.21,120.10, 119.94, 55.76, 55.56, 55.39, 40.61, 40.51, 32.02, 30.26, 30.18, 29.45, 24.13, 24.05, 23.99, 22.86, 22.80, 14.30. TOF/MALDI [M^+] calcd. for $C_{116}H_{162}Br$ 1636.4, found 1635.6. HRMS EI cald. for $C_{116}H_{162}Br$ 1634.1860, found 1634.1812.

General procedure E: Synthesis of 9-alkyl-oligofluorenylboronic acid (**F$_n$**)[59]

To a solution of 7'-bromo-9,9,9',9'-oligofluorene (**2.5**, **2.6**, **2.7, 2.8**, **4.7**, **4.8**, **4.10**, **4.11**, **4.12**) (1 eq) in dry tetrahydrofuran, n-BuLi (1.3 eq) was added dropwise under a N_2 atmosphere at -80 °C. The mixture was stirred at -80 °C for 10 min and then cooled down to -100 °C. Triisopropylborate (3 eq) was added and the reaction mixture was allowed to warm up to room temperature and stirred for 18 h. The reaction mixture was poured onto crushed ice, acidified with HCl to pH 2-3 when the TMS functionality was not present or quenched with water when it was. The mixture was then extracted with diethyl ether (4 times) and the combined organic fractions were washed with water, dried over anhydrous $MgSO_4$ and the solvent evaporated. The residue was purified by flash chromatography on a silica gel column with elution first by toluene to remove by-products and then with diethyl ether to recover the product.

9,9,9',9'-Tetrabutyl-2,2'-bifluoren-7-trimethylsilyl-2-boronic acid (**F_2 B**)

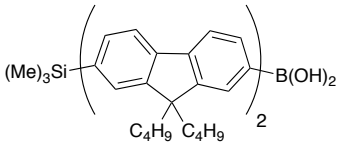

Using the general procedure E, the quantities used were: 7'-Bromo-9,9,9',9'-tetrabutyl-2,2'-bifluoren-7-yl)trimethylsilane (**2.5 B**) (10.41 g, $14.70 \cdot 10^{-3}$ mol), tetrahydrofuran (260 mL), n-BuLi (1.5 M solution in n-hexanes, 11.8 mL, $17.60 \cdot 10^{-3}$ mol), triisopropylborate (10.4 mL, $44.10 \cdot 10^{-3}$ mol). The product was afforded as a white foamy solid (7.99 g, $11.90 \cdot 10^{-3}$ mol, 81 %). ^{1}H NMR ($CDCl_3$) δ (ppm): 8.44-8.23 (2 H, m), 7.85-7.62 (2 H, m), 7.84-7.26 (6 H, m), 7.57-7.48 (2 H, m), 2.29-1.99 (8H, m), 1.56-1.07 (8 H, m), 0.86-0.64 (20 H, m), 0.34 (9 H, s). ^{13}C NMR ($CDCl_3$) δ (ppm): 152.88, 152.48, 152.19, 150.89, 150.65, 145.73, 144.40, 141.88, 141.82, 140.95, 140.88, 140.36, 139.57, 135.16, 132.72, 132.31, 130.31, 129.48, 128.28, 128.10, 126.64, 126.52, 122.00, 121.95, 121.12, 120.85, 120.50, 119.80, 119.48, 55.59, 55.51, 40.65, 40.41, 26.59, 26.54, 26.48, 23.56, 23.47, 14.29, 14.25, 14.22, -0.40. (MALDI/TOF, m/z): [M^+] calcd. for $C_{45}H_{59}BO_2Si$: 670.8; found, 670.9. Anal. calcd. for $C_{45}H_{59}BO_2Si$: C, 80.57; H, 8.86. Found: C, 81.52; H,8.35.

9,9,9',9',9'',9''-Hexabutyl-2,2'-terfluorenyl-7-trimethylsilyl-boronic acid (**F_3 B**)

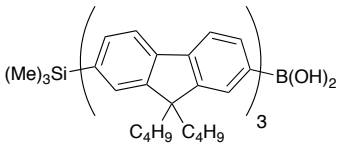

Using the general procedure E, the quantities used were: 2-bromo-9,9,9',9',9'',9''-hexabutyl-2,2'-terfluorenyl-7-trimethylsilane (**2.6 B**) (6.00 g, $6.11 \cdot 10^{-3}$ mol), tetrahydrofuran (170 mL), n-BuLi (1.52 M solution in n-hexanes, 5.2 mL, $7.94 \cdot 10^{-3}$ mol), triisopropylborate (4.2 mL, $18.32 \cdot 10^{-3}$ mol). The product was afforded as a white foamy solid (4.77 g, $5.04 \cdot 10^{-3}$ mol, 82 %). The compound could not be properly characterised as a boronic acid because it had trapped ether in the structure. It was converted to boronic ester for characterisation purposes (**F_3BE B**).

9,9,9',9',9'',9'',9''',9'''-Octabutyl-2,2'-quaterfluorenyl-7-trimehylsilboronic acid (**F_4 B**)

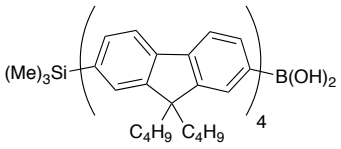

Using the general procedure E, the quantities used were: 7-bromo-9,9,9',9',9'',9'',9''',9'''-octabutyl-2-trimethylsilylquaterfluorene (**2.7 B**) (0.65 g, $5.20\cdot10^{-4}$ mol), tetrahydrofuran (170 mL), n-BuLi (2.2 M solution in n-hexanes, 0.30 mL, $6.70\cdot10^{-4}$ mol), triisopropylborate (0.36 mL, $1.5\cdot10^{-3}$ mol). The product was obtained as a white foamy solid (0.29 mg, $2.40\cdot10^{-4}$ mol, 46 %). ^{1}H NMR ($CDCl_3$) δ (ppm): 8.44-8.25 (1 H, m), 8.01-7.92 (1 H, m), 7.92-7.62 (20 H, m), 7.55-7.48 (2 H, m), 2.26-1.20 (16 H, m), 1.30-1.07 (16 H, m), 0.90-0.64 (40 H, m), 0.34 (9 H, s). (MALDI/TOF, m/z): [M^+] calcd. for $C_{87}H_{107}BO_2Si$: 1223.7; Found: 1224.0; Anal. calcd. for $C_{87}H_{107}BO_2Si$: C, 85.39; H, 8.81; Found: C, 85.40; H, 8.58.

9,9,9',9'-Tetrahexyl-2,2'-bifluorenyl-2-boronic acid (**F_2' H**)

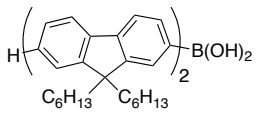

Using the general procedure E, the quantities used were: 7'-bromo-9,9,9',9'-tetrahexyl-2,2'-bifluorene (**4.10**) (6.20 g, $8.32\cdot10^{-3}$ mol), tetrahydrofuran (100 mL), n-BuLi (2 M solution in n-hexanes, 5.4 mL, $10.80\cdot10^{-3}$ mol), triisopropylborate (5.8 mL, $25.00\cdot10^{-3}$ mol). The product was afforded as a white foamy solid (4.65 g, $6.54\cdot10^{-3}$ mol, 79 %). ^{1}H NMR ($CDCl_3$) δ (ppm): 8.43-8.06 (2 H, m), 7.99-7.85 (2 H, m), 7.95-7.60 (6 H, m), 7.43-7.29 (3 H, m), 2.27-1.96 (8 H, m), 1.23-1.03 (24 H, m), 0.91-0.62 (20 H, m). The analysis was comparable with that from the literature. [59]

9,9,9',9'-Tetrahexyl-2,2'-bifluoren-7-trimethylsilyl-2-boronic acid (**F_2 H**)

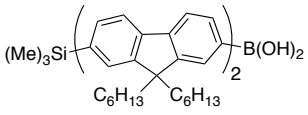

Using the general procedure E, the quantities used were: 7'-bromo-9,9,9',9'-tetrahexyl-2,2'-bifluoren-7-yl)trimethylsilane (**4.7**) (40.00 g, $48.9 \cdot 10^{-3}$ mol), tetrahydrofuran (500 mL), n-BuLi (2.43 M solution in n-hexanes, 26.1 mL, $63.6 \cdot 10^{-3}$ mol), triisopropylborate (33.8 mL, $146.7 \cdot 10^{-3}$ mol). The product was obtained as a white foamy solid (35.20 g, $44.96 \cdot 10^{-3}$ mol, 92 %). ^{1}H NMR ($CDCl_3$) δ (ppm): 8.41-8.10 (2 H, m), 7.97-7.61 (8 H, m), 7.56-7.47 (2 H, m), 2.29-1.96 (8 H, m), 1.21-1.05 (24 H, m), 0.84-0.67 (20 H, m), 0.34 (9 H, s). The analysis was comparable with that from the literature. [271]

9,9,9',9',9'',9''-Hexahexyl-2,2'-terfluorenyl-7-trimethylsilyl-boronic acid (**F_3 H**)

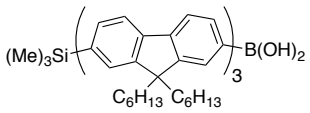

Using the general procedure E, the quantities used were: 2-bromo-9,9,9',9',9'',9''-hexahexyl-2,2'-terfluorenyl-7-trimethylsilane (**4.8**) (6.10 g, $5.30 \cdot 10^{-3}$ mol), tetrahydrofuran (76 mL), n-BuLi (2.42 M solution in n-hexanes, 2.9 mL, $6.89 \cdot 10^{-3}$ mol), triisopropylborate (3.7 mL, $15.90 \cdot 10^{-3}$ mol). The product was obtained as a white foamy solid (4.71 g, $4.22 \cdot 10^{-3}$ mol, 80 %). ^{1}H NMR ($CDCl_3$) δ (ppm): 8.46-8.24 (2 H, m), 8.00-7.74 (5 H, m), 7.77-7.60 (9 H, m), 7.56-7.45 (2 H, m), 2.30-1.94 (12 H, m), 1.21-1.04 (36 H, m), 0.88-0.68 (30 H, m), 0.33 (9 H, s). ^{13}C NMR ($CDCl_3$) δ (ppm): 152.61, 151.96, 151.87, 150.62, 150.34, 141.57, 140.79, 140.56, 140.09, 139.15, 132.00, 127.79, 126.40, 126.18, 121.69, 120.16, 119.16, 55.51, 55.39, 55.26, 40.51, 40.29, 31.68, 31.62, 31.51, 29.90, 29.82, 29.73, 24.02, 23.88, 22.72, 22.64, 14.17, -0.69. (MALDI/TOF, m/z): [M^+] calcd. for $C_{78}H_{107}BO_2Si$: 1114.8, Found: 1114.4; Anal. calcd. for $C_{78}H_{107}BO_2Si$: C, 85.36; H, 9.67; Found: C, 85.13; H, 9.86.

9,9,9',9',9'',9''-Hexahexyl-2,2'-terfluoren-7-ylboronic acid (**F_3' H**)

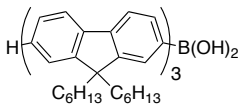

Using the general procedure E, the quantities used were: 7-bromo-9,9,9',9',9'',9''-hexahexyl-2,2'-terfluorene (**4.11**) (6.40 g, $5.93 \cdot 10^{-3}$ mol), tetrahydrofuran (75 mL), n-BuLi (1.54 M solution in n-hexanes, 5 mL, $7.71 \cdot 10^{-3}$ mol) triisopropylborate (4.1 mL, $17.80 \cdot 10^{-3}$ mol). The product was

obtained as a white foamy solid (5.19 g, 4.17 mmol, 84 %). ^{1}H NMR ($CDCl_3$) δ (ppm): 8.43-8.25 (2 H, m), 8.00-7.90 (2 H, m), 7.87-7.78 (3 H, m), 7.78-7.61 (9 H, m), 7.41-7.29 (3 H, m), 2.30-1.97 (12 H, m), 1.22-1.02 (36 H, m), 0.91-0.66 (30 H, m). The analysis was comparable with that from the literature. [59]

9,9,9',9',9'',9'',9''',9''',9''''-Octahexyl-2,2'-quaterfluoren-7-ylboronic acid (**F$_4$' H**)

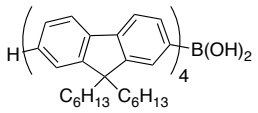

Using the general procedure E, the quantities used were: 7-bromo-9,9,9',9',9'',9'',9''',9''''-octahexyl-2,2'-quaterfluorene (**4.12**) (3.24 g, $2.30 \cdot 10^{-3}$ mol), tetrahydrofuran (40 mL), n-BuLi (2.4 M solution in n-hexanes, 1.25 mL, $2.99 \cdot 10^{-3}$ mol), triisopropylborate (1.60 mL, $6.89 \cdot 10^{-3}$ mol). The product was obtained as a white foamy solid (2.51 g, $1.82 \cdot 10^{-3}$ mol, 79 %). ^{1}H NMR ($CDCl_3$) δ (ppm): 8.43-8.13 (2H, m), 8.03-7.62 (20 H, s), 7.41-7.30 (3 H, m), 2.34-1.97 (16 H, m), 1.27-1.00 (48 H, m), 0.96-0.66 (40 H, m). The analysis was comparable with that from the literature. [59]

9,9,9',9'-Tetraoctyl-2,2'-bifluoren-7-trimethylsilyl-2-boronic acid (**F$_2$ O**)

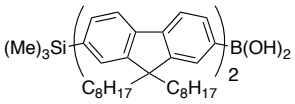

Using the general procedure E, the quantities used were: 7'-bromo-9,9,9',9'-tetraoctyl-2,2'-bifluoren-7-yl) trimethylsilane (**2.5 O**) (8.96 g, $9.62 \cdot 10^{-3}$ mol), tetrahydrofuran (100 mL), n-BuLi (1.95 M solution in n-hexanes, 6.41 mL, $12.51 \cdot 10^{-3}$ mol, triisopropylborate (6.7 mL, $28.86 \cdot 10^{-3}$ mol). The product was afforded as a white foamy solid (5.94 g, $6.63 \cdot 10^{-3}$ mol, 69 %). ^{1}H NMR ($CDCl_3$) δ (ppm): 8.38 (1 H, d, J = 7.6 Hz), 7.96 (1 H, d, J = 7.6 Hz), 7.93 (1 H, d, J = 8.0 Hz), 7.84 (1 H, d, J = 7.6 Hz), 7.77-7.68 (6 H, m), 7.56-7.93 (2 H, d, J = 8.8 Hz), 2.30-2.04 (8H, m), 1.26-1.07 (40 H, m), 0.88-0.75 (20 H, m), 0.36 (9 H, s). The analysis was comparable with that from the literature. [272]

9,9,9',9',9'',9''-Hexaoctyl-2,2'-terfluorenyl-7-trimethylsilyl-boronic acid (**F_3 O**)

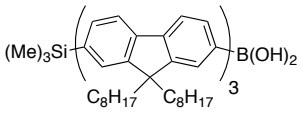

Using the general procedure E, the quantities used were: 2-bromo-9,9,9',9',9'',9''-hexaoctyl-2,2'-terfluorenyl-7-trimethylsilane (**2.6 O**) (8.00 g, $5.73 \cdot 10^{-3}$ mol), tetrahydrofuran (170 mL), n-BuLi (2.39 M solution in n-hexanes, 3.11 mL, $7.45 \cdot 10^{-3}$ mol), triisopropylborate (4 mL, $17.85 \cdot 10^{-3}$ mol). The product was obtained as a white foamy solid (1.61 g, $1.33 \cdot 10^{-3}$ mol, 98 %). ^{1}H NMR ($CDCl_3$) δ (ppm): 8.41-8.15 (2 H, m), 8.00-7.64 (14 H, m), 7.57-7.51 (2 H, m), 2.31-2.00 (12 H, m), 1.32-1.07 (60 H, m), 0.92-0.70 (30 H, m), 0.36 (9 H, s). ^{13}C NMR ($CDCl_3$) δ (ppm): 150. 47, 145.59, 141.77, 141.71, 140.90, 140.67, 140.61, 140.50, 140.23, 139.27, 136.07, 135.03, 132.13, 130.07, 127.95, 126.53, 126.47, 126.32, 125.81, 121.86, 121.80, 120.95, 120.27, 119.64, 119.29, 55.65, 55.53, 55.40, 40.68, 40.44, 32.08, 30.62, 30.38, 30.33, 30.23, 29.51, 29.45, 29.41, 24.22, 24.11, 22.90, 14.41, 14.35. (MALDI/TOF, m/z): calcd. for $C_{90}H_{131}BO_2Si$-BOH: 1238.9; Found: 1238.5 ($[M\text{-}B(OH)_2]^+$). Anal. calcd. for $C_{90}H_{131}BO_2Si$: C, 84.19; H, 10.28; Found: C, 83.90; H, 10.14.

9H,9H,9'H,9'H,9''H,9''H,9'''H,9'''H-Octaoctyl-2,2'-quaterfluoren-7-ylboronic acid (**F_4' O**)

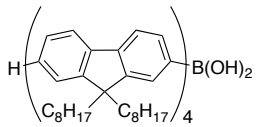

Using the general procedure E, the quantities used were: 7-bromo-9,9,9',9',9'',9'',9''',9'''-octaoctyl-2,2'-quaterfluorene (**2.8 O**) (0.41 g, $2.50 \cdot 10^{-4}$ mol), tetrahydrofuran (6 mL), n-BuLi (2.45 M solution in n-hexanes, 0.15 mL, $3.20 \cdot 10^{-4}$ mol), triisopropylborate (0.20 mL, $7.50 \cdot 10^{-4}$ mol). The product was obtained as a white foamy solid (0.37 g, $2.30 \cdot 10^{-4}$ mol, 73 %). ^{1}H NMR ($CDCl_3$) δ (ppm): 8.39 (1 H, d, J = 8.0 Hz), 8.31 (1 H, s), 8.10-7.62 (20 H, m), 7.41-7.30 (3 H, m), 2.32-1.98 (16 H, m), 1.28-1.02 (80 H, m), 0.92-0.67 (40 H, m). ^{13}C NMR ($CDCl_3$) δ (ppm): 125.90, 39.87, 31.29, 29.54, 28.71, 23.44, 22.10, 13.55. (MALDI/TOF, m/z): [M^+] calcd. for $C_{116}H_{163}BO_2$: 1600.4; found, 1601.0; Anal. calcd. for $C_{116}H_{163}BO_2$: C, 87.06; H, 10.27; Found: C, 87.32; H, 10.20.

9H,9H,9'H,9'H,9''H,9''H,9'''H,9'''H-Octaoctyl-2,2'-quaterfluorenyl-7-trimehylsilboronic acid (**F_4 O**)

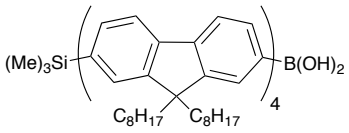

Using the general procedure E, the quantities used were: 7-bromo-9,9,9',9',9'',9'',9''',9'''-octaoctyl-2-trimethylsilylquaterfluorene (**2.7 O**) (1.50 g, $9.20 \cdot 10^{-4}$ mol), tetrahydrofuran (40 mL), n-BuLi (2.5 M solution in n-hexanes, 0.44 mL, $1.10 \cdot 10^{-3}$ mol), triisopropylborate (0.65 mL, $2.74 \cdot 10^{-3}$ mol). The product was obtained as a white foamy solid (0.68 g, $4.10 \cdot 10^{-4}$ mol, 44 %). ^{1}H NMR ($CDCl_3$) δ (ppm): 8.39 (1 H, d, J = 8.0 Hz), 8.30 (1 H, s), 8.10-7.60 (20 H, m), 7.55-7.48 (2 H, m), 2.29-1.98 (16 H, m), 1.32-1.04 (80 H, m), 0.93-0.66 (40 H, m), 0.34 (9 H, s). ^{13}C NMR ($CDCl_3$) δ (ppm): 125.80, 125.70, 121.10, 121.00, 119.60, 119.50, 109.50, 108.90, 103.70, 48.50, 39.90, 31.27, 29.43, 27.70, 23.40, 23.20, 22.08, 13.54.

General procedure F: Synthesis of 9,9-dialkyl-oligofluorenyl-boronic ester (**F_3BE B, F_4'BE H, F_4'BE O**)

9,9-Dialkyl-oligofluorenylboronic acid (**F_n-B(OH)$_2$** and **TMS-F_n-B(OH)$_2$**) (1 eq) and a diol (1.2 eq) were dissolved in dry toluene (10 mL) and the mixture was stirred at 120 °C for 18 h. Solvent evaporation yielded the white foamy product.

(9,9,9',9',9'',9''-Hexabutyl-7''-(4,4,5,5-tetramethyl-1,3,2-dioxaborolan-2-yl)-9*H*,9'*H*,9''*H*-[2,2':7',2''-terfluoren]-7-yl)trimethylsilane (**F_3BE B**)

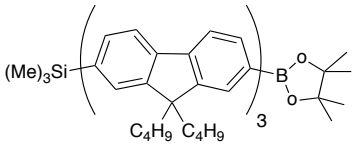

Using the general procedure F, the quantities used were: 9,9,9',9',9'',9''-hexabutyl-2,2'-terfluorenyl-7-trimethylsilyl-boronic acid (**F_3 B**) (0.30 g, $3.20 \cdot 10^{-4}$ mol), pinacol (45 mg, $3.80 \cdot 10^{-4}$ mol), toluene (10 mL). White foamy product (0.31 g, $2.99 \cdot 10^{-4}$ mol, 94%). ^{1}H NMR ($CDCl_3$) δ (ppm): 7.88-7.64 (16 H, m), 7.57-7.49 (2 H, m), 2.20-2.00 (12 H, m), 1.42 (12 H, s), 1.21-1.08 (12

H, m), 0.86-0.65 (30 H, m), 0.36 (9 H, s). ^{13}C NMR ($CDCl_3$) δ (ppm): 152.46, 152.15, 152.04, 144.16, 141.77, 141.26, 140.87, 140.82, 140.74, 140.68, 140.52, 140.43, 140.33, 138.38, 134.18, 132.20, 129.24, 127.98, 126.46, 126.33, 121.82, 120.71, 120.37, 120.32, 119.40, 119.35, 84.09, 55.60, 55.53, 55.38, 40.57, 40.49, 40.33, 26.47, 26.42, 26.35, 25.31, 23.44, 23.38, 14.19, 14.13, -0.48. (MALDI/TOF, m/z): [M^+] calcd. for $C_{72}H_{93}BO_2Si$: 1029.4; Found: 1029.5; Exact mass calcd. for $C_{72}H_{93}BO_2Si$: 1028.7047; Found: 1028.7044.

2-(9,9,9',9',9'',9'',9''',9'''-Octahexyl-9*H*,9'*H*,9''*H*,9'''*H*-[2,2':7',2'':7'',2'''-quaterfluoren]-7-yl)-1,3,2-dioxaborolane (**F_4'BE H**)

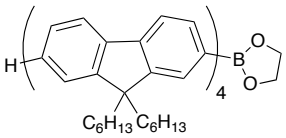

Using the general procedure F, the quantities used were: 9,9,9',9',9'',9'',9''',9'''-octahexyl-2,2'-quaterfluoren-7-ylboronic acid (**F_4' H**) (1.31 g, $9.54\cdot10^{-4}$ mol), toluene (20 mL), ethylene glycol (0.06 mL, $1.14\cdot10^{-3}$ mol). White foamy product (1.15 g, $8.22\cdot10^{-4}$ mol, 86 %). ^{1}H NMR ($CDCl_3$) δ (ppm): 8.50-8.32 (2 H, m), 8.06-8.66 (20 H, m), 7.45-7.33 (3 H, m), 2.36-1.96 (16 H, m), 1.26-1.07 (48 H, m), 0.99-0.71 (40 H, m). The analysis was comparable with that from the literature.[138]

9H,9H,9'H,9'H,9''H,9''H,9'''H,9'''H-Octaoctyl-2,2'-quaterfluoren-7-ylboronic acid (**F_4'BE H**)

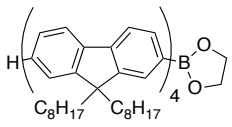

Using the general procedure F, the quantities used were: 9H,9H,9'H,9'H,9''H,9''H,9'''H,9'''H-octaoctyl-2,2'-quaterfluorenyl-7-trimethylsilyl-boronic acid (**F_4' H**) (0.18 g, $1.11\cdot10^{-4}$ mol), ethyleneglycol (0.07 mL, $1.33\cdot10^{-4}$ mol), toluene (30 mL). White foamy product (0.17 g, $1.06\cdot10^{-4}$ mol, 95%). ^{1}H NMR ($CDCl_3$) δ (ppm): 8.45-8.27 (1 H, m), 8.00-7.62 (21 H, m), 7.42-7.31 (3 H, m), 4.45 (2 H, s), 2.27-1.97 (16 H, m), 1.54 (2 H, s), 1.25-1.06 (80 H, m), 0.91-0.66 (40 H, m). ^{13}C NMR ($CDCl_3$) δ (ppm): 151.85, 151.52, 151.05, 150.33, 141.20, 140.85, 140.58, 140.06, 133.85, 129.12, 127.02, 126.82, 126.20, 125.56, 122.97, 121.54, 120.46, 120.00, 119.75, 119.44, 66.09, 55.38, 55.21, 40.42, 31.83, 30.37, 30.08, 29.25, 23.96, 23.87, 22.63, 11.10.

(MALDI/TOF, m/z): [M^+] calcd. for $C_{118}H_{165}BO_2$: 1626.4; found, 1626.5; Anal. calcd. for $C_{118}H_{165}BO_2$: C, 87.14; H, 10.23; Found: C, 86.75; H, 10.47.

10,15-Dihydro-5H-diindeno[1,2-*a*;1',2'-*c*]fluorene] (**2.1**)

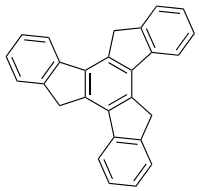

1-Indanone (13.60 g, 104 mmol) was added to a mixture of acetic acid (60 mL) and concentrated hydrochloric acid (30 mL). The solution was stirred for 16 h at 100 °C, then poured onto ice. The precipitate was washed with water, acetone and dichloromethane to yield a white powder (9.73 g, 28.4 mmol, 80%). ^{1}H NMR ($CDCl_3$) δ (ppm): 7.97 (3 H, d, J = 7.2 Hz), 7.70 (3H, d, J = 7.6 Hz), 7.51 (3 H, t, J = 7.6 Hz), 7.40 (3 H, t, J = 7.6 Hz), 4.29 (6 H, s). The analysis was comparable with that from the literature. [66]

General procedure G: Synthesis of hexaalkyltruxene (**T0 B**, **T0 O**) [59]

To a stirred suspension of truxene (**2.1**) (1 eq) in tetrahydrofuran (5.4 mL per gram) under nitrogen, n-BuLi (3.8 eq) was added dropwise at 0 °C over 30 min, not allowing the temperature to rise over 15 °C. The solid was dissolved and the colour changed to deep red. The solution was stirred at room temperature for 30 min and 1-bromoalkane (3.8 eq) was added over 10 min at 0 °C. The mixture was stirred at room temperature for 4 h and a second portion of BuLi (3.8 eq) was added dropwise at 0 °C over 30 min. After 30 min stirring at room temperature, 1-bromoalkane (3.8 eq) was added over 10 min at 0 °C and the reaction mixture was stirred at room temperature for 18 h (TLC monitoring). Upon reaction completion, it was quenched with saturated aqueous ammonium chloride and extracted with petroleum ether (5 times). The combined organic fractions were washed with water, dried over anhydrous $MgSO_4$, and the solvent evaporated. The material was purified by column chromatography on silica gel, eluting with petroleum ether to yield the product.

Hexabutyltruxene **T0 B**

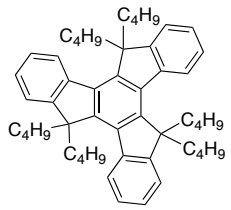

Using the general procedure G, the quantities used were: truxene (**2.1**) (3.19 g, $9.31 \cdot 10^{-3}$ mol), tetrahydrofuran (50 mL), n-BuLi (1.6 M solution in n-hexane, 22 mL, $35.2 \cdot 10^{-3}$ mol x 2), 1-bromobutane (3.8 mL, $35.6 \cdot 10^{-3}$ mol x 2). The product was obtained as a yellow powder (5.29 g, $7.73 \cdot 10^{-3}$ mol, 84 %). ^{1}H NMR ($CDCl_3$) δ (ppm): 8.39 (3 H, d, J = 7.2 Hz), 7.49 (3 H, d, J = 7.0 Hz), 7.45-7.35 (6 H, m), 3.01–3.00 (6 H, m), 2.15-2.05 (6 H, m), 0.94-0.86 (12 H, m), 0.47-0.30 (30 H, t, J = 7.6 Hz). The analysis was comparable with that from the literature. [116]

Hexaoctyltruxene (**T0 O**)

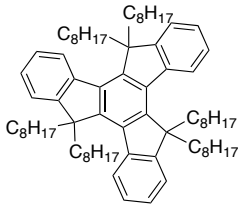

Using the general procedure G, the quantities used were: truxene (**2.1**) (3.19 g, $9.31 \cdot 10^{-3}$ mol), tetrahydrofuran (50 mL), n-BuLi (1.6 M solution in n-hexane, 22 mL, $35.2 \cdot 10^{-3}$ mol x 2), 1-bromooctane (6.3 mL, $35.6 \cdot 10^{-3}$ mol x 2). The product was obtained as a yellow solid (7.67 g, $7.57 \cdot 10^{-3}$ mol, 81 %). ^{1}H NMR ($CDCl_3$) δ (ppm): 8.36 (3 H, d, J = 8.0 Hz), 7.47 (3 H, d, J = 8.0 Hz), 7.41-7.34 (6 H, m), 2.99–2.92 (6 H, m), 2.11-2.04 (6 H, m), 1.08-0.85 (60 H, m), 0.74 (18 H, t, J = 8.0 Hz), 0.52-0.49 (12 H, m). ^{13}C NMR ($CDCl_3$) δ (ppm): 153.15, 144.53, 139.85, 137.82, 125.79, 125.44, 124.12, 121.67, 55.05, 36.37, 31.30, 29.36, 28.76, 28.58, 23.47, 22.02, 13.53. (MALDI/TOF, m/z): [M^+] calcd for $C_{75}H_{114}$ 1015.0; found 1015.0. Anal. calcd. for $C_{75}H_{114}$: C, 88.69; H, 11.31. Found: C, 89.18; H, 11.53.

General procedure H: Synthesis of tribromohexaalkyltruxene (**2.2 B**, **2.2 O**) [59]

Bromine (5.3 eq) was added to a stirred solution of hexaalkyltruxene (**T0**) (1 eq) in dichloromethane (10 mL per gram) over 5 min at room temperature and under protection from light. After 12 h stirring, excess bromine was removed by bubbling N_2 through the solution and washing the reaction mixture with a cold aqueous solution of Na_2SO_3. The mixture was extracted with dichloromethane (5 times), washed with aqueous sodium carbonate solution and then with water. The combined organic fractions were washed with water, dried over anhydrous $MgSO_4$ and treated with activated carbon to remove the red colour. The solvent was evaporated to afford the crude product, that was recrystallized from hexane.

Tribromohexabutyltruxene (**2.2 B**)

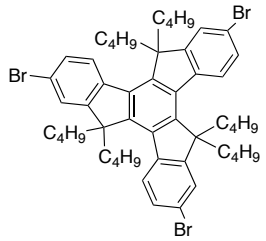

Using the general procedure H, the quantities used were: bromine (2 mL, $41.4 \cdot 10^{-3}$ mol), hexabutyltruxene (**T0 B**) (5.13 g, $7.50 \cdot 10^{-3}$ mol), dichloromethane (50 mL). The product was obtained as a white-yellowish crystalline solid was obtained (5.11 g, $5.55 \cdot 10^{-3}$ mol, 74%). ^{1}H NMR ($CDCl_3$) δ (ppm): 8.20 (3 H, d, J = 8.0 Hz), 7.58 (3 H, s), 7.53 (3 H, d, J = 8.0 Hz), 2.91–2.84 (6 H, m), 2.08-2.01 (6 H, m), 0.99-0.84 (12 H, m), 0.55 (30 H, m). (MALDI/TOF, m/z): [M^+] calcd. for $C_{51}H_{63}Br_3$ 915.8; found 916.6. Anal. calcd. for $C_{51}H_{63}Br_3$: C, 66.89; H, 6.93, Br, 26.18. Found: C, 67.25; H, 7.02, Br, 26.62. The analysis was comparable with that from the literature. [116]

Tribromohexaoctyltruxene (**2.2. O**)

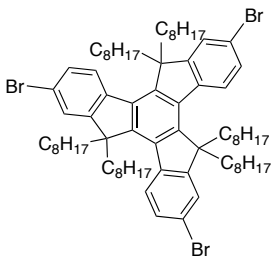

Using the general procedure H, the quantities used were: bromine (2.2 mL, $47.8 \cdot 10^{-3}$ mol), hexaoctyltruxene (**T0 O**) (7.47 g, $7.36 \cdot 10^{-3}$ mol), dichloromethane (50 mL). The product was obtained as a white crystalline solid was obtained (8.04 g, $6.43 \cdot 10^{-3}$ mol, 87 %). ^{1}H NMR ($CDCl_3$) δ (ppm): 8.19 (3 H, d, *J* = 8.0 Hz), 7.58 (3 H, d, *J* = 6.0 Hz), 7.52 (3 H, d, *J* = 8.0 Hz), 2.88–2.80 (6 H, m), 2.06-1.98 (6 H, m), 1.12-0.85 (60 H, m), 0.76 (18 H, t, *J* = 8.0 Hz), 0.38-0.58 (12 H, m). ^{13}C NMR ($CDCl_3$) δ (ppm): 36.72, 31.78, 29.68, 29.18, 29.02, 14.04. (MALDI/TOF, m/z): [M^+] calcd. for $C_{75}H_{111}Br_3$ 1252.4; found, 1251.9. Anal. calcd. for $C_{75}H_{111}Br_3$: C, 71.93; H, 8.93, Br; 19.40. Found: C, 71.93; H, 9.02; Br, 19.23.

General procedure I: Synthesis of Tris(7-trimethylsilyloligofluorenyltruxene) (**TnTMS**) by Suzuki cross-coupling (**T1TMS**, **T2TMS**, **T3TMS**, **T4TMS** (**B**, **O**))

A mixture of tribromohexaalkyltruxene (**2.2**) (1 eq), $Pd(PPh_3)_4$ (0.09 eq per position), 9,9-dialkyl-2-oligofluorenyl-7-trimethylsilyl-boronic acid (**F_n**) (1.6 eq per position) and $Ba(OH)_2 \cdot 8H_2O$ (1.5 eq per boronic acid functionality) was dissolved in anhydrous tetrahydrofuran or dimethoxyethane. The solution was degassed with N_2, followed by the addition of water and the system was stirred under N_2 at 70 °C for 18 h. The reaction was quenched with a saturated aqueous solution of NH_4Cl and extracted with dichloromethane (5 times). The combined organic fractions were washed with water and dried over anhydrous $MgSO_4$. The crude product was purified by column chromatography on silica gel eluting with petroleum ether:dichloromethane, to recover a colourless oil that was dissolved in the minimum amount of dichloromethane and reprecipitated from methanol to yield the product as a white solid.

Tris(7-trimethylsilylfluorenyltruxene) (butyl) (**T1TMS B**)

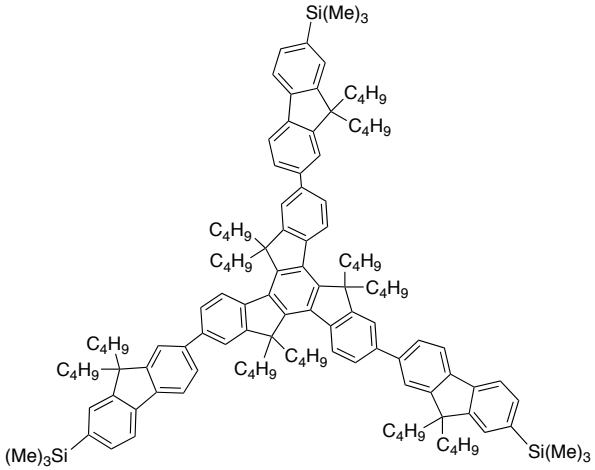

Using the general procedure I, the quantities used were: tribromohexabutyltruxene (**2.2 B**) (0.50 g, $5.50 \cdot 10^{-4}$ mol), $Pd(PPh_3)_4$ (0.16 g, $1.40 \cdot 10^{-4}$ mol), 9,9-dibutyl-2-fluorenyl-7-trimethylsilyl-boronic acid (**F_1 B**) (1.04 g, $2.62 \cdot 10^{-3}$ mol), $Ba(OH)_2 \cdot 8H_2O$ (1.31 g, $4.02 \cdot 10^{-3}$ mol), tetrahydrofuran (25 mL), water (2.25 mL). Column chromatography eluting with petroleum ether:dichloromethane (20:1). The product was obtained as a white solid (640 mg, $4.24 \cdot 10^{-4}$ mol, 77 %). The product was used without further purification.

Tris(7-trimethylsilylbifluorenyltruxene) (butyl) (**T2TMS B**)

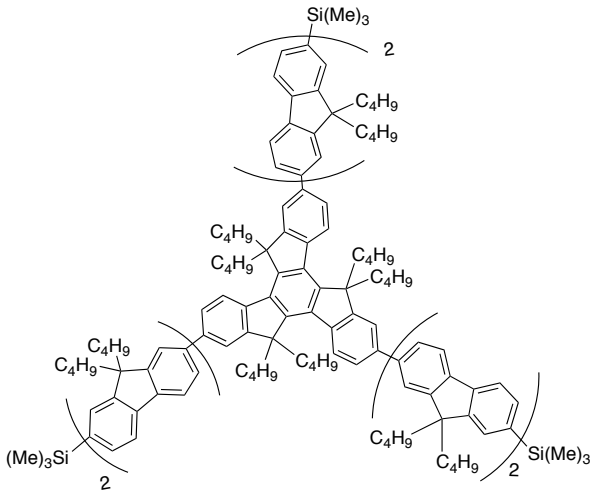

Using the general procedure I, the quantities used were: tribromohexabutyltruxene (**2.2 B**) (0.34 g, $3.75 \cdot 10^{-4}$ mol), $Pd(PPh_3)_4$ (0.11 g, $9.8 \cdot 10^{-5}$ mol), 9,9,9',9'-tetrabutyl-2,2'-bifluorenyl-7-trimethylsilyl-boronic acid (**F_2 B**) (1.20 g, $1.79 \cdot 10^{-3}$ mol), $Ba(OH)_2 \cdot 8H_2O$ (0.89 g, $2.74 \cdot 10^{-3}$ mol),

tetrahydrofuran (18 mL), water (1.6 mL). Column chromatography eluting with petroleum ether:toluene (20:1), increasing the polarity gradually until petroleum ether:toluene (6:1). The product was obtained as a creamy solid (0.90 g, $3.53 \cdot 10^{-4}$ mol, 94 %). ^{1}H NMR ($CDCl_3$) δ (ppm): 8.55 (3 H, d, J = 8.4 Hz), 7.93-7.76 (21 H, m), 7.78-7.64, (15 H, m), 7.58-7.48 (6 H, m), 3.22-3.03 (6 H, b.s.), 2.39-1.98 (30 H, m), 1.24-1.10 (24 H, m), 1.07-0.93 (16 H, m), 0.90-0.60 (68 H, m), 0.53 (18 H, t, J = 7.2 Hz), 0.36 (27 H, s). (MALDI/TOF, m/z): [M^+] calcd. for $C_{186}H_{234}Si_3$: 2554.1; found, 2554.2. Anal. calcd. for $C_{186}H_{234}Si_3$: C, 87.47; H, 9.23. Found: C, 85.60; H, 8.54.

Tris(7-trimethylsilylterfluorenyltruxene) (butyl) (**T3TMS B**)

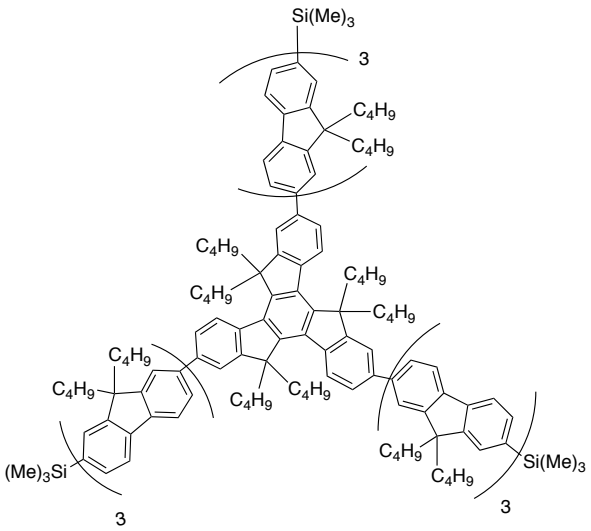

Using the general procedure I, the quantities used were: tribromohexabutyltruxene (**2.2 B**) (279 mg, $3.14 \cdot 10^{-4}$ mol), $Pd(PPh_3)_4$ (99 mg, $8.50 \cdot 10^{-5}$ mol), 9,9,9',9',9'',9''-hexabutyl-2,2'-terfluorenyl-7-trimethylsilyl-boronic acid (**F_3 B**) (1.42 g, $1.50 \cdot 10^{-3}$ mol), $Ba(OH)_2 \cdot 8H_2O$ (746 mg, $2.29 \cdot 10^{-3}$ mol), tetrahydrofuran (24 mL), water (2.25 mL). Column chromatography on silica gel eluting with petroleum ether:dichloromethane (6:1) to recover the product as a creamy solid (613 mg, $1.81 \cdot 10^{-4}$ mol, 58 %). ^{1}H NMR ($CDCl_3$) δ (ppm): 8.56 (3 H, d, J = 8.4 Hz), 7.94-7.79 (27 H, m), 7.78-7.64, (27 H, m), 7.56-7.50 (6 H, m), 3.05-3.25 (6 H, m), 2.38-1.99 (42 H, m), 1.28-0.95 (48 H, m), 0.90-0.70 (102 H, m), 0.73 (18 H, t, J = 5.6 Hz), 0.35 (27 H, s). (MALDI/TOF, m/z): [M^+] calcd. for $C_{249}H_{306}Si_3$:3383.35; found, 3383.89. Anal. calcd. for $C_{249}H_{306}Si_3$: C, 88.4; H, 9.1. Found: C, 87.47; H, 9.11.

Tris(7-trimethylsilylquaterfluorenyltruxene) (butyl) (**T4TMS B**)

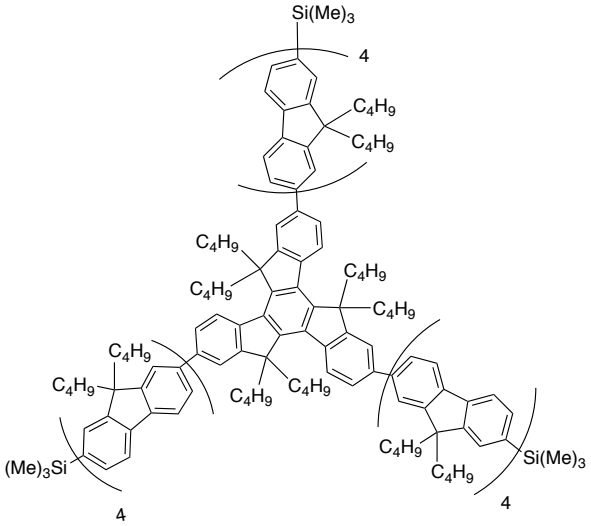

Using the general procedure I, the quantities used were: tribromohexabutyltruxene (**2.2 B**) (41 mg, $4.54 \cdot 10^{-5}$ mol), $Pd(PPh_3)_4$ (13 mg, $1.18 \cdot 10^{-5}$ mol), 9,9,9',9',9'',9'',9''',9''',9''''-octabutyl-2,2'-terfluorenyl-7-trimethylsilyl-boronic acid (**F_4 B**) (265 mg, $2.17 \cdot 10^{-4}$ mol), $Ba(OH)_2 \cdot 8H_2O$ (108 mg, $3.31 \cdot 10^{-3}$ mol), tetrahydrofuran (23 mL), water (0.32 mL). Column chromatography on silica gel eluting with petroleum ether:dichloromethane gradient elution (from 10:1 to 5:1) to recover the product as a creamy solid (97 mg, $2.31 \cdot 10^{-5}$ mol, 51 %). ^{1}H NMR ($CDCl_3$) δ (ppm): 8.59 (3 H, d, J = 8.5 Hz), 8.00-7.64 (72 H, m), 7.60-7.50 (6 H, m), 3.32-3.01 (6 H, m), 2.42-2.02 (54 H, m), 1.33-1.10 (54 H, m), 1.10-0.97 (12 H, m), 0.97-0.52 (144 H, m), 0.34 (27 H, s). ^{13}C NMR ($CDCl_3$) δ (ppm): 154.51, 151.87, 151.74, 150.22, 145.38, 141.46, 140.58, 140.51, 140.38, 140.10, 140.05, 139.71, 139.48, 139.07, 138.29, 131.89, 127.67, 126.16, 126.02, 125.25, 121.51, 121.29, 120.62, 120.06, 119.04, 55.88, 55.38, 55.32, 55.07, 40.40, 40.28, 40.02, 36.97, 29.74, 26.76, 26.20, 26.12, 23.20, 23.16, 23.06, 13.98, 13.93, 13.88, 13.81, 13.75, 13.69, -0.81. (MALDI/TOF, m/z): [M^+] calcd. for $C_{312}H_{387}Si_3$: 4212.6; found, 4212.7. Anal. calcd. for $C_{312}H_{387}Si_3$: C, 88.96; H, 9.04. Found: C, 63.00; H, 5.90.

Tris(7-trimethylsilylfluorenyltruxene) (octyl) (**T1TMS O**)

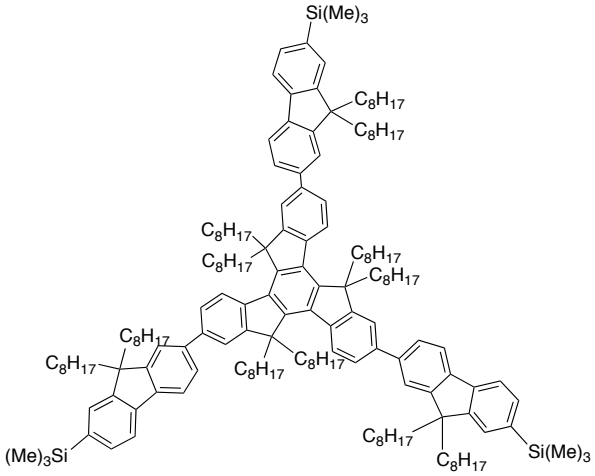

Using the general procedure I, the quantities used were: tribromohexaoctyltruxene (**2.2 O**) (200 mg, $1.6 \cdot 10^{-4}$ mol), $Pd(PPh_3)_4$ (48 mg, $4.20 \cdot 10^{-5}$ mol), 9,9-dioctyl-2-fluorenyl-7-trimethylsilyl-boronic acid (**F_1 O**) (387 mg, $7.60 \cdot 10^{-4}$ mol), $Ba(OH)_2 \cdot 8H_2O$ (380 mg, $1.70 \cdot 10^{-4}$ mol), dimethoxyethane (9.80 mL), water (0.77 mL). Column chromatography eluting with petroleum ether:toluene (20:1), to recover the product as colourless oil (265 mg, $1.17 \cdot 10^{-4}$ mol, 69 %). ^{1}H NMR ($CDCl_3$) δ (ppm): 8.59 (3 H, d, J = 8.4 Hz), 7.96-7.78 (18 H, m), 7.66-7.54 (6 H, m), 3.28-3.05 (6 H, m), 2.41-2.23 (6 H, m), 2.16 (12 H, t, J = 8 Hz), 1.28-0.95 (120 H, m), 0.95-0.67 (60 H, m), 0.42 (27 H, s). (MALDI/TOF, m/z): [M^+] calcd. for $C_{171}H_{258}Si_3$: 2396.4; found, 2396.9.

Tris(7-trimethylsilylbifluorenyltruxene) (octyl) (**T2TMS O**)

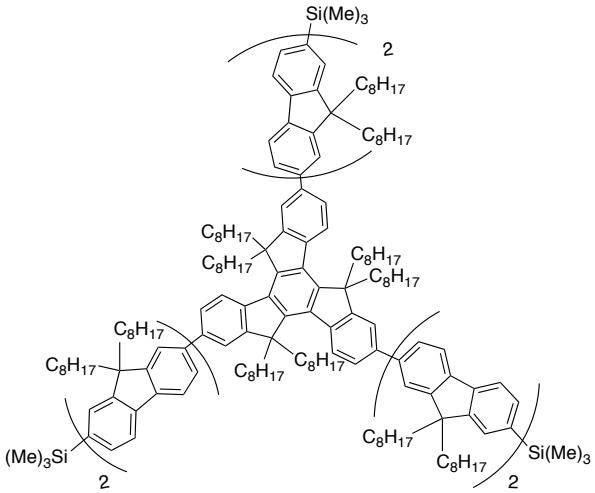

Using the general procedure I, the quantities used were: tribromohexaoctyltruxene (**2.2 O**) (950 mg, $7.60 \cdot 10^{-4}$ mol), $Pd(PPh_3)_4$ (228 mg, $2.00 \cdot 10^{-4}$ mol), 9,9,9',9'-tetraoctyl-2,2'-bifluorenyl-7-trimethylsilyl-boronic acid (**F_2 O**) (3.25 g, $3.62 \cdot 10^{-3}$ mol), $Ba(OH)_2 \cdot 8H_2O$ (1.80 g, $5.54 \cdot 10^{-3}$ mol), dimethoxyethane (31.5 mL), water (4.3 mL). Column chromatography on silica gel eluting with petroleum ether:toluene (20:1), increasing the polarity with petroleum ether:toluene (10:1). The product was obtained as a creamy solid (1.87 g, $5.25 \cdot 10^{-4}$ mol, 69 %). ^{1}H NMR ($CDCl_3$) δ (ppm): 8.59 (3 H, d, J = 8.0 Hz), 7.88-7.66 (36 H, m), 7.65-7.51 (6 H, m), 3.36-3.03 (6 H, m), 2.46-1.98 (30 H, m), 1.46-0.65 (270 H, m), 0.40 (27 H, s). ^{13}C NMR ($CDCl_3$) δ (ppm): 153.97, 151.36, 151.30, 151.27, 149.72, 144.74, 140.96, 140.18, 140.10, 139.84, 139.65, 139.59, 139.17, 139.06, 138.50, 137.70, 131.38, 127.19, 125.66, 125.56, 124.78, 124.47, 121.04, 120.78, 120.05, 119.52, 118.54, 76.84, 76.52, 76.20, 55.38, 54.91, 54.64, 40.03, 39.69, 36.66, 31.35, 31.31, 29.61, 29.47, 28.82, 28.77, 28.69, 28.64, 28.61, 23.66, 23.46, 23.35, 22.14, 22.04, 13.59, 13.53, -1.32. (MALDI/TOF, m/z): calcd. for $C_{258}H_{378}Si_3$: 3564.0; found, 3450.5 ($[M-C_8H_{17}]^+$). Anal. calcd. for $C_{258}H_{378}Si_3$: C, 86.95; H, 10.69. Found: C, 85.69; H, 9.18.

Tris(7-trimethylsilylterfluorenyltruxene) (octyl) (**T3TMS O**)

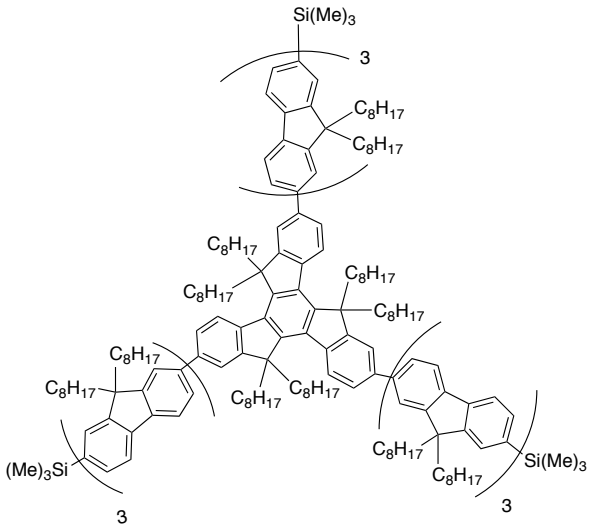

Using the general procedure I, the quantities used were: tribromohexaoctyltruxene (**2.2 O**) (150 mg, $1.20 \cdot 10^{-4}$ mol), $Pd(PPh_3)_4$ (36 mg, $3.10 \cdot 10^{-5}$ mol), 9,9,9',9',9'',9''-hexaoctyl-2,2'-terfluorenyl-7-trimethylsilyl-boronic acid (**F_3 O**) (763 mg, $5.70 \cdot 10^{-4}$ mol), $Ba(OH)_2 \cdot 8H_2O$ (280 mg, $8.60 \cdot 10^{-4}$ mol), thetrahydrofuran (5.8 mL), water (0.58 mL). Column chromatography on silica gel eluting with petroleum ether:toluene (20:1), increasing the polarity with petroleum ether:toluene (10:1). The product was obtained as a creamy solid (562 mg, $1.19 \cdot 10^{-4}$ mol, 99

%). ^{1}H NMR ($CDCl_3$) δ (ppm): 8.55 (3 H, d, J = 8.4 Hz), 7.95-7.78 (27 H, m), 7.78-7.63 (27 H, m), 7. 59-7.48 (6 H, m), 3.23-3.00 (6 H, m), 2.48-2.00 (42 H, m), 1.25-1.92 (240 H, m), 1.92-0.63 (120 H, m), 0.36 (27 H, s). ^{13}C NMR ($CDCl_3$) δ (ppm): 151.32, 125.66, 121.01, 119.45, 39.65, 31.33, 31.28, 29.54, 29.44, 28.76, 28.72, 28.66, 28.61, 23.44, 22.10, 22.01, 13.55, 13.51, -1,35. (MALDI/TOF, m/z): [M^+] calcd. for $C_{345}H_{498}Si_3$: 4729.9; found, 4727.5. Anal. calcd. for $C_{345}H_{498}Si_3$: C, 87.61; H, 10.61. Found: C, 87.55; H, 11.04.

Tris(7-bromobifluorenyltruxene) (octyl) (**T2Br O**)

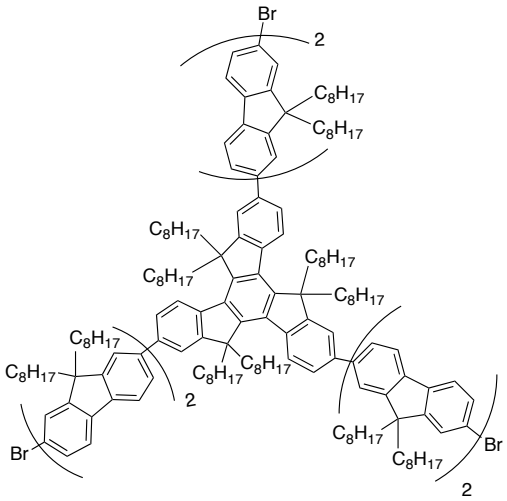

Tris(7-trimethylsilylbifluorenyltruxene) (octyl) (**T2TMS O**) (500 mg, $1.40\cdot10^{-4}$ mol) and sodium acetate (35 mg, $4.20\cdot10^{-4}$ mol) were dissolved in dry tetrahydrofuran (14 mL) under nitrogen and the reaction mixture was protected from the light and cooled down to 0 °C for 30 minutes. Br_2 (0.05 mL, $9.80\cdot10^{-4}$ mol) was added dropwise and the reaction mixture was stirred at 0 °C for 30 minutes. It was then quenched with triethylamine (0.45 mL) followed by the addition of 1M Na_2SO_3 (aq) (18 mL). The reaction mixture was washed with water and extracted with dichloromethane (5 times). The combined organic fractions were washed with a saturated solution of $NaHCO_3$ (aq), dried over $MgSO_4$ and solvent evaporated to yield a crude oil. It was then dissolved in the minimum amount of toluene and filtered through a silica plug to remove polar biproducts. After solvent evaporation the residue was dissolved in the minimum amount of dichloromethane and reprecipitated from methanol to yield the product as a creamy powder (457 mg, $1.28\cdot10^{-4}$ mol, 91 %). ^{1}H NMR ($CDCl_3$) δ (ppm): 8.51 (3 H, d, J = 8.0 Hz), 7.91-7.56 (36 H, m), 7.54-7.44 (6 H, m), 3.19-2.99 (6 H, m), 2.36-1.88 (30 H, m), 1.26-0.63 (270 H, m). ^{13}C NMR ($CDCl_3$) δ (ppm): 152.90, 151.50, 140.30, 139.60 137.91, 138.20, 126.00, 125.60, 125.30, 121.51, 121.20, 120.92, 120.50, 119.80, 119.50, 99.70, 99.10, 97.40, 88.50, 55.80, 54.80, 39.50, 37.10, 36.40, 31.32, 31.27, 29.56, 29.45, 29.79, 28.79, 28.74, 28.69, 28.58, 22.10,

22.01, 13.56, 13.50. (MALDI/TOF, m/z): [M^+] calcd. for $C_{249}H_{351}Br_3$: 3584.16; found, 3495.12 ([M-Br]$^+$). Anal. calcd. for $C_{249}H_{351}Br_3$: C, 83.4; H, 9.87; Br, 6.7. Found: C, 82.83; H, 9.50; Br, 6.21.

General procedure J: Synthesis of Tris(oligofluorenyltruxene) (**Tn**) (**T1**, **T2**, **T3**, **T4** (**B** and **O**))

Tris(7-trimethylsilyloligofluorenyltruxene) (**TnTMS**) (1 eq) was dissolved in dichloromethane (39 mL per gram) and CF_3COOH (5 eq per position) added. The mixture was stirred at room temperature for 2 h under nitrogen. Basic work up was carried out with water (2 times), saturated aqueous $NaHCO_3$ solution (2 times) and a final washing with water. The organic fraction was dried over anhydrous $MgSO_4$ and filtered through a silica plug to remove polar by-products. The colourless oil was dissolved in the minimum amount of dichloromethane and precipitated from methanol to yield the product as a white solid.

Tris(fluorenyltruxene) (butyl) (**T1 B**)

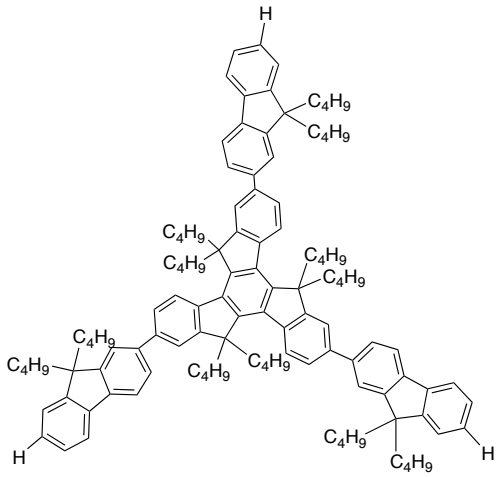

Using the general procedure J, the quantities used were: tris(7-trimethylsilylfluorenyltruxene) (butyl) (**T1TMS B**) (640 mg, $4.24 \cdot 10^{-4}$ mol), dichloromethane (25 mL), CF_3COOH (0.45 mL, $6.37 \cdot 10^{-3}$ mol). The product was obtained as a white solid (505 mg, $3.93 \cdot 10^{-4}$ mmol, 93 %). ^{1}H NMR ($CDCl_3$) δ (ppm): 8.50 (3 H, d, J = 8.0 Hz), 7.85-7.65 (18 H, m), 7.41-7.27 (9 H, m), 3.15-2.98 (6 H, m), 2.30-1.95 (18 H, m), 1.20-1.13 (12 H, m), 1.13-0.88 (12 H, m), 0.80-0.40 (60 H, m). ^{13}C NMR ($CDCl_3$) δ (ppm): 153.93, 151.02, 150.51, 144.79, 140.37, 139.97, 139.47, 139.12, 138.93, 137.72, 126.31, 125.46, 124.51, 122.45, 120.66, 120.02, 119.45, 119.24, 55.31, 54.66, 39.81, 36.39, 26.19, 25.56, 22.63, 22.47, 13.40, 13.34. (MALDI/TOF, m/z): [M^+] calcd for

$C_{114}H_{138}$ 1508.1; found 1508.0. Anal. calcd. for $C_{114}H_{138}$: C, 90.78; H, 9.22. Found: C, 90.65; H, 9.26.

Tris(bifluorenyltruxene) (butyl) (**T2 B**)

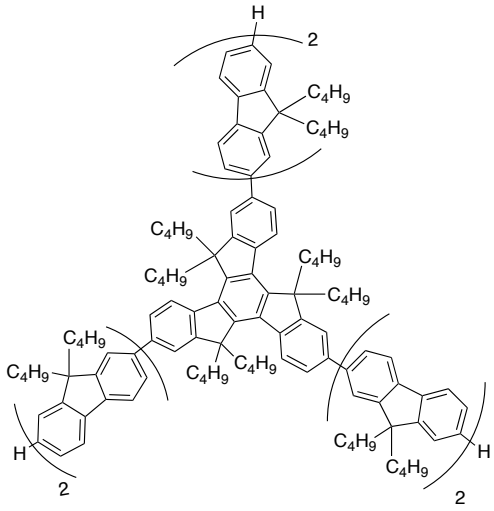

Using the general procedure J, the quantities used were: tris(7-trimethylsilylbifluorenyltruxene) (butyl) (**T2TMS B**) (882 mg, $3.45 \cdot 10^{-4}$ mol), dichloromethane (38 mL), CF_3COOH (0.37 mL, 5.18 mmol). The product was obtained as a white solid (725 mg, $3.10 \cdot 10^{-4}$ mol, 90 %). ^{1}H NMR ($CDCl_3$) δ (ppm): 8.56 (3 H, d, J = 8.0 Hz), 7.93-6.65 (36 H, m), 7.58-7.30 (9 H, m), 3.21-3.06 (6 H, m), 2.37-2.00 (30 H, m), 1.30-1.10 (24 H, m), 1.10-0.94 (16 H, m), 0.92-0-60 (68 H, m), 0.55 (18 H, t, J = 7.4 Hz). ^{13}C NMR ($CDCl_3$): δ 153.97, 151.37, 151.31,c151.01, 150.53, 144.84, 140.32, 140.00, 139.94, 139.89, 139.67, 139.58, 139.49, 139.17, 139.94, 137.75, 126.53, 126.32, 125.60, 125.51, 124.72, 124.56, 122.46, 120.98, 120.91, 120.75, 119.56, 119.51, 119.42, 119.24, 55.34, 54.84, 54.62, 39.86, 39.73, 36.43, 26.22, 25.67, 25.56, 22.67, 22.61, 22.50, 13.47, 13.44, 13.39, 13.33, 13.30, -1.33. (MALDI/TOF, m/z): [M^+] calcd. for $C_{177}H_{210}$: 2337.56; found, 2337.66. Anal. calcd. for $C_{177}H_{210}$: C, 90.94; H, 9.06. Found: C, 90.48; H, 8.81.

Tris(terfluorenyltruxene) (butyl) (**T3 B**)

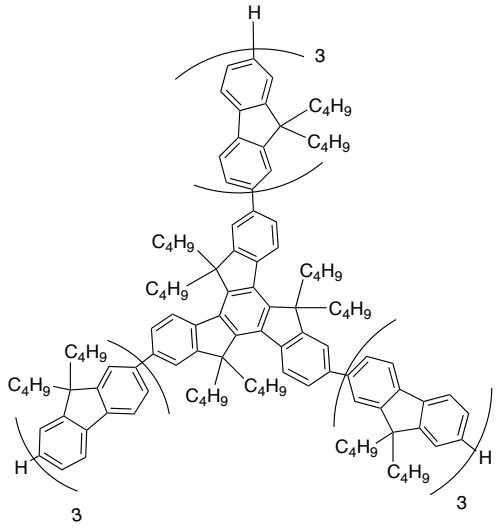

Using the general procedure J, the quantities used were: tris(7-trimethylsilylterfluorenyltruxene) (butyl) (**T3TMS B**) (571 mg, $1.69 \cdot 10^{-4}$ mol), dichloromethane (10 mL), CF_3COOH (0.18 mL, $2.53 \cdot 10^{-3}$ mol). The product was obtained as a white solid (459 mg, $1.45 \cdot 10^{-4}$ mol, 86 %). ^1H NMR ($CDCl_3$) δ (ppm): 8.56 (3 H, d, J = 8.0 Hz), 7.95-7.79 (27 H, m), 7.79-7.64 (27 H, m), 7.43-7.30 (9 H, m), 3.30-3.04 (6 H, m), 2.38-1.99 (42 H, m), 1.30-1.09 (36 H, m), 1.09-0.95 (12 H, m), 0.92-0.50 (120 H, m). ^{13}C NMR ($CDCl_3$) δ (ppm): 150.52, 144.85, 140.31, 139.98, 139.92, 139.67, 139.62, 139.57, 139.51, 139.18, 138.94, 126.31, 125.63,125.50, 122.45, 120.99, 120.90, 120.76, 119.50, 119.41, 119.24, 55.35, 54.84, 54.79, 54.62, 39.86, 39.73, 26.23, 25.67, 25.55, 22.67, 22.69, 22.51, 13.44, 13.39, 13.33. (MALDI/TOF, m/z): [M^+] calcd. for $C_{240}H_{282}$: 3166.8; found, 3167.6. Anal. calcd. for $C_{240}H_{282}$: C, 91.02; H, 8.98. Found: C, 90.67; H, 8.02.

Tris(quaterfluorenyltruxene) (butyl) (**T4 B**)

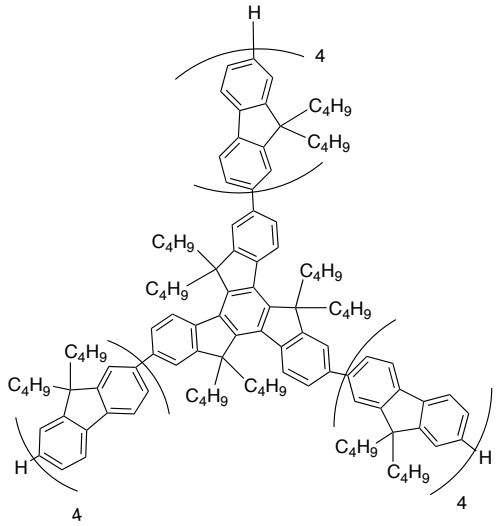

Using the general procedure J, the quantities used were: tris(7-trimethylsilylquaterfluorenyltruxene) (butyl) (**T4TMS B**) (76 mg, $1.81 \cdot 10^{-5}$ mol), dichloromethane (5 mL), CF_3COOH (0.5 mL, $7.14 \cdot 10^{-3}$ mol). The product was obtained as a white solid (72 mg, $1.79 \cdot 10^{-5}$ mol, 98 %). ^{1}H NMR ($CDCl_3$) δ (ppm): 8.56 (3 H, d, J = 8.0 Hz), 7.93-7.79 (33 H, m), 7.79-7.64 (39 H, m), 7.43-7.31 (9 H, m), 3.24-3.06 (6 H, m), 2.40-1.97 (54 H, m), 1.30-1.10 (54 H, m), 1.10-1.07 (12 H, m), 1.02-0.50 (144 H, m). ^{13}C NMR ($CDCl_3$) δ (ppm): 151.34, 150.99, 150.00, 140.31, 139.97, 139.56, 137.50, 125.63, 122.45, 120.99, 120.90, 119.51,119.22, 54.84, 54.78, 54.62, 39.72, 25.67, 25.55, 22.67, 22.62, 22.50, 13.43, 13.38, 13.34. (MALDI/TOF, m/z): [M^+] calcd. for $C_{303}H_{354}$: 3996.5; found, 3996.7. Anal. calcd. for $C_{303}H_{354}$: C, 91.07; H, 8.93. Found: C, 90.95; H, 8.76.

Tris(fluorenyltruxene) (octyl) (**T1 O**)

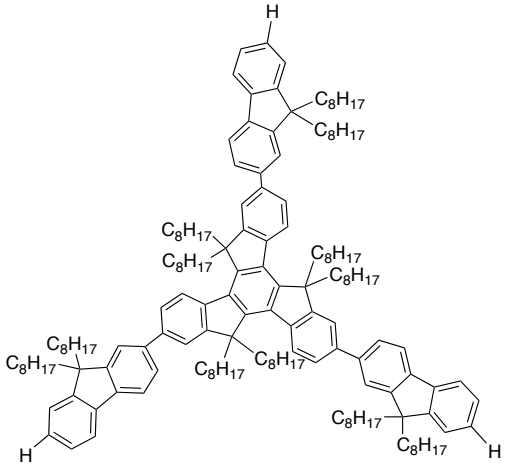

Using the general procedure J, the quantities used were: tris(7-trimethylsilylbifluorenyltruxene) (octyl) (**T1TMS O**) (511 mg, $2.35 \cdot 10^{-4}$ mol), dichloromethane (9.6 mL), CF_3COOH (0.33 mL, $3.20 \cdot 10^{-3}$ mol). The product was obtained as a colourless oil (431 mg, $1.98 \cdot 10^{-4}$ mmol, 93 %). ^{1}H NMR ($CDCl_3$) δ (ppm): 8.52 (3 H, d, J = 8.4 Hz), 7.87-7.73 (18 H, m), 7.43-7.30 (9 H, m), 3.16-3.00 (6 H, m), 2.11-2.15 (6 H, m), 2.15-1.96 (12 H, m), 1.19-0.59 (180 H, m). ^{13}C NMR ($CDCl_3$) δ (ppm): 151.20, 150.80, 150.50, 139.11, 138.90, 138.60, 126.60, 126.30, 125.60, 124.90, 123.60, 122.60, 120.20, 119.50, 119.80, 119.20, 55.50, 54.71, 40.20, 36.80, 31.31, 29.58, 29.40, 28.74, 28.56, 23.60, 23.34, 22.10, 21.99, 13-56, 13.48. (MALDI/TOF, m/z): [M^+] calcd. for $C_{162}H_{234}$: 2181.6; found, 2181.7. Anal. calcd. for $C_{162}H_{234}$: C, 89.19; H, 10.81. Found: C, 88.94; H, 10.81.

Tris(bifluorenyltruxene) (octyl) (**T2 O**)

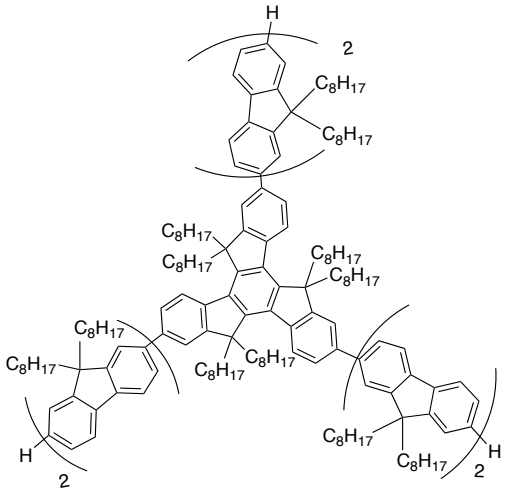

Using the general procedure J, the quantities used were: tris(7-trimethylsilylbifluorenyltruxene) (**T2TMS O**) (471 mg, $1.32 \cdot 10^{-4}$ mol), dichloromethane (6 mL), CF_3COOH (0.14 mL, $1.98 \cdot 10^{-3}$ mol). The product was obtained as a creamy solid (411 mg, $1.13 \cdot 10^{-4}$ mol, 93 %). ^{1}H NMR ($CDCl_3$) δ (ppm): 8.52 (3 H, d, J = 8.0 Hz), 7.90-7.62 (36 H, m), 7.41-7.30 (9 H, m), 3.18-2.98 (6 H, m), 2.35-1.95 (30 H, m), 1.30-0.60 (270 H, m). ^{13}C NMR ($CDCl_3$) δ (ppm): 153.98, 151.36, 151.30, 151.27, 149.72, 144.74, 140.96, 140.18, 140.10, 139.84, 139.65, 139.59, 139.17, 139.06, 138.59, 137.70, 131.38, 127.19, 125.66, 125.56, 124.78, 124.47, 121.04, 120.78, 120.05, 119.52, 118.54, 55.38, 54.91, 54.64, 40.03, 39.69, 36.66, 31.35, 31.31, 29.60, 29.47, 28.82, 28.77, 28.69, 28.65, 28.61, 23.66, 23.46, 23.35, 22.14, 22.11, 22.08, 22.04, 13.59, 13.53, -1.32. (MALDI/TOF, m/z) calcd. for $C_{247}H_{334}$: 3347.5; found, 3324.1 ([M-C_8H_{17}]$^+$). Anal. calcd. for $C_{247}H_{334}$: C, 89.34; H, 10.66. Found: C, 88.92; H, 10.96.

Tris(terfluorenyltruxene) (octyl) (**T3 O**)

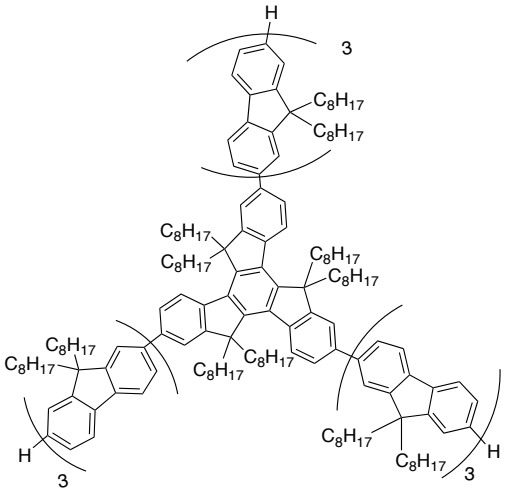

Using the general procedure J, the quantities used were: tris(9,9,9',9',9'',9''-hexaoctyl-2-trimethylsilyl-terfluorenyl)-5,5,10,10,15,15-hexaoctyltruxene (**T3TMS O**) (562 mg, $1.20 \cdot 10^{-5}$ mol), dichloromethane (20 mL), CF_3COOH (0.13 mL, $3.55 \cdot 10^{-4}$ mol). The product was obtained as a creamy solid (511 mg, $1.11 \cdot 10^{-5}$ mol, 94 %). ^{1}H NMR ($CDCl_3$) δ (ppm): 8.58 (3 H, d, J = 7.2 Hz), 8.50-7.60 (54 H, m), 7.47-7.32 (9 H, m), 3.35-2.95 (6 H, m), 2.48-1.97 (42 H, m), 1.45-0.65 (360 H, m). ^{13}C NMR ($CDCl_3$) δ (ppm): 151.31, 150.99, 150.52, 140.31, 140.03, 139.94, 139.61, 137.65, 125.67, 122.45, 121.00, 119.47, 54.90, 54.85, 54.68, 39.90, 31.35, 31.31, 29.56, 28.83, 28.79, 28.74, 28.62, 23.44, 23.34, 22.15, 22.05, 13.60. (MALDI/TOF, m/z): [M^+] calcd. for $C_{336}H_{474}$: 4498.3; found, 4498.7. Anal. calcd. for $C_{336}H_{474}$: C, 89.45; H, 10.55. Found: C, 88.29; H, 11.02.

Tris(quaterfluorenyltruxene) (octyl) (**T4 O**)

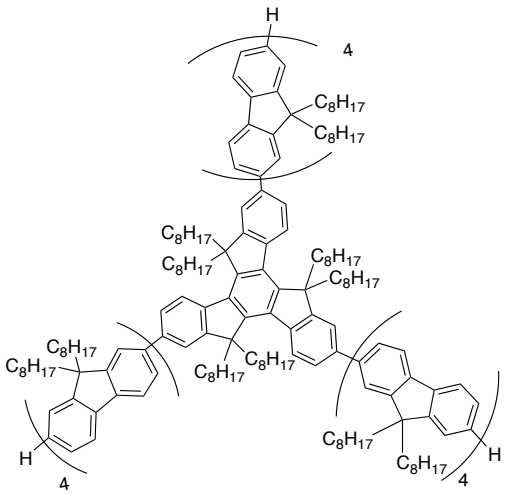

A mixture of tribromohexaoctyltruxene (**2.2**) (301 mg, $2.40 \cdot 10^{-4}$ mol), $Pd(PPh_3)_4$ (73 mg, $6.30 \cdot 10^{-5}$ mol), 9,9,9',9',9'',9'',9''',9'''-octaoctyl-2,2'-quaterfluorenylboronic acid (**F_4' O**) (1.84 g, $1.15 \cdot 10^{-3}$ mol) and $Ba(OH)_2 \cdot 8H_2O$ (571 mg, $1.76 \cdot 10^{-3}$ mol) was dissolved in anhydrous thetrahydrofuran (14 mL). The solution was degassed with N_2, followed by the addition of water (1.35 mL) and the system was stirred under N_2 at 70 °C for 18 h. The reaction was quenched with an aqueous solution of NH_4Cl (100 mL) and extracted with (7 x 100 mL) of dichloromethane. The combined organic fractions were washed with water (300 mL), dried over anhydrous $MgSO_4$ and the solvent evaporated to yield 2.20 g of brown oil. The crude product was purified by column chromatography on silica gel eluting with petroleum ether:toluene (10:1) to recover the product as a creamy solid that was dissolved in the minimum amount of dichloromethane and reprecipitated from methanol (780 mg, $1.37 \cdot 10^{-4}$ mol, 57 %). ^{1}H NMR ($CDCl_3$) δ (ppm): 8.53 (3 H, d, J = 6.0 Hz), 7.93-7.54 (72 H, m), 7.40-7.28 (9 H, m), 3.22-2.96 (6 H, b.s.), 2.39-1.90 (54 H, m), 1.28-0.64 (450 H, m). ^{13}C NMR ($CDCl_3$) δ (ppm): 152.14, 151.81, 151.34, 141.13, 140.86, 140.82, 140.66, 140.44, 140.36, 139.85, 127.11, 126.48, 126.36, 123.26, 121.83, 120.28, 120.03, 55.18, 55.72, 55.66, 55.50, 40.70, 37.43, 32.15, 32.11, 30.36, 30.26, 29.62, 29.58, 29.53, 29.41, 24.25, 24.26, 22.94, 22.91, 22.84, 14.37, 14.33. (MALDI/TOF, m/z): [M^+] calcd. for $C_{423}H_{594}$: 5679.2; found, 5679.8. Anal. calcd. for $C_{423}H_{594}$: C, 89.46; H, 10.54. Found: C, 88.21; H, 10.79.

Tris(hexafluorenyltruxene) (octyl) (**T6 O**)

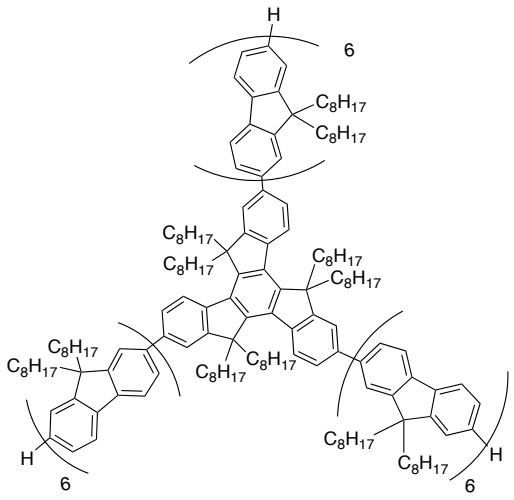

A mixture of tris(7-bromobifluorenyltruxene) (**T2Br O**) (291 mg, $8.00 \cdot 10^{-5}$ mol), $Pd(PPh_3)_4$ (24 mg, $2.10 \cdot 10^{-5}$ mol), 9,9,9',9',9'',9'',9''',9'''-octaoctyl-2,2'-quaterfluorenylboronic acid (**F_4' O**) (620 mg, $3.90 \cdot 10^{-4}$ mol) and $Ba(OH)_2 \cdot 8H_2O$ (193 mg, $5.90 \cdot 10^{-4}$ mol) was dissolved in anhydrous thetrahydrofuran (15 mL). The solution was degassed with N_2, followed by the addition of water (1.35 mL) and the system was stirred under N_2 at 70 °C for 18 h. The reaction was quenched with an aqueous solution of NH_4Cl (100 mL) and extracted with (7 x 100 mL) of dichloromethane. The combined organic fractions were washed with water (300 mL), dried over anhydrous $MgSO_4$ and the solvent evaporated to yield 0.88 g of brown oil. The crude product was purified by column chromatography on silica gel eluting initially with petroleum ether:toluene (10:1) and increasing the polarity to petroleum ether:toluene (20:1) to recover the product. It was dissolved in the minimum amount of dichloromethane and reprecipitated from methanol to obtain a creamy solid. (446 mg, $5.62 \cdot 10^{-5}$ mol, 69 %). ^{1}H NMR ($CDCl_3$) δ (ppm): 8.63-8.43 (3 H, b.s.), 8.00-7.56 (108 H, m), 7.40-7.28 (9 H, m), 3.22-2.96 (6 H, m), 2.33-1.96 (72 H, m), 1.28-0.64 (636 H, m). ^{13}C NMR ($CDCl_3$) δ (ppm): 152.18, 151.84, 151.37, 141.17, 140.88, 140.69, 140.39, 127.13, 126.52, 126.39, 127.13, 126.52, 126.39, 127.13, 126.52, 126.39, 123.30, 121.86, 120.31, 120.06, 74.06, 56.21, 55.76, 55.70, 55.53, 40.74, 32.19, 32.14, 30.40, 30.30, 29.65, 29.62, 29.57, 29.45, 24.28, 24.19, 22.95, 22.88, 14.40, 14.37. (MALDI/TOF, m/z): [M^+] calcd. for $C_{597}H_{834}$: 8012.0; found, 8013.8. Anal. calcd. for $C_{597}H_{834}$: C, 89.51; H, 10.49. Found: C, 89.21; H, 10.87.

Ethyl 3-oxo-3-(4'-bromophenyl)propionate (**4.2**) [273]

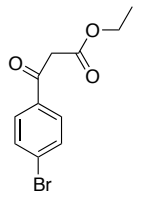

Under a nitrogen atmosphere, diethylcarbonate (48 mL, 0.40 mol) was added over NaH (6.94 g, 0.17 mol, previously washed with dry hexane) and the mixture was suspended in dry toluene (300 mL). 4'-Bromoacetophenone (**4.1**) (13.57 g, $66.70 \cdot 10^{-3}$ mol) was dissolved in dry toluene (100 mL) and this solution was added dropwise to the reaction mixture over 1 h. The reaction mixture was stirred under nitrogen at 83 °C for 18 h. The reaction mixture was quenched with glacial acetic acid (30 mL), it was poured onto a water-ice mixture and it was acidified with HCl (20 mL). The aqueous layer was extracted with ethyl acetate (2 x 90 mL) and the combined organic fractions were dried over $MgSO_4$ and the solvent evaporated to yield a yellow oil. The crude product was purified by Kugelrohr distillation (112 °C, 0.07 mm Hg), with further purification by column chromatography on silica gel, eluting with hexane:ethyl acetate (15:1) yielding the product as a colourless oil (11.79 g, $44 \cdot 10^{-3}$ mol, 65 %). ^{1}H NMR ($CDCl_3$) δ (ppm): 7.82 (2 H, d, J = 8.4 Hz), 7.63 (2 H, d, J = 8.4 Hz), 4.18 (2 H, q, J = 7.2 Hz), 3.93 (2 H, s), 1.25 (3 H, t, J = 7.2 Hz). The analysis was comparable with that from the literature.[273]

2,3-Bis(4-bromobenzoyl)succinate (**4.3**) [191]

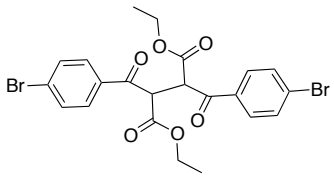

Br_2 (1.1 mL, $21 \cdot 10^{-3}$ mol) was dissolved in dichloromethane (33 mL) and the solution was added dropwise over a solution of ethyl 3-oxo-3-(4'-bromophenyl)propionate (**4.2**) (5.59 g, $21 \cdot 10^{-3}$ mol) in dichloromethane (33 mL). The reaction mixture was stirred for 30 minutes and was washed with water and aqueous $NaHCO_3$. The organic fraction was dried over $MgSO_4$ and solvent evaporated to yield a colourless oil, that was dissolved in dry dichloromethane (16 mL) and set aside ("solution 1").

A solution of ethyl 3-oxo-3-(4'-bromophenyl)propionate (**4.2**) (5.54 g, $21 \cdot 10^{-3}$ mol) in

dichloromethane (12 mL) was added over a solution of NaH (0.82 g, $21 \cdot 10^{-3}$ mol) in dichloromethane (22 mL). The mixture was refluxed for 15 minutes and "solution 1" was added to the reaction mixture followed by further refux under nitrogen for 3 h. The reaction mixture was washed with water and brine and the organic layer was dried over $MgSO_4$ and the solvent was evaporated. The colourless oil was washed with cold ethanol and the product precipitated as a white powder (7.59 g, $14 \cdot 10^{-3}$ mol, 68%). ^{1}H NMR ($CDCl_3$) δ (ppm): 8.05 (4 H, d, J = 8.0 Hz), 7.68 (4 H, d, J = 8.0 Hz), 4.54 (2 H, s), 4.00 (4 H, q, *J* = 7.2 Hz), 1.00 (6 H, t, *J* = 7.0 Hz). The analysis was comparable with that from the literature.[191]

3,6-Bis(4'-bromophenyl)furo[3,4-c]furane-1,4-dione (**BrDFF**) [191]

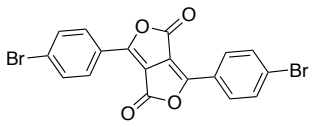

Diethyl 2,3-bis(4-bromobenzoyl)succinate (**4.3**) (7.54 g, $13.96 \cdot 10^{-3}$ mol) was slowly heated in vacuo (290-300 °C), cooled down (220-230 °C), and heated once more. The brown melted material was refluxed with methanol (50 mL), the solvent was evaporated and the residue was recrystallised from toluene (100 mL). The orange solid was purified by flash column chromatography on silica gel eluting with chloroform initially and finally recovering the product (fluorescent fraction) with ethyl acetate due to the insolubility of the material in chloroform. The product was obtained as dark orange needles (2.03 g, $4.54 \cdot 10^{-3}$ mol, 33 %). Melting point: >300 °C. ^{1}H NMR ($CDCl_3$) δ (ppm): 8.13 (4H, d, J = 7.2 Hz), 7.72 (4H, J = 6.8 Hz). The analysis was comparable with that from the literature.[191]

2,3,5,6-Tetrakis(4-bromophenyl)pyrrolo[3,4-c]pyrrole-1,4(2H,5H)-dione (**DPPBr$_4$**)[274]

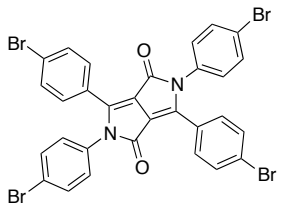

A mixture of 3,6-bis(4'-bromophenyl)furo[3,4-c]furane-1,4-dione (**BrDFF**) (500 mg, $1.12 \cdot 10^{-3}$ mol), p-bromoaniline (596 mg, $3.36 \cdot 10^{-3}$ mol) and dicyclohexylcarbodiimide (700 mg, $3.36 \cdot 10^{-3}$ mol), was suspended in chloroform (250 mL). One drop of trifluoroacetic acid was added and the reaction mixture was stirred for 6 days at room temperature (all the solids dissolved). After solvent removal, the dark orange residue was washed with methanol and a red solid was obtained. It was then purified by flash column chromatography on silica gel eluting with toluene. A small fraction of the starting material could not be separated and the product was recrystallised from methanol to yield an orange powder (210 mg, $2.78 \cdot 10^{-4}$ mol, 25 %). ^{1}H NMR ($CDCl_3$) δ (ppm): 7.56 (4 H, d, J = 8.7 Hz), 7.52 (4 H, d, J = 8.9 Hz), 7.47 (4 H, d, J = 8.9 Hz), 7.06 (4 H, d, J = 8.6 Hz). The analysis was comparable with that from the literature. [274]

2,3,5,6-Tetrakis(4-(9,9,9',9',9'',9'',9''',9'''-octaoctyl-9H,9'H,9''H,9'''-[2,2';7',2'';7'',2'''] quaterfluorene-7-yl)phenyl)-pyrrolo[3,4-c]pyrrole-1,4(2H,5H)-dione (**Star-DPP octyl**)[138]

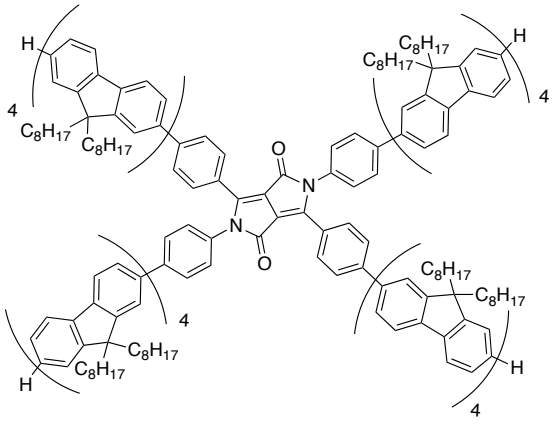

A mixture of 2,3,5,6-tetrakis(4-bromophenyl)pyrrolo[3,4-c]pyrrole-1,4(2H,5H)-dione (**DPPBr$_4$**) (30 mg, $3.9 \cdot 10^{-5}$ mol), $Pd(PPh_3)_4$ (5 mg, $5 \cdot 10^{-6}$ mol) and 9,9,9',9',9'',9'',9''',9'''-octaoctyl-9H,9'H,9''H,9'''H-[2,2':7',2'':7'',2'''-quaterfluoren]-7-yl) boronic acid (**F$_4$' O**) (374 mg, $2.34 \cdot 10^{-4}$

mol) was dissolved in anhydrous toluene (12 mL). The solution was degassed and heated to 100 °C under N_2, followed by the addition of a 0.2 M aqueous solution of K_2CO_3 (1.17 mL, $2.34 \cdot 10^{-4}$ mol) and the system was refluxed under N_2 for 67 h (TLC monitoring). After aqueous work up, the crude mixture was subjected to two flash column chromatographies on silica eluting with petroleum ether:dichloromethane (7:3) to recover a solid that was dissolved in the minimum amount of dichloromethane and reprecipitated from methanol to yield the product as an intense red solid (103 mg, $1.54 \cdot 10^{-5}$ mol, 40 %). ^{1}H NMR ($CDCl_3$) δ (ppm): 7.99 (4 H, d, *J* = 8.4 Hz), 7.91-7.62 (96 H, m), 7.48 (4 H, d, *J* = 8.4 Hz), 7.42-7.31 (12 H, m), 2.40-1.93 (64 H, m), 1.24-1.04 (320 H, m), 0.90-0.66 (160 H, m). ^{13}C NMR ($CDCl_3$) δ (ppm): 161.81, 151.43, 151.32, 150.99, 150.53, 143.90, 140.62, 140.38, 140.32, 140.05, 139.99, 139.84, 139.61, 139.55, 139.49, 139.23, 138.39, 138.08, 130.02, 127.36, 126.50, 126.29, 125.66, 125.54, 122.45, 121.01, 120.92, 119.67, 119.46, 119.37, 119.21, 110.45, 54.90, 54.85, 54.69, 39.88, 31.35, 31.29, 31.23, 29.54,28.72, 23.43, 23.34, 22.16, 22.10, 22.06, 22.03, 22.01,21.92, 13.61, 13.55. (MALDI/TOF, m/z): [M^+] calcd. for $C_{494}H_{660}N_2O_2$: 6658.5; found, 6661.3. Anal. calcd. for $C_{494}H_{660}N_2O_2$: C, 89.11; H, 9.99; N, 0.42. Found: C, 88.6; H, 10.05; N, 0.66.

3,6-Bis(4-bromophenyl)-2,5-bis(2-hexyldecyl)pyrrolo[3,4-c]pyrrole-1,4(2H,5H)-dione (**DPPBr$_2$-c**)[275]

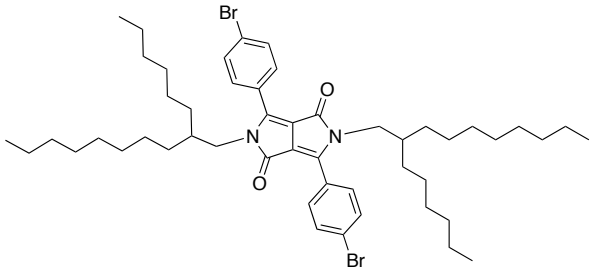

Under nitrogen, 1,4-diketo-3,6-bis(4-bromophenyl)pyrrolo[3,4-c]pyrrol (**4.4**) (250 mg, $5.60 \cdot 10^{-4}$ mol) and KO^{t}Bu (130 mg, $1.21 \cdot 10^{-3}$ mol) were suspended in dry dimethylsulfoxide (20 mL). The mixture was heated up to 60 °C and stirred for 30 minutes. 1-Bromo-2-hexyldecane (1.03 g, $3.36 \cdot 10^{-3}$ mol) was added dropwise over 90 min and the mixture was allowed to react at 60 °C for 20 h. It was then diluted with toluene (100 mL) and washed with water and brine. Drying the organic layer with $MgSO_4$ and evaporating the solvent yielded 910 mg of red oil. The crude product was purified by column chromatography on silica gel eluting with hexane:dichloromethane 1:1. The clean product was dissolved in the minimum amount of dichloromethane and reprecipitated from methanol to yield a pale orange solid (55 mg,

$6.14 \cdot 10^{-5}$ mol, 11 %). ^{1}H NMR ($CDCl_3$) δ (ppm): 7.64 (8 H, s), 3.70 (4 H, d, J = 7.2 Hz), 1.49 (2 H, d, J = 19.2 Hz), 1.24–1.05 (48 H, m), 0.89–0.80 (12 H, m). The analysis was comparable with that from the literature. [276]

3,6-Bisphenyl-2,5-bis(4-bromophenyl)pyrrolo[3,4-c]pyrrole-1,4(2H,5H)-dione (**DPPBr$_2$-c MOD**)[274]

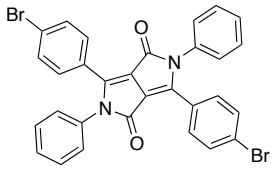

A mixture of 3,6-Bis(4'-bromophenyl)furo[3,4-c]furane-1,4-dione (**BrDFF**) (500 mg, 1.12 mmol), aniline (0.3 mL, 3.36 mmol) and dicyclohexylcarbodiimide (700 mg, 3.36 mmol), was suspended in chloroform (250 mL). One drop of trifluoroacetic acid was added and the reaction mixture was stirred for 2 days at room temperature (all the solids dissolved). The reaction mixture was washed with water (200 mL), $NaHCO_3$ (200 mL) and water (200 mL) and the organic fraction was dried over $MgSO_4$ and solvent evaporated to yield 464 mg of red solid. It was then purified twice by column chromatography on silica gel eluting with hot toluene. The product was recrystallised from toluene to yield an orange powder (400 mg, $6.68 \cdot 10^{-4}$ mol, 60 %). ^{1}H NMR ($CDCl_3$) δ (ppm): 7.54 (2 H, d, J = 8.8 Hz), 7.47-7.35 (5 H, m), 7.20 (2 H, d, J = 8.8 Hz). ^{13}C NMR ($CDCl_3$) δ (ppm): 131.70, 131.27, 129.32, 128.25, 128.02. (MALDI/TOF, m/z): [M^+] calcd. for $C_{30}H_{18}Br_2N_2O_2$: 598.3; found, 598.7. Anal. calcd. for $C_{30}H_{18}Br_2N_2O_2$: C, 60.23; H, 3.03; N, 4.68. Found: C, 60.54; H, 2.94; N, 4.31.

General method for the synthesis of linear conjugated bis(oligofluorene) DPPs (**Linear-c DPP octyl** and **Linear-c DPP MOD hexyl**)[138]

A mixture of the DPP core (1 eq), $Pd(PPh_3)_4$ (0.08 eq per position), 2-(9,9,9',9',9'',9'',9''', 9'''-octaalkyl- 9H,9'H,9''H,9H'''-[2,2';7',2'';7'',2''']quaterfluorene-7-yl) -1,3,2-dioxaborolane (1.6 eq per position) and anhydrous K_3PO_4 (1.7 eq per boronic acid functionality) was dissolved in anhydrous dimethylformamide (3 mL). The solution was degassed and stirred under N_2 at 80 °C for 40 h (TLC monitoring). After aqueous work up, the crude mixture was subjected to flash

column chromatography on silica gel. The red solid was dissolved in the minimum amount of dichloromethane and precipitated from methanol to obtain the product.

3,6-Bis(4-(9,9,9',9',9'',9'',9''',9'''-octaoctyl-9H,9'H,9''H,9H'''-[2,2';7',2'';7'',2''']quaterfluorene-7-yl)phenyl)-2,5-bis(2-hexyldecyl)pyrrolo[3,4-c]pyrrole-1,4(2H,5H)-dione (**Linear-c DPP octyl**)

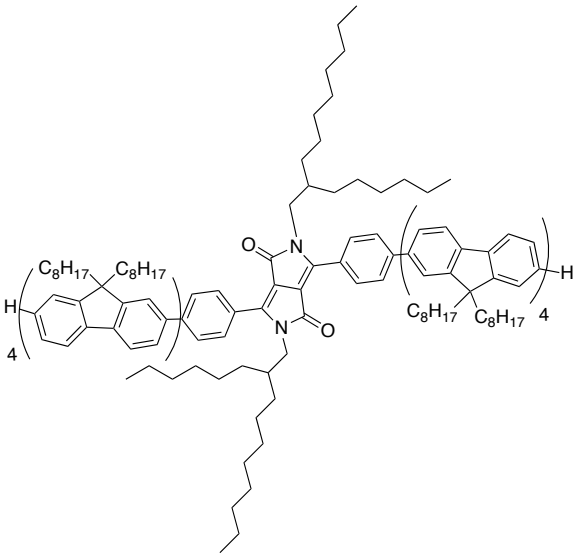

3,6-Bis(4-bromophenyl)-2,5-bis(2-hexyldecyl)pyrrolo[3,4-c]pyrrole-1,4(2H,5H)-dione (**DPPBr$_2$-c**) (27.6 mg, $3.09\cdot10^{-5}$ mol), $Pd(PPh_3)_4$ (6 mg, $5.25\cdot10^{-6}$ mol), 2-(9,9,9',9',9'',9'',9''', 9'''-octaoctyl-9H,9'H,9''H,9H'''-[2,2';7',2'';7'',2''']quaterfluorene-7-yl) -1,3,2-dioxaborolane (**F$_4$'BE O**) (161 mg, $9.88\cdot10^{-5}$ mol), anhydrous K_3PO_4 (36 mg, $1.71\cdot10^{-4}$ mol). Two flash column chromatography eluting with petroleum ether:dichloromethane (6:3) for the first column, and petroleum ether:toluene 1:2 for the second one. The product was obtained as an intense red solid (85 mg, $2.22\cdot10^{-5}$ mol, 72 %). ^{1}H NMR ($CDCl_3$) δ (ppm): 7.98 (4 H, d, J = 8.4 Hz), 7.92-7.74 (20 H, m), 7.74-7.63 (28 H, m), 7.42-7.30 (6 H, m), 3.86 (4 H, b.s.), 2.25-1.93 (32 H, m), 1.71 (2 H, b.s.), 1.25-1.06 (200 H, m), 0.91-0.68 (100 H, m). ^{13}C NMR ($CDCl_3$) δ (ppm): 162.45, 151.41, 151.32, 150.99, 150.52, 147.82, 140.31, 140.05, 139.99, 139.83, 139.49, 138.28, 128.72, 126.90, 126.30, 125.67, 122.44, 121.01, 119.66, 119.46, 119.20, 54.85, 54.68, 39.88, 31.40, 31.29, 29.54, 29.43, 29.03, 28.81, 28.71, 25.67, 25.61, 23.43, 23.33, 22.18, 22.13, 22.10, 13.62, 13.59, 13.55. (MALDI/TOF, m/z): [M^+] calcd. for $C_{282}H_{396}N_2O_2$: 3846.2; found, 3846.8. Anal. calcd. for $C_{282}H_{396}N_2O_2$: C, 88.06; H, 10.38; N, 0.73. Found: C, 86.57; H, 10.06; N, 0.60.

3,6-Bis(4-(9,9,9',9',9'',9'',9''',9'''-octaoctyl-9H,9'H,9''H,9H'''-[2,2';7',2'';7'',2''']quaterfluorene-7-yl)phenyl)-2,5-bisphenylpyrrolo[3,4-c]pyrrole-1,4(2H,5H)-dione (**Linear-c DPP MOD hexyl**)

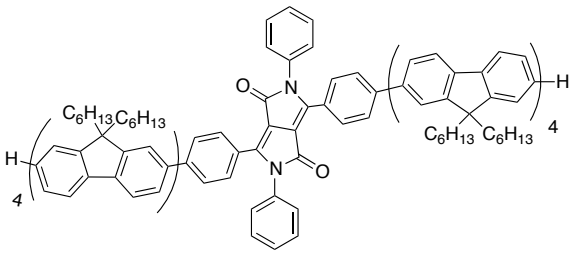

3,6-Bisphenyl-2,5-bis(4-bromophenyl)pyrrolo[3,4-c]pyrrole-1,4(2H,5H)-dione (**DPPBr$_2$-c MOD**) (35 mg, $5.85\cdot10^{-5}$ mol), $Pd(PPh_3)_4$ (12 mg, $9.94\cdot10^{-6}$ mol), 2-(9,9,9',9',9'',9'',9''',9'''-octahexyl-9H,9'H,9''H,9'''-[2,2';7',2'';7'',2''']quaterfluorene-7-yl) -1,3,2-dioxaborolane (**F$_4$'BE H**) (262 mg, $1.87\cdot10^{-4}$ mol), anhydrous K_3PO_4 (69 mg, $3.25\cdot10^{-4}$ mol). Three flash columns were performed to purify the compound eluting with hexane:dichloromethane (6:4 for the first column, 1:1 for the second and 4:6 for the third). The product was obtained as an intense red solid (152 mg, $4.89\cdot10^{-5}$ mol, 84 %). ^{1}H NMR (CD_2Cl_2) δ (ppm): 7.88-7.73 (20 H, m), 7.71-7.58 (32 H), 7.52-7.28 (16 H, m), 2.25-1.94 (32 H, m), 1.20-0.99 (96 H, m), 0.83-0.60 (80 H, m). ^{13}C NMR (CD_2Cl_2) δ (ppm): 152.37, 148.38, 145.57, 142.63, 142.34, 142.05, 141.99, 141.92, 141.68, 141.62, 141.57, 141.32, 140.03, 137.75, 131.90, 130.71, 129.66, 129.50, 128.58, 128.33, 128.23, 127.85, 127.62, 127.50, 124.53, 123.04, 121.71, 121.51, 121.40, 121.20, 112.38, 56.95, 56.75, 41.89, 33.05, 33.01, 31.20, 25.44, 25.38, 24.14, 24.11, 24.07, 15.33. (MALDI/TOF, m/z): [M$^+$] calcd. for $C_{230}H_{276}N_2O_2$: 3100.7; found, 3101.7. Anal. calcd. for $C_{230}H_{276}N_2O_2$: C, 89.09; H, 8.97; N, 0.90. Found: C, 88.14; H, 9.02; N, 0.65.

General procedure K: Synthesis of tetrakis (oligofluorene) tetraphenylethenes by Suzuki cross-coupling (**TPE1**, **TPE4**) [155]

A mixture of tetra-4-bromophenylethene (**TPEBr$_4$**) (1 eq), $Pd(PPh_3)_4$ (0.1 eq per position), 9,9-dihexyl-2,2'-fluorenylboronic acid (1.6 eq per position) and $Ba(OH)_2\cdot8H_2O$ (1.5 eq per boronic acid functionality) was dissolved in anhydrous thetrahydrofuran (20 mL). The solution was degassed with N_2, followed by the addition of water (0.6 mL) and the system was stirred under N_2 at 70 °C for 18 h. The reaction was quenched with an aqueous solution of NH_4Cl (50 mL) and extracted with dichloromethane (4 x 50 mL). The combined organic fractions were washed with water (100 mL), dried over anhydrous $MgSO_4$ and the solvent evaporated to yield a dark

green oil. The crude product was purified by column chromatography on silica gel. The material was dissolved in the minimum amount of dichloromethane and reprecipitated from methanol to yield the product.

1,1,2,2-Tetrakis(4-(9,9-dihexyl-9*H*-fluoren-2-yl)phenyl)ethene **TPE1**

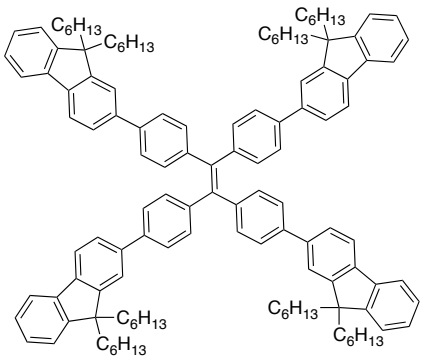

Using the general procedure K, the quantities used were: **$TPEBr_4$** (75 mg, $1.16\cdot10^{-4}$ mol), $Pd(PPh_3)_4$ (53 mg, $4.63\cdot10^{-5}$ mol), 9,9-dihexyl-2,2'-fluorenylboronic acid (**F_1' H**) (278 mg, $7.36\cdot10^{-4}$ mol), $Ba(OH)_2\cdot8H_2O$ (366 mg, $1.13\cdot10^{-3}$ mol). Column chromatography hexane:dichloromethane (9:1). The product was obtained as a bright yellow powder (153 mg, $9.21\cdot10^{-5}$ mol, 80 %). ^{1}H NMR (CD_2Cl_2) δ (ppm): 7.83-7.65 (8 H, m), 7.64-7.46 (16 H, m), 7.42-7.18 (20 H, m), 1.98 (16 H, q, J = 6.6 Hz), 1.23-0.92 (48 H, m), 0.72 (24 H, t, J = 7.0 Hz), 0.69-0.50 (16 H, m). ^{13}C NMR (CD_2Cl_2) δ (ppm): 151.51, 151.03, 143.06, 140.79, 140.58, 140.40, 139.54, 139.29, 132.02, 127.09, 126.80, 126.38, 125.68, 122.97, 121.17, 119.92, 119.68, 55.23, 40.42. 31.55, 29.70, 23.83. 22.60, 13.81. (MALDI/TOF, m/z): [M^+] calcd. for $C_{426}H_{532}$: 1662.5; found, 1661.21. Anal. calcd. for $C_{126}H_{148}$: C, 91.03; H, 8.97;. Found: C, 90.66; H, 9.30.

1,1,2,2-Tetrakis(4-(9,9,9',9',9'',9'',9''',9'''-octahexyl-9*H*,9'*H*,9''*H*,9'''*H*-[2,2':7',2'':7'',2'''-quaterfluoren]-7-yl)phenyl)ethene **TPE4**

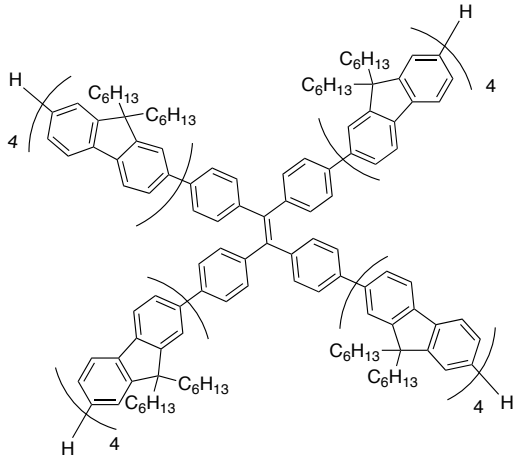

Using the general procedure K, the quantities used were: **$TPEBr_4$** (69.8 mg, $1.08\cdot10^{-4}$ mol), $Pd(PPh_3)_4$ (50 mg, $4.31\cdot10^{-5}$ mol), 9,9,9',9',9'',9'',9''',9'''-octahexyl-2,2'-quaterfluorenylboronic acid (**F_4' H**) (960 mg, $6.85\cdot10^{-4}$ mol), $Ba(OH)_2\cdot8H_2O$ (341 mg, $1.05\cdot10^{-3}$ mol). Column chromatography petroleum ether:toluene (9:1) stabilised with triethylamine (1%). The product was obtained as a bright yellow solid (549 mg, $9{,}72\cdot10^{-5}$ mol, 90 %). ^{1}H NMR ($CDCl_3$) δ (ppm): 7.86-7.58 (96 H, m), 7.42-7.29 (16 H, m), 2.30-1.90 (64 H, m), 1.20-1.05 (192 H, m), 0.90-0.55 (160 H, m). ^{13}C NMR ($CDCl_3$) δ (ppm): 152.14, 151.81, 151.34, 141.12, 140.87, 140.82, 140.66, 140.51, 140.35, 139.83, 139.72, 132.47, 127.35, 127.12, 236.80, 126.48, 126.37, 126.25, 123.26, 121.84, 121.76, 121.47, 120.32, 120.23, 120.06, 55.66, 55.60, 40.71, 31.82, 31.80, 30.04, 30.01, 24.17, 22.94, 22.91, 14.38. (MALDI/TOF, m/z): [M^+] calcd. for $C_{426}H_{532}$: 5652.8; found, 5652.2. Anal. calcd. for $C_{426}H_{532}$: C, 90.51; H, 9.49;. Found: C, 90.00; H, 9.89.

10-(4-Bromophenyl)-5,5-difluoro-1,3,7,9-tetramethyl-5*H*-dipyrrolo[1,2-*c*:2',1'-*f*][1,3,2]diazaborinin-4-ium-5-uide (**6.3**)[277]

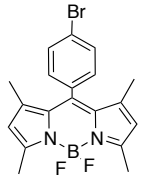

4-Bromobenzaldehyde (**6.1**) (2.38 g, $13 \cdot 10^{-3}$ mol) was dissolved in dry dichloromethane (1 L) and 2,4-dimethylpyrrole (**6.2**) (2.50 g, $26 \cdot 10^{-3}$ mol) was added, followed by the addition of 9 drops of trifluoroacetic acid (TFA). The reaction mixture was protected from the light and stirred at room temperature for 18 h. 2,3-Dichloro-5,6-dicyano-1,4-benzoquinone (DDQ) (3.56 g, $15 \cdot 10^{-3}$ mol) was added and the reaction mixture was stirred for 4 h. *N,N*-diisopropylethylamine (18 mL, $1.02 \cdot 10^{-3}$ mol) was added and the mixture was stirred for 10 minutes. BF_3OEt_2 (26 mL, 207 mmol) was slowly added and the reaction mixture was stirred overnight. The reaction mixture was filtered through a silica plug and most of the solvent was evaporated until 200 mL of the solution remained. It was then washed with water and brine and the organic fractions were dried over $MgSO_4$ and the solvent evaporated to yield 3.40 g of crude product. Purification by column chromatography on silica gel, eluting with hexane:ethyl acetate (10:1) yielded the product as a dark orange solid (2.46 g, $6.10 \cdot 10^{-3}$ mol, 47 %). ^{1}H NMR ($CDCl_3$) δ (ppm): 7.67 (2 H, d, J = 8.0 Hz), 7.20 (2 H, d, J = 8.0 Hz), 6.02 (2 H, s), 2.58 (6 H, s), 1.44 (6 H, s). The analysis was comparable with that from the literature.[277]

2,8-Dibromo-10-(4-bromophenyl)-5,5-difluoro-1,3,7,9-tetramethyl-5H-dipyrrolo[1,2-c:2',1'-f][1,3,2]diazaborinin-4-ium-5-uide (**6.4**)

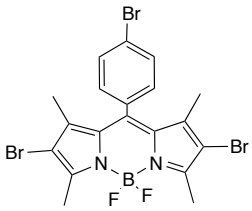

10-(4-Bromophenyl)-5,5-difluoro-1,3,7,9-tetramethyl-5*H*-dipyrrolo[1,2-*c*:2',1'-*f*][1,3,2]diazaborinin-4-ium-5-uide (**6.3**) (500 mg, $1.24 \cdot 10^{-3}$ mol) was dissolved in dry dichloromethane (20 mL) and the solution was protected from the light. *N*-Bromosuccinimide (596 mg, $3.35 \cdot 10^{-3}$ mol) was quickly added and the reaction mixture was degassed and stirred for 18 hours under nitrogen. The reaction was quenched with water and washed further water. The organic fraction was dried over $MgSO_4$ and solvent evaporated. The crude product was purified by column chromatography on silica gel eluting with hexane:dichloromethane (7:3). The product was obtained as a red solid (441 mg, $7.86 \cdot 10^{-4}$ mol, 63 %). m.p. 133-135 °C. ^{1}H NMR (CD_2Cl_2) δ (ppm): 7.69 (2 H, d, J = 8.4 Hz), 7.19 (2 H, d, J = 8.4 Hz), 2.56 (6 H, s), 1.41 (6 H, s). ^{13}C NMR (CD_2Cl_2) δ (ppm): 154.32, 140.84, 140.69, 133.36, 132.92, 132.89, 130.31, 129.90, 129.87, 129.84, 123.96, 111.91, 13.86, 13.58. (MALDI/TOF, m/z): [M^+] calcd. for

$C_{19}H_{16}BBr_3F_2N_2$: 560.9; found, 559.8. Anal. calcd. for $C_{19}H_{16}BBr_3F_2N_2$: C, 40.69; H, 2.88; N, 4.99. Found: C, 40.15; H, 2.38; N, 4.94.

General procedure L: Synthesis of T-shaped tris(oligofluorene) BODIPYs by Suzuki cross-coupling (**T-B1**, **T-B1TMS**, **T-B2**, **T-B3**) [99]

2,8-Dibromo-10-(4-bromophenyl)-5,5-difluoro-1,3,7,9-tetramethyl-5H-dipyrrolo[1,2-c:2',1'-f][1,3,2]diazaborinin-4-ium-5-uide (**6.4**) (1 eq), 9,9'-dihexyloligofluorenyl-2-boronic acid (1.2 eq per position minimum), $Pd_2(dba)_3$ (0.03 eq per position minimum) and $P(^tBu)_3HBF_4$ (2 eq per Pd catalyst) were dissolved in dry tetrahydrofuran (20 mL). An aqueous solution of K_3PO_4 (1.44 M, 1.20 eq per boronic acid functionality) was added to the previous solution and the reaction mixture was degassed and heated up to 70 °C. The reaction was refluxed under nitrogen for 48 h. It was then dissolved in dichloromethane (50 mL) and washed with water (3 x 50 mL). The organic layer was dried over $MgSO_4$, filtered and the solvents evaporated under reduced pressure. The crude product was purified by column chromatography on silica gel eluting with hexane:dichloromethane. The product was dissolved in the minimum amount of dichloromethane and precipitated from methanol to yield the product.

2,8-Bis(9,9-dihexyl-9H-fluoren-2-yl)-10-(4-(9,9-dihexyl-9H-fluoren-2-yl)phenyl)-5,5-difluoro-1,3,7,9-tetramethyl-5H-dipyrrolo[1,2-c:2',1'-f][1,3,2]diazaborinin-4-ium-5-uide (**T-B1**)

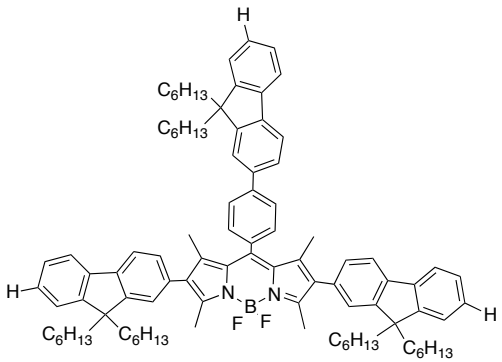

Using the general procedure L, the quantities used were: (**6.4**) (88 mg, $1.50 \cdot 10^{-4}$ mol), 9,9'-dihexylfluorenyl-2-boronic acid (**F_1' H**) (210 mg, $5.50 \cdot 10^{-4}$ mol), $Pd_2(dba)_3$ (20 mg, $2.18 \cdot 10^{-5}$ mol), $P(^tBu)_3xHBF_4$ (36 mg, $1.24 \cdot 10^{-4}$ mol), K_3PO_4 1.44 M (0.5 mL, $6.60 \cdot 10^{-4}$ mol). Column hexane:dichloromethane (3:1). The product was obtained as an intense pink powder (120 mg, $9.08 \cdot 10^{-5}$ mol, 60 %). ^1H NMR ($CDCl_3$) δ (ppm): 7.86 (2 H, d, J = 8.0 Hz), 7.78 (1 H, d, J = 7.6 Hz),

7.72 (5 H, d, *J* = 8.2 Hz), 7.67-7.63 (2 H, m), 7.51 (2 H, d, *J* = 8.4 Hz), 7.39-7.29 (9 H, m), 7.20-7.15 (4 H, m), 2.63 (6 H, s), 2.10-1.95 (12 H, m), 1.51 (6 H, s), 1.18-0.98 (36 H, m), 0.79-0.60 (30 H, m). ^{13}C NMR ($CDCl_3$) δ (ppm): 140.28, 140.02, 139.60, 138.51, 138.21, 133.90, 133.71, 131.70, 130.99, 128.24, 128.15, 127.26, 126.76, 126.58, 126.35, 126.29, 125.48, 124.25, 12.46, 122.34, 120.58, 119.53, 119.36, 119.16, 119.00, 54.73, 54.56, 39.84, 31.00, 30.97, 29.18, 29.11, 23.24, 22.05, 22.02, 21.99, 21.96, 13.51, 13.48, 13.44, 13.02, 12.74. (MALDI/TOF, m/z): [M^+] calcd. for $C_{94}H_{115}BF_2N_2$: 1321.7; found, 1321.6. Anal. calcd. for $C_{94}H_{115}BF_2N_2$: C, 85.42; H, 8.77; N, 2.12. Found: C, 82.94; H, 8.33; N, 1.83.

2,8-Bis(9,9-dihexyl-7-(trimethylsilyl)-9H-fluoren-2-yl)-10-(4-(9,9-dihexyl-7-(trimethylsilyl)-9H-fluoren-2-yl)phenyl)-5,5-difluoro-1,3,7,9-tetramethyl-5H-dipyrrolo[1,2-c:2',1'-f][1,3,2]diazaborinin-4-ium-5-uide (**T-B1TMS**)

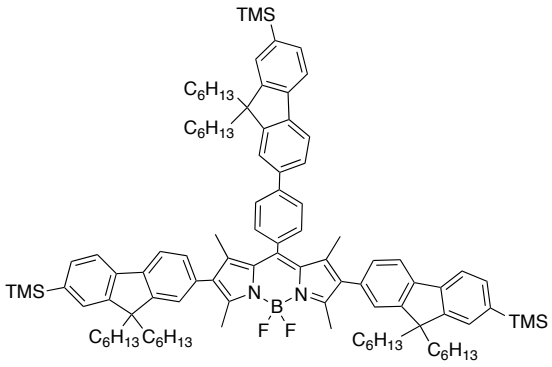

Using the general procedure L, the quantities used were: (**6.4**) (260 mg, $4.60\cdot10^{-4}$ mol), 9,9'-dihexylfluorenyl-7-trimethylsilyl-2-boronic acid (**F_1 H**) (835 mg, $1.87\cdot10^{-3}$ mol), $Pd_2(dba)_3$ (40 mg, $4.37\cdot10^{-5}$ mol), $P(^tBu)_3xHBF_4$ (50 mg, $1.72\cdot10^{-4}$ mol), K_3PO_4 1.44 M (1.6 mL, $2.25\cdot10^{-3}$ mol). Column chromatography hexane:dichloromethane (5:3). The product was dissolved in the minimum amount of dichloromethane and precipitated from methanol to yield an intense pink powder (478 mg, $3.11\cdot10^{-4}$ mol, 68 %). ^{1}H NMR ($CDCl_3$) *δ* (ppm): 7.86 (2 H, d, *J* = 8.0 Hz), 7.78 (1 H, d, *J* = 8.0 Hz), 7.74-7.67 (5 H, m), 7.67-7.62 (2 H, m), 7.54-7.43 (8 H, m), 7.09-7.03 (4 H, m), 2.62 (6 H, s), 2.10-1.91 (12 H, m), 1.50 (6 H, s), 1.07-1.95 (36 H, m), 0.75-0.60 (30 H, m), 0.32 (27 H, s). ^{13}C NMR ($CDCl_3$) *δ* (ppm): 154.35, 151.95, 151.16, 150.23, 150.17, 142.37, 142.24, 141.52, 141.28, 141.17, 140.25, 139.60, 139.35, 139.06, 134.53, 134.24, 132.50, 131.99, 131.58, 128.85, 128.81, 127.86, 127.78, 126.05, 125.08, 121.36, 120.20, 119.68, 119.15, 118.98, 55.32, 55.14, 40.17, 31.49, 29.59, 23.83, 22.55, 22.51, 13.82, 13.39, 13.17.

(MALDI/TOF, m/z): [M^+] calcd. for $C_{103}H_{139}BF_2N_2Si_3$: 1538.3; 1537.4. Anal. calcd. for $C_{103}H_{139}BF_2N_2Si_3$: C, 80.42; H, 9.11; N, 1.82. Found: C, 70.01; H, 8.11; N, 1.36.

5,5-Difluoro-1,3,7,9-tetramethyl-2,8-bis(9,9,9',9'-tetrahexyl-9H,9'H-[2,2'-bifluoren]-7-yl)-10-(4-(9,9,9',9'-tetrahexyl-9H,9'H-[2,2'-bifluoren]-7-yl)phenyl)-5H-dipyrrolo[1,2-c:2',1'-f][1,3,2]diazaborinin-4-ium-5-uide (**T-B2**)

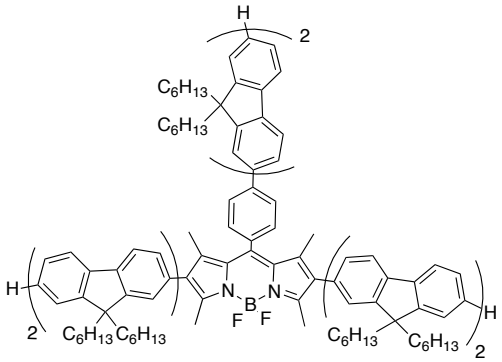

Using the general procedure L, the quantities used were: (**6.4**) (90 mg, $1.60\cdot10^{-4}$ mol), 9,9,9',9'-tetrahexyl-2,2'-bifluorenyl-2-boronic acid (**F_2' H**) (513 mg, $7.20\cdot10^{-4}$ mol), $Pd_2(dba)_3$ (20 mg, $2.18\cdot10^{-5}$ mol), $P(^tBu)_3xHBF_4$ (36 mg, $1.24\cdot10^{-4}$ mol), K_3PO_4 1.44 M (0.60 mL, $8.60\cdot10^{-4}$ mol). Column chromatography hexane:dichloromethane (7:3). The product was obtained as an intense pink powder (108 mg, $4.66\cdot10^{-5}$ mol, 30 %). ^{1}H NMR ($CDCl_3$) δ (ppm): 7.90 (2 H, d, J = 8.4 Hz), 7.85-7.73 (12 H, m), 7.71-7.60 (14 H, m), 7.54 (2 H, d, J = 8.4 Hz), 7.40-7.30 (9 H, m), 7.24-7.18 (4 H, m), 2.66 (6 H, s), 2.18-1.99 (24 H, m), 1.51 (6 H, s), 1.20-1.02 (72 H, m), 0.85-0.30 (60 H, m). ^{13}C NMR ($CDCl_3$) δ (ppm): 152.43, 151.93, 151.78, 151.39, 151.30, 141.09, 140.91, 140.71, 140.64, 140.28, 140.12, 132.55, 127.10, 126.64, 125.21, 123.24, 121.68, 120.20, 120.04, 55.69, 55.53, 55.41, 40.68, 31.78, 31.74, 30.00, 29.90, 24.08, 22.88, 22.81, 14.33, 13.60. (MALDI/TOF, m/z): [M^+] calcd. for $C_{169}H_{211}BF_2N_2$: 2319.30; found, 2318.19. Anal. calcd. for $C_{169}H_{211}BF_2N_2$: C, 87.52; H, 9.17; N, 1.21. Found: C, 85.34; H, 8.83; N, 0.86.

5,5-Difluoro-2,8-bis(9,9,9',9',9'',9''-hexahexyl-9H,9'H,9''H-[2,2':7',2''-terfluoren]-7-yl)-10-(4-(9,9,9',9',9'',9''-hexahexyl-9H,9'H,9''H-[2,2':7',2''-terfluoren]-7-yl)phenyl)-1,3,7,9-tetramethyl-5H-dipyrrolo[1,2-c:2',1'-f][1,3,2]diazaborinin-4-ium-5-uide (**T-B3**)

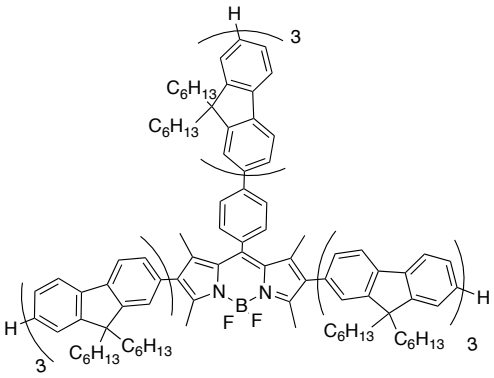

Using the general procedure L, the quantities used were: (**6.4**) (100 mg, $1.78 \cdot 10^{-4}$ mol), 9,9,9',9',9'',9''-hexahexyl-2,2'-terfluorenyl-2-boronic acid (**F_3' H**) (887 mg, $8.50 \cdot 10^{-4}$ mol), $Pd_2(dba)_3$ (49 mg, $5.35 \cdot 10^{-5}$ mol), $P(^tBu)_3xHBF_4$ (31 mg, $1.07 \cdot 10^{-4}$ mol), K_3PO_4 1.44 M (0.88 mL, $1.27 \cdot 10^{-3}$ mol). Column chromatography hexane:dichloromethane (7:3). The product was obtained as an intense pink powder (295 mg, $8.92 \cdot 10^{-5}$ mol, 50 %). ^{1}H NMR (CD_2Cl_2) δ (ppm): 7.92 (2 H, d, J = 8.4 Hz), 7.85-7.77 (15 H, m), 7.76-7.71 (5 H, m), 7.71-7.64 (24 H, m), 7.56 (2 H, d, J = 8.0 Hz), 7.40-7.28 (9 H, m), 7.26-7.19 (4 H, m), 2.60 (6 H, s), 2.18-1.87 (36 H, m), 1.55 (6 H, s), 1.16-1.00 (108 H, m), 0.81-0.63 (90 H, m). ^{13}C NMR (CD_2Cl_2) δ (ppm): 140.92, 140.65, 140.57, 140.50, 140.21, 140.14, 139.97, 139.38, 138.95, 134.56, 134.29, 132.43, 131.63, 128.97, 127.89, 127.13, 126.90, 126.19, 126.07, 125.09, 123.10, 121.58, 121.35, 120.19, 119.95, 119.76, 55.52, 55.41, 55.33, 40.44, 31.60, 29.76, 29.74, 29.70, 24.00, 23.96, 22.65, 22.59, 13.86, 13.22. (MALDI/TOF, m/z): [M^+] calcd. for $C_{244}H_{307}BF_2N_2$: 3316.9; found 3316.2. Anal. calcd. for $C_{244}H_{307}BF_2N_2$: C, 88.35; H, 9.33; N, 0.84. Found: C, 87.63; H, 9.08 N, 0.74.

2,8-Bis(7-bromo-9,9-dihexyl-9H-fluoren-2-yl)-10-(4-(7-bromo-9,9-dihexyl-9H-fluoren-2-yl)phenyl)-5,5-difluoro-1,3,7,9-tetramethyl-5H-dipyrrolo[1,2-c:2',1'-f][1,3,2]diazaborinin-4-ium-5-uide (**T-B1Br**)

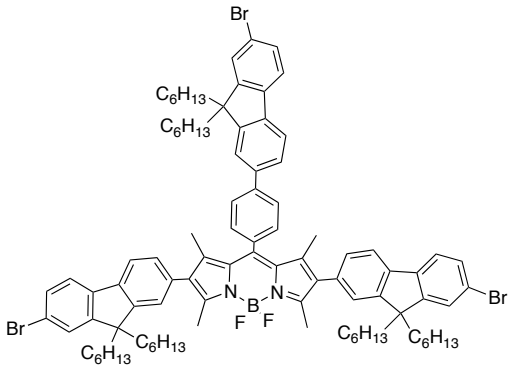

2,8-Bis(9,9-dihexyl-7-(trimethylsilyl)-9H-fluoren-2-yl)-10-(4-(9,9-dihexyl-7-(trimethylsilyl)-9H-fluoren-2-yl)phenyl)-5,5-difluoro-1,3,7,9-tetramethyl-5H-dipyrrolo[1,2-c:2',1'-f][1,3,2]diazaborinin-4-ium-5-uide (**T-B1TMS**) (400 mg, $2.60 \cdot 10^{-4}$ mol) and sodium acetate (66 mg, $7.80 \cdot 10^{-4}$ mol) were dissolved in dry tetrahydrofuran (16 mL). The solution was covered from light and cooled to 0 ^{o}C. A solution of bromine in dichloromethane (1.94 M, 1.3 mL, $2.60 \cdot 10^{-3}$ mol) was added to the previous solution. The reaction was stirred in the dark at 0 ^{o}C for 30 min. The reaction was quenched with an aqueous saturated sodium sulphite solution and the mixture was dissolved in dichloromethane. The solvents were evaporated and the product was purified by column chromatography on silica gel eluting with hexane:dichloromethane (7:3). The product was dissolved in the minimum amount of dichloromethane and precipitated from methanol to yield a bright pink solid (224 mg, $1.44 \cdot 10^{-4}$ mol, 55 %). ^{1}H NMR (CD_2Cl_2) δ (ppm): 7.86 (2 H, d, J = 8.4 Hz), 7.75 (1 H, d, J = 8.4 Hz), 7.70 (2 H, d, J = 8.5 Hz), 7.67-7.62 (2 H, m), 7.62-7.55 (3 H, m), 7.54-7.42 (8 H, m), 7.20-7.13 (4 H, m), 2.54 (6 H, s), 2.08-1.87 (12 H, m), 1.48 (6 H, s), 1.02-1.93 (36 H, m), 0.75-0.67 (18 H, m), 0.67-0.53 (12 H, m). ^{13}C NMR (CD_2Cl_2) δ (ppm): 151.42, 150.65, 142.22, 140.10, 139.87, 139.43, 139.38, 139.21, 134.39, 134.35, 132.93, 131.58, 130.12, 130.06, 129.08, 128.89, 127.91, 126.44, 126.39, 126.31, 125.03, 121.31, 121.16, 121.10, 120.27, 119.76, 55.77, 55.59, 40.37, 40.28, 31.58, 29.69, 29.63, 23.86, 22.64, 22.58, 13.86, 13.83, 13.80, 13.39, 13.16. (MALDI/TOF, m/z): [M^+] calcd. for $C_{94}H_{112}BBr_3F_2N_2$: 1558.4; found, 1558.2. Anal. calcd. for $C_{94}H_{112}BBr_3F_2N_2$: C, 72.45; H, 7.24; N, 1.80. Found: C, 66.09; H, 6.07; N, 1.68.

5,5-Difluoro-2,8-bis(9,9,9',9',9'',9'',9''',9'''-octahexyl-9H,9'H,9''H,9H'''-[2,2':7',2''-quaterfluoren]-7-yl)-10-(4-(9,9,9',9',9'',9'',9''',9'''-octahexyl-9H,9'H,9''H,9'''H-[2,2':7',2''-terfluoren]-7-yl)phenyl)-1,3,7,9-tetramethyl-5H-dipyrrolo[1,2-c:2',1'-f][1,3,2]diazaborinin-4-ium-5-uide (**T-B4**)

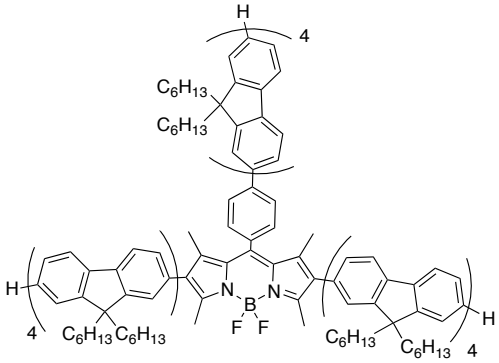

2,8-Bis(7-bromo-9,9-dihexyl-9H-fluoren-2-yl)-10-(4-(7-bromo-9,9-dihexyl-9H-fluoren-2-yl)phenyl)-5,5-difluoro-1,3,7,9-tetramethyl-5H-dipyrrolo[1,2-c:2',1'-f][1,3,2]diazaborinin-4-ium-5-uide (**T-B1Br**) (100 mg, $6.42 \cdot 10^{-5}$ mol), 9,9,9',9',9'',9''-hexahexyl-2,2'-terfluoren-7-trimethylsilyl-2-boronic acid (**F_3' H**) (311 mg, $3.06 \cdot 10^{-4}$ mol) and $Pd(PPh_3)_4$ (22 mg, $1.92 \cdot 10^{-5}$ mol) were dissolved in dry tetrahydrofuran (20 mL). An aqueous solution of K_3PO_4 (1.44 M, 0.64 mL, $9.17 \cdot 10^{-4}$ mol) was added to the previous solution and the reaction mixture was degassed and heated up to 70 °C. The reaction was refluxed under nitrogen for 3 days. The reaction mixture was quenched with water, diluted in dichloromethane and washed with water and brine. The organic layer was dried over $MgSO_4$, filtered and the solvents evaporated under reduced pressure. The crude product was purified by column chromatography on silica gel eluting with hexane:dichloromethane (7:3). The product was dissolved in the minimum amount of dichloromethane and precipitated from methanol to yield an intense pink powder (59 mg, $1.37 \cdot 10^{-5}$ mol, 21 %). ^{1}H NMR (CD_2Cl_2) δ (ppm): 7.90 (2 H, d, J = 8.0 Hz), 7.84-7.74 (20 H, m), 7.74-7.61 (41 H, m), 7.53 (2 H, d, J = 8.0 Hz), 7.39-7.24 (10 H, m), 7.23-7.16 (4 H, m), 2.58 (6 H, s), 2.20-1.89 (48 H, m), 1.52 (6 H, s), 1.16-0.98 (144 H, m), 0.80-0.67 (120 H, m). ^{13}C NMR (CD_2Cl_2) δ (ppm): 151.65, 151.31,151.17, 142.40, 142.28, 140.93, 140.67, 140.60, 140.52, 140.21, 140.16, 139.99, 138.97, 134.57, 134.31, 132.45, 131.64, 128.92, 127.92, 126.09, 125.11, 123.11, 121.65, 121.36, 120.22, 120.08, 119.97, 119.77, 55.60, 55.54, 55.42, 55.34, 40.46, 31.62, 29.77, 29.71, 24.03, 23.97, 22.72, 22.70, 22.66, 22.63, 22.61, 22.58, 13.88, 13.45, 13.24. (MALDI/TOF, m/z): [M^+] calcd. for $C_{319}H_{403}BF_2N_2$: 4314.4; found 4314.9. Anal. calcd. for $C_{319}H_{403}BF_2N_2$: C, 80.88; H, 9.41; N, 0.65. Found: C, 85.69; H, 9.18; N, 0.64.

General procedure M: Synthesis of Y-shaped tris(oligofluorene) BODIPYs by Suzuki cross-coupling (**Y-B1, Y-B2, Y-B3, Y-B4**)

10-(4-Bromophenyl)-3,7-dichloro-5,5-difluoro-5*H*-dipyrrolo[1,2-*c*:2',1'-*f*][1,3,2]diazaborinin-4-ium-5-uide (**6.5**) (1 eq), 9,9'-dihexyloligofluorenyl-2-boronic acid (**F_n' H**) (1.6 eq per position minimum) and (A-^{ta}Phos)$_2$PdCl$_2$ (0.1 eq per position) were dissolved in dry tetrahydrofuran (20 mL). An aqueous solution of K_3PO_4 (1.44 M, 1.5 eq per boronic acid functionality) was added and the reaction mixture was degassed and heated up to 70 °C. It was refluxed under nitrogen for several hours. The reaction mixture was quenched with water, diluted in dichloromethane and washed with brine and water. The combined organic fractions were dried over $MgSO_4$ and the solvent was evaporated. The crude product was purified by column chromatography on silica gel eluting with hexane:dichloromethane (10:3). The product was dissolved in the minimum amount of dichloromethane and precipitated from methanol to yield a dark green powder.

3,7-Bis(9,9-dihexyl-9*H*-fluoren-2-yl)-10-(4-(9,9-dihexyl-9*H*-fluoren-2-yl)phenyl)-5,5-difluoro-5*H*-dipyrrolo[1,2-*c*:2',1'-*f*][1,3,2]diazaborinin-4-ium-5-uide (**Y-B1**)

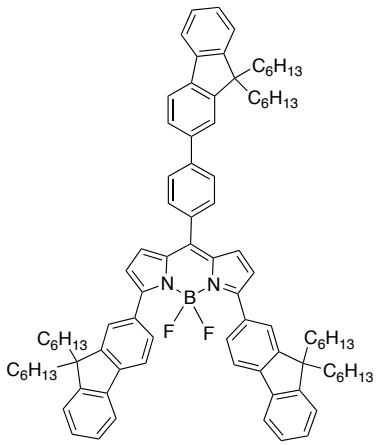

Using the general procedure L, the quantities used were: (**6.5**) (150 mg, $3.61\cdot10^{-4}$ mol), 9,9'-dihexylfluorenyl-2-boronic acid (**F_1' H**) (651 mg, $1.72\cdot10^{-3}$ mol), (A-^{ta}Phos)$_2$PdCl$_2$ (77 mg, $1.08\cdot10^{-4}$ mol), K_3PO_4 1.44 M (1.80 mL, $2.58\cdot10^{-3}$ mol). Refluxed under nitrogen for 36 hours. The product was obtained as a dark green powder (122 mg, $9.64\cdot10^{-5}$ mol, 27 %). ^{1}H NMR (CD_2Cl_2) δ (ppm): 8.04 (2 H, dd, *J* = 8.0 Hz, 1.2 Hz), 7.94 (2 H, d, *J* = 8.4 Hz), 7.84 (3 H, d, *J* = 8.4 Hz), 7.79-7.70 (9 H, m), 7.42-7.29 (9 H, m), 7.05 (2 H, d, *J* = 4.4 Hz), 6.80 (2 H, d, *J* = 4.0 Hz), 2.10-1.94 (12 H, m), 1.18-0.94 (36 H, m), 0.76-0.53 (30 H, m). ^{13}C NMR (CD_2Cl_2) δ (ppm):

151.64, 151.24, 150.70, 143.58, 142.96, 142.68, 141.39, 140.69, 140.64, 138.91, 136.74, 133.43, 131.49, 131.39, 130.59, 128.67, 127.66, 127.45, 127.04, 126.99, 126.92, 126.12, 124.22, 123.15, 123.12, 121.70, 121.16, 120.27, 120.23, 119.95, 119.45, 55.40, 55.35, 40.48, 40.29, 31.64, 31.57, 29.80, 29.76, 23.97, 23.85, 22.67, 22.64, 22.61, 13.85. (MALDI/TOF, m/z): [M^+] calcd. for $C_{90}H_{107}BF_2N_2$: 1265.6; found 1264.2. Anal. calcd. for $C_{90}H_{107}BF_2N_2$: C, 85.41; H, 8.52; N, 2.21. Found: C, 84.91; H, 8.38; N, 2.09.

5,5-Difluoro-3,7-bis(9,9,9',9'-tetrahexyl-9*H*,9'*H*-[2,2'-bifluoren]-7-yl)-10-(4-(9,9,9',9'-tetrahexyl-9*H*,9'*H*-[2,2'-bifluoren]-7-yl)phenyl)-5*H*-dipyrrolo[1,2-*c*:2',1'-*f*][1,3,2]diazaborinin-4-ium-5-uide (**Y-B2**)

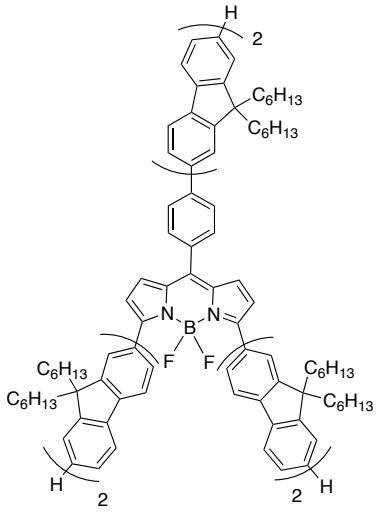

Using the general procedure L, the quantities used were: (**6.5**) (100 mg, $2.40\cdot10^{-4}$ mol), 9,9,9',9'-tetrahexyl-2,2'-bifluorenyl-2-boronic acid (**F_2' H**) (815 mg, $1.15\cdot10^{-3}$ mol), (A-^{ta}Phos)$_2PdCl_2$ (51 mg, $7.22\cdot10^{-5}$ mol, K_3PO_4 1.44 M (1.20 mL, $1.72\cdot10^{-3}$ mol). Refluxed under nitrogen for 48 hours. The product was obtained as a dark green powder (82 mg, $3.64\cdot10^{-5}$ mol, 15 %). ^{1}H NMR (CD_2Cl_2) δ (ppm): 8.10 (2 H, d, *J* = 8.0 Hz), 7.95-7.62 (32 H, m), 7.43-7.26 (9 H, m), 7.08 (2 H, d, *J* = 4.4 Hz), 6.84 (2 H, d, *J* = 4.4 Hz), 2.23-1.91 (24 H, m), 1.19-0.99 (72 H, m), 0.85-0.60 (60 H, m). ^{13}C NMR (CD_2Cl_2) δ (ppm): 159.09, 152.45, 152.17, 152.04, 151.66, 151.18, 151.04, 143.69, 142.90, 142.41, 141.23, 141.11, 140.99, 140.91, 140.57, 140.54, 140.51, 139.91, 139.86, 138.93, 136.81, 133.49, 131.55, 131.41, 130.62, 128.83, 127.15, 127.07, 126.90, 126.26, 126.12, 124.30, 123.10, 121.76, 121.67, 121.64, 121.21, 120.57, 120.34, 120.26, 119.95, 119.78, 119.56, 55.60, 55.55, 55.36, 55.33, 40.51, 40.43, 31.64, 31.61, 31.58, 29.76, 24.05, 23.94, 22.69, 22.64, 13.90, 13.86. (MALDI/TOF, m/z): [M^+] calcd. for

$C_{165}H_{203}BF_2N_2$: 2263.2; found 2262.1. Anal. calcd. for $C_{165}H_{203}BF_2N_2$: C, 87.56; H, 9.04; N, 1.24. Found: C, 86.76; H, 8.86; N, 1.21.

5,5-Difluoro-3,7-bis(9,9,9',9',9'',9''-hexahexyl-9*H*,9'*H*,9''*H*-[2,2':7',2''-terfluoren]-7-yl)-10-(4-(9,9,9',9',9'',9''-hexahexyl-9*H*,9'*H*,9''*H*-[2,2':7',2''-terfluoren]-7-yl)phenyl)-5*H*-dipyrrolo[1,2-*c*:2',1'-*f*][1,3,2]diazaborinin-4-ium-5-uide (**Y-B3**)

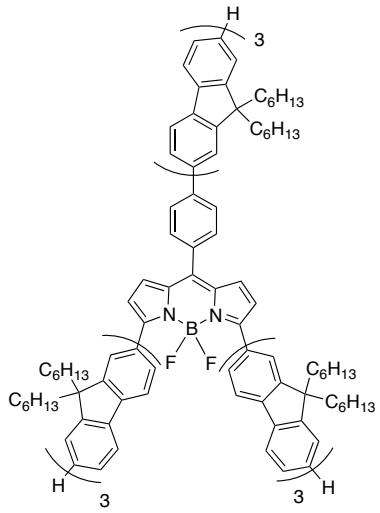

Using the general procedure L, the quantities used were: (**6.5**) (150 mg, $3.61\cdot10^{-4}$ mol), 9,9,9',9',9'',9''-hexahexyl-2,2'-bifluorenyl-2-boronic acid (**F_3' H**) (1.80 g, $1.72\cdot10^{-3}$ mol), (A-^{ta}Phos)$_2PdCl_2$ (77 mg, $1.08\cdot10^{-4}$ mol), K_3PO_4 1.44 M (1.79 mL, $2.58\cdot10^{-3}$ mol). Refluxed under nitrogen for 48 hours. The product was obtained as a dark green powder (356 mg, $1.09\cdot10^{-4}$ mol, 30 %). ^{1}H NMR (CD_2Cl_2) δ (ppm): 8.10 (2 H, d, *J* = 8.0 Hz), 7.95-7.63 (50 H, m), 7.41-7.28 (9 H, m), 7.09 (2 H, d, *J* = 4.4 Hz), 6.85 (2 H, d, *J* = 4.4 Hz), 2.23-1.96 (36 H, m), 1.21-1.00 (108 H, m), 0.85-0.60 (90 H, m). ^{13}C NMR (CD_2Cl_2) δ (ppm): 159.09, 152.48, 152.19, 152.06, 151.95, 151.63, 151.16, 151.05, 143.59, 143.41, 141.22, 140.93, 140.67, 140.59, 140.50, 140.27, 140.13, 139.90, 138.94, 136.83, 131.55, 131.43, 127.13, 126.90, 126.24, 126.08, 124.33, 123.10, 121.68, 121.58, 120.59, 120.07, 119.96, 119.76, 119.58, 55.56, 55.52, 55.33, 40.44, 31.65, 31.62, 31.59, 29.77, 23.96, 22.70, 22.65, 13.87. (MALDI/TOF, m/z): [M^+] calcd. for $C_{240}H_{299}BF_2N_2$: 3260.8; found 3260.0. Anal. calcd. for $C_{240}H_{299}BF_2N_2$: C, 88.40; H, 9.24; N, 0.88. Found: C, 87.86; H, 9.59; N, 0.84.

5,5-Difluoro-3,7-bis(9,9,9',9',9'',9'',9''',9''')-octahexyl-9*H*,9'*H*,9''*H*,9'''*H*-[2,2':7',2'''-quaterfluoren]-7-yl)-10-(4-(9,9,9',9',9'',9'',9'''-octahexyl-9*H*,9'*H*,9''*H*,9'''H-[2,2':7',2'''-quaterfluoren]-7-yl)phenyl)-5*H*-dipyrrolo[1,2-*c*:2',1'-*f*][1,3,2]diazaborinin-4-ium-5-uide (**Y-B4**)

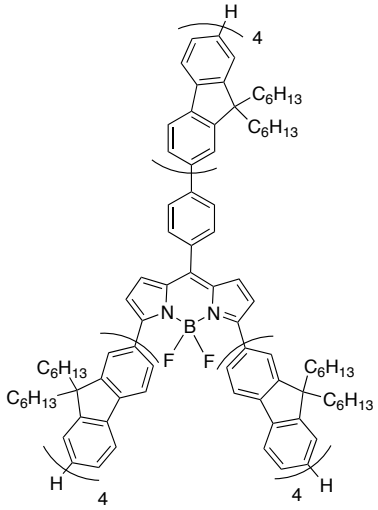

Using the general procedure L, the quantities used were: (**6.5**) (85 mg, $2.05 \cdot 10^{-4}$ mol), 9,9,9',9',9'',9'',9''',9'''-octahexyl-2,2'-quaterfluorenyl-2-boronic acid (**F_4' H**) (1.34 g, $9.78 \cdot 10^{-4}$ mol), (A-^{ta}Phos)$_2$PdCl$_2$ (44 mg, $6.15 \cdot 10^{-5}$ mol), K_3PO_4 1.44 M (1.02 mL, $1.47 \cdot 10^{-3}$ mol). It was refluxed under nitrogen for 24 hours. The product was obtained as a dark green powder (62 mg, $1.45 \cdot 10^{-5}$ mol, 7 %). ^{1}H NMR (CD_2Cl_2) δ (ppm): 8.11 (2 H, d, J = 8 Hz), 7.98-7.62 (68 H, m), 7.43-7.27 (9 H, m), 7.09 (2 H, d, J = 4.4 Hz), 6.81 (2 H, d, J = 4.4 Hz), 2.29-1.93 (48 H, m), 1.20-1.00 (144 H, m), 0.85-0.60 (120 H, m). ^{13}C NMR (CD_2Cl_2) δ (ppm): 159.01, 152.50, 151.95, 151.63, 151.16, 151.05, 143.60, 142.41, 141.22, 140.92, 140.65, 140.59, 140.50, 140.27, 140.15, 139.94, 139.90, 138.94, 136.82, 133.49, 131.55, 131.43, 127.13, 126.89, 126.19, 126.97, 124.32, 123.10, 121.63, 121.58, 121.22, 120.60, 120.28, 120.06, 119.95, 119.75, 119.57, 55.55, 55.52, 55.32, 40.44, 31.60, 29.76, 24.01, 23.95, 22.64, 13.87. (MALDI/TOF, m/z): [M^+] calcd. for $C_{315}H_{395}BF_2N_2$: 4258.3; found: 4257.7. Anal. calcd. for $C_{315}H_{395}BF_2N_2$: C, 88.85; H, 9.35; N, 0.66. Found: C, 87.32; H, 9.21; N, 0.50.

8 References

1. P. Atkins and J. d. Paula, *Atkins Physical Chemistry*, Oxford University Press, Oxford, 2006.
2. S. Eliott, *The Physics of Chemistry and Solids*, Wiley-Backwell, 1998.
3. A. Rockett, *The Materials Science of Semiconductors*, Springer Science+Business Media, LLC, New York, 2008.
4. V. Coropceanu, J. Cornil, D. A. da Silva Filho, Y. Olivier, R. Silbey and J.-L. Bredas, *Chem. Rev.*, 2007, **107**, 926-952.
5. A. C. Grimsdale, K. L. Chan, R. E. Martin, P. G. Jokisz and A. B. Holmes, *Chem. Rev.*, 2009, **109**, 897-1091.
6. J. Roncali, *Macromol. Rapid Commun.*, 2007, **28**, 1761-1775.
7. S. W. Thomas, III, G. D. Joly and T. M. Swager, *Chem. Rev.*, 2007, **107**, 1339-1386.
8. Y. Yamashita, *Sci. Tech. Adv. Mater.*, 2009, **10**, 024313-024322.
9. N. R. Armstrong, W. N. Wang, D. M. Alloway, D. Placencia, E. Ratcliff and M. Brumbach, *Macromol. Rapid Commun.*, 2009, **30**, 717-731.
10. X. Zhu and C. Ahn, *Conf Proc IEEE Eng Med Biol Soc*, 2004, **3**, 1968-1971.
11. S. Moller, S. R. Forrest, C. Perlov, W. Jackson and C. Taussig, *J. Appl. Phys.*, 2003, **94**, 7811-7819.
12. J. Roncali, *Chem. Rev.*, 1997, **97**, 173-205.
13. E. E. Havinga, W. Tenhoeve and H. Wynberg, *Polym. Bull.*, 1992, **29**, 119-126.
14. W. Brüttig, *Physics of Organic Semiconductors*, Wiley-VCH, Weinheim, Germany, 2005.
15. A. Koehler and H. Baessler, *Materials Science & Engineering R-Reports*, 2009, **66**, 71-109.
16. U. Mitschke and P. Bauerle, *J. Mater. Chem.*, 2000, **10**, 1471-1507.
17. H. H. Jaffe and A. L. Miller, *J. Chem. Educ.*, 1966, **43**, 469.
18. D. H. Williams and I. Fleming, *Spectroscopic methods in organic chemistry*, McGraw-Hill, Madenhead, 1995.
19. A. Bernanose, M. Comte and P. Vouaux, *J. Chim. Phys. Phys.- Chim. Biol.*, 1953, **50**, 64-68.
20. C. W. Tang and S. A. Vanslyke, *Appl. Phys. Lett.*, 1987, **51**, 913-915.
21. C. Adachi, T. Tsutsui and S. Saito, *Appl. Phys. Lett.*, 1990, **56**, 799-801.
22. R. H. Friend, R. W. Gymer, A. B. Holmes, J. H. Burroughes, R. N. Marks, C. Taliani, D. D. C. Bradley, D. A. Dos Santos, J. L. Bredas, M. Logdlund and W. R. Salaneck, *Nature*, 1999, **397**, 121-128.
23. A. E. Siegman, *Lasers*, University Science Books, Mill Valley, 1986.
24. O. Svelto, *Principles of Lasers*, 4th edn., Plenum Press, New York, 1998.
25. I. D. W. Samuel and G. A. Turnbull, *Chem. Rev.*, 2007, **107**, 1272-1295.
26. J. Hecht, *Understanding lasers*, 2nd edn., IEEE Press, Piscataway, NY, 1993.
27. G. P. Agrawal, *Semiconductor Lasers: Past, Present, Future.*, AIP, Woodbury, NY, 1995.
28. U. Scherf, S. Riechel, U. Lemmer and R. F. Mahrt, *Curr. Opin. Solid State Mater. Sci.*, 2001, **5**, 143-154.
29. W. H. Knox, R. L. Fork, M. C. Downer, R. H. Stolen, C. V. Shank and J. A. Valdmanis, *Appl. Phys. Lett.*, 1985, **46**, 1120-1121.
30. B. H. Soffer, McFarland, B. B., *Appl. Phys. Lett.*, 1967, **10**, 266.
31. N. Karl, *Phys. Status Solidi A*, 1972, **13**, 651-655.
32. O. S. Avanesjan, V. A. Benderskii, V. K. Brikenstein, V. L. Broude, L. I. Korshunov, A. G. Lavrushko and Tartakovskii, II, *Mol. Cryst. Liq. Cryst.*, 1974, **29**, 165-174.

33. D. Moses, *Appl. Phys. Lett.*, 1992, **60**, 3215-3216.
34. N. Tessler, *Adv. Mater.*, 1999, **11**, 363-370.
35. V. G. Kozlov and S. R. Forrest, *Curr. Opin. Solid State Mater. Sci.*, 1999, **4**, 203-208.
36. G. A. Turnbull, P. Andrew, W. L. Barnes and I. D. W. Samuel, *Phys. Rev. B: Condens. Matter*, 2003, **67**, 165107-165115.
37. J. R. Lawrence, G. A. Turnbull, I. D. W. Samuel, G. J. Richards and P. L. Burn, *Opt. Lett.*, 2004, **29**, 869-871.
38. D. Astruc, E. Boisselier and C. Ornelas, *Chem. Rev.*, **110**, 1857-1959.
39. T. Spehr, R. Pudzich, T. Fuhrmann and J. Salbeck, *Org. Electron.*, 2003, **4**, 61-69.
40. M. Goossens, A. Ruseckas, G. A. Turnbull and I. D. W. Samuel, *Appl. Phys. Lett.*, 2004, **85**, 31-33.
41. D. Amarasinghe, A. Ruseckas, A. E. Vasdekis, M. Goossens, G. A. Turnbull and I. D. W. Samuel, *Appl. Phys. Lett.*, 2006, **89**.
42. C. W. Tang, S. A. Vanslyke and C. H. Chen, *J. Appl. Phys.*, 1989, **65**, 3610-3616.
43. B. Kraabel, V. I. Klimov, R. Kohlman, S. Xu, H. L. Wang and D. W. McBranch, *Phys. Rev. B: Condens. Matter*, 2000, **61**, 8501-8515.
44. U. Rauscher, H. Bassler, D. D. C. Bradley and M. Hennecke, *Phys. Rev. B: Condens. Matter*, 1990, **42**, 9830-9836.
45. A. K. Sheridan, A. R. Buckley, A. M. Fox, A. Bacher, D. D. C. Bradley and I. D. W. Samuel, *J. Appl. Phys.*, 2002, **92**, 6367-6371.
46. J. Pina, J. S. de Melo, H. D. Burrows, A. L. Macanita, F. Galbrecht, T. Bunnagel and U. Scherf, *Macromolecules*, 2009, **42**, 1710-1719.
47. G. Tsiminis, Y. Wang, P. E. Shaw, A. L. Kanibolotsky, I. F. Perepichka, M. D. Dawson, P. J. Skabara, G. A. Turnbull and I. D. W. Samuel, *Appl. Phys. Lett.*, 2009, **94**, 233304.
48. L. Persano, S. Molle, S. Girardo, A. A. R. Neves, A. Camposeo, R. Stabile, R. Cingolani and D. Pisignano, *Adv. Funct. Mater.*, 2008, **18**, 2692-2698.
49. J. R. Lawrence, G. A. Turnbull and I. D. W. Samuel, *Appl. Phys. Lett.*, 2003, **82**, 4023-4025.
50. I. D. W. Samuel, E. B. Namdas and G. A. Turnbull, *Nature Photon.*, 2009, **3**, 546-549.
51. G. Tsiminis, A. Ruseckas, I. D. W. Samuel and G. A. Turnbull, *Appl. Phys. Lett.*, 2009, **94**, 253304-253307.
52. D. Schneider, T. Rabe, T. Riedl, T. Dobbertin, M. Kroger, E. Becker, H. H. Johannes, W. Kowalsky, T. Weimann, J. Wang, P. Hinze, A. Gerhard, P. Stossel and H. Vestweber, *Adv. Mater.*, 2005, **17**, 31-34.
53. G. Heliotis, D. D. C. Bradley, M. Goossens, S. Richardson, G. A. Turnbull and I. D. W. Samuel, *Appl. Phys. Lett.*, 2004, **85**, 6122-6124.
54. D. Amarasinghe, A. Ruseckas, G. A. Turnbull and I. D. W. Samuel, *Prod. IEEE*, 2009, **97**, 1637-1650.
55. D. T. McQuade, A. E. Pullen and T. M. Swager, *Chem. Rev.*, 2000, **100**, 2537-2574.
56. J. S. Yang and T. M. Swager, *J. Am. Chem. Soc.*, 1998, **120**, 11864-11873.
57. H. A. Ho, K. Dore, M. Boissinot, M. G. Bergeron, R. M. Tanguay, D. Boudreau and M. Leclerc, *J. Am. Chem. Soc.*, 2005, **127**, 12673-12676.
58. Y. L. Tang, F. He, M. H. Yu, F. D. Feng, L. L. An, H. Sun, S. Wang, Y. L. Li and D. B. Zhu, *Macromol. Rapid Commun.*, 2006, **27**, 389-392.
59. A. L. Kanibolotsky, R. Berridge, P. J. Skabara, I. F. Perepichka, D. D. C. Bradley and M. Koeberg, *J. Am. Chem. Soc.*, 2004, **126**, 13695-13702.
60. Y. Wang, G. Tsiminis, Y. Yang, A. Ruseckas, A. L. Kanibolotsky, I. F. Perepichka, P. J. Skabara, G. A. Turnbull and I. D. W. Samuel, *Synth. Met.*, 2010, **160**, 1397-1400.
61. A. L. Kanibolotsky, I. F. Perepichka and P. J. Skabara, *Chem. Soc. Rev.*, 2010, **39**, 2695-2728.
62. J. Roncali, P. Leriche and A. Cravino, *Adv. Mater.*, 2007, **19**, 2045-2060.

63. A. L. Kanibolotsky, J. C. Forgie, G. J. McEntee, M. M. A. Talpur, P. J. Skabara, T. D. J. Westgate, J. J. W. McDouall, M. Auinger, S. J. Coles and M. B. Hursthouse, *Chem. Eur. J.*, 2009, **15**, 11581-11593.
64. B. Gomez-Lor, O. de Frutos, P. A. Ceballos, T. Granier and A. M. Echavarren, *Eur. J. Org. Chem.*, 2001, 2107-2114.
65. Y. Wu, X. Hao, J. Wu, J. Jin and X. Ba, *Macromolecules*, 2010, **43**, 731-738.
66. B. Gomez-Lor, E. Gonzalez-Cantalapiedra, M. Ruiz, S. de Frutos, D. J. Cardenas, A. Santos and A. M. Echavarren, *Chem. Eur. J.*, 2004, **10**, 2601-2608.
67. L.-L. Li, P. Hu, B.-Q. Wang, W.-H. Yu, Y. Shimizu and K.-Q. Zhao, *Liq. Cryst.*, 2010, **37**, 499-506.
68. C. Moberg, *Angew. Chem. Int. Ed.*, 1998, **37**, 248-268.
69. O. de Frutos, T. Granier, B. Gomez-Lor, J. Jimenez-Barbero, A. Monge, E. Gutierrez-Puebla and A. M. Echavarren, *Chem. Eur. J.*, 2002, **8**, 2879-2890.
70. K.-P. Tseng, M.-T. Kao, T. W. T. Tsai, C.-H. Hsu, J. C. C. Chan, J.-J. Shyue, S.-S. Sun and K.-T. Wong, *Chem. Commun.*, 2012, **48**, 3515-3517.
71. J. Pei, J. L. Wang, X. Y. Cao, X. H. Zhou and W. B. Zhang, *J. Am. Chem. Soc.*, 2003, **125**, 9944-9945.
72. M. S. Yuan, Z. Q. Liu and Q. Fang, *J. Org. Chem.*, 2007, **72**, 7915-7922.
73. S. Diring, R. Ziessel, F. Barigelletti, A. Barbieri and B. Ventura, *Chem. Eur. J.*, 2010, **16**, 9226-9236.
74. S. Diring, B. Ventura, A. Barbieri and R. Ziessel, *Dalton Trans.*, 2012, **41**, 13090-13096.
75. S. Diring, F. Puntoriero, F. Nastasi, S. Campagna and R. Ziessel, *J. Am. Chem. Soc.*, 2009, **131**, 6108-6110.
76. Y. Shi, M. Liang, L. Wang, H. Han, L. You, Z. Sun and S. Xue, *ACS Appl. Mater. Interfaces*, 2013, **5**, 144-153.
77. L. Yu, J. Xi, H. T. Chan, T. Su, L. J. Antrobus, B. Tong, Y. Dong, W. K. Chan and D. L. Phillips, *J. Phys. Chem. C*, 2013, **117**, 2041-2052.
78. J.-M. Koenen, S. Jung, A. Patra, A. Helfer and U. Scherf, *Adv. Mater.*, 2012, **24**, 681-686.
79. L. Sanchez, N. Martin, E. Gonzalez-Cantalapiedra, A. M. Echavarren, G. M. A. Rahman and D. M. Guldi, *Org. Lett.*, 2006, **8**, 2451-2454.
80. M.-A. Tehfe, F. Dumur, B. Graff, J.-L. Clement, D. Gigmes, F. Morlet-Savary, J.-P. Fouassier and J. Lalevee, *Macromolecules*, 2013, **46**, 736-746.
81. B. Du, D. Fortin and P. D. Harvey, *J. Inorg. Organomet. Polym. Mater.*, 2013, **23**, 81-88.
82. Y. P. Xie, X. F. Zhang, Y. Xiao, Y. D. Zhang, F. Zhou, J. Qi and J. L. Qu, *Chem. Commun.*, 2012, **48**, 4338-4340.
83. S. Beaupre, P.-L. T. Boudreault and M. Leclerc, *Adv. Mater.*, 2010, **22**, E6-E27.
84. J. Zaumseil, C. L. Donley, J. S. Kim, R. H. Friend and H. Sirringhaus, *Adv. Mater.*, 2006, **18**, 2708-2712.
85. G. Heliotis, R. Xia, D. D. C. Bradley, G. A. Turnbull, I. D. W. Samuel, P. Andrew and W. L. Barnes, *Appl. Phys. Lett.*, 2003, **83**, 2118-2120.
86. S. Y. Cho, A. C. Grimsdale, D. J. Jones, S. E. Watkins and A. B. Holmes, *J. Am. Chem. Soc.*, 2007, **129**, 11910-11911.
87. M. Sims, D. D. C. Bradley, M. Ariu, M. Koeberg, A. Asimakis, M. Grell and D. G. Lidzey, *Adv. Funct. Mater.*, 2004, **14**, 765-781.
88. M. R. Craig, M. M. de Kok, J. W. Hofstraat, A. Schenning and E. W. Meijer, *J. Mater. Chem.*, 2003, **13**, 2861-2862.
89. R. E. Martin and F. Diederich, *Angew. Chem. Int. Ed.*, 1999, **38**, 1350-1377.
90. S. W. Culligan, Y. H. Geng, S. H. Chen, K. Klubek, K. M. Vaeth and C. W. Tang, *Adv. Mater.*, 2003, **15**, 1176-1180.
91. Y. H. Geng, S. W. Culligan, A. Trajkovska, J. U. Wallace and S. H. Chen, *Chem. Mater.*, 2003, **15**, 542-549.

92. Z. Q. Gao, Z. H. Li, P. F. Xia, M. S. Wong, K. W. Cheah and C. H. Chen, *Adv. Funct. Mater.*, 2007, **17**, 3194-3199.
93. L. S. Chinelatto, Jr., J. del Barrio, M. Pinol, L. Oriol, M. A. Matranga, M. P. De Santo and R. Barberi, *J. Photochem. Photobiol., A*, 2010, **210**, 130-139.
94. T. Yasuda, K. Fujita, T. Tsutsui, Y. H. Geng, S. W. Culligan and S. H. Chen, *Chem. Mater.*, 2005, **17**, 264-268.
95. I. I. Perepichka, I. F. Perepichka, M. R. Bryce and L. O. Palsson, *Chem. Commun.*, 2005, 3397-3399.
96. C. van der Pol, M. R. Bryce, M. Wielopolski, C. Atienza-Castellanos, D. M. Guldi, S. Filippone and N. Martin, *J. Org. Chem.*, 2007, **72**, 6662-6671.
97. E. Leary, M. Teresa Gonzalez, C. van der Pol, M. R. Bryce, S. Filippone, N. Martin, G. Rubio-Bollinger and N. Agrait, *Nano Lett.*, 2011, **11**, 2236-2241.
98. M. Wielopolski, G. d. M. Rojas, C. van der Pol, L. Brinkhaus, G. Katsukis, M. R. Bryce, T. Clark and D. M. Guldi, *Acs Nano*, 2010, **4**, 6449-6462.
99. N. J. Findlay, C. Orofino-Pena, J. Bruckbauer, S. E. T. Elmasly, S. Arumugam, A. R. Inigo, A. L. Kanibolotsky, R. W. Martin and P. J. Skabara, *J. Mater. Chem. C*, 2013, **1**, 2249-2256.
100. M. P. Aldred, C. Li, G.-F. Zhang, W.-L. Gong, A. D. Q. Li, Y. Dai, D. Ma and M.-Q. Zhu, *J. Mater. Chem.*, 2012, **22**, 7515-7528.
101. X. J. Feng, P. L. Wu, K. F. Li, M. S. Wong and K. W. Cheah, *Chem. Eur. J.*, 2011, **17**, 2518-2526.
102. W.-J. Li, B. Liu, Y. Qian, L.-H. Xie, J. Wang, S.-B. Li and W. Huang, *Polym. Chem.*, 2013, **4**, 1796-1802.
103. A. Kaeser, I. Fischer, R. Abbel, P. Besenius, D. Dasgupta, M. A. J. Gillisen, G. Portale, A. L. Stevens, L. M. Herz and A. P. H. J. Schenning, *Acs Nano*, 2013, **7**, 408-416.
104. P. Chen, R. A. Lalancette and F. Jaekle, *J. Am. Chem. Soc.*, 2011, **133**, 8802-8805.
105. C.-G. Zhen, Y.-F. Dai, W.-J. Zeng, Z. Ma, Z.-K. Chen and J. Kieffer, *Adv. Funct. Mater.*, 2011, **21**, 699-707.
106. Q. Yan, Y. Fan and D. Zhao, *Macromolecules*, 2012, **45**, 133-141.
107. H. Zhou, R. Lu, X. Zhao, X. Qiu, P. Xue, X. Liu and X. Zhang, *Tetrahedron Lett.*, 2010, **51**, 5287-5290.
108. W. Y. Lai, R. D. Xia, Q. Y. He, P. A. Levermore, W. Huang and D. D. C. Bradley, *Adv. Mater.*, 2009, **21**, 355-360.
109. K. M. Omer, A. L. Kanibolotsky, P. J. Skabara, I. F. Perepichka and A. J. Bard, *J. Phys. Chem. B*, 2007, **111**, 6612-6619.
110. A. J. C. Kuehne, D. Elfstrom, A. R. Mackintosh, A. L. Kanibolotsky, B. Guilhabert, E. Gu, I. F. Perepichka, P. J. Skabara, M. D. Dawson and R. A. Pethrick, *Adv. Mater.*, 2009, **21**, 781-785.
111. A. Hernandez-Santana, A. R. Mackintosh, B. Guilhabert, A. L. Kanibolotsky, M. D. Dawson, P. J. Skabara and D. Graham, *J. Mater. Chem.*, 2011, **21**, 14209-14212.
112. M. Wu, Z. Gong, A. J. C. Kuehne, A. L. Kanibolotsky, Y. J. Chen, I. F. Perepichka, A. R. Mackintosh, E. Gu, P. J. Skabara, R. A. Pethrick and M. D. Dawson, *Opt. Express*, 2009, **17**, 16436-16443.
113. B. Guilhabert, N. Laurand, J. Herrnsdorf, Y. Chen, A. R. Mackintosh, A. L. Kanibolotsky, E. Gu, P. J. Skabara, R. A. Pethrick and M. D. Dawson, *J. Opt.*, 2010, **12**, 035503-035508.
114. J. Herrnsdorf, B. Guilhabert, Y. Chen, A. L. Kanibolotsky, A. R. Mackintosh, R. A. Pethrick, P. J. Skabara, E. Gu, N. Laurand and M. D. Dawson, *Opt. Express*, 2010, **18**, 25535-25545.
115. B. Guilhabert, N. Laurand, J. Herrnsdorf, Y. Chen, A. L. Kanibolotsky, C. Orofino, P. J. Skabara and M. D. Dawson, *IEEE Photon. J.*, 2012, **4**, 684-690.

116. H. Zhou, X. Zhao, T. Huang, R. Lu, H. Zhang, X. Qi, P. Xue, X. Liu and X. Zhang, *Org. Biomol. Chem.*, 2011, **9**, 1600-1607.
117. W. B. Zhang, W. H. Jin, X. H. Zhou and J. Pei, *Tetrahedron*, 2007, **63**, 2907-2914.
118. S. C. Yuan, Q. J. Sun, T. Lei, B. Du, Y. F. Li and J. Pei, *Tetrahedron*, 2009, **65**, 4165-4172.
119. Q. Q. Chen, F. Liu, Z. Ma, B. Peng, W. Wei and W. Huang, *Synlett*, 2007, 3145-3148.
120. Y. M. Sun, K. Xiao, Y. Q. Liu, J. L. Wang, J. Pei, G. Yu and D. B. Zhu, *Adv. Funct. Mater.*, 2005, **15**, 818-822.
121. J. L. Wang, X. F. Duan, B. Jiang, L. B. Gan, J. Pei, C. He and Y. F. Li, *J. Org. Chem.*, 2006, **71**, 4400-4410.
122. T. L. Zhen-Ming Tang, Jing-Liang Wang, Juguo Ma, Jian Pei, *J. Org. Chem.*, 2010, **75**, 3644-3655.
123. J.-L. Wang, Y.-T. Chan, C. N. Moorefield, J. Pei, D. A. Modarelli, N. C. Romano and G. R. Newkome, *Macromol. Rapid Commun.*, 2010, **31**, 850-855.
124. X. H. Zhou, J. C. Yan and J. Pei, *Org. Lett.*, 2003, **5**, 3543-3546.
125. G. Tsiminis, N. A. Montgomery, A. L. Kanibolotsky, A. Ruseckas, I. F. Perepichka, P. J. Skabara, G. A. Turnbull and I. D. W. Samuel, *Semicond. Sci. Technol.*, 2012, **27**.
126. Y. Zou, J. Zou, T. Ye, H. Li, C. Yang, H. Wu, D. Ma, J. Qin and Y. Cao, *Adv. Funct. Mater.*, 2013, **23**, 1781-1788.
127. J. S. Yang, H. H. Huang and J. H. Ho, *J. Phys. Chem. B*, 2008, **112**, 8871-8878.
128. J. S. Yang, Y. R. Lee, J. L. Yan and M. C. Lu, *Org. Lett.*, 2006, **8**, 5812-5816.
129. H.-H. Huang, C. Prabhakar, K.-C. Tang, P.-T. Chou, G.-J. Huang and J.-S. Yang, *J. Am. Chem. Soc.*, 2011, **133**, 8028-8039.
130. J. S. Yang, H. H. Huang, Y. H. Liu and S. M. Peng, *Org. Lett.*, 2009, **11**, 4942-4945.
131. W. Y. Lai, Q. Y. He, R. Zhu, Q. Q. Chen and W. Huang, *Adv. Funct. Mater.*, 2008, **18**, 265-276.
132. P. A. Levermore, R. Xia, W. Lai, X. H. Wang, W. Huang and D. D. C. Bradley, *Journal of Physics D-Applied Physics*, 2007, **40**, 1896-1901.
133. F. Liu, W. Y. Lai, C. Tang, H. B. Wu, Q. Q. Chen, B. Peng, W. Wei, W. Huang and Y. Cao, *Macromol. Rapid Commun.*, 2008, **29**, 659-664.
134. R. D. Xia, W. Y. Lai, P. A. Levermore, W. Huang and D. D. C. Bradley, *Adv. Funct. Mater.*, 2009, **19**, 2844-2850.
135. B. S. Li, J. Li, Y. Q. Fu and Z. S. Bo, *J. Am. Chem. Soc.*, 2004, **126**, 3430-3431.
136. T. Xu, R. Lu, X. Liu, P. Chen, X. Qiu and Y. Zhao, *J. Org. Chem.*, 2008, **73**, 1809-1817.
137. Q. D. Liu, J. P. Lu, J. F. Ding, M. Day, Y. Tao, P. Barrios, J. Stupak, K. Chan, J. J. Li and Y. Chi, *Adv. Funct. Mater.*, 2007, **17**, 1028-1036.
138. A. L. Kanibolotsky, F. Vilela, J. C. Forgie, S. E. T. Elmasly, P. J. Skabara, K. Zhang, B. Tieke, J. McGurk, C. R. Belton, P. N. Stavrinou and D. D. C. Bradley, *Adv. Mater.*, 2011, **23**, 2093-2097.
139. T. Zhang, R. Wang, L. Wang, Q. Wang and J. Li, *Dyes Pigm.*, 2013, **97**, 155-161.
140. D. Katsis, Y. H. Geng, J. J. Ou, S. W. Culligan, A. Trajkovska, S. H. Chen and L. J. Rothberg, *Chem. Mater.*, 2002, **14**, 1332-1339.
141. S. Jeeva and S. C. Moratti, *Synthesis-Stuttgart*, 2007, 3323-3328.
142. A. C. A. Chen, J. U. Wallace, S. K. H. Wei, L. C. Zeng and S. H. Chen, *Chem. Mater.*, 2006, **18**, 204-213.
143. K.-Y. Pu, K. Li and B. Liu, *Adv. Mater.*, 2010, **22**, 643-646.
144. C. D. Simpson, J. S. Wu, M. D. Watson and K. Mullen, *J. Mater. Chem.*, 2004, **14**, 494-504.
145. *The Porphyrin Handbook, Volume 1, Synthesis and Organic Chemistry*, Academic Press, San Diego, 1999.
146. *The Porphyrin Handbook, Volume 15: Phthalocyanine Synthesis*, Academic Press, Amsterdam, 2003.

147. M. Tavasli, S. Bettington, M. R. Bryce, H. A. Al Attar, F. B. Dias, S. King and A. P. Monkman, *J. Mater. Chem.*, 2005, **15**, 4963-4970.
148. J. H. Jo, C. Y. Chi, S. Hoger, G. Wegner and D. Y. Yoon, *Chem. Eur. J.*, 2004, **10**, 2681-2688.
149. J. Grimme, M. Kreyenschmidt, F. Uckert, K. Mullen and U. Scherf, *Adv. Mater.*, 1995, **7**, 292-295.
150. M. Moreno Oliva, J. Casado, J. T. Lopez Navarrete, R. Berridge, P. J. Skabara, A. L. Kanibolotsky and I. F. Perepichka, *J. Phys. Chem. B*, 2007, **111**, 4026-4035.
151. N. A. Montgomery, J.-C. Denis, S. Schumacher, A. Ruseckas, P. J. Skabara, A. Kanibolotsky, M. J. Paterson, I. Galbraith, G. A. Turnbull and I. D. W. Samuel, *J. Phys. Chem. A*, 2011, **115**, 2913-2919.
152. Y. Yang, G. A. Turnbull and I. D. W. Samuel, *Adv. Funct. Mater.*, 2010, **20**, 2093-2097.
153. Y. Wang, B. R. Rae, R. K. Henderson, Z. Gong, J. McKendry, E. Gu, M. D. Dawson, G. A. Turnbull and I. D. W. Samuel, *Aip Advances*, 2011, **1**, 032115-032124.
154. Y. Wang, N. B. McKeown, K. J. Msayib, G. A. Turnbull and I. D. W. Samuel, *Sensors*, 2011, **11**, 2478-2487.
155. C. R. Belton, A. L. Kanibolotsky, J. Kirkpatrick, C. Orofino, S. E. T. Elmasly, P. N. Stavrinou, P. J. Skabara and D. D. C. Bradley, *Adv. Funct. Mater.*, 2013, **23**, 2792-2804.
156. J. Cornil, I. Gueli, A. Dkhissi, J. C. Sancho-Garcia, E. Hennebicq, J. P. Calbert, V. Lemaur, D. Beljonne and J. L. Bredas, *J. Chem. Phys.*, 2003, **118**, 6615-6623.
157. M. T. Bernius, M. Inbasekaran, J. O'Brien and W. S. Wu, *Adv. Mater.*, 2000, **12**, 1737-1750.
158. N. Tokmoldin, N. Griffiths, D. D. C. Bradley and S. A. Haque, *Adv. Mater.*, 2009, **21**, 3475-3478.
159. D. Kabra, L. P. Lu, M. H. Song, H. J. Snaith and R. H. Friend, *Adv. Mater.*, 2010, **22**, 3194-3198.
160. R. Xia, G. Heliotis, P. N. Stavrinou and D. D. C. Bradley, *Appl. Phys. Lett.*, 2005, **87**, 031104.
161. M. Voigt, J. Chappell, T. Rowson, A. Cadby, M. Geoghegan, R. A. L. Jones and D. G. Lidzey, *Org. Electron.*, 2005, **6**, 35-45.
162. M. S. Liu, X. Z. Jiang, S. Liu, P. Herguth and A. K. Y. Jen, *Macromolecules*, 2002, **35**, 3532-3538.
163. D.-Y. Chung, J. Huang, D. D. C. Bradley and A. J. Campbell, *Org. Electron.*, 2010, **11**, 1088-1095.
164. G. Heliotis, R. Xia, D. D. C. Bradley, G. A. Turnbull, I. D. W. Samuel, P. Andrew and W. L. Barnes, *J. Appl. Phys.*, 2004, **96**, 6959-6965.
165. J. Huang, Q. Liu, J.-H. Zou, X.-H. Zhu, A.-Y. Li, J.-W. Li, S. Wu, J. Peng, Y. Cao, R. Xia, D. D. C. Bradley and J. Roncali, *Adv. Funct. Mater.*, 2009, **19**, 2978-2986.
166. M. Wang, X. Hu, P. Liu, W. Li, X. Gong, F. Huang and Y. Cao, *J. Am. Chem. Soc.*, 2011, **133**, 9638-9641.
167. J. Nelson, *Mater. Today*, 2011, **14**, 462-470.
168. L. Huo, J. Hou, S. Zhang, H.-Y. Chen and Y. Yang, *Angew. Chem. Int. Ed.*, 2010, **49**, 1500-1503.
169. H. Zhou, L. Yang, A. C. Stuart, S. C. Price, S. Liu and W. You, *Angew. Chem. Int. Ed.*, 2011, **50**, 2995-2998.
170. J. M. Winfield, A. Van Vooren, M.-J. Park, D.-H. Hwang, J. Cornil, J.-S. Kim and R. H. Friend, *J. Chem. Phys.*, 2009, **131**, 035104.
171. K. G. Jespersen, W. J. D. Beenken, Y. Zaushitsyn, A. Yartsev, M. Andersson, T. Pullerits and V. Sundstrom, *J. Chem. Phys.*, 2004, **121**, 12613-12617.
172. J. M. Winfield, C. L. Donley, R. H. Friend and J.-S. Kim, *J. Appl. Phys.*, 2010, **107**, 024902.
173. R. L. Martin, *J. Chem. Phys.*, 2003, **118**, 4775-4777.

174. Y. W. Soon, T. M. Clarke, W. Zhang, T. Agostinelli, J. Kirkpatrick, C. Dyer-Smith, I. McCulloch, J. Nelson and J. R. Durrant, *Chem. Sci.*, 2011, **2**, 1111-1120.
175. R. Xia, P. N. Stavrinou, D. D. C. Bradley and Y. Kim, *J. Appl. Phys.*, 2012, **111**.
176. M. Kasha, *Discuss. Faraday Soc.*, 1950, **9**, 14-19.
177. D. G. Farnum, G. Mehta, G. G. I. Moore and F. P. Siegal, *Tetrahedron Lett.*, 1974, 2549-2552.
178. Z. M. Hao and A. Iqbal, *Chem. Soc. Rev.*, 1997, **26**, 203-213.
179. B. Tieke, A. R. Rabindranath, K. Zhang and Y. Zhu, *Beilstein J. Org. Chem.*, 2010, **6**, 830-845.
180. C. B. Nielsen, M. Turbiez and I. McCulloch, *Adv. Mater.*, 2013, **25**, 1859-1880.
181. D. Chandran and K.-S. Lee, *Macromol. Res.*, 2013, **21**, 272-283.
182. Z. Qiao, Y. Xu, S. Lin, J. Peng and D. Cao, *Synth. Met.*, 2010, **160**, 1544-1550.
183. K. Zhang, B. Tieke, F. Vilela and P. J. Skabara, *Macromol. Rapid Commun.*, 2011, **32**, 825-830.
184. C. H. Woo, P. M. Beaujuge, T. W. Holcombe, O. P. Lee and J. M. J. Frechet, *J. Am. Chem. Soc.*, 2010, **132**, 15547-15549.
185. H. Bronstein, Z. Chen, R. S. Ashraf, W. Zhang, J. Du, J. R. Durrant, P. S. Tuladhar, K. Song, S. E. Watkins, Y. Geerts, M. M. Wienk, R. A. J. Janssen, T. Anthopoulos, H. Sirringhaus, M. Heeney and I. McCulloch, *J. Am. Chem. Soc.*, 2011, **133**, 3272-3275.
186. L. Dou, W.-H. Chang, J. Gao, C.-C. Chen, J. You and Y. Yang, *Adv. Mater.*, 2013, **25**, 825-831.
187. B. Carsten, J. M. Szarko, L. Lu, H. J. Son, F. He, Y. Y. Botros, L. X. Chen and L. Yu, *Macromolecules*, 2012, **45**, 6390-6395.
188. W. K. Chan, Y. M. Chen, Z. H. Peng and L. P. Yu, *J. Am. Chem. Soc.*, 1993, **115**, 11735-11743.
189. Y. Zhu, A. R. Rabindranath, T. Beyerlein and B. Tieke, *Macromolecules*, 2007, **40**, 6981-6989.
190. Y. Zhu, I. Heim and B. Tieke, *Macromol. Chem. Phys.*, 2006, **207**, 2206-2214.
191. K. Zhang and B. Tieke, *Macromolecules*, 2008, **41**, 7287-7295.
192. D. R. Cao, Q. L. Liu, W. J. Zeng, S. H. Han, J. B. Peng and S. P. Liu, *J. Polym. Sci. A Polym. Chem*, 2006, **44**, 2395-2405.
193. A. B. Tamayo, M. Tantiwiwat, B. Walker and T.-Q. Nguyen, *J. Phys. Chem. C*, 2008, **112**, 15543-15552.
194. M. Tantiwiwat, A. Tamayo, N. Luu, X.-D. Dang and T.-Q. Nguyen, *J. Phys. Chem. C*, 2008, **112**, 17402-17407.
195. A. B. Tamayo, B. Walker and T.-Q. Nguyen, *J. Phys. Chem. C*, 2008, **112**, 11545-11551.
196. A. B. Tamayo, X.-D. Dang, B. Walker, J. Seo, T. Kent and T.-Q. Nguyen, *Appl. Phys. Lett.*, 2009, **94**, 103301.
197. B. Walker, A. B. Tomayo, X.-D. Dang, P. Zalar, J. H. Seo, A. Garcia, M. Tantiwiwat and T.-Q. Nguyen, *Adv. Funct. Mater.*, 2009, **19**, 3063-3069.
198. S. Izawa, K. Hashimoto and K. Tajima, *Synth. Met.*, 2012, **162**, 2201-2205.
199. J. Huang, C. Zhan, X. Zhang, Y. Zhao, Z. Lu, H. Jia, B. Jiang, J. Ye, S. Zhang, A. Tang, Y. Liu, Q. Pei and J. Yao, *ACS Appl. Mater. Interfaces*, 2013, **5**, 2033-2039.
200. A. Tang, L. Li, Z. Lu, J. Huang, H. Jia, C. Zhan, Z. a. Tan, Y. Li and J. Yao, *J. Mater. Chem. A*, 2013, **1**, 5747-5757.
201. Z. Zhao, J. W. Y. Lam and B. Z. Tang, *J. Mater. Chem.*, 2012, **22**, 23726-23740.
202. J. D. Luo, Z. L. Xie, J. W. Y. Lam, L. Cheng, H. Y. Chen, C. F. Qiu, H. S. Kwok, X. W. Zhan, Y. Q. Liu, D. B. Zhu and B. Z. Tang, *Chem. Commun.*, 2001, 1740-1741.
203. Y. Hong, J. W. Y. Lam and B. Z. Tang, *Chem. Commun.*, 2009, 4332-4353.
204. Y. Hong, J. W. Y. Lam and B. Z. Tang, *Chem. Soc. Rev.*, 2011, **40**, 5361-5388.

205. J. W. Chen, C. C. W. Law, J. W. Y. Lam, Y. P. Dong, S. M. F. Lo, I. D. Williams, D. B. Zhu and B. Z. Tang, *Chem. Mater.*, 2003, **15**, 1535-1546.
206. X. Fan, J. Sun, F. Wang, Z. Chu, P. Wang, Y. Dong, R. Hu, B. Z. Tang and D. Zou, *Chem. Commun.*, 2008, 2989-2991.
207. Y. Ren, J. W. Y. Lam, Y. Q. Dong, B. Z. Tang and K. S. Wong, *J. Phys. Chem. B*, 2005, **109**, 1135-1140.
208. Z. Li, Y. Dong, B. X. Mi, Y. H. Tang, M. Haussler, H. Tong, Y. P. Dong, J. W. Y. Lam, Y. Ren, H. H. Y. Sung, K. S. Wong, P. Gao, I. D. Williams, H. S. Kwok and B. Z. Tang, *J. Phys. Chem. B*, 2005, **109**, 10061-10066.
209. A. Qin, J. W. Y. Lam and B. Z. Tang, *Prog. Polym. Sci.*, 2012, **37**, 182-209.
210. R. Hu, J. W. Y. Lam, J. Liu, H. H. Y. Sung, I. D. Williams, Z. Yue, K. S. Wong, M. M. F. Yuen and B. Z. Tang, *Polym. Chem.*, 2012, **3**, 1481-1489.
211. Y. Xu, L. Chen, Z. Guo, A. Nagai and D. Jiang, *J. Am. Chem. Soc.*, 2011, **133**, 17622-17625.
212. Y. Liu, X. Chen, Y. Lv, S. Chen, J. W. Y. Lam, F. Mahtab, H. S. Kwok, X. Tao and B. Z. Tang, *Chem. Eur. J.*, 2012, **18**, 9929-9938.
213. C. Y. K. Chan, Z. Zhao, J. W. Y. Lam, J. Liu, S. Chen, P. Lu, F. Mahtab, X. Chen, H. H. Y. Sung, H. S. Kwok, Y. Ma, I. D. Williams, K. S. Wong and B. Z. Tang, *Adv. Funct. Mater.*, 2012, **22**, 378-389.
214. Z. Zhao, S. Chen, J. W. Y. Lam, P. Lu, Y. Zhong, K. S. Wong, H. S. Kwok and B. Z. Tang, *Chem. Commun.*, 2010, **46**, 2221-2223.
215. W. Z. Yuan, P. Lu, S. Chen, J. W. Y. Lam, Z. Wang, Y. Liu, H. S. Kwok, Y. Ma and B. Z. Tang, *Adv. Mater.*, 2010, **22**, 2159-+.
216. H. Li, Z. Chi, X. Zhang, B. Xu, S. Liu, Y. Zhang and J. Xu, *Chem. Commun.*, 2011, **47**, 11273-11275.
217. J. Zhou, Z. Chang, Y. Jiang, B. He, M. Du, P. Lu, Y. Hong, H. S. Kwok, A. Qin, H. Qiu, Z. Zhao and B. Z. Tang, *Chem. Commun.*, 2013, **49**, 2491-2493.
218. Z. Chang, Y. Jiang, B. He, J. Chen, Z. Yang, P. Lu, H. S. Kwok, Z. Zhao, H. Qiu and B. Z. Tang, *Chem. Commun.*, 2013, **49**, 594-596.
219. V. S. Vyas, M. Banerjee and R. Rathore, *Tetrahedron Lett.*, 2009, **50**, 6159-6162.
220. V. S. Vyas and R. Rathore, *Chem. Commun.*, 2010, **46**, 1065-1067.
221. X. Luo, J. Li, C. Li, L. Heng, Y. Q. Dong, Z. Liu, Z. Bo and B. Z. Tang, *Adv. Mater.*, 2011, **23**, 3261-3265.
222. H. Li, Z. Chi, B. Xu, X. Zhang, X. Li, S. Liu, Y. Zhang and J. Xu, *J. Mater. Chem.*, 2011, **21**, 3760-3767.
223. S.-J. Yoon, J. W. Chung, J. Gierschner, K. S. Kim, M.-G. Choi, D. Kim and S. Y. Park, *J. Am. Chem. Soc.*, 2010, **132**, 13675-13683.
224. L. Bu, M. Sun, D. Zhang, W. Liu, Y. Wang, M. Zheng, S. Xue and W. Yang, *J. Mater. Chem. C*, 2013, **1**, 2028-2035.
225. J. Shi, N. Chang, C. Li, J. Mei, C. Deng, X. Luo, Z. Liu, Z. Bo, Y. Q. Dong and B. Z. Tang, *Chem. Commun.*, 2012, **48**, 10675-10677.
226. A. M. Brouwer, *Pure Appl. Chem.*, 2011, **83**, 2213-2228.
227. G. Ulrich, R. Ziessel and A. Harriman, *Angew. Chem. Int. Ed.*, 2008, **47**, 1184-1201.
228. A. Loudet and K. Burgess, *Chem. Rev.*, 2007, **107**, 4891-4932.
229. A. Treibs and F.-H. Kreuzer, *Liebigs Ann. Chem.*, 1968, **718**, 208-223.
230. N. Boens, V. Leen and W. Dehaen, *Chem. Soc. Rev.*, 2012, **41**, 1130-1172.
231. http://www.invitrogen.com/site/us/en/home/References/Molecular-Probes-The-Handbook/Fluorophores-and-Their-Amine-Reactive-Derivatives/BODIPY-Dye-Series.html, Accessed 16th June, 2013.

232. M. J. Ortiz, I. Garcia-Moreno, A. R. Agarrabeitia, G. Duran-Sampedro, A. Costela, R. Sastre, F. Lopez Arbeloa, J. Banuelos Prieto and I. Lopez Arbeloa, *PCCP*, 2010, **12**, 7804-7811.
233. J. Banuelos, I. J. Arroyo-Cordoba, I. Valois-Escamilla, A. Alvarez-Hernandez, E. Pena-Cabrera, R. Hu, B. Z. Tang, I. Esnal, V. Martinez and I. Lopez Arbeloa, *R. Soc. Chem. Adv.*, 2011, **1**, 677-684.
234. J. Chen, A. Burghart, A. Derecskei-Kovacs and K. Burgess, *J. Org. Chem.*, 2000, **65**, 2900-2906.
235. J. Banuelos, V. Martin, C. F. Azael Gomez-Duran, I. J. Arroyo Cordoba, E. Pena-Cabrera, I. Garcia-Moreno, A. Costela, M. Eugenio Perez-Ojeda, T. Arbeloa and I. Lopez Arbeloa, *Chem. Eur. J.*, 2011, **17**, 7261-7270.
236. I. Garcia-Moreno, F. Amat-Guerri, M. Liras, A. Costela, L. Infantes, R. Sastre, F. L. Arbeloa, J. B. Prieto and I. L. Arbeloa, *Adv. Funct. Mater.*, 2007, **17**, 3088-3098.
237. A. C. Benniston and G. Copley, *PCCP*, 2009, **11**, 4124-4131.
238. S. G. Awuah and Y. You, *R. Soc. Chem. Adv.*, 2012, **2**, 11169-11183.
239. A. Kamkaew, S. H. Lim, H. B. Lee, L. V. Kiew, L. Y. Chung and K. Burgess, *Chem. Soc. Rev.*, 2013, **42**, 77-88.
240. S. Kolemen, O. A. Bozdemir, Y. Cakmak, G. Barin, S. Erten-Ela, M. Marszalek, J.-H. Yum, S. M. Zakeeruddin, M. K. Nazeeruddin, M. Graetzel and E. U. Akkaya, *Chem. Sci.*, 2011, **2**, 949-954.
241. T. Rousseau, A. Cravino, E. Ripaud, P. Leriche, S. Rihn, A. De Nicola, R. Ziessel and J. Roncali, *Chem. Commun.*, 2010, **46**, 5082-5084.
242. L. Bonardi, H. Kanaan, F. Camerel, P. Jolinat, P. Retailleau and R. Ziessel, *Adv. Funct. Mater.*, 2008, **18**, 401-413.
243. M. A. H. Alamiry, A. C. Benniston, G. Copley, K. J. Elliott, A. Harriman, B. Stewart and Y.-G. Zhi, *Chem. Mater.*, 2008, **20**, 4024-4032.
244. A. B. Nepomnyashchii and A. J. Bard, *Acc. Chem. Res.*, 2012, **45**, 1844-1853.
245. B. C. Popere, A. M. Della Pelle and S. Thayumanavan, *Macromolecules*, 2011, **44**, 4767-4776.
246. V. R. Donuru, G. K. Vegesna, S. Velayudham, S. Green and H. Liu, *Chem. Mater.*, 2009, **21**, 2130-2138.
247. C. Thivierge, A. Loudet and K. Burgess, *Macromolecules*, 2011, **44**, 4012-4015.
248. D. Collado, J. Casado, S. R. Gonzalez, J. T. L. Navarrete, R. Suau, E. Perez-Inestrosa, T. M. Pappenfus and M. M. M. Raposo, *Chem. Eur. J.*, 2011, **17**, 498-507.
249. A. Poirel, A. De Nicola and R. Ziessel, *Org. Lett.*, 2012, **14**, 5696-5699.
250. Y. Hayashi, S. Yamaguchi, W. Y. Cha, D. Kim and H. Shinokubo, *Org. Lett.*, 2011, **13**, 2992-2995.
251. Y. Cakmak and E. U. Akkaya, *Org. Lett.*, 2009, **11**, 85-88.
252. N. Sakamoto, C. Ikeda, M. Yamamura and T. Nabeshima, *Chem. Commun.*, 2012, **48**, 4818-4820.
253. S. Diring and R. Ziessel, *Tetrahedron Lett.*, 2009, **50**, 1203-1208.
254. H. Sugimoto, M. Muto, T. Tanaka and A. Osuka, *Eur. J. Org. Chem.*, 2011, 71-77.
255. A. S. Guram, X. Wang, E. E. Bunel, M. M. Faul, R. D. Larsen and M. J. Martinelli, *J. Org. Chem.*, 2007, **72**, 5104-5112.
256. T. Rohand, W. Qin, N. Boens and W. Dehaen, *Eur. J. Org. Chem.*, 2006, 4658-4663.
257. V. Leen, E. Braeken, K. Luckermans, C. Jackers, M. Van der Auweraer, N. Boens and W. Dehaen, *Chem. Commun.*, 2009, 4515-4517.
258. B. Verbelen, V. Leen, L. Wang, N. Boens and W. Dehaen, *Chem. Commun.*, 2012, **48**, 9129-9131.
259. C. Y. Chi and G. Wegner, *Macromol. Rapid Commun.*, 2005, **26**, 1532-1537.

260. A. B. Nepomnyashchii, M. Broering, J. Ahrens and A. J. Bard, *J. Am. Chem. Soc.*, 2011, **133**, 8633-8645.
261. C. W. Wan, A. Burghart, J. Chen, F. Bergstrom, L. B. A. Johansson, M. F. Wolford, T. G. Kim, M. R. Topp, R. M. Hochstrasser and K. Burgess, *Chem. Eur. J.*, 2003, **9**, 4430-4441.
262. G. W. T. M. J. Frisch, H. B. Schlegel, G. E. Scuseria, M. A. Robb, J. R. Cheeseman, G. Scalmani, V. Barone, B. Mennucci, G. A. Petersson, H. Nakatsuji, M. Caricato, X. Li, H. P. Hratchian, A. F. Izmaylov, J. Bloino, G. Zheng, J. L. Sonnenberg, M. Hada, M. Ehara, K. Toyota, R. Fukuda, J. Hasegawa, M. Ishida, T. Nakajima, Y. Honda, O. Kitao, H. Nakai, T. Vreven, J. A. Montgomery, Jr., J. E. Peralta, F. Ogliaro, M. Bearpark, J. J. Heyd, E. Brothers, K. N. Kudin, V. N. Staroverov, R. Kobayashi, J. Normand, K. Raghavachari, A. Rendell, J. C. Burant, S. S. Iyengar, J. Tomasi, M. Cossi, N. Rega, J. M. Millam, M. Klene, J. E. Knox, J. B. Cross, V. Bakken, C. Adamo, J. Jaramillo, R. Gomperts, R. E. Stratmann, O. Yazyev, A. J. Austin, R. Cammi, C. Pomelli, J. W. Ochterski, R. L. Martin, K. Morokuma, V. G. Zakrzewski, G. A. Voth, P. Salvador, J. J. Dannenberg, S. Dapprich, A. D. Daniels, Ö. Farkas, J. B. Foresman, J. V. Ortiz, J. Cioslowski, D. J. Fox, Gaussian, Inc., Wallingford CT, Editon edn., 2009.
263. P. T. A. Galek, N. C. Handy, A. J. Cohen and G. K. L. Chan, *Chem. Phys. Lett.*, 2005, **404**, 156-163.
264. A. Schafer, C. Huber and R. Ahlrichs, *J. Chem. Phys.*, 1994, **100**, 5829-5835.
265. A. V. Marenich, C. J. Cramer and D. G. Truhlar, *J. Phys. Chem. B*, 2009, **113**, 6378-6396.
266. M. Ranger, D. Rondeau and M. Leclerc, *Macromolecules*, 1997, **30**, 7686-7691.
267. G. Hughes, C. S. Wang, A. S. Batsanov, M. Fern, S. Frank, M. R. Bryce, I. F. Perepichka, A. P. Monkman and B. P. Lyons, *Org. Biomol. Chem.*, 2003, **1**, 3069-3077.
268. N. Lin, X. Y. Liu, Y. Y. Diao, H. Xu, C. Chen, X. Ouyang, H. Yang and W. Ji, *Adv. Funct. Mater.*, 2012, **22**, 361-368.
269. G. Saikia and P. K. Iyer, *J. Org. Chem.*, 2010, **75**, 2714-2717.
270. Z. H. Li, M. S. Wong, H. Fukutani and Y. Tao, *Org. Lett.*, 2006, **8**, 4271-4274.
271. X. F. Yu, S. Lu, C. Ye, T. C. Li, T. X. Liu, S. Y. Liu, Q. L. Fan, E. Q. Chen and W. Huang, *Macromolecules*, 2006, **39**, 1364-1375.
272. Q. Wang, Y. Qu, H. Tian, Y. Geng and F. Wang, *Macromolecules*, 2011, **44**, 1256-1260.
273. J. M. Holub, K. O'Toole-Colin, A. Getzel, A. Argenti, M. A. Evans, D. C. Smith, G. A. Dalglish, S. Rifat, D. L. Wilson, B. M. Taylor, U. Miott, J. Glersaye, K. S. Lam, B. J. McCranor, J. D. Berkowitz, R. B. Miller, J. R. Lukens, K. Krumpe, J. T. Gupton and B. S. Burnham, *Molecules*, 2004, **9**, 135-157.
274. K. Zhang, B. Tieke, J. C. Forgie, F. Vilela, J. A. Parkinson and P. J. Skabara, *Polymer*, 2010, **51**, 6107-6114.
275. K. Zhang, B. Tieke, J. C. Forgie and P. J. Skabara, *Macromol. Rapid Commun.*, 2009, **30**, 1834-1840.
276. S.-Y. Liu, M.-M. Shi, J.-C. Huang, Z.-N. Jin, X.-L. Hu, J.-Y. Pan, H.-Y. Li, A. K. Y. Jen and H.-Z. Chen, *J. Mater. Chem. A*, 2013, **1**, 2795-2805.
277. X. Zhang, Y. Xiao and X. Qian, *Org. Lett.*, 2008, **10**, 29-32.

9 Appendix - NMRs of final compounds

T1 B

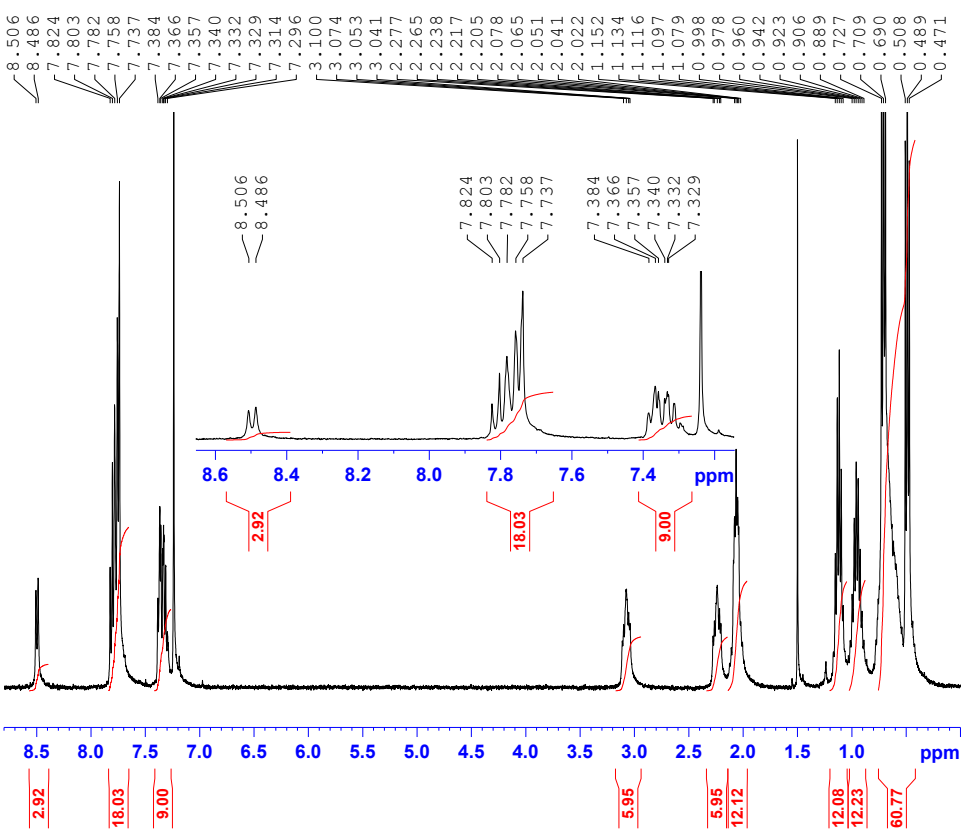


```
NAME          D143746 CO41 I H, C
EXPNO                    1
PROCNO                   1
Date_             20110328
Time                 15.56
INSTRUM              spect
PROBHD    5 mm QNP 1H/13
PULPROG               zg30
TD                   32564
SOLVENT              CDCl3
NS                      16
DS                       2
SWH               8223.685 Hz
FIDRES            0.252539 Hz
AQ                1.9799412 sec
RG                     406
DW                  60.800 usec
DE                   6.50 usec
TE                  300.0 K
D1                2.00000000 sec
TD0                      1

======== CHANNEL f1 ========
NUC1                    1H
P1                   9.40 usec
PL1                 -4.00 dB
PL1W           19.93825150 W
SFO1          400.1324710 MHz
SI                   32768
SF            400.1300185 MHz
WDW                     EM
SSB                      0
LB                    0.30 Hz
GB                       0
PC                    1.00
```

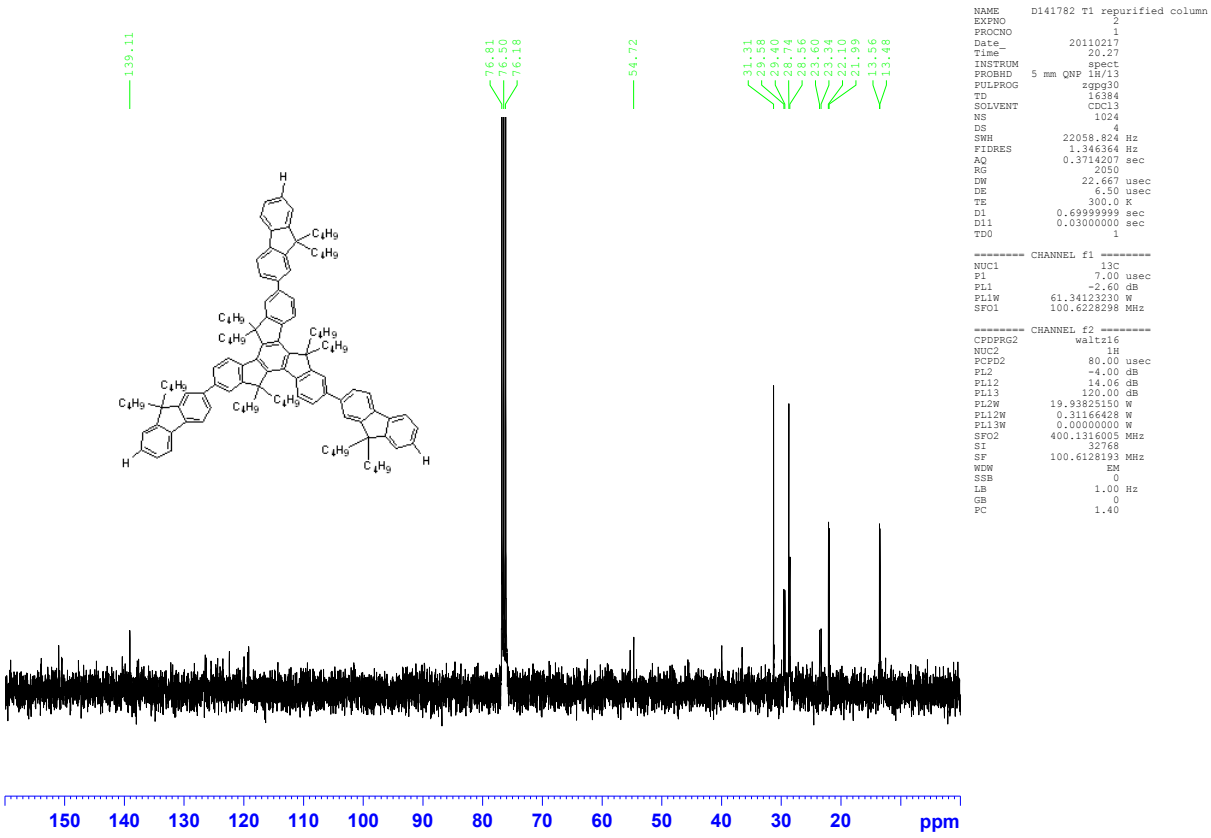


```
NAME        D141782 T1 repurified column
EXPNO                2
PROCNO               1
Date_         20110217
Time_            20.27
INSTRUM          spect
PROBHD   5 mm QNP 1H/13
PULPROG         zgpg30
TD               16384
SOLVENT          CDCl3
NS                1024
DS                   4
SWH          22058.824 Hz
FIDRES        1.346364 Hz
AQ            0.3714207 sec
RG                2050
DW              22.667 usec
DE               6.50 usec
TE              300.0 K
D1           0.69999999 sec
D11          0.03000000 sec
TD0                  1

======== CHANNEL f1 ========
NUC1               13C
P1                7.00 usec
PL1              -2.60 dB
PL1W       61.34123230 W
SFO1      100.6228298 MHz

======== CHANNEL f2 ========
CPDPRG2         waltz16
NUC2               1H
PCPD2            80.00 usec
PL2              -4.00 dB
PL12             14.06 dB
PL13            120.00 dB
PL2W       19.93825150 W
PL12W       0.31166428 W
PL13W       0.00000000 W
SFO2      400.1316005 MHz
SI               32768
SF        100.6128193 MHz
WDW                EM
SSB                 0
LB               1.00 Hz
GB                  0
PC               1.40
```

T2 B

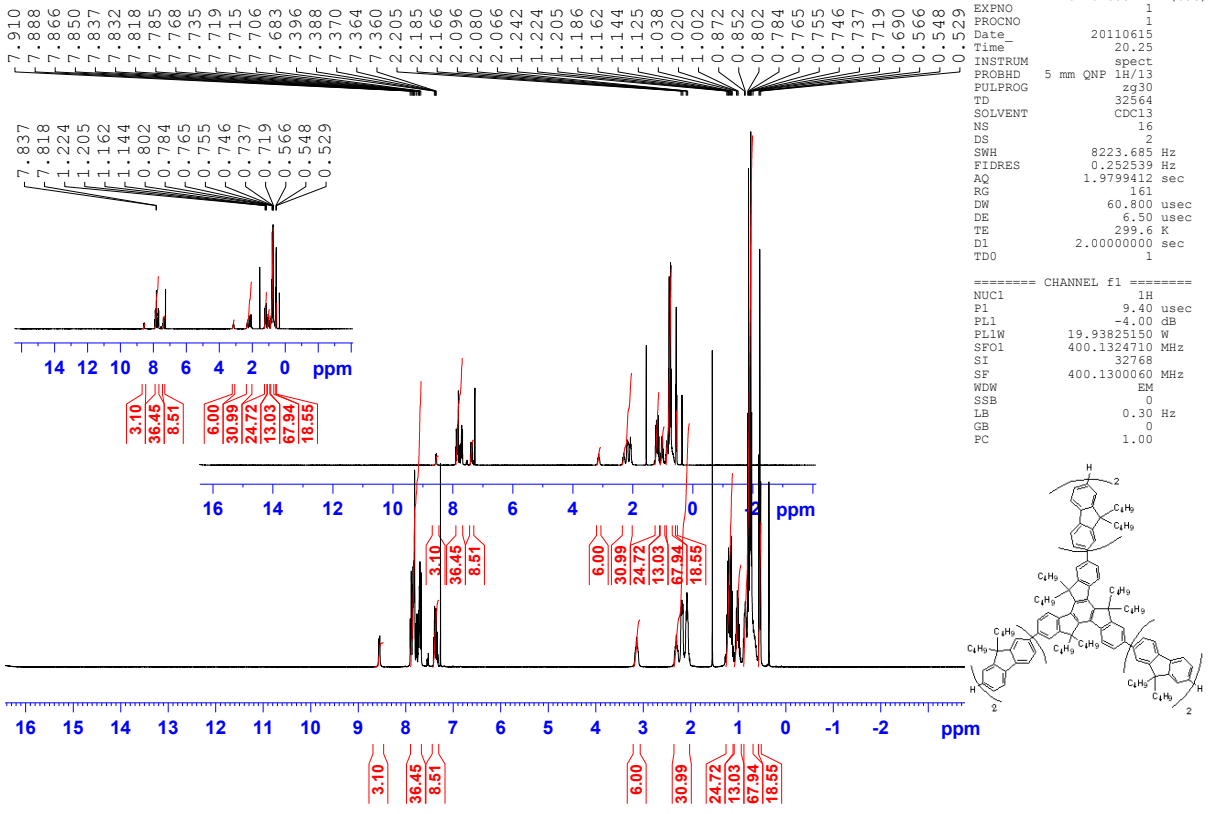


```
NAME        D146228 CO51I T2(but)
EXPNO                1
PROCNO               1
Date_         20110615
Time_            20.25
INSTRUM          spect
PROBHD   5 mm QNP 1H/13
PULPROG          zg30
TD               32564
SOLVENT          CDCl3
NS                  16
DS                   2
SWH           8223.685 Hz
FIDRES        0.252539 Hz
AQ            1.9799412 sec
RG                 161
DW              60.800 usec
DE               6.50 usec
TE              299.6 K
D1           2.00000000 sec
TD0                  1

======== CHANNEL f1 ========
NUC1                1H
P1                9.40 usec
PL1              -4.00 dB
PL1W       19.93825150 W
SFO1      400.1324710 MHz
SI               32768
SF        400.1300060 MHz
WDW                EM
SSB                 0
LB               0.30 Hz
GB                  0
PC               1.00
```

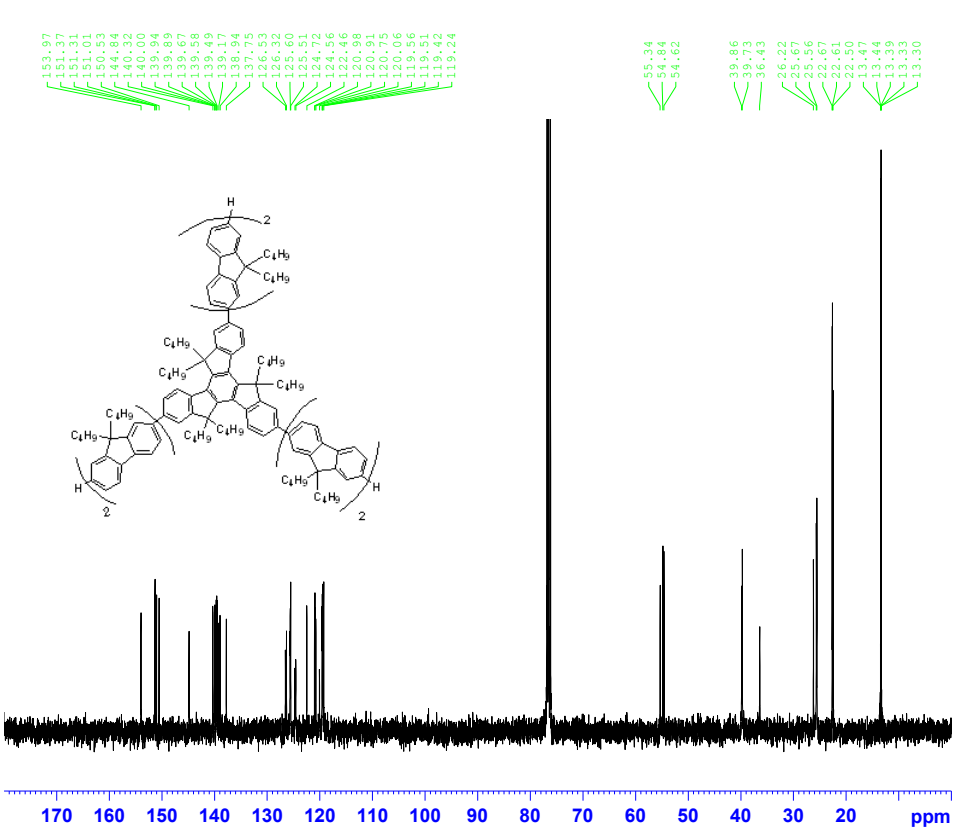


```
NAME        D146228 CO51I T2(but)
EXPNO                          2
PROCNO                         1
Date_                   20110615
Time_                      21.42
INSTRUM                    spect
PROBHD     5 mm QNP 1H/13
PULPROG                 zgpg30
TD                         16384
SOLVENT                  CDCl3
NS                          4056
DS                             4
SWH                  22058.824 Hz
FIDRES                1.346364 Hz
AQ                    0.3714207 sec
RG                          2050
DW                        22.667 usec
DE                          6.50 usec
TE                         299.6 K
D1                    0.69999999 sec
D11                   0.03000000 sec
TD0                            1

======== CHANNEL f1 ========
NUC1                         13C
P1                          7.00 usec
PL1                        -2.60 dB
PL1W                 61.34123230 W
SFO1                100.6228298 MHz

======== CHANNEL f2 ========
CPDPRG2                 waltz16
NUC2                         1H
PCPD2                      80.00 usec
PL2                        -4.00 dB
PL12                       14.06 dB
PL13                      120.00 dB
PL2W                19.93825150 W
PL12W                0.31166428 W
PL13W                0.00000000 W
SFO2                400.1316005 MHz
SI                          32768
SF                  100.6128193 MHz
WDW                            EM
SSB                            0
LB                          1.00 Hz
GB                             0
PC                          1.40
```

T3 B

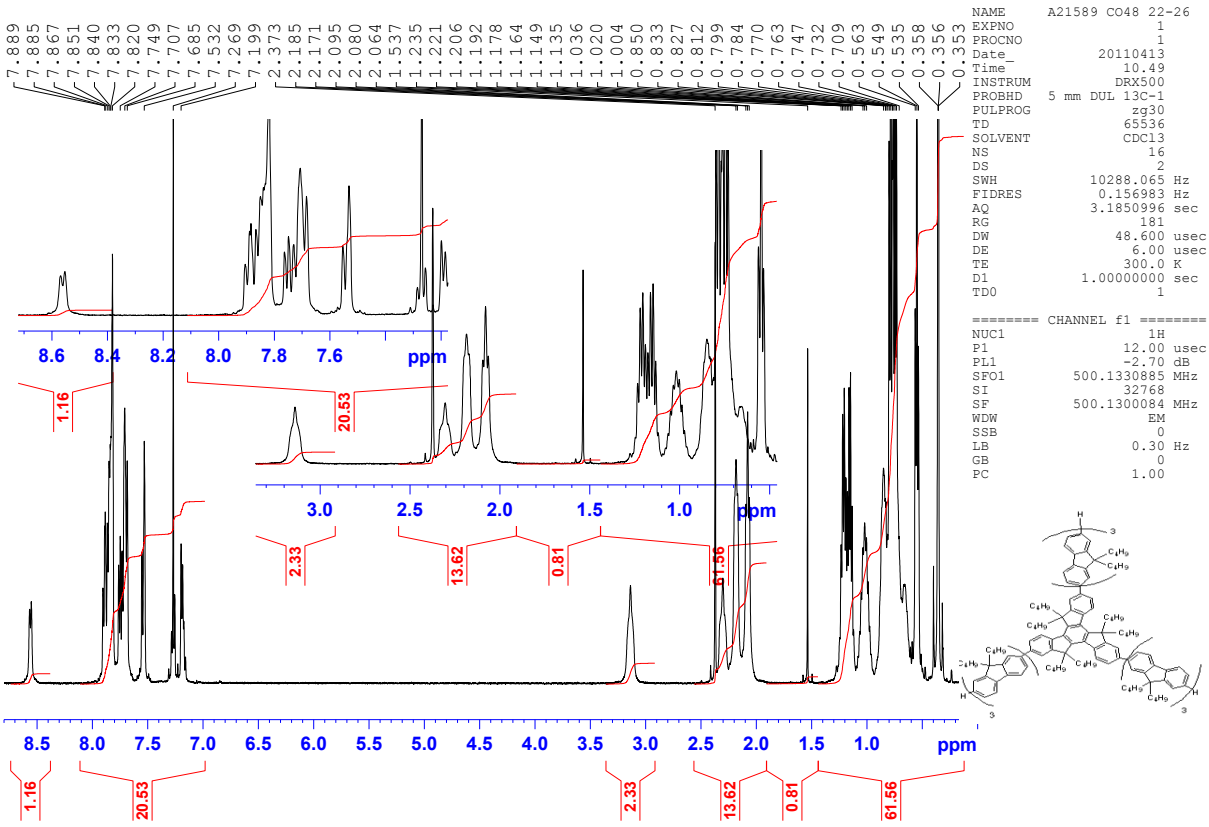


```
NAME        A21589 CO48 22-26
EXPNO                          1
PROCNO                         1
Date_                   20110413
Time_                      10.49
INSTRUM                   DRX500
PROBHD     5 mm DUL 13C-1
PULPROG                    zg30
TD                         65536
SOLVENT                  CDCl3
NS                            16
DS                             2
SWH                  10288.065 Hz
FIDRES                0.156983 Hz
AQ                    3.1850996 sec
RG                           181
DW                        48.600 usec
DE                          6.00 usec
TE                         300.0 K
D1                    1.00000000 sec
TD0                            1

======== CHANNEL f1 ========
NUC1                          1H
P1                         12.00 usec
PL1                        -2.70 dB
SFO1                500.1330885 MHz
SI                          32768
SF                  500.1300084 MHz
WDW                            EM
SSB                            0
LB                          0.30 Hz
GB                             0
PC                          1.00
```

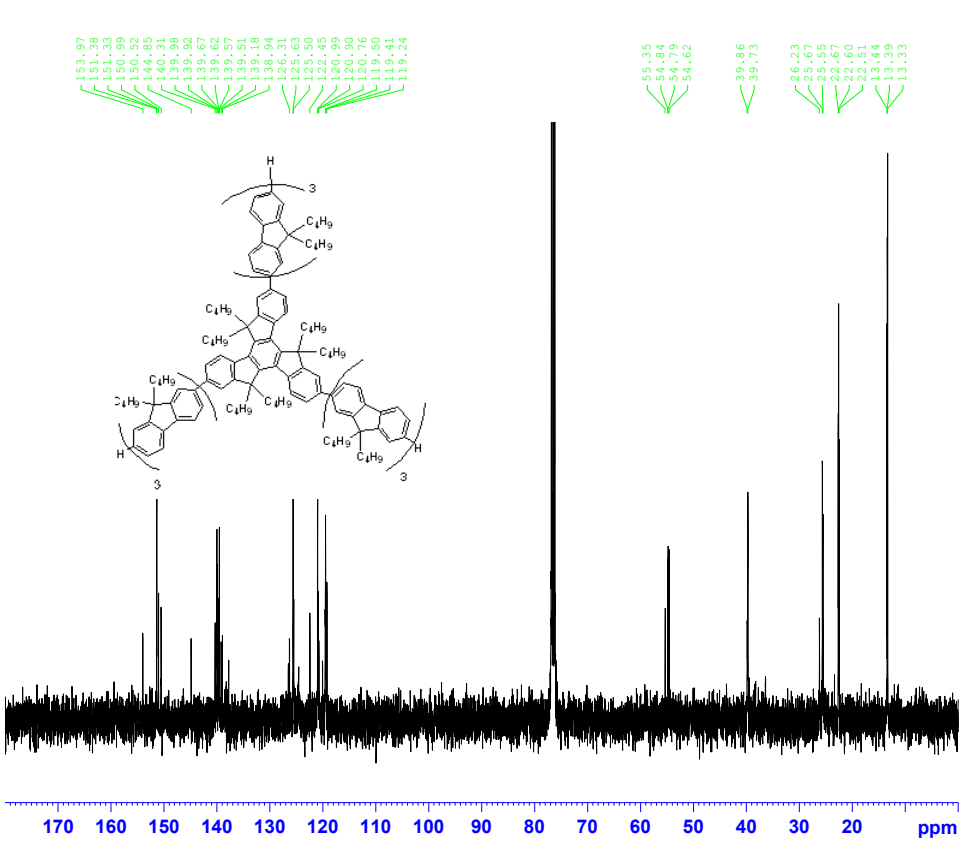


```
NAME        D146229 CO58 T3(but)
EXPNO                          2
PROCNO                         1
Date_                   20110615
Time                       23.04
INSTRUM                    spect
PROBHD     5 mm QNP 1H/13
PULPROG                  zgpg30
TD                        16384
SOLVENT                   CDCl3
NS                         4056
DS                            4
SWH                   22058.824 Hz
FIDRES                 1.346364 Hz
AQ                     0.3714207 sec
RG                         2050
DW                       22.667 usec
DE                         6.50 usec
TE                        299.2 K
D1                    0.69999999 sec
D11                   0.03000000 sec
TD0                            1

======== CHANNEL f1 ========
NUC1                         13C
P1                          7.00 usec
PL1                        -2.60 dB
PL1W                61.34123230 W
SFO1                100.6228298 MHz

======== CHANNEL f2 ========
CPDPRG2                 waltz16
NUC2                         1H
PCPD2                      80.00 usec
PL2                        -4.00 dB
PL12                       14.06 dB
PL13                      120.00 dB
PL2W                19.93825150 W
PL12W                0.31166428 W
PL13W                0.00000000 W
SFO2                400.1316005 MHz
SI                         32768
SF                  100.6128193 MHz
WDW                           EM
SSB                            0
LB                          1.00 Hz
GB                             0
PC                          1.40
```

T1 O

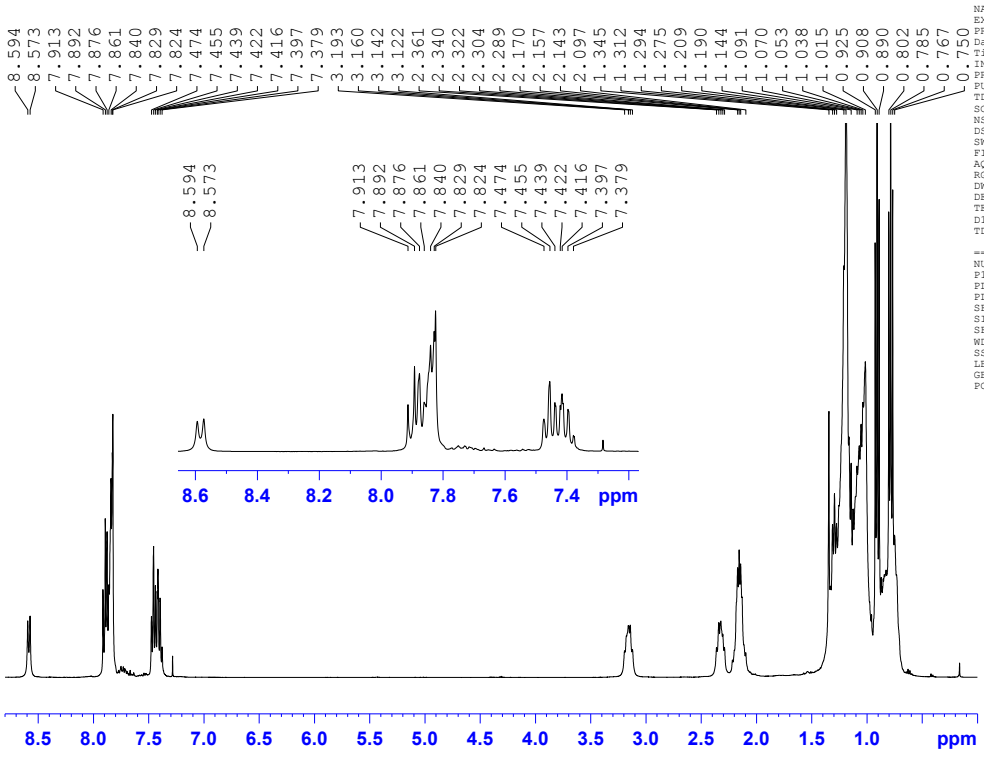


```
NAME        D139546 T1 filtrate acetone
EXPNO                          1
PROCNO                         1
Date_                   20101216
Time                       15.25
INSTRUM                    spect
PROBHD     5 mm QNP 1H/13
PULPROG                    zg30
TD                        32564
SOLVENT                   CDCl3
NS                           16
DS                            2
SWH                    8223.685 Hz
FIDRES                 0.252539 Hz
AQ                     1.9799412 sec
RG                          14.2
DW                        60.800 usec
DE                         6.50 usec
TE                        300.0 K
D1                    2.00000000 sec
TD0                            1

======== CHANNEL f1 ========
NUC1                         1H
P1                          9.40 usec
PL1                        -4.00 dB
PL1W                19.93825150 W
SFO1                400.1324710 MHz
SI                         32768
SF                  400.1300000 MHz
WDW                           EM
SSB                            0
LB                          0.30 Hz
GB                             0
PC                          1.00
```

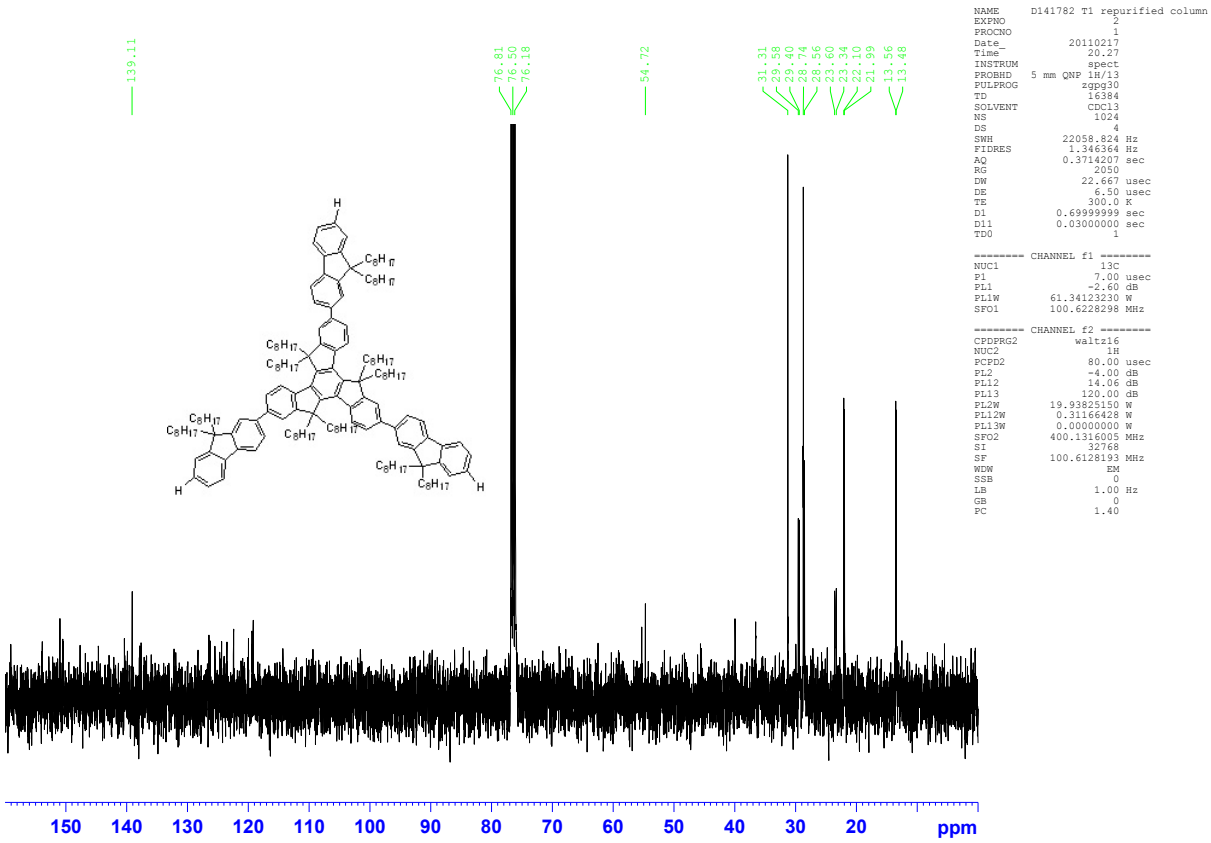


```
NAME          D141782 T1 repurified column
EXPNO                                    2
PROCNO                                   1
Date_                             20110217
Time_                                20.27
INSTRUM                              spect
PROBHD       5 mm QNP 1H/13
PULPROG                           zgpg30
TD                                   16384
SOLVENT                           CDCl3
NS                                    1024
DS                                       4
SWH                           22058.824 Hz
FIDRES                         1.346364 Hz
AQ                            0.3714207 sec
RG                                    2050
DW                               22.667 usec
DE                                6.50 usec
TE                                300.0 K
D1                           0.69999999 sec
D11                          0.03000000 sec
TD0                                      1

======== CHANNEL f1 ========
NUC1                                  13C
P1                                 7.00 usec
PL1                               -2.60 dB
PL1W                       61.34123230 W
SFO1                      100.6228298 MHz

======== CHANNEL f2 ========
CPDPRG2                       waltz16
NUC2                                  1H
PCPD2                             80.00 usec
PL2                               -4.00 dB
PL12                              14.06 dB
PL13                             120.00 dB
PL2W                       19.93825150 W
PL12W                       0.31166428 W
PL13W                       0.00000000 W
SFO2                      400.1316005 MHz
SI                                   32768
SF                        100.6128193 MHz
WDW                                  EM
SSB                                   0
LB                                 1.00 Hz
GB                                    0
PC                                 1.40
```

T2 O

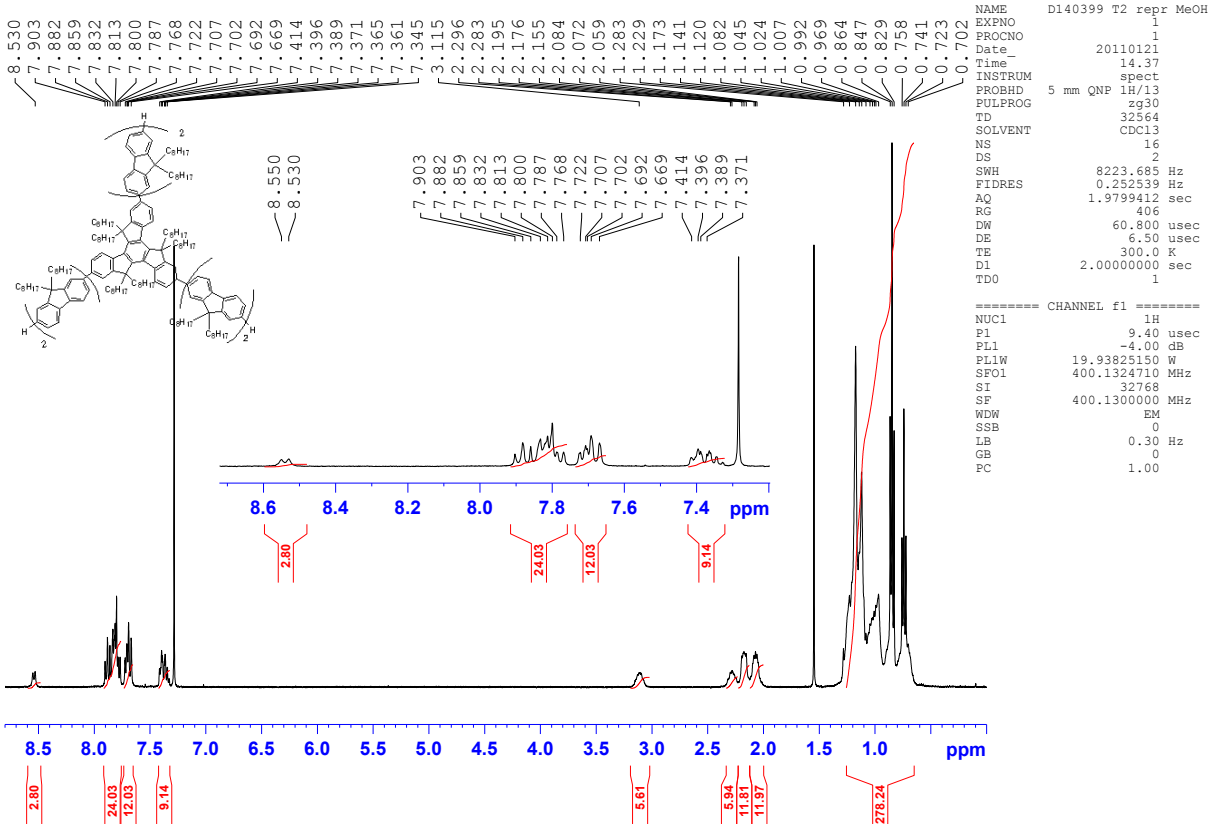


```
NAME          D140399 T2 repr MeOH
EXPNO                                    1
PROCNO                                   1
Date_                             20110121
Time                                14.37
INSTRUM                              spect
PROBHD       5 mm QNP 1H/13
PULPROG                             zg30
TD                                   32564
SOLVENT                           CDCl3
NS                                      16
DS                                       2
SWH                            8223.685 Hz
FIDRES                         0.252539 Hz
AQ                            1.9799412 sec
RG                                     406
DW                               60.800 usec
DE                                6.50 usec
TE                                300.0 K
D1                           2.00000000 sec
TD0                                      1

======== CHANNEL f1 ========
NUC1                                  1H
P1                                 9.40 usec
PL1                               -4.00 dB
PL1W                       19.93825150 W
SFO1                      400.1324710 MHz
SI                                   32768
SF                        400.1300000 MHz
WDW                                  EM
SSB                                   0
LB                                 0.30 Hz
GB                                    0
PC                                 1.00
```

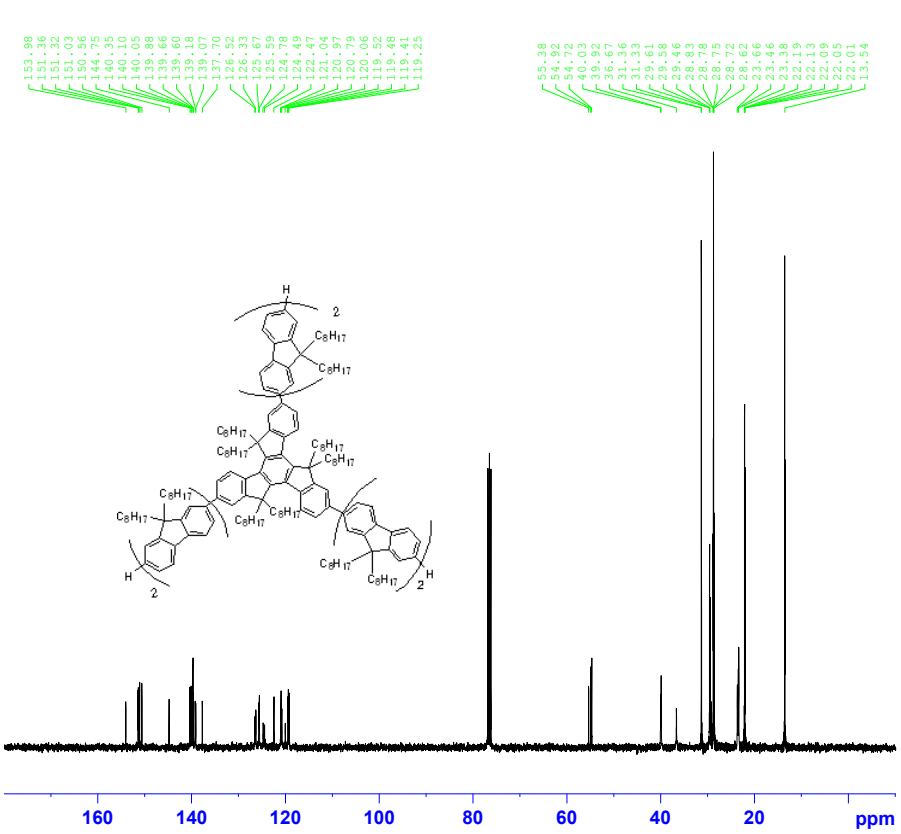

```
NAME          D137563 T2
EXPNO                2
PROCNO               1
Date_         20101026
Time              15.13
INSTRUM           spect
PROBHD   5 mm QNP 1H/13
PULPROG         zgpg30
TD               16384
SOLVENT          CDCl3
NS                1024
DS                   4
SWH          22058.824 Hz
FIDRES        1.346364 Hz
AQ            0.3714207 sec
RG                2050
DW              22.667 usec
DE               6.50 usec
TE              300.0 K
D1            0.69999999 sec
D11           0.03000000 sec
TD0                  1

======== CHANNEL f1 ========
NUC1               13C
P1                7.00 usec
PL1              -2.60 dB
PL1W       61.34123230 W
SFO1      100.6228298 MHz

======== CHANNEL f2 ========
CPDPRG2         waltz16
NUC2                1H
PCPD2            80.00 usec
PL2              -4.00 dB
PL12             14.06 dB
PL13            120.00 dB
PL2W       19.93825150 W
PL12W       0.31166428 W
PL13W       0.00000000 W
SFO2      400.1316005 MHz
SI               32768
SF        100.6128193 MHz
WDW                 EM
SSB                  0
LB                1.00 Hz
GB                   0
PC                1.40
```

T3 O

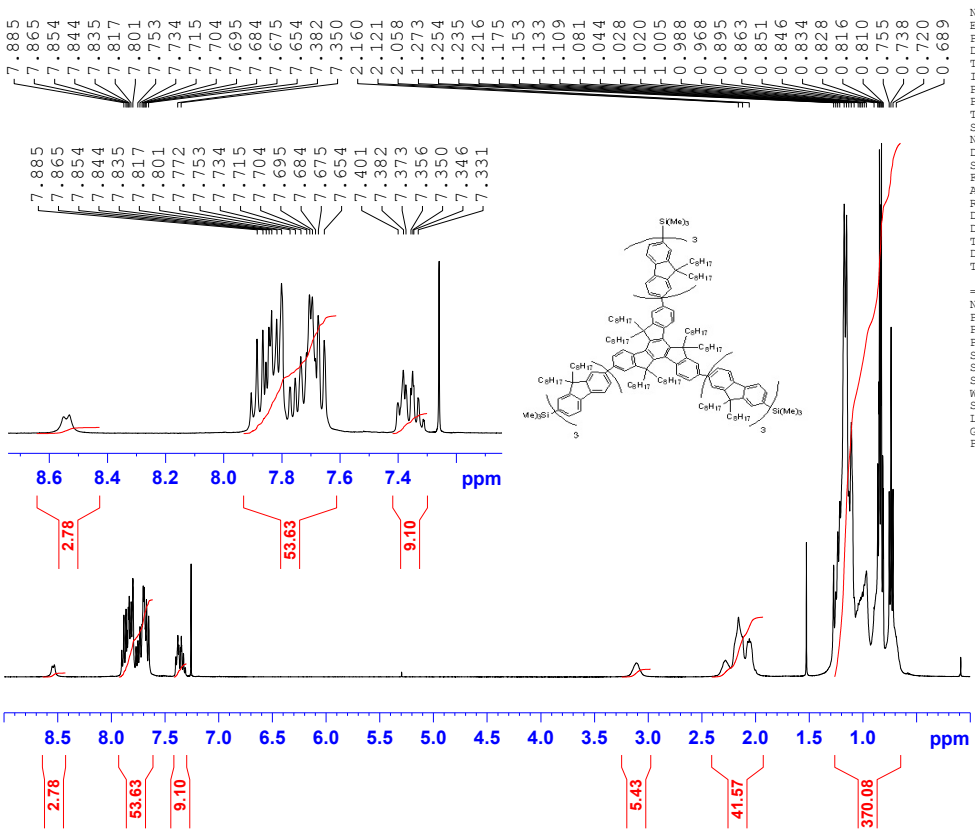

```
NAME      D131870 CO21 fracs 3-6
EXPNO                1
PROCNO               1
Date_         20100416
Time              11.03
INSTRUM           spect
PROBHD   5 mm QNP 1H/13
PULPROG           zg30
TD               32564
SOLVENT          CDCl3
NS                  16
DS                   2
SWH          8223.685 Hz
FIDRES       0.252539 Hz
AQ           1.9799412 sec
RG                  57
DW              60.800 usec
DE               6.50 usec
TE              300.0 K
D1           2.00000000 sec
TD0                  1

======== CHANNEL f1 ========
NUC1                1H
P1                9.40 usec
PL1              -4.00 dB
PL1W       19.93825150 W
SFO1      400.1324710 MHz
SI               32768
SF        400.1300097 MHz
WDW                 EM
SSB                  0
LB                0.30 Hz
GB                   0
PC                1.00
```

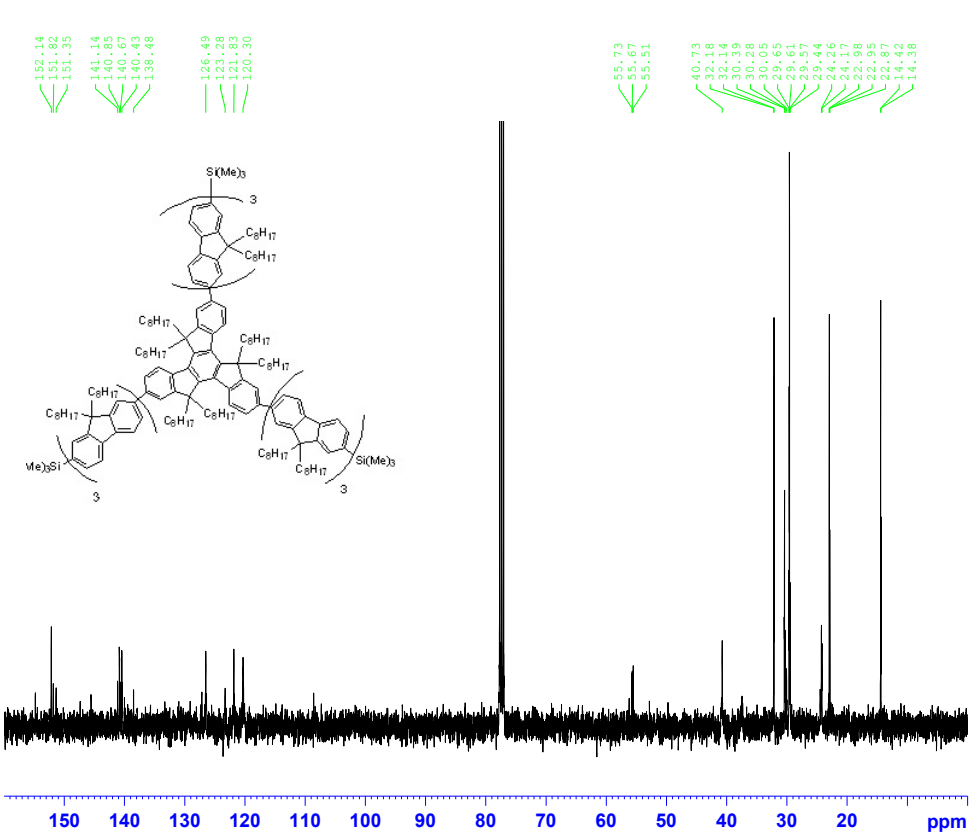


```
NAME        D133493 CO21 13C NMR
EXPNO                 1
PROCNO                1
Date_          20100611
Time              13.18
INSTRUM           spect
PROBHD    5 mm QNP 1H/13
PULPROG          zgpg30
TD                16384
SOLVENT           CDCl3
NS                 1024
DS                    4
SWH           22058.824 Hz
FIDRES         1.346364 Hz
AQ             0.3714207 sec
RG                 2050
DW               22.667 usec
DE                6.50 usec
TE                295.2 K
D1            0.69999999 sec
D11           0.03000000 sec
TD0                   1

======== CHANNEL f1 ========
NUC1                 13C
P1                  7.00 usec
PL1                -2.60 dB
PL1W         61.34123230 W
SFO1        100.6228298 MHz

======== CHANNEL f2 ========
CPDPRG2          waltz16
NUC2                 1H
PCPD2             80.00 usec
PL2               -4.00 dB
PL12              14.06 dB
PL13             120.00 dB
PL2W         19.93825150 W
PL12W         0.31166428 W
PL13W         0.00000000 W
SFO2        400.1316005 MHz
SI                32768
SF          100.6127363 MHz
WDW                  EM
SSB                   0
LB                 1.00 Hz
GB                    0
PC                 1.40
```

T4 O

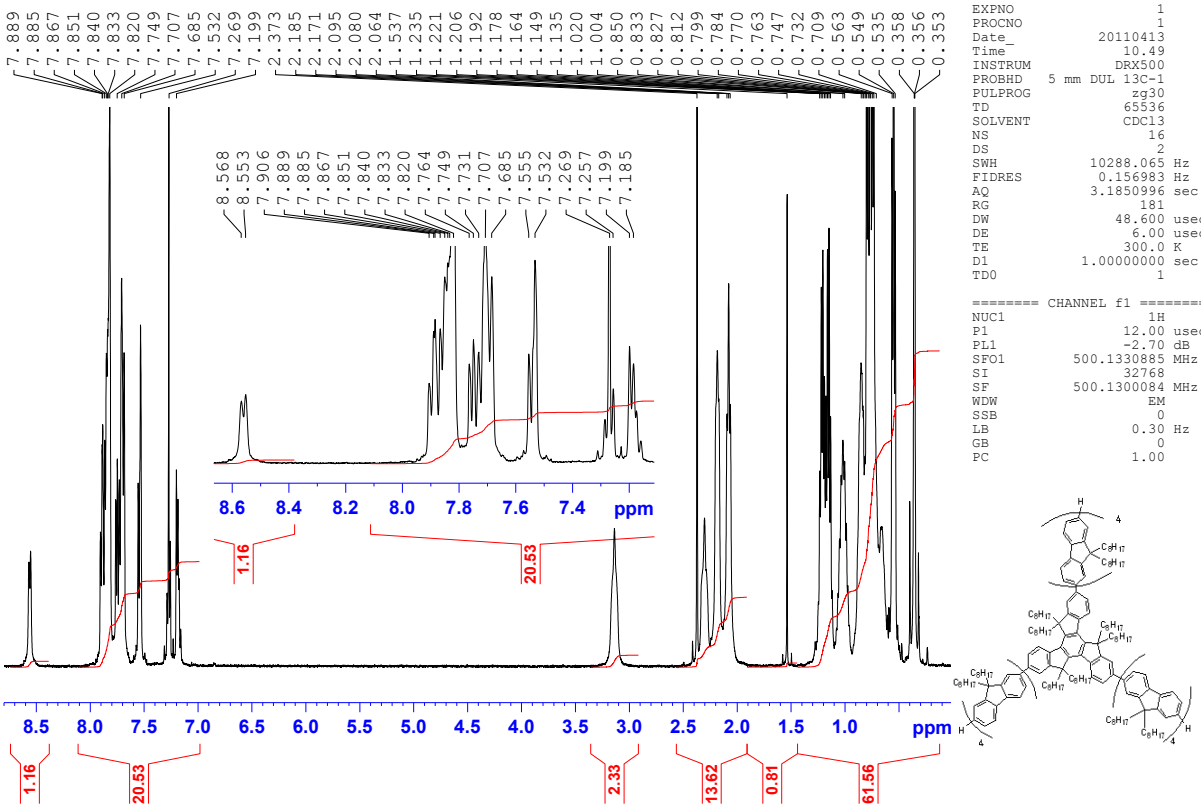


```
NAME        A21589 CO48 22-26
EXPNO                 1
PROCNO                1
Date_          20110413
Time              10.49
INSTRUM          DRX500
PROBHD    5 mm DUL 13C-1
PULPROG          zg30
TD               65536
SOLVENT          CDCl3
NS                   16
DS                    2
SWH           10288.065 Hz
FIDRES         0.156983 Hz
AQ             3.1850996 sec
RG                 181
DW               48.600 usec
DE                6.00 usec
TE                300.0 K
D1            1.00000000 sec
TD0                   1

======== CHANNEL f1 ========
NUC1                 1H
P1                12.00 usec
PL1               -2.70 dB
SFO1        500.1330885 MHz
SI                32768
SF          500.1300084 MHz
WDW                  EM
SSB                   0
LB                 0.30 Hz
GB                    0
PC                 1.00
```

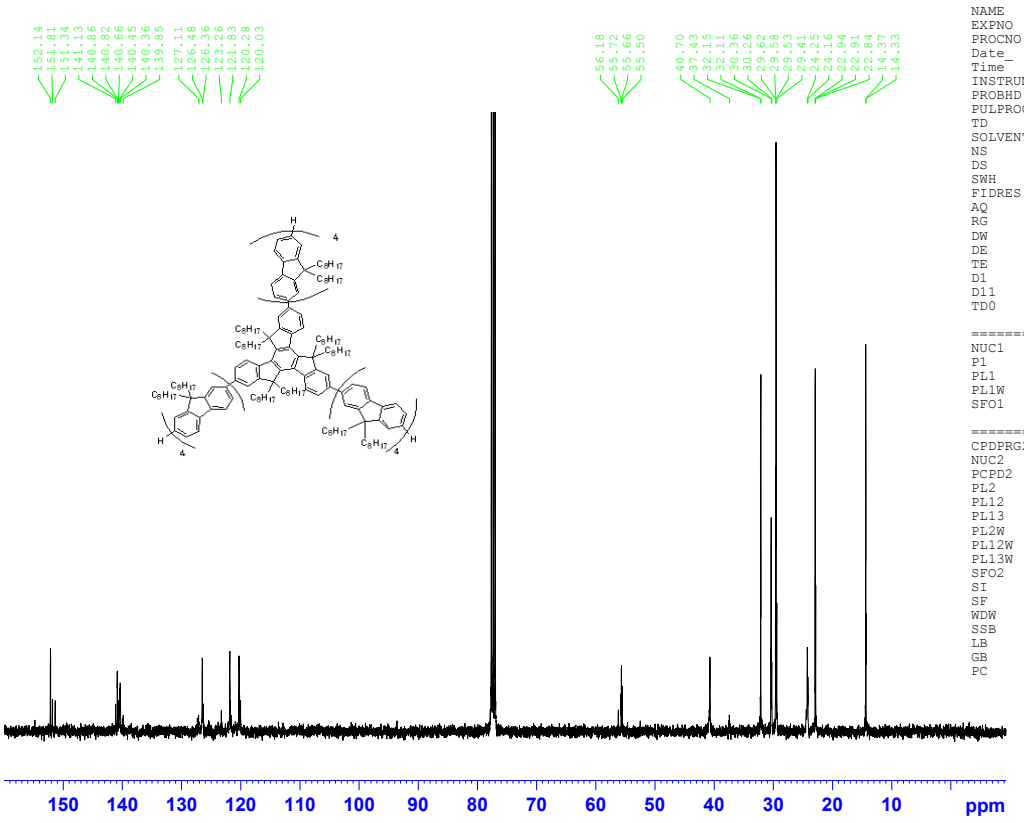


```
NAME        D180055 CO34 C
EXPNO                    1
PROCNO                   1
Date_             20130430
Time                 2.36
INSTRUM             spect
PROBHD   5 mm QNP 1H/13
PULPROG          zgpg30
TD                  16384
SOLVENT             CDCl3
NS                   4024
DS                      4
SWH          22058.824 Hz
FIDRES        1.346364 Hz
AQ            0.3714207 sec
RG                   2050
DW              22.667 usec
DE               6.50 usec
TE              300.0 K
D1           0.69999999 sec
D11          0.03000000 sec
TD0                      1

======== CHANNEL f1 ========
NUC1                   13C
P1                  7.00 usec
PL1                -2.60 dB
PL1W        61.34123230 W
SFO1       100.6228298 MHz

======== CHANNEL f2 ========
CPDPRG2          waltz16
NUC2                   1H
PCPD2              80.00 usec
PL2                -4.00 dB
PL12               14.06 dB
PL13              120.00 dB
PL2W        19.93825150 W
PL12W        0.31166428 W
PL13W        0.00000000 W
SFO2       400.1316005 MHz
SI                 32768
SF         100.6127376 MHz
WDW                   EM
SSB                    0
LB                  1.00 Hz
GB                     0
PC                  1.40
```

T6 O

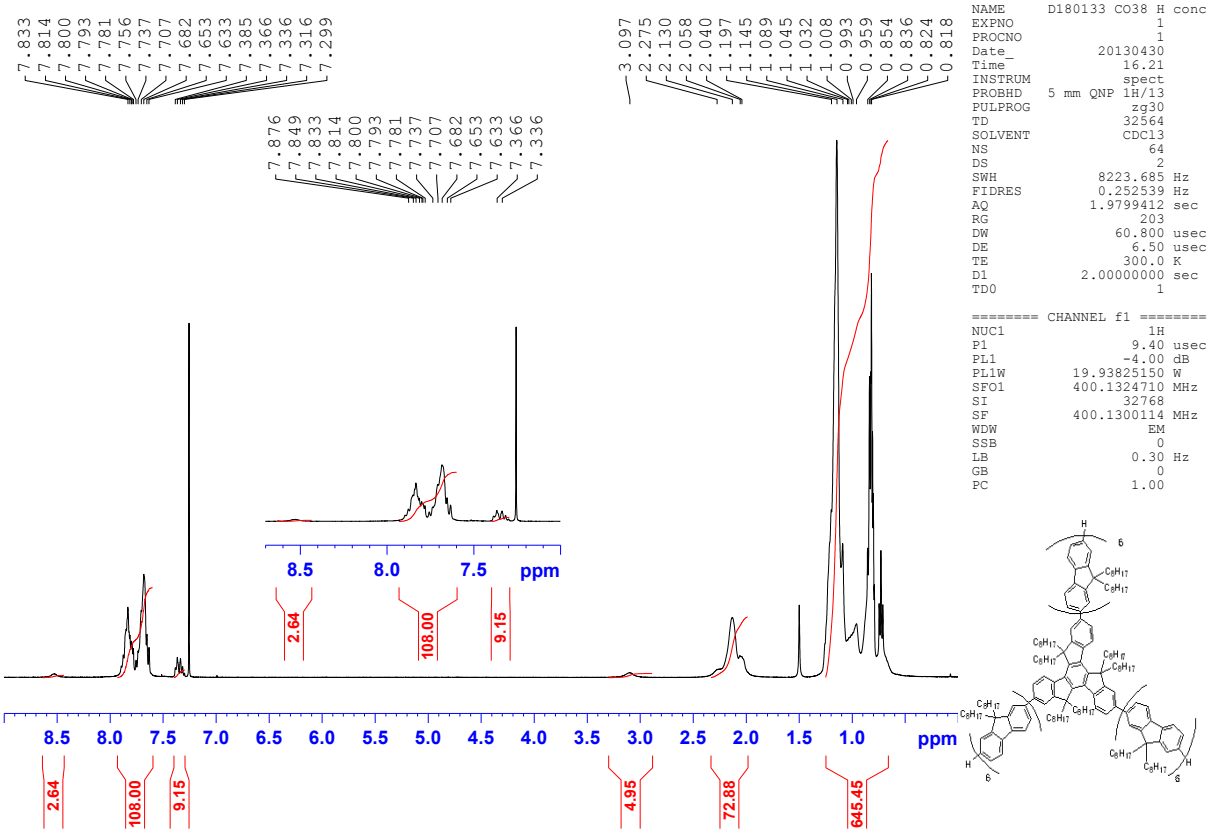


```
NAME        D180133 CO38 H conc
EXPNO                    1
PROCNO                   1
Date_             20130430
Time                16.21
INSTRUM             spect
PROBHD   5 mm QNP 1H/13
PULPROG             zg30
TD                  32564
SOLVENT             CDCl3
NS                     64
DS                      2
SWH           8223.685 Hz
FIDRES        0.252539 Hz
AQ            1.9799412 sec
RG                    203
DW              60.800 usec
DE               6.50 usec
TE              300.0 K
D1           2.00000000 sec
TD0                      1

======== CHANNEL f1 ========
NUC1                   1H
P1                  9.40 usec
PL1                -4.00 dB
PL1W        19.93825150 W
SFO1       400.1324710 MHz
SI                 32768
SF         400.1300114 MHz
WDW                   EM
SSB                    0
LB                  0.30 Hz
GB                     0
PC                  1.00
```

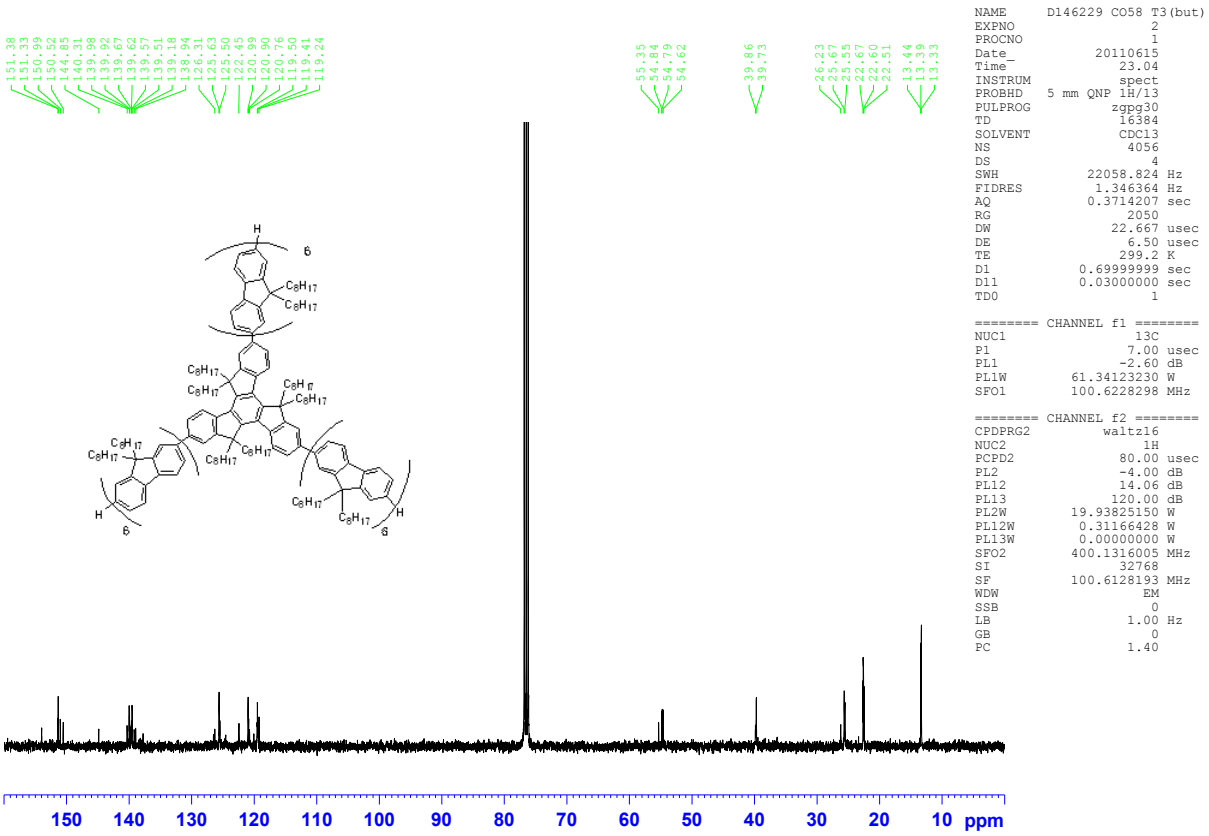
151.38
151.33
150.99
150.82
140.85
140.31
139.98
139.92
139.67
139.62
139.57
139.51
139.18
138.94
126.31
125.63
125.50
122.45
120.99
120.90
120.76
119.50
119.41
119.24
55.35
54.84
54.79
54.62
39.86
39.73
26.23
25.67
25.55
22.67
22.60
22.51
13.44
13.39
13.33
NAME D146229 CO58 T3(but)
EXPNO 2
PROCNO 1
Date_ 20110615
Time 23.04
INSTRUM spect
PROBHD 5 mm QNP 1H/13
PULPROG zgpg30
TD 16384
SOLVENT CDCl3
NS 4056
DS 4
SWH 22058.824 Hz
FIDRES 1.346364 Hz
AQ 0.3714207 sec
RG 2050
DW 22.667 usec
DE 6.50 usec
TE 299.2 K
D1 0.69999999 sec
D11 0.03000000 sec
TD0 1
======== CHANNEL f1 ========
NUC1 13C
P1 7.00 usec
PL1 -2.60 dB
PL1W 61.34123230 W
SFO1 100.6228298 MHz
======== CHANNEL f2 ========
CPDPRG2 waltz16
NUC2 1H
PCPD2 80.00 usec
PL2 -4.00 dB
PL12 14.06 dB
PL13 120.00 dB
PL2W 19.93825150 W
PL12W 0.31166428 W
PL13W 0.00000000 W
SFO2 400.1316005 MHz
SI 32768
SF 100.6128193 MHz
WDW EM
SSB 0
LB 1.00 Hz
GB 0
PC 1.40
150 140 130 120 110 100 90 80 70 60 50 40 30 20 10 ppm

Star DPP

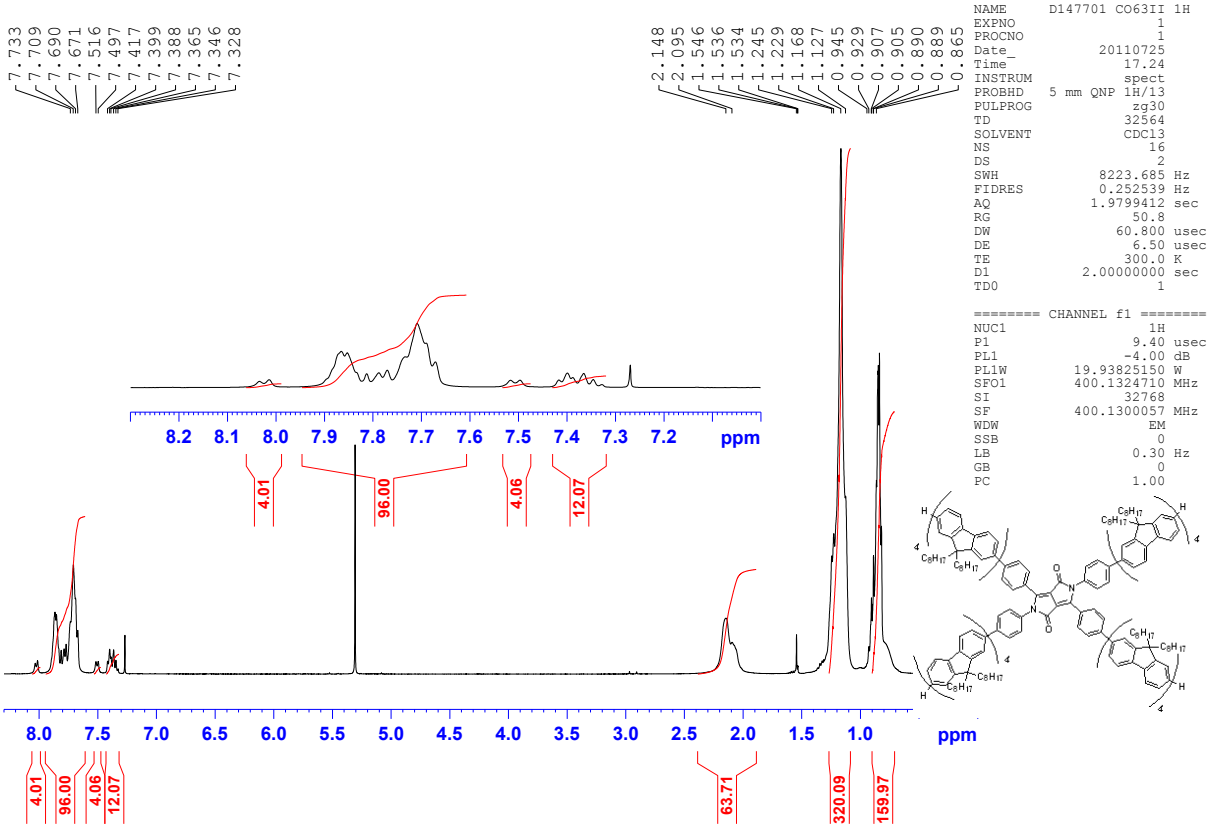
7.733
7.709
7.690
7.671
7.516
7.497
7.417
7.399
7.388
7.365
7.346
7.328
2.148
2.095
1.546
1.536
1.534
1.245
1.229
1.168
1.127
0.945
0.929
0.907
0.905
0.890
0.889
0.865
NAME D147701 CO63II 1H
EXPNO 1
PROCNO 1
Date_ 20110725
Time 17.24
INSTRUM spect
PROBHD 5 mm QNP 1H/13
PULPROG zg30
TD 32564
SOLVENT CDCl3
NS 16
DS 2
SWH 8223.685 Hz
FIDRES 0.252539 Hz
AQ 1.9799412 sec
RG 50.8
DW 60.800 usec
DE 6.50 usec
TE 300.0 K
D1 2.00000000 sec
TD0 1
======== CHANNEL f1 ========
NUC1 1H
P1 9.40 usec
PL1 -4.00 dB
PL1W 19.93825150 W
SFO1 400.1324710 MHz
SI 32768
SF 400.1300057 MHz
WDW EM
SSB 0
LB 0.30 Hz
GB 0
PC 1.00
8.2 8.1 8.0 7.9 7.8 7.7 7.6 7.5 7.4 7.3 7.2 ppm
4.01
96.00
4.06
12.07
8.0 7.5 7.0 6.5 6.0 5.5 5.0 4.5 4.0 3.5 3.0 2.5 2.0 1.5 1.0 ppm
4.01
96.00
4.06
12.07
63.71
320.09
159.97

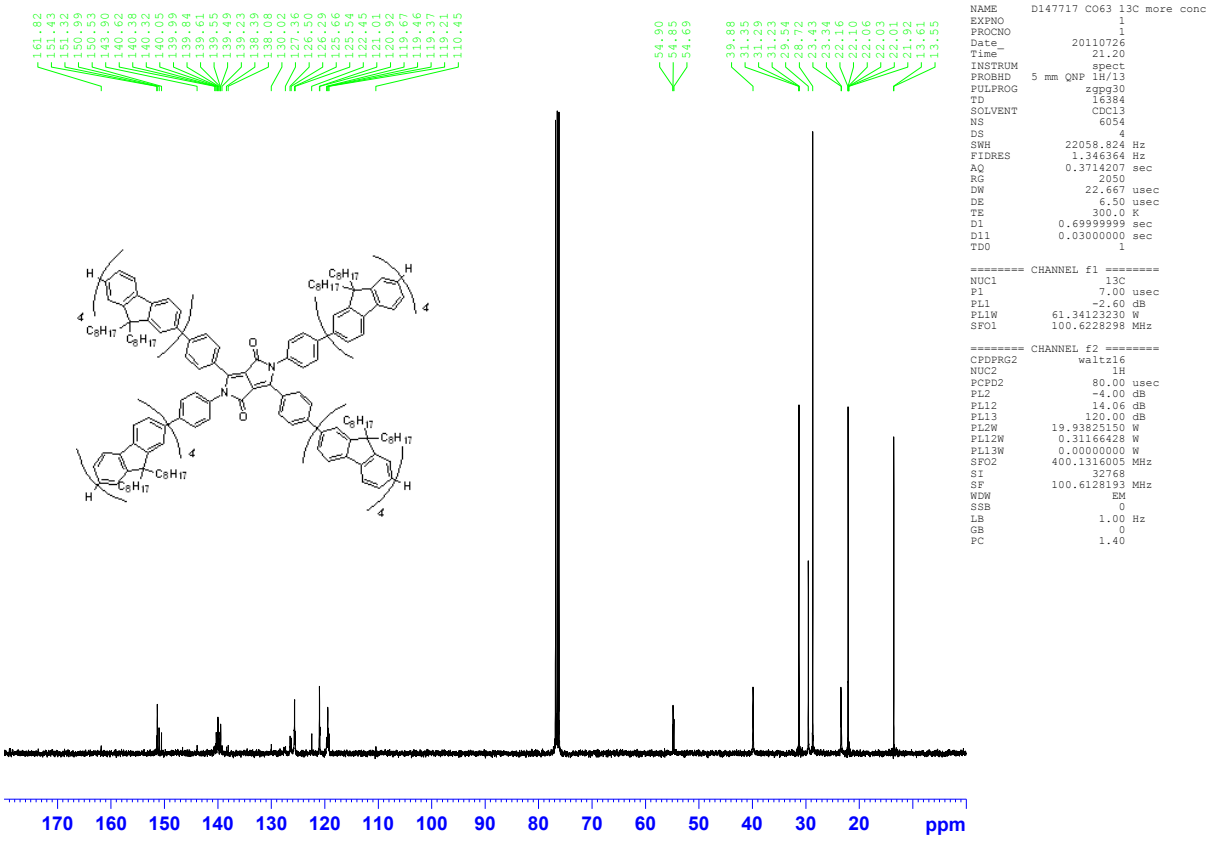
NAME D147717 CO63 13C more conc
EXPNO 1
PROCNO 1
Date_ 20110726
Time 21.20
INSTRUM spect
PROBHD 5 mm QNP 1H/13
PULPROG zgpg30
TD 16384
SOLVENT CDCl3
NS 6054
DS 4
SWH 22058.824 Hz
FIDRES 1.346364 Hz
AQ 0.3714207 sec
RG 2050
DW 22.667 usec
DE 6.50 usec
TE 300.0 K
D1 0.69999999 sec
D11 0.03000000 sec
TD0 1
======== CHANNEL f1 ========
NUC1 13C
P1 7.00 usec
PL1 -2.60 dB
PL1W 61.34123230 W
SFO1 100.6228298 MHz
======== CHANNEL f2 ========
CPDPRG2 waltz16
NUC2 1H
PCPD2 80.00 usec
PL2 -4.00 dB
PL12 14.06 dB
PL13 120.00 dB
PL2W 19.93825150 W
PL12W 0.31166428 W
PL13W 0.00000000 W
SFO2 400.1316005 MHz
SI 32768
SF 100.6128193 MHz
WDW EM
SSB 0
LB 1.00 Hz
GB 0
PC 1.40
ppm

Linear-c DPP

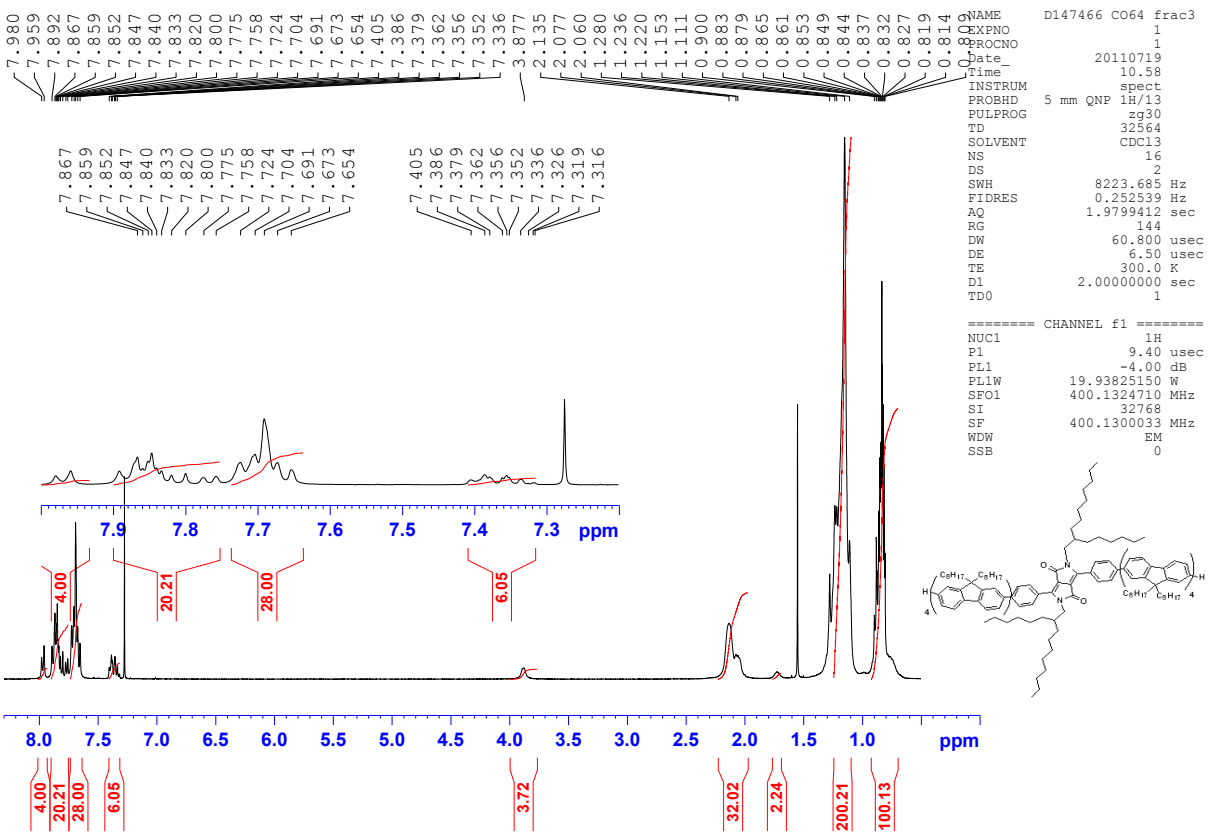
NAME D147466 CO64 frac3
EXPNO 1
PROCNO 1
Date_ 20110719
Time 10.58
INSTRUM spect
PROBHD 5 mm QNP 1H/13
PULPROG zg30
TD 32564
SOLVENT CDCl3
NS 16
DS 2
SWH 8223.685 Hz
FIDRES 0.252539 Hz
AQ 1.9799412 sec
RG 144
DW 60.800 usec
DE 6.50 usec
TE 300.0 K
D1 2.00000000 sec
TD0 1
======== CHANNEL f1 ========
NUC1 1H
P1 9.40 usec
PL1 -4.00 dB
PL1W 19.93825150 W
SFO1 400.1324710 MHz
SI 32768
SF 400.1300033 MHz
WDW EM
SSB 0
ppm
4.00
20.21
28.00
6.05
3.72
32.02
2.24
200.21
100.13

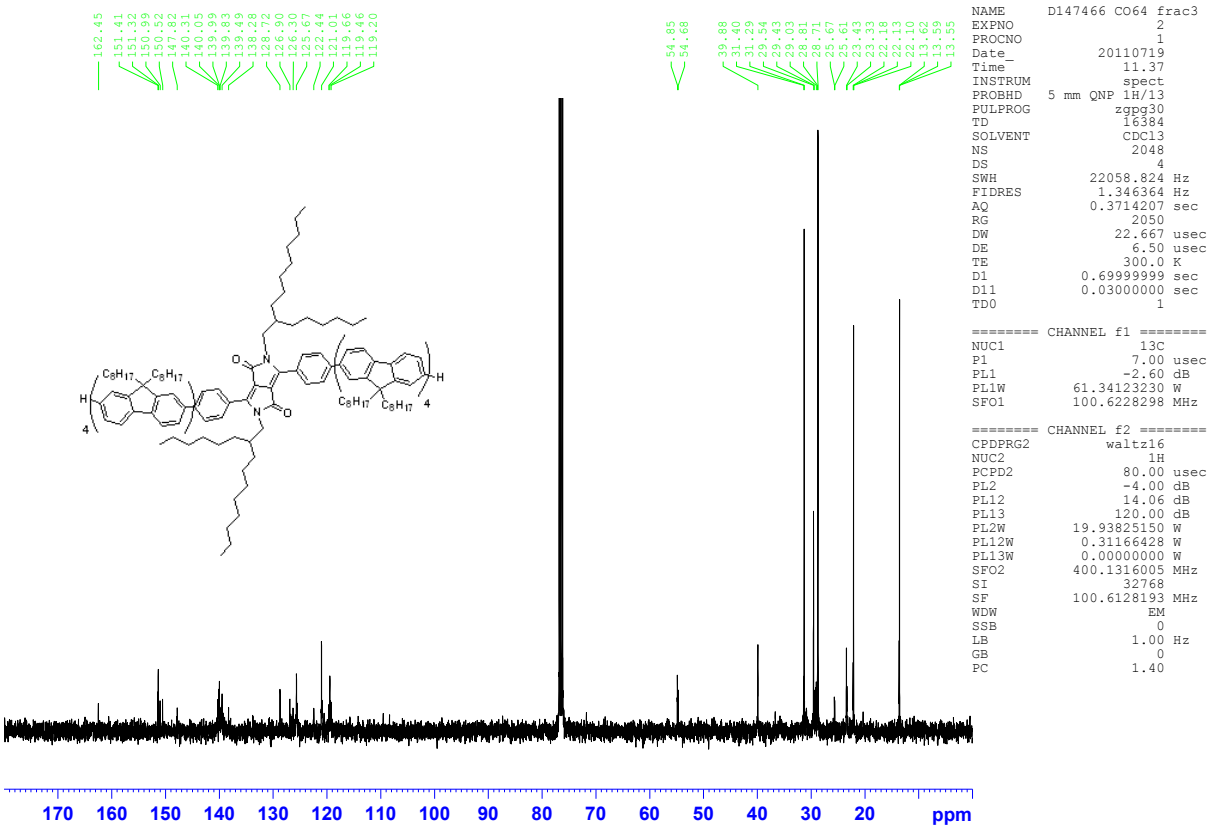

Linear-c DPP MOD

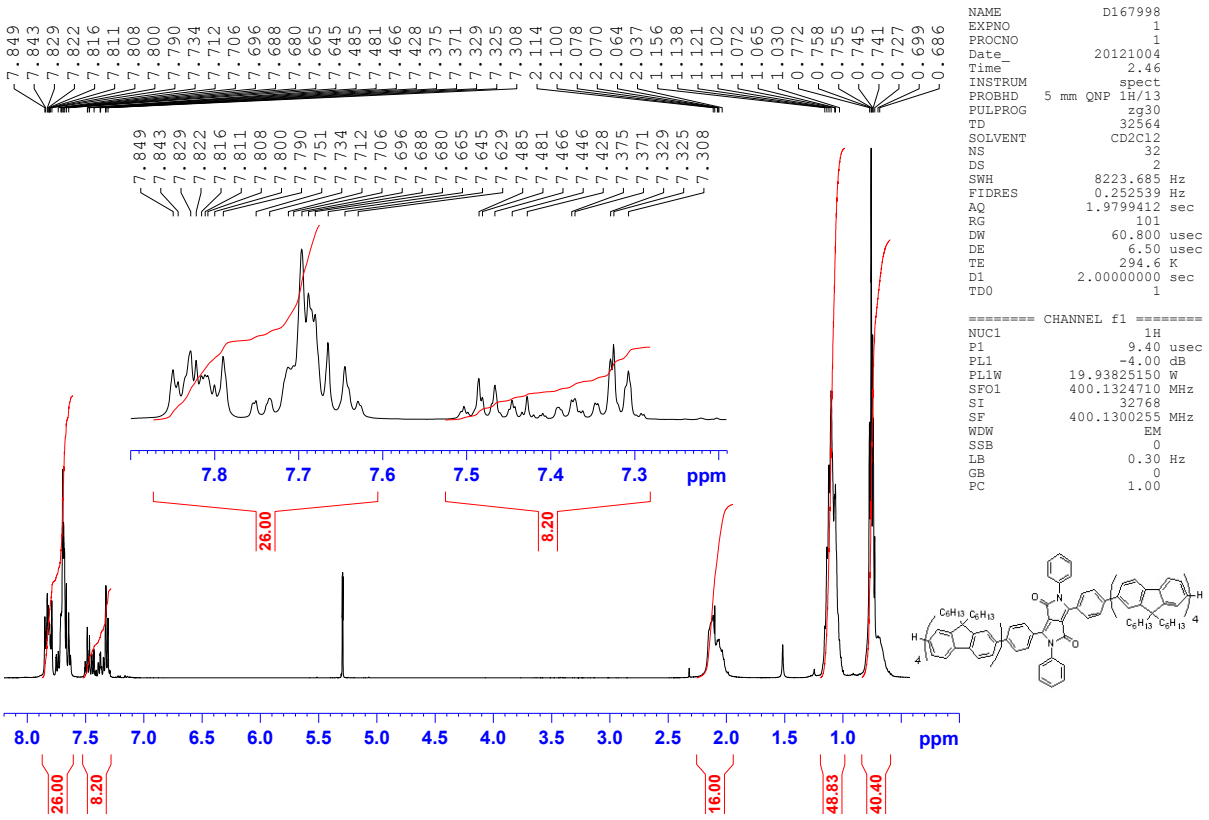

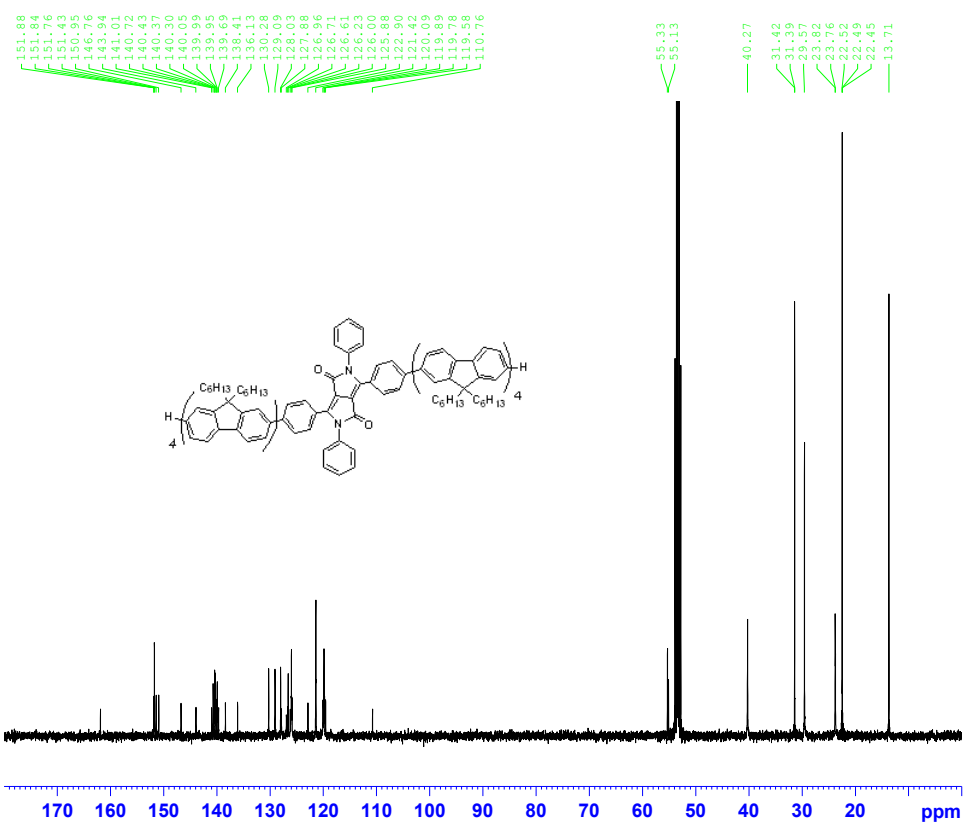
151.88
151.84
151.76
151.43
150.95
146.76
143.94
141.01
140.72
140.43
140.37
140.30
140.05
139.99
139.95
139.69
138.41
136.13
130.28
129.09
128.03
127.88
126.96
126.71
126.23
126.00
125.88
122.90
121.42
120.09
119.89
119.78
119.58
110.76
55.33
55.13
40.27
31.42
31.39
29.57
23.82
23.76
22.52
22.49
22.45
13.71
NAME D167998
EXPNO 2
PROCNO 1
Date_ 20121004
Time 4.04
INSTRUM spect
PROBHD 5 mm QNP 1H/13
PULPROG zgpg30
TD 16384
SOLVENT CD2Cl2
NS 4096
DS 4
SWH 22058.824 Hz
FIDRES 1.346364 Hz
AQ 0.3714207 sec
RG 2050
DW 22.667 usec
DE 6.50 usec
TE 294.7 K
D1 0.69999999 sec
D11 0.03000000 sec
TD0 1
======== CHANNEL f1 ========
NUC1 13C
P1 7.00 usec
PL1 -2.60 dB
PL1W 61.34123230 W
SFO1 100.6228298 MHz
======== CHANNEL f2 ========
CPDPRG2 waltz16
NUC2 1H
PCPD2 80.00 usec
PL2 -4.00 dB
PL12 14.06 dB
PL13 120.00 dB
PL2W 19.93825150 W
PL12W 0.31166428 W
PL13W 0.00000000 W
SFO2 400.1316005 MHz
SI 32768
SF 100.6127766 MHz
WDW EM
SSB 0
LB 1.00 Hz
GB 0
PC 1.40
170 160 150 140 130 120 110 100 90 80 70 60 50 40 30 20 ppm

TPE1

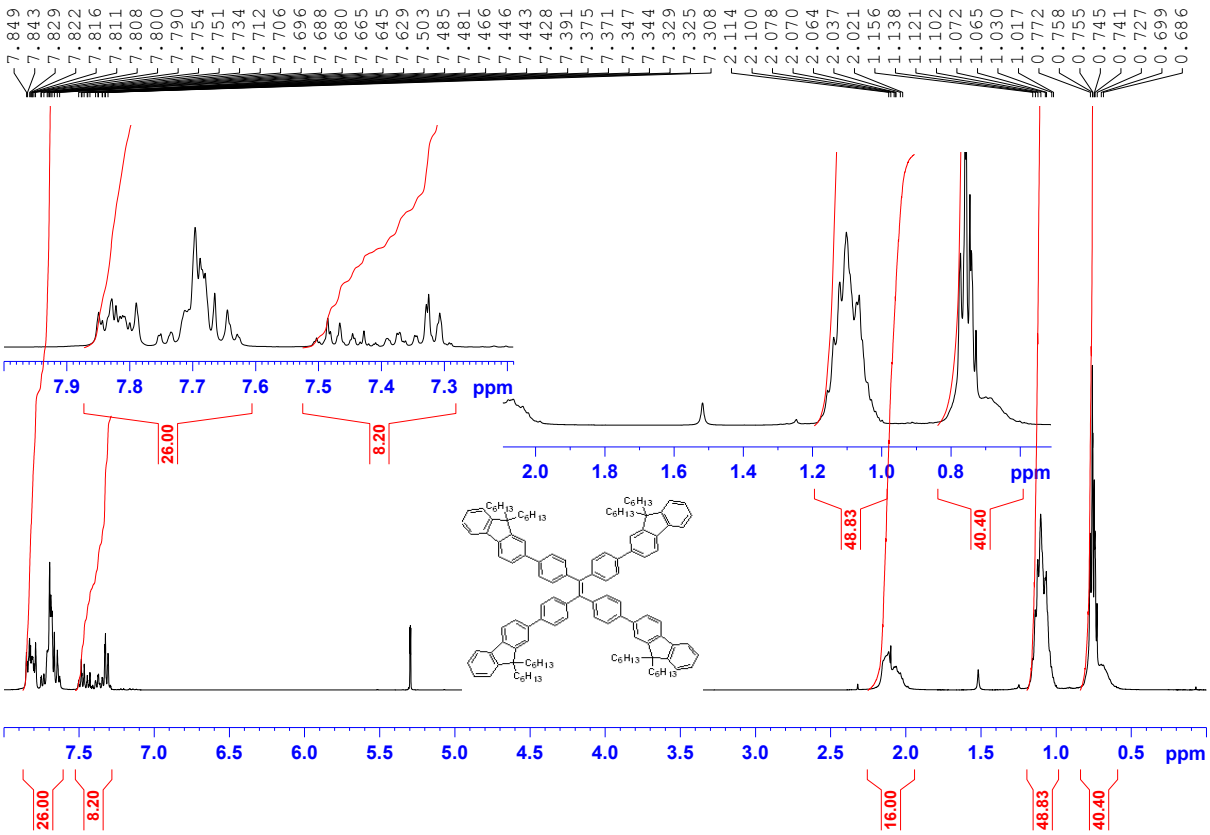
7.849
7.843
7.829
7.822
7.816
7.811
7.808
7.800
7.790
7.754
7.751
7.734
7.712
7.706
7.696
7.688
7.680
7.665
7.645
7.629
7.503
7.485
7.481
7.466
7.446
7.443
7.428
7.391
7.375
7.371
7.347
7.344
7.329
7.325
7.308
2.114
2.100
2.078
2.070
2.064
2.037
2.021
1.156
1.138
1.121
1.102
1.072
1.065
1.030
1.017
0.772
0.758
0.755
0.745
0.741
0.727
0.699
0.686
7.9 7.8 7.7 7.6 7.5 7.4 7.3 ppm
26.00
8.20
2.0 1.8 1.6 1.4 1.2 1.0 0.8 ppm
48.83
40.40
7.5 7.0 6.5 6.0 5.5 5.0 4.5 4.0 3.5 3.0 2.5 2.0 1.5 1.0 0.5 ppm
26.00
8.20
16.00
48.83
40.40

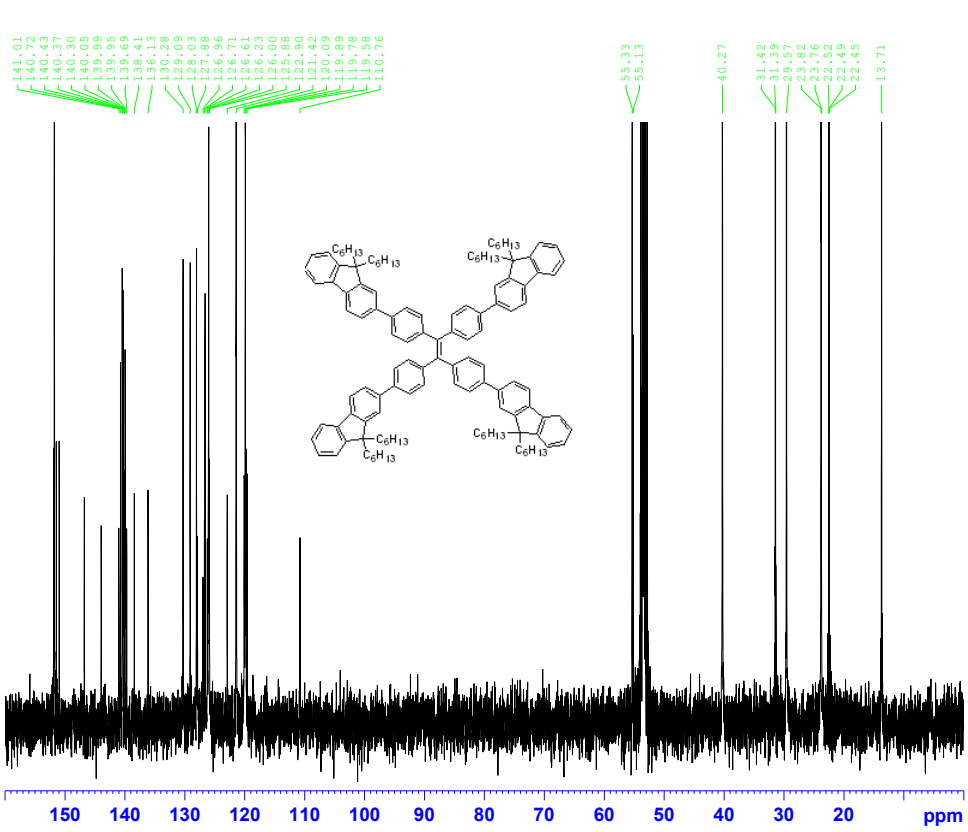


```
NAME                D167998
EXPNO                     2
PROCNO                    1
Date_              20121004
Time                   4.04
INSTRUM               spect
PROBHD    5 mm QNP 1H/13
PULPROG              zgpg30
TD                    16384
SOLVENT              CD2Cl2
NS                     4096
DS                        4
SWH               22058.824 Hz
FIDRES             1.346364 Hz
AQ                 0.3714207 sec
RG                     2050
DW                   22.667 usec
DE                    6.50 usec
TE                   294.7 K
D1                0.69999999 sec
D11               0.03000000 sec
TD0                       1

======== CHANNEL f1 ========
NUC1                    13C
P1                     7.00 usec
PL1                   -2.60 dB
PL1W           61.34123230 W
SFO1          100.6228298 MHz

======== CHANNEL f2 ========
CPDPRG2            waltz16
NUC2                    1H
PCPD2                80.00 usec
PL2                  -4.00 dB
PL12                 14.06 dB
PL13                120.00 dB
PL2W           19.93825150 W
PL12W           0.31166428 W
PL13W           0.00000000 W
SFO2          400.1316005 MHz
SI                    32768
SF            100.6127766 MHz
WDW                      EM
SSB                       0
LB                     1.00 Hz
GB                        0
PC                     1.40
```

TPE4

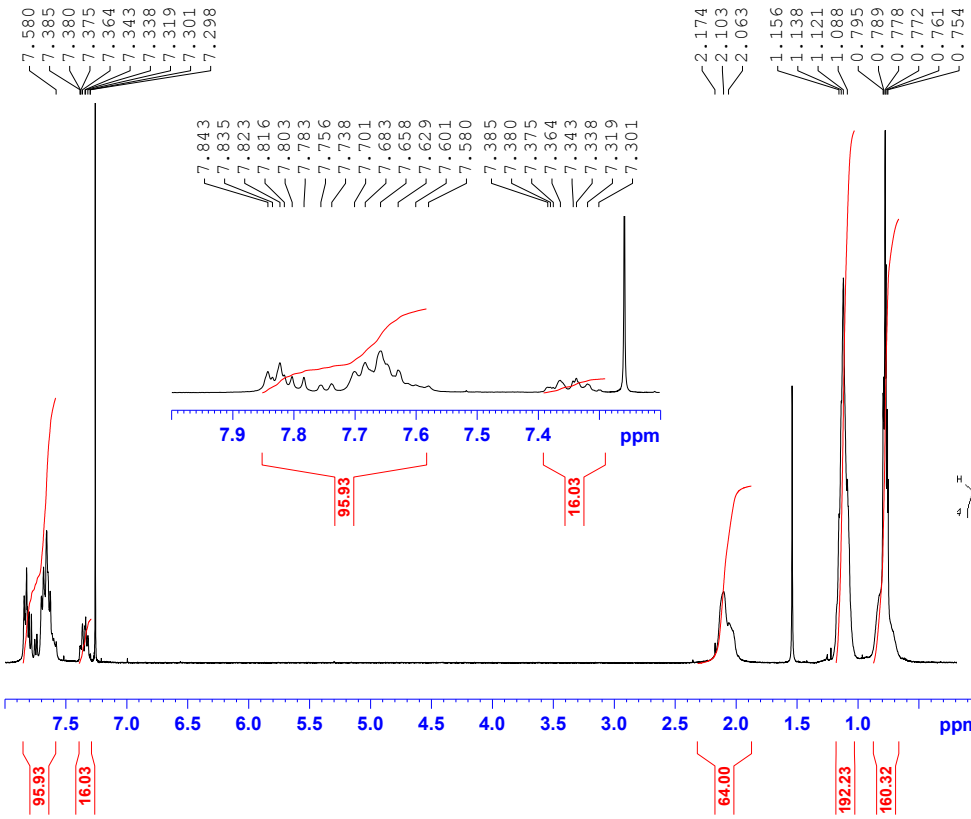


```
NAME      D168801 CO104 1Hdiluted
EXPNO                   1
PROCNO                  1
Date_            20121020
Time                7.03
INSTRUM            spect
PROBHD  5 mm QNP 1H/13
PULPROG             zg30
TD                 32564
SOLVENT            CDCl3
NS                    16
DS                     2
SWH              8223.685 Hz
FIDRES           0.252539 Hz
AQ               1.9799412 sec
RG                   406
DW                60.800 usec
DE                 6.50 usec
TE                294.3 K
D1             2.00000000 sec
TD0                    1

======== CHANNEL f1 ========
NUC1                   1H
P1                  9.40 usec
PL1                -4.00 dB
PL1W        19.93825150 W
SFO1       400.1324710 MHz
SI                 32768
SF         400.1300103 MHz
WDW                   EM
SSB                    0
LB                  0.30 Hz
GB                     0
PC                  1.00
```

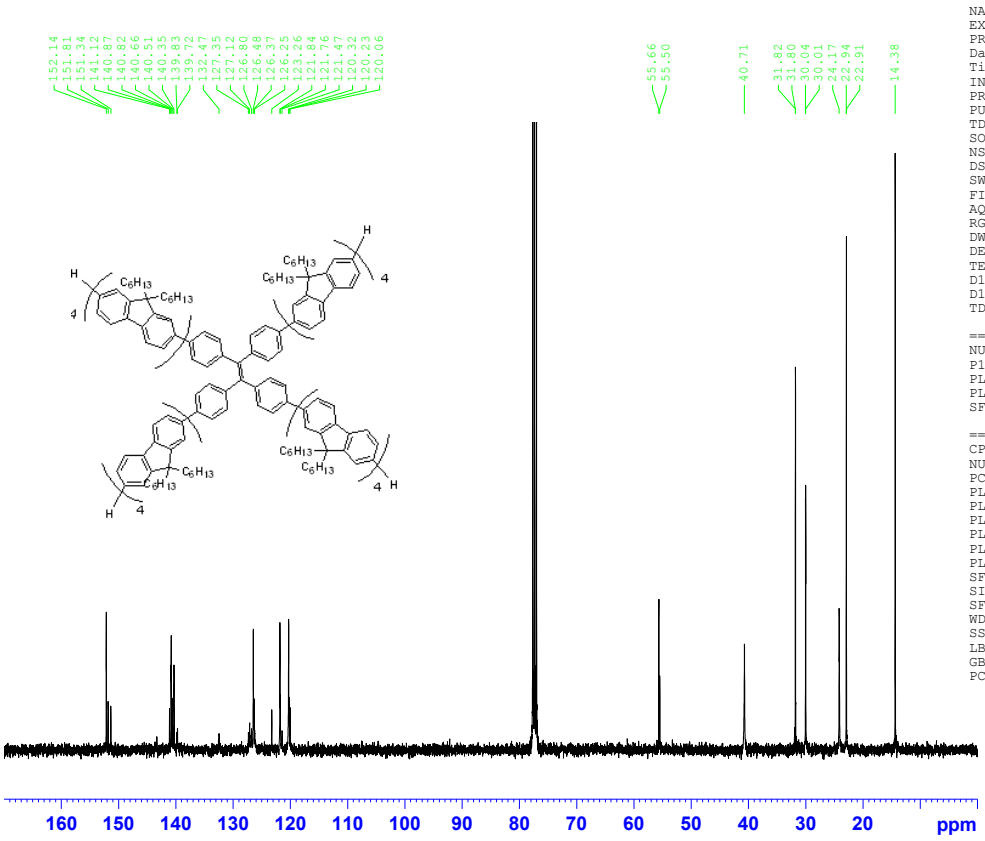


```
NAME                D168685
EXPNO                     2
PROCNO                    1
Date_              20121019
Time                  3.17
INSTRUM              spect
PROBHD    5 mm QNP 1H/13
PULPROG             zgpg30
TD                   16384
SOLVENT              CDCl3
NS                    6144
DS                       4
SWH              22058.824 Hz
FIDRES            1.346364 Hz
AQ                0.3714207 sec
RG                     2050
DW                  22.667 usec
DE                    6.50 usec
TE                  294.0 K
D1                0.69999999 sec
D11               0.03000000 sec
TD0                       1

======== CHANNEL f1 ========
NUC1                    13C
P1                    7.00 usec
PL1                  -2.60 dB
PL1W          61.34123230 W
SFO1          100.6228298 MHz

======== CHANNEL f2 ========
CPDPRG2            waltz16
NUC2                    1H
PCPD2                80.00 usec
PL2                  -4.00 dB
PL12                 14.06 dB
PL13                120.00 dB
PL2W          19.93825150 W
PL12W          0.31166428 W
PL13W          0.00000000 W
SFO2          400.1316005 MHz
SI                    32768
SF            100.6127365 MHz
WDW                      EM
SSB                       0
LB                     1.00 Hz
GB                        0
PC                     1.40
```

T-B1

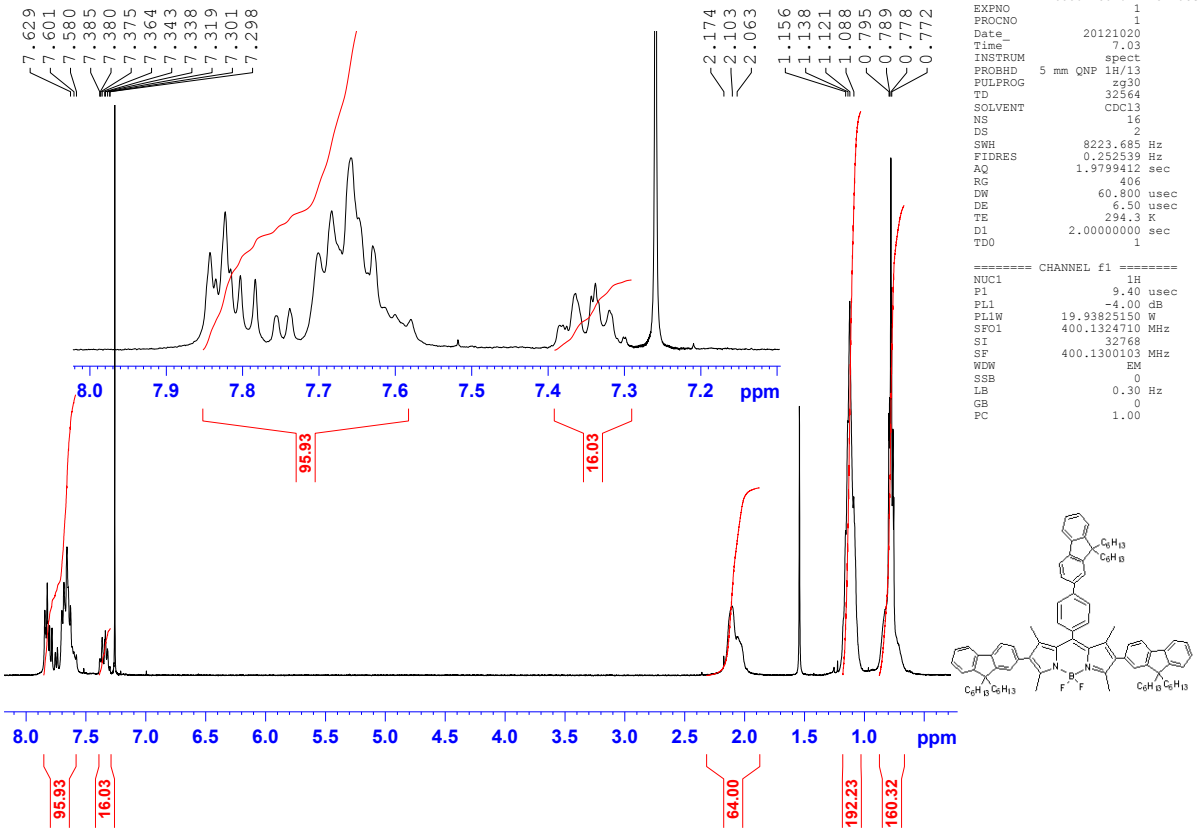


```
NAME      D168801 CO104 1Hdiluted
EXPNO                     1
PROCNO                    1
Date_              20121020
Time                  7.03
INSTRUM              spect
PROBHD    5 mm QNP 1H/13
PULPROG               zg30
TD                   32564
SOLVENT              CDCl3
NS                      16
DS                       2
SWH               8223.685 Hz
FIDRES            0.252539 Hz
AQ                1.9799412 sec
RG                     406
DW                  60.800 usec
DE                    6.50 usec
TE                  294.3 K
D1                2.00000000 sec
TD0                       1

======== CHANNEL f1 ========
NUC1                    1H
P1                    9.40 usec
PL1                  -4.00 dB
PL1W          19.93825150 W
SFO1          400.1324710 MHz
SI                    32768
SF            400.1300103 MHz
WDW                      EM
SSB                       0
LB                     0.30 Hz
GB                        0
PC                     1.00
```

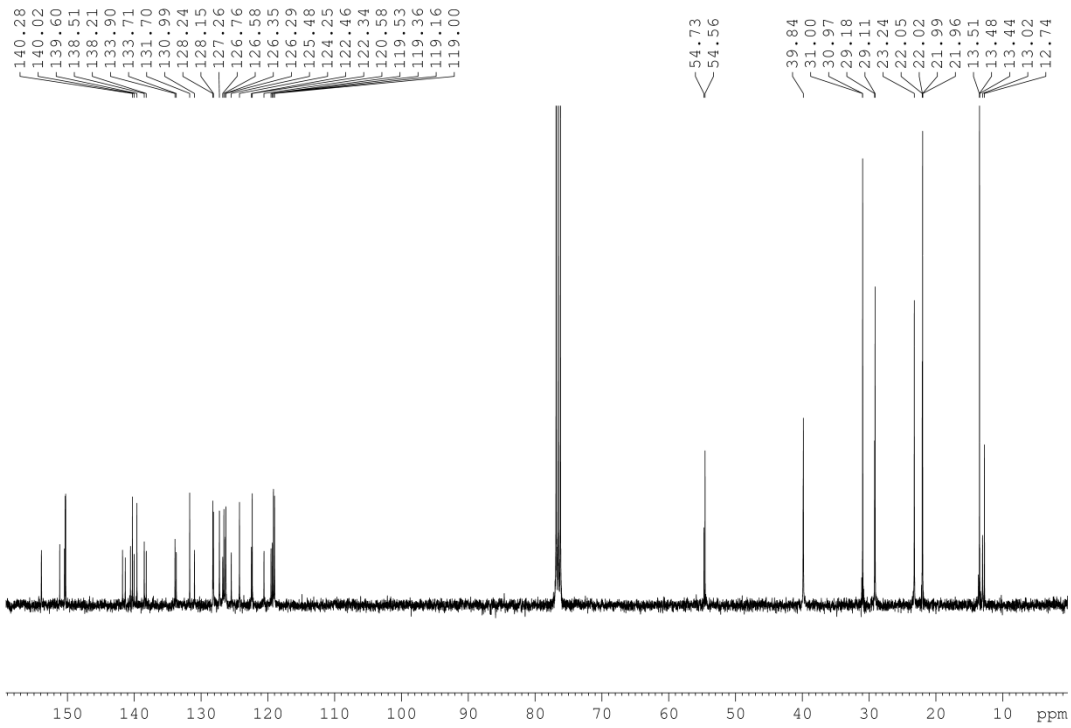
140.28
140.02
139.60
138.51
138.21
133.90
133.71
131.70
130.99
128.24
128.15
127.26
126.76
126.58
126.35
126.29
125.48
124.25
122.46
122.34
120.58
119.53
119.36
119.16
119.00
54.73
54.56
39.84
31.00
30.97
29.18
29.11
23.24
22.05
22.02
21.99
21.96
13.51
13.48
13.44
13.02
12.74
150 140 130 120 110 100 90 80 70 60 50 40 30 20 10 ppm

T-B2

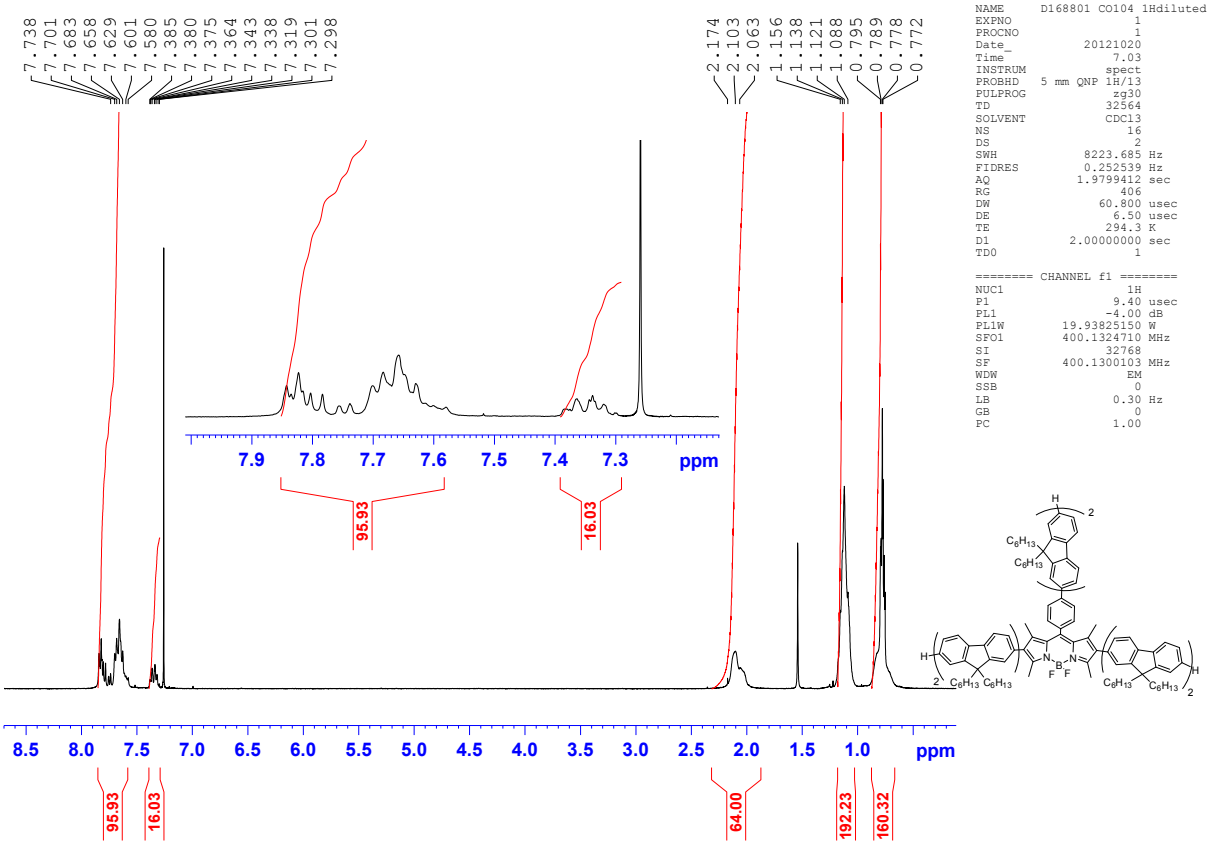
7.738
7.701
7.683
7.658
7.629
7.601
7.580
7.385
7.380
7.375
7.364
7.343
7.338
7.319
7.301
7.298
2.174
2.103
2.063
1.156
1.138
1.121
1.088
0.795
0.789
0.778
0.772
7.9 7.8 7.7 7.6 7.5 7.4 7.3 ppm
95.93
16.03
8.5 8.0 7.5 7.0 6.5 6.0 5.5 5.0 4.5 4.0 3.5 3.0 2.5 2.0 1.5 1.0 ppm
95.93
16.03
64.00
192.23
160.32
NAME D168801 CO104 1Hdiluted
EXPNO 1
PROCNO 1
Date_ 20121020
Time 7.03
INSTRUM spect
PROBHD 5 mm QNP 1H/13
PULPROG zg30
TD 32564
SOLVENT CDCl3
NS 16
DS 2
SWH 8223.685 Hz
FIDRES 0.252539 Hz
AQ 1.9799412 sec
RG 406
DW 60.800 usec
DE 6.50 usec
TE 294.3 K
D1 2.00000000 sec
TD0 1
======== CHANNEL f1 ========
NUC1 1H
P1 9.40 usec
PL1 -4.00 dB
PL1W 19.93825150 W
SFO1 400.1324710 MHz
SI 32768
SF 400.1300103 MHz
WDW EM
SSB 0
LB 0.30 Hz
GB 0
PC 1.00

T-B3

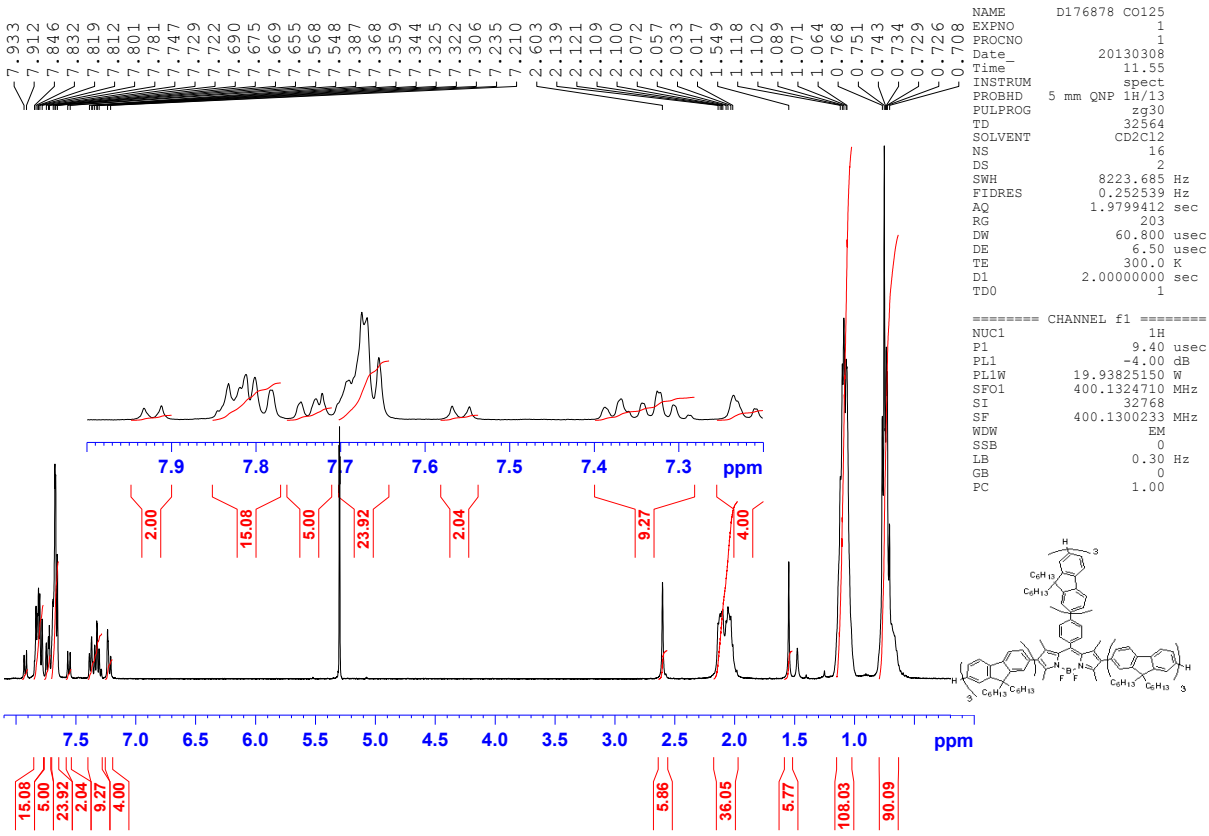
7.933 7.912 7.846 7.832 7.819 7.812 7.801 7.781 7.747 7.729 7.722 7.690 7.675 7.669 7.655 7.568 7.548 7.387 7.368 7.359 7.344 7.325 7.322 7.306 7.235 7.210 2.603 2.139 2.121 2.109 2.100 2.072 2.057 2.033 2.017 1.549 1.118 1.102 1.089 1.071 1.064 0.768 0.751 0.743 0.734 0.729 0.726 0.708
NAME D176878 CO125
EXPNO 1
PROCNO 1
Date_ 20130308
Time 11.55
INSTRUM spect
PROBHD 5 mm QNP 1H/13
PULPROG zg30
TD 32564
SOLVENT CD2Cl2
NS 16
DS 2
SWH 8223.685 Hz
FIDRES 0.252539 Hz
AQ 1.9799412 sec
RG 203
DW 60.800 usec
DE 6.50 usec
TE 300.0 K
D1 2.00000000 sec
TD0 1
======== CHANNEL f1 ========
NUC1 1H
P1 9.40 usec
PL1 -4.00 dB
PL1W 19.93825150 W
SFO1 400.1324710 MHz
SI 32768
SF 400.1300233 MHz
WDW EM
SSB 0
LB 0.30 Hz
GB 0
PC 1.00
7.9 7.8 7.7 7.6 7.5 7.4 7.3 ppm
2.00 15.08 5.00 23.92 2.04 9.27 4.00
7.5 7.0 6.5 6.0 5.5 5.0 4.5 4.0 3.5 3.0 2.5 2.0 1.5 1.0 ppm
15.08 5.00 23.92 2.04 9.27 4.00 5.86 36.05 5.77 108.03 90.09

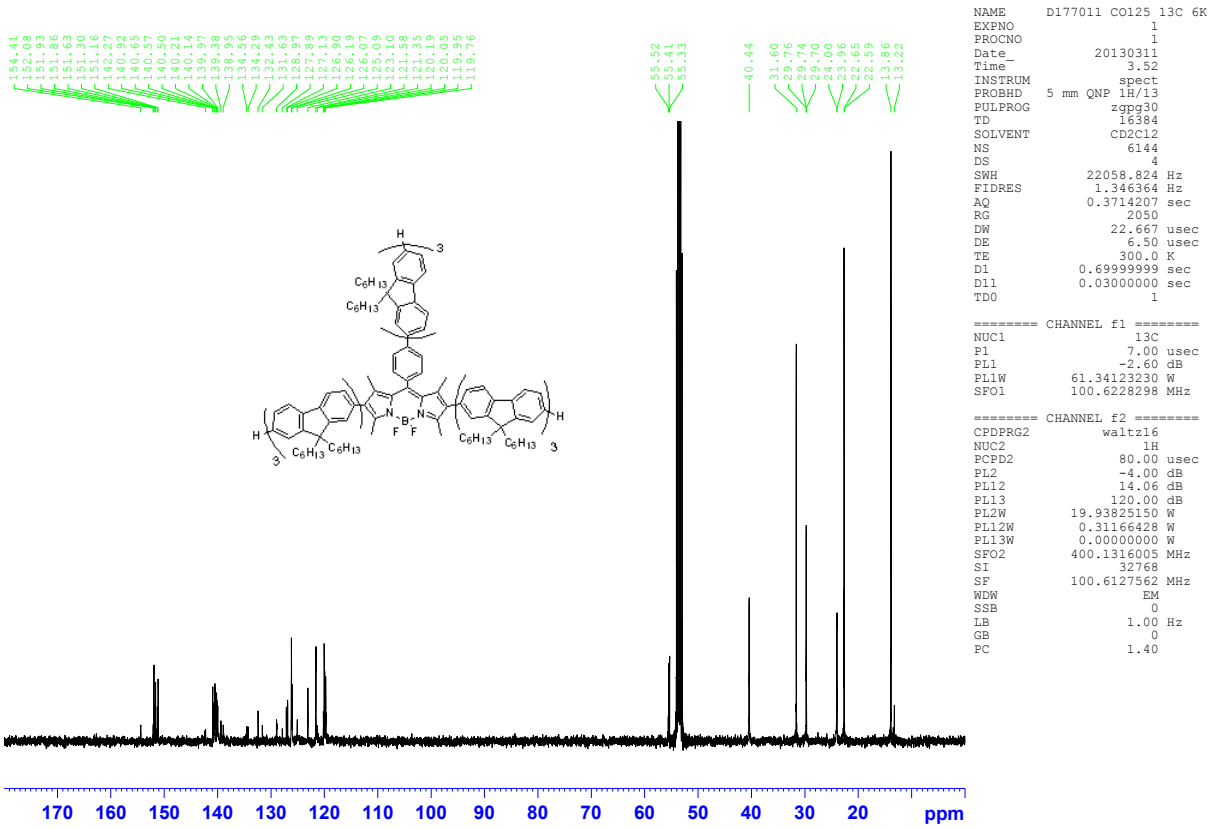
154.41 152.08 151.93 151.86 151.63 151.30 151.16 142.27 140.92 140.65 140.57 140.21 140.14 139.97 139.38 138.95 134.56 134.29 132.43 131.63 128.97 127.89 127.13 126.90 126.19 126.07 125.09 123.10 121.58 121.35 120.19 120.05 119.95 119.76
55.52 55.41 55.33
40.44
31.60 29.76 29.74 29.70 24.00 23.96 22.65 22.59 13.86 13.22
NAME D177011 CO125 13C 6K
EXPNO 1
PROCNO 1
Date_ 20130311
Time 3.52
INSTRUM spect
PROBHD 5 mm QNP 1H/13
PULPROG zgpg30
TD 16384
SOLVENT CD2Cl2
NS 6144
DS 4
SWH 22058.824 Hz
FIDRES 1.346364 Hz
AQ 0.3714207 sec
RG 2050
DW 22.667 usec
DE 6.50 usec
TE 300.0 K
D1 0.69999999 sec
D11 0.03000000 sec
TD0 1
======== CHANNEL f1 ========
NUC1 13C
P1 7.00 usec
PL1 -2.60 dB
PL1W 61.34123230 W
SFO1 100.6228298 MHz
======== CHANNEL f2 ========
CPDPRG2 waltz16
NUC2 1H
PCPD2 80.00 usec
PL2 -4.00 dB
PL12 14.06 dB
PL13 120.00 dB
PL2W 19.93825150 W
PL12W 0.31166428 W
PL13W 0.00000000 W
SFO2 400.1316005 MHz
SI 32768
SF 100.6127562 MHz
WDW EM
SSB 0
LB 1.00 Hz
GB 0
PC 1.40
170 160 150 140 130 120 110 100 90 80 70 60 50 40 30 20 ppm

T-B4

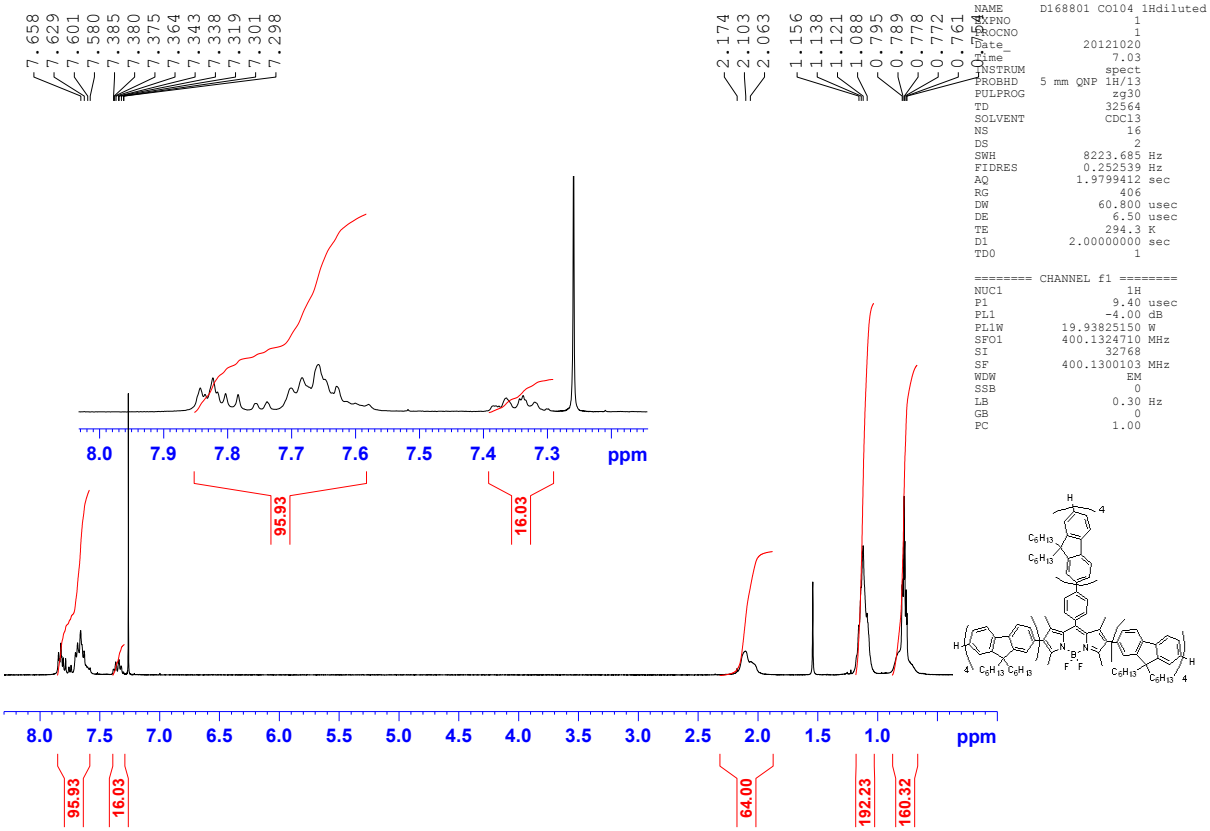
7.658 7.629 7.601 7.580 7.385 7.380 7.375 7.364 7.343 7.338 7.319 7.301 7.298
2.174 2.103 2.063 1.156 1.138 1.121 1.088 0.795 0.789 0.778 0.772 0.761
NAME D168801 CO104 1Hdiluted
EXPNO 1
PROCNO 1
Date_ 20121020
Time 7.03
INSTRUM spect
PROBHD 5 mm QNP 1H/13
PULPROG zg30
TD 32564
SOLVENT CDCl3
NS 16
DS 2
SWH 8223.685 Hz
FIDRES 0.252539 Hz
AQ 1.9799412 sec
RG 406
DW 60.800 usec
DE 6.50 usec
TE 294.3 K
D1 2.00000000 sec
TD0 1
======== CHANNEL f1 ========
NUC1 1H
P1 9.40 usec
PL1 -4.00 dB
PL1W 19.93825150 W
SFO1 400.1324710 MHz
SI 32768
SF 400.1300103 MHz
WDW EM
SSB 0
LB 0.30 Hz
GB 0
PC 1.00
8.0 7.9 7.8 7.7 7.6 7.5 7.4 7.3 ppm
95.93
16.03
8.0 7.5 7.0 6.5 6.0 5.5 5.0 4.5 4.0 3.5 3.0 2.5 2.0 1.5 1.0 ppm
95.93
16.03
64.00
192.23
160.32

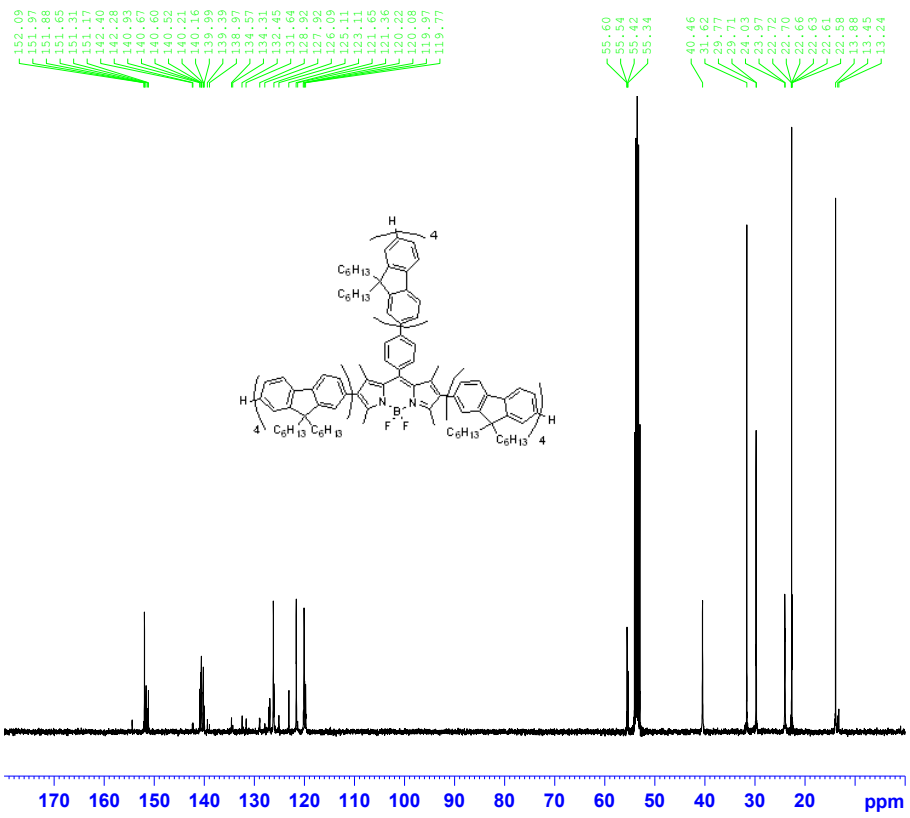


```
NAME        D177222 CO124 13C  8K
EXPNO                1
PROCNO               1
Date_         20130313
Time_            23.57
INSTRUM          spect
PROBHD   5 mm QNP 1H/13
PULPROG         zgpg30
TD               16384
SOLVENT          CD2Cl2
NS                8000
DS                   4
SWH          22058.824 Hz
FIDRES        1.346364 Hz
AQ            0.3714207 sec
RG                2050
DW              22.667 usec
DE               6.50 usec
TE              300.0 K
D1           0.69999999 sec
D11          0.03000000 sec
TD0                  1

======== CHANNEL f1 ========
NUC1               13C
P1                7.00 usec
PL1              -2.60 dB
PL1W       61.34123230 W
SFO1      100.6228298 MHz

======== CHANNEL f2 ========
CPDPRG2         waltz16
NUC2                1H
PCPD2            80.00 usec
PL2              -4.00 dB
PL12             14.06 dB
PL13             120.00 dB
PL2W       19.93825150 W
PL12W       0.31166428 W
PL13W       0.00000000 W
SFO2      400.1316005 MHz
SI               32768
SF        100.6127558 MHz
WDW                 EM
SSB                  0
LB                1.00 Hz
GB                   0
PC                1.40
```

Y-B1

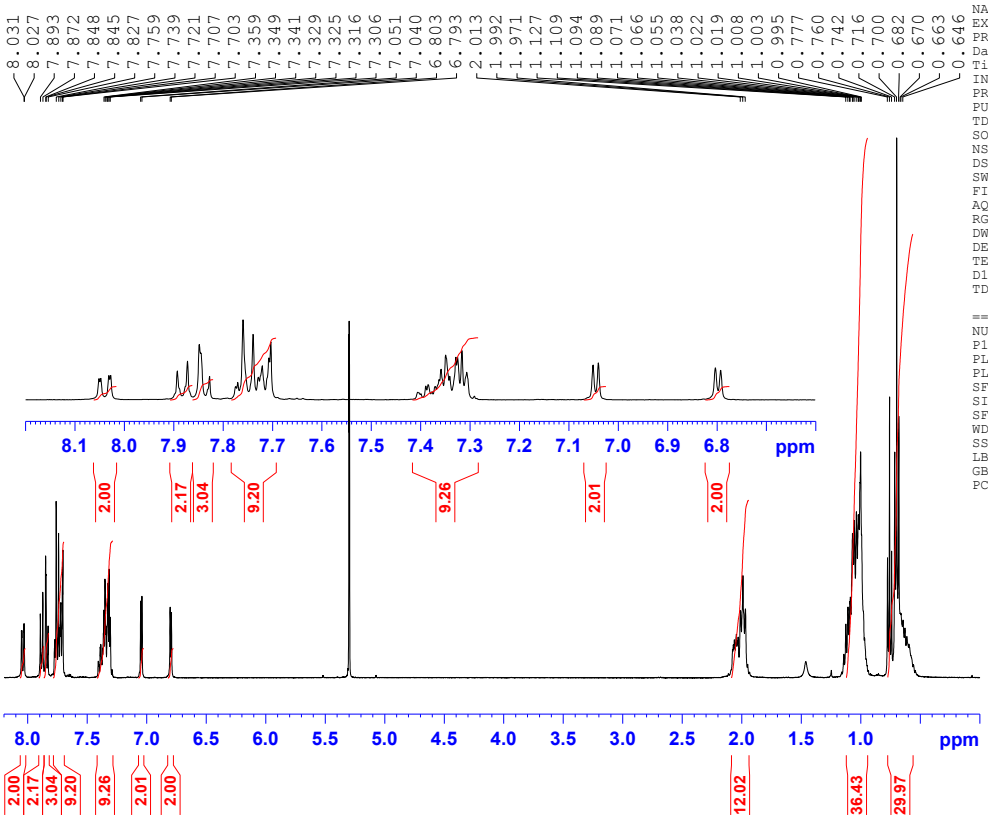


```
NAME        D177004 CO122
EXPNO                1
PROCNO               1
Date_         20130310
Time_            16.24
INSTRUM          spect
PROBHD   5 mm QNP 1H/13
PULPROG          zg30
TD               32564
SOLVENT          CD2Cl2
NS                  64
DS                   2
SWH           8223.685 Hz
FIDRES        0.252539 Hz
AQ            1.9799412 sec
RG                 406
DW              60.800 usec
DE               6.50 usec
TE              300.0 K
D1           2.00000000 sec
TD0                  1

======== CHANNEL f1 ========
NUC1                1H
P1                9.40 usec
PL1              -4.00 dB
PL1W       19.93825150 W
SFO1      400.1324710 MHz
SI               32768
SF        400.1300233 MHz
WDW                 EM
SSB                  0
LB                0.30 Hz
GB                   0
PC                1.00
```

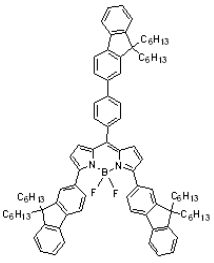

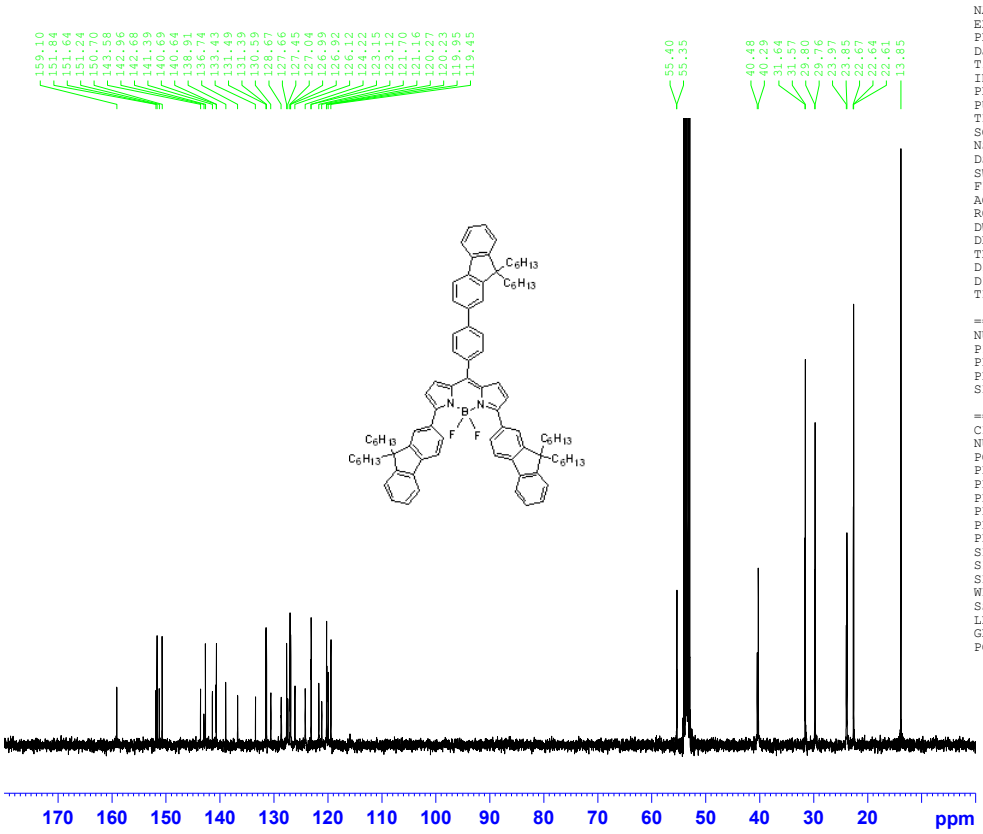


```
NAME        D177010 CO122 13C 6K
EXPNO                         1
PROCNO                        1
Date_                  20130311
Time                       1.52
INSTRUM                   spect
PROBHD    5 mm QNP 1H/13
PULPROG                  zgpg30
TD                        16384
SOLVENT                 CD2Cl2
NS                          6144
DS                             4
SWH                  22058.824 Hz
FIDRES                1.346364 Hz
AQ                    0.3714207 sec
RG                         2050
DW                       22.667 usec
DE                         6.50 usec
TE                        300.0 K
D1                   0.69999999 sec
D11                  0.03000000 sec
TD0                           1

======== CHANNEL f1 ========
NUC1                        13C
P1                         7.00 usec
PL1                       -2.60 dB
PL1W                61.34123230 W
SFO1               100.6228298 MHz

======== CHANNEL f2 ========
CPDPRG2                 waltz16
NUC2                        1H
PCPD2                     80.00 usec
PL2                       -4.00 dB
PL12                      14.06 dB
PL13                     120.00 dB
PL2W                19.93825150 W
PL12W                0.31166428 W
PL13W                0.00000000 W
SFO2               400.1316005 MHz
SI                         32768
SF                 100.6127562 MHz
WDW                           EM
SSB                            0
LB                          1.00 Hz
GB                             0
PC                          1.40
```

Y-B2

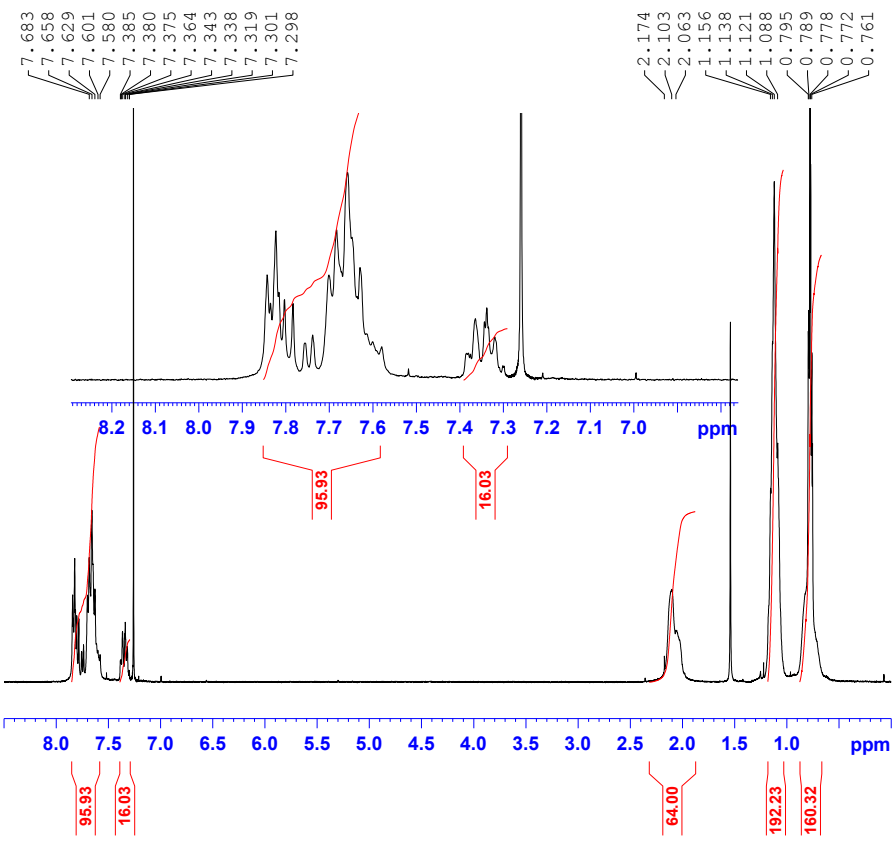


```
NAME        D168801 CO104 1Hdiluted
EXPNO                         1
PROCNO                        1
Date_                  20121020
Time                       7.03
INSTRUM                   spect
PROBHD    5 mm QNP 1H/13
PULPROG                   zg30
TD                        32564
SOLVENT                 CDCl3
NS                           16
DS                            2
SWH                   8223.685 Hz
FIDRES                0.252539 Hz
AQ                    1.9799412 sec
RG                          406
DW                       60.800 usec
DE                         6.50 usec
TE                        294.3 K
D1                   2.00000000 sec
TD0                           1

======== CHANNEL f1 ========
NUC1                        1H
P1                         9.40 usec
PL1                       -4.00 dB
PL1W                19.93825150 W
SFO1               400.1324710 MHz
SI                         32768
SF                 400.1300103 MHz
WDW                           EM
SSB                            0
LB                          0.30 Hz
GB                             0
PC                          1.00
```

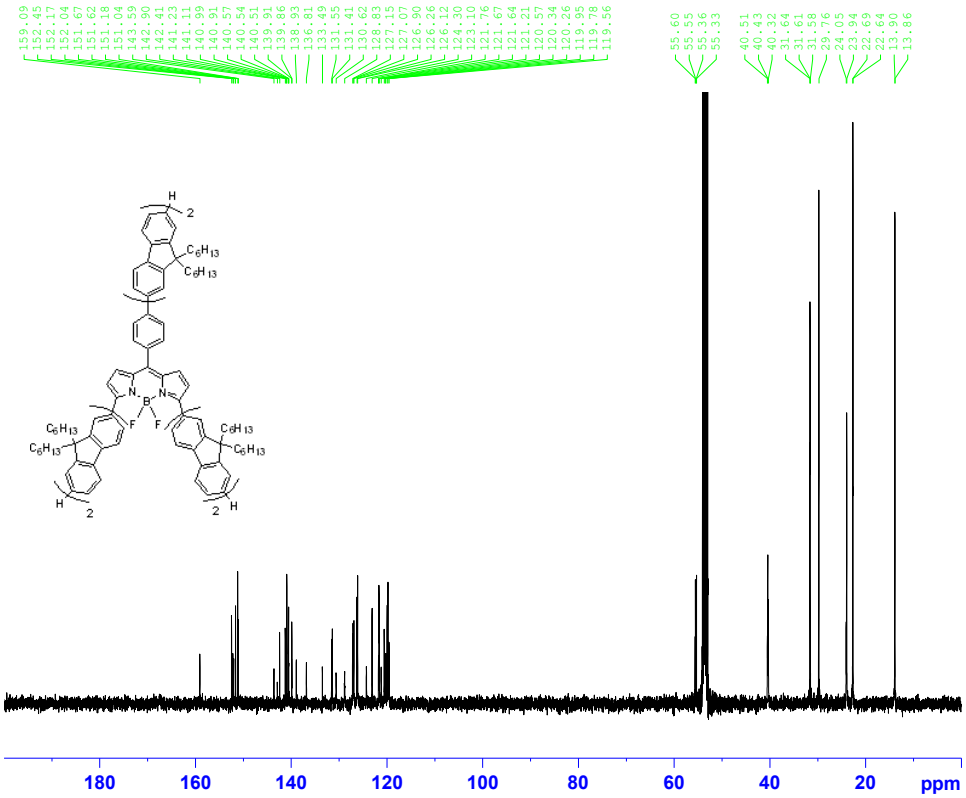
159.09
152.45
152.17
151.84
151.62
151.18
151.04
143.59
142.90
142.41
141.23
141.11
140.99
140.91
140.57
140.54
140.51
139.91
139.86
138.93
136.81
133.49
131.55
131.41
130.62
128.83
127.15
127.07
126.90
126.26
126.12
124.30
123.10
121.76
121.64
121.21
120.57
120.34
120.26
119.95
119.78
119.56
55.60
55.55
55.36
55.33
40.51
40.43
40.32
31.64
31.61
31.58
29.76
24.05
23.94
22.69
22.64
13.90
13.86
NAME D177434 CO126 13C
EXPNO 2
PROCNO 1
Date_ 20130315
Time 22.40
INSTRUM spect
PROBHD 5 mm QNP 1H/13
PULPROG zgpg30
TD 16384
SOLVENT CD2Cl2
NS 10240
DS 4
SWH 22058.824 Hz
FIDRES 1.346364 Hz
AQ 0.3714207 sec
RG 2050
DW 22.667 usec
DE 6.50 usec
TE 300.0 K
D1 0.69999999 sec
D11 0.03000000 sec
TD0 1
======== CHANNEL f1 ========
NUC1 13C
P1 7.00 usec
PL1 -2.60 dB
PL1W 61.34123230 W
SFO1 100.6228298 MHz
======== CHANNEL f2 ========
CPDPRG2 waltz16
NUC2 1H
PCPD2 80.00 usec
PL2 -4.00 dB
PL12 14.06 dB
PL13 120.00 dB
PL2W 19.93825150 W
PL12W 0.31166428 W
PL13W 0.00000000 W
SFO2 400.1316005 MHz
SI 32768
SF 100.6127556 MHz
WDW EM
SSB 0
LB 1.00 Hz
GB 0
PC 1.40
180
160
140
120
100
80
60
40
20
ppm

Y-B3

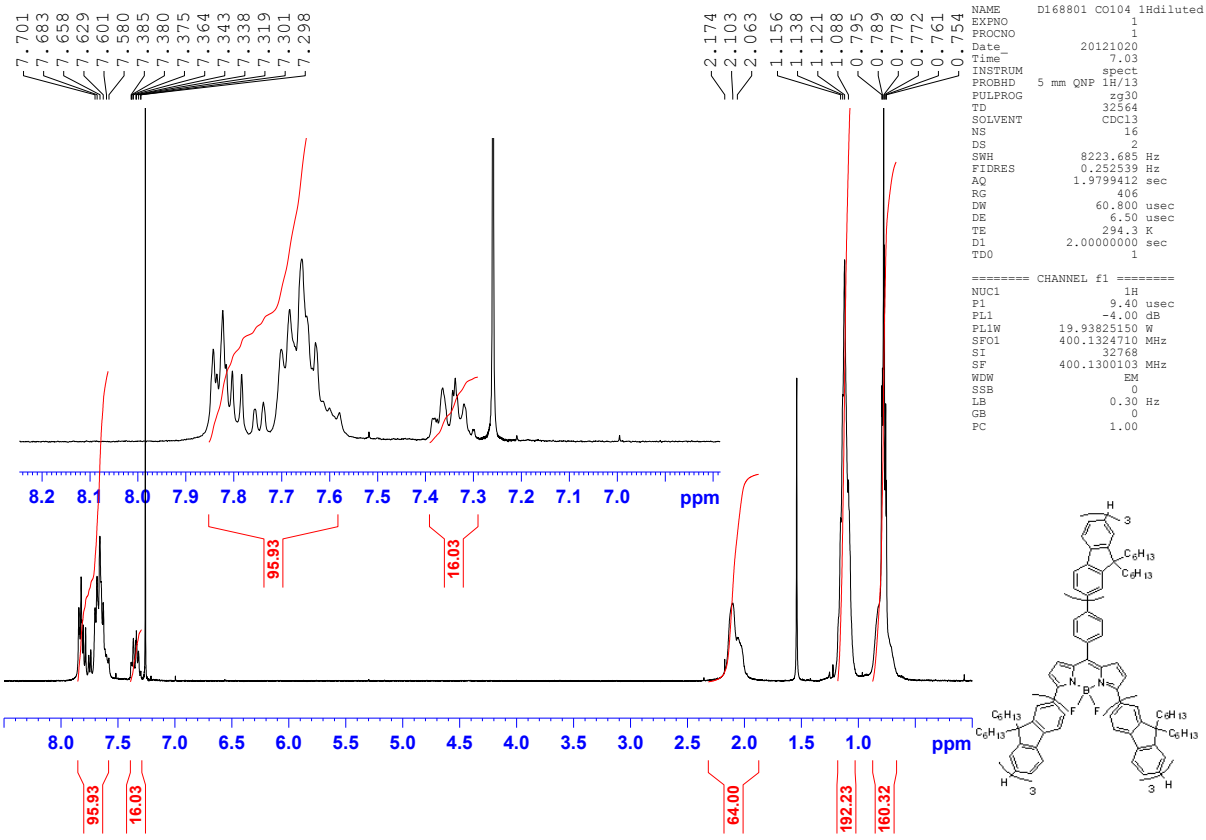
7.701
7.683
7.658
7.629
7.601
7.580
7.385
7.380
7.375
7.364
7.343
7.338
7.319
7.301
7.298
2.174
2.103
2.063
1.156
1.138
1.121
1.088
0.795
0.789
0.778
0.772
0.761
0.754
NAME D168801 CO104 1Hdiluted
EXPNO 1
PROCNO 1
Date_ 20121020
Time 7.03
INSTRUM spect
PROBHD 5 mm QNP 1H/13
PULPROG zg30
TD 32564
SOLVENT CDCl3
NS 16
DS 2
SWH 8223.685 Hz
FIDRES 0.252539 Hz
AQ 1.9799412 sec
RG 406
DW 60.800 usec
DE 6.50 usec
TE 294.3 K
D1 2.00000000 sec
TD0 1
======== CHANNEL f1 ========
NUC1 1H
P1 9.40 usec
PL1 -4.00 dB
PL1W 19.93825150 W
SFO1 400.1324710 MHz
SI 32768
SF 400.1300103 MHz
WDW EM
SSB 0
LB 0.30 Hz
GB 0
PC 1.00
8.2
8.1
8.0
7.9
7.8
7.7
7.6
7.5
7.4
7.3
7.2
7.1
7.0
ppm
95.93
16.03
8.0
7.5
7.0
6.5
6.0
5.5
5.0
4.5
4.0
3.5
3.0
2.5
2.0
1.5
1.0
ppm
95.93
16.03
64.00
192.23
160.32

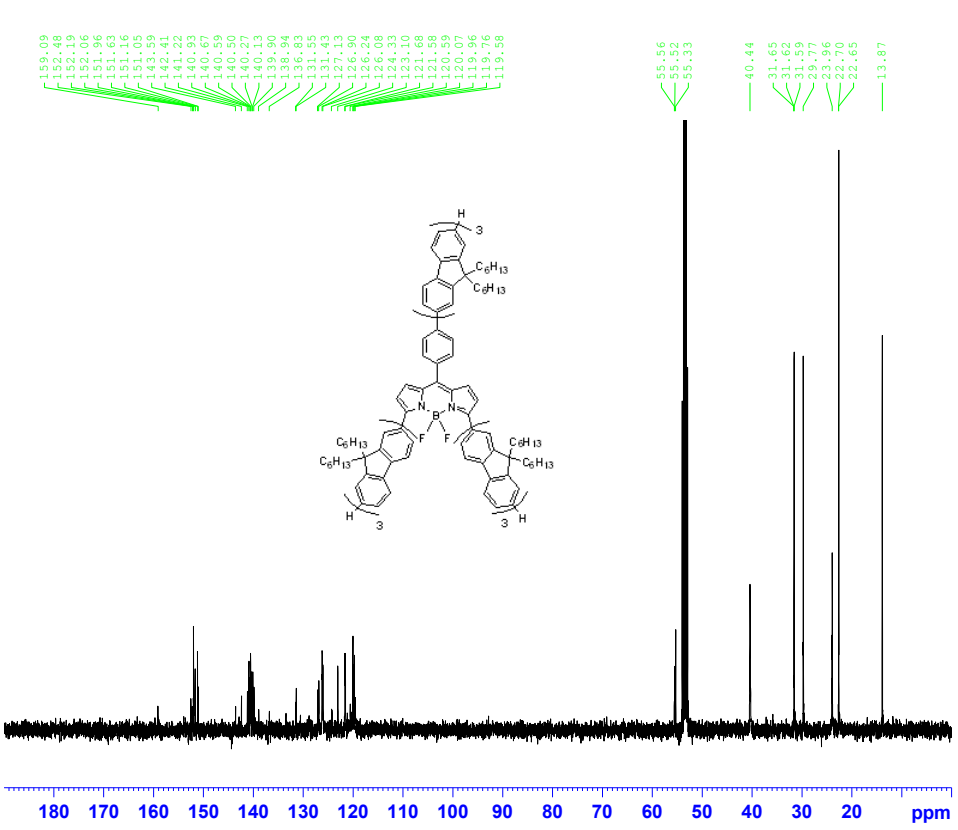


```
NAME          D177329 128 13C
EXPNO                      1
PROCNO                     1
Date_               20130314
Time                    9.53
INSTRUM                 spect
PROBHD    5 mm QNP 1H/13
PULPROG               zgpg30
TD                     16384
SOLVENT              CD2Cl2
NS                       1024
DS                          4
SWH                22058.824 Hz
FIDRES              1.346364 Hz
AQ                  0.3714207 sec
RG                       2050
DW                     22.667 usec
DE                      6.50 usec
TE                     300.0 K
D1                 0.69999999 sec
D11                0.03000000 sec
TD0                        1

======== CHANNEL f1 ========
NUC1                      13C
P1                       7.00 usec
PL1                     -2.60 dB
PL1W               61.34123230 W
SFO1              100.6228298 MHz

======== CHANNEL f2 ========
CPDPRG2              waltz16
NUC2                      1H
PCPD2                  80.00 usec
PL2                    -4.00 dB
PL12                   14.06 dB
PL13                  120.00 dB
PL2W               19.93825150 W
PL12W               0.31166428 W
PL13W               0.00000000 W
SFO2              400.1316005 MHz
SI                       32768
SF                100.6127570 MHz
WDW                         EM
SSB                          0
LB                        1.00 Hz
GB                           0
PC                        1.40
```

Y-B4

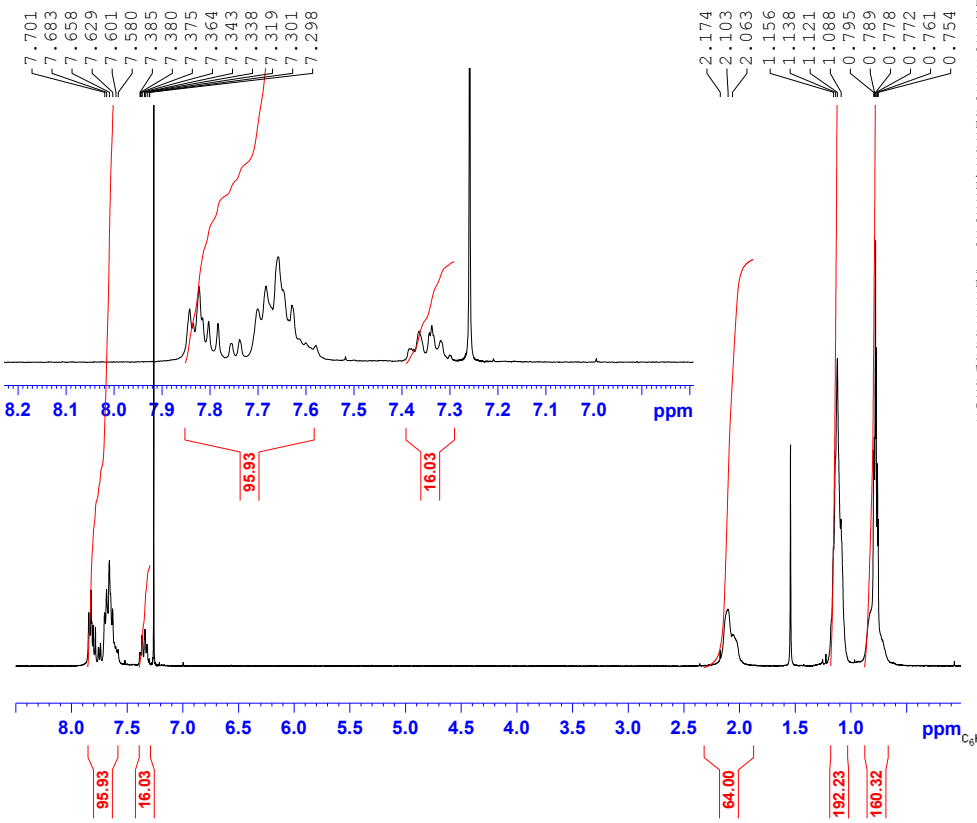


```
NAME          D168801 CO104 1Hdiluted
EXPNO                      1
PROCNO                     1
Date_               20121020
Time                    7.03
INSTRUM                 spect
PROBHD    5 mm QNP 1H/13
PULPROG                 zg30
TD                     32564
SOLVENT              CDCl3
NS                         16
DS                          2
SWH                8223.685 Hz
FIDRES             0.252539 Hz
AQ                 1.9799412 sec
RG                       406
DW                     60.800 usec
DE                      6.50 usec
TE                     294.3 K
D1                 2.00000000 sec
TD0                        1

======== CHANNEL f1 ========
NUC1                       1H
P1                       9.40 usec
PL1                     -4.00 dB
PL1W               19.93825150 W
SFO1              400.1324710 MHz
SI                       32768
SF                400.1300103 MHz
WDW                         EM
SSB                          0
LB                        0.30 Hz
GB                           0
PC                        1.00
```

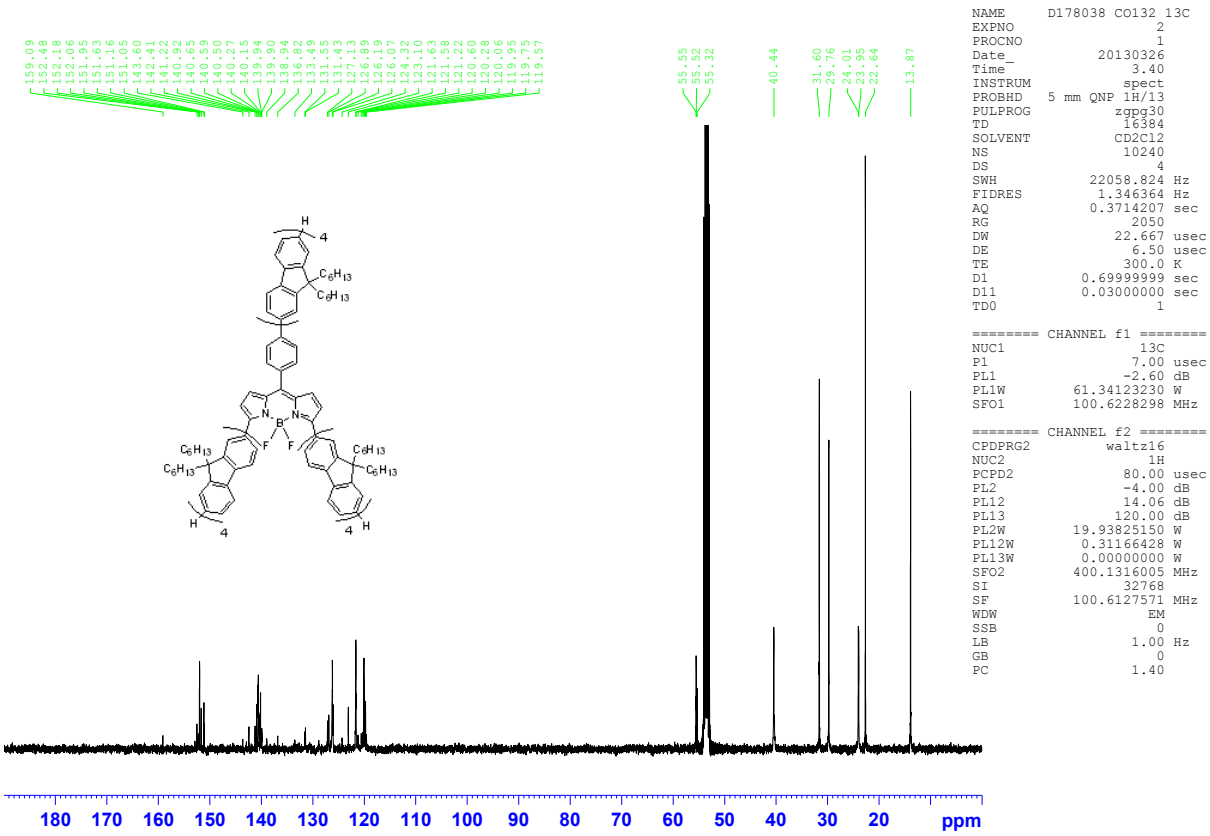


```
NAME        D178038 CO132 13C
EXPNO                   2
PROCNO                  1
Date_            20130326
Time                3.40
INSTRUM            spect
PROBHD    5 mm QNP 1H/13
PULPROG           zgpg30
TD                 16384
SOLVENT            CD2Cl2
NS                 10240
DS                     4
SWH            22058.824 Hz
FIDRES          1.346364 Hz
AQ              0.3714207 sec
RG                  2050
DW                22.667 usec
DE                 6.50 usec
TE                300.0 K
D1             0.69999999 sec
D11            0.03000000 sec
TD0                     1

======== CHANNEL f1 ========
NUC1                  13C
P1                   7.00 usec
PL1                 -2.60 dB
PL1W          61.34123230 W
SFO1         100.6228298 MHz

======== CHANNEL f2 ========
CPDPRG2           waltz16
NUC2                   1H
PCPD2                80.00 usec
PL2                 -4.00 dB
PL12                14.06 dB
PL13               120.00 dB
PL2W          19.93825150 W
PL12W          0.31166428 W
PL13W          0.00000000 W
SFO2         400.1316005 MHz
SI                   32768
SF           100.6127571 MHz
WDW                     EM
SSB                      0
LB                    1.00 Hz
GB                       0
PC                    1.40
```